

WRANGELLIA FLOOD BASALTS IN ALASKA, YUKON, AND  
BRITISH COLUMBIA: EXPLORING THE GROWTH AND MAGMATIC HISTORY  
OF A LATE TRIASSIC OCEANIC PLATEAU

By

ANDREW R. GREENE

A THESIS SUBMITTED IN PARTIAL FULFILLMENT OF  
THE REQUIREMENTS FOR THE DEGREE OF

DOCTOR OF PHILOSOPHY

in

THE FACULTY OF GRADUATE STUDIES

(Geological Sciences)

UNIVERSITY OF BRITISH COLUMBIA

(Vancouver)

August 2008

©Andrew R. Greene, 2008

## ABSTRACT

The Wrangellia flood basalts are parts of an oceanic plateau that formed in the eastern Panthalassic Ocean (ca. 230-225 Ma). The volcanic stratigraphy presently extends >2300 km in British Columbia, Yukon, and Alaska. The field relationships, age, and geochemistry have been examined to provide constraints on the construction of oceanic plateaus, duration of volcanism, source of magmas, and the conditions of melting and magmatic evolution for the volcanic stratigraphy.

Wrangellia basalts on Vancouver Island (Karmutsen Formation) form an emergent sequence consisting of basal sills, submarine flows (>3 km), pillow breccia and hyaloclastite (<1 km), and subaerial flows (>1.5 km). Karmutsen stratigraphy overlies Devonian to Permian volcanic arc (~380-355 Ma) and sedimentary sequences and is overlain by Late Triassic limestone. The Karmutsen basalts are predominantly homogeneous tholeiitic basalt (6-8 wt% MgO); however, the submarine part of the stratigraphy, on northern Vancouver Island, contains picritic pillow basalts (9-20 wt% MgO). Both lava groups have overlapping initial  $\epsilon_{\text{Hf}}$  and  $\epsilon_{\text{Nd}}$ , indicating a common, ocean island basalt (OIB)-type Pacific mantle source similar to the source of basalts from the Ontong Java and Caribbean Plateaus. The major-element chemistry of picrites indicates extensive melting (23-27%) of anomalously hot mantle (~1500°C), which is consistent with an origin from a mantle plume head.

Wrangellia basalts extend ~450 km across southern Alaska (Wrangell Mountains and Alaska Range) and through southwest Yukon where <3.5 km of mostly subaerial flows (Nikolai Formation) are bounded by Pennsylvanian to Permian volcanic (312-280 Ma) and sedimentary strata, and Late Triassic limestone. The vast majority of the Nikolai basalts are LREE-enriched high-Ti basalt (1.6-2.4 wt%  $\text{TiO}_2$ ) with uniform plume-type Pacific mantle isotopic compositions. However, the lowest ~400 m of stratigraphy in the Alaska Range, and lower stratigraphy in Yukon, is light rare earth element (LREE)-depleted low-Ti basalt (0.4-1.2 wt%  $\text{TiO}_2$ ) with pronounced negative-HFSE anomalies and high  $\epsilon_{\text{Hf}}$  values that are decoupled from Nd and displaced well above the OIB mantle array. The low-Ti basalts indicate subduction-modified mantle was involved in the formation of basalts exposed in Alaska and Yukon, possibly from mechanical and thermal erosion of the base of the lithosphere from an impinging mantle plume head.

## TABLE OF CONTENTS

<b>Abstract.....</b>	<b>ii</b>
<b>Table of Contents .....</b>	<b>iii</b>
<b>List of Tables .....</b>	<b>vii</b>
<b>List of Figures.....</b>	<b>ix</b>
<b>Acknowledgements .....</b>	<b>xv</b>
<b>Dedication .....</b>	<b>xvi</b>
<b>Co-authorship statement .....</b>	<b>xvii</b>

### CHAPTER 1

<b>Introduction.....</b>	<b>1</b>
Introduction and motivation for this study .....	2
The Wrangellia oceanic plateau.....	7
Methodology and rationale for this study .....	10
Previous research .....	11
The importance of LIPs and mantle plumes .....	12
An overview of the four manuscripts in this dissertation and additional references ...	15
Contributions to this project.....	18
References.....	19

### CHAPTER 2

#### **Wrangellia Flood Basalts on Vancouver Island: Significance of**

#### **Picritic and Tholeiitic Lavas for the Melting History and Magmatic**

<b>Evolution of a Major Oceanic Plateau .....</b>	<b>26</b>
Introduction.....	27
Geologic setting .....	28
Wrangellia on Vancouver Island .....	28
Age of the Karmutsen Formation .....	31
Volcanic stratigraphy and petrography .....	31
Sample preparation and analytical methods .....	37
Whole-rock chemistry.....	44
Major- and trace-element compositions.....	44
Sr-Nd-Hf-Pb isotopic compositions.....	56
Alteration .....	62
Olivine accumulation in picritic lavas .....	63
Discussion .....	63
Melting conditions and major-element composition of primary magmas .....	65
Source of Karmutsen lavas .....	68
REE modeling: Dynamic melting and source mineralogy .....	71
Magmatic evolution of Karmutsen tholeiitic basalts .....	75
Conclusions.....	78
Acknowledgements.....	79
References.....	79

## **CHAPTER 3**

### **Wrangellia Flood Basalts in Alaska: A Record of Plume-Lithosphere**

<b>Interaction in a Late Triassic Accreted Oceanic Plateau .....</b>	<b>86</b>
Introduction.....	87
Geologic setting .....	89
Wrangellia in Alaska.....	89
Wrangell Mountains.....	89
Eastern Alaska Range .....	91
Age of the Nikolai Formation.....	93
Volcanic stratigraphy and petrography .....	93
Whole-rock chemistry.....	104
Major- and trace-element compositions.....	104
Sr-Nd-Hf-Pb isotopic compositions.....	115
Alteration .....	115
Flood basalt chemostratigraphy .....	123
Discussion.....	125
Source of Nikolai basalts .....	125
Lithospheric involvement in derivation of the low-titanium basalts .....	128
Nature of underlying Paleozoic arc lithosphere.....	128
Trace-element and isotopic source constraints of the low titanium basalts...	129
Origin of decoupled Hf and Nd isotopic compositions of	
low-titanium basalts .....	134
Melting conditions and estimated major-element composition of	
primary low-Ti magma .....	138
Conclusions.....	142
Acknowledgements.....	143
References.....	143

## **CHAPTER 4**

### **Geochemistry of Flood Basalts from the Yukon (Canada) Segment of the**

<b>Accreted Wrangellia Oceanic Plateau .....</b>	<b>151</b>
Introduction.....	152
Geologic setting and age constraints.....	153
Field relations and petrography .....	156
Whole-rock chemistry.....	161
Major- and trace-element compositions.....	161
Sr-Nd-Hf-Pb isotopic compositions.....	171
Discussion.....	171
Effects of alteration and comparison to Nikolai basalts in Alaska .....	171
Relationship between chemistry and stratigraphic position.....	179
Source characteristics of Nikolai basalts in Yukon .....	180
Melting of arc mantle in formation of the low-titanium basalts .....	182
Conclusion .....	188
Acknowledgements.....	189
References.....	189



## **CHAPTER 5**

### **The Age and Volcanic Stratigraphy of the Accreted Wrangellia Oceanic**

<b>Plateau in Alaska, Yukon and British Columbia.....</b>	<b>195</b>
Introduction.....	196
Wrangellia flood basalts: The volcanic stratigraphy of an accreted oceanic plateau .....	198
Geographic distribution and aerial extent of the Wrangellia flood basalts.....	200
Geologic history of Wrangellia.....	200
Stratigraphy of Wrangellia.....	203
Wrangellia of southern Alaska.....	203
Talkeetna Mountains and eastern Alaska Range .....	205
Wrangell Mountains.....	209
Wrangellia in southwest Yukon.....	215
Wrangellia in southeast Alaska.....	218
Wrangellia in the Queen Charlotte Islands (Haida Gwaii) .....	221
Wrangellia on Vancouver Island .....	222
Central and southern Vancouver Island.....	222
Northern Vancouver Island.....	228
Geochronology of Wrangellia.....	233
Previous geochronology for Wrangellia flood basalts and related plutonic rocks .....	233
Information about samples analyzed by $^{40}\text{Ar}/^{39}\text{Ar}$ in this study .....	235
$^{40}\text{Ar}/^{39}\text{Ar}$ geochronological results .....	236
Summary of isotopic age determinations for Wrangellia flood basalts.....	243
Paleontological studies.....	243
Discussion .....	245
Overview of geology and age of Northern and Southern Wrangellia.....	245
Eruption environment for Wrangellia flood basalts.....	248
Northern Wrangellia .....	248
Southern Wrangellia .....	249
The accumulation and subsidence of the Wrangellia flood basalts .....	251
Conclusion .....	254
Acknowledgements.....	255
References.....	255

## **CHAPTER 6**

<b>Conclusions.....</b>	<b>266</b>
Conclusions and Directions for Future Research.....	267
References.....	271

<b>Appendices.....</b>	<b>272</b>
Appendix A. Geologic map of the Mount Arrowsmith area .....	273
Appendix B. XRF whole-rock analyses of a subset of Karmutsen basalts, Vancouver Island, B.C.....	274
Appendix C. PCIGR trace-element analyses of Karmutsen basalts, Vancouver Island, B.C.....	276
Appendix D. Sample preparation and analytical methods for Alaska samples .....	279
Appendix E. Sample preparation and analytical methods for Yukon samples.....	284
Appendix F. Major element (wt% oxide) and trace element (ppm) abundances in whole rock samples of Late Paleozoic Station Creek Formation, Yukon.....	288
Appendix G. Previous research on Wrangellia.....	290
Appendix H. $^{40}\text{Ar}/^{39}\text{Ar}$ analytical methods.....	306
Appendix I. Analytical results of reference material from Actlabs whole-rock analyses for Vancouver Island and Yukon .....	308
Appendix J. Description of supplementary electronic files on CD-ROM .....	310

## **Supplementary electronic files on CD-ROM**

### **Supplementary data files (SD)**

- SD 1- Endnote database for Wrangellia (.enl file)
- SD 2- Reference list for Wrangellia (.doc file)
- SD 3- Geochemistry for  $^{40}\text{Ar}/^{39}\text{Ar}$  samples (.xls file)
- SD 4-  $^{40}\text{Ar}/^{39}\text{Ar}$  analytical data (.xls file)
- SD 5- Wrangellia ages and biostratigraphy (.xls file)

### **Supplementary Google Earth files (SGE)**

- SGE 1- Mapped Wrangellia flood basalts (.kmz file)
- SGE 2- Major faults in Alaska and Yukon (.kml file)
- SGE 3- Major faults in southwest B.C. (.kml file)
- SGE 4- Alaska sample locations (.kml file)
- SGE 5- Yukon sample locations (.kml file)
- SGE 6- Vancouver Island sample locations (.kml file)
- SGE 7- Alaska Range photograph locations (.kmz file)
- SGE 8- Wrangell Mountains photograph locations (.kmz file)
- SGE 9- Yukon photograph locations (.kmz file)
- SGE 10- Vancouver Island photograph locations (.kmz file)

### **Supplementary photo files (SP)**

- SP 1- Alaska Range photographs (.pdf file)
- SP 2- Wrangell Mountains photographs (.pdf file)
- SP 3- Ed MacKevett Jr. Wrangell Mountains photographs (.pdf file)
- SP 4- Yukon photographs (.pdf file)
- SP 5- Vancouver Island photos (.pdf file)

Greene\_2008\_PhD\_dissertation\_UBC (.pdf file of complete dissertation)

## **LIST OF TABLES**

### **CHAPTER 2**

Table 2.1	Summary of petrographic characteristics and phenocryst proportions of Karmutsen basalts on Vancouver Island, B.C.....	39
Table 2.2	Major element (wt% oxide) and trace element (ppm) abundances in whole rock samples of Karmutsen basalts, Vancouver Island, B.C.....	46
Table 2.3	Sr and Nd isotopic compositions of Karmutsen basalts, Vancouver Island, B.C.....	59
Table 2.4	Hf isotopic compositions of Karmutsen basalts, Vancouver Island, B.C. ....	60
Table 2.5	Pb isotopic compositions of Karmutsen basalts, Vancouver Island, B.C. ....	61
Table 2.6	Estimated primary magma compositions for Karmutsen basalts and other oceanic plateaus/islands.....	67

### **CHAPTER 3**

Table 3.1	Summary of petrographic characteristics and phenocryst proportions of Nikolai basalts in Alaska.....	102
Table 3.2	Major element (wt% oxide) and trace element (ppm) abundances in whole rock samples of Nikolai basalts, Alaska.....	106
Table 3.3	Sr and Nd isotopic compositions of Nikolai basalts, Alaska.....	118
Table 3.4	Hf isotopic compositions of Nikolai basalts, Alaska.....	119
Table 3.5	Pb isotopic compositions of Nikolai basalts, Alaska.....	120
Table 3.6	Estimated primary magma compositions for Nikolai basalts and other oceanic plateaus/islands.....	141

### **CHAPTER 4**

Table 4.1	Summary of petrographic characteristics and phenocryst proportions of Nikolai basalts in Yukon.....	160
Table 4.2	Major element (wt% oxide) and trace element (ppm) abundances in whole rock samples of Nikolai basalts, Yukon.....	163

Table 4.3	Sr and Nd isotopic geochemistry of Nikolai basalts, Yukon. ....	174
Table 4.4	Hf isotopic compositions of Nikolai basalts, Yukon. ....	175
Table 4.5	Pb isotopic compositions of Nikolai basalts, Yukon. ....	176
<b>CHAPTER 5</b>		
Table 5.1	Areal extent and volumetric estimates for the Wrangellia flood basalts .....	201
Table 5.2	Compilation of previous geochronology of Wrangellia flood basalts and associated plutonic rocks.....	234
Table 5.3	$^{40}\text{Ar}/^{39}\text{Ar}$ dating results for 13 samples of Wrangellia flood basalts and 6 samples from the Wrangellia Terrane. ....	241
Table 5.4	Comparison of geology and ages of Northern and Southern Wrangellia. ....	246

## **LIST OF FIGURES**

### **CHAPTER 1**

Figure 1.1 Distribution of Phanerozoic LIPs on Earth. ....	3
Figure 1.2 Schematic diagrams of mantle plumes in the Earth's interior.....	4
Figure 1.3 "Pin-pricking" the giant Ontong Java Plateau.....	6
Figure 1.4 Map showing distribution of Wrangellia flood basalts in Alaska, Yukon, and British Columbia. ....	8
Figure 1.5 Estimated distribution of the continental landmasses in the Middle to Late Triassic (~226 Ma). ....	9
Figure 1.6 Age difference between peak eruption ages of LIPs from the last 260 Myr versus the age of a stratigraphic boundary. ....	14
Figure 1.7 Photographs showing the different modes of transportation used for field work in remote areas of Alaska, Yukon, and BC as part of this project.....	17

### **CHAPTER 2**

Figure 2.1 Simplified map of Vancouver Island showing the distribution of the Karmutsen Formation. ....	30
Figure 2.2 Geologic map and stratigraphy of the Schoen Lake Provincial Park and Karmutsen Range areas. ....	33
Figure 2.3 Photographs of picritic and tholeiitic pillow basalts from the Karmutsen Range area (Alice and Nimpkish Lake area), northern Vancouver Island.....	34
Figure 2.4 Photographs showing field relations from the Schoen Lake Provincial Park area, northern Vancouver Island. ....	35
Figure 2.5 Photomicrographs of picritic pillow basalts, Karmutsen Formation, northern Vancouver Island. ....	38
Figure 2.6 Whole-rock major-element, Ni, and LOI variation diagrams for the Karmutsen Formation. ....	45
Figure 2.7 Whole-rock REE and trace-element concentrations for the Karmutsen Formation. ....	53

Figure 2.8 Whole-rock trace-element concentrations and ratios for the Karmutsen Formation. ....	55
Figure 2.9 Whole-rock Sr, Nd, and Hf isotopic compositions for the Karmutsen Formation. ....	57
Figure 2.10 Pb isotopic compositions of leached whole-rock samples by MC-ICP-MS for the Karmutsen Formation. ....	58
Figure 2.11 Relationship between abundance of olivine phenocrysts and whole-rock MgO contents for Keogh Lake picrites. ....	64
Figure 2.12 Estimated primary magma compositions for three Keogh Lake picrites using the forward and inverse modeling technique of Herzberg <i>et al.</i> (2007). ....	66
Figure 2.13 Comparison of age-corrected (230 Ma) Sr-Nd-Hf-Pb isotopic compositions for Karmutsen flood basalts on Vancouver Island to age-corrected OIB and MORB. ....	69
Figure 2.14 Evolution of $\epsilon_{\text{Hf}}$ with time for picritic and tholeiitic lavas for the Karmutsen Formation. ....	72
Figure 2.15 Trace-element modeling results for incongruent dynamic mantle melting for picritic and tholeiitic lavas from the Karmutsen Formation. ....	74
Figure 2.16 Forward fractional crystallization modeling results for major elements from MELTS (Ghiorso & Sack, 1995) compared to picritic and tholeiitic lavas from the Karmutsen Formation. ....	77
 <b>CHAPTER 3</b>	
Figure 3.1 Simplified map of south-central Alaska showing the distribution of the Nikolai Formation. ....	90
Figure 3.2 Geologic map and stratigraphy of the Wrangell Mountains, Alaska. ....	92
Figure 3.3 Photographs of the base of the Nikolai Formation in the Wrangell Mountains, Alaska. ....	94
Figure 3.4 Photograph of ~1000 m of continuous flood basalt stratigraphy at the top of the Nikolai Formation along Glacier Creek in the Wrangell Mountains, Alaska. ....	95
Figure 3.5 Photographs showing the top of the Nikolai Formation in the Wrangell Mountains, Alaska. ....	97

Figure 3.6 Simplified geologic map and stratigraphy of the Amphitheater Mountains, Alaska. ....	98
Figure 3.7 Photographs of the base of the Nikolai Formation in the Amphitheater Mountains, east-central Alaska Range (Tangle Lakes, West), Alaska. ....	99
Figure 3.8 Geologic map and stratigraphy of the Clearwater Mountains, Alaska.....	101
Figure 3.9 Representative photomicrographs of Nikolai basalts, Alaska. ....	103
Figure 3.10 Whole-rock major-element and Ni variation diagrams vs. MgO for the Nikolai Formation in Alaska with data for the Nikolai Formation in Yukon. ....	105
Figure 3.11 Whole-rock REE and trace-element concentrations for the Nikolai Formation in Alaska.....	113
Figure 3.12 Whole-rock trace-element concentration variations and ratios for the Nikolai Formation in Alaska, with data for the Nikolai Formation in Yukon. ....	114
Figure 3.13 Whole-rock Sr, Nd, and Hf isotopic compositions for the Nikolai Formation in Alaska.....	116
Figure 3.14 Pb isotopic compositions of leached whole-rock samples by MC-ICP-MS for the Nikolai Formation in Alaska. ....	117
Figure 3.15 Loss-on-ignition versus MgO and isotopic ratios for the Nikolai Formation in Alaska.....	122
Figure 3.16 Chemostratigraphy of the Nikolai Formation in three areas of Alaska (Clearwater, Amphitheater, and Wrangell Mountains). ....	124
Figure 3.17 Comparison of age-corrected (230 Ma) Sr-Nd-Hf isotopic compositions for Nikolai basalts in Alaska to age-corrected OIB and MORB. ....	126
Figure 3.18 Comparison of Pb isotopic compositions of the Nikolai Formation in Alaska to OIB and MORB. ....	127
Figure 3.19 Trace-element ratios and isotopic compositions of the Nikolai Formation in Alaska.....	130
Figure 3.20 Th-Nb and Ti-Yb proxies of the Nikolai Formation in Alaska with data compilation and modeling results. ....	132

Figure 3.21	Global Hf-Nd isotope systematics with age-corrected data of the Nikolai Formation in Alaska.....	136
Figure 3.22	Comparison of initial Hf, Nd, and Sr isotopic compositions of the Nikolai Formation in Alaska to Pacific arcs (Tonga-Kermadec, Mariana, Vanuatu, New Britain) and Pacific MORB.....	137
Figure 3.23	Estimated primary magma compositions for two picrites from the Nikolai Formation using the forward and inverse modeling technique of Herzberg <i>et al.</i> (2007).....	140

## CHAPTER 4

Figure 4.1	Simplified map of southwest Yukon showing the distribution of the Nikolai Formation.....	154
Figure 4.2	Geologic map and stratigraphy of the northern part of the Kluane Ranges, Yukon. ....	155
Figure 4.3	Photographs of the Nikolai Formation in the Kluane Ranges, Yukon. ....	158
Figure 4.4	Photomicrographs of representative Nikolai basalts in southwest Yukon.....	159
Figure 4.5	Whole-rock major-element variation diagrams for the Nikolai Formation in Yukon with data for the Nikolai Formation in Alaska.....	162
Figure 4.6	Whole-rock REE and trace-element concentrations for the Nikolai Formation in Kluane Ranges, Yukon.....	170
Figure 4.7	Whole-rock trace-element concentrations for the Nikolai Formation in Yukon, with data for the Nikolai Formation in Alaska.....	172
Figure 4.8	Whole-rock Sr, Nd, and Hf isotopic compositions for the Nikolai Formation in Yukon, with fields for the Nikolai Formation in Alaska.....	173
Figure 4.9	Comparison of trace-element compositions of the Nikolai basalts in Yukon to averages for basalts from Alaska. ....	178
Figure 4.10	Comparison of age-corrected (230 Ma) Sr-Nd-Hf isotopic compositions of the Nikolai Formation in Yukon and Alaska to age-corrected OIB and MORB. ....	181
Figure 4.11	Th-Nb and Ti-Yb systematics for the Nikolai Formation in Yukon with data compilation and modeling results. ....	183



Figure 4.12 Trace-element ratios of high- and low-titanium basalts of the Nikolai Formation in Yukon with Paleozoic arc samples and fields for Nikolai basalts in Alaska. ....	184
Figure 4.13 Schematic diagrams of two stages of melting of Nikolai basalts in Yukon and Alaska that produced the low- and high-titanium basalts in Yukon and Alaska. ....	185
Figure 4.14 Trace-element abundances of low-titanium basalts from Yukon compared to arc mantle compositions of the Early to Middle Jurassic Talkeetna arc and incongruent dynamic melting modeling results. ....	187
 <b>CHAPTER 5</b>	
Figure 5.1 Map showing the distribution of Phanerozoic large igneous provinces. ....	197
Figure 5.2 Simplified map showing the distribution of Wrangellia flood basalts in Alaska, Yukon, and British Columbia. ....	199
Figure 5.3 Simplified map of eastern south-central Alaska showing the distribution of Wrangellia flood basalts and stratigraphic columns. ....	204
Figure 5.4 Geology and magnetic map of the Amphitheater Mountains. ....	207
Figure 5.5 Photographs of base of Nikolai Formation in Tangle Lakes area of the Amphitheater Mountains. ....	208
Figure 5.6 Photographs of the base of Nikolai Formation north of Skolai Creek in Wrangell-St. Elias National Park. ....	210
Figure 5.7 Photographs of flood basalts in the Glacier Creek area in Wrangell-St. Elias National Park and map of the southern part of the Wrangell Mountains. ....	211
Figure 5.8 Photographs of the top of the Nikolai Formation around Hidden Lake Creek in Wrangell-St. Elias National Park. ....	212
Figure 5.9 Photographs and map of the Nikolai Formation in southwest Yukon. ....	216
Figure 5.10 Simplified map of southeast Alaska showing the distribution of Triassic basalts that may be correlative with Wrangellia flood basalts. ....	219
Figure 5.11 Simplified map of Vancouver Island showing the distribution of the Karmutsen Formation. ....	223

Figure 5.12	Field notes, photographs, and geologic map for the Schoen Lake area, Vancouver Island.....	226
Figure 5.13	Generalized geology and photographs of Buttle Lake area, Vancouver Island. ....	227
Figure 5.14	Generalized geology of the Karmutsen Formation on northern Vancouver Island in the Port Alice-Robson Bight area.....	229
Figure 5.15	Photographs of intra-Karmutsen sedimentary lens near the top of the Karmutsen southwest of Nimpkish Lake, northern Vancouver Island. ....	231
Figure 5.16	Photographs from near Holberg Inlet, northern Vancouver Island. ....	232
Figure 5.17	$^{40}\text{Ar}/^{39}\text{Ar}$ age spectra for 6 analyses of plagioclase separates from Vancouver Island. ....	237
Figure 5.18	$^{40}\text{Ar}/^{39}\text{Ar}$ age spectra of 1 biotite and 2 plagioclase separates from Yukon. ....	238
Figure 5.19	$^{40}\text{Ar}/^{39}\text{Ar}$ age spectra for 6 analyses of plagioclase separates from Alaska.....	239
Figure 5.20	$^{40}\text{Ar}/^{39}\text{Ar}$ age spectra for 6 analyses of hornblende separates from Alaska.....	240
Figure 5.21	$^{40}\text{Ar}/^{39}\text{Ar}$ and U/Pb ages of Wrangellia flood basalts and plutonic rocks.....	244
Figure 5.22	Summary of geochronology and biostratigraphy for Wrangellia.....	247

## ACKNOWLEDGEMENTS

This project has involved help from numerous people who I am extremely grateful to. James Scoates and Dominique Weis proposed and guided this study. I am grateful for the opportunity they gave me and for their enthusiastic guidance and support.

I also have greatly appreciated help from Graham Nixon of the BC Geological Survey and Steve Israel of the Yukon Geological Survey. Advice was also offered from Jeanine Schmidt (USGS Anchorage), David Brew (USGS Menlo Park), Nick Massey (BCGS), Mikkel Schau, and Don Carlisle.

Kelly and Natalie Bay of Wrangell Mountain Air in McCarthy, Alaska provided extensive knowledge of the Wrangell Mountains. Jeff Trop (Bucknell University) and Danny Rosenkrans (Wrangell-St. Elias National Park) offered assistance with backcountry advice about Wrangell-St. Elias National Park.

Great thanks go to Bruno Kieffer, Frederico Henriques, and James Scoates for help with field work and making time in the field lots of fun.

Katrin Breitsprecher was helpful with reviewing and discussions. Bruno Kieffer, Jane Barling, and Bert Mueller provided training for analytical work.

I would also like to thank Mark Jellinek and Jim Mortensen for being a part of my thesis committee and posing thought-provoking questions that inspired me to explore different areas.

## DEDICATION

This dissertation is dedicated to my Mom and Dad, Sue and Art Greene.  
It is special to share this achievement with them.



## **CO-AUTHORSHIP STATEMENT**

The four manuscripts in this dissertation are all co-authored by colleagues. My supervisors James Scoates and Dominique Weis are co-authors on each of the manuscripts and they significantly contributed to each manuscript. Their contributions included ideas, advice, comments, and reviewing, as well as financial support. The contributions from other co-authors on each manuscript are described below.

### **CHAPTER 2**

#### **Wrangellia flood basalts on Vancouver Island: Significance of picritic and tholeiitic lavas for the melting history and magmatic evolution of a major oceanic plateau**

Authors: Andrew R. Greene, James S. Scoates, Dominique Weis, Graham T. Nixon, Bruno Kieffer

Bruno Kieffer analyzed a suite of 24 samples from Vancouver Island for isotopic and trace-element compositions.

Graham Nixon helped with field work and advice on field relationships and geochemistry.

### **CHAPTER 3**

#### **Wrangellia flood basalts in Alaska: A record of plume-lithosphere interaction in a Late Triassic accreted oceanic plateau**

Authors: Andrew R. Greene, James S. Scoates, and Dominique Weis

James Scoates and Dominique Weis contributed to many aspects of this manuscript.

### **CHAPTER 4**

#### **Geochemistry of flood basalts from the Yukon (Canada) segment of the accreted Wrangellia oceanic plateau**

Authors: Andrew R. Greene, James S. Scoates, Dominique Weis, Steve Israel

Steve Israel assisted with field work, and contributed funding for field work and analytical data. Steve provided major- and trace-element whole-rock analyses of twenty-six samples of Nikolai basalt and 8 Station Creek samples.

### **CHAPTER 5**

#### **The age and volcanic stratigraphy of the accreted Wrangellia oceanic plateau in Alaska, Yukon and British Columbia**

Authors: Andrew R. Greene, James S. Scoates, Dominique Weis, Erik C. Katvala, Steve Israel, and Graham T. Nixon

Erik Katvala assisted with field work on Vancouver Island, provided fossil determinations, and helped with revisions on the manuscript.

Steve Israel contributed a single  $^{40}\text{Ar}/^{39}\text{Ar}$  age date and provided revisions on the manuscript.

Graham Nixon offered advice and revisions on the manuscript.

# **CHAPTER 1**

## **Introduction**

## INTRODUCTION AND MOTIVATION FOR THIS STUDY

The largest melting events on Earth have led to the formation of transient large igneous provinces (LIPs). LIPs are features that can extend over millions of square kilometers of the Earth's surface and consist of flood basalt sequences up to 6 km thick. These voluminous outpourings of lava occur over short intervals of geologic time (i.e. several million years) and have been linked to major changes in the global climate and biosphere in Earth history.

This project is an extensive field and geochemical study of one of the major transient LIPs on Earth, the Triassic Wrangellia oceanic plateau. Transient and persistent LIPs cover large areas of the oceans and continents (Fig. 1.1). Approximately 13 major transient LIPs have formed in the last 260 Myr (Courtilot & Renne, 2003), including the Siberian (ca. 251 Ma) and Deccan traps (ca. 65 Ma); volcanism usually takes place in less than a few million years. Examples of persistent LIPs, or hotspots, are Ninetyeast Ridge and the Hawaiian-Emperor chain, where volcanism occurs over tens of millions of years.

Large igneous province is an umbrella term that includes continental flood basalts (CFBs), volcanic rifted margins, oceanic plateaus, and aseismic ridges (Saunders, 2005). Common attributes of these provinces are that they form from an unusually high magmatic flux, they are mostly basaltic in composition, and they are not directly associated to seafloor spreading processes. The origin of most LIPs is best explained by mantle plumes. Mantle plumes are buoyant upwellings of hot mantle that may rise through the surrounding mantle as large spherical heads fed by narrower conduits (Griffiths & Campbell, 1990), or a variety of plume shapes, possibly without heads (Farnetani & Samuel, 2005). Transient LIPs are the initial eruptive products that form from melting of a new mantle plume head at the base of the lithosphere, and persistent LIPs form from melting within the narrower plume tail (Campbell, 2005) (Fig. 1.2).

Continental flood basalts are closely associated with continental breakup. The formation of the Paraná-Etendeka (ca. 133 Ma) preceded the opening of the South Atlantic Ocean and formation of the North Atlantic Volcanic Province (ca. 62-60 Ma) preceded the opening of the North Atlantic Ocean. The Ethiopian traps (ca. 30 Ma) are an example of the eruption of flood basalts prior to rifting of Arabia and Africa. CFBs are at least 1 km thick and greater than 100,000 km<sup>2</sup> and are emplaced as hundreds (or over a

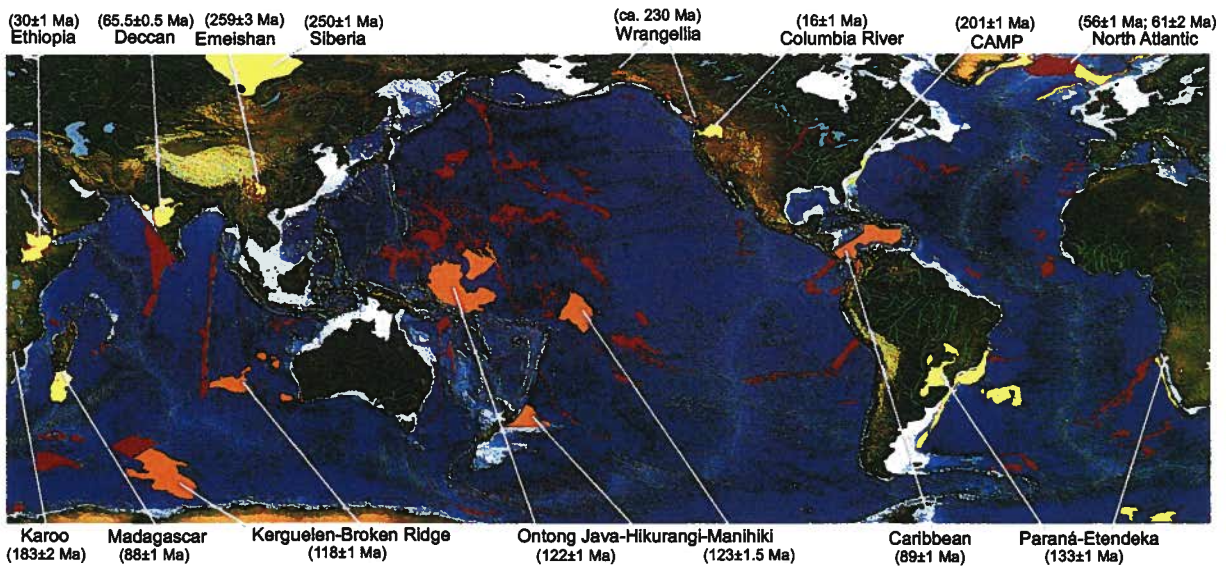


**Figure 1.1** Distribution of Phanerozoic LIPs on Earth. Transient LIPs are indicated in yellow (continental) and orange (oceanic) with peak eruption ages. Persistent LIPs are mostly in red. Map modified from base map by A. Goodlife and F. Martinez in Mahoney and Coffin (1997). The peak eruption ages of each LIP are from the compiled references within Courtillot and Renne (2003) and Taylor (2006).



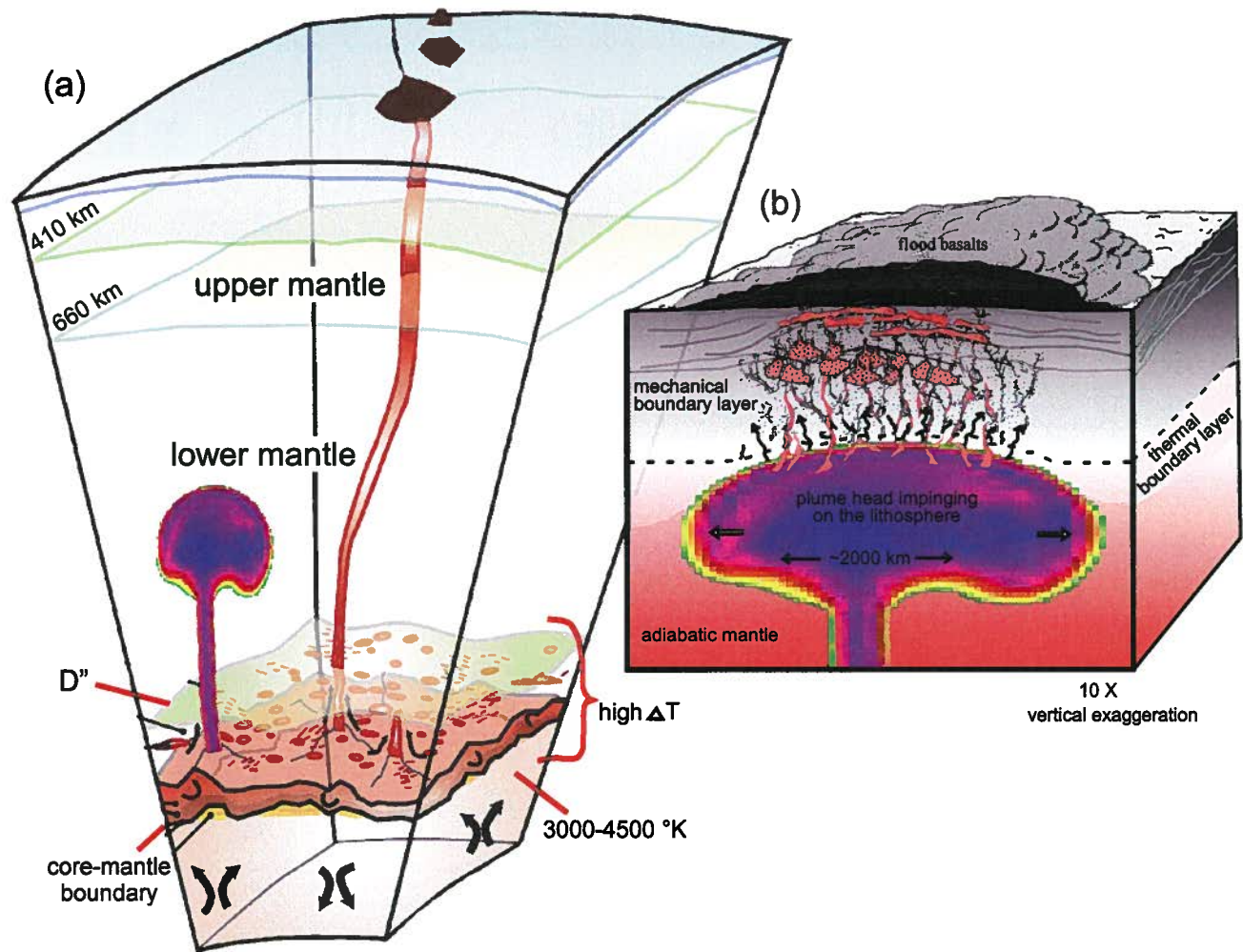


**Figure 1.2** Schematic diagrams of mantle plumes in the Earth's interior. (a) A view of the deep-mantle complexities beneath the central Pacific Ocean showing the Hawaiian hotspot, a D'' high-velocity reflector, and heterogeneity at the base of the lower mantle where mantle plumes may originate. Mantle plume head is hypothetical. Drawing modified from Garnero (2004) with parts of a plume model by Farnetani and Samuel (2005). (b) A drawing of a model of plume-lithosphere interaction beneath oceanic lithosphere that produces basalts erupted in an oceanic plateau. Dashed line marks the base of the mechanical boundary layer. Arrows indicate flattening of the plume head. Model developed primarily after work of Saunders et al. (1992). Parts of the diagrams were adapted from a drawing by J. Holden in Fodor (1987) and a plume model by Farnetani and Samuel (2005).

thousand) of inflated compound pahoehoe flow fields that form a tabular flow stratigraphy (Self *et al.*, 1997). CFBs have been well-studied due to their accessibility as subaerial land-based features.

Oceanic plateaus are not nearly as well-studied as CFBs because they are mostly submerged in the oceans. Several extant oceanic plateaus in the ocean basins have been broken up by seafloor spreading since their formation (Fig. 1.1). The Ontong Java, Manihiki and Hikurangi plateaus may have formed together at ca. 120 Ma and together cover ~1% Earth's surface (Taylor, 2006). Ontong Java ( $2 \times 10^6$  km<sup>2</sup> in area; 30-35 km thick) formed from the largest magmatic event recorded on Earth and covers an area of the western Pacific Ocean comparable to the size of western Europe, or approximately one-third the size of the conterminous United States (Fitton *et al.*, 2004). The Kerguelen ( $2 \times 10^6$  km<sup>2</sup> in area; 20 km thick) and Broken Ridge Plateaus formed together, beginning ca. 118 Ma, and have since been separated by seafloor spreading along the Southeast Indian Ridge (Weis & Frey, 2002; Fig. 1.1). An important feature of the basalts erupted in some oceanic plateaus is that they are unaffected by continental lithosphere and are thus better suited for understanding the composition of the mantle source of LIPs than CFBs.

The basalt stratigraphy of oceanic plateaus remains largely unsampled because of the difficulty in sampling more than the uppermost few hundred meters of flows from drilling ships (Fig. 1.3). For example, the Ontong Java Plateau, which rises to depths of 1700 m below sea level, has been the focus of several Deep Sea Drilling Project (DSDP; Site 289) and Ocean Drilling Program (ODP; Leg 192, Sites 803 and 807) legs to sample the basaltic basement of the plateau (Fig. 1.3; Mahoney *et al.*, 2001). These efforts have been described as “pin-pricking the elephant” (Tejada *et al.*, 2004); drilling of Ontong Java has only penetrated a maximum 338 m of approximately 6 km or more of the basalt stratigraphy (Mahoney *et al.*, 2001). Drilling of the Kerguelen Plateau has only penetrated a maximum 233 m of the basalt stratigraphy (Frey *et al.*, 2000). Ocean drilling of extant plateaus submerged in the ocean is an extremely difficult and expensive tool to study oceanic plateaus.

The most efficient and comprehensive way to study oceanic plateaus is by observing and sampling exposures of oceanic plateaus where they have been accreted at

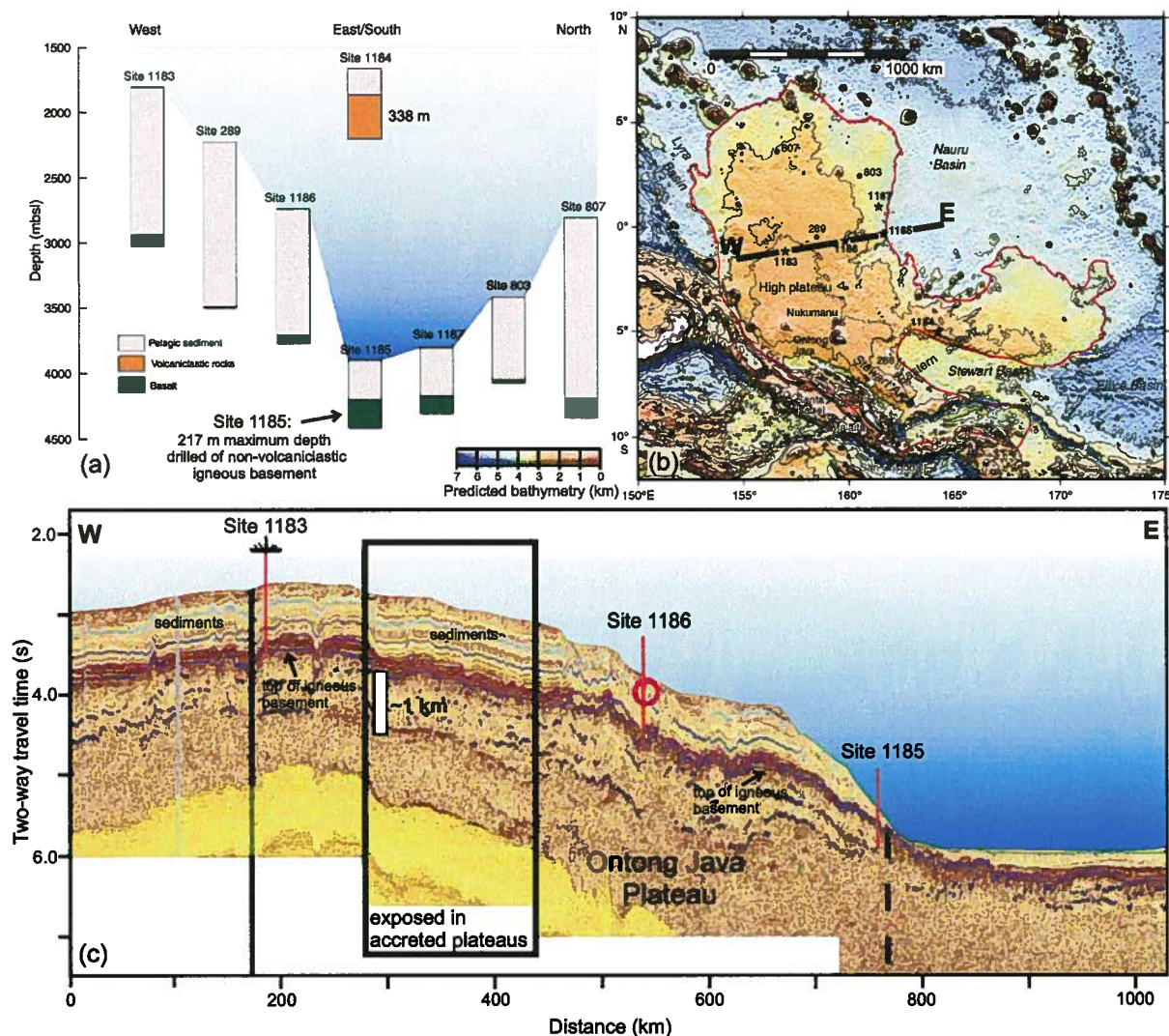


**Figure 1.3** “Pin-pricking” the giant Ontong Java Plateau. (a) Representation of drilled stratigraphic sections from 8 DSDP and ODP drilling sites (locations shown in panel b). Diagram adapted from Mahoney *et al.* (2001). The most volcanic rock sampled from drilling is 338 m of volcaniclastic rock at Site 1184 and 217 m of pillowed and massive basalt at Site 1185. (b) Predicted bathymetry (after Smith & Sandwell, 1997) of the Ontong Java Plateau and surrounding region showing the location of drill sites from ODP Leg 192 (stars) and previous drill sites (white and black circles). Map adapted from Mahoney *et al.* (2001). The broken black line (labeled W-E) indicates a transect where multichannel seismic reflection (MCS) investigations acquired data for the plateau by R/V Hakuho Maru KH98-1 Leg 2 in 1998 (shown in panel c). (c) Composite east-west MCS transects of the Ontong Java Plateau with reflecting horizons (location shown in panel b). Figure modified from Inoue *et al.* (2008). Sediments and the top of the igneous basement are indicated. Vertical red lines indicate depth of drilling at 3 labelled sites on the transect. Red circle indicates location of ‘eye structure’ (see Inoue *et al.*, 2008). Vertical exaggeration = ~100:1. This figure serves to illustrate the difficulty of sampling and studying extant oceanic plateaus in the ocean basins. The black rectangle in panel c indicates the extent of stratigraphy that is exposed and accessible in obducted oceanic plateaus on land, such as the Wrangellia oceanic plateau.

continental margins or accreted onto island arcs, as in the case of the Ontong Java Plateau and the Solomon island arc. However, Phanerozoic examples of accreted oceanic plateaus are rare. Accreted sections of flood basalts around the Caribbean Sea and in Central and South America are several kilometers thick in areas (e.g. Kerr *et al.*, 1998; Révillon *et al.*, 1999; Kerr, 2003). Several small sections of the Ontong Java Plateau are exposed on land in the Solomon Islands (Tejada *et al.*, 1996; Babbs, 1997; Petterson *et al.*, 1999; Tejada *et al.*, 2002). These are the two major oceanic plateaus where obducted parts of the plateau have been studied.

## **THE WRANGELLIA OCEANIC PLATEAU**

Wrangellia flood basalts in the Pacific Northwest of North America are part of one of the best exposed accreted oceanic plateaus on Earth and can provide information about oceanic plateaus that is rarely accessible elsewhere on Earth. Wrangellia flood basalts formed as part of a transient LIP in the Middle to Late Triassic, with accretion to western North America occurring either in the Late Jurassic or Early Cretaceous. Although their original areal distribution was likely considerably larger, current exposures of the flood basalts extend over 2300 km in British Columbia (BC), Yukon, and Alaska (Fig. 1.4). Parts of the entire volcanic stratigraphy, from the base to the top, are accessible for close examination on land. From a geochemical perspective, the Wrangellia flood basalts have remained relatively poorly studied and have been the focus of only one study in the last twenty years using modern analytical geochemistry (Lassiter *et al.*, 1995).

In this study, the Wrangellia oceanic plateau has been intensively studied to establish the stratigraphical and geochemical architecture of an oceanic plateau and the nature of the episodic melting events that lead to the formation of oceanic plateaus. The Wrangellia flood basalts erupted mostly within the Late Ladinian and Carnian stages of the Triassic (ca. 230 Ma; e.g. Carlisle & Suzuki, 1974; Parrish & McNicoll, 1992), as the continents were gathered into a great landmass referred to as Pangaea (Fig. 1.5). They erupted atop different-aged Paleozoic arc volcanic and marine sedimentary sequences and are overlain by Late Triassic limestone. Paleontological and paleomagnetic studies indicate that the Wrangellia flood basalts probably erupted in the eastern Panthalassic



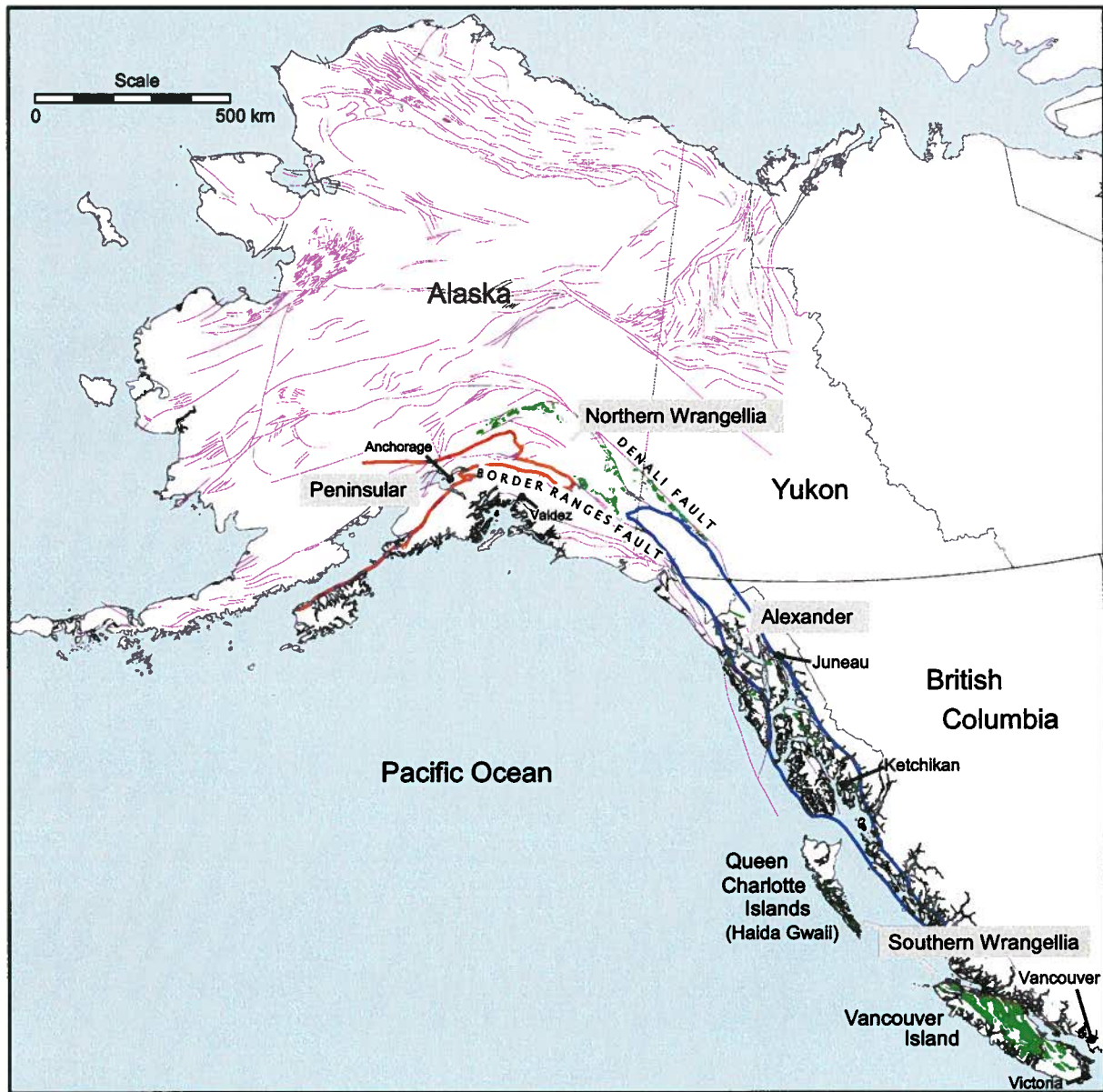


**Figure 1.4** Map showing distribution of Wrangellia flood basalts in Alaska, Yukon, and British Columbia. Map derived from Wilson *et al.* (1998), Israel (2004), Massey *et al.* (2005a, b), Wilson *et al.* (2005), and Brew (2007, written comm.). Outlines for the Peninsular and Alexander Terranes are shown in orange and blue, respectively. As labeled, the Wrangellia Terrane is referred to as Northern and Southern Wrangellia in this study. Major faults in Alaska and parts of Yukon and BC are shown with purple lines. The Wrangellia, Alexander, Peninsular terranes, which are part of the Wrangellia Composite Terrane, share similar elements or have a linked geologic history [as defined by Plafker *et al.* (1989), Nokleberg *et al.* (1994), Plafker and Berg (1994), and Plafker *et al.* (1994)]. Geochronology from a single pluton in Alaska is proposed to link the Proterozoic to Triassic Alexander Terrane to Wrangellia by late Pennsylvanian time (Gardner *et al.*, 1988). The Wrangellia and Peninsular Terranes may have been in close proximity by the Late Triassic or Early Jurassic (Rioux *et al.*, 2007).

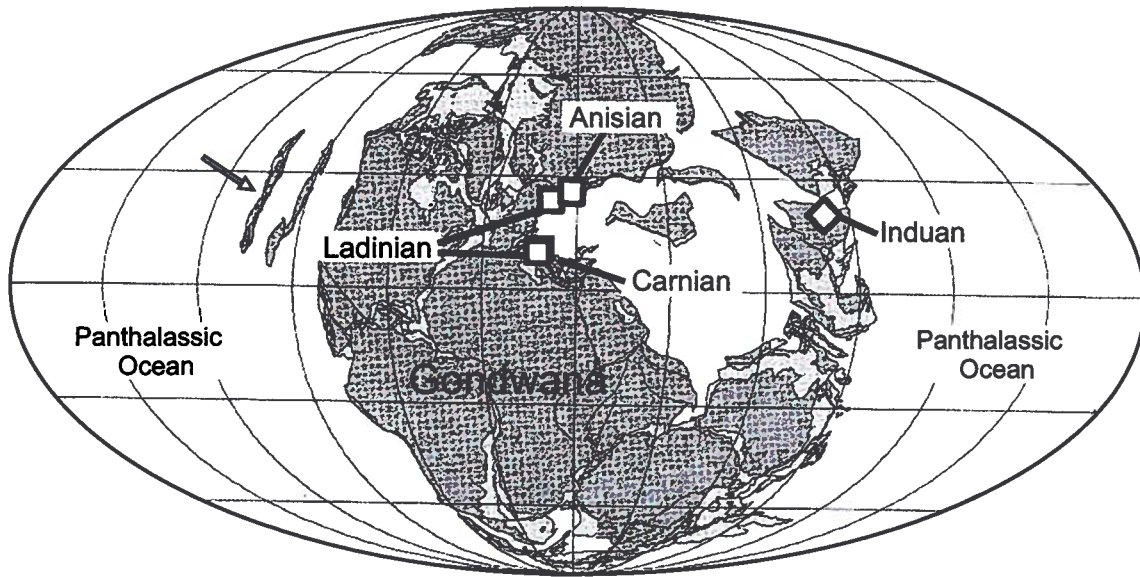


**Figure 1.5** Estimated distribution of the continental landmasses in the Middle to Late Triassic (~226 Ma). Map modified from Ogg (2004), based on the reconstruction of Scotese (2004). Global Stratotype Sections and Points (GSSP) are indicated for stages of the Triassic. Blue arrow indicates estimated location of the Wrangellia oceanic plateau.

Ocean in equatorial latitudes (Jones *et al.*, 1977; Katvala & Henderson, 2002). The eruption of Wrangellia flood basalts broadly coincides with major biotic and environmental changes worldwide that occurred at the end of Carnian time (Furin *et al.*, 2006). A global-scale environmental crisis, referred to as the Reingrabener turnover, occurred in the Carnian (e.g. Furin *et al.*, 2006). This event is preserved by the collapse of rimmed carbonate platforms, a global shift in sedimentological and geochemical proxies, and a strong radiation of several groups, including scleractinian reef builders, calcareous nannoplankton, and dinosaurs (Furin *et al.*, 2006 and references therein). The accretion of the Wrangellia oceanic plateau to western North America was a major tectonic event and represents a significant addition of oceanic mantle-derived material to the North American crust (Condie, 2001).

The volcanic stratigraphy of the Wrangellia plateau is defined as the Karmutsen Formation on Vancouver and Queen Charlotte Islands (Haida Gwaii), and as the Nikolai Formation in southwest Yukon and south-central Alaska (Fig. 1.4). On Vancouver Island, the volcanic stratigraphy is a tripartite succession of submarine, volcanoclastic, and subaerial flows approximately 6 km thick. In Alaska and Yukon, the volcanic stratigraphy is predominantly massive subaerial flows with a small proportion of submarine flows along the base. Smaller elements in southeast Alaska may be correlative with the Wrangellia flood basalts.

Rapid eruption of the Wrangellia flood basalts is supported by the absence of intervening sediments between the flows, except in the uppermost part of the stratigraphy as volcanism waned. Paleomagnetic measurements of the Wrangellia flood basalts have not revealed any magnetic reversals, which also testifies to the short duration of eruptions (Hillhouse, 1977; Yole & Irving, 1980; Hillhouse & Coe, 1994).

## **METHODOLOGY AND RATIONALE FOR THIS STUDY**

This study represents the first comprehensive study of the Wrangellia oceanic plateau. The integration of geochemical, volcanological, stratigraphic, and geochronological results provide constraints on the formation of the Wrangellia oceanic plateau. The volcanological and stratigraphic studies yield insights about the emplacement of flows, eruptive environment, original tectonic setting, and construction

of the plateau. The geochronological and paleontological studies allow for estimation of the age and duration of volcanism. The petrologic and geochemical studies provide information about the composition of the source, conditions of melting, and the magmatic evolution of lavas that formed the Wrangellia plateau. The interpretation of these different results will help to develop our understanding of the physical and chemical processes that occur in mantle plumes, as they decompress and impinge on the base of oceanic lithosphere and produce the basaltic magmas which erupt through oceanic lithosphere and form oceanic plateaus. The contributions in the four major chapters in this dissertation (described below) address some of the enduring questions about the origin of oceanic plateaus.

## **PREVIOUS RESEARCH**

In the 1970s, Jones and co-workers (1977) defined the fault-bound blocks of crust that contain diagnostic Triassic flood basalts in BC, Yukon, and Alaska as Wrangellia, named after the type section in the Wrangell Mountains of Alaska. Early paleomagnetic and paleontological studies of Wrangellia indicated long-distance displacement of the basalts from equatorial latitudes (Hillhouse, 1977) and similar *Daonella* bivalves were found in sediments directly beneath the flood basalts on Vancouver Island and in the Wrangell Mountains (Jones *et al.*, 1977). A back-arc setting was initially proposed for the formation of Karmutsen basalts on Vancouver and Queen Charlotte Islands based on major- and trace-element geochemistry of 12 samples (Barker *et al.*, 1989). Richards and co-workers (1991) proposed a plume initiation model for the Wrangellia flood basalts based on evidence of rapid uplift prior to volcanism, lack of evidence of rifting associated with volcanism (few dikes and abundant sills), and the short duration and high eruption rate of volcanism. A geochemical study of 36 samples of Wrangellia flood basalts, 29 samples from Buttle Lake on Vancouver Island and 9 samples from the Wrangell Mountains in Alaska, was undertaken by Lassiter and co-workers (1995) as part of the only modern geochemical and isotopic study of Wrangellia flood basalts until the initiation of this project. Lassiter and co-workers (1995) suggested mixing of a plume-type source with low Nb/Th arc-type mantle could reproduce variations in the Wrangellia flood basalts.



## THE IMPORTANCE OF LIPS AND MANTLE PLUMES

Since the recognition of oceanic plateaus in the early 1970s (Edgar *et al.*, 1971; Donnelly, 1973; Kroenke, 1974), there have been significant advances in our understanding of oceanic plateaus. A wide range of scientific approaches have been used to study oceanic plateaus; however, we only partially understand the physical and chemical processes that lead to the formation of oceanic plateaus.

Oceanic plateaus have formed for at least the last several hundred million years and likely well back into Earth history. Archean and Proterozoic greenstone belts have been interpreted to be remnants of oceanic plateaus (e.g. Kerr, 2003) and komatiites (>18 wt % MgO, with spinifex-textured olivines) may be the high-temperature melting products of ancient mantle plumes (e.g. Arndt & Nesbet, 1982) and some Phanerozoic plume heads (e.g. Storey *et al.*, 1991). Phanerozoic oceanic plateaus may form from mantle plumes that originate at the core-mantle boundary (Campbell, 2005). The large temperature and density contrasts that exist between the outer core and mantle are expected to produce an unstable boundary layer above the core that episodically leads to the formation of mantle plumes (Jellinek & Manga, 2004). Oceanic plateaus are thus the surface manifestations of a major mode of heat loss from the interior of the Earth. The geochemical study of flood basalts is one important way by which we gain information about mantle plumes rising from their origin to the eruption of their melting products at the Earth's surface.

Although mantle plumes are considered the strongest hypothesis for the origin of LIPs, there are a number of alternative interpretations: meteorite impacts (Rogers, 1982), enhanced convection at the edge of continental cratons (King & Anderson, 1998), delamination of lithosphere causing rapid mantle upwelling (Elkins-Tanton, 2005), and melting of fertile eclogitic mantle (Korenaga, 2005). One example of evidence that mantle plumes are responsible for the formation of most LIPs is the high melt production rates that form LIPs, which make them difficult to explain by an origin related to plate tectonic processes (Jellinek & Manga, 2004). Perhaps the best evidence for the high source temperatures required to explain the melting that produces LIPs is the presence of picrites (e.g. Saunders, 2005), with MgO between 12 and 18 wt % and 1-2 wt % Na<sub>2</sub>O + K<sub>2</sub>O (Le Bas, 2000). In this study, high-Mg picritic lavas have been discovered for the

first time within the Wrangellia oceanic plateau on northern Vancouver Island and in Alaska and modeling of their compositions indicate high source temperatures and high degrees of melting.

The eruption of basalts in LIPs has the potential to significantly affect the composition of the atmosphere and oceans by releasing large amounts of gas (primarily CO<sub>2</sub> and SO<sub>2</sub>) and aerosols that may trigger heating via runaway greenhouse effect or cooling via the spread of stratospheric sulphate aerosols that backscatter and absorb the sun's radiation (e.g. Rampino & Stothers, 1988; Wignall, 2001). Although CO<sub>2</sub> emissions in LIPs are small compared to the amount of CO<sub>2</sub> present in the atmosphere and the land-ocean-atmosphere flux of CO<sub>2</sub>, the gradual buildup of CO<sub>2</sub> from LIP eruptions may tip the balance enough to initiate release of other greenhouse gases, such as methane hydrates on the seafloor (Saunders, 2005). The release of SO<sub>2</sub> in LIP eruptions is incomparable to inputs at any other time during the Phanerozoic (Self *et al.*, 2006). The eruption of a single <2400 km<sup>3</sup> flow field is estimated to release as much as 6,500 Tg a<sup>-1</sup> for a 10-year duration, which is enormous compared to the background amount of S in the atmosphere (<1 Tg) (Self *et al.*, 2006). In the oceans, a series of variables that are consequences of large releases of CO<sub>2</sub> lead to warmer polar waters, decreased solubility of CO<sub>2</sub> and O<sub>2</sub>, and increased biogenic productivity in surface waters (e.g. Kerr, 2005). These effects can potentially lead to a shutdown of the ocean circulation system and anoxic conditions. It is likely that the eruption of Wrangellia flood basalts would have significantly affected the chemical composition of the ocean and atmosphere.

The close correlation between major mass extinctions in Earth history and the formation of most transient LIPs suggests a causal link between LIP eruptions and environmental change (Rampino & Stothers, 1988; Fig. 1.6). The three most recent large diversity depletion events in the Phanerozoic (Permian-Triassic, Triassic-Jurassic, Cretaceous-Tertiary) coincide with the timing of peak volcanic activity in the formation of a continental flood basalt province (Siberia, Central Atlantic Magmatic Province (CAMP), and Deccan, respectively) (Courtillot & Renne, 2003). The eruption of the Siberian traps may have played a key role in the End Permian extinction event because of the high proportion of pyroclastic eruptions and intrusion of magmas into carbon- and methane-bearing strata (Wignall, 2001). Recent studies of the CAMP and the Deccan

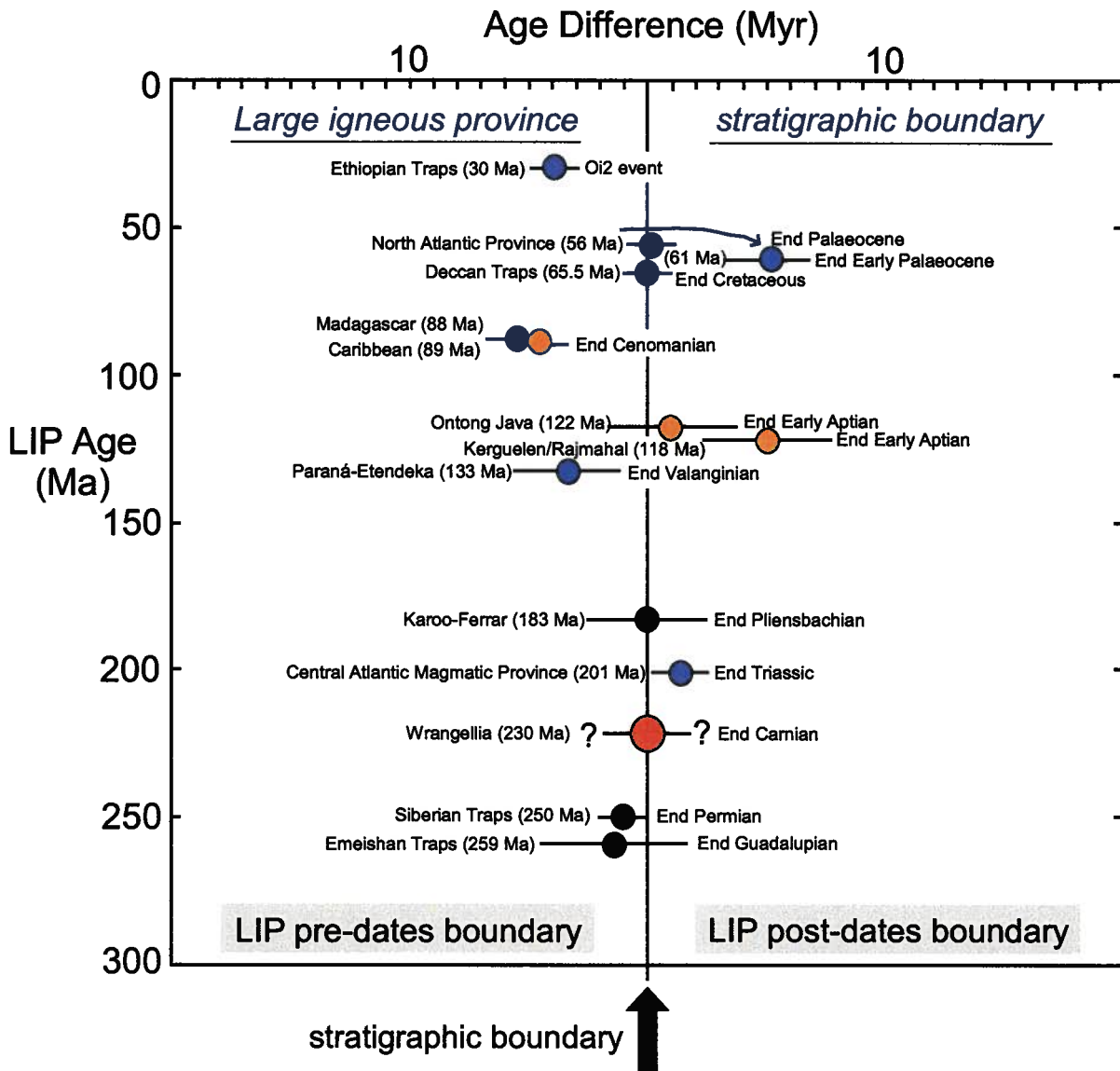


**Figure 1.6** Age difference between peak eruption ages of LIPs from the last 260 Myr versus the age of a stratigraphic boundary associated with major sudden environmental changes. Diagram modified from Kelley (2007). Ages are mostly from the compilation of Courtillot and Renne (2003). The possible connection between Wrangellia and a climatic and biotic crisis recognized in the Carnian is hypothetical and needs to be explored further (Furin *et al.*, 2006).

Traps support a close temporal relationship between the End Triassic and End Cretaceous extinctions, respectively.

A recent study by Courtillot and Olsen (2007) suggests there may be a connection between magnetic superchrons, where the Earth's magnetic field does not reverse polarity for abnormally long periods of time (30-50 Myr), and the timing of mantle plumes. The ~50 Myr long Kaiman Long Reverse Superchron (310 to 260 Ma) ended ~10 Myr before eruption of the Siberian Traps and the ~35 Myr long Cretaceous Long Normal Superchron (118 to 83 Ma) ended ~18 Myr before eruption of the Deccan Traps (Courtillot & Olsen, 2007). Courtillot and Olsen (2007) suggest a mechanism whereby a major change in heat flow at the core-mantle boundary may lead to the end of a superchron and cause initiation of "killer" mantle plumes.

Along with aerially-extensive flood basalt sequences, radiating dike swarms are impressive aspects of transient LIPs which extend >2800 km and are a major mode of lateral transport of LIP magmas in the crust. Radiating dike swarms are diagnostic of major magmatic events linked to mantle plumes and associated continental break-up and serve as indicators of plume centers and magma transport (Ernst *et al.*, 2001). Dike swarms have been identified in every Mesozoic and Cenozoic CFB on Earth and are expected to form in oceanic plateaus (Ernst & Buchan, 2003). Where the flood basalts are largely eroded, such as the CAMP, dike swarms can be used to reconstruct plate motions and identify plume events through Earth's history (Ernst & Buchan, 1997).

There are many important and fascinating aspects of LIPs. The study of LIPs holds great relevance in a variety of large-scale Earth processes and this study provides constraints which help to further our understanding of these geological phenomena.

## **AN OVERVIEW OF THE FOUR CHAPTERS IN THIS DISSERTATION AND ADDITIONAL REFERENCES**

The chapters in this dissertation were written in manuscript form for submission to major international geological journals. Three of the first four manuscripts are detailed studies of the Wrangellia flood basalts from different regions of western North America (Vancouver Island, Alaska, and Yukon). These three manuscripts parallel one another in that similar analytical techniques are used, but each study has distinct results and

interpretations. Each study involved extensive field work using different modes of transportation in remote areas of western North America (Fig. 1.7). Additional contributions from this project that are not included in the dissertation are four government geological survey papers (Greene *et al.*, 2005b, 2005c, 2006c; Nixon *et al.*, 2008b) and eight abstracts to international geological conferences (Greene *et al.*, 2005a, 2006a, 2006b, 2007a, 2007b, 2007c, 2008a, 2008b). Contributions to other conference proceedings include studies of platinum-group elements (Scoates *et al.*, 2006, 2007, 2008) and stratigraphic successions of Wrangellia flood basalts (Nixon *et al.*, 2008a).

The first manuscript in this dissertation is a comprehensive study of the Karmutsen Formation on Vancouver Island, which has major implications for the evolution of this large oceanic plateau. Karmutsen basalts on Vancouver Island comprise one of the thickest and most complete examples of the volcanic stratigraphy of an emergent oceanic plateau on Earth. My co-authors and I examine the field relationships, stratigraphy, petrography, and geochemical and isotopic compositions of the Karmutsen Formation to assess the nature of the mantle source and to evaluate the melting history and subsequent magmatic evolution of basalts involved in the construction of this major oceanic plateau.

The second manuscript is a study of the Nikolai Formation in Alaska. This study integrates field relationships in widespread areas of Alaska and geochemistry of continuous sections of volcanic stratigraphy to understand the physical and chemical processes that occur as a mantle plume head impinges on the base of oceanic arc lithosphere. This information provides insights into the temporal and spatial variation of the magmas in a major oceanic plateau that result from plume-lithosphere interaction.

The third manuscript is a field, petrographic, and geochemical study of Nikolai basalts in Yukon, where volcanic stratigraphy and bounding sedimentary sequences are similar to Alaska. Nikolai basalts in Yukon are more altered than their counterparts in Alaska and a comparative geochemical study of Nikolai basalts from Yukon and Alaska allows for analysis of the effects of alteration and regional differences in basalts erupted in the northern part of Wrangellia. This study also examines the geochemistry of the underlying Paleozoic arc sequences and their role in the generation of the Nikolai basalts.

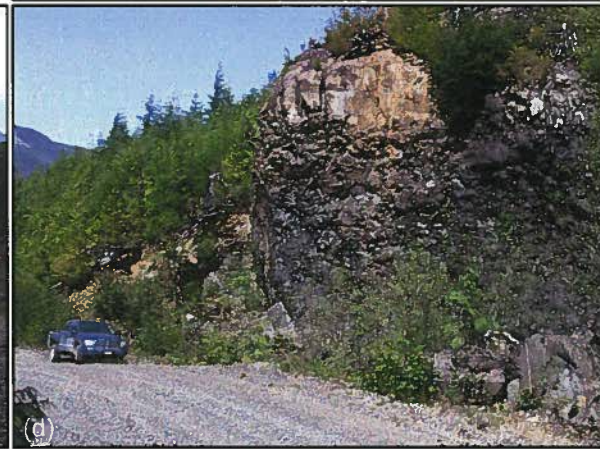
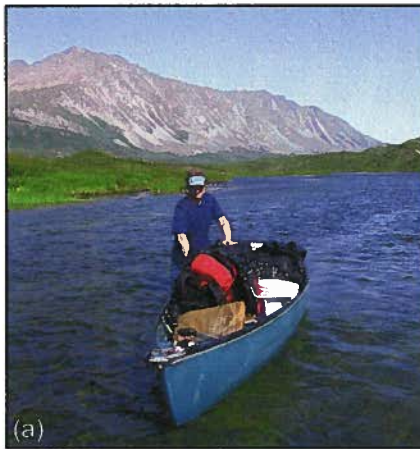


**Figure 1.7** Photographs showing the different modes of transportation used for field work in remote areas of Alaska, Yukon, and BC as part of this project. (a) Canoe access to the Amphitheater Mountains in the Alaska Range, Alaska. (b) Helicopter access in the Kluane Ranges, southwest Yukon. (c) Transportation by Super Cub in Wrangell-St. Elias National Park, Alaska. (d) Four-wheel drive vehicle access on logging roads on northern Vancouver Island. Photograph by Graham Nixon.

The fourth manuscript is a stratigraphic and geochronological study of Wrangellia flood basalts from throughout BC, Yukon, and Alaska. This synthesis integrates observations from field work and dozens of government geological survey reports and maps to provide detailed descriptions of the volcanic stratigraphy and the pre- and post-volcanic rock stratigraphy of Wrangellia. This overview is presented in the form of stratigraphic columns and descriptions, compiled geologic maps, photographic databases, interactive Google Earth files, and a review and compilation of previous research on Wrangellia. The maps, photographs, and archiving of information are presented differently than in the previous chapters and offer users interactive electronic tools to visualize and explore information about the Wrangellia oceanic plateau. This work, in combination with  $^{40}\text{Ar}/^{39}\text{Ar}$  geochronology of flood basalts throughout Wrangellia, provides an over-arching contribution that brings together past and present research on Wrangellia in a new light.

## **CONTRIBUTIONS TO THIS PROJECT**

This project benefited from the assistance of many people. Assistance with field work in Alaska, Yukon, and BC was provided by Bruno Kieffer, Frederico Henriques, and James Scoates. Advice for field work was provided by Graham Nixon (British Columbia Geological Survey), Nick Massey (British Columbia Geological Survey), Don Carlisle, Steve Israel (Yukon Geological Survey), Jeanine Schmidt (United States Geological Survey-Anchorage), David Brew (United States Geological Survey-Menlo Park), Danny Rosenkrans (Wrangell-St. Elias National Park), and Jeff Trop (Bucknell University). Isotopic and trace-element analyses for a suite of 24 samples on Vancouver Island were made by Bruno Kieffer and Jane Barling. Bruno Kieffer, Jane Barling, and Bert Mueller also provided training for analytical work for Yukon and Alaska samples at the Pacific Centre for Isotopic and Geochemical Research (PCIGR). The analyses for  $^{40}\text{Ar}/^{39}\text{Ar}$  geochronology were carried out by Tom Ullrich from samples that were crushed, separated, picked, and leached by me.

This project was made possible from funding provided by the BC & Yukon Chamber of Mines (Association of Mineral Exploration BC) from the 2004 Rocks to Riches Program, the BC Geological Survey, the Yukon Geological Survey, and by

NSERC Discovery Grants to James Scoates and Dominique Weis. The author was also supported by a University Graduate Fellowship at UBC. Major- and trace-element analyses for this project were performed by Activation Laboratories (ActLabs) in Ontario, Canada and at the Ronald B. Gilmore X-Ray Fluorescence Laboratory (XRF) at the University of Massachusetts. Claude Herzberg (Rutgers University), Julian Pearce (Cardiff University), and Haibo Zou (University of California Los Angeles) offered assistance with geochemical modeling. My supervisors, James Scoates and Dominique Weis, offered invaluable assistance and guidance with all aspects of this project.

## REFERENCES

- Arndt, N. T. & Nisbet, E. G. (1982). Geochemistry of Munro township basalt. In: Arndt, N. T. & Nisbet, E. G. (eds.) *Komatiites*. Allen and Unwin: Winchester, MA, pp. 19-27.
- Babbs, T. L. (1997). Geochemical and petrological investigations of the deeper portions of the Ontong Java Plateau: Malaita, Solomon Islands. Unpublished Ph.D. dissertation, Leicester University, U.K., 254 pp.
- Barker, F., Brown, A. S., Budahn, J. R. & Plafker, G. (1989). Back-arc with frontal-arc component origin of Triassic Karmutsen basalt, British Columbia, Canada. *Chemical Geology* **75**, 81-102.
- Brew, D. A. C. (2007, written comm.). Unpublished map showing the distribution of the Late Triassic Wrangellia, Hyd Group, and Perserverance group rocks in southeastern Alaska, scale 1:600,000 (Based on Brew, D. A. (Compiler), Unpublished bedrock geologic map of southeastern Alaska.)
- Campbell, I. H. (2005). Large igneous provinces and the mantle plume hypothesis. *Elements* **1**, 265-269.
- Carlisle, D. & Suzuki, T. (1974). Emergent basalt and submergent carbonate-clastic sequences including the Upper Triassic Dilleri and Welleri zones on Vancouver Island. *Canadian Journal of Earth Sciences* **11**, 254-279.
- Condie, K. C. (2001). *Mantle Plumes and Their Record in Earth History*. Cambridge University Press: Cambridge, 306 p.
- Courtillot, V. & Olsen, P. E. (2007). Mantle plumes link magnetic superchrons to Phanerozoic mass depletion events. *Earth and Planetary Science Letters* **260**, 495-504.
- Courtillot, V. E. & Renne, P. R. (2003). On the ages of flood basalt events. *Comptes Rendus Geoscience* **335**, 113-140.
- Donnelly, T. W. (1973). Late Cretaceous basalts from the Caribbean: a possible flood basalt province of vast size. *EOS* **54**, 1004.
- Edgar, N. T., Ewing, J. I. & Hennion, J. (1971). Seismic refraction and reflection in the Caribbean Sea. *American Association of Petroleum Geologists Bulletin* **55**, 833-870.



- Elkins-Tanton, L. (2005). Continental magmatism caused by lithospheric delamination. In: Foulger, G. R., Natland, J. H., Presnall, D. C. & Anderson, D. L. (eds.) *Plates, Plumes and Paradigms*. Geological Society of America Special Paper 388, pp. 449-462.
- Ernst, R. E. & Buchan, K. L. (1997). Giant radiating dyke swarms: Their use in identifying pre-Mesozoic large igneous provinces and mantle plumes. In: Mahoney, J. J. & Coffin, M. F. (eds.) *Large Igneous Provinces: Continental, Oceanic, and Planetary Flood Volcanism*. American Geophysical Union Geophysical Monograph 100, pp. 297-333.
- Ernst, R. E. & Buchan, K. L. (2003). Recognizing mantle plumes in the geologic record. *Annual Review of Earth and Planetary Sciences* **31**, 469-523.
- Ernst, R. E., Grosfils, E. B. & Mège, D. (2001). Giant dike swarms: Earth, Venus and Mars. *Annual Review of Earth and Planetary Science* **29**, 489- 534.
- Farnetani, C. G. & Samuel, H. (2005). Beyond the thermal plume paradigm. *Geophysical Research Letters* **32**(L07311), doi:10.1029/2005GL022360.
- Fitton, J. G., Mahoney, J. J., Wallace, P. J. & Saunders, A. D. (eds.) (2004). *Origin and Evolution of the Ontong Java Plateau*. Geological Society of London Special Publication 229. 374 pp.
- Fodor, R. V. (1987). Low- and high-TiO<sub>2</sub> flood basalts of southern Brazil: origin from picritic parentage and a common mantle source. *Earth and Planetary Science Letters* **84**, 423-430.
- Frey, F. A., et al. (2000). Origin and evolution of a submarine large igneous province: the Kerguelen Plateau and Broken Ridge, southern Indian Ocean. *Earth and Planetary Science Letters* **176**, 73-89.
- Furin, S., Preto, N., Rigo, M., Roghi, G., Gianolla, P., Crowley, J. L. & Bowring, S. A. (2006). High-precision U-Pb zircon age from the Triassic of Italy: Implications for the Triassic time scale and the Carnian origin of calcareous nannoplankton and dinosaurs. *Geology* **34**(12), 1009-1012, 10.1130/g22967a.1.
- Gardner, M. C., Bergman, S. C., Cushing, G. W., MacKevett, E. M., Jr., Plafker, G., Campbell, R. B., Dodds, C. J., McClelland, W. C. & Mueller, P. A. (1988). Pennsylvanian pluton stitching of Wrangellia and the Alexander terrane, Wrangell Mountains, Alaska. *Geology* **16**, 967-971.
- Garnero, E. J. (2004). A new paradigm for Earth's core-mantle boundary. *Science* **304**, 834-836.
- Greene, A., Scoates, J. S., Weis, D. & Kieffer, B. (2006a). Wrangellia Flood Basalts: Exploring the architecture and composition of an accreted oceanic plateau. *Geological Society of America Cordilleran Section* Anchorage, Alaska. 38: 5, p. 25.
- Greene, A. R., Scoates, J. S., Weis, D. & Kieffer, B. (2006b). Wrangellia Flood Basalts: Exploring the architecture and composition of an accreted oceanic plateau. *Geological Association of Canada 2006 Annual Meeting*, Montreal, Quebec.
- Greene, A. R., Scoates, J. S., Nixon, G. T. & Weis, D. (2006c). Picritic lavas and basal sills in the Karmutsen flood basalt province, Wrangellia, northern Vancouver Island. In: Grant, B. (ed.) *Geological Fieldwork 2005*. British Columbia Ministry of Energy, Mines and Petroleum Resources Paper 2006-1, pp. 39-52.

- Greene, A. R., Scoates, J. S. & Weis, D. (2005a). Wrangellia Terrane in B.C. and Yukon: Where are its Ni-Cu-PGE deposits? *Cordilleran Mineral Roundup Expo*, Vancouver, BC.
- Greene, A. R., Scoates, J. S. & Weis, D. (2005b). Wrangellia Terrane on Vancouver Island: Distribution of flood basalts with implications for potential Ni-Cu-PGE mineralization. In: Grant, B. (ed.) *Geological Fieldwork 2004*. British Columbia Ministry of Energy, Mines and Petroleum Resources Paper 2005-1, pp. 209-220.
- Greene, A. R., Scoates, J. S. & Weis, D. (2008a). Wrangellia flood basalts in Alaska: A record of plume-lithosphere interaction in a Late Triassic accreted oceanic plateau. *Goldschmidt 2008 Conference*, Vancouver, BC.
- Greene, A. R., Scoates, J. S., Weis, D. & Israel, S. (2005c). Flood basalts of the Wrangellia Terrane, southwest Yukon: Implications for the formation of oceanic plateaus, continental crust and Ni-Cu-PGE mineralization. In: Emond, D. S., Lewis, L. L. & Bradshaw, G. D. (eds.) *Yukon Exploration and Geology 2004*. Yukon Geological Survey, pp. 109-120.
- Greene, A. R., Scoates, J. S., Weis, D., Israel, S., Nixon, G. T. & Kieffer, B. (2007a). Geochemistry and geochronology of the Wrangellia Flood Basalts in British Columbia, Yukon, and Alaska. *Cordilleran Mineral Roundup Expo*, Vancouver, BC.
- Greene, A. R., Scoates, J. S., Weis, D. & Nixon, G. T. (2007b). Significance of picritic and tholeiitic lavas within Wrangellia Flood Basalts on Vancouver Island for the melting history and magmatic evolution of a major oceanic plateau. *AGU 2007 Fall Meeting* San Francisco, CA. Abstract V33A-1153
- Greene, A. R., Scoates, J. S., Weis, D. & Nixon, G. T. (2008b). Picritic and tholeiitic lavas within Wrangellia Flood Basalts on Vancouver Island for the melting history and magmatic evolution of a major oceanic plateau. *Cordilleran Tectonics Workshop*, Vancouver, BC.
- Greene, A. R., Weis, D. & Scoates, J. S. (2007c). Wrangellia Flood Basalts: Exploring the architecture and composition of an accreted oceanic plateau. *Geological Association of Canada, NUNA 2007 Conference: The Pulse of the Earth and Planetary Evolution*, Sudbury, Ontario.
- Griffiths, R. W. & Campbell, I. H. (1990). Stirring and structure in mantle starting plumes. *Earth and Planetary Science Letters* **99**, 66-78.
- Hillhouse, J. W. (1977). Paleomagnetism of the Triassic Nikolai Greenstone, McCarthy Quadrangle, Alaska. *Canadian Journal of Earth Sciences* **14**, 2578-3592.
- Hillhouse, J. W. & Coe, R. S. (1994). Paleomagnetic data from Alaska. In: Plafker, G. & Berg, H. C. (eds.) *The Geology of Alaska*. Geological Society of America Geology of North America G-1, pp. 797-812.
- Inoue, H., Coffin, M. F., Nakamura, Y., Mochizuki, K. & Kroenke, L. W. (2008). Intrabasement reflections of the Ontong Java Plateau: Implications for plateau construction. *Geochemistry Geophysics Geosystems* **9**(Q04014), doi:10.1029/2007GC001780.
- Israel, S. (2004). Geology of Southwestern Yukon (1:250 000 scale). *Yukon Geological Survey Open File 2004-16*.

- Jellinek, A. M. & Manga, M. (2004). Links between long-lived hotspots, mantle plumes, D", and plate tectonics. *Reviews of Geophysics* **42**(RG3002), doi:10.1029/2003RG000144.
- Jones, D. L., Silberling, N. J. & Hillhouse, J. (1977). Wrangellia; a displaced terrane in northwestern North America. *Canadian Journal of Earth Sciences* **14**(11), 2565-2577.
- Katvala, E. C. & Henderson, C. M. (2002). Conodont sequence biostratigraphy and paleogeography of the Pennsylvanian-Permian Mount Mark and Fourth Lake Formations, southern Vancouver Island. In: Hills, L. V., Henderson, C. M. & Bamber, E. W. (eds.) *Carboniferous and Permian of the World*. Canadian Society of Petroleum Geologists Memoir 19, pp. 461-478.
- Kelley, S. (2007). The geochronology of large igneous provinces, terrestrial impact craters, and their relationship to mass extinctions on Earth. *Journal of the Geological Society of London* **164**, 923-936.
- Kerr, A. C. (2003). Oceanic Plateaus. In: Rudnick, R. (ed.) *The Crust*. Elsevier Science: Oxford Treatise on Geochemistry Vol. 3 Holland, H. D. & Turekian, K. K. (eds.), pp. 537-565.
- Kerr, A. C. (2005). Oceanic LIPs: The kiss of death. *Elements* **1**(5), 289-292.
- Kerr, A. C., Tarney, J., Nivia, A., Marriner, G. F. & Saunders, A. D. (1998). The internal structure of oceanic plateaus: inferences from obducted Cretaceous terranes in western Columbia and the Caribbean. *Tectonophysics* **292**, 173-188.
- King, S. D. & Anderson, D. L. (1998). Edge-driven convection. *Earth and Planetary Science Letters* **160**, 289-296.
- Korenaga, J. (2005). Why did not the Ontong Java Plateau form subaerially? *Earth and Planetary Science Letters* **234**, 385- 399.
- Kroenke, L. W. (1974). Origin of continents through development and coalescence of oceanic flood basalt plateaus. *Eos* **55**, 443.
- Lassiter, J. C., DePaolo, D. J. & Mahoney, J. J. (1995). Geochemistry of the Wrangellia flood basalt province: Implications for the role of continental and oceanic lithosphere in flood basalt genesis. *Journal of Petrology* **36**(4), 983-1009.
- Le Bas, M. J. (2000). IUGS reclassification of the high-Mg and picritic volcanic rocks. *Journal of Petrology* **41**(10), 1467-1470.
- Mahoney, J. J. & Coffin, M. F. (eds.) (1997). *Large Igneous Provinces: Continental, Oceanic, and Planetary Flood Volcanism*. AGU Geophysical Monograph 100. 438 pp.
- Mahoney, J. J., Fitton, J. G., Wallace, P. J. & al., e. (2001). Proceedings of the Ocean Drilling Program, Initial Reports Volume 192. Available from World Wide Web: [http://odp.pangaea.de/publications/192\\_IR/VOLUME/CHAPTERS/IR192\\_01.PDF](http://odp.pangaea.de/publications/192_IR/VOLUME/CHAPTERS/IR192_01.PDF).
- Massey, N. W. D., MacIntyre, D. G., Desjardins, P. J. & Cooney, R. T. (2005a). Digital Geology Map of British Columbia: Tile NM9 Mid Coast, B.C. *B.C. Ministry of Energy and Mines* Geofile 2005-2.
- Massey, N. W. D., MacIntyre, D. G., Desjardins, P. J. & Cooney, R. T. (2005b). Digital Geology Map of British Columbia: Tile NM10 Southwest B.C. *B.C. Ministry of Energy and Mines* Geofile 2005-3.

- Nixon, G. T., Larocque, J., Greene, A. R. & Scoates, J. S. (2008a). Stratigraphic setting and metallogenic significance of high-Mg lavas in the Karmutsen flood basalts, northern Vancouver Island, British Columbia. *GAC-MAC 2008*, Quebec City, Quebec.
- Nixon, G. T., Laroque, J., Pals, A., Styan, J., Greene, A. R. & Scoates, J. S. (2008b). High-Mg lavas in the Karmutsen flood basalts, northern Vancouver Island (NTS 092L): Stratigraphic setting and metallogenic significance. In: Grant, B. (ed.) *Geological Fieldwork 2007*. B.C. Ministry of Energy, Mines and Petroleum Resources Paper 2008-1, pp. 175-190.
- Nokleberg, W. J., Plafker, G. & Wilson, F. H. (1994). Geology of south-central Alaska. In: Plafker, G. & Berg, H. C. (eds.) *The Geology of North America*. Geological Society of America: Boulder, CO The Geology of Alaska G-1, pp. 311-366.
- Ogg, J. G. (2004). The Triassic Period. In: Gradstein, F. M., Ogg, J. G. & Smith, A. G. (eds.) *A Geologic Time Scale 2004*. Cambridge University Press: Cambridge, pp. 271-306.
- Parrish, R. R. & McNicoll, V. J. (1992). U-Pb age determinations from the southern Vancouver Island area, British Columbia. *Geological Survey of Canada*. Radiogenic Age and Isotopic Studies: Report 5 Paper 91-2, 79-86 p.
- Petterson, M. G., Babbs, T., Neal, C. R., Mahoney, J. J., Saunders, A. D., Duncan, R. A., Tolia, D., Magu, R., Qopoto, C., Mahoa, H. & Natogga, D. (1999). Geological-tectonic framework of Solomon Islands, SW Pacific: crustal accretion and growth within an intra-oceanic setting. *Tectonophysics* **301**, 35-60.
- Plafker, G. & Berg, H. C. (1994). Overview of the geology and tectonic evolution of Alaska. In: G., P. & H.C., B. (eds.) *The Geology of North America*. Geological Society of America: Boulder, CO The Geology of Alaska G-1, pp. 989-1021.
- Plafker, G., Moore, J. C. & Winkler, G. R. (1994). Geology of the southern Alaska margin. In: Plafker, G. & Berg, H. C. (eds.) *The Geology of North America*. Geological Society of America: Boulder, CO The Geology of Alaska G-1, pp. 389-449.
- Plafker, G., Nokleberg, W. J. & Lull, J. S. (1989). Bedrock geology and tectonic evolution of the Wrangellia, Peninsular, and Chugach terranes along the Trans-Alaskan Crustal Transect in the northern Chugach Mountains and southern Copper River basin, Alaska. *Journal of Geophysical Research* **94**, 4,255-4,295.
- Rampino, M. R. & Stothers, R. B. (1988). Flood basalt volcanism during the past 250 million years. *Science* **241**, 663-668.
- Révilion, S., Arndt, N. T., Hallot, E., Kerr, A. C. & Tarney, J. (1999). Petrogenesis of picrites from the Caribbean Plateau and the North Atlantic magmatic province. *Lithos* **49**, 1-21.
- Richards, M. A., Jones, D. L., Duncan, R. A. & DePaolo, D. J. (1991). A mantle plume initiation model for the Wrangellia flood basalt and other oceanic plateaus. *Science* **254**, 263-267.
- Rioux, M., Hacker, B., Mattinson, J., Kelemen, P., Blusztajn, J. & Gehrels, G. (2007). Magmatic development of an intra-oceanic arc: High-precision U-Pb zircon and whole-rock isotopic analyses from the accreted Talkeetna arc, south-central Alaska. *Geological Society of America Bulletin* **119**(9-10), 1168-1184, 10.1130/b25964.1.

- Rogers, G. (1982). Oceanic plateaus as meteorite impact signatures. *Nature* **299**, 341-342.
- Saunders, A. D. (2005). Large igneous provinces: Origin and environmental consequences. *Elements* **1**, 259-263.
- Saunders, A. D., Storey, M., Kent, R. W. & Norry, M. J. (1992). Consequences of plume-lithosphere interactions. In: Storey, B. C., Alabaster, T. & Pankhurst, R. J. (eds.) *Magmatism and the Causes of Continental Breakup*. Geological Society of London Special Publication 68: London, pp. 41-60.
- Scoates, J. S., Greene, A. R. & Weis, D. (2006). Platinum group element geochemistry of the Karmutsen flood basalt province, Wrangellia terrane, Vancouver Island. *Geological Society of America Cordilleran Section*, Anchorage, Alaska. 38: 5, p. 26.
- Scoates, J. S., Greene, A. R. & Weis, D. (2008). Platinum group element geochemistry of large igneous provinces. *Goldschmidt 2008 Conference*, Vancouver, BC.
- Scoates, J. S., Greene, A. R., Weis, D., Israel, S. & Nixon, G. T. (2007). PGE geochemistry and sulphide saturation state of the Triassic Wrangellia basalts, Vancouver Island and Yukon. *Cordilleran Mineral Roundup Expo*, Vancouver, BC.
- Scotese, C. R. (2004). PALEOMAP project. <http://www.scotese.com/research.htm>.
- Self, S., T., T. & L., K. (1997). Emplacement of continental flood basalt lava flows. In: Mahoney, J. J. & Coffin, M. F. (eds.) *Large Igneous Provinces: Continental, Oceanic, and Planetary Flood Volcanism*. American Geophysical Union: Washington. Geophysical Monograph 100, pp. 381-410.
- Self, S., Widdowson, M., Thordarson, T. & Jay, A. E. (2006). Volatile fluxes during flood basalt eruptions and potential effects on the global environment: A Deccan perspective. *Earth and Planetary Science Letters* **248**, 518-532.
- Smith, W. H. F. & Sandwell, D. T. (1997). Global Sea Floor Topography from Satellite Altimetry and Ship Depth Soundings. *Science* **277**, 1956-1962.
- Storey, M., Mahoney, J. J., Kroenke, L. W. & Saunders, A. D. (1991). Are oceanic plateaus sites of komatiite formation? *Geology* **19**, 376-379.
- Taylor, B. (2006). The single largest oceanic plateau: Ontong Java-Manihiki-Hikurangi. *Earth and Planetary Science Letters* **241**(3-4), 372-380.
- Tejada, M. L. G., Mahoney, J. J., Castillo, P. R., Ingle, S. P., Sheth, H. C. & Weis, D. (2004). Pin-pricking the elephant: evidence on the origin of the Ontong Java Plateau from Pb-Sr-Hf-Nd isotopic characteristics of ODP Leg 192 basalts. In: Fitton, J. G., Mahoney, J. J., Wallace, P. J. & Saunders, A. D. (eds.) *Origin and Evolution of the Ontong Java Plateau*. Geological Society of London, Special Publication 229, pp. 133-150.
- Tejada, M. L. G., Mahoney, J. J., Duncan, R. A. & Hawkins, M. P. (1996). Age and geochemistry of basement and alkalic rocks of Malaita and Santa Isabel, Solomon Islands, Southern Margin of Ontong Java Plateau. *Journal of Petrology* **37**(2), 361-394.
- Tejada, M. L. G., Mahoney, J. J., Neal, C. R., Duncan, R. A. & Petterson, M. G. (2002). Basement geochemistry and geochronology of Central Malaita, Solomon Islands, with implications for the origin and evolution of the Ontong Java Plateau. *Journal of Petrology* **43**(3), 449-484.

- Weis, D. & Frey, F. A. (2002). Submarine basalts of the northern Kerguelen plateau: interaction between the Kerguelen plume and the southeast Indian Ridge revealed at ODP Site 1140. *Journal of Petrology* **43**(7), 1287-1309.
- Wignall, P. B. (2001). Large igneous provinces and mass extinctions. *Earth-Science Reviews* **53**, 1-33.
- Wilson, F. H., Dover, J. D., Bradley, D. C., Weber, F. R., Bundtzen, T. K. & Haeussler, P. J. (1998). Geologic map of Central (Interior) Alaska. *U. S. Geological Survey Open-File Report 98-133-A*. <http://wrgis.wr.usgs.gov/open-file/of98-133-a/>.
- Wilson, F. H., Labay, K. A., Shew, N. B., Preller, C. C., Mohadjer, S. & Richter, D. H. (2005). Digital Data for the Geology of Wrangell-Saint Elias National Park and Preserve, Alaska *U. S. Geological Survey Open-File Report 2005-1342*, <http://pubs.usgs.gov/of/2005/1342/>.
- Yole, R. W. & Irving, E. (1980). Displacement of Vancouver Island, paleomagnetic evidence from the Karmutsen Formation. *Canadian Journal of Earth Sciences* **17**, 1210-1228.

## **CHAPTER 2**

### **Wrangellia Flood Basalts on Vancouver Island: Significance of Picritic and Tholeiitic Lavas for the Melting History and Magmatic Evolution of a Major Oceanic Plateau**

<sup>1</sup>A version of this chapter has been submitted for publication.

## INTRODUCTION

The largest magmatic events on Earth have led to the formation of oceanic plateaus. Oceanic plateaus are transient large igneous provinces (LIPs) that cover up to two million square kilometers of the ocean floor and form crustal emplacements 20-40 km thick with submarine or subaerial flood basalt sequences six or more kilometers thick (Coffin & Eldholm, 1994). LIPs typically form in one or more pulses lasting less than a few million years. Three key aspects of LIPs are that they form from unusually high melt production rates, they are predominantly basaltic in composition, and their formation is often not directly attributable to seafloor spreading processes (e.g. Saunders, 2005). The high melt production rates are best explained by high mantle source temperatures of rapidly upwelling mantle (i.e. mantle plumes) and direct evidence of high mantle temperatures is eruption of high-MgO, near-primary lavas (Kerr & Mahoney, 2007). Studies of oceanic plateaus may provide important information about their construction and growth history, the temperature and depth of melting of the mantle source, the volume of magma and melt production rates, and the composition of the mantle source. Combined, this information serves to constrain aspects of the mantle plume hypothesis from the origin of components in the source to emplacement of voluminous lava sequences. From a geochemical perspective, study of oceanic plateaus is important because the lavas erupted in oceanic plateaus are generally unaffected by continental contamination.

Presently, one of the great challenges in studying oceanic plateaus in the ocean basins is the difficulty in sampling more than the uppermost few hundred meters of flows (e.g. Kerguelen, Ontong Java, etc.). Accreted sections of oceanic plateaus (e.g. Caribbean, Ontong Java) provide an opportunity to closely examine their volcanic stratigraphy. Wrangellia flood basalts in the Pacific Northwest of North America are parts of an immense LIP that erupted in a marine setting and accreted to western North America in the Late Jurassic or Early Cretaceous (Richards *et al.*, 1991). Although their original areal distribution was likely considerably larger, current exposures of the flood basalts extend in a thin belt over 2300 km in British Columbia (BC), Yukon, and Alaska and retain a large part of their original stratigraphic thickness (~6 km on Vancouver Island; ~3.5 km in Alaska). The present extent of the Wrangellia oceanic plateau



remnants is primarily a result of transform fault motions that occurred along western North America after accretion, rather than an indication of the original size of the plateau. The flood basalts erupted in the Middle to Late Triassic (~231-225 Ma; Richards *et al.*, 1991) atop different-aged Paleozoic arc volcanic and marine sedimentary sequences and are overlain by Late Triassic limestone. On Vancouver Island, a tripartite succession of flood basalts includes submarine, volcanoclastic, and subaerial flows formed as part of an enormous emergent oceanic plateau. Richards *et al.* (1991) proposed a plume initiation model for the Wrangellia flood basalts based on evidence of rapid uplift prior to volcanism, lack of evidence of rifting associated with volcanism (i.e. few dikes and abundant sills), and the short duration and high eruption rate of volcanism. Wrangellia flood basalts are perhaps the most extensive accreted remnants of an oceanic plateau in the world where parts of the entire volcanic stratigraphy are exposed, but they have been the focus of only one study in the last 20 years using multiple types of isotopic and geochemical data (Lassiter *et al.*, 1995).

In this study, we examine the field relationships, stratigraphy, petrography, major and trace elements, and Sr-Nd-Hf-Pb isotopic compositions of Wrangellia flood basalts from different areas of Vancouver Island to assess the nature of the mantle source and to evaluate the melting history and subsequent magmatic evolution of basalts involved in the construction of this major oceanic plateau. The geochemistry of picritic and tholeiitic basalts that form the volcanic stratigraphy of this oceanic plateau offers a view of the melting history of plume-derived magmas that does not involve continental lithosphere and where source heterogeneity does not have a major role. This study is one part of a large research project on the nature, origin and evolution of the Triassic Wrangellia flood basalts in British Columbia, Yukon and Alaska.

## **GEOLOGIC SETTING**

### **Wrangellia on Vancouver Island**

Wrangellia flood basalts form the core of the Wrangellia terrane, or Wrangellia, one of the largest outboard terranes accreted to western North America (Jones *et al.*, 1977). Middle to Late Triassic flood basalts extend in a discontinuous belt from Vancouver and Queen Charlotte Islands (Karmutsen Formation), through southeast

Alaska and southwest Yukon, and into the Wrangell Mountains, Alaska Range, and Talkeetna Mountains in east and central Alaska (Nikolai Formation) (Fig. 2.1).

Wrangellia covers approximately 80% of Vancouver Island, which is 460 km long by 130 km wide (Fig. 2.1). Wrangellia is the uppermost sheet of a stack of southwest-vergent thrust sheets that form the crust of Vancouver Island and has a cumulative thickness of >10 km (Monger & Journeay, 1994). Pre-Karmutsen units of Wrangellia on Vancouver Island are Devonian arc sequences of the Sicker Group and Mississippian to Early Permian siliciclastic and carbonate rocks of the Buttle Lake Group (Muller, 1980; Sutherland-Brown *et al.*, 1986). The Paleozoic formations have varied estimated thicknesses (~2-5 km) (Muller, 1980; Massey, 1995a) and are only exposed on central and southern Vancouver Island (Fig. 2.1). The Karmutsen Formation is overlain by the shallow-water Quatsino Limestone (30-750 m) and deeper-water Parson Bay Formation (~600 m), which is intercalated with and overlain by Bonanza arc volcanics (169-202 Ma; Nixon *et al.*, 2006b). Bonanza arc plutonic rocks (167-197 Ma) also intrude the Karmutsen Formation and are some of the youngest units of Wrangellia that formed prior to accretion with North America (Nixon *et al.*, 2006b). Following accretion, Wrangellia units were intruded by the predominantly Cretaceous Coast Plutonic Complex (Wheeler & McFeely, 1991).

The Karmutsen Formation (19,142 km<sup>2</sup>, based on mapped areas from digital geologic maps) is composed of basal sediment-sill complexes, a lower member of pillowed and unpillowed submarine flows, a middle member of mostly pillow breccia and hyaloclastite, and an upper member of predominantly massive subaerial flows (Carlisle & Suzuki, 1974). The pillow basalts directly overlie thick sediment-sill complexes composed of mafic sills intruding Middle Triassic pelagic sediments and Late Paleozoic formations. The boundary between pillow breccia/hyaloclastite and massive lava flows represents the transition from a submarine to a subaerial eruptive environment. The uppermost flows of the Karmutsen are intercalated and overlain by shallow-water limestone and local occurrences of submarine flows occur within the upper subaerial member. The Karmutsen Formation and Wrangellia on Vancouver Island were the focus of mapping efforts and stratigraphic descriptions by Carlisle (Carlisle, 1963; Carlisle, 1972; Carlisle & Suzuki, 1974) and Muller (Muller *et al.*, 1974; Muller, 1977). Recent

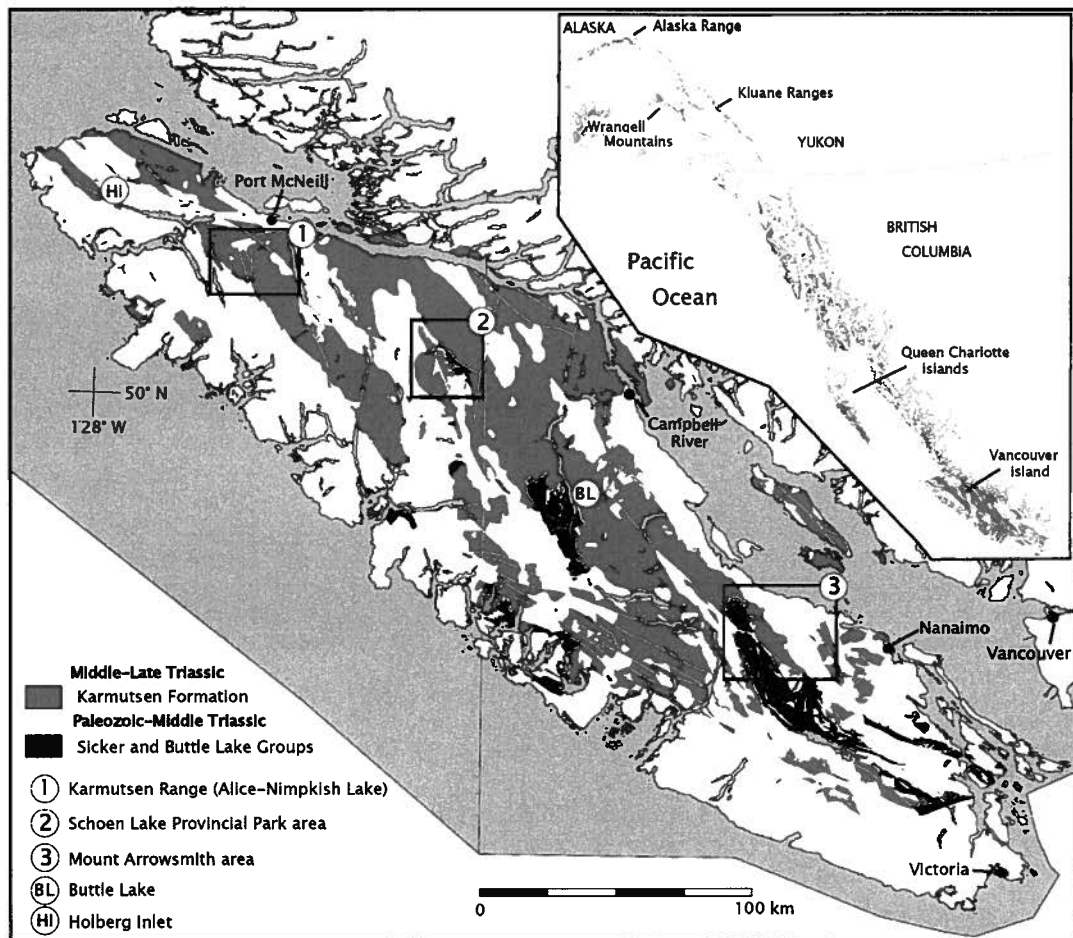


**Figure 2.1** Simplified map of Vancouver Island showing the distribution of the Karmutsen Formation (gray) and underlying Paleozoic formations (black; after Massey *et al.*, 2005a, 2005b). The main areas of field study are indicated with boxes or circles with capital letters (see legend). Ocean is light gray. The inset shows the extent of the Wrangellia flood basalts (gray) in British Columbia, Yukon, and Alaska.

descriptions of the Karmutsen Formation on northern Vancouver Island have been made during regional mapping studies (1:50,000 scale) on northern Vancouver Island by Nixon *et al.* (Nixon *et al.*, 2006b; Nixon & Orr, 2007; Nixon *et al.*, 2008).

### **Age of the Karmutsen Formation**

The age and duration of Karmutsen volcanism are constrained by fossils in the underlying and overlying sedimentary units and by three U-Pb isotopic age determinations on intrusive rocks that are likely related to the Karmutsen volcanics. *Daonella*-bearing shale 100-200 m below the base of the pillow basalts on Schoen Mountain and *Halobia*-rich shale interlayered with flows in the upper part of the Karmutsen indicate eruption of the flood basalts in the Upper Ladinian (Middle Triassic) to Upper Carnian (Late Triassic; Carlisle and Suzuki, 1974). The only published U-Pb age is based on a single concordant analysis of a multi-grain baddeleyite fraction from a gabbro on southern Vancouver Island that yielded a  $^{206}\text{Pb}/^{238}\text{U}$  age of  $227.3 \pm 2.6$  Ma (Parrish & McNicoll, 1992). Two unpublished  $^{206}\text{Pb}/^{238}\text{U}$  baddeleyite ages, also from a gabbro on southern Vancouver Island, are  $226.8 \pm 0.5$  Ma (5 fractions) and  $228.4 \pm 2.5$  (2 fractions; Sluggett, 2003).

### **VOLCANIC STRATIGRAPHY AND PETROGRAPHY**

Field studies undertaken on Vancouver Island in 2004-2006 explored the volcanic stratigraphy of the Karmutsen flood basalts in three main areas: the Karmutsen Range (between Alice and Nimpkish lakes), the area around Schoen Lake Provincial Park, and around Mount Arrowsmith (Greene *et al.*, 2005; Greene *et al.*, 2006), and also around Holberg Inlet, on northernmost Vancouver Island, and Buttle Lake (Fig. 2.1). The character and thickness of the flood basalt sequences vary locally, although the tripartite succession of the Karmutsen Formation appears to be present throughout Vancouver Island. The stratigraphic thicknesses for the pillow, pillow breccia, and massive flow members are estimated at ~2600 m, 1100 m, and 2900 m, respectively, in the type area around Buttle Lake (Surdam, 1967); on northern Vancouver Island estimated thicknesses are >3000 m, 400-1500 m, and >1500 m, respectively (Nixon *et al.*, 2008); on Mount

Arrowsmith and nearby areas on southern Vancouver Island estimates are 1100 m, 950 m, and 1200 m, respectively (Yorath *et al.*, 1999; Fig. 2.1).

Picritic pillow lavas occur west of the Karmutsen Range on northern Vancouver Island, in a roughly triangular-shaped area (~30 km across) bounded by Keogh, Maynard and Sara lakes (Figs 2.2 and 2.3; Greene *et al.*, 2006; Nixon *et al.*, 2008). Excellent exposures of picritic pillow lavas occur in roadcuts along the north shore of Keogh Lake, the type locality (Greene *et al.*, 2006). The Keogh Lake picrites mostly form pillowed flow units (<15 m thick), with pillows and tubes of varied dimensions (typically <1 m wide), and unpillowed flows. Numerous thermal contraction features in the pillows are filled with quartz-carbonate, such as drain-back ledges, tortoise-shell jointing, and interpillow voids containing spalled rims (Fig. 2.3; Greene *et al.*, 2006). The picritic pillow basalts are not readily distinguishable in the field from basalt, except by their density and non-magnetic character and minor interpillow quartz-carbonate. Recent fieldwork and mapping indicates that the picrites occur mostly near the transition between pillow lava emplacement and hyaloclastite deposition (Nixon *et al.*, 2008).

In and around Schoen Lake Provincial Park, there is a well-preserved sediment-sill complex at the base of the Karmutsen Formation (Figs 2.2 and 2.4). Middle Triassic marine sedimentary rocks overlie Pennsylvanian to Permian limestone and siliceous sedimentary rocks, and both successions are intruded by mafic sills related to the overlying flood basalts (Carlisle, 1972). Carlisle (1972) estimated the sediment-sill complex to be approximately 600-900 m thick with a total thickness of 150-200 m of pre-intrusive sedimentary rocks. The Triassic sedimentary rocks range from thinly-bedded siliceous and calcareous shale to banded chert and finely-laminated, *Daonella*-bearing shale (Carlisle, 1972). The basal sediment-sill complex is immediately overlain by thick successions of submarine flows (Fig. 2.4). Basal sills and pre-Karmutsen sediments are also exposed around Buttle Lake.

Exposures with large vertical relief around Mount Arrowsmith (Appendix A) and Buttle Lake preserve thick successions of pillow basalt, breccias, and subaerial flows and there are rarely sediments between flows or in interpillow voids. Unpillowed submarine flows interspersed with pillowed flows are locally recognizable by irregular, hackly columnar jointing. The massive subaerial flows form monotonous sequences marked

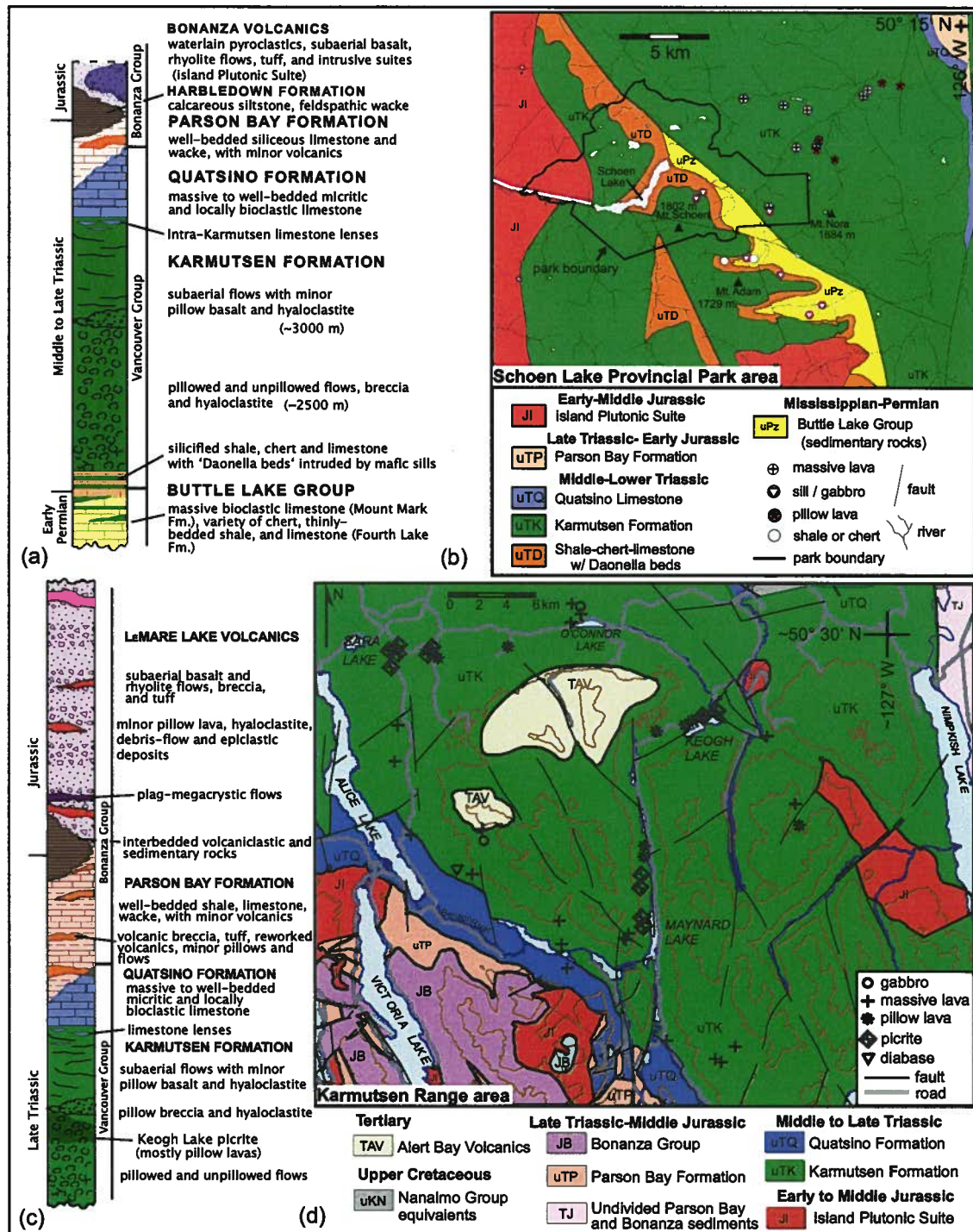


**Figure 2.2** Geologic map and stratigraphy of the Schoen Lake Provincial Park and Karmutsen Range areas (locations shown in Figure 2.1, northern Vancouver Island). (a) Stratigraphic column depicts units exposed in the Schoen Lake area, derived from Carlisle (1972) and fieldwork. (b) Generalized geology for the Schoen Lake area with sample locations. Map derived from Massey *et al.* (2005a). The exposures in the Schoen Lake area are the lower volcanic stratigraphy and base of the Karmutsen Formation. (c) Stratigraphic column for geology in the Alice-Nimpkish Lake area, derived from Nixon & Orr (2007). (d) Geologic map from mapping of Nixon & Orr (2006a) and Nixon *et al.* (2008). Sample sites and lithologies are denoted in the legend. The Keogh Lake picrites are exposed near Keogh, Sara, and Maynard lakes and areas to the east of Maynard Lake (Nixon *et al.*, 2008).



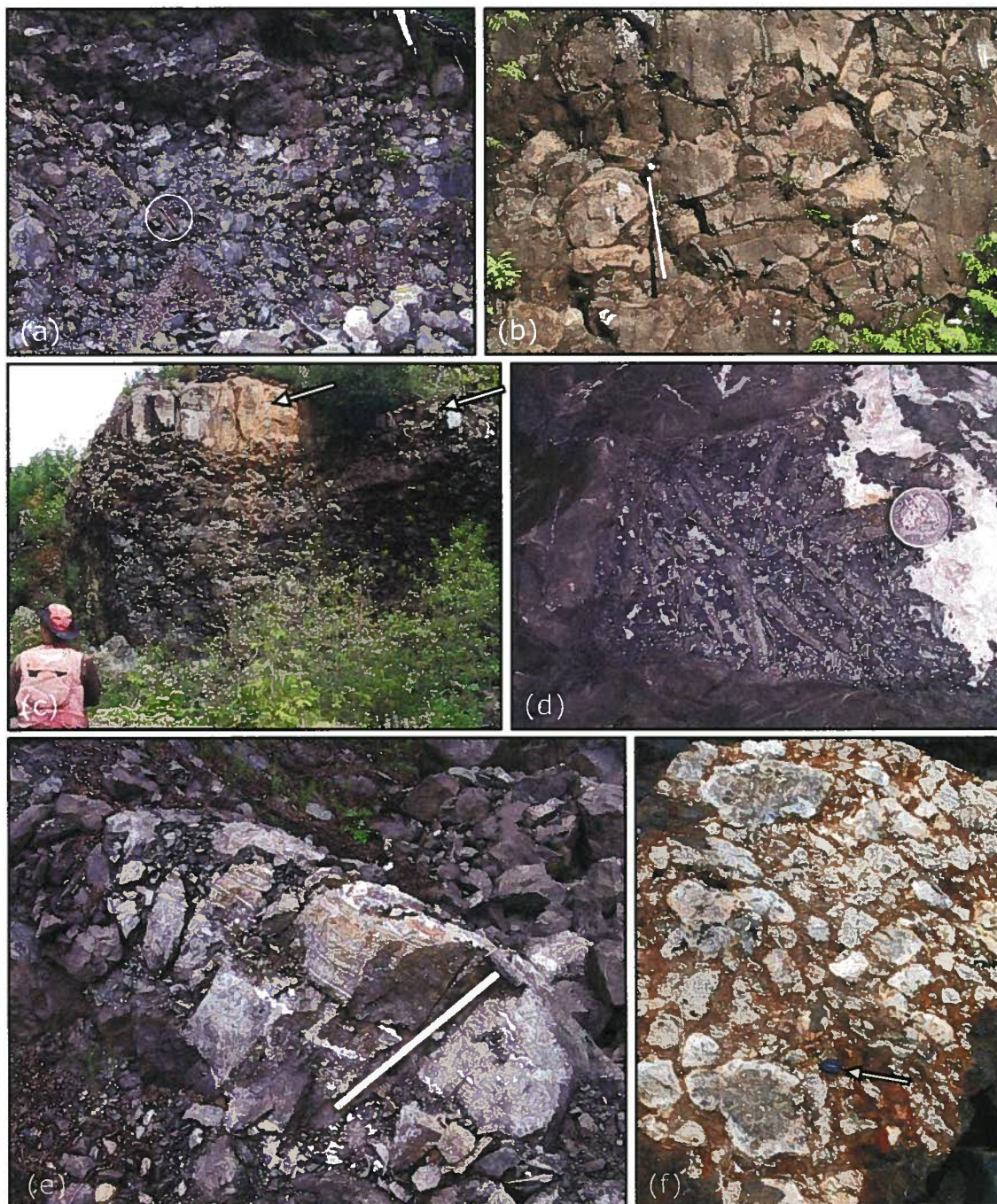


**Figure 2.3** Photographs of picritic and tholeiitic pillow basalts from the Karmutsen Range area (Alice and Nimpkish Lake area), northern Vancouver Island. (a) Stack of dense, closely packed, asymmetric picritic pillows with radial vesicle infillings (circled sledgehammer ~80 cm long for scale). (b) Picritic pillow basalts in cross-section near Maynard Lake. Note vesicular upper margin to pillows. (c) Unpillowed submarine flow with coarse, hackly columns (marked with arrows) draped over high-MgO pillow basalt. (d) Spalled rims from pillows filling voids between tholeiitic pillow basalt (coin for scale). (e) Cross-section of a large picritic pillow lobe with infilling of quartz-carbonate in cooling-contraction cracks (sledgehammer for scale). (f) High-MgO pillow breccia stratigraphically between submarine and subaerial flows (lens cap for scale ~7 cm diameter).



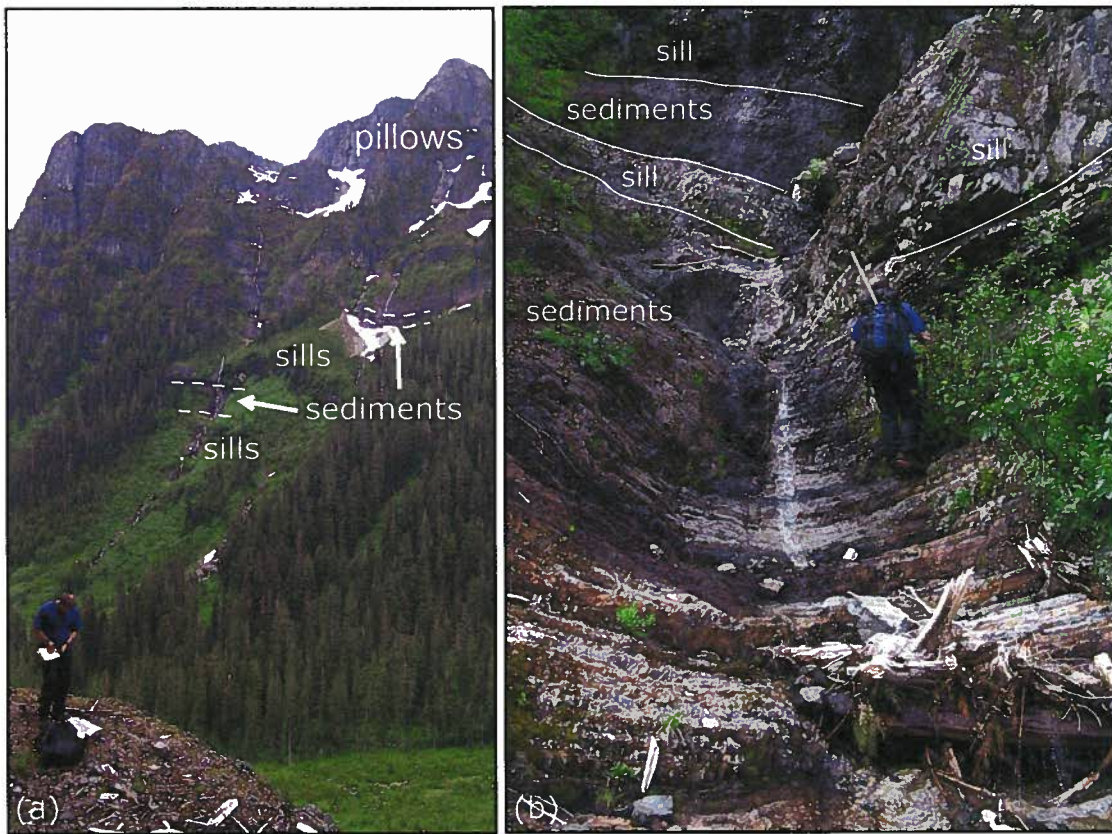


**Figure 2.4** Photographs showing field relations from the Schoen Lake Provincial Park area, northern Vancouver Island. (a) Sediment-sill complex at the base of the Karmutsen Formation on the north side of Mount Adam (see Fig. 2.2 for location). (b) Interbedded mafic sills and deformed, finely-banded chert and shale with calcareous horizons, from location between Mt. Adam and Mt. Schoen.



Arrowsmith and nearby areas on southern Vancouver Island estimates are 1100 m, 950 m, and 1200 m, respectively (Yorath *et al.*, 1999; Fig. 2.1).

Picritic pillow lavas occur west of the Karmutsen Range on northern Vancouver Island, in a roughly triangular-shaped area (~30 km across) bounded by Keogh, Maynard and Sara lakes (Figs 2.2 and 2.3; Greene *et al.*, 2006; Nixon *et al.*, 2008). Excellent exposures of picritic pillow lavas occur in roadcuts along the north shore of Keogh Lake, the type locality (Greene *et al.*, 2006). The Keogh Lake picrites mostly form pillowed flow units (<15 m thick), with pillows and tubes of varied dimensions (typically <1 m wide), and unpillowed flows. Numerous thermal contraction features in the pillows are filled with quartz-carbonate, such as drain-back ledges, tortoise-shell jointing, and interpillow voids containing spalled rims (Fig. 2.3; Greene *et al.*, 2006). The picritic pillow basalts are not readily distinguishable in the field from basalt, except by their density and non-magnetic character and minor interpillow quartz-carbonate. Recent fieldwork and mapping indicates that the picrites occur mostly near the transition between pillow lava emplacement and hyaloclastite deposition (Nixon *et al.*, 2008).

In and around Schoen Lake Provincial Park, there is a well-preserved sediment-sill complex at the base of the Karmutsen Formation (Figs 2.2 and 2.4). Middle Triassic marine sedimentary rocks overlie Pennsylvanian to Permian limestone and siliceous sedimentary rocks, and both successions are intruded by mafic sills related to the overlying flood basalts (Carlisle, 1972). Carlisle (1972) estimated the sediment-sill complex to be approximately 600-900 m thick with a total thickness of 150-200 m of pre-intrusive sedimentary rocks. The Triassic sedimentary rocks range from thinly-bedded siliceous and calcareous shale to banded chert and finely-laminated, *Daonella*-bearing shale (Carlisle, 1972). The basal sediment-sill complex is immediately overlain by thick successions of submarine flows (Fig. 2.4). Basal sills and pre-Karmutsen sediments are also exposed around Buttle Lake.

Exposures with large vertical relief around Mount Arrowsmith (Appendix A) and Buttle Lake preserve thick successions of pillow basalt, breccias, and subaerial flows and there are rarely sediments between flows or in interpillow voids. Unpillowed submarine flows interspersed with pillowed flows are locally recognizable by irregular, hackly columnar jointing. The massive subaerial flows form monotonous sequences marked

mainly by amygdaloidal horizons and brecciated flow tops are rarely observed. A single locality with well-preserved pahoehoe flow features is exposed north of Holberg Inlet (Nixon & Orr, 2007; Nixon *et al.*, 2008). There is no evidence of significant detrital material from a continental source in sediments associated with the flood basalts anywhere on Vancouver Island. The uppermost Karmutsen flows are interbedded with thin (>4 m) lenses of limestone, and rarely siliciclastic sedimentary rocks (Nixon *et al.*, 2006b). Plagioclase-phyric (>0.8 mm) trachytic-textured flows are also commonly found near the top of the Karmutsen Formation (Nixon *et al.*, 2006b).

A total of 129 samples were collected from the Karmutsen Formation on Vancouver Island and 63 samples were selected for geochemical work based on the relative degree of alteration and geographic distribution of the samples. Fifty-six of these samples have been divided into four groups based on petrography (Table 2.1) and geochemistry, including tholeiitic basalt, picrite, high-MgO basalt, and coarse-grained mafic rocks. The tholeiitic basalts are dominantly glomeroporphyritic with an intersertal to intergranular groundmass (Table 2.1). Plagioclase forms most of the phenocrysts and glomerocrysts and the groundmass is fine-grained plagioclase microlites, clinopyroxene granules, small grains of Fe-Ti oxide, devitrified glass, and secondary minerals; there is no fresh glass. The picritic and high-MgO basaltic lavas exhibit plagioclase and clinopyroxene with spherulitic morphologies with abundant euhedral olivine phenocrysts (Fig. 2.5; Table 2.1). Only olivine is strongly altered and is completely pseudomorphically replaced by talc/tremolite. Plagioclase and clinopyroxene phenocrysts are not present in the high-MgO samples. The coarse-grained mafic rocks are characterized petrographically by subophitic texture with average grain size typically >1mm, and are generally non-glomeroporphyritic. The coarse-grained mafic rocks are mostly from the interiors of massive flows, although some may be from sills.

## **SAMPLE PREPARATION AND ANALYTICAL METHODS**

Only the freshest rocks in the field were sampled and only the least altered samples were selected for chemical and isotopic analysis based on thorough petrographic inspection. Sixty-three of the 129 collected samples (including 7 non-Karmutsen

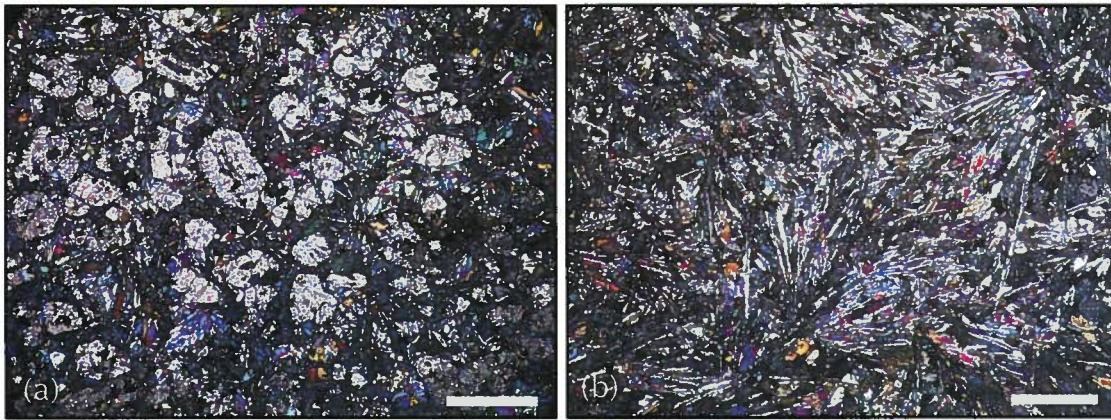


**Figure 2.5** Photomicrographs of picritic pillow basalts, Karmutsen Formation, northern Vancouver Island. Scale bars are 1 mm long. (a) Picrite with abundant euhedral olivine pseudomorphs from Keogh Lake type locality (Fig. 2.2) in cross-polarized transmitted light (sample 4722A4; 19-19.8 wt % MgO, 4 analyses). Samples contain dense clusters (24-42 vol %) of olivine pseudomorphs (<2 mm) in a groundmass of curved and branching sheaves of acicular plagioclase and intergrown with clinopyroxene and altered glass. In many cases, plagioclase nucleated on the edges of the olivine phenocrysts. (b) Sheaves of intergrown plagioclase and clinopyroxene in aphyric picrite pillow lava from west of Maynard Lake (Fig. 2.2) in cross-polarized transmitted light (sample 4723A2; 10.8 wt % MgO).

Table 2.1 Summary of petrographic characteristics and phenocryst proportions of Karmutsen basalts on Vancouver Island, B.C.

Sample <sup>a</sup>	Area <sup>b</sup>	Flow <sup>c</sup>	Group <sup>d</sup>	Texture <sup>e</sup>	vol% Of Plag	Cpx	Ox	Alteration <sup>f</sup>	Note <sup>h</sup>
4718A1	MA	PIL	THOL	Intersertal	20	5		3	few plag glcr <2 mm, cpx <1 mm
4718A2	MA	PIL	THOL	Intersertal, glomero	15			1	plag glcr <2 mm, very fresh
4718A5	MA	FLO	THOL	Intersertal, glomero	10			2	mottled, few plag glcr <4 mm
4718A6	MA	BRE	THOL	porphyritic	20			2	plag 5-6 mm, sericite alteration
4718A7	MA	PIL	THOL	glomero	10			3	plag glcr <3 mm
4719A2	MA	PIL	THOL	porphyritic, intersertal	5			3	plag glcr <2 mm
4719A3	MA	PIL	THOL	glomero	10			2	plag glcr <3 mm
4720A2	SL	BRE	THOL	glomero	5			3	plag glcr <2 mm
4720A3	SL	FLO	THOL	glomero	3			3	plag glcr <3 mm
4720A4	SL	FLO	THOL	glomero	5			1	plag glcr <5 mm, slightly cg, very fresh
4720A5	SL	FLO	THOL	seriate	20			3	plag glcr <2 mm, plag needles and laths
4720A8	SL	FLO	THOL	glomero	20			2	plag glcr <2 mm, plag needles and laths
4720A9	SL	FLO	THOL	glomero	10			2	plag glcr <1.5 mm
4721A1	SL	PIL	THOL	glomero	15			3	plag glcr <1.5 mm, plag needles aligned
4721A2	SL	FLO	THOL	glomero	10			1	plag glcr <3 mm, very fresh
4721A3	SL	FLO	THOL	glomero	20			3	plag glcr <2 mm, plag needles
4721A4	SL	FLO	THOL	glomero, ophimottled	20	5		1	plag glcr <1.5 mm, cpx <1 mm (olk), very fresh
4721A5	SL	FLO	THOL	glomero, ophimottled	5	15		3	plag glcr <1.5 mm, cpx <1 mm (olk)
4722A2	KR	FLO	THOL	Intergranular, Intersertal	1			1	few plag phenos <2 mm
4723A10	KR	FLO	THOL	Intergranular	5	3	10	3	few plag glcr <1 mm, ox 0.5-1 mm
4724A5	SL	FLO	THOL	porphyritic	25			3	plag 7-8 mm
5614A10	KR	FLO	THOL	Intergranular, Intersertal	2		5	3	ox <0.5 mm
5614A11	KR	FLO	THOL	Intergranular, Intersertal	5		7	3	ox 0.5-1 mm
5614A13	KR	FLO	THOL	Intergranular, porphyritic	5		5	3	ox 0.5-1 mm
5615A1	KR	PIL	THOL	aphytic, Intersertal	1			2	f.g., no phenos
5615A8	KR	PIL	THOL	Intergranular			3	1	f.g., abundant small ox, very fresh
5615A10	KR	PIL	THOL	Intergranular	3			3	2 plag glcr <4 mm
5616A2	KR	FLO	THOL	intergranular, Intersertal	5		7	3	ox 0.2-0.5 mm
5618A1	QI	FLO	THOL	Intergranular	3	2	10	3	ox 0.5-2 mm, c.g., plag laths >2 mm
93G171	KR	PIL	PIC	subophitic	23				ol <2.3 mm, cpx <1.5 mm, partially enc plag
4722A4	KR	PIL	PIC	cumulus, Intergranular	35	10		3	ol <1.5 mm, cpx <2 mm enc plag
4723A3	KR	PIL	PIC	spherulitic	31			3	ol <1 mm, swtl plag <1.5 mm
4723A4	KR	PIL	PIC	Intergranular, Intersertal	0			3	swtl plag <1 mm, no ol phenos
4723A13	KR	PIL	PIC	spherulitic	24			3	swtl plag <1 mm
5614A1	KR	PIL	PIC	spherulitic	24			1	ol <1.5 mm, swtl plag <1 mm
5615A7	KR	PIL	PIC	cumulus, Intergranular	42	10		1	ol <1.5 mm, cpx <1.5 mm enc plag
5615A12	KR	PIL	PIC	spherulitic	13			1	ol <2 mm, swtl plag <1 mm
5616A1	KR	PIL	PIC	Intergranular, Intersertal	25			1	ol <2 mm
4723A2	KR	PIL	HI-MG	spherulitic	0			3	swtl plag <2 mm, no ol phenos
5614A3	KR	PIL	HI-MG	spherulitic, intrafasciculate	12			1	ol <1.5 mm, swtl plag <2 mm
5614A5	KR	BRE	HI-MG	porphyritic, ophimottled	13			2	ol <2 mm, cpx <2 mm enc plag
5616A7	KR	PIL	HI-MG	Intersertal	2			2	ol <2 mm, plag needles <1 mm
4722A5	KR	FLO	OUTLIER	Intersertal				3	mottled, very f.g., v. small pl needles
5615A11	KR	PIL	OUTLIER	Intersertal				3	mottled, very f.g., v. small pl needles
4720A6	SL	FLO	CG	subophitic		15		1	plag glcr <3 mm, cpx <3 mm
4720A7	SL	FLO	CG	subophitic		25		1	plag chad <1.5 mm, cpx olk <2 mm, very fresh
4720A10	SL	SIL	CG	subophitic, intrafasciculate			5	3	plag chad <2 mm, cpx olk <3 mm, ox <1 mm, c.g.
4724A3	SL	FLO	CG	ophimottled, subophitic	5	30	5	3	plag glcr 4-5 mm, cpx olk <2 mm, ox <1 mm
5614A14	KR	SIL	CG	Intergranular		10	5	3	plag <1 mm, cpx <2 mm
5614A15	KR	SIL	CG	subophitic		25	3	1	plag <1 mm, cpx olk <3 mm, ox <0.2 mm
5615A5	KR	GAB	CG	Intergranular, plag-phyric	30		5	3	ox <0.5 mm, plag laths <4 mm
5615A6	KR	GAB	CG	Intergranular, plag-phyric	15		10	3	plag <3 mm, ox 0.5-1.5 mm
5616A3	KR	GAB	CG	subophitic		25	5	1	plag laths <1 mm, cpx olk <2 mm, ox 0.5-1 mm
5617A1	SL	SIL	CG	Intergranular, intergrowths		30		3	plag <3 mm, cpx <5 mm, cpx-plag intergrowths
5617A5	SL	SIL	CG	Intergranular, Intersertal	1			1	plag <1 mm, f.g., mottled
5617A4	SL	SIL	MIN	Intersertal			5	3	f.g.

<sup>a</sup>Sample number: last digit year, month, day, Initial, sample station (except 93G171). <sup>b</sup>MA, Mount Arrowsmith; SL, Schoen Lake; KR, Karmutsen Range. <sup>c</sup>PIL, pillow; BRE, breccia; FLO, flow; SIL, sill; GAB, gabbro. <sup>d</sup>THOL, tholeiitic basalt; PIC, picrite; HI-MG, high-MgO basalt; CG, coarse-grained; MIN, mineralized sill. <sup>e</sup>glomero, glomeroporphyritic. <sup>f</sup>Olivine modes for picrites based on area calculations from scans (see Olivine accumulation in picritic lavas section and Figure 2.13). <sup>g</sup>Visual alteration index based primarily on degree of plagioclase alteration and presence of secondary minerals (1, least altered; 3, most altered). Plagioclase phenocrysts commonly altered to albite, pumpellyite, and chlorite; olivine is altered to talc, tremolite, and clinoclase (determined using the Rietveld method of X-ray powder diffraction); clinopyroxene is unaltered; Fe-Ti oxide commonly replaced by sphene. <sup>h</sup>glcr, glomerocrysts; f.g., fine-grained; c.g., coarse-grained; olk, olkocryst; chad, chadacryst; enc, enclosing, swtl, swallow-tail. Mineral abbreviations: ol, olivine pseudomorphs; plag, plagioclase; cpx, clinopyroxene; ox, oxides (includes ilmenite + titanomagnetite).

samples) were crushed (400 g) into small pieces <2 mm in diameter in a Rocklabs hydraulic piston crusher between WC-plates to minimize contamination. The coarse-crush was mixed and 100 g was powdered in a planetary mill using agate jars and balls cleaned with quartz sand between samples.

#### *ActLabs Analytical Methods*

The major- and trace-element compositions of the whole rock powders were determined at Activation Laboratories Ltd. (Actlabs) in Ancaster, Ontario. Analytical techniques and detection limits are also available from Actlabs ([http://www.actlabs.com/methsub\\_code4ere.htm](http://www.actlabs.com/methsub_code4ere.htm)). The particular analytical method for each of the elements analyzed is indicated in Table 2.2. For the major elements, a 0.2 g sample was mixed with a mixture of lithium metaborate/lithium tetraborate and fused in a graphite crucible. The molten mixture was poured into a 5% HNO<sub>3</sub> solution and shaken until dissolved (~30 minutes). The samples were analyzed for major oxides and selected trace elements on a combination simultaneous/sequential Thermo Jarrell-Ash Enviro II inductively coupled plasma optical emission spectrometer (ICP-OES). Internal calibration was achieved using a variety of international reference materials (e.g. W-2, BIR-1, DNC-1) and independent control samples. Additional trace elements were analyzed by both the INAA (instrumental neutron activation analysis) and ICP-MS (inductively couple plasma mass spectrometry) methods. For the INAA analyses, 1.5-2.5 g of sample was weighed into small polyethylene vials and irradiated with control international reference material CANMET WMS-1 and NiCr flux wires at a thermal neutron flux of  $7 \times 10^{12} \text{ n cm}^{-2} \text{ s}^{-1}$  in the McMaster Nuclear Reactor. Following a 7-day waiting period, the samples were measured on an Ortec high-purity Ge detector linked to a Canberra Series 95 multichannel analyzer. Activities for each element were decay- and weight-corrected and compared to a detector calibration developed from multiple international certified reference materials. For the ICP-MS analyses, 0.25 g of sample was digested in HF, followed by a mixture of HNO<sub>3</sub> and HClO<sub>4</sub>, heated and taken to dryness. The samples were brought back into solution with HCl. Samples were analyzed using a Perkin Elmer Optima 3000 ICP. In-lab standards or certified reference materials

(e.g. W-2, BIR-1, DNC-1) were used for quality control. A total of 15 blind duplicates were analyzed to assess reproducibility and the results were within analytical error.

#### *University of Massachusetts XRF Analytical Methods*

Fourteen sample duplicate powders (high-MgO basalts and picrites) were also analyzed at the Ronald B. Gilmore X-Ray Fluorescence (XRF) Laboratory at the University of Massachusetts. Major elements were measured on a fused La-bearing lithium borate glass disc using a Siemens MRS-400 spectrometer with a Rh X-ray tube operating at 2700 W. Trace element concentrations (Rb, Sr, Ba, Ce, Nb, Zr, Y, Pb, Zn, Ga, Ni, Cr, V) were measured on a separate powder pellet using a Philips PW2400 sequential spectrometer using a Rh X-ray tube. Loss-on-ignition (LOI) and ferrous iron measurements were made as described by Rhodes and Vollinger (2004). Precision and accuracy estimates for the data are described by Rhodes (1996) and Rhodes and Vollinger (2004). Results for each sample are the average of two separate analyses (shown in Appendix B).

#### *PCIGR Analytical Methods*

A subset of 19 samples was selected for high-precision trace-element analysis and Sr, Nd, Pb, and Hf isotopic analysis at the Pacific Centre for Isotopic and Geochemical Research (PCIGR) at the University of British Columbia (UBC). Samples were selected from the 63 samples analyzed for whole-rock chemistry at ActLabs, based on major- and trace-element chemistry, alteration (low LOI and petrographic alteration index), and sample location. Samples were prepared for trace-element analysis at the PCIGR by the technique described by Pretorius *et al.* (2006) on unleached rock powders. Sample powders (~100 mg) were weighed in 7 mL screw-top Savillex® beakers and dissolved in 1 mL ~14N HNO<sub>3</sub> and 5 mL 48% HF on a hotplate for 48 hours at 130°C with periodic ultrasonication. Samples were dried and redissolved in 6 mL 6N HCl on a hotplate for 24 hours and then dried and redissolved in 1 mL concentrated HNO<sub>3</sub> for 24 hours before final drying. Trace element abundances were measured with a Thermo Finnigan Element2 High Resolution-Inductively Coupled Plasma-Mass Spectrometer (HR-ICP-MS) following the procedures described by Pretorius *et al.* (2006) within 24 hours of

redissolution. High field strength elements (HFSE) and large ion lithophile elements (LILE) were measured in medium resolution mode at 2000x dilution using a PFA teflon spray chamber washed with Aqua Regia for 3 minutes between samples. Rare earth elements (REE) were measured in high resolution mode, and U and Pb in low resolution mode, at 2000x dilution using a glass spray chamber washed with 2% HNO<sub>3</sub> between samples. Total procedural blanks and reference materials (BCR-2, BHVO-2) were analyzed with the batch of samples. Indium was used as an internal standard in all samples and standard solutions. Background and standard solutions were analyzed after every 5 samples to detect memory effects and mass drift. Results for PCIGR trace-element analyses are shown in Appendix C.

Sample digestion for purification of Sr, Nd, Hf, and Pb for column chemistry began by weighing each sample powder (400-500 mg) prior to leaching. All samples were leached with 6N HCl and placed in an ultrasonic bath for 15 minutes. Samples were rinsed two times with 18 mega  $\Omega$ -cm H<sub>2</sub>O between each leaching step (15 total) until the supernatant was clear (following the technique of Mahoney, 1987). Samples were then dried on a hotplate for 24 hours and weighed again. Sample solutions were then prepared by dissolving ~100-250 mg of the leached powder dissolved in 1 mL ~14N HNO<sub>3</sub> and 10 mL 48% HF on a hotplate for 48 hours at 130°C with periodic ultrasonication. Samples were dried and redissolved in 6 mL 6N HCl on a hotplate for 24 hours and then dried. Pb was separated using anion exchange columns and the discard was used for Sr, REE, and Hf separation. Nd was separated from the other REE and Hf required two additional purification steps. Detailed procedures for column chemistry for separating Sr, Nd, and Pb at the PCIGR are described in Weis *et al.* (2006) and Hf purification is described in Weis *et al.* (2007). Sr and Nd isotope ratios were measured on a Thermo Finnigan Triton Thermal Ionization Mass Spectrometer (TIMS) in static mode with relay matrix rotation on a single Ta and double Re-Ta filament, respectively. Four to 5 filaments per barrel of 21 were occupied by standards (NBS 987 for Sr and LaJolla for Nd) for each barrel where samples were run. Sample Sr and Nd isotopic compositions were corrected for mass fractionation using  $^{86}\text{Sr}/^{88}\text{Sr} = 0.1194$  and  $^{146}\text{Nd}/^{144}\text{Nd} = 0.7219$ . Each sample was then normalized using the barrel average of the reference material relative to the values of  $^{143}\text{Nd}/^{144}\text{Nd} = 0.511858$  and  $^{87}\text{Sr}/^{86}\text{Sr} = 0.710248$  (Weis *et al.*, 2006). During the course of

the Vancouver Island analyses, the La Jolla Nd standard gave an average value of  $0.511856 \pm 6$  (n=7) and NBS987 standard gave an average of  $0.710240 \pm 8$  (n=11) ( $2\sigma$  error is reported as times  $10^6$ ).  $^{147}\text{Sm}/^{144}\text{Nd}$  ratio errors are approximately ~1.5%, or ~0.006. United States Geological Survey (USGS) reference material BHVO-2 was processed with the samples and yielded Sr and Nd isotopic ratios of  $0.703460 \pm 7$  and  $0.512978 \pm 6$ , respectively. These are in agreement with the published values of  $0.703479 \pm 20$  and  $0.512984 \pm 11$ , respectively (Weis *et al.*, 2006).

Pb and Hf isotopic compositions were analyzed by static multi-collection on a Nu Plasma (Nu Instruments) Multiple Collector-Inductively Coupled Plasma-Mass Spectrometer (MC-ICP-MS). The detailed analytical procedure for Pb isotopic analyses on the Nu Plasma at the PCIGR is described in Weis *et al.* (2006). The configuration for Pb analyses allows for collection of Pb, Tl, and Hg together. Tl and Hg are used to monitor instrumental mass discrimination and isobaric overlap, respectively. All sample solutions were analyzed with approximately the same Pb/Tl ratio (~4) as the reference material NIST SRM 981. To accomplish this, a small aliquot of each sample solution from the Pb columns was analyzed on the Element2 to determine the precise amount of Pb available for analysis on the Nu Plasma. The SRM 981 standard was run after every two samples on the Nu Plasma. During the time samples were run, analyses of the SRM 981 Pb reference material gave values of  $^{206}\text{Pb}/^{204}\text{Pb}=16.9403 \pm 22$ ,  $^{207}\text{Pb}/^{204}\text{Pb}=15.4958 \pm 23$ , and  $^{208}\text{Pb}/^{204}\text{Pb}=36.7131 \pm 64$  (n=61;  $2\sigma$  error is reported as times  $10^4$ ); these values are in excellent agreement with reported TIMS triple-spike values of Galer & Abouchami (1998). Fractionation-corrected Pb isotopic ratios were further corrected by the sample-standard bracketing method or the ln-ln correction method described by White *et al.* (2000) and Blichert-Toft *et al.* (2003). Leached powders of USGS reference material BHVO-2 yielded Pb isotopic ratios of  $^{206}\text{Pb}/^{204}\text{Pb}=18.6454 \pm 8$ ,  $^{207}\text{Pb}/^{204}\text{Pb}=15.4910 \pm 5$ , and  $^{208}\text{Pb}/^{204}\text{Pb}=38.2225 \pm 14$  and BCR-2 yielded  $^{206}\text{Pb}/^{204}\text{Pb}=18.8046 \pm 6$ ,  $^{207}\text{Pb}/^{204}\text{Pb}=15.6251 \pm 8$ , and  $^{208}\text{Pb}/^{204}\text{Pb}=38.8349 \pm 6$  ( $2\sigma$  error is reported as times  $10^4$ ). These values are in agreement with leached residues of BHVO-2 and BCR-2 from Weis *et al.*, (2006).

Hf isotopic compositions were analyzed following the procedures detailed in Weis *et al.* (2007). The configuration for Hf analyses monitored Lu mass 175 and Yb



mass 172 to allow for interference correction to masses 174 and 176. Hf isotopic ratios were normalized internally for mass fractionation to a  $^{179}\text{Hf}/^{177}\text{Hf}$  ratio of 0.7325 using an exponential correction. Standards were run after every two samples and sample results were normalized to the ratio of the in-run daily average and a  $^{176}\text{Hf}/^{177}\text{Hf}$  ratio for JMC-475 of 0.282160. During the course of analyses, the Hf standard JMC-475 gave an average value  $0.282167 \pm 9$  (n=130). USGS reference materials BCR-2 and BHVO-2 were processed with the samples and yielded Hf isotopic ratios of  $0.282867 \pm 5$  and  $0.283100 \pm 5$ , respectively. Published values for BCR-2 and BHVO-2 are  $0.282871 \pm 7$  and  $0.283104 \pm 8$ , respectively (Weis *et al.*, 2007).

## WHOLE-ROCK CHEMISTRY

### Major- and trace-element compositions

The most abundant type of lava in the Karmutsen Formation is tholeiitic basalt with a restricted range of major- and trace-element compositions. The tholeiitic basalts have similar compositions to the coarse-grained mafic rocks, and both groups are distinct from the picrites and high-MgO basalts (Fig. 2.6). The tholeiitic basalts have lower MgO (5.7-7.7 wt % MgO) and higher TiO<sub>2</sub> (1.4-2.2 wt % TiO<sub>2</sub>) than the picrites (13.0-19.8 wt % MgO, 0.5-0.7 wt % TiO<sub>2</sub>) and high-MgO basalts (9.1-11.6 wt % MgO, 0.5-0.8 wt % TiO<sub>2</sub>) (Fig. 2.6; Table 2.2). Almost all data plot within the tholeiitic field in a total alkalis versus silica plot, although there has been substantial K-loss in most samples from the Karmutsen Formation (Fig. 2.7), and the tholeiitic basalts generally have higher SiO<sub>2</sub>, Na<sub>2</sub>O+K<sub>2</sub>O, CaO, and FeO<sub>T</sub> (total iron expressed as FeO) than the picrites. The tholeiitic basalts also have noticeably lower LOI (mean  $1.72 \pm 1.3$  wt %) than the picrites (mean  $5.39 \pm 0.8$  wt %) and high-MgO basalts (mean  $3.84 \pm 1.5$  wt %; Fig. 2.6) reflecting the presence of abundant altered olivine phenocrysts in the latter groups. Ni concentrations are significantly higher for the picrites (339-755 ppm) and high-MgO basalts (122-551 ppm) than the tholeiitic basalts (58-125 ppm, except for one anomalous sample) and coarse-grained rocks (70-213 ppm) (Fig. 2.6; Table 2.2). An anomalous tholeiitic pillowed flow (3 samples; outlier in Tables 2.1 and 2.2), from near the picrite type locality at Keogh Lake, and a mineralized sill (disseminated sulfide), from the basal

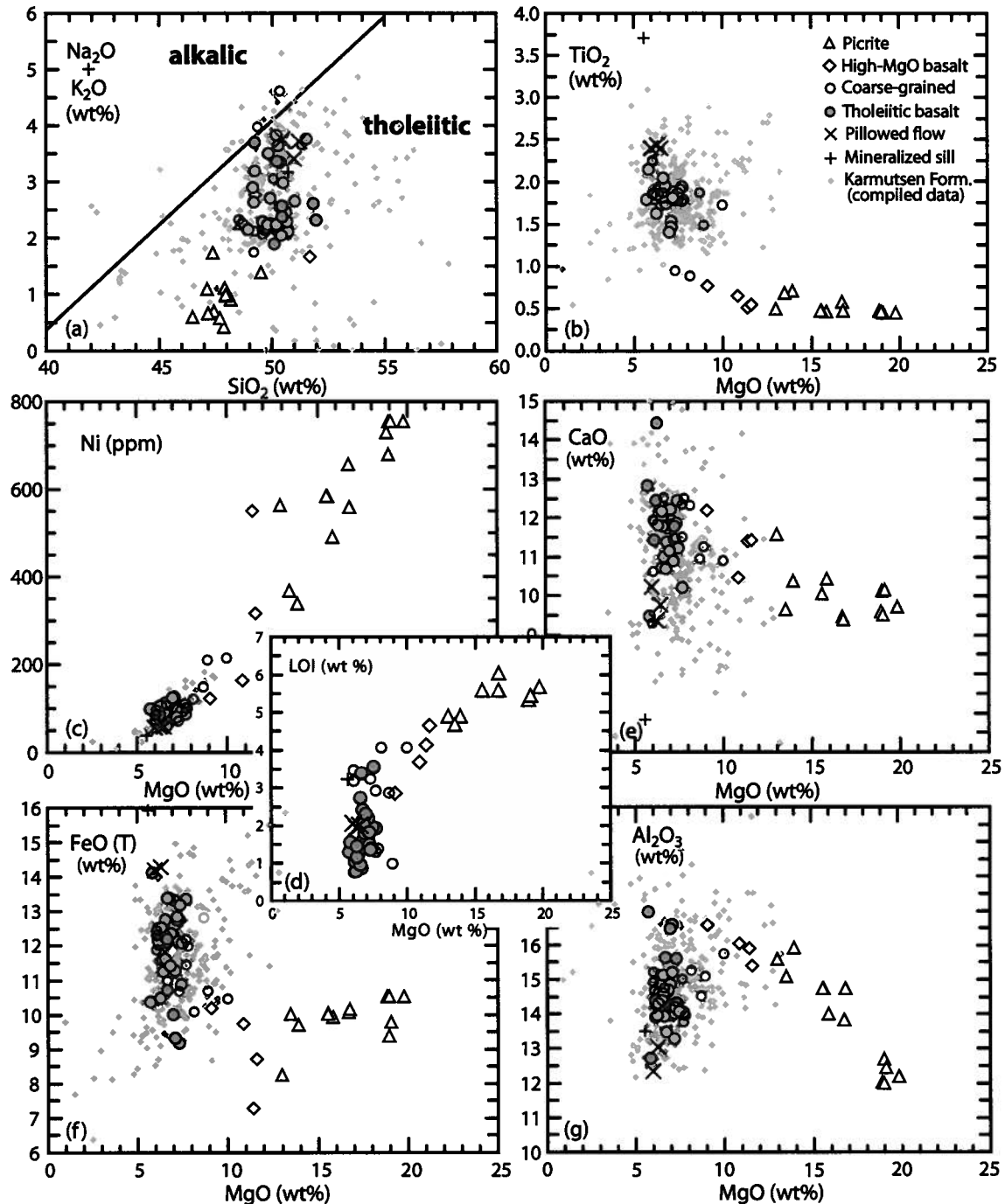


**Figure 2.6** Whole-rock major-element, Ni, and LOI variation diagrams for the Karmutsen Formation. New samples from this study (Table 2.2) are shown by symbols with black outlines (see legend). Previously-published analyses are shown in small gray symbols without black outlines. The boundary of the alkaline and tholeiitic fields is that of MacDonald and Katsura (1964). Total iron expressed as FeO, LOI is loss-on-ignition, and oxides are plotted on an anhydrous, normalized basis. References for the 322 compiled analyses for the Karmutsen Formation are G. Nixon (unpublished data), Barker *et al.* (1989), Kuniyoshi (1972), Lassiter *et al.* (1995), Massey (1995a; 1995b), Muller *et al.* (1974); Surdam (1967), and Yorath *et al.* (1999). Note that the compiled data set has not been filtered; many of the samples with high SiO<sub>2</sub> (>52 wt %) are probably not Karmutsen flood basalts, but younger Bonanza basalts and andesites. Three pillowed flow samples (x) and a mineralized sill (+) are distinguished separately because of their anomalous chemistry. Coarse-grained samples are indicated separately and generally have subophitic texture. Three tholeiitic basalt samples (4724A5, 4718A5, 4718A6) with >16 wt % Al<sub>2</sub>O<sub>3</sub> contain 10-25 modal % of large plagioclase phenocrysts (7-8 mm) or glomerocrysts (>4 mm).

Table 2.2 Major element (wt% oxide) and trace element (ppm) abundances in whole rock samples of Karmutsen basalts, Vancouver Island, B.C.

Sample	4718A1	4718A2(1)	4718A2(2)	4718A5	4718A6	4718A7	4719A2	4719A3	4720A2	4720A3
Group	THOL	THOL	THOL	THOL	THOL	THOL	THOL	THOL	THOL	THOL
Area	MA	MA	MA	MA	MA	MA	MA	MA	SL	SL
Flow	Pillow	Pillow	Pillow	Flow	Breccia	Pillow	Pillow	Pillow	Breccia	Flow
UTM EW	5455062	5455150	5455150	5455459	5455518	5455280	5454625	5454625	5567712	5567305
UTM NS	384113	384260	384260	383424	383237	382261	381761	381761	708686	707890
Unnormalized Major Element Oxides (Weight %):										
SiO <sub>2</sub>	47.93	48.65	49.07	48.41	48.69	48.44	49.68	49.08	49.24	48.47
TiO <sub>2</sub>	1.646	1.857	1.835	1.402	1.359	1.487	1.705	1.676	1.577	1.716
Al <sub>2</sub> O <sub>3</sub>	14.41	14.30	14.15	15.89	15.92	14.74	14.93	14.06	13.54	13.52
Fe <sub>2</sub> O <sub>3</sub> *	12.29	12.07	12.48	9.90	10.74	12.13	9.75	12.21	11.30	11.61
MnO	0.171	0.183	0.181	0.155	0.157	0.167	0.185	0.178	0.212	0.185
MgO	6.25	6.21	6.16	6.81	6.74	6.89	6.98	6.55	6.09	7.12
CaO	10.22	11.85	11.70	11.31	10.76	11.56	10.96	10.94	14.00	11.94
Na <sub>2</sub> O	3.22	2.28	2.25	2.51	2.89	2.39	2.23	2.24	2.12	2.18
K <sub>2</sub> O	0.24	0.18	0.14	0.35	0.34	0.24	0.27	0.31	0.10	0.29
P <sub>2</sub> O <sub>5</sub>	0.15	0.14	0.15	0.10	0.12	0.12	0.08	0.13	0.12	0.12
LOI	2.72	1.38	1.22	2.17	2.28	1.64	1.97	1.63	1.15	1.95
Total	99.24	99.09	99.33	99.01	99.98	99.81	98.75	99.00	99.45	99.11
Trace Elements (ppm):										
La	7.88	9.03	8.72	6.50	6.58	6.10	7.17	7.02	7.20	7.88
Ce	19.0	22.2	21.6	15.5	16.2	15.4	18.0	17.7	17.3	19.0
Pr	2.71	3.10	3.02	2.15	2.20	2.23	2.62	2.52	2.42	2.72
Nd	13.0	15.2	14.5	10.7	11.2	11.4	13.2	12.5	12.2	13.5
Sm	3.57	4.11	4.05	3.03	3.13	3.42	3.67	3.66	3.43	3.85
Eu	1.40	1.57	1.48	1.18	1.20	1.25	1.47	1.39	1.33	1.47
Gd	4.39	4.77	4.87	3.59	3.64	3.90	4.32	4.24	4.12	4.48
Tb	0.76	0.82	0.82	0.63	0.64	0.68	0.76	0.74	0.71	0.78
Dy	4.55	5.02	4.79	3.80	3.87	4.12	4.68	4.41	4.28	4.78
Ho	0.90	0.99	0.96	0.77	0.78	0.84	0.94	0.89	0.87	0.95
Er	2.57	2.79	2.72	2.20	2.27	2.34	2.66	2.45	2.48	2.69
Tm	0.36	0.40	0.39	0.32	0.32	0.33	0.37	0.35	0.34	0.38
Yb	2.15	2.39	2.32	1.90	1.96	2.00	2.23	2.11	2.05	2.33
Lu	0.31	0.33	0.32	0.27	0.27	0.28	0.30	0.30	0.29	0.33
Sc	40.7	41.3	40.4	38.9	38.3	40.2	42.8	42.8	41.1	46.2
V	328	351	353	285	279	317	341	341	325	344
Cr	93	146	125	290	297	252	130	131	151	168
Co	48.7	49.9	48.9	46.1	45.4	51.4	53.1	53.4	50.5	56.2
Ni	87	90	88	125	122	115	94	103	83	93
Cu	177	201	198	167	158	159	180	168	167	184
Zn	83	91	91	77	73	82	86	87	79	88
Ga	19	19	20	17	19	18	16	18	19	17
Ge	1.6	1.5	1.4	1.1	1.5	1.5	0.7	1.5	1.9	1.1
Rb	4	2	2	6	6	4	5	5		6
Sr	418	231	228	282	332	263	281	286	192	214
Y	25	28	28	22	22	24	26	26	25	27
Zr	86	97	94	72	71	77	86	83	83	90
Nb	8.4	10.1	10.0	7.0	6.8	6.5	7.4	7.3	7.9	8.6
Cs	0.7	0.3	0.2	0.5	0.5	0.2	0.2	0.2		0.2
Ba	173	50	49	71	98	62	143	133	28	81
Hf	2.6	2.8	2.8	2.0	2.2	2.1	2.6	2.5	2.4	2.6
Ta	0.59	0.68	0.65	0.45	0.46	0.41	0.53	0.49	0.51	0.60
Pb	4	7	7	10	4	6	7	11	7	9
Th	0.65	0.74	0.72	0.52	0.53	0.54	0.61	0.61	0.57	0.64
U	0.20	0.23	0.24	0.17	0.16	0.17	0.22	0.19	0.18	0.20

Abbreviations for group are: THOL, tholeiitic basalt; PIC, picrite; HI-MG, high MgO basalt; CG, coarse-grained (sill or gabbro); MIN SIL, mineralized sill; OUTLIER, anomalous pillowed flow in plots. Abbreviations for area are: MA, Mount Arrowsmith; SL, Schoen Lake; KR, Karmutsen Range; QI, Quadra Island. Sample locations are given using the Universal Transverse Mercator (UTM) coordinate system (NAD83; zones 9 and 10). Analyses were performed at Activation Laboratory (ActLabs). Fe<sub>2</sub>O<sub>3</sub>\* is total iron expressed as Fe<sub>2</sub>O<sub>3</sub>. LOI is loss-on-ignition. All major elements, Sr, V, and Y were measured by ICP quadrupole OES on solutions of fused samples; Cu, Ni, Pb, and Zn were measured by total dilution ICP; Cs, Ga, Ge, Hf, Nb, Rb, Ta, Th, U, Zr, and REE were measured by magnetic-sector ICP on solutions of fused samples; Co, Cr, and Sc were measured by INAA. Blanks are below detection limit. \*Ni concentrations for these high-MgO samples by XRF. See Appendices B and C for complete XRF data and PCIGR trace element data, respectively. Major elements for sample 93G17 are normalized, anhydrous. Samples from Quadra Island are not shown in figures.

Sample	4720A4	4720A5	4720A5	4720A6	4720A7(1)	4720A7(2)	4720A8	4720A9	4720A10	4721A1
Group	THOL	THOL	THOL	CG	CG	CG	THOL	THOL	CG	THOL
Area	SL	SL	SL	SL	SL	SL	SL	SL	SL	SL
Flow	Flow	Flow	Breccia	Flow	Flow	Flow	Flow	Flow	Sill	Pillow
UTM EW	5566984	5563304	5563304	5566161	5566422	5566422	5566800	5564002	5560585	5563843
UTM NS	707626	705978	705978	704411	703056	703056	700781	703739	702230	704932
<i>Unnormalized Major Element Oxides (Weight %):</i>										
SiO <sub>2</sub>	49.16	50.25	48.88	48.90	49.60	49.53	48.02	48.06	47.38	48.17
TiO <sub>2</sub>	1.776	1.736	1.781	1.799	1.811	1.809	1.768	1.767	0.829	1.890
Al <sub>2</sub> O <sub>3</sub>	14.00	13.43	13.84	14.21	14.34	14.36	14.34	14.11	14.42	14.96
Fe <sub>2</sub> O <sub>3</sub> *	13.30	13.03	13.46	11.78	13.37	13.39	13.18	13.73	10.58	11.40
MnO	0.194	0.175	0.179	0.195	0.199	0.199	0.195	0.185	0.161	0.180
MgO	6.39	5.93	6.12	6.40	5.93	5.94	6.73	6.35	7.69	6.39
CaO	11.85	11.05	11.43	12.08	11.69	11.68	11.37	11.61	11.66	11.75
Na <sub>2</sub> O	1.86	2.12	2.16	1.82	1.97	1.97	1.97	2.08	2.77	1.93
K <sub>2</sub> O	0.14	0.12	0.14	0.31	0.15	0.13	0.11	0.11	0.12	0.10
P <sub>2</sub> O <sub>5</sub>	0.15	0.15	0.16	0.12	0.16	0.15	0.15	0.16	0.06	0.13
LOI	0.93	1.44	1.42	1.38	0.75	0.75	1.91	1.37	4.07	2.11
Total	99.75	99.42	99.56	99.00	99.97	99.90	99.73	99.52	99.75	99.01
<i>Trace Elements (ppm):</i>										
La	8.44	7.81	8.07	7.75	7.84	7.74	6.86	7.06	2.24	7.31
Ce	20.5	18.8	19.5	19.0	19.0	19.3	17.5	17.3	5.6	18.9
Pr	2.88	2.63	2.73	2.71	2.67	2.74	2.54	2.46	0.85	2.78
Nd	14.3	13.1	13.5	13.9	13.3	13.7	12.6	12.3	4.8	13.5
Sm	4.07	3.68	3.87	4.03	3.86	3.89	3.72	3.51	1.76	4.06
Eu	1.49	1.43	1.45	1.43	1.42	1.43	1.37	1.36	0.75	1.47
Gd	4.70	4.60	4.74	4.62	4.73	4.66	4.40	4.19	2.58	4.72
Tb	0.81	0.79	0.83	0.81	0.81	0.82	0.77	0.75	0.50	0.81
Dy	4.90	4.77	4.92	5.01	4.95	4.97	4.86	4.62	3.38	4.99
Ho	0.99	0.96	0.98	1.01	1.01	1.01	0.98	0.93	0.76	1.03
Er	2.81	2.80	2.79	2.89	2.92	2.89	2.78	2.65	2.31	2.96
Tm	0.39	0.40	0.40	0.41	0.42	0.40	0.40	0.37	0.34	0.41
Yb	2.31	2.47	2.46	2.51	2.49	2.44	2.51	2.27	2.16	2.50
Lu	0.33	0.35	0.35	0.36	0.34	0.35	0.35	0.33	0.31	0.36
Sc	42.9	41.0	44.5	43.4	44.2		42.0	44.0	49.9	44.4
V	349	354	362	363	366	367	362	362	288	378
Cr	122	133	156	152	154		155	166	311	158
Co	53.7	50.8	54.8	52.5	52.6		54.5	55.5	49.5	54.8
Ni	92	99	105	107	97	85	116	112	121	106
Cu	202	174	185	188	212	210	218	187	134	208
Zn	92	90	93	96	93	94	109	90	64	86
Ga	20	19	19	18	19	19	19	18	14	18
Ge	1.6	1.6	1.6	1.2	1.6	1.7	1.8	1.4	1.4	1.3
Rb	2	1	1	10	2	2		1	2	2
Sr	179	183	188	155	173	174	174	196	130	174
Y	27	28	28	27	29	28	28	28	21	30
Zr	97	93	92	94	94	93	95	88	38	97
Nb	9.1	8.6	8.2	8.7	8.6	8.7	8.3	7.8	1.7	8.5
Cs	0.2	0.1	0.1	0.9	0.3	0.3	0.2	0.1	0.3	0.6
Ba	34	37	38	39	45	43	33	35	68	36
Hf	2.7	2.7	2.6	2.7	2.7	2.8	2.7	2.6	1.2	2.9
Ta	0.60	0.57	0.56	0.57	0.56	0.55	0.55	0.53	0.09	0.58
Pb	7	8	8	7	14	6	8	8		14
Th	0.68	0.63	0.61	0.64	0.61	0.61	0.62	0.61	0.24	0.68
U	0.20	0.21	0.19	0.21	0.19	0.19	0.19	0.18	0.11	0.22

Sample	4721A2	4721A3	4721A4	4721A5	4722A2(1)*	4722A2(2)*	4722A2(3)*	4722A2(4)*	4722A4(1)*	4722A4(2)*
Group	THOL	THOL	THOL	THOL	THOL	THOL	THOL	THOL	PIC	PIC
Area	SL	SL	SL	SL	KR	KR	KR	KR	KR	KR
Flow	Flow	Flow	Flow	Flow	Flow	Flow	Flow	Flow	Pillow	Pillow
UTM EW	5563936	5564229	5564285	5564343	5590769	5590769	5590769	5590769	5595528	5595528
UTM NS	704941	704928	704896	705008	634318	634318	634318	634318	629490	629490
<i>Unnormalized Major Element Oxides (Weight %):</i>										
SiO <sub>2</sub>	49.56	48.17	49.49	49.37	48.33	48.67	47.23	48.16	43.85	43.84
TiO <sub>2</sub>	1.770	1.768	1.791	1.806	1.799	1.816	1.783	1.782	0.425	0.425
Al <sub>2</sub> O <sub>3</sub>	13.92	14.16	13.98	13.98	13.59	13.74	13.77	13.62	11.56	11.74
Fe <sub>2</sub> O <sub>3</sub> *	13.07	13.24	13.13	13.53	13.75	13.05	14.13	13.76	10.11	9.65
MnO	0.174	0.183	0.176	0.201	0.185	0.187	0.187	0.187	0.161	0.158
MgO	6.06	6.61	6.46	5.98	6.97	7.02	7.09	7.09	17.74	17.51
CaO	12.15	11.30	11.76	11.59	11.42	11.42	11.43	11.48	9.43	9.36
Na <sub>2</sub> O	2.01	2.03	1.92	1.92	2.03	2.05	2.02	2.08	0.53	0.53
K <sub>2</sub> O	0.09	0.15	0.12	0.15	0.14	0.13	0.06	0.14	0.10	0.13
P <sub>2</sub> O <sub>5</sub>	0.16	0.14	0.14	0.15	0.15	0.14	0.14	0.12	0.04	0.00
LOI	0.76	1.78	0.87	1.04	1.48	1.34	1.38	1.37	5.45	5.33
Total	99.73	99.53	99.85	99.71	99.84	99.56	99.22	99.79	99.39	98.66
<i>Trace Elements (ppm):</i>										
La	7.86	7.42	7.21	7.62	6.95	7.34	7.65	6.95	1.06	0.96
Ce	19.2	18.3	17.9	18.8	17.8	18.5	19.3	17.8	2.6	2.5
Pr	2.70	2.66	2.57	2.73	2.53	2.64	2.94	2.67	0.41	0.38
Nd	13.5	13.3	13.0	13.9	12.9	12.7	13.6	13.3	2.6	2.3
Sm	3.84	3.84	3.81	3.91	3.72	3.66	4.05	3.77	0.92	0.84
Eu	1.46	1.40	1.38	1.47	1.41	1.42	1.55	1.42	0.38	0.37
Gd	4.47	4.59	4.28	4.73	4.42	4.62	4.76	4.59	1.40	1.42
Tb	0.79	0.79	0.77	0.83	0.77	0.77	0.83	0.80	0.30	0.30
Dy	4.75	4.88	4.77	5.12	4.61	4.60	4.92	4.77	2.16	2.17
Ho	0.96	0.98	0.97	1.04	0.94	0.94	0.92	0.95	0.49	0.50
Er	2.72	2.82	2.80	2.99	2.65	2.70	2.64	2.69	1.53	1.54
Tm	0.38	0.39	0.40	0.42	0.38	0.38	0.389	0.37	0.24	0.23
Yb	2.35	2.42	2.40	2.55	2.32	2.27	2.41	2.28	1.58	1.52
Lu	0.32	0.35	0.34	0.35	0.32	0.34	0.349	0.34	0.23	0.23
Sc	42.1	42.3	42.2	39.7	39.2	29.2	41.6	41.5	38.3	40.1
V	351	364	364	367	365	365	362	362	201	189
Cr	118	164	151	122	143	98	162	165	1710	1830
Co	51.6	54.9	53.3	46.5	50.0	37.7	55.7	53.5	80.3	84.6
Ni	91	115	108	90	107	105	93	93	755	755
Cu	195	206	211	210	189	189	178	174	92	83
Zn	90	87	92	92	104	103	98	94	77	55
Ga	19	19	19	19	19	19	20	17	10	9
Ge	1.7	1.3	1.7	1.6	1.4	1.5	1.5	1.2	1.0	0.7
Rb	1	1	1	1	2	2	2	2	5	4
Sr	187	162	160	171	190	193	178	190	100	97
Y	26	28	29	29	27	28	26	27	16	13
Zr	97	95	95	96	96	87	94	102	16	19
Nb	9.0	8.5	8.6	8.5	8.3	8.4	8.5	8.5	0.7	0.9
Cs	0.2	0.4	0.3	0.2	0.2	0.2	0.4	0.2	2.8	2.7
Ba	39	34	28	34	34	34	28	33	19	18
Hf	2.8	2.8	2.7	2.9	2.8	2.6	2.8	2.8	0.5	0.6
Ta	0.60	0.57	0.55	0.59	0.55	0.54	0.6	0.57	0.09	0.03
Pb	8	9	9	5	11	12	91	7	4	4
Th	0.69	0.62	0.62	0.67	0.66	0.64	0.59	0.68	0.10	0.11
U	0.21	0.20	0.19	0.20	0.19	0.20	0.23	0.15	0.05	0.03

Sample	4722A4(3)*	4722A5(1)*	4722A5(2)*	4723A2*	4723A3*	4723A4*	4723A10	4723A13(1)*	4723A13(2)*	4724A3
Group	PIC	OUTLIER	OUTLIER	HI-MG	PIC	PIC	THOL	PIC	PIC	CG
Area	KR	KR	KR	KR	KR	KR	KR	KR	KR	SL
Flow	Pillow	Flow	Flow	Pillow	Pillow	Pillow	Flow	Pillow	Pillow	Flow
UTM EW	5595528	5595029	5595029	5588266	5588274	5586081	5578863	5599233	5599233	5581870
UTM NS	629490	627605	627605	626698	626641	626835	630940	616507	616507	704472
<i>Unnormalized Major Element Oxides (Weight %):</i>										
SiO <sub>2</sub>	42.94	48.95	48.45	46.73	44.41	44.39	50.03	44.62	44.71	49.08
TiO <sub>2</sub>	0.42	2.295	2.333	0.611	0.539	0.663	2.083	0.443	0.442	1.457
Al <sub>2</sub> O <sub>3</sub>	11.26	13.61	12.51	15.24	12.75	14.93	12.31	13.71	13.75	14.77
Fe <sub>2</sub> O <sub>3</sub> *	10.82	12.56	15.24	10.26	10.33	10.11	15.21	10.38	10.37	11.60
MnO	0.161	0.188	0.191	0.158	0.148	0.139	0.223	0.138	0.138	0.128
MgO	18.28	6.18	5.99	10.27	15.42	13.02	5.66	14.47	14.48	8.73
CaO	8.98	9.33	8.99	9.93	8.73	9.73	9.19	9.37	9.36	11.02
Na <sub>2</sub> O	0.54	3.26	3.30	2.26	0.78	1.56	2.94	0.86	0.86	1.99
K <sub>2</sub> O	0.02	0.30	0.30	0.38	0.07	0.07	0.70	0.06	0.07	0.15
P <sub>2</sub> O <sub>5</sub>	0.03	0.13	0.19	0.06	0.05	0.06	0.18	0.05	0.05	0.12
LOI	5.7	2.00	1.95	3.70	5.61	4.91	1.55	5.59	5.59	0.98
Total	99.16	98.80	99.45	99.60	98.83	99.58	100.07	99.68	99.81	100.02
<i>Trace Elements (ppm):</i>										
La	1.08	8.77	9.46	1.94	1.80	1.78	8.93	1.40	1.36	5.57
Ce	2.6	23.0	25.2	5.0	4.5	4.5	21.5	3.4	3.4	14.3
Pr	0.43	3.37	3.68	0.74	0.67	0.71	3.10	0.52	0.51	2.09
Nd	2.5	17.2	17.9	4.2	3.8	4.1	15.5	3.0	2.9	10.4
Sm	0.87	5.20	5.21	1.41	1.27	1.48	4.20	1.00	1.01	2.98
Eu	0.405	1.74	1.79	0.52	0.51	0.63	1.62	0.46	0.44	1.21
Gd	1.45	6.39	6.63	2.09	1.86	2.16	5.21	1.71	1.69	3.85
Tb	0.3	1.11	1.20	0.42	0.37	0.42	0.90	0.36	0.35	0.65
Dy	2.11	6.59	7.08	2.91	2.60	2.79	5.40	2.54	2.50	4.01
Ho	0.47	1.34	1.39	0.67	0.59	0.60	1.11	0.59	0.56	0.81
Er	1.54	3.85	3.94	2.10	1.86	1.79	3.23	1.89	1.79	2.27
Tm	0.242	0.55	0.57	0.32	0.29	0.26	0.45	0.29	0.28	0.33
Yb	1.62	3.31	3.48	2.06	1.85	1.67	2.71	1.89	1.84	1.98
Lu	0.244	0.45	0.51	0.31	0.28	0.25	0.39	0.29	0.28	0.28
Sc	36.4	38.7	33.1	47.2	41.0	38.1	38.3	43.5		35.1
V	194	481	495	261	218	235	496	219	222	287
Cr	1750	79.7	59.0	358	1570	725	34.2	1370		352
Co	80	45.6	40.7	48.8	72.9	60.4	47.1	72.2		52.4
Ni	755	59	59	163	656	339	61	583	583	209
Cu	83	116	114	111	110	106	306	142	98	208
Zn	55	106	103	61	60	63	107	106	62	83
Ga	11	17	20	13	12	13	20	12	12	19
Ge	1.2	0.7	1.3	1.2	1.1	1.1	1.6	1.2	1.3	1.6
Rb	6	6	6	10	2	2	12	2	1	2
Sr	93	225	229	271	64	132	299	73	73	167
Y	15	39	39	20	17	18	32	16	17	23
Zr	16	127	126	33	29	36	110	24	22	73
Nb	0.7	10.0	10.6	1.5	1.3	1.1	9.7	0.8	0.7	6.5
Cs	5.8	0.3	0.4	6.5	0.9	0.8	0.4	0.7	0.7	0.3
Ba	27	87	88	84	15	20	152	13	13	55
Hf	0.6	3.7	3.7	1.0	0.9	1.0	3.1	0.7	0.7	2.1
Ta		0.67	0.70	0.08	0.06	0.05	0.65	0.04	0.04	0.42
Pb	22	6	7		4		5	8		7
Th	0.09	1.08	1.08	0.23	0.20	0.10	0.77	0.15	0.14	0.43
U	0.07	0.38	0.39	0.10	0.09	0.05	0.27	0.08	0.07	0.16

Sample	4724A3	5614A1*	5614A3*	5614A5*	5614A10	5614A11	5614A13	5614A14	5614A15	5615A1
Group	THOL	PIC	HI-MG	HI-MG	THOL	THOL	THOL	CG	CG	THOL
Area	SL	KR	KR	KR	KR	KR	KR	KR	KR	KR
Flow	Flow	Pillow	Pillow	Breccia	Flow	Flow	Flow	Sill	Flow	Pillow
UTM EW	5580653	5599183	5599183	5599192	5595261	5593546	5588018	5588246	5589935	5599424
UTM NS	704736	616472	616472	614756	615253	615098	618867	618183	615917	620187
<i>Unnormalized Major Element Oxides (Weight %):</i>										
SiO <sub>2</sub>	48.08	46.24	48.43	47.1	46.69	48.06	47.78	46.17	46.2	47.61
TiO <sub>2</sub>	1.729	0.471	0.477	0.512	1.761	1.741	1.86	1.773	1.605	1.873
Al <sub>2</sub> O <sub>3</sub>	16.39	14.57	14.9	14.52	13.32	13.35	12.91	13.8	14.77	13.55
Fe <sub>2</sub> O <sub>3</sub> *	11.13	8.57	7.59	9.12	12.72	12.96	14.23	13.53	10.89	14.34
MnO	0.196	0.145	0.134	0.135	0.168	0.187	0.211	0.136	0.123	0.188
MgO	5.54	12.11	10.66	10.92	7.09	6.38	6.47	8.25	9.37	7.42
CaO	12.38	10.81	10.68	10.78	10.62	10.51	10.24	10.41	10.22	9.86
Na <sub>2</sub> O	2.01	1.3	1.51	2.1	3.49	3.23	2.91	2.01	1.55	2.87
K <sub>2</sub> O	0.10	0.01	0.06	0.01	0.01	0.44	0.44	0.21	0.08	0.21
P <sub>2</sub> O <sub>5</sub>	0.15	0.04	0.04	0.05	0.14	0.13	0.15	0.14	0.13	0.15
LOI	1.29	4.91	4.13	4.67	3.53	2.39	2.02	2.87	4.07	1.92
Total	99.01	99.14	98.6	99.89	99.43	99.37	99.21	99.3	99.03	100
<i>Trace Elements (ppm):</i>										
La	7.98	1.79	1.71	0.91	8.04	7.23	8.51	7.31	6.88	8.17
Ce	19.4	4.3	4.0	2.5	19.7	18.0	20.9	18.7	17.6	20.2
Pr	2.72	0.65	0.59	0.43	2.96	2.68	3.08	2.81	2.68	3.01
Nd	13.3	3.4	3.2	2.7	13.7	12.3	14.7	13.2	12.5	14.3
Sm	3.69	1.11	1.09	1.02	3.88	3.6	4.2	3.89	3.43	4.12
Eu	1.42	0.501	0.483	0.526	1.44	1.39	1.59	1.47	1.34	1.58
Gd	4.58	1.74	1.71	1.6	4.47	4.24	4.79	4.61	4.03	4.88
Tb	0.75	0.37	0.37	0.34	0.79	0.77	0.87	0.81	0.7	0.85
Dy	4.53	2.67	2.66	2.35	4.59	4.57	5.12	4.76	4.11	5.01
Ho	0.89	0.6	0.59	0.52	0.85	0.89	0.98	0.9	0.76	0.94
Er	2.54	1.87	1.87	1.67	2.47	2.53	2.83	2.55	2.18	2.7
Tm	0.36	0.297	0.292	0.27	0.37	0.36	0.413	0.375	0.324	0.404
Yb	2.26	2.01	1.99	1.8	2.27	2.26	2.54	2.35	2	2.51
Lu	0.32	0.308	0.312	0.267	0.325	0.329	0.375	0.336	0.29	0.365
Sc	34.4	45	48.8	43.7	43.8	43.8	42.4	39.3	32.3	44.5
V	299	222	217	206	354	362	372	332	271	380
Cr	207	1370	1420	797	195	76	71.9	328	400	172
Co	43.1	68.7	76.1	68.6	48.9	53.6	51.5	58.9	56.8	57.4
Ni	98	564	551	315	93	67	65	147	213	86
Cu	198	104	111	96	134	181	165	83	111	182
Zn	76	53	51	48	80	93	102	86	72	84
Ga	21	11	12	13	20	17	20	20	19	19
Ge	1.5	0.9	0.8	0.9	1.4	0.9	1.6	1.3	1.1	1.3
Rb						9	8	3		5
Sr	272	120	130	141	86	381	274	283	183	287
Y	25	18	17	16	26	27	29	28	23	29
Zr	92	22	24	19	90	86	98	91	86	98
Nb	8.6	0.7	0.8	0.5	8.1	8.0	9.0	8.2	7.7	8.6
Cs	0.1	0.4	0.4		0.8	0.4	0.1	0.1	0.2	0.9
Ba	32	18	20	9	11	80	85	62	32	39
Hf	2.7	0.7	0.7	0.6	2.7	2.5	2.9	2.8	2.6	3.0
Ta	0.60				0.6	0.5	0.7	0.5	0.5	0.6
Pb		26	28	29	97	97	98	94	82	97
Th	0.69	0.15	0.17	0.08	0.75	0.62	0.66	0.54	0.52	0.64
U	0.25	0.11	0.11	0.06	0.3	0.24	0.26	0.21	0.22	0.27

Sample	5615A5	5615A6	5615A7(1)*	5615A7(2)*	5615A8	5615A10	5615A11	5615A12*	5616A1*	5616A2
Group	CG	CG	PIC	PIC	THOL	THOL	OUTLIER	PIC	PIC	THOL
Area	KR	KR	KR	KR	KR	KR	KR	KR	KR	KR
Flow	Flow	Sill	Pillow	Pillow	Pillow	Pillow	Pillow	Pillow	Pillow	Flow
UTM EW	5601095	5601095	5595569	5595569	5595513	5595376	5595029	5586126	5598448	5585731
UTM NS	624103	624103	629573	629573	629434	629069	627605	626824	616507	623077
<i>Unnormalized Major Element Oxides (Weight %):</i>										
SiO <sub>2</sub>	47.76	46.53	47.16	45.73	48.31	47.29	49.08	45.35	43.7	48.72
TiO <sub>2</sub>	2.125	2.119	0.466	0.442	1.745	1.807	2.304	0.643	0.439	1.939
Al <sub>2</sub> O <sub>3</sub>	14.41	14.06	11.84	11.48	13.45	13.7	11.86	14.07	13.66	13.21
Fe <sub>2</sub> O <sub>3</sub> *	12.5	13.01	11.54	11.22	13.48	14.23	15.2	10.4	10.47	14.11
MnO	0.191	0.177	0.172	0.166	0.196	0.195	0.215	0.142	0.158	0.235
MgO	5.71	5.7	18.59	18.19	6.78	6.77	5.73	12.56	15.55	6.29
CaO	8.81	10	9.45	9.14	11.77	10.65	9.84	9	8.71	11.19
Na <sub>2</sub> O	4.16	3.64	0.42	0.41	1.8	2.58	3.25	2.11	0.98	2.49
K <sub>2</sub> O	0.2	0.09	0.01	0.16	0.03	0.21	0.04	0.02	0.04	0.01
P <sub>2</sub> O <sub>5</sub>	0.18	0.19	0.03	0.05	0.14	0.14	0.22	0.06	0.04	0.16
LOI	3.17	3.45		2.86	1.74	1.57	2.07	4.68	6.05	3.38
Total	99.2	98.96	99.67	99.84	99.43	99.14	99.81	99.02	99.8	99.66
<i>Trace Elements (ppm):</i>										
La	11.6	11.7	1.09	1.02	7.32	7.34	6.41	1.73	1.52	8.87
Ce	28.4	26.9	2.7	2.6	18.4	18.5	17.3	4.7	3.6	21.0
Pr	4.01	3.95	0.44	0.41	2.69	2.84	2.89	0.77	0.55	3.02
Nd	17.7	17.7	2.5	2.4	12.9	13.2	15.6	4.4	3.0	14.4
Sm	4.74	4.76	0.88	0.85	3.78	3.92	5.06	1.47	1.02	4.16
Eu	1.78	1.73	0.381	0.361	1.47	1.48	1.88	0.607	0.454	1.59
Gd	5.49	5.32	1.42	1.35	4.4	4.65	6.19	2.13	1.57	4.81
Tb	0.93	0.93	0.3	0.3	0.79	0.81	1.13	0.42	0.34	0.86
Dy	5.49	5.31	2.16	2.12	4.65	4.79	6.65	2.78	2.44	5.07
Ho	1.02	0.98	0.49	0.46	0.89	0.91	1.24	0.59	0.55	0.92
Er	2.91	2.86	1.55	1.46	2.58	2.58	3.67	1.78	1.73	2.72
Tm	0.441	0.43	0.253	0.236	0.379	0.38	0.547	0.267	0.268	0.413
Yb	2.75	2.73	1.71	1.58	2.34	2.42	3.44	1.75	1.77	2.62
Lu	0.392	0.391	0.247	0.245	0.339	0.348	0.493	0.269	0.277	0.378
Sc	35.7	38.5	39.2	39.5	40.4	39.8	43.8	38.3	37.5	41.6
V	381	376	224	222	353	363	520	215	204	401
Cr	127	164	1910	1850	173	166	107	906	3000	76
Co	39.4	43.7	87.1	89.3	53	52.4	53.4	67.2	67.9	50.8
Ni	73	85	729	680	96	94	56	368	559	58
Cu	105	148	86	80	175	185	208	83	77	210
Zn	86	102	57	54	88	86	94	50	53	85
Ga	21	21	10	10	20	20	18	14	12	22
Ge	1.4	1.4	1.1	0.9	1.4	1.3	0.7	1.1	1.1	1.6
Rb		2	6	6	2	9		2		
Sr	128	170	124	120	194	279	143	189	112	67
Y	32	31	15	15	28	28	39	16	16	30
Zr	116	121	16	15	91	96	124	35	22	100
Nb	12.7	13.0	0.9	0.7	8.0	8.5	9.9	1.4	0.9	9.2
Cs	0.2		4.4	4.5	0.6	1.3	0.1	0.6	0.8	
Ba	36	34	27	24	39	61	20	15	20	8
Hf	3.4	3.5	0.6	0.5	2.7	2.8	3.8	1.1	0.7	2.9
Ta	0.9	0.9			0.6	0.6	0.7			0.6
Pb	110	118	24	22	91	92	113	34	22	96
Th	0.92	0.93	0.1	0.08	0.59	0.61	1.01	0.09	0.14	0.83
U	0.34	0.33	0.07	0.07	0.22	0.24	0.41	0.07	0.1	0.25



Sample	5616A3	5616A7	5617A1	5617A4	5617A5(1)*	5617A5(2)*	5618A1	5618A3	5618A4	93G171
Group	CG	HI-MG	CG	MIN SIL	CG	CG	THOL	THOL	THOL	PIC
Area	KR	KR	SL	SL	SL	SL	QI	QI	QI	KR
Flow	Flow	Pillow	Sill	Sill	Sill	Sill	Flow	Pillow	Breccia	Pillow
UTM EW	5584647	5589833	5580375	5557712	5557712	5557712	5557892	5552258	5552258	5599395
UTM NS	623236	626879	702240	700905	700905	700905	338923	341690	341690	616613
<i>Unnormalized Major Element Oxides (Weight %):</i>										
SiO <sub>2</sub>	48.77	48.75	49.1	48.06	49.31	47.4	48.81	47.9	40.29	47.93
TiO <sub>2</sub>	1.814	0.732	0.901	3.505	1.713	1.71	1.749	1.362	2.159	0.461
Al <sub>2</sub> O <sub>3</sub>	14.23	15.92	13.72	12.79	13.39	13.33	12.82	13.79	16.27	14.02
Fe <sub>2</sub> O <sub>3</sub> *	12.85	10.88	11.34	16.78	12.39	12.71	13.81	11.62	18.1	9.9
MnO	0.185	0.153	0.16	0.164	0.174	0.174	0.211	0.158	0.28	0.19
MgO	7.28	8.7	8.99	5.25	7.5	7.46	6.96	6.57	9.7	15.8
CaO	10.92	11.69	10.96	6.48	12.01	11.93	10.54	12.08	6.78	10.42
Na <sub>2</sub> O	1.86	2.12	3.46	2.31	1.83	1.8	2.76	3.13	0.58	1.02
K <sub>2</sub> O	0.16	0.07	0.03	0.69	0.22	0.17	0.5	0.12	0.52	0.11
P <sub>2</sub> O <sub>5</sub>	0.13	0.04	0.08	0.35	0.13	0.14	0.14	0.1	0.18	0.08
LOI	2.92	2.86	3.23	3.22	1.28	1.38	1.8	3.17	4.77	
Total	99.14	99.91	99.97	99.6	99.95	98.21	99.9	99.99	99.63	100.00
<i>Trace Elements (ppm):</i>										
La	7.14	1.51	2.84	22.3	8.13	7.94	7.72	6.57	10.7	1.4
Ce	17.9	3.8	6.9	51.5	19.7	19.2	19.1	15.4	24.3	3.6
Pr	2.72	0.59	1.1	7.19	2.89	2.85	2.85	2.22	3.48	0.56
Nd	12.9	3.5	6.1	32.7	13.3	13.3	13.5	10.5	15.9	2.9
Sm	3.82	1.36	2.14	8.86	3.83	3.77	3.98	2.98	4.53	1.23
Eu	1.47	0.638	0.888	3.33	1.45	1.43	1.47	1.21	2.04	0.47
Gd	4.49	2.05	3.05	9.84	4.36	4.32	4.56	3.56	5.64	2.10
Tb	0.79	0.43	0.63	1.64	0.75	0.75	0.79	0.63	0.99	0.32
Dy	4.66	2.9	4.19	9.58	4.35	4.25	4.71	3.84	5.95	2.38
Ho	0.9	0.61	0.86	1.78	0.83	0.81	0.88	0.75	1.15	0.64
Er	2.6	1.91	2.65	5.06	2.37	2.31	2.56	2.16	3.36	2.11
Tm	0.373	0.305	0.415	0.73	0.341	0.342	0.375	0.331	0.495	0.297
Yb	2.35	2.02	2.66	4.56	2.13	2.14	2.36	2.12	3.11	1.97
Lu	0.34	0.302	0.401	0.637	0.304	0.298	0.342	0.296	0.455	0.282
Sc	40	50.7	54.5	44.2	40.8	37.7	42.9	41.8	54.2	
V	349	270	327	517	342	338	367	313	499	140
Cr	317	346	210	64.4	274	255	114	194	159	606
Co	52.6	56.7	46.8	38.3	51.8	47.6	53	46	62	
Ni	110	122	70	39	98	97	79	67	68	491
Cu	164	111	160	232	161	160	25	125	109	91
Zn	87	51	69	160	77	76	89	92	75	57
Ga	20	15	16	27	19	19	19	18	24	
Ge	1.3	1	1.3	2	1.1	0.7	1.5	1.5	1.3	
Rb	3			21	7	7	8	3	10	
Sr	237	181	58	197	255	254	227	170	220	
Y	25	19	27	52	24	23	27	21	38	13
Zr	91	26	45	229	89	86	89	67	112	24
Nb	8.1	1.1	2.1	19.7	8.9	8.5	8.1	6.6	9.8	0.9
Cs	1.2	0.3	0.2	1.2	0.2	0.2	0.4		0.6	
Ba	39	23	12	771	38	37	103	17	109	20
Hf	2.7	0.8	1.4	6.4	2.6	2.5	2.7	2	3.3	0.8
Ta	0.6		0.1	1.4	0.6	0.6	0.8	0.5	0.7	0.1
Pb	93	37	48	151	85	83	83	66	65	
Th	0.52	0.14	0.28	2.09	0.61	0.57	0.57	0.45	0.71	0.15
U	0.23	0.09	0.16	0.88	0.23	0.25	0.22	0.22	0.34	

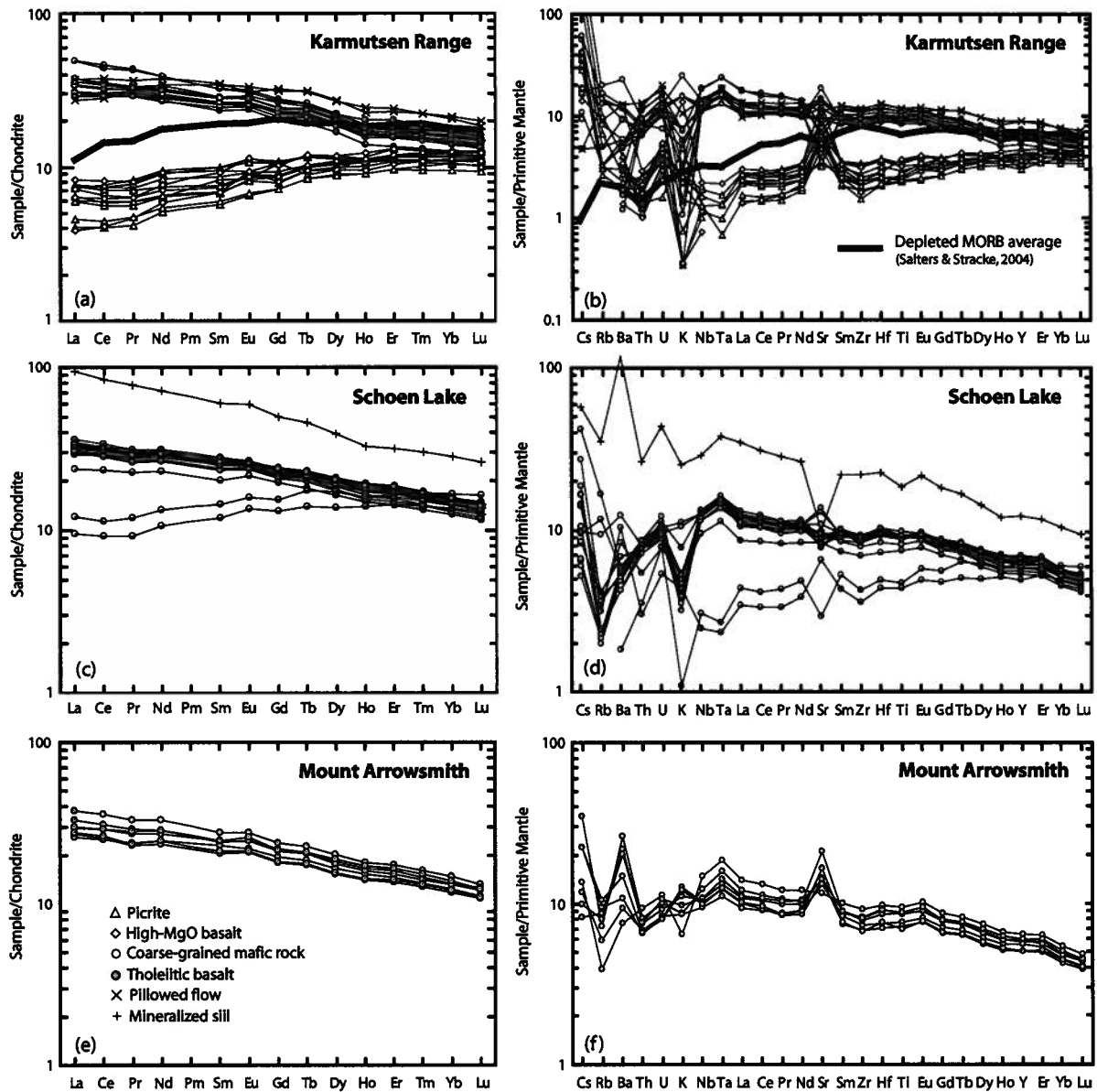


**Figure 2.7** Whole-rock REE and other incompatible-element concentrations for the Karmutsen Formation. (a), (c), and (e) are chondrite-normalized REE patterns for samples from each of the three main field areas on Vancouver Island. (b), (d), and (f) are primitive mantle-normalized trace-element patterns for samples from each of the three main field areas. All normalization values are from McDonough and Sun (1995). Note the clear distinction between LREE-enriched tholeiitic basalts and LREE-depleted picrites, the effects of alteration on the LILE (especially loss of K and Rb), and the different range for the vertical scale in panel b (extends down to 0.1).

sediment-sill complex at Schoen Lake, are distinguished by higher  $\text{TiO}_2$  and  $\text{FeO}_T$  than the main group of tholeiitic basalts. The tholeiitic basalts are similar in major-element composition to previously published results for samples from the Karmutsen Formation; however, the Keogh Lake picrites, which encompass the picritic and high-MgO basalt pillow lavas, extend to ~20 wt % MgO (Fig. 2.6, and references therein).

The tholeiitic basalts from the Karmutsen Range form a tight range of parallel light rare earth element (LREE)-enriched patterns ( $\text{La/Yb}_{\text{CN}}=2.1\text{-}2.4$ ; mean  $2.2 \pm 0.2$ ), whereas the picrites and high-MgO basalts from the Karmutsen Range form a range of parallel LREE-depleted patterns ( $\text{La/Yb}_{\text{CN}}=0.3\text{-}0.7$ ; mean  $0.6 \pm 0.2$ ) with lower REE abundances than the tholeiitic basalts (Fig. 2.7). Tholeiitic basalts from the Schoen Lake and Mount Arrowsmith areas have similar REE patterns to samples from the Karmutsen Range (Schoen Lake-  $\text{La/Yb}_{\text{CN}}=2.1\text{-}2.6$ ; mean  $2.3 \pm 0.3$ ; Mount Arrowsmith-  $\text{La/Yb}_{\text{CN}}=1.9\text{-}2.5$ ; mean  $2.2 \pm 0.4$ ), and the coarse-grained mafic rocks have similar REE patterns to the tholeiitic basalts ( $\text{La/Yb}_{\text{CN}}=2.1\text{-}2.9$ ; mean  $2.5 \pm 0.8$ ). Two LREE-depleted coarse-grained mafic rocks from the Schoen Lake area have similar REE patterns ( $\text{La/Yb}_{\text{CN}}=0.7$ ) to the picrites from the Keogh Lake area, indicating that this distinctive suite of rocks is exposed as far south as Schoen Lake (Fig. 2.7). The anomalous pillowed flow from the Karmutsen Range has lower  $\text{La/Yb}_{\text{CN}}$  (1.3-1.8) than the main group of tholeiitic basalts from the Karmutsen Range (Fig. 2.7). The mineralized sill from the Schoen Lake area is distinctly LREE-enriched ( $\text{La/Yb}_{\text{CN}}=3.3$ ) with the highest REE abundances ( $\text{La}_{\text{CN}}=94.0$ ) of all Karmutsen samples, which may reflect contamination by adjacent sediment.

The primitive mantle-normalized trace-element patterns (Fig. 2.7), and trace-element variations and ratios (Fig. 2.8), highlight the differences in trace-element concentrations between the four main groups of Karmutsen flood basalts on Vancouver Island. The tholeiitic basalts from all three areas have relatively smooth, parallel trace-element patterns; some samples have small positive Sr anomalies, relative to Nd and Sm, and many samples have prominent negative K anomalies relative to U and Nb, reflecting K-loss during alteration (Fig. 2.7). The large ion lithophile elements (LILE) in the tholeiitic basalts (mainly Rb and K, not Cs) are depleted relative to HFSE and LREE, and LILE segments, especially for the Schoen Lake area (Fig. 2.7d), are remarkably parallel.

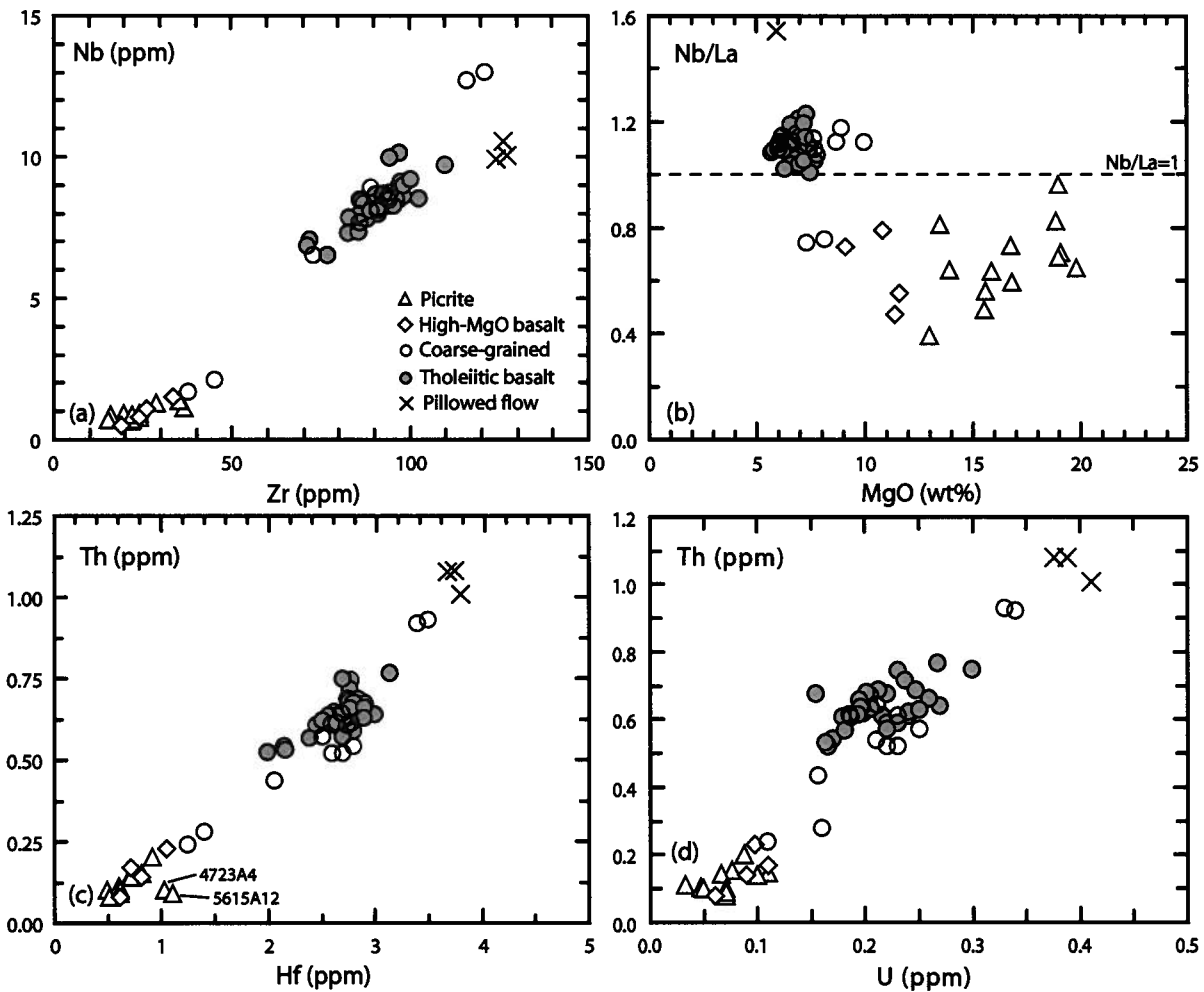


**Figure 2.8** Whole-rock trace-element concentrations and ratios for the Karmutsen Formation (except panel b is versus MgO). (a) Nb vs. Zr. (b) Nb/La vs. MgO. (c) Th vs. Hf. (d) Th vs. U. There is a clear distinction between the tholeiitic basalts and picrites in Nb and Zr, both in concentration and the slope of each trend.

The picrites and high-MgO basalts form a tight band of parallel trace-element patterns and are depleted in HFSE and LREE with positive Sr anomalies and relatively low Rb. The coarse-grained mafic rocks from the Karmutsen Range have identical trace-element patterns to the tholeiitic basalts. Samples from the Schoen Lake area have similar trace-element patterns to the Karmutsen Range, except for the two LREE-depleted coarse-grained mafic rocks and the mineralized sill (Fig. 2.7d).

### **Sr-Nd-Hf-Pb isotopic compositions**

The nineteen samples of the Karmutsen Formation from the four main groups, selected on the basis of major and trace-element variation, stratigraphic position, and location to cover the range of these parameters, have indistinguishable age-corrected Hf and Nd isotope ratios and distinct ranges of Sr isotopic compositions (Fig. 2.9). The tholeiitic basalts, picrites, high-MgO basalt, and coarse-grained mafic rocks have initial  $\epsilon_{\text{Hf}} = +8.7$  to  $+12.6$  and  $\epsilon_{\text{Nd}} = +6.6$  to  $+8.8$  corrected for *in situ* radioactive decay since 230 Ma (Fig. 2.9; Tables 2.3 and 2.4). All the Karmutsen samples form a well-defined linear array in a Lu-Hf isochron diagram corresponding to an age of  $241 \pm 15$  Ma (Fig. 2.9). This is within error of the accepted age of the Karmutsen Formation and indicates that the Hf isotope systematics have behaved as a closed system since ca. 230 Ma. The anomalous pillowed flow has similar initial  $\epsilon_{\text{Hf}}$  (+9.8) and slightly lower initial  $\epsilon_{\text{Nd}}$  (+6.2) than the other Karmutsen samples. The picrites and high-MgO basalt have higher initial  $^{87}\text{Sr}/^{86}\text{Sr}$  (0.70398-0.70518) than the tholeiitic basalts (initial  $^{87}\text{Sr}/^{86}\text{Sr} = 0.70306$ -0.70381) and the coarse-grained mafic rocks (initial  $^{87}\text{Sr}/^{86}\text{Sr} = 0.70265$ -0.70428) overlap the ranges of the picrites and tholeiitic basalts (Fig. 2.9; Table 2.3).

The measured Pb isotopic compositions of the tholeiitic basalts are more radiogenic than those of the picrites and the most magnesian Keogh Lake picrites have the least radiogenic Pb isotopic compositions. The range of initial Pb isotope ratios for the picrites is  $^{206}\text{Pb}/^{204}\text{Pb} = 18.142$ -18.580,  $^{207}\text{Pb}/^{204}\text{Pb} = 15.547$ -15.562, and  $^{208}\text{Pb}/^{204}\text{Pb} = 37.873$ -38.257 and the range for the tholeiitic basalts is  $^{206}\text{Pb}/^{204}\text{Pb} = 18.782$ -19.098,  $^{207}\text{Pb}/^{204}\text{Pb} = 15.570$ -15.584, and  $^{208}\text{Pb}/^{204}\text{Pb} = 37.312$ -38.587 (Fig. 2.10; Table 2.5). The coarse-grained mafic rocks overlap the range of initial Pb isotopic compositions for the tholeiitic basalts with  $^{206}\text{Pb}/^{204}\text{Pb} = 18.652$ -19.155,  $^{207}\text{Pb}/^{204}\text{Pb} = 15.568$ -15.588, and

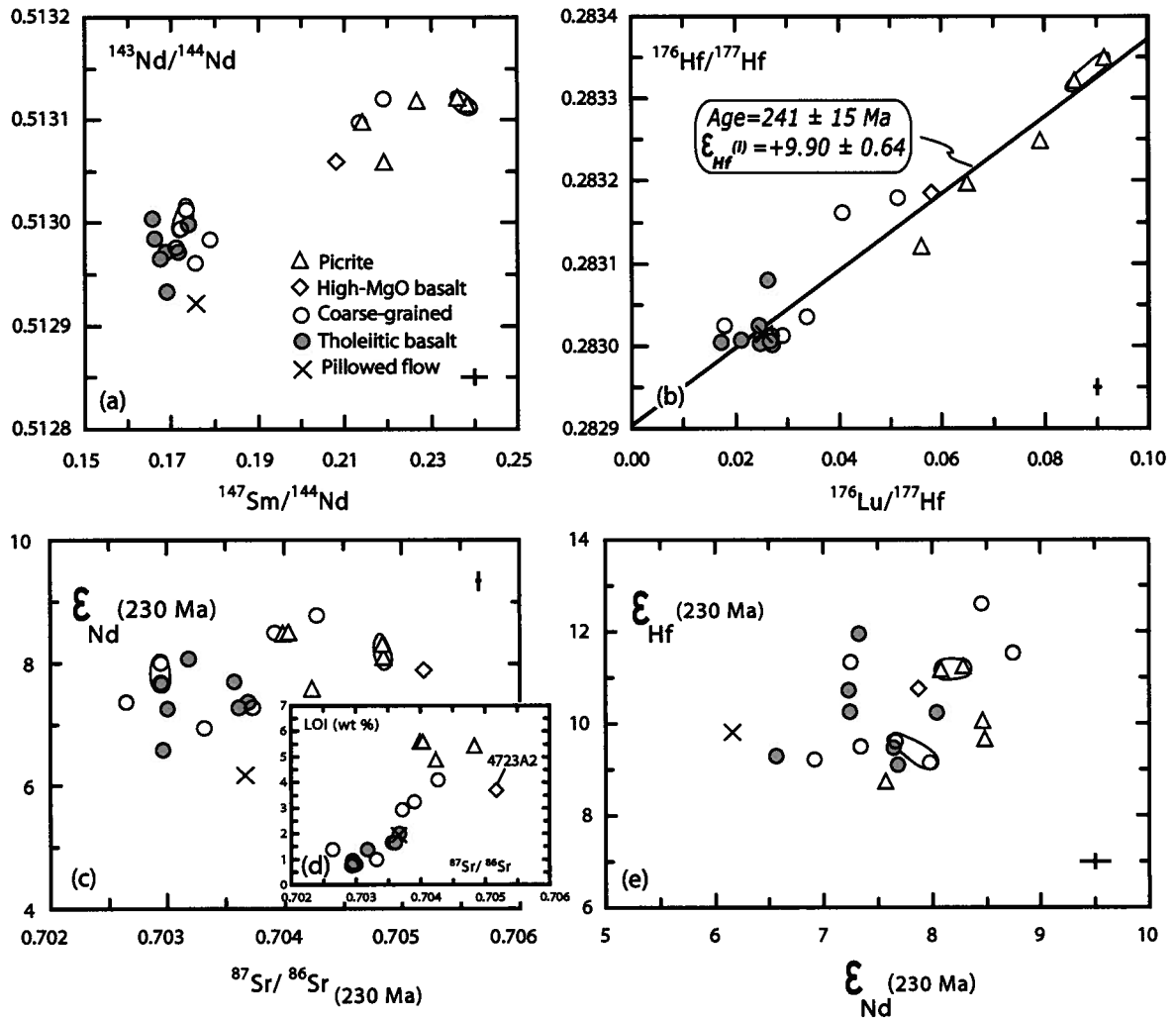


**Figure 2.9** Whole-rock Sr, Nd, and Hf isotopic compositions for the Karmutsen Formation. (a)  $^{143}\text{Nd}/^{144}\text{Nd}$  vs.  $^{147}\text{Sm}/^{144}\text{Nd}$ . (b)  $^{176}\text{Hf}/^{177}\text{Hf}$  vs.  $^{176}\text{Lu}/^{177}\text{Hf}$ . The slope of the best-fit line for all samples corresponds to an age of  $241 \pm 15$  Ma. (c) Initial  $\epsilon_{\text{Nd}}$  vs.  $^{87}\text{Sr}/^{86}\text{Sr}$ . Age correction to 230 Ma. (d) LOI vs.  $^{87}\text{Sr}/^{86}\text{Sr}$ . (e) Initial  $\epsilon_{\text{Hf}}$  vs.  $\epsilon_{\text{Nd}}$ . Average  $2\sigma$  error bars are shown in a corner of each panel. Complete chemical duplicates, shown in Tables 2.3 and 2.4 (samples 4720A7 and 4722A4), are circled in each plot.

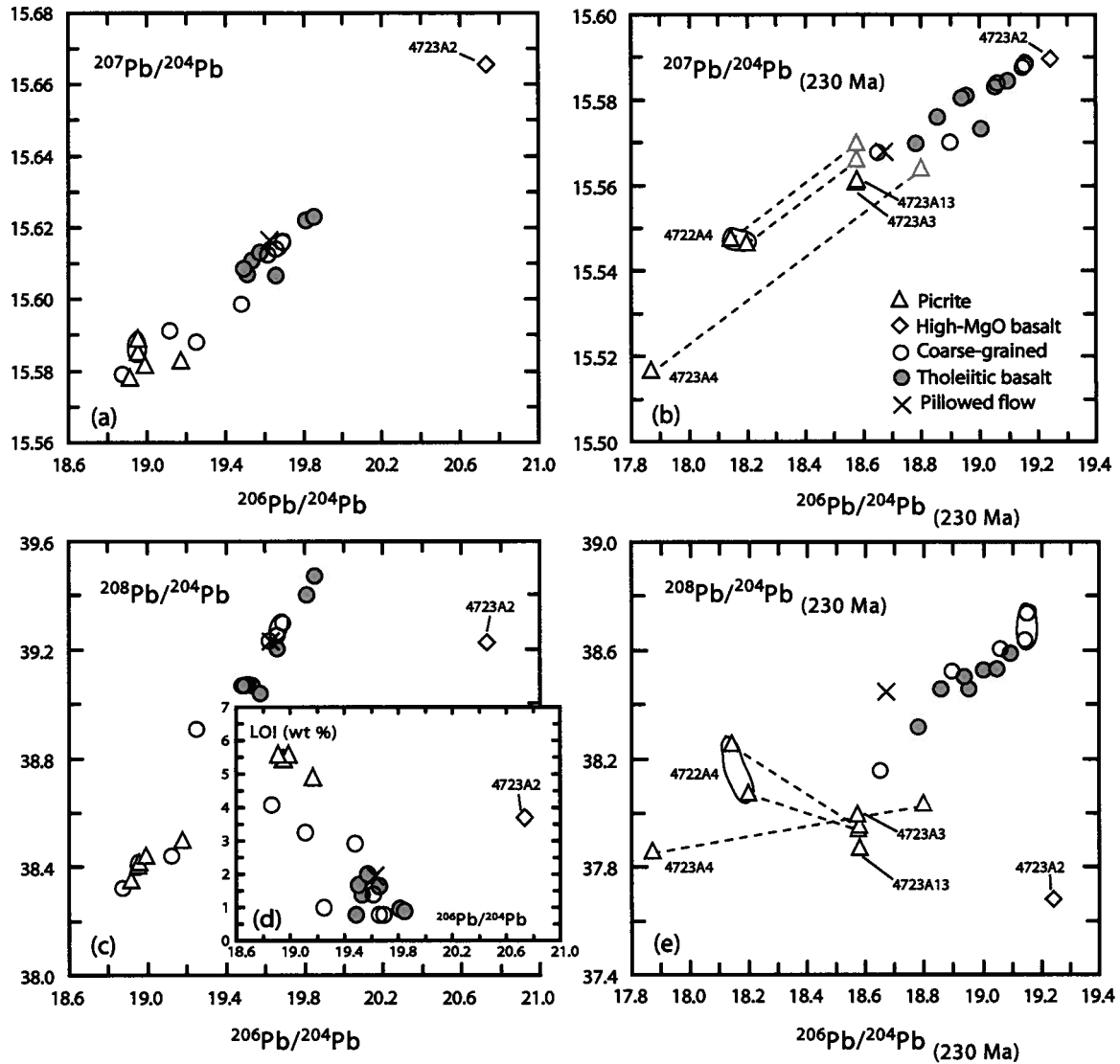


**Figure 2.10** Pb isotopic compositions of leached whole-rock samples measured by MC-ICP-MS for the Karmutsen Formation. Error bars are smaller than symbols. (a) Measured  $^{207}\text{Pb}/^{204}\text{Pb}$  vs.  $^{206}\text{Pb}/^{204}\text{Pb}$ . (b) Initial  $^{207}\text{Pb}/^{204}\text{Pb}$  vs.  $^{206}\text{Pb}/^{204}\text{Pb}$ . Age correction to 230 Ma. (c) Measured  $^{208}\text{Pb}/^{204}\text{Pb}$  vs.  $^{206}\text{Pb}/^{204}\text{Pb}$ . (d) LOI vs.  $^{206}\text{Pb}/^{204}\text{Pb}$ . (e) Initial  $^{208}\text{Pb}/^{204}\text{Pb}$  vs.  $^{206}\text{Pb}/^{204}\text{Pb}$ . Complete chemical duplicates, shown in Table 2.5 (samples 4720A7 and 4722A4), are circled in each plot. The dashed lines in panels b and e show the differences in age-corrections for two picrites (4723A4, 4722A4) using the measured U, Th, and Pb concentrations for each sample (black triangles) and the age-corrections when concentrations are used from the two picrites (4723A3, 4723A13) that appear to be least affected by alteration.

Table 2.3 Sr and Nd isotopic geochemistry of Karmutsen basalts, Vancouver Island, B.C.

Sample	Group <sup>a</sup>	Area <sup>b</sup>	Rb	Sr	<sup>87</sup> Sr/ <sup>86</sup> Sr	2σ <sub>m</sub>	<sup>87</sup> Rb/ <sup>86</sup> Sr	<sup>87</sup> Sr/ <sup>86</sup> Sr <sub>i</sub>	230 Ma	Sm	Nd	<sup>143</sup> Nd/ <sup>144</sup> Nd	2σ <sub>m</sub>	ε <sub>Nd</sub>	<sup>147</sup> Sm/ <sup>144</sup> Nd	<sup>143</sup> Nd/ <sup>144</sup> Nd <sub>i</sub>	ε <sub>Nd(t)</sub>
		(ppm)		(ppm)						(ppm)	(ppm)					230 Ma	
4718A2	THOL	MA	1.28	202	0.703247	6	0.0183	0.70319	4.60	16.8	0.513004	6	7.1	0.1656	0.51275	8.1	
4718A7	THOL	MA	3.78	283	0.703702	8	0.0387	0.70358	4.79	16.6	0.512988	6	7.0	0.1742	0.51274	7.7	
4719A2	THOL	MA	3.27	244	0.703811	9	0.0387	0.70368	4.48	16.1	0.512972	6	6.5	0.1688	0.51272	7.3	
4719A3	THOL	MA	3.49	229	0.703757	6	0.0441	0.70361	4.22	14.8	0.512972	6	6.5	0.1718	0.51271	7.2	
4720A4	THOL	SL	2.54	215	0.703066	8	0.0341	0.70295	5.77	21.0	0.512984	7	6.7	0.1682	0.51273	7.6	
4721A2	THOL	SL	1.58	209	0.703076	7	0.0220	0.70300	4.05	14.6	0.512965	7	6.4	0.1675	0.51271	7.2	
4721A4	THOL	SL	1.65	172	0.703062	7	0.0277	0.70297	5.48	19.6	0.512833	6	5.8	0.1691	0.51268	6.6	
4722A5	OUTLIER	KR	4.46	191	0.703877	7	0.0678	0.70366	6.10	21.0	0.512922	6	5.5	0.1756	0.51266	6.2	
4720A6	CG	SL	6.11	123	0.703121	9	0.1438	0.70265	4.75	16.8	0.512976	7	6.6	0.1711	0.51272	7.3	
4720A7	CG	SL	2.18	157	0.703078	6	0.0401	0.70285	4.96	17.3	0.513012	6	7.3	0.1735	0.51275	8.0	
4720A7(dup)	CG	SL	1.79	140	0.703067	9	0.0369	0.70295	4.56	16.0	0.512984	6	6.9	0.1722	0.51273	7.7	
4720A10	CG	SL	0.11	60	0.704294	7	0.0055	0.70428	2.05	5.7	0.513120	7	9.4	0.2191	0.51279	8.7	
4724A3	CG	SL	1.44	135	0.703421	8	0.0310	0.70332	3.84	13.2	0.512961	6	6.3	0.1757	0.51270	6.9	
5616A3	CG	KR	3.00	237	0.703849	7	0.0366	0.70373	3.82	12.9	0.512983	6	6.7	0.1790	0.51271	7.2	
5617A1	CG	SL	2.00	58	0.704241	7	0.0988	0.70391	2.14	6.06	0.513097	7	9.0	0.2135	0.51278	8.5	
4722A4	PIC	KR	3.16	77	0.705220	8	0.1184	0.70483	1.07	2.70	0.513115	6	9.3	0.2384	0.51276	8.1	
4722A4(dup)	PIC	KR	3.16	77	0.705214	7	0.1184	0.70483	0.97	2.48	0.513122	6	9.4	0.2361	0.51277	8.3	
4723A3	PIC	KR	1.65	69	0.704209	9	0.0696	0.70398	2.09	5.91	0.513098	7	9.0	0.2142	0.51278	8.5	
4723A4	PIC	KR	1.43	110	0.704352	8	0.0375	0.70423	2.14	5.90	0.513060	10	8.2	0.2192	0.51273	7.6	
4723A13	PIC	KR	0.67	63	0.704132	8	0.0312	0.70403	1.33	3.54	0.513118	7	9.4	0.2268	0.51278	8.5	
4723A2	HI-MG	KR	8.23	269	0.705466	7	0.0885	0.70518	1.99	5.79	0.513059	8	8.2	0.2081	0.51275	7.9	

<sup>a</sup> THOL, tholeiitic basalt, CG, coarse-grained mafic rock, PIC, picrite, HI-MG, high-MgO basalt; OUTLIER, anomalous pillowed flow in plots. <sup>b</sup> Abbreviations for area are: KR, Karmutsen Range, SL, Schoen Lake, MA, Mount Arrowsmith. (dup) Indicates complete chemistry duplicate. All isotopic and elemental analyses carried out at the PCIGR; the complete trace element analyses are shown in Appendix C.



Table 2.4 Hf isotopic compositions of Karmutsen basalts, Vancouver Island, B.C.

Sample	Group <sup>a</sup>	Area <sup>b</sup>	Lu (ppm)	Hf (ppm)	<sup>177</sup> Hf/ <sup>176</sup> Hf	2σ <sub>m</sub>	ε <sub>Hf</sub>	<sup>176</sup> Lu/ <sup>177</sup> Hf	<sup>177</sup> Hf/ <sup>176</sup> Hf <sub>t</sub>	ε <sub>Hf(t)</sub>
230 Ma										
4718A2	THOL	MA	0.38	2.53	0.283007	4	8.3	0.0211	0.28291	10.2
4718A7	THOL	MA	0.46	2.41	0.283001	7	8.1	0.0271	0.28288	9.1
4719A2	THOL	MA	0.40	2.16	0.283079	5	10.9	0.0262	0.28296	12.0
4719A3	THOL	MA	0.37	2.12	0.283024	9	8.9	0.0246	0.28291	10.2
4720A4	THOL	SL	0.53	3.04	0.283002	7	8.1	0.0247	0.28289	9.5
4721A2	THOL	SL	0.36	2.99	0.283004	10	8.2	0.0173	0.28293	10.7
4721A4	THOL	SL	0.53	2.79	0.283006	6	8.3	0.0268	0.28289	9.3
4722A5	OUTLIER	KR	0.56	3.15	0.283015	6	8.6	0.0254	0.28290	9.8
4720A6	CG	SL	0.45	2.38	0.283012	5	8.5	0.0269	0.28289	9.5
4720A7	CG	SL	0.46	2.23	0.283012	6	8.5	0.0291	0.28288	9.1
4720A7(dup)	CG	SL	0.43	2.35	0.283012	4	8.5	0.0260	0.28290	9.6
4720A10	CG	SL	0.36	1.00	0.283179	7	14.4	0.0515	0.28295	11.5
4724A3	CG	SL	0.34	1.41	0.283035	8	9.3	0.0339	0.28288	9.2
5616A3	CG	KR	0.34	2.70	0.283024	7	8.9	0.0179	0.28294	11.3
5617A1	CG	SL	0.40	1.40	0.283161	4	13.8	0.0407	0.28298	12.6
4722A4	PIC	KR	0.29	0.48	0.283321	10	19.4	0.0857	0.28294	11.2
4722A4(dup)	PIC	KR	0.29	0.45	0.283350	11	20.4	0.0915	0.28294	11.3
4723A3	PIC	KR	0.45	0.98	0.283197	6	15.0	0.0649	0.28291	10.1
4723A4	PIC	KR	0.35	0.90	0.283121	26	12.3	0.0561	0.28287	8.7
4723A13	PIC	KR	0.35	0.63	0.283250	7	16.9	0.0791	0.28290	9.7
4723A2	HI-MG	KR	0.43	1.06	0.283186	7	14.7	0.0579	0.28293	10.8

<sup>a</sup> THOL, tholeiitic basalt, CG, coarse-grained mafic rock, PIC, picrite, HI-MG, high-MgO basalt; OUTLIER, anomalous pillowed flow in plots. <sup>b</sup> Abbreviations for area are: KR, Karmutsen Range, SL, Schoen Lake, MA, Mount Arrowsmith. (dup) indicates complete chemistry duplicate. All isotopic and elemental analyses carried out at the PCIGR; the complete trace element analyses are shown in Appendix C.

Table 2.5 Pb isotopic compositions of Karmutsen basalts, Vancouver Island, B.C.

Sample	Group <sup>a</sup>	Area <sup>b</sup>	U (ppm)	Th (ppm)	Pb (ppm)	<sup>208</sup> Pb/ <sup>204</sup> Pb	2σ <sub>m</sub>	<sup>207</sup> Pb/ <sup>204</sup> Pb	2σ <sub>m</sub>	<sup>206</sup> Pb/ <sup>204</sup> Pb	2σ <sub>m</sub>	<sup>238</sup> U/ <sup>204</sup> Pb	<sup>235</sup> U/ <sup>204</sup> Pb	<sup>232</sup> Th/ <sup>204</sup> Pb	<sup>206</sup> Pb/ <sup>204</sup> Pb	<sup>207</sup> Pb/ <sup>204</sup> Pb	<sup>208</sup> Pb/ <sup>204</sup> Pb
4718A2	THOL	MA	0.18	0.56	0.71	19.5369	0.0021	15.6105	0.0017	39.0684	0.0035	16.0	0.116	53.2	18.957	15.581	38.455
4718A7	THOL	MA	0.17	0.52	0.54	19.5133	0.0016	15.6070	0.0015	39.0697	0.0042	20.1	0.146	65.7	18.782	15.570	38.312
4719A2	THOL	MA	0.18	0.47	0.68	19.5780	0.0015	15.6130	0.0012	39.0359	0.0032	17.6	0.127	46.4	18.940	15.581	38.501
4719A3	THOL	MA	0.14	0.45	0.52	19.6814	0.0017	15.6066	0.0015	39.2027	0.0042	18.0	0.131	58.8	19.007	15.573	38.524
4720A4	THOL	SL	0.21	0.72	0.65	19.8169	0.0012	15.6218	0.0010	39.3997	0.0026	21.0	0.153	75.7	19.053	15.583	38.527
4721A2	THOL	SL	0.25	0.72	0.91	19.4972	0.0019	15.6084	0.0015	39.0681	0.0039	17.6	0.127	53.1	18.859	15.576	38.454
4721A4	THOL	SL	0.17	0.61	0.54	19.8552	0.0009	15.6229	0.0008	39.4709	0.0020	20.9	0.151	76.7	19.098	15.584	38.587
4722A5	OUTLIER	KR	0.33	0.82	0.81	19.6272	0.0016	15.6164	0.0012	39.2322	0.0034	26.3	0.191	68.0	18.673	15.568	38.448
4720A6	CG	SL	0.13	0.45	0.56	19.6209	0.0017	15.6124	0.0013	39.2307	0.0039	15.4	0.112	54.4	19.062	15.584	38.603
4720A7	CG	SL	0.13	0.48	0.61	19.6640	0.0009	15.6138	0.0006	39.2547	0.0019	14.2	0.103	53.5	19.149	15.588	38.638
4720A7(dup)	CG	SL	0.14	0.44	0.61	19.6951	0.0006	15.6157	0.0006	39.2975	0.0022	14.9	0.108	48.8	19.154	15.588	38.735
4720A10	CG	SL	0.05	0.11	0.51	18.8745	0.0018	15.5788	0.0016	38.3176	0.0042	6.1	0.044	14.3	18.652	15.568	38.153
4724A3	CG	SL	0.09	0.30	0.60	19.2520	0.0014	15.5880	0.0013	39.9072	0.0032	9.7	0.070	33.6	18.900	15.570	38.519
5816A3	CG	KR				19.4845	0.0007	15.5986	0.0006	39.0679	0.0015						
5817A1	CG	SL				19.1202	0.0007	15.5910	0.0006	38.4401	0.0016						
4722A4	PIC	KR	0.05	0.07	0.17	18.9514	0.0017	15.5852	0.0017	38.4063	0.0041	20.8	0.151	28.8	18.197	15.547	38.074
4722A4(dup)	PIC	KR	0.05	0.03	0.16	18.9539	0.0013	15.5890	0.0012	38.4186	0.0029	22.4	0.162	14.1	18.142	15.548	38.257
4723A3	PIC	KR	0.06	0.19	0.32	18.9873	0.0012	15.5820	0.0011	38.4434	0.0027	11.4	0.083	38.8	18.573	15.561	37.996
4723A4	PIC	KR	0.05		0.09	19.1733	0.0013	15.5832	0.0012	38.4984	0.0033	35.9	0.261	55.5	17.868	15.517	37.858
4723A13	PIC	KR	0.03	0.11	0.18	18.9131	0.0011	15.5784	0.0011	38.3518	0.0030	9.2	0.067	41.5	18.580	15.561	37.873
4723A2	HI-MG	KR	0.06	0.19	0.09	20.7321	0.0037	15.6656	0.0030	39.2295	0.0073	41.0	0.298	134.7	19.242	15.590	37.676

<sup>a</sup> THOL, tholeiitic basalt; CG, coarse-grained mafic rock; PIC, picrite; HI-MG, high-MgO basalt; OUTLIER, anomalous pillowed flow in plots. <sup>b</sup> Abbreviations for area are: KR, Karmutsen Range, SL, Schoen Lake, MA, Mount Arrowsmith. (dup) indicates complete chemistry duplicate. All isotopic and elemental analyses carried out at the PCIGR; the complete trace element analyses shown in Appendix C.

$^{208}\text{Pb}/^{204}\text{Pb} = 38.153\text{--}38.735$ . One high-MgO basalt has the highest initial  $^{206}\text{Pb}/^{204}\text{Pb}$  (19.242) and  $^{207}\text{Pb}/^{204}\text{Pb}$  (15.590), and the lowest initial  $^{208}\text{Pb}/^{204}\text{Pb}$  (37.676). The Pb isotopic ratios for Karmutsen samples define broadly linear relationships in Pb isotope plots. The age-corrected Pb isotopic compositions of several picrites have been affected by U and Pb (and/or Th) mobility during alteration (Fig. 2.10).

## ALTERATION

The Karmutsen basalts have retained most of their original igneous structures and textures; however, secondary alteration and low-grade metamorphism generated zeolitic- and prehnite-pumpellyite-bearing mineral assemblages (Table 2.1) (Cho *et al.*, 1987), which have primarily affected the distribution of the LILE and the Sr isotopic systematics. The Keogh Lake picrites show the strongest effects of alteration and have higher LOI (up to 5.5 wt %), variable LILE, and higher measured Sr, Nd, and Hf and lower measured Pb isotope ratios than tholeiitic basalts. As a result, Sr and Pb isotopes show a relationship with LOI (Figs 2.9 and 2.10), whereas Nd and Hf isotopic compositions do not correlate with LOI (not shown). The relatively high initial Sr isotopic compositions for high-MgO lavas (up to 0.7052) likely resulted from an increase in  $^{87}\text{Sr}/^{86}\text{Sr}$  through addition of seawater Sr (e.g. Hauff *et al.*, 2003). High-MgO lavas from the Caribbean plateau have similarly high  $^{87}\text{Sr}/^{86}\text{Sr}$  compared to basalts (Révillon *et al.*, 2002). The correction for *in situ* decay on initial Pb isotopic ratios has been affected by mobilization of U and Pb (and/or Th) in whole rocks since their formation. A thorough acid leaching during sample preparation was used that has been shown to effectively remove alteration phases (Weis *et al.*, 2006; Nobre Silva *et al.*, submitted). The HFSE abundances for tholeiitic and picritic basalts exhibit clear linear correlations in binary diagrams (Fig. 2.8), whereas plots of LILE versus HFSE are highly scattered (not shown) due to the mobility of some of the alkali and alkaline earth LILE (Cs, Rb, Ba, K) and Sr for most samples during alteration.

The degree of alteration in the Karmutsen samples does not appear to be related to eruption environment or depth of burial. Pillow rims are compositionally different from pillow cores (Surdam, 1967; Kuniyoshi, 1972), and aquagene tuffs are chemically different from isolated pillows within pillow breccia, but submarine and subaerial basalts

exhibit a similar degree of alteration. There is no clear correlation between the submarine and subaerial basalts and some commonly used chemical alteration indices [e.g. Ba/Rb vs.  $K_2O/P_2O_5$  (Huang & Frey, 2005)]. There is also no definitive correlation between the petrographic alteration index (Table 2.1; 1-least altered, 3-intensely altered) and chemical alteration indices, although 10 of 13 tholeiitic basalts with the highest K and LILE abundances have a petrographic alteration index of 3.

## **OLIVINE ACCUMULATION IN PICRITIC LAVAS**

Geochemical trends and petrographic characteristics indicate that accumulation of olivine played an important role in the formation of the Keogh Lake picrites on northern Vancouver Island. The Keogh Lake picrites show a strong linear correlation in plots of  $Al_2O_3$ ,  $TiO_2$ , Sc, Yb, and Ni versus MgO and many of the picrites have abundant clusters of olivine pseudomorphs (Table 2.1; Fig. 2.11). There is a strong linear correlation between modal percent olivine and whole-rock magnesium content for the Keogh Lake picrites (Fig. 2.11). Magnesium contents range between 10 and 19 wt % MgO and the proportion of olivine phenocrysts in these samples varies from 0 to 42 vol % (Fig. 2.11). With a few exceptions, the size range and median size of the olivine phenocrysts in most samples is comparable. The clear correlation between proportion of olivine phenocrysts and whole-rock magnesium contents indicates that accumulation of olivine was directly responsible for the high MgO contents (>10 wt %) for most of the picritic lavas.

## **DISCUSSION**

The Wrangellia oceanic plateau on Vancouver Island was constructed in a three-layered structure of mostly tholeiitic basalt with a restricted range of composition. The plateau formed rapidly during a single phase (ca. 230 Ma) and hiatuses between eruptions were not long-lasting so there was very little accumulation of sediments. The pillowed and unpillowed flows that built up the submarine volcanic edifice from the deep seafloor resulted primarily from different effusive rates and local topography. Some of the unpillowed flows represent master tubes for the delivery of lava to distal parts of submarine flow fields. Abundant picritic pillow lavas erupted during the middle and latter stages of submarine growth (Nixon *et al.*, 2008), in areas of the plateau exposed on

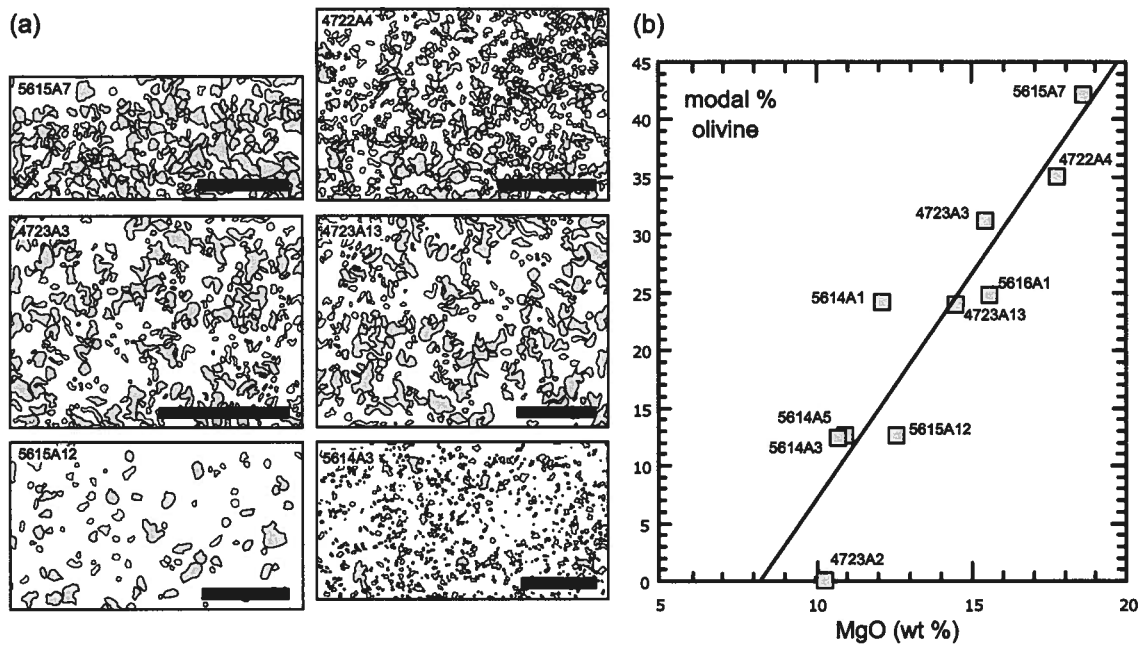


**Figure 2.11** Relationship between abundance of olivine phenocrysts and whole-rock MgO contents for Keogh Lake picrites. (a) Tracings of olivine grains (gray) in six high-MgO samples made from high resolution (2400 dpi) scans of petrographic thin-sections. Scale bars are 10 mm in length and sample numbers are indicated in upper left. (b) Modal % olivine vs. whole-rock MgO. Black line is the best-fit line for ten high-MgO samples. The areal proportion of olivine was calculated from raster images of olivine grains using ImageJ® image analysis software, which provides an acceptable estimation of the modal abundance (e.g. Chayes, 1954).

northern Vancouver Island. The overlying volcanoclastic units formed as a consequence of eruption in shallow water. A broad subaerial platform was constructed of well-layered sheet flows and, as volcanism waned, local interflow carbonate deposits developed, along with plagioclase megacrystic flows and local volcanoclastic deposits. The geochemical and stratigraphic relationships observed in the Karmutsen Formation on Vancouver Island provide constraints on the construction of oceanic plateaus, the source of magmas for a plume head impinging on oceanic lithosphere, and the conditions of melting and subsequent magmatic evolution of basaltic magmas involved in the formation of an oceanic plateau. Studies of the formation of this oceanic plateau in the following sections examine the (1) temperature and extent of melting of picritic lavas; (2) composition of the mantle source; (3) the depth of melting and residual mineralogy in the source region; and (4) low-pressure evolution of the Karmutsen basalts.

### **Melting conditions and major-element composition of primary magmas**

The primary melts to most flood basalt provinces are believed to be picritic (e.g. Cox, 1980) and they have been found in many continental and oceanic flood basalt provinces worldwide [e.g. Siberia; Karoo; Parana-Etendeka; Caribbean; Deccan (Saunders, 2005)]. Near-primary picritic lavas with low total alkali abundances require high-degree partial melting of the mantle source (e.g. Herzberg & O'Hara, 2002). The Keogh Lake picrites from northern Vancouver Island are the best candidates for least-modified partial melts of the mantle plume source, despite having accumulated olivine phenocrysts, and can be used to estimate conditions of melting and the composition of primary magmas for the Karmutsen Formation. Herzberg *et al.* (2007) have provided a thorough description of a technique for inverse and forward modeling for estimating mantle temperature, melt fraction, primary magma composition, and source residue composition using major elements.

The estimated melting conditions and primary magma compositions for the picritic lavas of the Karmutsen Formation, and a brief summary of the modeling method, are presented in Figure 2.12 and Table 2.6. If Karmutsen picritic lavas were derived from accumulated fractional melting of fertile peridotite, the primary magmas would have contained 15-17 wt % MgO and ~10 wt % CaO (Fig. 2.12; Table 2.6), formed from 23-

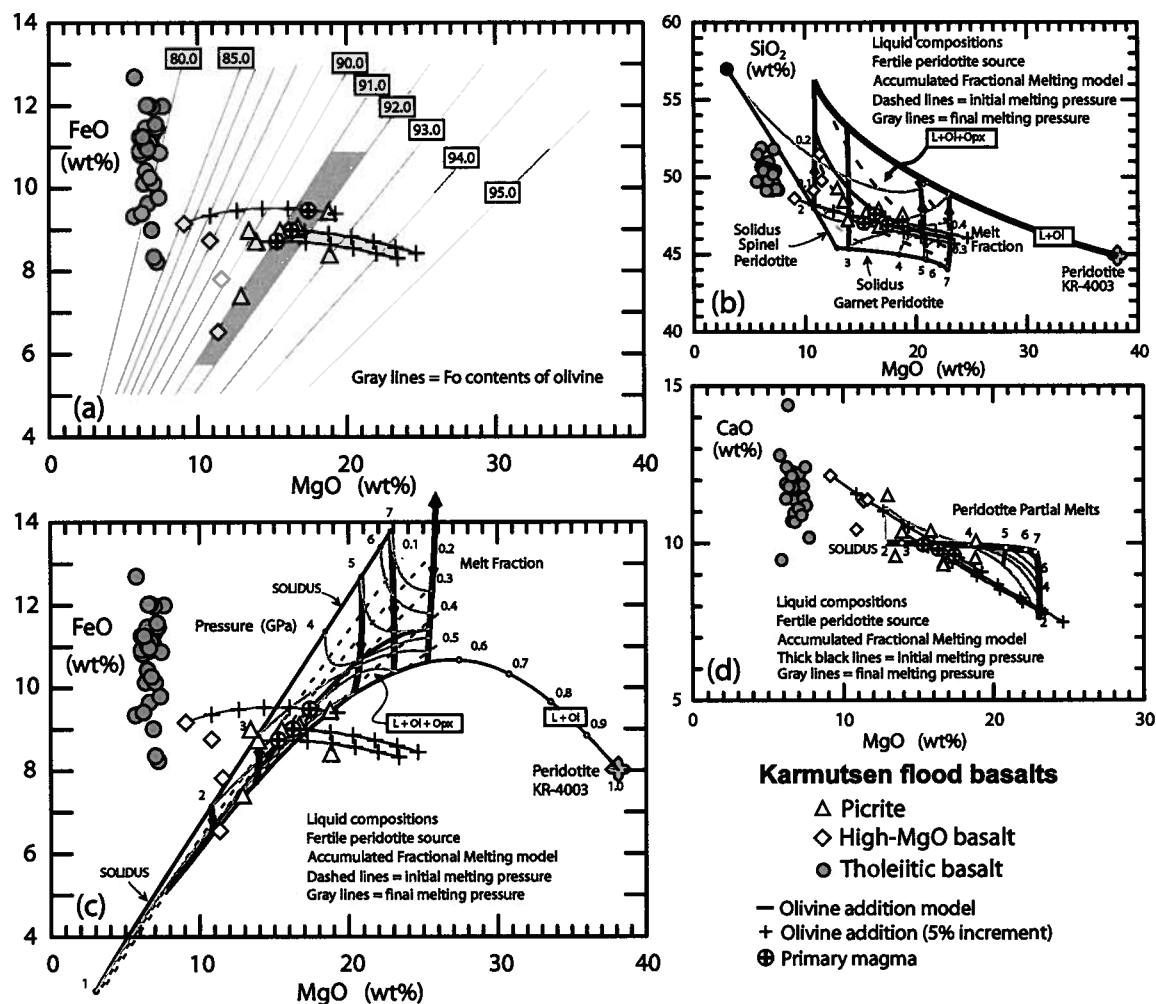


**Figure 2.12** Estimated primary magma compositions for three Keogh Lake picrites (samples 4723A4, 4723A13, 5616A7) using the forward and inverse modeling technique of Herzberg *et al.* (2007). Karmutsen compositions and modeling results are overlain on diagrams provided by C. Herzberg. (a) Whole-rock FeO vs. MgO for Karmutsen samples from this study. Total iron estimated to be FeO is 0.90. Gray lines show olivine compositions that would precipitate from liquid of a given MgO-FeO composition. Black lines with crosses show results from olivine addition (inverse model) using PRIMELT1 (Herzberg *et al.*, 2007). (b) SiO<sub>2</sub> vs. MgO with Karmutsen lavas and model results. (c) FeO vs. MgO with Karmutsen lava compositions and results of forward model for accumulated fractional melting of fertile peridotite. (d) CaO vs. MgO with Karmutsen lava compositions and model results. To briefly summarize the technique [see Herzberg *et al.* (2007) for complete description], potential parental magma compositions for the high-MgO lava series were selected (highest MgO and appropriate CaO) and, using PRIMELT1 software, olivine was incrementally added to the selected compositions to show an array of potential primary magma compositions (inverse model). Then, using PRIMELT1, the results from the inverse model were compared to a range of accumulated fractional melts for fertile peridotite, derived from parameterization of the experimental results of Walter (1998) (forward model; Herzberg & O'Hara, 2002). A melt fraction was sought that was unique to both the inverse and forward models (Herzberg *et al.*, 2007). A unique solution was found when there was a common melt fraction for both models in FeO-MgO and CaO-MgO-Al<sub>2</sub>O<sub>3</sub>-SiO<sub>2</sub> (CMAS) projection space. This modeling assumes olivine was the only phase crystallizing and ignores chromite precipitation, and possible augite fractionation in the mantle (Herzberg & O'Hara, 2002). Results are best for a residue of spinel lherzolite (not pyroxenite). The presence of accumulated olivine in samples of Keogh Lake picrites used as starting compositions does not significantly affect the results because we are modeling addition of olivine. The tholeiitic basalts cannot be used for modeling because they are all plag + cpx + ol saturated.

Table 2.6 Estimated primary magma compositions for Karmutsen basalts and other oceanic plateaus/islands

Sample	4723A4	4723A13	5616A7	93G171	Average	OJP <sup>a</sup>	Mauna Kea <sup>b</sup>	Gorgona <sup>c</sup>
(Weight %):								
SiO <sub>2</sub>	47.0	47.6	46.9	47.8	47.3	48.0	46.3	46.1
TiO <sub>2</sub>	0.68	0.46	0.60	0.46	0.55	0.62	1.93	0.56
Al <sub>2</sub> O <sub>3</sub>	15.3	14.3	13.0	13.9	14.1	12.3	9.6	11.7
Cr <sub>2</sub> O <sub>3</sub>	0.10	0.20	0.04	0.09	0.11	0.07	0.26	0.16
Fe <sub>2</sub> O <sub>3</sub>	1.03	1.08	0.89	1.09	1.02	0.90	1.08	1.18
FeO	8.7	9.0	9.5	8.9	9.0	9.2	10.3	10.1
MnO	0.15	0.15	0.16	0.19	0.16	0.17	0.18	0.18
MgO	15.3	16.3	17.4	16.1	16.3	16.8	18.3	18.8
CaO	9.9	9.8	9.6	10.3	9.9	10.3	10.1	10.0
Na <sub>2</sub> O	1.59	0.90	1.74	1.01	1.31	1.36	1.67	1.04
K <sub>2</sub> O	0.07	0.06	0.05	0.11	0.07	0.08	0.41	0.03
NiO	0.05	0.08	0.08	0.07	0.07	0.10	0.08	0.11
Eruption T(°C)	1354	1375	1397	1369	1374	1382	1415	1422
Potential T(°C)	1467	1491	1517	1486	1490	1500		1606
Fo content (olivine)	91.2	91.2	91.6	91.2	91.3	90.5	91.4	90.6
Melt fraction	0.23	0.27	0.26	0.27	0.26	0.27		0.28
%ol addition	4.2	2.5	24.3	0.8	7.9	18		

<sup>a</sup> Ontong Java primary magma composition for accumulated fraction melting (AFM) from Herzberg (2004).

<sup>b</sup> Mauna Kea primary magma composition is average of 4 samples in Table 1 of Herzberg (2006).

<sup>c</sup> Gorgona primary magma composition for AFM for 1F, fertile source, in Table 4 of Herzberg and O'Hara (2002).

Total iron estimated to be FeO is 0.90.



27% partial melting, and would have crystallized olivine with a Fo content of ~91 (Fig. 2.12; Table 2.6). Calculated mantle temperatures for the Karmutsen picrites (~1490°C) indicate melting from anomalously hot mantle (100-200°C) compared to ambient mantle that produces mid-ocean ridge basalt (MORB; ~1280-1400°C; Herzberg *et al.*, 2007). Several picrites are near-primary melts and required very little addition of olivine (e.g. sample 93G171, with measured 15.8 wt % MgO). These temperature and melting estimates of the Karmutsen picrites in this study are consistent with the decompression of hot mantle peridotite in an actively convecting plume head (i.e. plume initiation model).

The estimated primary magma compositions and melting conditions for some other LIPs (e.g. the Ontong Java Plateau) are similar to estimates for the Karmutsen Formation (Table 2.6). Herzberg (2004) found that primary magma compositions for Ontong Java basalts, assuming a peridotite source, would contain ~17 wt % MgO and ~10 wt % CaO (Table 2.6), and these magmas would have formed by 27% melting with mantle potential temperatures of ~1500°C, and first melting occurring at ~3.6 GPa. Fitton & Godard (2004) estimated 30% partial melting of the Ontong Java lavas based on the Zr contents of primary magmas calculated by incremental addition of equilibrium olivine to analyses of Kroenke-type basalt. If a considerable amount of eclogite was involved in the formation of the Ontong Java Plateau, the excess temperatures estimated by Herzberg *et al.* (2007) may not be required (Korenaga, 2005). Estimated primary magmas for Mauna Kea and Gorgona have higher MgO (18-19 wt % MgO) and comparable CaO (10 wt % CaO) (Table 2.6; Herzberg (2006)).

### **Source of Karmutsen lavas**

Karmutsen samples have isotopic compositions belonging to the field of ocean island basalts (OIB) and provide a sampling of the Pacific mantle ca. 230 Ma (Fig. 2.13). The Karmutsen tholeiitic basalts have initial  $\epsilon_{\text{Nd}}$  and  $^{87}\text{Sr}/^{86}\text{Sr}$  that fall within the range of basalts from the Caribbean Plateau (e.g. Kerr *et al.*, 1996; Kerr *et al.*, 1997; Hauff *et al.*, 2000; Kerr, 2003), a range of Hawaiian isotope data (e.g. Frey *et al.*, 2005), and lie within and just above the range for the Ontong Java Plateau (Tejada *et al.*, 2004; Fig 2.13). Karmutsen tholeiitic basalts with the highest initial  $\epsilon_{\text{Nd}}$  and lowest initial  $^{87}\text{Sr}/^{86}\text{Sr}$  lie just below the field for northern East Pacific Rise (EPR) MORB (e.g. Niu *et al.*, 1999;

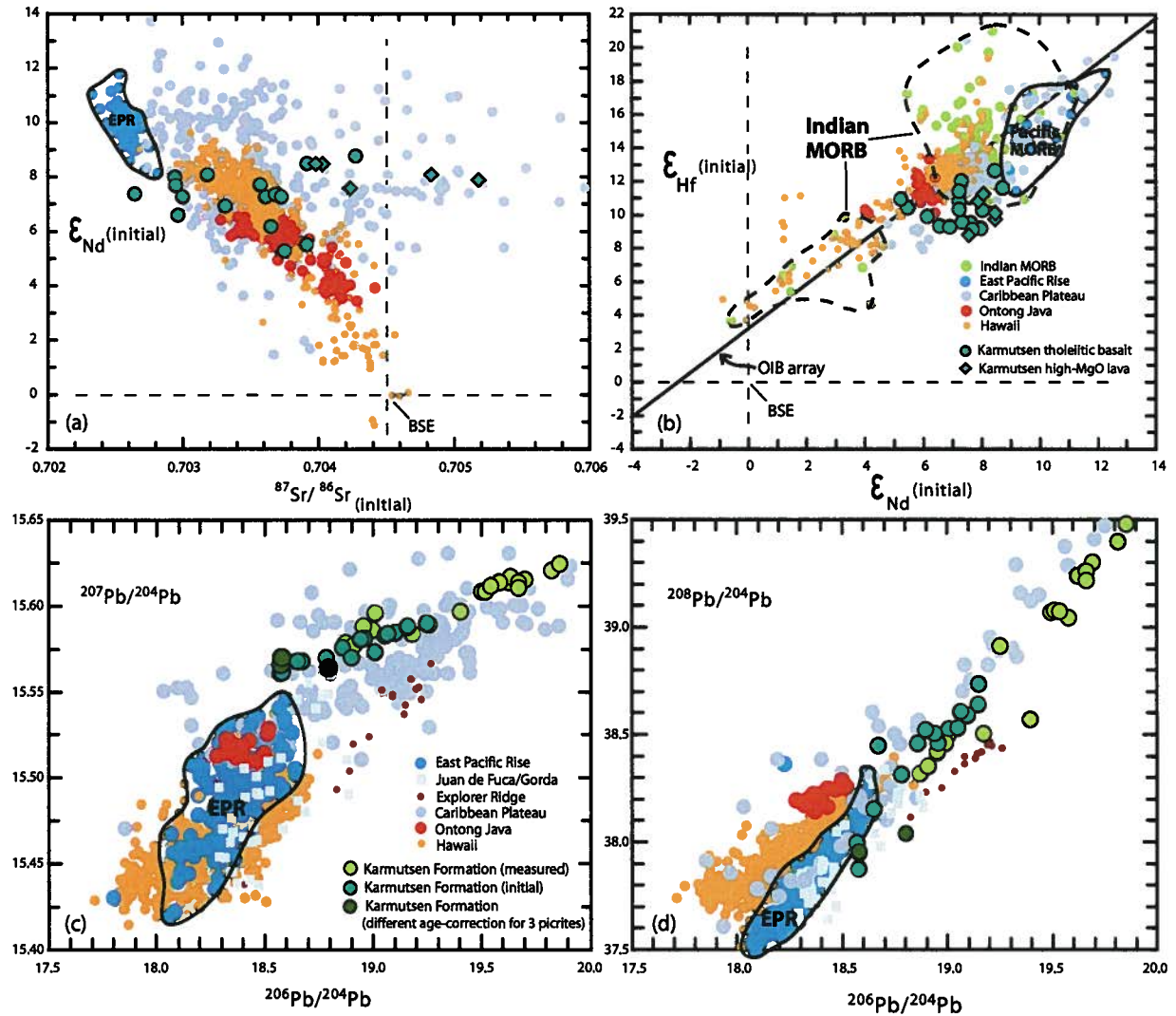


**Figure 2.13** Comparison of age-corrected (230 Ma) Sr-Nd-Hf-Pb isotopic compositions for Karmutsen flood basalts on Vancouver Island to age-corrected OIB and MORB. (a) Initial  $\epsilon_{Nd}$  vs.  $^{87}Sr/^{86}Sr$ . (b) Initial  $\epsilon_{Hf}$  vs.  $\epsilon_{Nd}$ . Both fields with dashed lines are Indian MORB. (c) Measured and initial  $^{207}Pb/^{204}Pb$  vs.  $^{206}Pb/^{204}Pb$ . (d) Measured and initial  $^{208}Pb/^{204}Pb$  vs.  $^{206}Pb/^{204}Pb$ . Most of the compiled data was extracted from the GEOROC database (<http://georoc.mpch-mainz.gwdg.de/georoc/>). Data for Ontong Java from Mahoney *et al.* (1993), Babbs (1997), and Tejada *et al.* (2004); Indian MORB from Salters (1996), Kempton *et al.* (2002), and Janney *et al.* (2005); Pacific MORB from Mahoney *et al.* (1992, 1994), Nowell *et al.* (1998), Salters and White (1998), and Chauvel and Blichert-Toft (2001); Explorer Ridge data from Cousens and Weis (pers. comm., 2007); OIB array line from Vervoort *et al.* (1999). EPR is East Pacific Rise. Several high-MgO samples affected by secondary alteration were not plotted for clarity in Pb isotope plots. Dashed lines indicate Bulk Silicate Earth (BSE). An extended reference list is available upon request.

Regelous *et al.*, 1999). Initial Hf and Nd isotopic compositions place the Karmutsen basalts on the edge of the field of OIB (age-corrected), with slightly higher initial  $\epsilon_{\text{Nd}}$  and similar initial  $\epsilon_{\text{Hf}}$  to Ontong Java, and slightly lower initial  $\epsilon_{\text{Hf}}$  and similar initial  $\epsilon_{\text{Nd}}$  to the range of compositions for Hawaii and the Caribbean Plateau (Fig. 2.13). Karmutsen samples are slightly offset to the low side of the OIB array (Vervoort *et al.*, 1999), slightly overlap the low  $\epsilon_{\text{Hf}}$  end of a field for Indian MORB (Kempton *et al.*, 2002; Janney *et al.*, 2005), and samples with the highest initial  $\epsilon_{\text{Hf}}$  and  $\epsilon_{\text{Nd}}$  lie just at the edge of the presently defined field for Pacific MORB (Mahoney *et al.*, 1992, 1994; Nowell *et al.*, 1998; Chauvel & Blichert-Toft, 2001). Karmutsen Pb isotope ratios overlap a broad range for the Caribbean Plateau and the linear trends for Karmutsen samples intersect fields for EPR MORB, Hawaii, and Ontong Java in  $^{208}\text{Pb}$ - $^{206}\text{Pb}$  space, but do not intersect these fields in  $^{207}\text{Pb}$ - $^{206}\text{Pb}$  space (Fig. 2.13). The more radiogenic  $^{207}\text{Pb}/^{204}\text{Pb}$  for a given  $^{206}\text{Pb}/^{204}\text{Pb}$  of Karmutsen basalts indicate they are isotopically enriched in comparison to EPR MORB, Hawaii, and Ontong Java.

The Hf-Nd isotopic geochemistry of volcanic rocks of the Karmutsen Formation on Vancouver Island indicates an isotopically rather uniform mantle source. The Hf and Nd isotopic compositions of Karmutsen basalts indicate long-term depletion of the more highly incompatible elements in the mantle source and are distinct from MORB; they are less depleted than the source of MORB and there is no clear evidence of involvement of MORB-type mantle. The limited variation of Hf and Nd isotopic compositions is slightly greater than in the isotopically very uniform mantle source of Ontong Java. Small-scale heterogeneities in the mantle source of Karmutsen lavas may have been diluted by the high degrees of partial melting, similar to Ontong Java (Tejada *et al.*, 2004). Lassiter *et al.* (1995) suggested that mixing of a plume-type source with  $\epsilon_{\text{Nd}} +6$  to  $+7$  with arc material with low Nb/Th could reproduce variations in the Karmutsen basalts, but the absence of low Nb/La ratios in most of the basalts restricts the amount of arc lithospheric involvement (based on major and trace elements and Sr, Nd, and Pb isotopic compositions for a suite of 29 samples from Buttle Lake in Strathcona Provincial Park on central Vancouver Island; Fig. 2.1). The isotopic composition and trace-element ratios of Karmutsen basalts in this study do not indicate significant involvement of Paleozoic arc

lithosphere on Vancouver Island. There are no clear HFSE-depletions in Karmutsen tholeiitic basalts.

The Sr-Nd-Hf-Pb isotope systematics for Karmutsen basalts distinguish the source of Karmutsen basalts from MORB and some OIB. The Hf and Nd isotope systematics provide the firmest constraints on the character of the source for Karmutsen lavas. The Lu/Hf ratios of the picritic lavas (mean 0.08) are considerably higher than in tholeiitic basalts (mean 0.02), but the small range of initial  $\epsilon_{\text{Hf}}$  for the two lava suites suggests that these differences in trace-element compositions were not long-lived, and do not correspond to intrinsic differences in the mantle plume source. Evolution of Hf isotopes with time shows that if the picritic and tholeiitic lavas originally had a similar range of  $\epsilon_{\text{Hf}}$  it would take  $\sim 155$  m.y. for Hf isotope ratios to evolve so there would be no overlap in  $\epsilon_{\text{Hf}}$  (Fig. 2.14); this is similar to a concept emphasized by Arndt *et al.* (1997) using Nd isotopes of lavas from Gorgona Island. Therefore, it is unlikely that the picrites had high Lu/Hf ratios long before ascent of the plume and the different Lu/Hf ratios likely developed during the melting process within the plume during ascent. The similar initial Hf and Nd isotopic ratios of the picrites and tholeiitic basalts preclude the limited isotopic range being simply the result of mixing of magmas. The slightly different Pb isotope ratios of the picrites and tholeiitic basalts are at least partly a result of alteration-related effects. As observed in the Caribbean Plateau, the radiogenic Pb in Karmutsen basalts is systematically different than in MORB, Ontong Java, and OIB from Hawaii, but Hf and Nd isotope compositions indicate a homogeneous, OIB-type enriched mantle source.

#### **REE modeling: Dynamic melting and source mineralogy**

The combination of isotopic and trace-element geochemistry of picritic and tholeiitic Karmutsen lavas indicates that differences in trace elements may have originated from different melting histories within a predominantly homogeneous, depleted (but not MORB) mantle source. Dynamic melting models simulate progressive decompression melting where some of the melt fraction is retained by the residue and only when the degree of partial melting is greater than the critical mass porosity, and the source becomes permeable, is excess melt extracted from the residue (Zou, 1998). For the

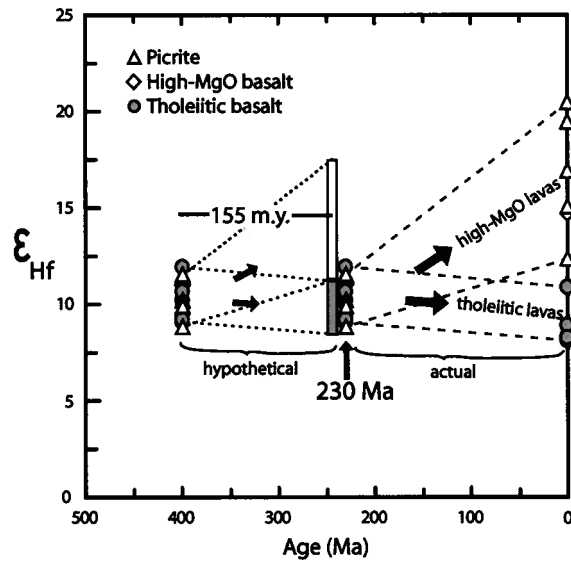


**Figure 2.14** Evolution of  $\epsilon_{\text{Hf}}$  with time for picritic and tholeiitic lavas for the Karmutsen Formation. The different Lu/Hf ratios of the Karmutsen lavas likely originated during melting processes within the plume. For example, if the picritic and tholeiitic lavas possessed the Lu/Hf ratios that they did at 230 Ma more than 155 m.y. before their formation, they would have evolved to have a different range of Hf isotopic compositions by 230 Ma (shown by the gray and white vertical boxes for tholeiitic and picritic lavas, respectively). This is shown by hypothetical compositions at 400 Ma (using  $\epsilon_{\text{Hf}}(230 \text{ Ma})$  for each sample) and  $\epsilon_{\text{Hf}}$  evolution trends using  $^{176}\text{Lu}/^{177}\text{Hf}$  for each sample. Picritic lavas have high Lu/Hf ratios so they accumulate radiogenic Hf within a relatively short geologic timespan. Decay constant of  $1.87 \times 10^{-11} \text{ yr}^{-1}$  used from Scherer *et al.* (2001). Error bars are smaller than symbols.

Karmutsen lavas, evolution of trace element concentrations was simulated using the incongruent dynamic melting model developed by Zou & Reid (2001). Melting of the mantle at pressures greater than ~1 GPa involves incongruent melting (e.g. Longhi, 2002) with olivine being produced during reaction of cpx + opx + sp for spinel peridotites. Modeling was separated into two intervals of melting, for a garnet lherzolite (gt lherz) and spinel lherzolite (sp lherz) source, using coefficients for incongruent melting reactions based on experiments on lherzolite melting (e.g. Kinzler & Grove, 1992; Longhi, 2002). The model solutions are non-unique and a range in degree of melting, partition coefficients, melt reaction coefficients, and proportion of mixed source components is possible to achieve acceptable solutions.

The LREE-depleted high-MgO lavas require melting of a depleted spinel lherzolite source (Fig. 2.15). The modeling results indicate a high degree of melting (22-25%), similar to results from major-element modeling using PRIMELT1 (discussed above), from a LREE-depleted source, and melting of garnet was probably not involved in formation of the high-MgO lavas. The enriched tholeiitic basalts involved melting of both garnet and spinel lherzolite and represent aggregate melts produced from continuous melting throughout the depth of the melting column (Fig. 2.15), which were subsequently homogenized and fractionated in magma chambers at low pressure. The modeling results indicate that these aggregate melts would have involved lesser proportions of enriched, small-degree melts (1-6% melting) generated at depth and greater amounts of depleted, high-degree melts (12-25%) generated at lower pressure (ratio of gt lherz to sp lherz melt would have been approximately 1 to 3, or 1 to 4; see Fig. 2.15). The degree of melting was high (23-27%), similar to the degree of partial melting of primary melts that erupted as the Keogh Lake picrites, from a source that was likely depleted in LREE.

Although the modeling results indicate that the depleted high-MgO Karmutsen lavas were formed from high-degree partial melting within the spinel lherzolite stability field (~0.9-2.5 GPa), the source was not necessarily more depleted in incompatible trace elements than the source of the tholeiitic lavas. It is possible that early high-pressure, low-degree melting left a residue within parts of the plume (possibly the hotter, interior portion) that was depleted in trace elements (e.g. Elliott *et al.*, 1991); further decompression and high-degree melting of such depleted regions could then have

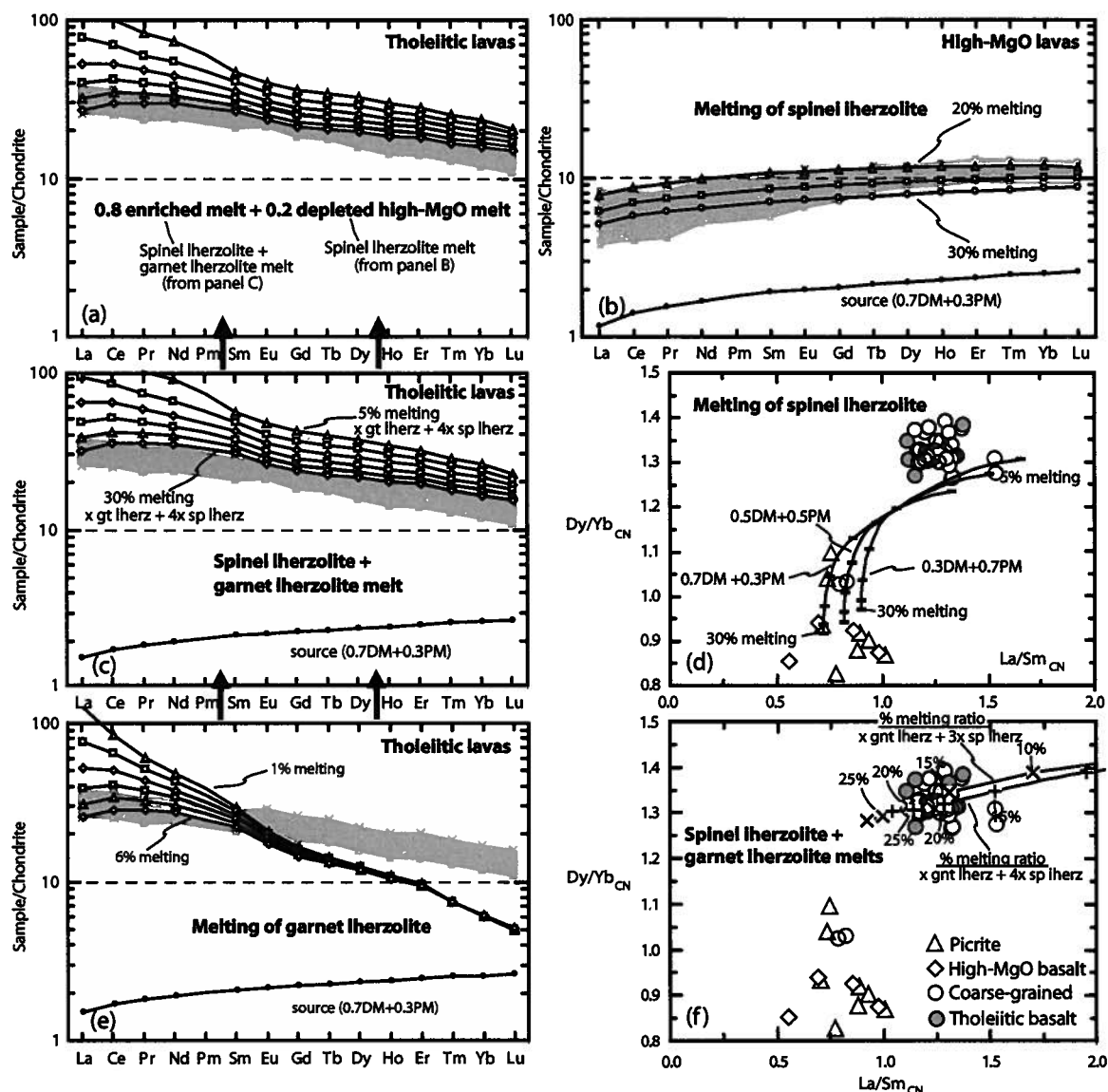


**Figure 2.15** Trace-element modeling results for incongruent dynamic mantle melting for picritic and tholeiitic lavas from the Karmutsen Formation. Three steps of modeling for tholeiitic lavas are shown (order of modeling is shown going upwards from panel e to c to a, following the arrows): (e) Melting of garnet lherzolite, (c) Mixing of garnet and spinel lherzolite melts, and (a) Mixing of enriched tholeiitic and depleted picritic melts. (b) Melting of spinel lherzolite for high-MgO lavas. Shaded field is the range of REE patterns for Karmutsen tholeiitic basalts in panels a, c, and e and for picrites in panel b. Patterns with symbols in panels a, b, c, and e are modeling results (patterns are 5% melting increments in panels a and c and 1% increments in panel e). Abbreviations are: PM, primitive mantle; DM, depleted MORB mantle; gt lherz, garnet lherzolite; sp lherz, spinel lherzolite. The ratios of percent melting for garnet and spinel lherzolite are indicated in panel c. A range of proportion of source components (0.7DM:0.3PM to 0.9DM:0.1PM) can reproduce the variation in high-MgO lavas. (d)  $Dy/Yb_{CN}$  vs.  $La/Sm_{CN}$  for results of spinel lherzolite melting modeling and Karmutsen samples. Tickmarks are 5% increments and proportions of mantle source components are labelled next to curves. (f)  $Dy/Yb_{CN}$  vs.  $La/Sm_{CN}$  for results of spinel lherzolite + garnet lherzolite melting modeling and Karmutsen samples. Melting modeling uses the formulation of Zou & Reid (2001), an example calculation is shown in their Appendix. PM from McDonough & Sun (1995) and DM from Salters & Stracke (2004). Melt reaction coefficients of spinel lherzolite from Kinzler & Grove (1992) and garnet lherzolite from Walter (1998). Partition coefficients from Salters & Stracke (2004) and Shaw (2000) were kept constant. Source mineralogy for spinel lherzolite (0.18cpx:0.27opx:0.52ol:0.03sp) from Kinzler (1997) and for garnet lherzolite (0.34cpx:0.08opx:0.53ol:0.05gt) from Salters & Stracke (2004). A source composition with mantle components up to 0.3 PM and 0.7 depleted mantle can reproduce REE patterns similar to those of the high-MgO lavas, with best fits for a melt fraction of 0.22-0.25. Concentrations of tholeiitic basalts cannot easily be reproduced from an entirely primitive or depleted source. A range of source compositions (0.7DM:0.3PM to 0.3DM:0.7PM) and garnet and spinel lherzolite melt mixtures generate similar results ( $x$  gt lherz +  $3x$  sp lherz to  $x$  gt lherz +  $4x$  sp lherz; where  $x$  is percent melting in the interval of modeling; the ratio of the respective melt proportions in the aggregate melt was kept constant).

generated the depleted high-MgO Karmutsen lavas. However, the modeling results indicate that this earlier melting was not necessary for their formation, depending on the original trace-element composition of the source. Shallow, high-degree melting would preferentially sample depleted regions, whereas deeper, low-degree melting may not sample more refractory, depleted regions (e.g. Caribbean; Escuder-Virueze *et al.*, 2007). Decompression melting within the mantle plume initiated within the garnet stability field at high mantle potential temperature ( $T_p > 1450^\circ\text{C}$ ) and proceeded beneath oceanic arc lithosphere within the spinel field where more extensive degrees of melting could occur.

### **Magmatic evolution of Karmutsen tholeiitic basalts**

Primary magmas in LIPs leave extensive coarse-grained residues within or below the crust and these mafic and ultramafic plutonic sequences represent a significant proportion of the original magma that partially crystallized at depth (e.g. Farnetani *et al.*, 1996). For example, seismic and petrological studies of Ontong Java (e.g. Farnetani *et al.*, 1996), combined with the use of MELTS (Ghiorso & Sack, 1995), indicate that the volcanic sequence may have been only ~40% of the total magma reaching the Moho. Neal *et al.* (1997) estimated between 7 and 14 km of cumulate thickness corresponding with 11 to 22 km of flood basalt, depending on the presence of pre-existing oceanic crust and the total crustal thickness (25-35 km), and that 30-45% fractional crystallization took place for Ontong Java magmas. Interpretations of seismic velocity measurements suggest the presence of pyroxene and gabbroic cumulates ~9-16 km thick beneath the Ontong Java Plateau (e.g. Hussong *et al.*, 1979).

Wrangellia is characterized by high crustal velocities in seismic refraction lines, which is indicative of mafic plutonic rocks extending to depth beneath Vancouver Island (Clowes *et al.*, 1995). Wrangellia crust is ~25-30 km thick beneath Vancouver Island and is underlain by a strongly reflective zone of high velocity and density that has been interpreted as a major shear zone where lower Wrangellia lithosphere was detached (Clowes *et al.*, 1995). The vast majority of Karmutsen flows are evolved tholeiitic lavas (e.g. low MgO, high FeO/MgO) indicating an important role for partial crystallization of melts at low pressure, and a significant portion of the crust beneath Vancouver Island has seismic properties that are consistent with crystalline residues from partially crystallized



Karmutsen magmas. To test the proportion of the primary magma that fractionated within the crust, MELTS (Ghiorso & Sack, 1995) was used to simulate fractional crystallization using several estimated primary magma compositions from modeling results using PRIMELT1. The major-element composition of primary magmas could not be estimated for the tholeiitic basalts due to extensive plag + cpx + ol fractionation, and thus the MELTS modeling of the picrites is used as a proxy for the evolution of major elements in the volcanic sequence. A pressure of 1 kbar was used with variable water contents (anhydrous and 0.2 wt % H<sub>2</sub>O), calculated at the quartz-fayalite-magnetite (QFM) oxygen buffer. Experimental results from Ontong Java indicate that most crystallization occurs in magma chambers shallower than 6 km deep (<2 kbar; Sano & Yamashita, 2004); however, some crystallization may take place at greater depths (3-5 kbar; Farnetani *et al.*, 1996).

A selection of the MELTS results are shown in Figure 2.16. Olivine and spinel crystallize at high temperature until ~15-20 wt % of the liquid mass has fractionated, and the residual magma contains 9-10 wt % MgO (Fig. 2.16). At 1235-1225°C, plagioclase begins crystallizing and between 1235 and 1190°C olivine ceases crystallizing and clinopyroxene saturates (Fig. 2.16). As expected, the addition of clinopyroxene and plagioclase to the crystallization sequence causes substantial changes in the composition of the residual liquid; FeO and TiO<sub>2</sub> increase and Al<sub>2</sub>O<sub>3</sub> and CaO decrease, while the decrease in MgO lessens considerably (Fig. 2.16). In general, the compositions of the predicted residual liquids follow trends for compositions of Karmutsen lavas, but miss some of the low MgO, high CaO basalts (some of which are due to plag accumulation). Also, trends in Al<sub>2</sub>O<sub>3</sub> and CaO of Karmutsen basalts are not clearly decreasing with decreasing MgO. Increasing the crystallization pressure slightly and water content of the melts does not systematically improve the match to the observed data.

The MELTS results indicate that a significant proportion of crystallization takes place before plagioclase (~15-20% crystallization) and clinopyroxene (~35-45% crystallization) join the crystallization sequence. These results suggest >45% crystallization of primary magmas occurred (estimated from residual liquid % in Fig. 2.16) and, if the original flood basalt stratigraphy on Vancouver Island was ~6 km, at least an equivalent amount of complementary plutonic rocks should have crystallized.

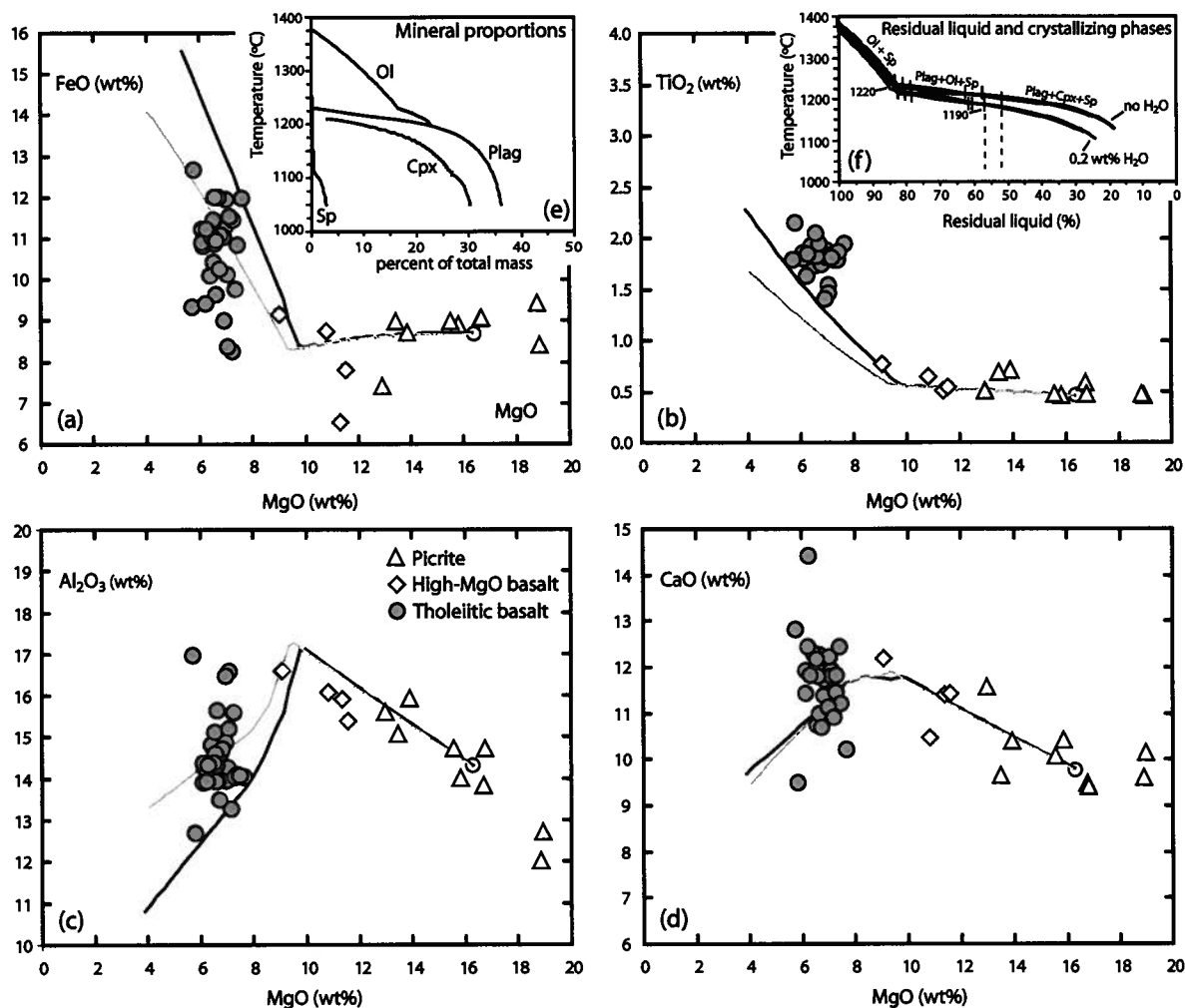


**Figure 2.16** Forward fractional crystallization modeling results for major elements from MELTS (Ghiorso & Sack, 1995) compared to picritic and tholeiitic lavas from the Karmutsen Formation. (a), (b), (c), and (d) are major-element compositions of residual liquids compared to Karmutsen lava compositions. For clarity, the results are only shown for one starting composition (white circle), using the composition of the estimated primary magma for the high-MgO lava series from the modeling technique of Herzberg *et al.* (2007) for sample 4723A13, as shown in Fig. 2.12. The estimated primary magmas for samples 4723A3 and 93G171 yield similar results. A pressure of 1 kbar was used with no H<sub>2</sub>O and 0.2 wt % H<sub>2</sub>O, calculated at QFM. Black line is anhydrous and grey line is 0.2 wt % H<sub>2</sub>O. The end-point for the anhydrous result is at 78% fractionation and 1130°C and the end-point for the result with 0.2 wt % H<sub>2</sub>O is 75% fractionation and 1110°C. (e) Mineral proportions of crystallized phases from one MELT run (sample 4723A13) with no H<sub>2</sub>O. (f) Percent residual liquid vs. temperature labelled with intervals of crystallizing phases.

The Karmutsen basalts and their plutonic residues thus represent a significant addition of crust (perhaps >12 km thickness), previously thickened by Paleozoic arc activity.

## CONCLUSION

The Karmutsen Formation covers ~20,000 km<sup>2</sup> of Vancouver Island, British Columbia, and was constructed as a large oceanic plateau during a single phase over a geologically short interval (ca. 230 Ma). The tripartite volcanic stratigraphy on Vancouver Island is upwards of 6 km of submarine flows, volcanoclastic deposits, and massive sheet flows; these volcanological differences are primarily related to the eruption environment (deep-water, shallow-water, subaerial). The rapid growth of the plateau prevented intervening sediments from accumulating, except in the uppermost stratigraphy where isolated limestone lenses commonly associated with pillowed and volcanoclastic basalts preserve a record of the subsidence history of the plateau.

The Wrangellia plateau on Vancouver Island was constructed dominantly of tholeiitic basalt with a restricted major- and trace-element, and isotopic, composition. Picritic pillow basalts erupted in the middle to latter portion of the submarine phase. Modeling results of Karmutsen picrites indicate melting of anomalously hot mantle (~1500°C) and extensive degrees of partial melting (23-27%) and are consistent with a plume initiation model. The lavas that built the volcanic edifice were derived from an isotopically relatively uniform depleted mantle source distinct from the source of MORB. There are compositional similarities between the source of Karmutsen basalts on Vancouver Island and the sources of ocean islands (e.g. Hawaii) and plateaus (e.g. Ontong Java) in the Pacific Ocean. The Karmutsen basalts erupted atop Paleozoic arc volcanic sequences, but there is no clear evidence from our work on Vancouver Island of significant involvement of arc or continental material in formation of the basalts. Picrites formed from melting of spinel lherzolite with a depleted mantle isotopic composition similar to the source of the tholeiitic basalt. The tholeiitic basalts underwent extensive low-pressure fractionation (<2-3 kbar) and seismic work indicates some of the Wrangellia crust beneath Vancouver Island may correspond to the plutonic residues of the Karmutsen Formation.

## ACKNOWLEDGEMENTS

We would like to thank Nick Arndt for helping us get this project started and Nick Massey for insights into Vancouver Island geology. We would also like to thank Claude Herzberg for his kind help with modeling techniques. We are grateful to Mikkel Schau for his insight and enthusiasm during fieldwork. Jane Barling assisted with analyses by MC-ICP-MS. Funding was generously provided by the Rocks to Riches Program administered by the BC & Yukon Chamber of Mines in 2004, by the BC Geological Survey in 2005, and by NSERC Discovery Grants to J. Scoates and D. Weis. A. Greene was supported by a University Graduate Fellowship at UBC.

## REFERENCES

- Babbs, T. L. (1997). Geochemical and petrological investigations of the deeper portions of the Ontong Java Plateau: Malaita, Solomon Islands. Unpublished Ph.D. dissertation, Leicester University, U.K.
- Barker, F., Brown, A. S., Budahn, J. R. & Plafker, G. (1989). Back-arc with frontal-arc component origin of Triassic Karmutsen basalt, British Columbia, Canada. *Chemical Geology* **75**, 81-102.
- Blichert-Toft, J., Weis, D., Maerschalk, C., Agranier, A. & Albarède, F. (2003). Hawaiian hot spot dynamics as inferred from the Hf and Pb isotope evolution of Mauna Kea volcano. *Geochemistry Geophysics Geosystems* **4**(2), 1-27, doi:10.1029/2002GC000340.
- Carlisle, D. (1963). Pillow breccias and their aquagene tuffs, Quadra Island, British Columbia. *Journal of Geology* **71**, 48-71.
- Carlisle, D. (1972). Late Paleozoic to Mid-Triassic sedimentary-volcanic sequence on Northeastern Vancouver Island. *Geological Society of Canada Paper*. Report of Activities 72-1, Part B, 24-30 p.
- Carlisle, D. & Suzuki, T. (1974). Emergent basalt and submergent carbonate-clastic sequences including the Upper Triassic Dilleri and Welleri zones on Vancouver Island. *Canadian Journal of Earth Sciences* **11**, 254-279.
- Chauvel, C. & Blichert-Toft, J. (2001). A hafnium isotope and trace element perspective on melting of the depleted mantle. *Earth and Planetary Science Letters* **190**, 137-151.
- Chayes, F. (1954). The theory of thin-section analysis. *Journal of Geology* **62**, 92-101.
- Cho, M., Liou, J. G. & Maruyama, S. (1987). Transition from the zeolite to prehnite-pumpellyite facies in the Karmutsen metabasites, Vancouver Island, British Columbia. *Journal of Petrology* **27**(2), 467-494.
- Clowes, R. M., Zelt, C. A., Amor, J. R. & Ellis, R. M. (1995). Lithospheric structure in the southern Canadian Cordillera from a network of seismic refraction lines. *Canadian Journal of Earth Sciences* **32**(10), 1485-1513.
- Coffin, M. F. & Eldholm, O. (1994). Large igneous provinces: Crustal structure, dimensions, and external consequences. *Reviews of Geophysics* **32**(1), 1-36.

- Escuder-Virueite, J., Pérez-Estaún, A., Contreras, F., Joubert, M., Weis, D., Ullrich, T. D. & Spadea, P. (2007). Plume mantle source heterogeneity through time: Insights from the Duarte Complex, Hispaniola, northeastern Caribbean. *Journal of Geophysical Research* **112**(B04203), doi:10.1029/2006JB004323.
- Farnetani, C. G., Richards, M. A. & Ghiorso, M. S. (1996). Petrological models of magma evolution and deep crustal structure beneath hotspots and flood basalt provinces. *Earth and Planetary Science Letters* **143**, 81-94.
- Fitton, J. G. & Godard, M. (2004). Origin and evolution of magmas on the Ontong Java Plateau. In: Fitton, J. G., Mahoney, J. J., Wallace, P. J. & Saunders, A. D. (eds.) *Origin and Evolution of the Ontong Java Plateau*. Special Publication 229 Geological Society, pp. 151-178.
- Frey, F. A., Huang, S., Blichert-Toft, J., Regelous, M. & Boyet, M. (2005). Origin of depleted components in basalt related to the Hawaiian hotspot: Evidence from isotopic and incompatible element ratios. *Geochemistry Geophysics Geosystems* **6**(1), 23, doi:10.1029/2004GC000757.
- Galer, S. J. G. & Abouchami, W. (1998). Practical application of lead triple spiking for correction of instrumental mass discrimination. *Mineralogical Magazine* **62A**, 491-492.
- Ghiorso, M. S. & Sack, R. O. (1995). Chemical mass transfer in magmatic processes, IV. A revised and internally consistent thermodynamic model for the interpolation and extrapolation of liquid-solid equilibria in magmatic systems at elevated temperatures and pressures. *Contributions to Mineralogy and Petrology* **119**, 197-212.
- Greene, A. R., Scoates, J. S., Nixon, G. T. & Weis, D. (2006). Picritic lavas and basal sills in the Karmutsen flood basalt province, Wrangellia, northern Vancouver Island. In: Grant, B. (ed.) *Geological Fieldwork 2005*. Paper 2006-1 British Columbia Ministry of Energy, Mines and Petroleum Resources, pp. 39-52.
- Greene, A. R., Scoates, J. S. & Weis, D. (2005). Wrangellia Terrane on Vancouver Island: Distribution of flood basalts with implications for potential Ni-Cu-PGE mineralization. In: Grant, B. (ed.) *Geological Fieldwork 2004*. Paper 2005-1 British Columbia Ministry of Energy, Mines and Petroleum Resources, pp. 209-220.
- Hauff, F., Hoernle, K. & Schmidt, A. (2003). Sr-Nd-Pb composition of Mesozoic Pacific oceanic crust (Site 1149 and 801, ODP Leg 185): Implications for alteration of ocean crust and the input into the Izu-Bonin-Mariana subduction system. *Geochemistry Geophysics Geosystems* **4**(8), doi:10.1029/2002GC000421.
- Hauff, F., Hoernle, K., Tilton, G., Graham, D. W. & Kerr, A. C. (2000). Large volume recycling of oceanic lithosphere over short time scales: geochemical constraints from the Caribbean Large Igneous Province. *Earth and Planetary Science Letters* **174**, 247-263.
- Herzberg, C. (2004). Partial melting below the Ontong Java Plateau. In: Fitton, J. G., Mahoney, J. J., Wallace, P. J. & Saunders, A. D. (eds.) *Origin and Evolution of the Ontong Java Plateau*. Special Publication 229 Geological Society, pp. 179-183.
- Herzberg, C. (2006). Petrology and thermal structure of the Hawaiian plume from Mauna Kea volcano. *Nature* **444**(7119), 605.

- Herzberg, C., Asimow, P. D., Arndt, N., Niu, Y., Leshner, C. M., Fitton, J. G., Cheadle, M. J. & Saunders, A. D. (2007). Temperatures in ambient mantle and plumes: Constraints from basalts, picrites, and komatiites. *Geochemistry Geophysics Geosystems* **8**(Q02006), doi:10.1029/2006GC001390.
- Herzberg, C. & O'Hara, M. J. (2002). Plume-associated ultramafic magmas of Phanerozoic age. *Journal of Petrology* **43**(10), 1857-1883.
- Huang, S. & Frey, F. A. (2005). Trace element abundances of Mauna Kea basalt from phase 2 of the Hawaii Scientific Drilling Project: Petrogenetic implications of correlations with major element content and isotopic ratios. *Geochemistry Geophysics Geosystems* **4**(6), 43, doi:10.1029/2002GC000322.
- Hussong, D. M., Wipperfurth, L. K. & Kroenke, L. W. (1979). The crustal structure of the Ontong Java and Manihiki Oceanic Plateaus. *Journal of Geophysical Research* **84**(B11), 6,003-6,010.
- Janney, P. E., Le Roex, A. P. & Carlson, R. W. (2005). Hafnium isotope and trace element constraints on the nature of mantle heterogeneity beneath the Central Southwest Indian Ridge (13°E to 47°E). *Journal of Petrology* **46**(12), 2427-2464, 10.1093/petrology/egi060.
- Jones, D. L., Silberling, N. J. & Hillhouse, J. (1977). Wrangellia; a displaced terrane in northwestern North America. *Canadian Journal of Earth Sciences* **14**(11), 2565-2577.
- Kempton, P. D., Pearce, J. A., Barry, T. L., Fitton, J. G., Langmuir, C. H. & Christie, D. M. (2002). Sr-Nd-Pb-Hf isotope results from ODP Leg 187: Evidence for mantle dynamics of the Australian-Antarctic Discordance and origin of the Indian MORB source. *Geochemistry Geophysics Geosystems* **3**(12), 1074, doi:10.1029/2002GC000320.
- Kerr, A. C. (2003). Oceanic Plateaus. In: Rudnick, R. (ed.) *The Crust*. Treatise on Geochemistry Vol. 3. Holland, H. D. & Turekian, K. K. (eds.) Elsevier Science: Oxford, pp. 537-565.
- Kerr, A. C. & Mahoney, J. J. (2007). Oceanic plateaus: Problematic plumes, potential paradigms. *Chemical Geology* **241**, 332-353.
- Kerr, A. C., Marriner, G. F., Tarney, J., Nivia, A., Saunders, A. D., Thirlwall, M. F. & Sinton, A. C. (1997). Cretaceous basaltic terranes in Western Columbia: Elemental, chronological and Sr-Nd isotopic constraints on petrogenesis. *Journal of Petrology* **38**(6), 677-702.
- Kerr, A. C., Tarney, J., Marriner, G. F., Klaver, G. T., Saunders, A. D. & Thirlwall, M. F. (1996). The geochemistry and petrogenesis of the Late-Cretaceous picrites and basalts of Curacao, Netherlands Antilles; a remnant of an oceanic plateau. *Contributions to Mineralogy and Petrology* **124**(1), 29-43.
- Kerr, A. C., Tarney, J., Nivia, A., Marriner, G. F. & Saunders, A. D. (1998). The internal structure of oceanic plateaus: inferences from obducted Cretaceous terranes in western Columbia and the Caribbean. *Tectonophysics* **292**, 173-188.
- Kinzler, R. J. (1997). Melting of mantle peridotite at pressures approaching the spinel to garnet transition: Application to mid-ocean ridge basalt petrogenesis. *Journal of Geophysical Research* **102**(B1), 853-874.
- Kinzler, R. J. & Grove, T. L. (1992). Primary magmas of mid-ocean ridge basalts 1. Experiments and methods. *Journal of Geophysical Research* **97**(B5), 6,885-6,906.

- Korenaga, J. (2005). Why did not the Ontong Java Plateau form subaerially? *Earth and Planetary Science Letters* **234**, 385- 399.
- Kuniyoshi, S. (1972). Petrology of the Karmutsen (Volcanic) Group, northeastern Vancouver Island, British Columbia. Unpublished Ph.D. dissertation, University of California, Los Angeles. 242 pp.
- Lassiter, J. C., DePaolo, D. J. & Mahoney, J. J. (1995). Geochemistry of the Wrangellia flood basalt province: Implications for the role of continental and oceanic lithosphere in flood basalt genesis. *Journal of Petrology* **36**(4), 983-1009.
- Longhi, J. (2002). Some phase equilibrium systematics of lherzolite melting: I. *Geochemistry Geophysics Geosystems* **3**(3), 10.1029/2001GC000204.
- MacDonald, G. A. & Katsura, T. (1964). Chemical composition of Hawaiian lavas. *Journal of Petrology* **5**, 82-133.
- Mahoney, J. J. (1987). An isotopic survey of Pacific oceanic plateaus: implications for their nature and origin. In: Keating, B. H., Fryer, P., Batiza, R. & Boehlert, G. W. (eds.) *Seamounts, Islands, and Atolls*. American Geophysical Union: Washington, D.C. Geophysical Monograph 43, pp. 207-220.
- Mahoney, J., LeRoex, A. P., Peng, Z., Fisher, R. L. & Natland, J. H. (1992). Southwestern Limits of Indian Ocean Ridge Mantle and the Origin of Low  $^{206}\text{Pb}/^{204}\text{Pb}$  Mid-Ocean Ridge Basalt: Isotope Systematics of the Central Southwest Indian Ridge (17°-50°E). *Journal of Geophysical Research* **97**(B13), 19771-19790.
- Mahoney, J., Storey, M., Duncan, R., Spencer, K. & Pringle, M. (1993). Geochemistry and age of the Ontong Java Plateau. In: Pringle, M., Sager, W. & Sliter, W. (eds.) *AGU Monograph on the Mesozoic Pacific: Geology, Tectonics, and Volcanism*. 77 AGU: Washington, pp. 233-261.
- Mahoney, J. J., Sinton, J. M., Kurz, M. D., MacDougall, J. D., Spencer, K. J. & Lugmair, G. W. (1994). Isotope and trace element characteristics of a super-fast spreading ridge: East Pacific rise, 13-23°S. *Earth and Planetary Science Letters* **121**, 173-193.
- Massey, N. W. D. (1995a). Geology and mineral resources of the Alberni-Nanaimo Lakes sheet, Vancouver Island 92F/1W, 92F/2E, and part of 92F/7E. *British Columbia Ministry of Energy, Mines and Petroleum Resources*. Paper 1992-2, 132 p.
- Massey, N. W. D. (1995b). Geology and mineral resources of the Cowichan Lake sheet, Vancouver Island 92C/16. *British Columbia Ministry of Energy, Mines and Petroleum Resources*. Paper 1992-3, 112 p.
- Massey, N. W. D., MacIntyre, D. G., Desjardins, P. J. & Cooney, R. T. (2005a). Digital Geology Map of British Columbia: Tile NM9 Mid Coast, B.C. *B.C. Ministry of Energy and Mines* Geofile 2005-2.
- Massey, N. W. D., MacIntyre, D. G., Desjardins, P. J. & Cooney, R. T. (2005b). Digital Geology Map of British Columbia: Tile NM10 Southwest B.C. *B.C. Ministry of Energy and Mines* Geofile 2005-3.
- McDonough, W. F. & Sun, S. (1995). The composition of the Earth. *Chemical Geology* **120**, 223-253.
- Monger, J. W. H. & Journeay, J. M. (1994). Basement geology and tectonic evolution of the Vancouver region. In: Monger, J. W. H. (ed.) *Geology and Geological*

- Hazards of the Vancouver Region, Southwestern British Columbia*. Geological Survey of Canada Bulletin, 481, pp. 3-25.
- Muller, J. E. (1977). Geology of Vancouver Island. *Geological Survey of Canada Open File Map 463*.
- Muller, J. E. (1980). The Paleozoic Sicker Group of Vancouver Island, British Columbia. *Geological Survey of Canada*. Paper 79-30, 22 p.
- Muller, J. E., Northcote, K. E. & Carlisle, D. (1974). Geology and mineral deposits of Alert Bay - Cape Scott map area, Vancouver Island, British Columbia. *Geological Survey of Canada, Paper 74-8*, 77.
- Neal, C. R., Mahoney, J. J., Kroenke, L. W., Duncan, R. A. & Petterson, M. G. (1997). The Ontong-Java Plateau. In: Mahoney, J. J. & Coffin, M. F. (eds.) *Large Igneous Provinces: Continental, Oceanic, and Planetary Flood Volcanism*. Geophysical Monograph 100 AGU: Washington, pp. 183-216.
- Niu, Y., Collerson, K. D., Batiza, R., Wendt, J. I. & Regelous, M. (1999). Origin of enriched-typed mid-ocean ridge basalt at ridges far from mantle plumes: The East Pacific Rise at 11°20'N. *Journal of Geophysical Research* **104**, 7067-7088.
- Nixon, G. T., Hammack, J. L., Koyanagi, V. M., Payie, G. J., Haggart, J. W., Orchard, M. J., Tozer, T., Friedman, R. M., D.A., A., Palfy, J. & Cordey, F. (2006a). Geology of the Quatsino – Port McNeill area, northern Vancouver Island. *BC Ministry of Energy, Mines and Petroleum Resources*. Geoscience Map 2006-2, scale 1:50 000.
- Nixon, G. T., Kelman, M. C., Stevenson, D., Stokes, L. A. & Johnston, K. A. (2006b). Preliminary geology of the Nimpkish map area (NTS 092L/07), northern Vancouver Island, British Columbia. In: Grant, B. & Newell, J. M. (eds.) *Geological Fieldwork 2005*. Paper 2006-1 British Columbia, Ministry of Energy, Mines and Petroleum Resources, pp. 135-152.
- Nixon, G. T., Laroque, J., Pals, A., Styant, J., Greene, A. R. & Scoates, J. S. (2008). High-Mg lavas in the Karmutsen flood basalts, northern Vancouver Island (NTS 092L): Stratigraphic setting and metallogenic significance. In: Grant, B. (ed.) *Geological Fieldwork 2007*. Paper 2008-1 British Columbia, Ministry of Energy, Mines and Petroleum Resources, pp. 175-190.
- Nixon, G. T. & Orr, A. J. (2007). Recent revisions to the Early Mesozoic stratigraphy of Northern Vancouver Island (NTS 102I; 092L) and metallogenic implications, British Columbia. In: Grant, B. (ed.) *Geological Fieldwork 2006*. Paper 2007-1 British Columbia, Ministry of Energy, Mines and Petroleum Resources, pp. 163-177.
- Nobre Silva, I. G., Weis, D., Barling, J. & Scoates, J. S. (submitted). Leaching systematics for the determination of high-precision Pb isotope compositions of ocean island basalts. *Geochemistry, Geophysics, Geosystems* 2007GC001891.
- Nowell, G. M., Kempton, P. D., Noble, S. R., Fitton, J. G., Saunders, A., Mahoney, J. J. & Taylor, R. N. (1998). High precision Hf isotope measurements of MORB and OIB by thermal ionisation mass spectrometry: insights into the depleted mantle. *Chemical Geology* **149**, 211-233.
- Parrish, R. R. & McNicoll, V. J. (1992). U-Pb age determinations from the southern Vancouver Island area, British Columbia. *Geological Survey of Canada*. Radiogenic Age and Isotopic Studies: Report 5 Paper 91-2, 79-86 p.



- Pretorius, W., Weis, D., Williams, G., Hanano, D., Kieffer, B. & Scoates, J. S. (2006). Complete trace elemental characterization of granitoid (USGSG-2, GSP-2) reference materials by high resolution inductively coupled plasma-mass spectrometry. *Geostandards and Geoanalytical Research* **30**(1), 39-54.
- Regelous, M., Niua, Y., Wendt, J. I., Batizab, R., Greiga, A. & Collerson, K. D. (1999). Variations in the geochemistry of magmatism on the East Pacific Rise at 10°30'N since 800 ka. *Earth and Planetary Science Letters* **168**, 45-63.
- Révilion, S., Chauvel, C., Arndt, N. T., Pik, R., Martineau, F., Fourcade, S. & Marty, B. (2002). Heterogeneity of the Caribbean plateau mantle source: Sr, O and He isotopic compositions of olivine and clinopyroxene from Gorgona Island. *Earth and Planetary Science Letters* **205**(1-2), 91.
- Rhodes, J. M. (1996). Geochemical stratigraphy of lava flows samples by the Hawaii Scientific Drilling Project. *Journal of Geophysical Research* **101**(B5), 11,729-11,746.
- Rhodes, J. M. & Vollinger, M. J. (2004). Composition of basaltic lavas sampled by phase-2 of the Hawaii Scientific Drilling Project: Geochemical stratigraphy and magma types. *Geochemistry Geophysics Geosystems* **5**(3), doi:10.1029/2002GC000434.
- Richards, M. A., Jones, D. L., Duncan, R. A. & DePaolo, D. J. (1991). A mantle plume initiation model for the Wrangellia flood basalt and other oceanic plateaus. *Science* **254**, 263-267.
- Salters, V. J. & White, W. (1998). Hf isotope constraints on mantle evolution. *Chemical Geology* **145**, 447-460.
- Salters, V. J. M. (1996). The generation of mid-ocean ridge basalts from the Hf and Nd isotope perspective. *Earth and Planetary Science Letters* **141**, 109-123.
- Salters, V. J. M. & Stracke, A. (2004). Composition of the depleted mantle. *Geochemistry Geophysics Geosystems* **5**(Q05B07), doi:10.1029/2003GC000597.
- Sano, T. & Yamashita, S. (2004). Experimental petrology of basement lavas from Ocean Drilling Program Leg 192: implications for differentiation processes in Ontong Java Plateau magmas. In: Fitton, J. G., Mahoney, J. J., Wallace, P. J. & Saunders, A. D. (eds.) *Origin and Evolution of the Ontong Java Plateau*. Special Publications 229 Geological Society, pp. 185-218.
- Saunders, A. D. (2005). Large igneous provinces: Origin and environmental consequences. *Elements* **1**, 259-263.
- Scherer, E., Munker, C. & Mezger, K. (2001). Calibration of the lutetium-hafnium clock. *Science* **293**(5530), 683-687, 10.1126/science.1061372.
- Sluggett, C. L. (2003). Uranium-lead age and geochemical constraints on Paleozoic and Early Mesozoic magmatism in Wrangellia Terrane, Saltspring Island, British Columbia. Unpublished B.Sc. thesis, University of British Columbia. 84 pp.
- Surdam, R. C. (1967). Low-grade metamorphism of the Karmutsen Group. Unpublished Ph.D. dissertation, University of California, Los Angeles. 288 pp.
- Sutherland-Brown, A., Yorath, C. J., Anderson, R. G. & Dom, K. (1986). Geological maps of southern Vancouver Island, LITHOPROBE I 92C/10, 11, 14, 16, 92F/1, 2, 7, 8. *Geological Survey of Canada*. Open File 1272.
- Tejada, M. L. G., Mahoney, J. J., Castillo, P. R., Ingle, S. P., Sheth, H. C. & Weis, D. (2004). Pin-pricking the elephant: evidence on the origin of the Ontong Java

- Plateau from Pb-Sr-Hf-Nd isotopic characteristics of ODP Leg 192 basalts. In: Fitton, J. G., Mahoney, J. J., Wallace, P. J. & Saunders, A. D. (eds.) *Origin and Evolution of the Ontong Java Plateau*. Geological Society of London, Special Publication 229, pp. 133-150.
- Vervoort, J. D., Patchett, P., Blichert-Toft, J. & Albarède, F. (1999). Relationships between Lu-Hf and Sm-Nd isotopic systems in the global sedimentary system. *Earth and Planetary Science Letters* **168**, 79-99.
- Walter, M. J. (1998). Melting of garnet peridotite and the origin of komatiite and depleted lithosphere. *Journal of Petrology* **39**(1), 29-60.
- Weis, D., Kieffer, B., Maerschalk, C., Barling, J., de Jong, J., Williams, G. A., Hanano, D., Mattielli, N., Scoates, J. S., Goolaerts, A., Friedman, R. A. & Mahoney, J. B. (2006). High-precision isotopic characterization of USGS reference materials by TIMS and MC-ICP-MS. *Geochemistry Geophysics Geosystems* **7**(Q08006), doi:10.1029/2006GC001283.
- Weis, D., Kieffer, B., Hanano, D., Silva, I. N., Barling, J., Pretorius, W., Maerschalk, C. & Mattielli, N. (2007). Hf isotope compositions of U.S. Geological Survey reference materials. *Geochemistry Geophysics Geosystems* **8**(Q06006), doi:10.1029/2006GC001473.
- Weis, D., Kieffer, B., Maerschalk, C., Barling, J., de Jong, J., Williams, G. A., Hanano, D., Mattielli, N., Scoates, J. S., Goolaerts, A., Friedman, R. A. & Mahoney, J. B. (2006). High-precision isotopic characterization of USGS reference materials by TIMS and MC-ICP-MS. *Geochemistry Geophysics Geosystems* **7**(Q08006), doi:10.1029/2006GC001283.
- Wheeler, J. O. & McFeely, P. (1991). Tectonic assemblage map of the Canadian Cordillera and adjacent part of the United States of America. *Geological Survey of Canada Map* 1712A.
- White, W. M., Albarède, F. & Télouk, P. (2000). High-precision analysis of Pb isotope ratios by multi-collector ICP-MS. *Chemical Geology* **167**, 257-270.
- Yorath, C. J., Sutherland Brown, A. & Massey, N. W. D. (1999). LITHOPROBE, southern Vancouver Island, British Columbia. *Geological Survey of Canada. LITHOPROBE, southern Vancouver Island, British Columbia Bulletin* **498**, 145 p.
- Zou, H. (1998). Trace element fractionation during modal and non-modal dynamic melting and open-system melting: A mathematical treatment. *Geochimica et Cosmochimica Acta* **62**(11), 1937-1945.
- Zou, H. & Reid, M. R. (2001). Quantitative modeling of trace element fractionation during incongruent dynamic melting. *Geochimica et Cosmochimica Acta* **65**(1), 153-162.

## **CHAPTER 3**

### **Wrangellia Flood Basalts in Alaska: A Record of Plume-Lithosphere Interaction in a Late Triassic Accreted Oceanic Plateau**

<sup>1</sup>A version of this chapter has been submitted for publication.

## INTRODUCTION

Oceanic plateaus and continental flood basalts (CFBs) are produced from the largest melting events recorded on Earth. Oceanic plateaus and CFBs are transient large igneous provinces (LIPs) that form from unusually high magmatic fluxes over several million years or less (Saunders, 2005). The presence of transient LIPs in a variety of tectonic settings attests to large thermal anomalies that are not directly attributable to seafloor spreading processes. A longstanding controversy in many transient LIPs worldwide is the role of the mantle lithosphere in generation of the basaltic magmas. CFBs have compositions that indicate involvement of subcontinental lithospheric mantle and continental crust (e.g. Peate & Hawkesworth, 1996). Compositional evidence of plume-lithosphere interaction in oceanic plateaus, however, remains elusive because oceanic plateaus are less accessible. Oceanic plateaus are enormous volcanic edifices (2-4 km high) that are isolated from continents and form upon mid-ocean ridges, extinct arcs, detached or submerged continental fragments, or intraplate settings (Coffin *et al.*, 2006). The basalts that form oceanic plateaus have a better chance of avoiding interaction with continental lithosphere than basalts erupted along the margins or in the interiors of continents (Kerr & Mahoney, 2007).

A significant issue in the geochemistry of flood basalt provinces has been the origin of high- and low-titanium basalts within the flood basalt stratigraphy (e.g. Arndt *et al.*, 1993). Numerous flood basalt provinces have been found to possess two or more distinguishable groups of basalts based on titanium contents [e.g. Siberia (Wooden *et al.*, 1993); Emeishan (Xu *et al.*, 2001); Karoo (Cox *et al.*, 1967); Ferrar (Hornig, 1993); Paraná-Etendeka (Peate, 1997); Deccan (Melluso *et al.*, 1995); Ethiopia (Pik *et al.*, 1998); Columbia River Basalts (Hooper & Hawkesworth, 1993)]. In several of these provinces, the high- and low-titanium basalts are geographically distributed, and in several provinces these different lava types have a distinct stratigraphic distribution. However, all of these LIPs formed upon continental crust and are thought to have involved interaction with metasomatized lithospheric mantle or continental crust during parts of their eruptive history.

The Wrangellia flood basalts in Alaska erupted in the eastern Panthalassic Ocean over <5 Myr in the Middle to Late Triassic, with accretion to western North America

occurring in the Late Jurassic or Early Cretaceous (Jones *et al.*, 1977). The Wrangellia flood basalts form thick successions of flood basalts bounded by marine sediments that extend over widespread areas of Alaska, Yukon, and British Columbia (>2300 km in length). In south-central Alaska, parts of the complete flood basalt stratigraphy overlie Late Paleozoic oceanic arc crust and marine sediments and are overlain by Late Triassic limestone. Most of the 3.5-4 km of flood basalts in Alaska erupted subaerially, however, in areas of Alaska there are pillowed and volcanoclastic basalts in the lower part of the volcanic stratigraphy.

The Wrangellia flood basalts in Alaska provide an exceptional opportunity to examine the volcanic stratigraphy of an accreted oceanic plateau. While Ocean Drilling Program (ODP) and Deep Sea Drilling Program (DSDP) legs have drilled extant oceanic plateaus in the ocean basins, the vast majority of the stratigraphic sequence of oceanic plateaus remains generally unsampled and undescribed. This study examines volcanic stratigraphy, petrography, and geochemistry of flood basalts in the Wrangell Mountains and Alaska Range in south-central Alaska to determine the source and origin of high- and low-titanium basalts in the accreted Wrangellia oceanic plateau and the role of the pre-existing Paleozoic oceanic arc lithosphere.

A mantle plume origin was proposed for Wrangellia flood basalts by Richards *et al.* (1991) based on the large volume of flood basalts erupted in a short duration, the absence of evidence of rifting, and evidence of uplift prior to eruption of the flood basalts. The only previous modern analytical study of the Wrangellia flood basalts in Alaska involved major- and trace-element chemistry, and Sr, Nd, and Pb isotopic analyses, of 9 basalts from the Wrangell Mountains (Lassiter *et al.*, 1995). This present study is part of a larger research project on the origin and evolution of the Triassic Wrangellia flood basalts in British Columbia, Yukon, and Alaska (Greene *et al.*, 2008, submitted-b). The generation of compositionally distinct basalts in part of the Wrangellia oceanic plateau has implications for the interaction of mantle plumes and oceanic mantle modified by subduction.

## GEOLOGIC SETTING

### Wrangellia in Alaska

The Wrangellia Terrane, or Wrangellia, was defined by Jones *et al.* (1977) as a set of fault-bound crustal blocks with similar stratigraphy along the margin of western North America (Fig. 3.1). The Wrangellia flood basalts have been mapped as the Nikolai Formation in Alaska and Yukon (Northern Wrangellia) and the Karmutsen Formation on Vancouver and Queen Charlotte Islands (Southern Wrangellia). Three key aspects of Wrangellia led Jones and co-workers (1977) to suggest these crustal blocks formed as part of a once-contiguous terrane: thick sections of tholeiitic flood basalts directly overlie shale with Middle to Late Ladinian *Daonella*; similar-aged Late Triassic limestones overlie the flood basalts; and paleomagnetic evidence indicated that eruption of the flood basalts occurred at low latitude. Wrangellia may have joined with parts of the Alexander Terrane, primarily in southeast Alaska, as early as the Late Pennsylvanian (Gardner *et al.*, 1988) and may have been in close proximity to the Peninsular Terrane of southern Alaska by the Late Triassic (Rioux *et al.*, 2007).

Wrangellia extends ~450 km in an arcuate belt in the Wrangell Mountains, Alaska Range, and Talkeetna Mountains in southern Alaska (Fig. 3.1). The northwest margin of Wrangellia is one of the most prominent geophysical features in south-central Alaska and is exposed along the Talkeetna Suture Zone (Glen *et al.*, 2007). The suture between Wrangellia and transitional crust to the northwest is well-defined geophysically by a series of narrow gravity and magnetic highs along the Talkeetna Suture Zone, between dense, strongly magnetic Wrangellia crust and less dense, weakly magnetic crust beneath flysch basins to the northwest (Glen *et al.*, 2007). This area lies directly in the axis of the major orocline of southern Alaska, where structures curve from northwest- to northeast-trending (e.g. Plafker *et al.*, 1994; Fig. 3.1). The Wrangellia terrane is bounded by the Denali Fault to the northeast and extends more than 300 km to the southeast in Yukon where Wrangellia stratigraphy is very similar to Alaska (Fig. 3.1).

### *Wrangell Mountains*

Wrangellia stratigraphy is well-exposed in a northwest-trending belt extending ~100 km along the southern flank of the Wrangell Mountains in Wrangell-St. Elias

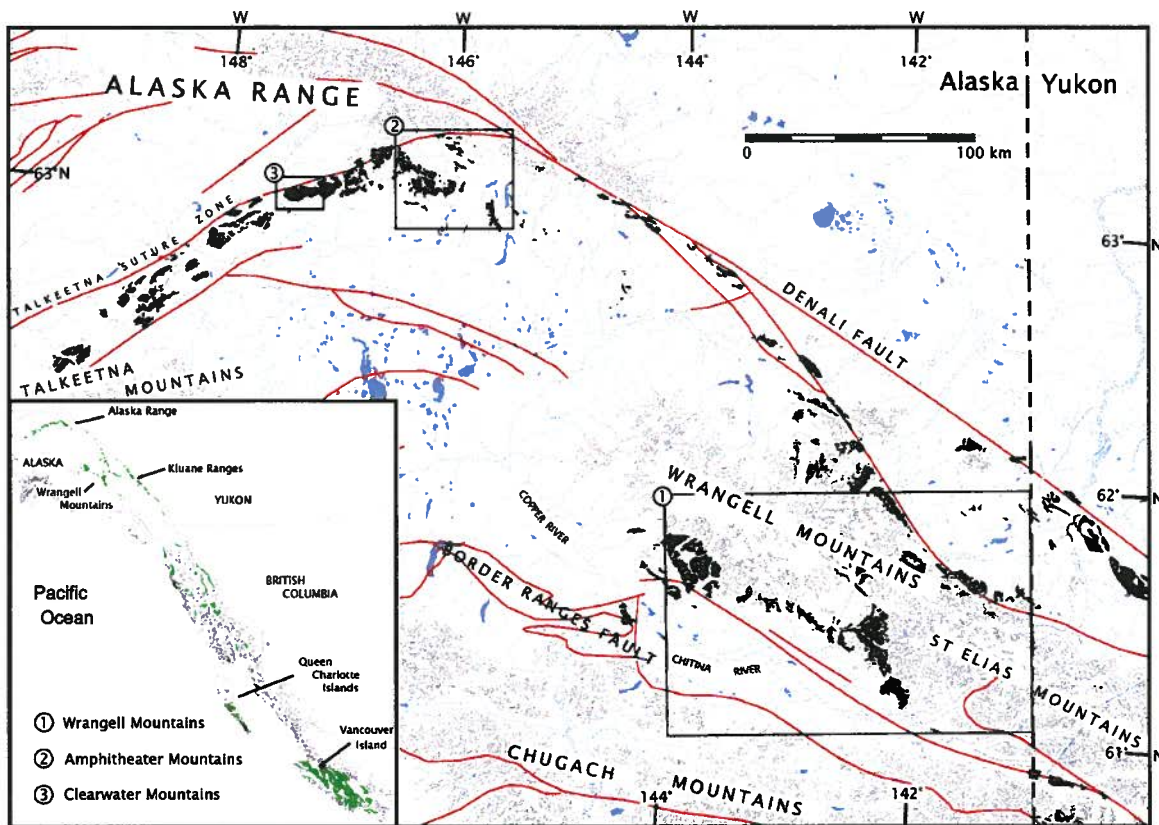


**Figure 3.1** Simplified map of south-central Alaska showing the distribution of the Nikolai Formation (black), derived from the GIS-based digital map compilations of Wilson *et al.* (1998, 2005) and Schmidt (pers. comm, 2006). The three main areas that were studied are outlined with boxes and indicated in the legend. The inset shows the extent of the Wrangellia flood basalts (green) in Alaska, Yukon, and British Columbia. The red lines are faults.

National Park (Fig. 3.2). The Nikolai Formation disconformably overlies the Skolai Group, which comprises Pennsylvanian to Early Permian volcanic arc sequences and marine sediments of the Station Creek and Hasen Creek Formations, respectively (Smith and MacKevett, 1970; Fig. 3.2). In most areas, Nikolai basalts unconformably overlie parts of the Hasen Creek Formation called the Golden Horn Limestone Lenticle (<250 m thick), which forms prominent yellow- and red-stained cliffs of bioclastic Early Permian limestone. Isolated lenses of *Daonella*-bearing Middle Triassic argillite (<100 m thick) lie between the top of the Golden Horn Limestone and the base of the Nikolai Formation (Smith and MacKevett, 1970). The Skolai Group is intruded by mafic and ultramafic intrusive bodies related to the Nikolai basalts. The Nikolai basalts cover ~1057 km<sup>2</sup> (4.2% of all Wrangellia flood basalts from Vancouver Island to central Alaska) within the McCarthy and Nabesna Quadrangles in Wrangell-St. Elias National Park and are approximately 3.5–4 km in total thickness. A cumulative thickness of over 3.5 km of marine sedimentary rocks, ranging in age from Late Triassic to Late Jurassic, overlies the Nikolai Formation in the Wrangell Mountains (MacKevett *et al.*, 1997). Volcanic successions of the Miocene to Holocene Wrangell volcanic field unconformably overlie Jurassic and Cretaceous sedimentary sequences (MacKevett, 1978; Richter *et al.*, 1990).

#### *Eastern Alaska Range*

The Nikolai Formation in the eastern Alaska Range and small areas of the Talkeetna Mountains covers 666 km<sup>2</sup> (2.6% of all Wrangellia flood basalts) mostly in the Mount Hayes and Healy Quadrangles, and is 3.5–4 km thick in the Amphitheater and Clearwater Mountains (Fig. 3.1). Volcanic and marine sedimentary sequences similar to the Late Paleozoic successions in the Wrangell Mountains underlie the Nikolai basalts in the Alaska Range (Nokleberg *et al.*, 1994). In the Amphitheater Mountains, a major feeder system for the Nikolai Formation stratigraphically underlies flood basalt stratigraphy within a well-preserved synform that contains exposures of mafic and ultramafic intrusive units. These are the most significant occurrence of plutonic rocks associated with flood basalts within Wrangellia. The upper part of the volcanic stratigraphy contains interbedded volcanic and sedimentary horizons (argillite and



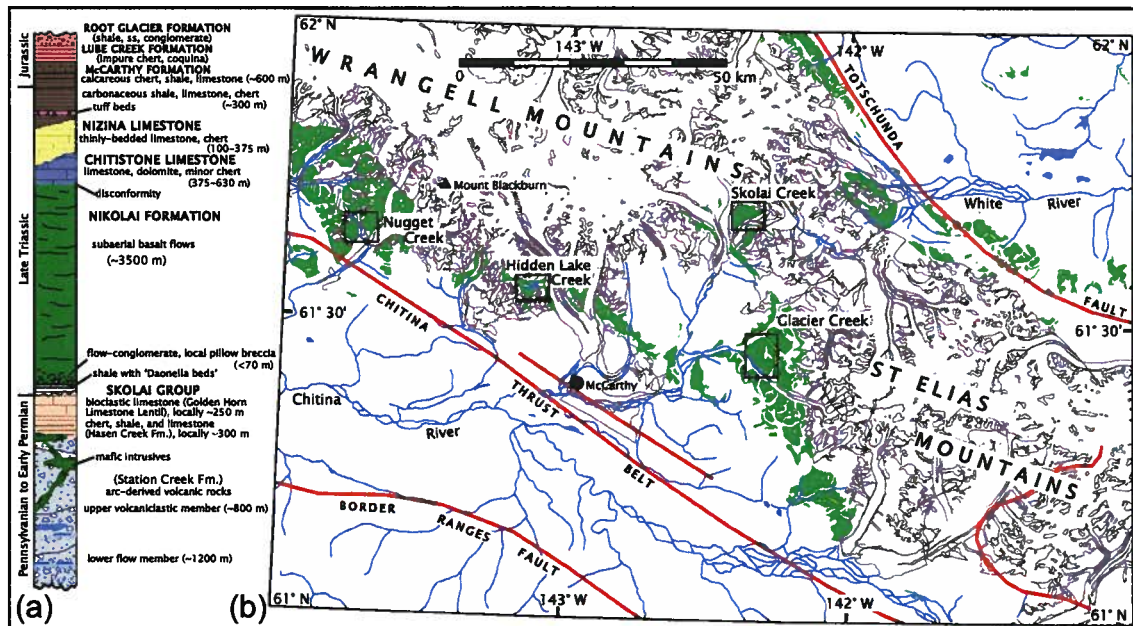


**Figure 3.2** Geologic map and stratigraphy of the Wrangell Mountains, Alaska (location shown in Figure 1). (a) Stratigraphic column depicts Late Paleozoic to Jurassic units on the south side of the Wrangell Mountains, derived from Smith and MacKevett (1970) and MacKevett (1978). (b) Simplified map showing the distribution of the Nikolai Formation (green) in the Wrangell Mountains, derived from the GIS-based digital map compilation of Wilson *et al.* (2005). The four areas of field study are outlined with labelled boxes. The red lines are faults.

limestone) that give way to fine-grained sedimentary strata, which are poorly exposed in the Amphitheater Mountains.

### **Age of the Nikolai Formation**

Biostratigraphy and geochronology provide bounds on the age and duration of emplacement of the Nikolai basalts. Fossil assemblages in finely laminated shale immediately beneath the Nikolai basalts in the Wrangell Mountains indicate a Middle to Late Ladinian age (McRoberts, pers. comm. 2007; Jones *et al.*, 1977) and fossils in limestone disconformably overlying the Nikolai Formation are Late Carnian to Early Norian (Armstrong & MacKevett, 1977; Plafker *et al.*, 1989). Five  $^{40}\text{Ar}/^{39}\text{Ar}$  plateau ages for hornblende and biotite from intrusive rocks in the Amphitheater Mountains in the Alaska Range interpreted to be comagmatic with Nikolai basalts indicate formation of these rocks at ~231-225 Ma (Bittenbender *et al.*, 2007; Schmidt & Rogers, 2007). Three Nikolai basalt samples from the Wrangell Mountains yielded  $^{40}\text{Ar}/^{39}\text{Ar}$  step-heating ages of  $228.3 \pm 5.2$ ,  $232.8 \pm 11.5$ , and  $232.4 \pm 11.9$  Ma (Lassiter, 1995).

## **VOLCANIC STRATIGRAPHY AND PETROGRAPHY**

Field studies in Alaska focussed in three general areas where parts of the entire flood basalt stratigraphy are well-exposed: the southern flank of the Wrangell Mountains, and the Amphitheater and Clearwater Mountains in the southern part of the eastern Alaska Range (Fig. 3.1).

In the Wrangell Mountains, field studies focussed in 4 areas: Skolai Creek, Glacier Creek, Hidden Lake Creek, and Nugget Creek (Fig. 3.2). The base of the Nikolai Formation is well-exposed near Skolai Creek, the type section for the underlying Paleozoic Skolai Group. At Skolai Creek, the base of the Nikolai Formation is basalt flow-conglomerate, pillow breccia, and minor pillow basalt. (Figs 3.2 and 3.3). Pebbles and cobbles comprise >30% of the basal flow-conglomerate and all the clasts appear to be derived from the underlying Skolai Group (Fig. 3.3). Middle to upper portions of the flood basalt stratigraphy are well-exposed above Glacier Creek, where massive maroon- and green-colored flows form monotonous sequences with amygdaloidal-rich horizons and no discernible erosional surfaces or sediments between flows (Fig. 3.4). The top of

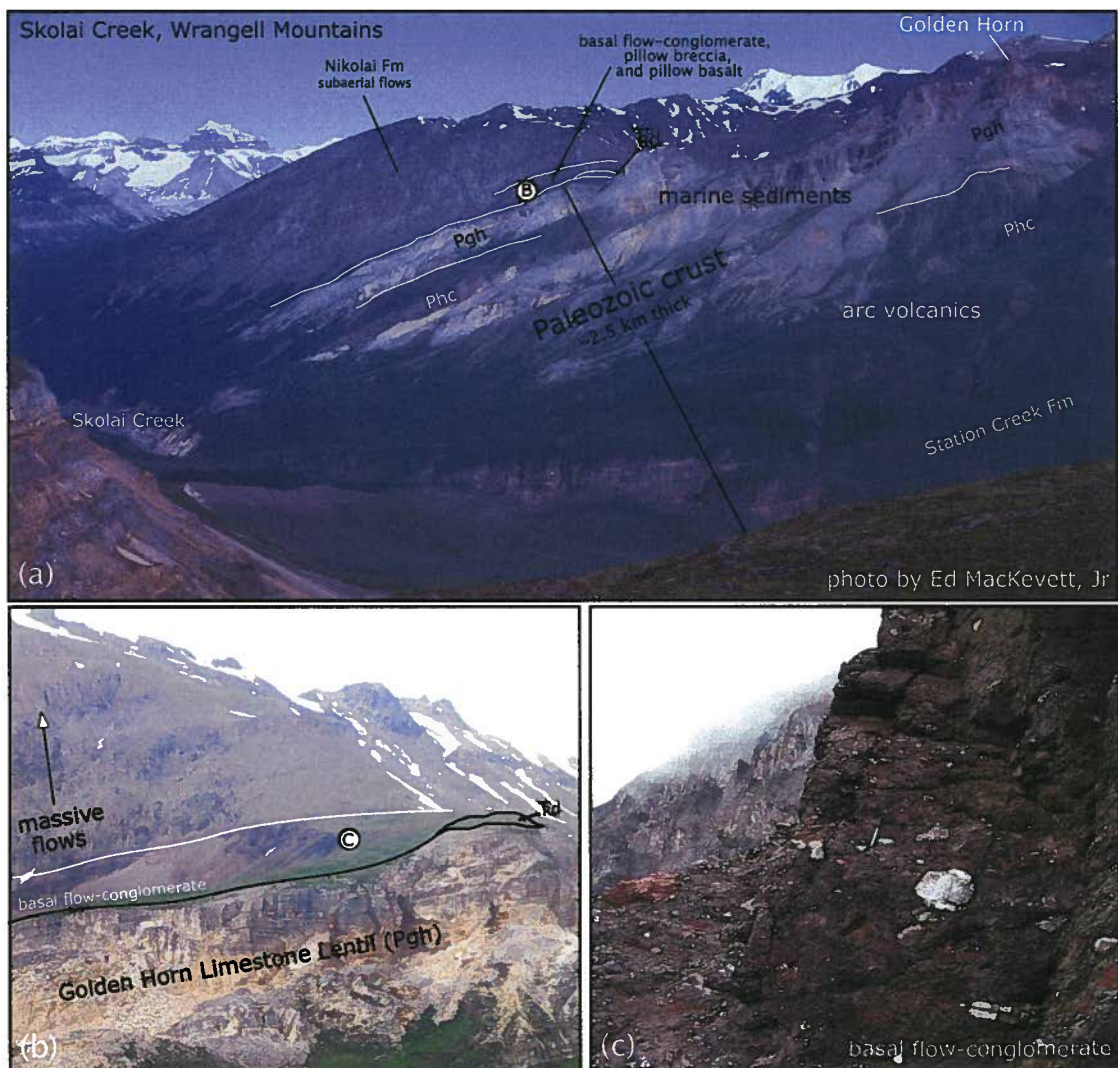


**Figure 3.3** Photographs of the base of the Nikolai Formation in the Wrangell Mountains, Alaska. (a) Westward-dipping Paleozoic arc volcanic rocks of the Station Creek Formation overlain by Early Permian shale and limestone (Phc-Hasen Creek Formation; Pgh-Golden Horn Limestone Lentil), isolated lenses of Middle Triassic 'Daonella-beds' (TRd), basalt flow-conglomerate with local pillows, and massive subaerial flows on the north side of Skolai Creek. Photograph by Ed MacKevett, Jr. (b) Close-up photograph of area b in photo a. (c) Close-up photograph of area c in photo b showing basal flow-conglomerate with clasts of rounded cobbles of white limestone (<20 cm) derived from Golden Horn Limestone Lentil and red basalt (<40 cm) from Station Creek Formation. Pen (14 cm) in middle of photo for scale.



**Figure 3.4** Photograph of ~1000 m of continuous flood basalt stratigraphy at the top of the Nikolai Formation along Glacier Creek in the Wrangell Mountains, Alaska. The yellow line marks the contact between Nikolai basalts and the overlying Chitistone Limestone.



the flood basalts are best exposed around Hidden Lake Creek where a sharp contact between Nikolai basalts and overlying Chitistone Limestone is mostly a smooth surface with minimal evidence of weathering (Fig. 3.5; Armstrong & MacKevett, 1982). Several occurrences of a thin zone (<1 m) of highly-oxidized subangular cobble-sized clasts of Nikolai basalt and minor thinly-bedded siltstone occur along the contact (Fig. 3.5).

In the Amphitheater Mountains, fieldwork concentrated in five areas: Glacier Gap Lake, Landmark Gap Lake, Tangle Lakes (West), Sugarloaf Mountain, and Rainy Creek (Fig. 3.6). The Amphitheater Mountains are formed of exceptionally well-preserved flood basalt sequences flanked by associated underlying mafic and ultramafic plutonic rocks. South of the Eureka Creek fault is a broad synform with approximately 3.5 km of basaltic flows with basal sill complexes exposed along the outer margins (Fig. 3.6). The lower ~500 m of volcanic stratigraphy are submarine flows and subaerial flows comprise most of the remainder of the volcanic stratigraphy. Within the synform, several north-south-trending, U-shaped glacial valleys (e.g. Lower Tangle Lakes) provide excellent cross-sectional exposures of sediment-sill complexes and the base of the flood basalt stratigraphy (Figs 3.6 and 3.7). The lowest part of over 1000 m of continuous volcanic stratigraphy consists of unfossiliferous shale and siliceous argillite (<4 m thick) interbedded with massive mafic sills (2-30 m thick), in turn overlain by pillow basalt (Fig. 3.7). The basal pillowed flow is 13 m thick and pillows are typically <1 m in diameter with sediment between pillows along the base of the flow. Sills interbedded with thinly bedded basaltic sandstone and minor hyaloclastite also occur slightly higher in the stratigraphy, within the submarine stratigraphy (Figs 3.6 and 3.7). Middle and upper sections of the Nikolai Formation are massive amygdaloidal flows (mostly <15 m thick) with no discernible erosional surfaces or sediments between flows.

A small segment of Wrangellia consisting of a heterogeneous assemblage of mafic and ultramafic plutonic and volcanic rocks forms a wedge between the Broxson Gulch Thrust and the Eureka Creek fault in the northern part of the Amphitheater Mountains (Fig. 3.6). A complex steeply-dipping sequence of picritic tuff and volcanoclastic rocks, mafic and ultramafic intrusives and dikes, and limestone occurs within several ridges near Rainy Creek. These units have distinct lithologic character from the volcanic stratigraphy of the Nikolai Formation south of the Eureka Creek Fault

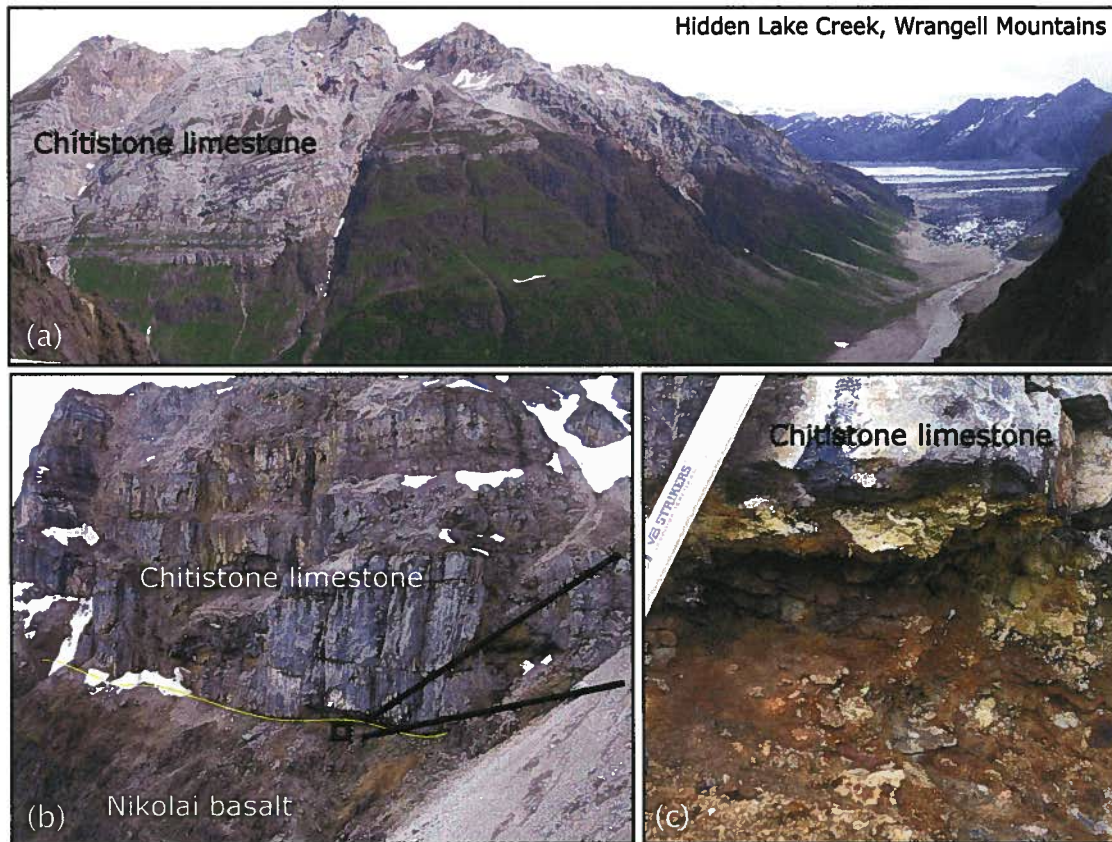


**Figure 3.5** Photographs showing the top of the Nikolai Formation in the Wrangell Mountains, Alaska. (a) Chitistone Limestone overlying the Nikolai Formation above Hidden Creek in the Wrangell Mountains. Faulting has offset the contact. (b) Close-up photograph of uppermost Nikolai flow and base of the Chitistone Limestone from where photo a was taken. (c) Cobbles <10 cm long along the contact between the Chitistone Limestone and Nikolai Formation. The oxidized cobbles are subangular, closely packed, aligned along their long axis, and are glomeroporphyritic basalt identical to the uppermost flows of the Nikolai Formation. Sledgehammer handle (4 cm wide) for scale.

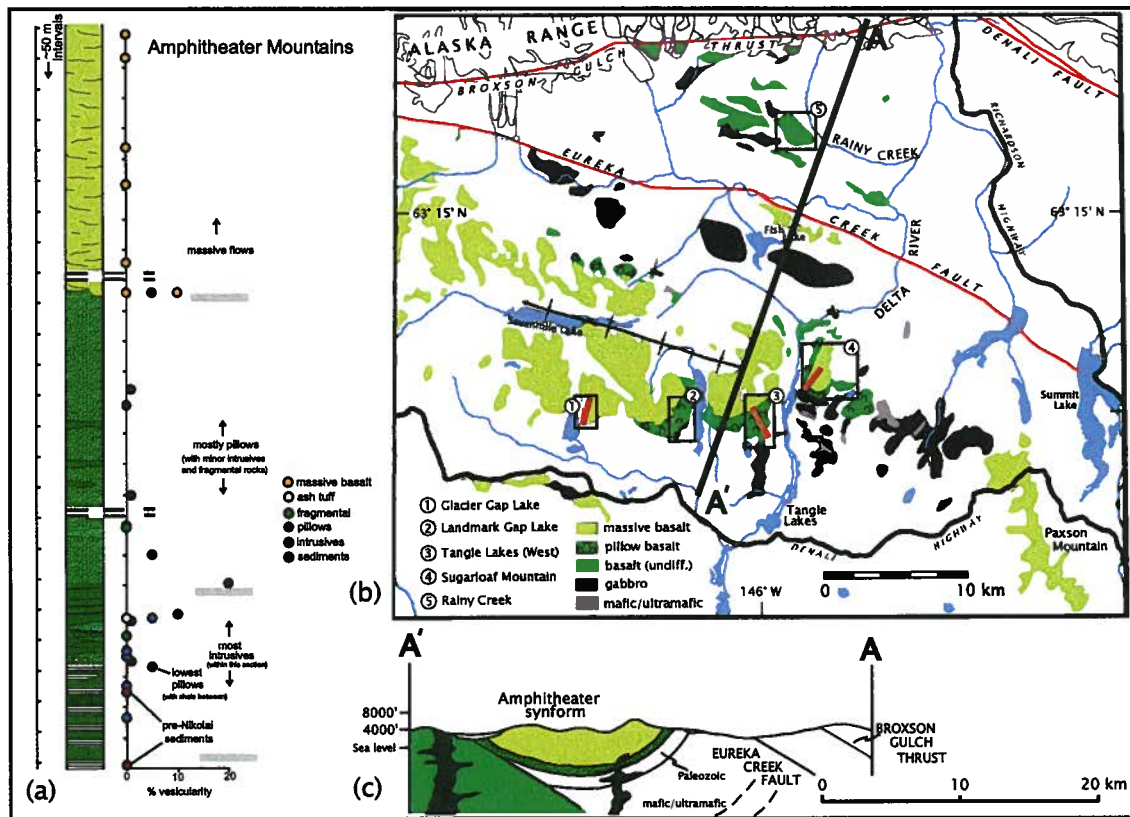


**Figure 3.6** Simplified geologic map and stratigraphy of the Amphitheater Mountains, Alaska (location shown in Figure 3.1). (a) Stratigraphic column with sample lithologies and estimated vesicularity for flood basalts from the lower part of the volcanic stratigraphy, derived from three traverses marked by red lines in b. Vesicularity estimated visually from thin-sections. (b) Generalized geology of the Nikolai Formation and related plutonic rocks in the Amphitheater Mountains. Five main field areas are outlined with numbered boxes (see legend). Map derived Nokleberg *et al.* (1992) and digital compilation of Wilson *et al.* (1998). (c) Schematic cross-section of Amphitheater Mountains from A to A' in panel b, adapted from Nokleberg *et al.* (1985).



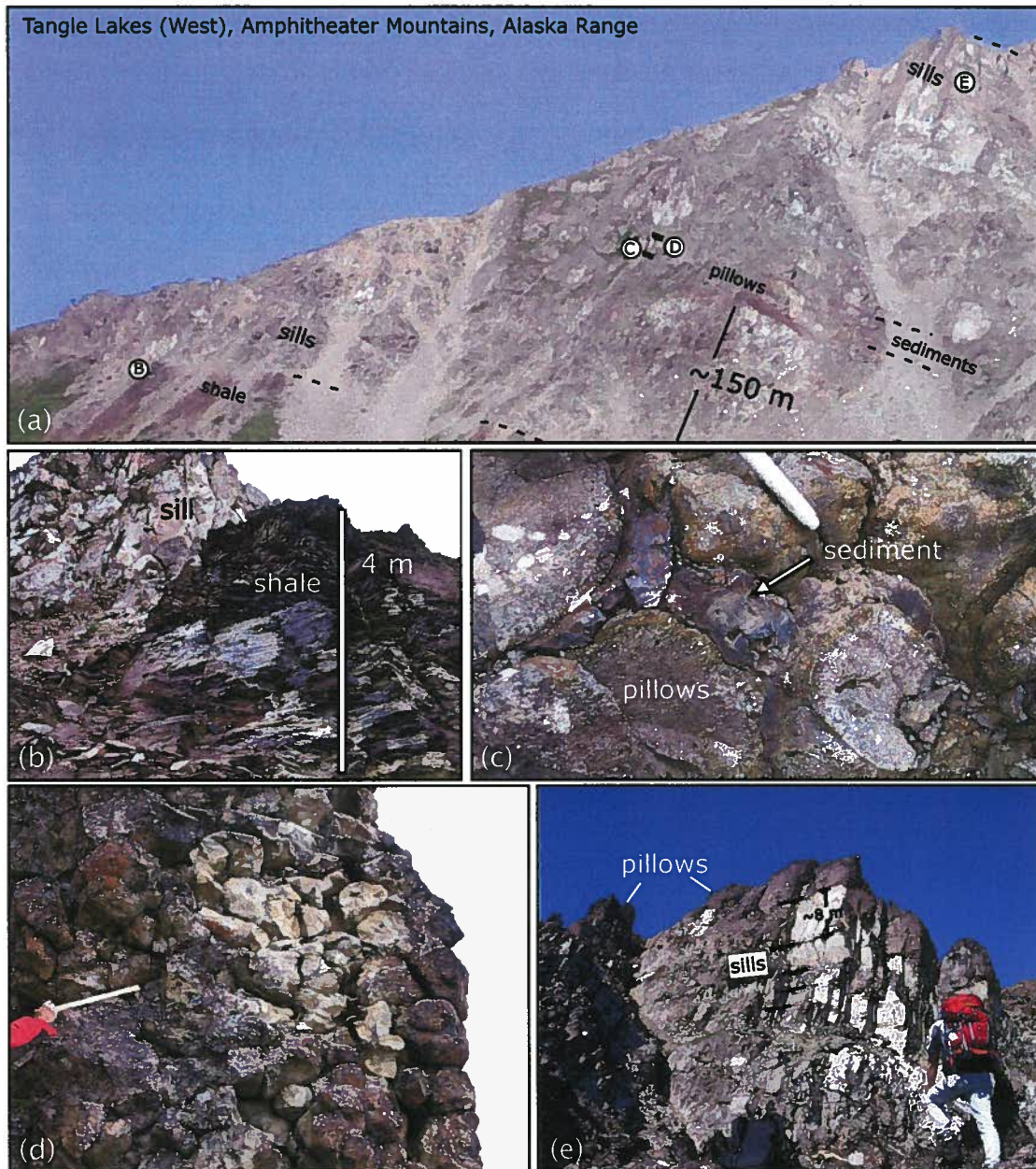


**Figure 3.7** Photographs of the base of the Nikolai Formation in the Amphitheater Mountains, east-central Alaska Range (Tangle Lakes, West), Alaska. (a) Basal sill and sediments beneath submarine flows. Letters denote locations of other photographs. (b) Fissile shale (~4 m thick) and a mafic sill from the lowermost exposure of shale. (c) Pillow basalt with shale between pillows lying directly above shale similar to photograph b. (d) Pillow basalt (pillow tubes are <1 m diameter in cross-section) in the lowermost flow (13 m thick) in the Tangle section. Photograph c is from the base of this flow. Sledgehammer (80 cm long) for scale. (e) Sequence of at least 4 massive sills (<8 m thick) interbedded with fine-grained tuff (<2 m thick). Tuff layers interbedded with sills contain plagioclase crystals (<0.5 mm), curvilinear shards, and local areas of volcanic breccia containing basaltic clasts with abundant small acicular plagioclase (<0.5 mm).



within the broad synform. A small suite of eight samples, including several highly altered olivine-bearing picritic tuffs, were collected for comparison to Nikolai basalts within the synform and are referred to as Rainy Creek picrites.

In the Clearwater Mountains, a small mountain range ~40 km west of the Amphitheater Mountains, the lowest level of exposure is pelagic sedimentary sequences interbedded with mafic sills, very similar to units in the Amphitheater Mountains (Fig. 3.8). The lowest flows of the Nikolai Formation are pillow basalt directly overlying thin beds of shale and argillite (<3 m thick) with sediment commonly filling interpillow voids in the lowermost pillows. Picritic pillow lavas have been found in the submarine stratigraphy in the Clearwater Mountains. Similar to the Amphitheater Mountains, the lower <400 m of the volcanic stratigraphy is submarine flows and the remainder of the stratigraphy is primarily subaerial flows. Upper parts of the volcanic stratigraphy contain subaerial flows (or sills) with columnar jointing, minor occurrences of tuff and volcanic breccia, and limestone and argillite lenses interbedded with flows are overlain by fine-grained sediments with diagnostic index fossils (bivalve *Halobia* and ammonoid *Tropite*; Smith, 1981).

A total of 111 samples of the Nikolai Formation and several Paleozoic, Late Mesozoic, and Cenozoic volcanic and sedimentary rocks were collected for petrography and geochemical analysis. Fifty-three of these samples were selected for geochemistry based on the visual degree of alteration (Table 3.1; 1-least altered, 3-intensely altered) and are grouped into high- and low-titanium basalts, sills, and picrites based on geochemistry.

The high- and low-titanium basalts have similar petrographic textures with simple mineralogy and aphyric or glomeroporphyritic texture (Fig. 3.9; Table 3.1). Half of the 26 high-titanium basalts are glomeroporphyritic and about half of the low-titanium basalts are aphyric (Table 3.1). Phenocrysts and glomerocrysts in the Nikolai Formation are almost exclusively plagioclase and the primary minerals in the groundmass are plagioclase, clinopyroxene, and Fe-Ti oxide, and olivine is rarely present (Fig. 3.9; Table 3.1). High-titanium basalts have a higher proportion of Fe-Ti oxide than low-titanium basalts (Table 3.1). Several of the uppermost flows in the Wrangell Mountains are plagioclase-rich (>50% plagioclase laths ~1mm long with ~5:1 aspect ratio) with

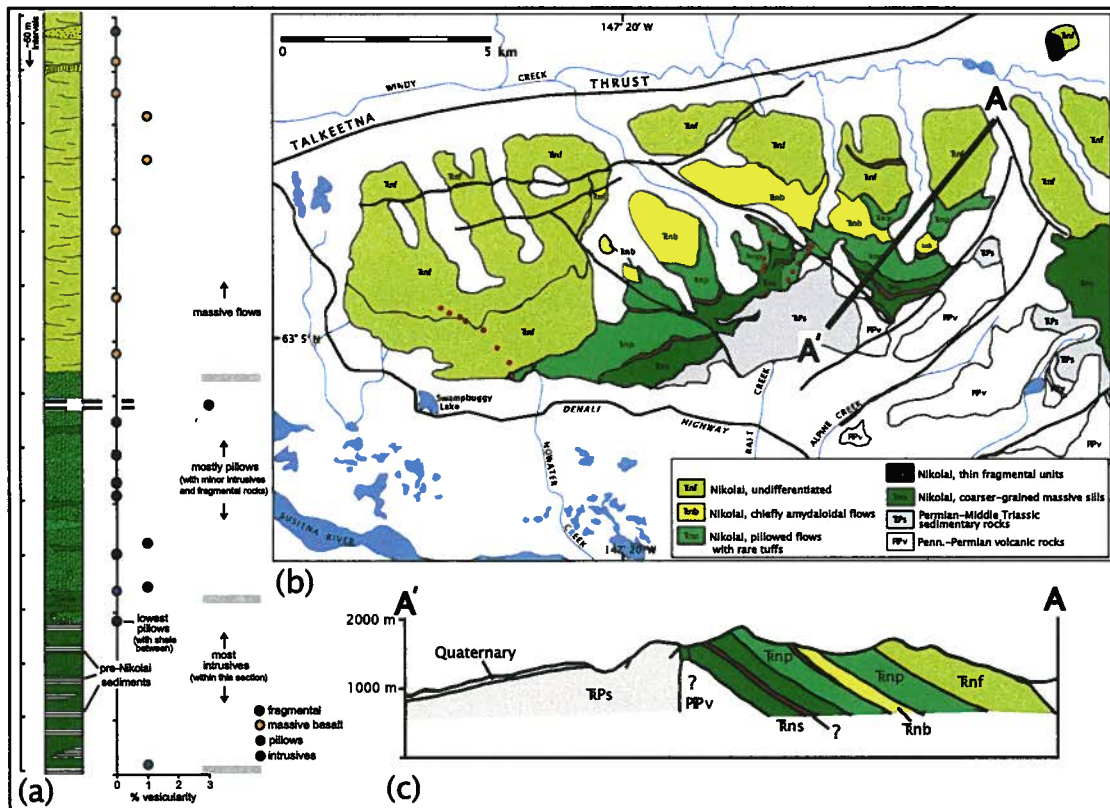


**Figure 3.8** Geologic map and stratigraphy of the Clearwater Mountains, Alaska. (a) Stratigraphic column with sample lithologies and estimated vesicularity for flood basalts from the lower part of the stratigraphy, derived from three traverses and maps of Smith (1973) and Silberling *et al.* (1981). Vesicularity estimated visually from thin-sections. (b) Generalized geology of the Nikolai Formation and related plutonic rocks in the Clearwater Mountains, adapted from Silberling *et al.* (1981). Sample locations are shown by red dots. Location of map shown in Figure 3.1. (c) Schematic cross-section of Clearwater Mountains from A to A' in panel b, adapted from Silberling *et al.* (1981).

Table 3.1 Summary of petrographic characteristics and phenocryst proportions of Nikolai basalts in Alaska

Sample <sup>a</sup>	Area <sup>b</sup>	Flow <sup>c</sup>	Group <sup>d</sup>	Texture <sup>e</sup>	vol% Ol <sup>f</sup>	Plag	Cpx	Ox	Alteration <sup>g</sup>	Note <sup>h</sup>
5710A2	WM	FLO	high-Ti	glomero	20				3	plag glcr <3 mm
5801A2	CL	FLO	high-Ti	glomero				20	1	abundant ox
5806A3	GG	FLO	high-Ti	aphyric, recrystallized				10	3	abundant ox, few relict phenos
5708A2	WM	FLO	high-Ti	trachytic, glomero	3			15	2	abundant ox, plag glcr <2 mm
5801A9	CL	PIL	high-Ti	aphyric, intersertal					3	aphyric
5725A2	TA	SIL??	high-Ti sill	glomero	15			10	2	plag glcr <2 mm, cpx <0.5 mm
5716A2	WM	FLO	high-Ti	intergranular, aphyric				10	2	plag laths <1.5 mm, plag-rich, secondary min
5806A5	GG	FLO	high-Ti	aphyric, intersertal				15	3	abundant ox, aphyric
5716A3	WM	FLO	high-Ti	plag-phyric, intersertal	30				3	abundant plag phenos and glcr <4 mm
5707A3	WM	FLO	high-Ti	intergranular, intersertal	3			10	3	few plag <2 mm
5710A3	WM	FLO	high-Ti	glomero, intergranular	10			15	3	plag glcr <3 mm, plag laths <1 mm, ox-rich
5719A6	WM	FLO	high-Ti	glomero, intergranular	10			15	2	abundant ox, plag glcr <3 mm, plag-rich
5719A5	WM	FLO	high-Ti	glomero, intergranular	10			15	1	abundant ox, plag glcr <3 mm, plag-rich
5801A5	CL	FLO	high-Ti	glomero, intergranular	15			20	2	abundant ox, plag glcr <2 mm
5806A6	GG	FLO	high-Ti	aphyric, intersertal					3	plag <0.5 mm, cpx <0.5 mm
5712A2	WM	FLO	high-Ti	glomero	5			15	2	plag glcr <3 mm, plag laths <0.5 mm
5726A1	TA	PIL	high-Ti	aphyric					2	vesicles 3%, very f.g., 1 plag glcr <3 mm
5726A6	TA	PIL	high-Ti	glomero, intersertal	20				2	plag glcr <2 mm, plag needles <0.5 mm
5725A4	TA	SIL??	high-Ti sill	aphyric, ophimottled				7	2	plag <0.5 mm, cpx <0.5 mm
5726A3	TA	FLO	high-Ti	intersertal	1			10	3	plag phenos <2 mm
5810A10	TA	PIL	high-Ti	aphyric, intersertal				5	1	plag <0.5 mm, cpx <0.5 mm
5715A1	WM	FLO	high-Ti	trachytic, glomero	20			10	1	plag glcr <3 mm, aligned pl <0.5 mm
5714A1	WM	FLO	high-Ti	trachytic, glomero	10			10	2	plag glcr <3 mm, aligned plag laths <0.5 mm
5716A1	WM	FLO	high-Ti	plag-phyric	5			5	3	plag <8 mm, very c.g., plag laths <1 mm
5726A2	TA	FLO	high-Ti	aphyric, intersertal				3	2	vesicles <0.5 mm, plag needles <0.5 mm
5714A3	WM	FLO	high-Ti	intergranular, glomero	10			3	3	c.g., abundant sec min, plag glcr <3 mm
5715A5	WM	FLO	low-Ti	relict glomero					3	altered, abundant sec min, plag glcr <3 mm
5801A8	CL	FLO	low-Ti	intergranular, aphyric				5	3	blocky ox <0.5 mm
5802A5	CL	PIL	low-Ti	intergranular, ophimottled				5	2	aphyric
5731A5	CL	PIL	low-Ti	intergranular, ophimottled					2	aphyric
5802A6	CL	SIL	low-Ti	intergranular			15	1	1	plag laths <1 mm, cpx <1.5 mm
5810A4	TA	SIL	low-Ti sill	glomero, intersertal	25				1	plag glcr <3 mm
5802A1	CL	PIL	low-Ti	intersertal			2		2	plag needles <0.5 mm, cpx <1.5 mm
5731A6	CL	PIL	low-Ti	intergranular, intersertal					3	plag <0.5 mm
5810A6	TA	PIL	low-Ti	glomero, intersertal	10				1	10% vesicles, plag glcr <3 mm
5727A3	TA	SIL	low-Ti sill	subophitic			5	3	3	plag <1 mm, cpx <1 mm, ox <0.5 mm
5810A1	TA	PIL	low-Ti	aphyric, intersertal					2	15% vesicles, tiny plag needles <0.3 mm
5727A5	TA	PIL	low-Ti	aphyric, intersertal				1	2	plag needles <0.5 mm
5727A7	TA	PIL	low-Ti	aphyric, intersertal				2	2	vesicular, plag needles <0.5 mm, cpx <0.5 mm
5810A2	TA	SIL	low-Ti sill	aphyric, intersertal				1	2	f.g., plag needles <0.5 mm
5727A2	TA	SIL	low-Ti sill	intergranular			5		3	plag laths <1 mm, cpx <1 mm
5731A3	CL	PIL	low-Ti	intergranular, intersertal	5				2	few ol <1.5 mm
5802A3	CL	PIL	low-Ti	aphyric, intersertal	2				2	few ol <1 mm
5727A6	TA	SIL	low-Ti sill	subophitic, ophimottled			20	1	2	cpx <2 mm enc plag <1 mm
5802A2	CL	PIL	low-Ti	variolithic					3	highly altered, glomero, aligned plag
5731A4	CL	PIL	low-Ti	subophitic, ophimottled				1	3	cpx <1 mm enc tiny plag needles
5811A1	TA	GAB	low-Ti sill	intergranular			15		2	cpx <2 mm filling interstices
5719A1	WM	BRE	basal	trachytic					2	calcite and qtz <3 mm, plag needles <1 mm
5802A4	CL	PIL	CWPIC	spherulitic	30				2	ol <2 mm, swt plag <1 mm
5808A3	RC	TUF	RCPIC	tuffaceous					3	
5808A8	RC	SIL	RC	tuffaceous				5	3	blocky ox <0.5 mm
5808A2	RC	TUF	RCPIC	tuffaceous					3	
5808A1	RC	TUF	RC	tuffaceous					3	
5808A6	RC	DIK	RC	intergranular					2	elongate hbl (<1.5 mm) with qtz cement

<sup>a</sup>Sample number: last digit year, month, day, initial, sample station (except 93G171). <sup>b</sup>WM, Wrangell Mountains; TA, Tangle Lake; GG, Glacier Gap Lake; CL, Clearwater Mountains; RC, Rainy Creek; <sup>c</sup>PIL, pillow; BRE, breccia; FLO, flow; SIL, sill; GAB, gabbro; TUF, tuff; DIK, dike. <sup>d</sup>basal, basal flow-conglomerate; RC, Rainy Creek; RCPIC, Rainy Creek picrite; CWPIC, Clearwater picrite. <sup>e</sup>glomero, glomeroporphyritic. <sup>f</sup>Modal proportions were visually estimated. <sup>g</sup>Visual alteration index based primarily on degree of plagioclase alteration and presence of secondary minerals (1, least altered; 3, most altered). Plagioclase is commonly replaced by epidote, chlorite, sericite, clinzoisite, and clay minerals and zoning is obscured in many samples due to albittization; clinopyroxene is mostly unaltered compared to plagioclase; Fe-Ti oxides are altered to sphene and leucosane minerals; amygdules (<20 volume %) are prevalent throughout most subaerial flows and are usually filled with quartz, calcite, epidote, prehnite and pumpellyite.

<sup>h</sup>glcr, glomerocrysts; f.g., fine-grained; c.g., coarse-grained; olk, swt, swallow-tail. Mineral abbreviations: ol, olivine pseudomorphs; plag, plagioclase; cpx, clinopyroxene; ox, oxides (includes ilmenite + titanomagnetite). High- and low-titanium basalts are listed from highest (top) to lowest (bottom) TiO<sub>2</sub> contents.



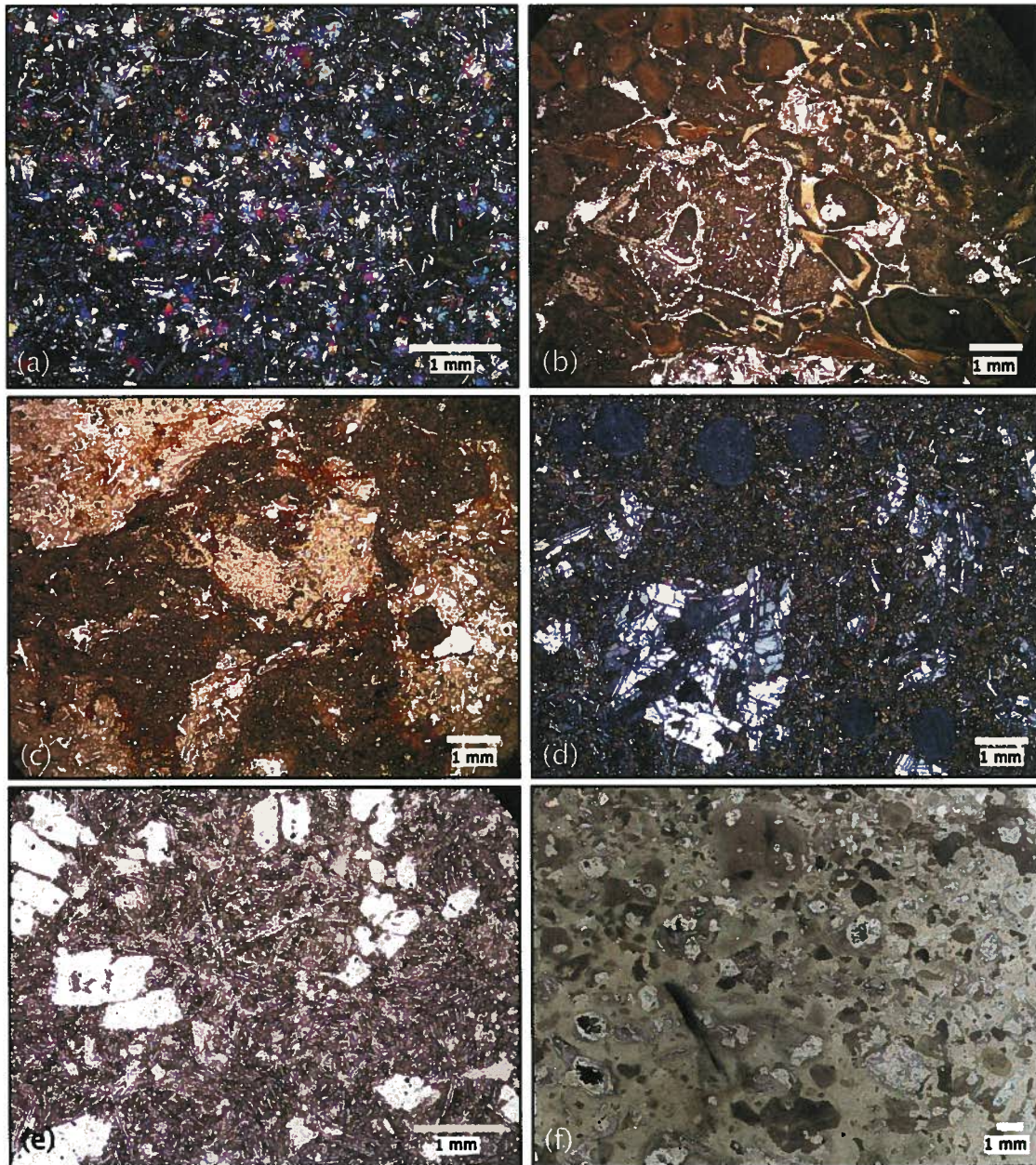


**Figure 3.9** Representative photomicrographs of Nikolai basalts, Alaska. (a) Aphyric pillow basalt from the Tangle Lake (West) in the Amphitheater Mountains in cross-polarized transmitted light (sample 5810A10). (b) Hyaloclastite from near the top of the submarine section at Tangle Lake (West) in plane-polarized transmitted light (sample 5810A9, no chemistry). (c) Hyaloclastite interbedded with sills from Tangle Lake (West) in plane-polarized transmitted light (sample 5810A3b, no chemistry). (d) Glomeroporphyritic pillow basalt with abundant amygdules (~10 vol %) from Tangle Lake (West) in cross-polarized transmitted light (sample 5810A6). (e) Variolitic picritic pillow basalt with olivine pseudomorphs (<2 mm) and acicular plagioclase with swallow-tail terminations from the Clearwater Mountains, in plane-polarized transmitted light (sample 5802A4). (f) Rainy Creek picritic tuff with pseudomorphed olivine phenocrysts, undeformed recrystallized angular and cusped shards, and lithic particles in a fine-grained matrix, in plane-polarized transmitted light (sample 5808A2). Some clasts appear to be clusters of grains, some of which contain thin green rims.

trachytic-like texture and abundant oxides. Picrite from the Clearwater Mountains preserve spherulitic textures with bow-tie and fan-shaped bundles of acicular plagioclase, typically with swallow-tail terminations. Olivine (<2 mm) pseudomorphed by secondary minerals comprises ~20 vol % of the picrite and plagioclase commonly radiates from the edges of olivine pseudomorphs and is intergrown with clinopyroxene. The sample preparation and analytical methods for whole-rock chemistry, major elements, trace elements, Sr, Nd, Hf, and Pb isotopes are described in Appendix D.

## **WHOLE-ROCK CHEMISTRY**

### **Major- and trace-element compositions**

The most noteworthy feature of the major-element chemistry of the Nikolai Formation is two clearly distinguishable groups of high- and low-titanium basalt (Fig. 3.10). The low-titanium basalts range from 0.4 to 1.2 wt %  $\text{TiO}_2$  and the high-titanium basalts range from 1.6 to 2.4 wt %  $\text{TiO}_2$  (Fig. 3.10; Table 3.2). The high-titanium basalts have a limited range in MgO (5.7-7.9 wt % MgO, except for one plagioclase-rich flow with 4.8 wt % MgO) and  $\text{SiO}_2$  (49.2-52.1 wt %), whereas the low-titanium basalts extend to higher MgO and have a significantly larger range in MgO (6.4-12.0 wt %) and  $\text{SiO}_2$  (46.7-52.2 wt %). Almost all of the Nikolai basalts in Alaska fall within the tholeiitic field in a total alkalis versus silica plot, with low-titanium basalts generally having lower total alkalis than the high-titanium basalts. The low-titanium basalts exhibit broadly decreasing trends of  $\text{TiO}_2$ ,  $\text{FeO}_T$ , and  $\text{Na}_2\text{O}$  with increasing MgO (Fig. 3.10) and have higher loss on ignition (LOI; mean LOI =  $2.7 \pm 1.3$  wt %) than the high-titanium basalts (mean LOI =  $1.9 \pm 1.5$  wt %; Table 3.2). Low-titanium basalts with >8 wt % MgO have higher concentrations of Ni than the high-titanium basalts and the three picrite samples have noticeably higher Ni concentrations (525-620 ppm) than all basalts (Fig. 3.10). Both the high- and low-titanium basalts have a large range in CaO, which appears to be independent of MgO variation. A single Clearwater picrite (13.6 wt % MgO) and two Rainy Creek picrites (15.5-16.2 wt % MgO) have higher MgO with similar  $\text{TiO}_2$ ,  $\text{FeO}_T$ , and alkali contents to the low-titanium basalts, however, the Rainy Creek picrites have notably lower  $\text{Al}_2\text{O}_3$  (Fig. 3.10). The basal flow-conglomerate from the Wrangell Mountains has distinct major-element chemistry compared to the other Nikolai basalts.



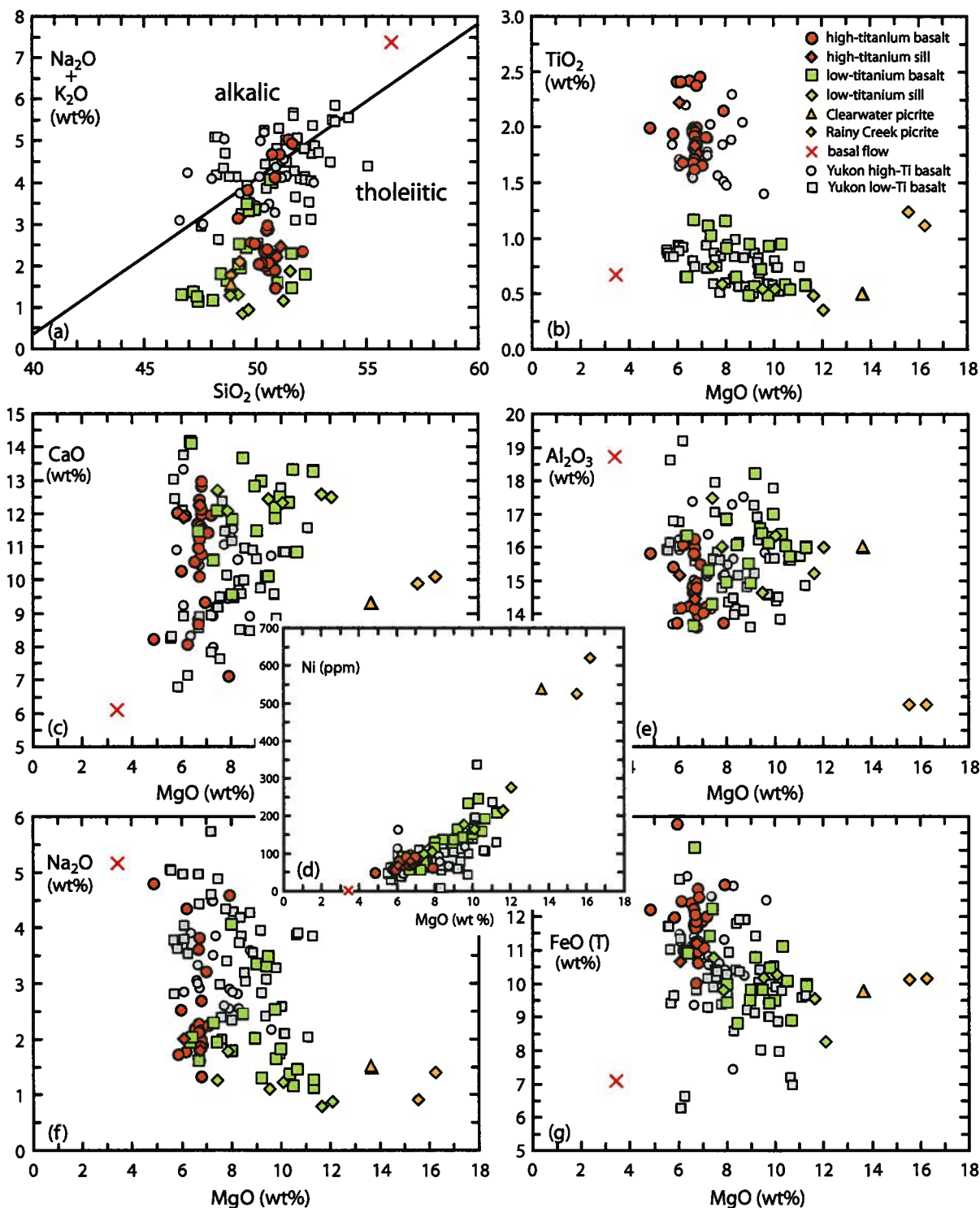


**Figure 3.10** Whole-rock major-element and Ni variation diagrams vs. MgO for the Nikolai Formation in Alaska with data for the Nikolai Formation in Yukon (see chapter 4). The boundary of the alkaline and tholeiitic fields is that of MacDonald and Katsura (1964). Total iron expressed as FeO, LOI is loss-on-ignition, and oxides are plotted on an anhydrous, normalized basis. Note the clear distinction between the high- and low-titanium basalts in panel b and the difference in alkali contents between the Nikolai basalts in Alaska and Yukon in panel a.

Table 3.2 Major element (wt% oxide) and trace element (ppm) abundances in whole rock samples of Nikolai basalts, Alaska.

SAMPLE	5707A3	5708A2	5710A2	5710A3	5712A2	5714A1	5714A3	5715A1 (1)	5715A1 (2)	5715A5
Group	HI-TI	HI-TI	HI-TI	HI-TI	HI-TI	HI-TI	HI-TI	HI-TI	HI-TI	LOW-TI
Area	WM	WM	WM	WM	WM	WM	WM	WM	WM	WM
Flow	FLO	FLO	FLO	FLO	FLO	FLO	FLO	FLO	FLO	FLO
UTM EW	6816521	6813830	6838676	6836850	6838178	6826371	6826390	6827794	6827794	6828050
UTM NS	430777	428595	356035	356266	353987	384783	384806	383399	383399	383641
Unnormalized Major Element Oxides (Weight %):										
SiO <sub>2</sub>	49.74	48.40	48.81	50.02	49.90	49.31	50.21	49.61	49.41	50.25
TiO <sub>2</sub>	1.96	2.36	2.4	1.95	1.89	1.66	1.6	1.69	1.68	1.14
Al <sub>2</sub> O <sub>3</sub>	13.37	13.49	15.21	14.45	13.76	15.58	16.01	15.56	15.75	16.69
Fe <sub>2</sub> O <sub>3</sub> *	14.05	16.14	12.94	13.39	13.76	13.21	10.99	13	12.97	10.39
MnO	0.27	0.27	0.23	0.18	0.24	0.17	0.16	0.2	0.2	0.18
MgO	6.69	5.89	6.85	6.56	6.74	6.6	6.64	6.63	6.62	7.94
CaO	10.61	10.09	9.16	8.56	11.35	10.8	9.97	11.09	11.04	9.48
Na <sub>2</sub> O	2.64	2.47	3.15	3.56	1.87	2.08	3.77	1.84	1.82	3.36
K <sub>2</sub> O	0.29	0.61	0.58	1.03	0.22	0.42	0.28	0.2	0.2	0.67
P <sub>2</sub> O <sub>5</sub>	0.16	0.23	0.21	0.18	0.16	0.15	0.14	0.15	0.14	0.09
LOI	1.68	1.41	2.37	2.47	1.28	2.39	3.12	0.84	1.84	3.57
Total	99.78	99.95	99.54	99.88	99.89	99.98	99.77	99.97	99.83	100.19
Trace elements (ppm):										
La		10.32			8.08			6.56	6.56	3.74
Ce		24.25			21.79			17.07	17.07	10.69
Pr		3.66			2.90			2.35	2.35	1.49
Nd		18.83			14.73			12.20	12.20	7.68
Sm		5.22			4.19			3.51	3.51	2.32
Eu		1.73			1.43			1.25	1.25	0.90
Gd		5.57			4.17			3.80	3.80	2.55
Tb		1.02			0.77			0.72	0.72	0.50
Dy		6.84			5.04			4.77	4.77	3.34
Ho		1.35			0.99			0.98	0.98	0.69
Er		4.02			2.85			2.86	2.86	1.98
Tm		0.61			0.33			0.36	0.36	0.25
Yb		3.58			2.37			2.59	2.59	1.77
Lu		0.53			0.36			0.40	0.40	0.28
Sc		44.06			42.52			41.17	41.17	38.50
V	362	411	349	337	346	329	276	354	352	249
Cr	165	62	167	119	133	156	282	165	167	460
Co		47			45			44	44	39
Ni	75	57	89	69	73	82	81	85	85	116
Cu		19			1067			126	126	64
Zn	121	176	126	108	113	109	88	110	111	68
Ga	19	20	21	19	19	19	17	20	19	15
Rb	3.4	9.7	6.1	15	2.2	5.2	2.6	1	1	8.5
Sr	237	162	263	481	184	334	394	184	184	437
Y	28.1	36.1	31.6	27.8	25.8	26.2	22.6	26	26.2	18.3
Zr	113	148	145	115	110	99	93	98	98	60
Nb	10.1	12.5	12.2	9.7	9.9	7.7	7.3	7.7	7.7	4.4
Cs		0.08			0.14			0.28	0.28	0.83
Ba	79	108	147	246	70	63	56	55	56	129
Hf		4.10			3.15			2.78	2.78	1.79
Ta		0.74			0.67			0.48	0.48	0.30
Pb		1.59			0.81			0.52	0.52	0.44
Th		0.98			0.72			0.64	0.64	0.34
U		0.31			0.20			0.19	0.19	0.09
La(XRF)	6	7	8	7	6	6	4	6	6	2
Ce(XRF)	21	27	24	22	21	16	13	17	16	8

Abbreviations for group are: HI-TI, high-titanium; LOW-TI, low-titanium; RC, Rainy Creek; RCPIC, Rainy Creek picrite; CWPIC, Clearwater picrite. Abbreviations for flow are: FLO, massive flow; PIL, pillow basalt; FLO-BRE, flow-conglomerate-pillow breccia; SIL, sill; TUF, tuff. Abbreviations for area are: WM, Wrangell Mountains; TANGLE, Tangle Lakes; GLAC, Glacier Gap Lake; CLEAR, Clearwater Mountains; RAINY, Rainy Creek. Sample locations are given using the Universal Transverse Mercator (UTM) coordinate system (NAD83; zones 6 and 7). XRF analyses were performed at University of Massachusetts Ronald B. Gilmore XRF Laboratory. Fe<sub>2</sub>O<sub>3</sub>\* is total iron expressed as Fe<sub>2</sub>O<sub>3</sub>. LOI is loss-on-ignition. Elements by XRF: Sc, V, Cr, Ni, Zn, Ga, Rb, Sr, Y, Zr, Nb, Ba. Elements by ICP-MS: REE, Co, Cu, Cs, Hf, Ta, Pb, Th, U.

SAMPLE	5716A1	5716A2	5716A3	5719A1	5719A5 (1)	5719A5 (2)	5719A6	5725A2	5725A4	5726A1
Group	HI-TI	HI-TI	HI-TI	LOW-TI	HI-TI	HI-TI	HI-TI	HI-TI	HI-TI	HI-TI
Area	WM	WM	WM	WM	WM	WM	WM	TANGLE	TANGLE	TANGLE
Flow	FLO	FLO	FLO	FLO-BRE	FLO	FLO	FLO	SIL	SIL	PIL
UTM EW	6824771	6824809	6825071	6840607	6840632	6840632	6840632	7001750	7002024	7002334
UTM NS	384884	384800	384853	430357	430204	430204	430204	556168	555867	553245
<i>Unnormalized Major Element Oxides (Weight %):</i>										
SiO <sub>2</sub>	50.89	50.52	50.76	55.72	49.54	49.62	49.76	50.53	50.43	49.01
TiO <sub>2</sub>	1.66	2.12	1.96	0.67	1.92	1.93	1.92	2.19	1.82	1.88
Al <sub>2</sub> O <sub>3</sub>	15.82	13.56	15.57	18.59	14.57	14.55	14.45	14.98	14.31	13.96
Fe <sub>2</sub> O <sub>3</sub> *	12.03	14.22	13.37	7.84	12.84	12.86	12.79	11.73	12.36	13.13
MnO	0.18	0.19	0.18	0.16	0.21	0.21	0.21	0.2	0.2	0.23
MgO	6.13	7.83	4.8	3.37	6.52	6.55	6.65	5.99	6.66	7.07
CaO	7.94	7.01	8.1	6.07	11.47	11.5	11.45	11.74	12.13	11.74
Na <sub>2</sub> O	4.26	4.52	4.71	5.14	2.01	2.02	2.12	1.99	1.78	2.26
K <sub>2</sub> O	0.58	0.08	0.23	2.18	0.29	0.3	0.24	0.46	0.42	0.25
P <sub>2</sub> O <sub>5</sub>	0.15	0.18	0.19	0.38	0.17	0.17	0.17	0.21	0.16	0.16
LOI	2.96	3.57	3.54	5.14	1.05	1.09	2.66	1.26	1.03	1.88
Total	99.64	100.23	99.87	100.12	99.54	99.71	99.76	100.02	100.27	99.69
<i>Trace elements (ppm):</i>										
La				18.10	9.13	9.13			8.57	7.52
Ce				36.95	21.43	21.43			21.35	19.80
Pr				4.56	3.05	3.05			3.00	2.74
Nd				20.65	16.26	16.26			15.16	14.35
Sm				4.26	4.45	4.45			4.30	4.07
Eu				1.31	1.48	1.48			1.43	1.08
Gd				3.96	4.58	4.58			4.32	4.15
Tb				0.52	0.79	0.79			0.77	0.74
Dy				3.40	5.31	5.31			4.89	4.92
Ho				0.66	0.97	0.97			0.94	0.91
Er				2.12	2.94	2.94			2.69	2.59
Tm				0.26	0.35	0.35			0.32	0.30
Yb				1.94	2.46	2.46			2.17	2.03
Lu				0.31	0.36	0.36			0.30	0.27
Sc				11.02	41.37	41.37			38.05	41.02
V	289	393	319	170	366	367	340	358	325	359
Cr	157	133	70	0	162	160	164	140	127	217
Co				16	42	42			42	42
Ni	66	61	47	1	77	76	78	68	80	90
Cu				25	167	167			160	138
Zn	94	97	82	83	104	104	104	96	101	110
Ga	15	17	21	17	19	19	19	20	20	17
Rb	5.8	0.6	2	25.4	5.8	5.9	4.1	16.2	16.5	2.1
Sr	321	56	97	158	200	200	275	213	207	239
Y	26.4	30.8	28.5	19.5	26.3	26.1	25.6	29.6	24.3	24.3
Zr	98	120	118	81	113	113	112	140	107	110
Nb	7.6	9.7	10.2	6.3	10.1	10	9.9	12.1	9.2	9.4
Cs				0.06	0.09	0.09			0.53	0.07
Ba	115	14	47	1277	94	91	85	245	83	191
Hf				2.30	3.23	3.23			3.08	2.66
Ta				0.36	0.63	0.63			0.57	0.52
Pb				2.96	0.85	0.85			0.66	0.95
Th				4.18	0.87	0.87			0.83	0.86
U				1.91	0.25	0.25			0.25	0.23
La(XRF)	4	4	7	17	7	8	8	8	5	5
Ce(XRF)	16	18	18	34	23	23	21	23	19	18



SAMPLE	5726A2	5726A3	5726A6	5727A2	5727A3	5727A5	5727A6 (1)	5727A6 (2)	5727A7	5731A3
Group	HI-TI	HI-TI	HI-TI	LOW-TI	LOW-TI	LOW-TI	LOW-TI	LOW-TI	LOW-TI	LOW-TI
Area	TANGLE	TANGLE	TANGLE	TANGLE	TANGLE	TANGLE	TANGLE	TANGLE	TANGLE	CLEAR
Flow	FLO	FLO	PIL	SIL	SIL	PIL	SIL	SIL	PIL	PIL
UTM EW	7002466	7002475	7002270	6999661	6999663	6999658	6999646	6999646	6999646	6993085
UTM NS	553936	553826	553495	550468	550377	550351	550324	550324	550270	483499
<i>Unnormalized Major Element Oxides (Weight %):</i>										
SiO <sub>2</sub>	51.41	49.90	50.11	50.70	50.97	47.43	48.89	48.89	46.13	50.94
TiO <sub>2</sub>	1.63	1.81	1.85	0.54	0.58	0.57	0.48	0.48	0.56	0.53
Al <sub>2</sub> O <sub>3</sub>	13.83	14.73	14.74	14.49	15.85	15.81	15.06	15.06	17.97	15.51
Fe <sub>2</sub> O <sub>3</sub> *	12.16	12.34	11.71	11.21	10.79	11.04	10.51	10.51	11.84	9.75
MnO	0.19	0.21	0.19	0.19	0.19	0.19	0.18	0.18	0.17	0.17
MgO	6.96	6.72	6.75	9.41	7.75	10.35	11.51	11.51	9.09	10.52
CaO	11.25	11.96	12.7	12.3	11.96	13.12	12.43	12.43	12.78	10.68
Na <sub>2</sub> O	2.2	1.95	1.94	1.09	1.76	1.06	0.79	0.79	1.19	1.22
K <sub>2</sub> O	0.11	0.09	0.13	0.06	0.1	0.09	0.05	0.05	0.1	0.22
P <sub>2</sub> O <sub>5</sub>	0.14	0.16	0.16	0.04	0.05	0.07	0.06	0.06	0.07	0.1
LOI	1.6	1.35	1.29	2.18	2.3	2.87	3	3	2.75	3.15
Total	99.88	99.87	100.28	100.03	100.00	99.73	99.96	99.96	99.90	99.64
<i>Trace elements (ppm):</i>										
La				1.13	1.13		1.25	1.27	2.56	
Ce				3.19	3.22		3.56	3.58	5.66	
Pr				0.49	0.51		0.54	0.56	0.80	
Nd				2.92	2.92		3.05	3.09	3.86	
Sm				1.22	1.23		1.11	1.13	1.30	
Eu				0.56	0.49		0.37	0.36	0.67	
Gd				1.47	1.47		1.33	1.37	1.63	
Tb				0.36	0.34		0.34	0.32	0.38	
Dy				2.62	2.60		2.35	2.37	2.80	
Ho				0.56	0.60		0.55	0.53	0.64	
Er				1.67	1.70		1.63	1.58	1.93	
Tm				0.22	0.22		0.21	0.21	0.25	
Yb				1.61	1.61		1.53	1.53	1.91	
Lu				0.27	0.26		0.25	0.24	0.33	
Sc				44.90	43.02		45.67	49.00	50.33	
V	324	332	333	242	254	257	233	233	268	217
Cr	118	148	136	555	269	455	521	521	199	605
Co				51	44		54	54	57	
Ni	79	84	85	178	106	157	214	214	163	191
Cu				96	116		98	96	131	
Zn	102	100	84	81	77	84	74	74	92	68
Ga	18	20	19	14	14	13	12	12	15	12
Rb	0.7	0.4	3.4	1.7	1.8	1.2	0.6	0.6	1.5	4.6
Sr	195	178	198	76	117	146	123	123	155	205
Y	22.2	24.6	24.7	15.1	15.5	15.8	14	14	17.2	17.2
Zr	94	106	109	23	24	17	15	15	20	38
Nb	8	9.2	9.4	0.9	0.9	1	0.8	0.8	0.8	2.2
Cs				0.36	0.28		0.12	0.12	0.23	
Ba	45	47	48	98	76	130	46	46	54	125
Hf				0.80	0.87		0.57	0.57	0.70	
Ta				0.04	0.05		0.04	0.04	0.05	
Pb				0.55	0.50		0.20	0.18	1.21	
Th				0.17	0.17		0.07	0.07	0.29	
U				0.07	0.07		0.03	0.03	0.10	
La(XRF)	6	7	6	0	1	1	1	1	2	4
Ce(XRF)	17	18	19	2	2	2	3	3	3	11

SAMPLE	5731A4	5731A5	5731A6	5801A2	5801A5	5801A8	5801A9	5802A1	5802A2	5802A3
Group	LOW-TI	LOW-TI	LOW-TI	HI-TI	HI-TI	LOW-TI	HI-TI	LOW-TI	LOW-TI	LOW-TI
Area	CLEAR	CLEAR	CLEAR	CLEAR	CLEAR	CLEAR	CLEAR	CLEAR	CLEAR	CLEAR
Flow	PIL	PIL	PIL	FLO	FLO	FLO	PIL	PIL	PIL	PIL
UTM EW	6993131	6993230	6993320	6992862	6992750	6992452	6992443	6993172	6993140	6993104
UTM NS	483495	483531	483566	480105	480328	480516	480528	483888	483867	483847
<i>Unnormalized Major Element Oxides (Weight %):</i>										
SiO <sub>2</sub>	48.61	48.12	49.13	50.00	49.75	50.82	49.97	49.18	49.94	47.76
TiO <sub>2</sub>	0.48	0.92	0.64	2.37	1.91	1.09	2.33	0.71	0.48	0.52
Al <sub>2</sub> O <sub>3</sub>	15.89	16.1	15.9	14.02	15.17	15.06	13.95	16.27	15.33	16.76
Fe <sub>2</sub> O <sub>3</sub> *	10.32	11.5	9.69	13.68	13.13	12.51	12.28	10.82	10.44	10.42
MnO	0.19	0.19	0.16	0.21	0.21	0.22	0.19	0.19	0.19	0.18
MgO	9.63	9.67	8.37	6.08	5.76	7.16	6.69	9.41	8.85	9.85
CaO	12	11.71	13.54	11.77	11.84	10.44	11.77	10	12.67	12.31
Na <sub>2</sub> O	1.87	1.35	2.13	1.74	1.69	1.99	1.85	2.82	1.88	1.2
K <sub>2</sub> O	0.63	0.28	0.29	0.13	0.28	0.27	0.38	0.63	0.11	0.59
P <sub>2</sub> O <sub>5</sub>	0.06	0.1	0.16	0.22	0.17	0.15	0.22	0.17	0.06	0.06
LOI	3.1	3.34	3.77	1.26	1.25	2.13	1.5	3.64	3.43	2.7
Total	99.68	99.94	100.01	100.22	99.91	99.71	99.63	100.20	99.95	99.65
<i>Trace elements (ppm):</i>										
La				12.70	8.65				3.00	
Ce				28.04	21.65				6.92	
Pr				4.14	3.07				1.00	
Nd				21.10	15.51				4.04	
Sm				5.55	4.25				1.31	
Eu				1.79	1.46				0.45	
Gd				5.49	4.40				1.57	
Tb				0.93	0.80				0.34	
Dy				6.21	5.22				2.53	
Ho				1.13	1.01				0.57	
Er				3.25	2.93				1.76	
Tm				0.37	0.35				0.23	
Yb				2.66	2.50				1.75	
Lu				0.38	0.36				0.39	
Sc				37.45	38.99				50.28	
V	232	256	237	386	358	285	330	265	247	242
Cr	373	578	412	211	58	69	129	360	364	346
Co				43	41				44	
Ni	141	232	137	80	56	56	81	142	127	151
Cu				207	182				89	
Zn	67	72	62	115	111	118	95	73	68	70
Ga	12	15	13	20	20	16	19	12	11	13
Rb	15.9	6.5	3.3	1.7	5.9	4.6	5	16.3	2.1	16.9
Sr	392	272	484	225	187	148	190	485	303	260
Y	13.8	20.4	16.2	29.4	26.2	26.7	24.8	18.1	15.3	14.9
Zr	26	45	35	146	113	59	109	40	23	29
Nb	1.4	1.6	2.8	13.1	10.3	3.9	9.4	3.1	1.3	1.7
Cs				0.12	0.09				0.30	
Ba	173	108	190	57	70	118	73	186	44	198
Hf				4.03	3.17				0.78	
Ta				0.76	0.61				0.08	
Pb				1.01	0.72				0.21	
Th				1.24	0.84				0.56	
U				0.36	0.24				0.20	
La(XRF)	3	2	6	9	7	6	5	6	3	4
Ce(XRF)	7	9	14	31	20	13	21	13	6	8

SAMPLE	5802A4 (1)	5802A4 (2)	5802A5	5802A6	5806A3	5806A5	5806A6	5808A1	5808A2	5808A3
Group	LOW-TI	CWPIC	LOW-TI	LOW-TI	HI-TI	HI-TI	HI-TI	RC	RCPIC	RCPIC
Area	CLEAR	CLEAR	CLEAR	CLEAR	GLAC	GLAC	GLAC	RAINY	RAINY	RAINY
Flow	PIL	PIL	PIL	SIL?	FLO	FLO	FLO	TUF	TUF	TUF
UTM EW	6993057	6993057	6993004	6992950	7000695	7000232	6999795	7021484	7021213	7021298
UTM NS	483801	483801	483762	483733	538926	538787	538622	556534	556314	556392
<i>Unnormalized Major Element Oxides (Weight %):</i>										
SiO <sub>2</sub>	48.26	48.28	46.68	51.77	49.67	49.86	50.25	49.93	46.44	46.89
TiO <sub>2</sub>	0.5	0.5	0.93	0.9	2.37	1.97	1.89	1.01	1.06	1.18
Al <sub>2</sub> O <sub>3</sub>	15.81	15.83	16.19	14.82	13.98	14.58	13.96	14.09	10.72	10.72
Fe <sub>2</sub> O <sub>3</sub> *	10.73	10.75	12.21	11	13.53	12.98	12.79	13.4	10.72	10.72
MnO	0.19	0.19	0.2	0.19	0.21	0.21	0.21	0.22	0.15	0.18
MgO	13.49	13.47	10.21	7.95	6.4	6.6	6.62	7.31	15.42	14.78
CaO	9.2	9.19	12.16	11.72	10.36	10.83	12.24	11.9	9.59	9.42
Na <sub>2</sub> O	1.48	1.51	1.23	1.47	2.14	2.25	1.59	1.61	1.34	0.88
K <sub>2</sub> O	0.05	0.05	0.12	0.3	0.68	0.57	0.29	0.31	0.35	1.12
P <sub>2</sub> O <sub>5</sub>	0.09	0.09	0.1	0.09	0.22	0.17	0.17	0.1	0.09	0.11
LOI	4.51	4.53	3.32	1.56	1.82	1.62	1.67	1.98	3.2	2.4
Total	99.80	99.86	100.03	100.21	99.56	100.02	100.01	99.88	99.86	100.01
<i>Trace elements (ppm):</i>										
La	5.18	5.18	3.58						5.99	6.52
Ce	12.40	12.40	9.28						15.32	18.08
Pr	1.48	1.48	1.32						1.96	2.33
Nd	6.61	6.61	6.68						9.85	11.57
Sm	1.69	1.69	2.19						2.69	3.01
Eu	0.51	0.51	0.84						0.94	1.09
Gd	1.84	1.84	2.53						2.77	3.02
Tb	0.40	0.40	0.54						0.51	0.54
Dy	2.62	2.62	3.76						3.25	3.23
Ho	0.56	0.56	0.79						0.66	0.63
Er	1.76	1.76	2.30						1.79	1.79
Tm	0.23	0.23	0.29						0.21	0.22
Yb	1.69	1.69	2.12						1.48	1.45
Lu	0.27	0.27	0.33						0.22	0.25
Sc	40.80	40.80	45.91						27.29	29.39
V	202	203	257	254	369	339	327	313	285.54	297.75
Cr	1596	1577	633	448	213	141	123	138	1327	1250
Co	60	60	58						67	63
Ni	539	538	244	128	89	87	78	76	620	525
Cu	78	78	103						123	79
Zn	74	74	82	85	119	112	101	111	60	63
Ga	13	13	16	16	21	20	19	16	13	13
Rb	0.4	0.5	3	8.8	13.9	11.8	4.9	5.8	6.11	26.43
Sr	183	184	252	188	215	208	205	185	126.86	92.53
Y	15.4	15.2	20.7	18.5	29.1	25.4	25.4	28.5	16.01	15.81
Zr	35	35	46	49	144	116	112	41	58.73	65.10
Nb	2	2.1	1.5	3	12.9	10.4	9.6	5.3	6.00	8.11
Cs	0.50	0.50	0.30						0.43	1.10
Ba	39	37	40	92	182	118	108	140	72	191
Hf	1.05	1.05	1.51						1.71	1.88
Ta	0.11	0.11	0.08						0.35	0.48
Pb	0.13	0.13	0.50						0.76	0.65
Th	0.89	0.89	0.34						0.70	1.06
U	0.32	0.32	0.11						0.26	0.38
La(XRF)	4	5	2	2	9	7	6	3	6	7
Ce(XRF)	7	11	4	4	27	21	19	7	15	18

SAMPLE	5808A6	5808A8	5810A1 (1)	5810A1 (2)	5810A2	5810A4	5810A6 (1)	5810A6 (2)	5810A10	5811A1
Group	RC	RC	LOW-TI	LOW-TI	LOW-TI	LOW-TI	LOW-TI	LOW-TI	HI-TI	LOW-TI
Area	RAINY	RAINY	TANGLE	TANGLE	TANGLE	TANGLE	TANGLE	TANGLE	TANGLE	TANGLE
Flow	DIK	SIL	PIL	PIL	SIL	SIL	PIL	PIL	PIL	SIL
UTM EW	7021445	7021631	6999686	6999686	6999760	6999733	6999748	6999748	7000019	6999515
UTM NS	556560	557160	550380	550380	550367	550310	550268	550268	550092	550374
<i>Unnormalized Major Element Oxides (Weight %):</i>										
SiO <sub>2</sub>	49.27	50.04	47.02	46.82	48.39	48.45	48.75	48.69	50.27	49.18
TiO <sub>2</sub>	0.93	1.14	0.57	0.57	0.54	0.73	0.64	0.64	1.74	0.35
Al <sub>2</sub> O <sub>3</sub>	14.71	13.39	15.84	15.8	16.2	17.2	16.2	16.1	14.61	15.84
Fe <sub>2</sub> O <sub>3</sub> *	10.76	15.35	10.94	10.96	11.32	11.81	12.01	12.03	12.04	9.09
MnO	0.2	0.25	0.18	0.18	0.2	0.2	0.24	0.24	0.19	0.17
MgO	8.88	6.57	11.23	11.16	9.96	7.32	6.34	6.26	6.71	11.93
CaO	11.31	11.27	13.14	13.09	12.21	12.5	13.95	13.98	12.81	12.38
Na <sub>2</sub> O	1.73	1.52	1.19	1.04	1.22	1.25	1.86	1.77	1.3	0.88
K <sub>2</sub> O	1.57	0.06	0.06	0.07	0.07	0.06	0.15	0.15	0.14	0.07
P <sub>2</sub> O <sub>5</sub>	0.27	0.11	0.07	0.07	0.06	0.12	0.08	0.08	0.15	0.05
LOI	2.16	1.96	2.68	2.65	2.62	2.19	1.73	1.72	1.49	3.27
Total	99.63	99.70	100.24	99.76	100.17	99.64	100.22	99.94	99.96	99.94
<i>Trace elements (ppm):</i>										
La			1.16	1.16	1.94	3.45	2.30	2.30	7.81	
Ce			3.40	3.40	4.53	8.87	5.88	5.88	20.71	
Pr			0.57	0.57	0.61	1.20	0.83	0.83	2.83	
Nd			3.31	3.31	3.21	6.12	4.52	4.52	13.98	
Sm			1.26	1.26	1.16	1.96	1.55	1.55	3.95	
Eu			0.43	0.43	0.46	0.73	0.51	0.51	1.45	
Gd			1.51	1.51	1.46	2.15	1.79	1.79	3.94	
Tb			0.36	0.36	0.35	0.45	0.42	0.42	0.76	
Dy			2.59	2.59	2.53	3.28	2.94	2.94	4.63	
Ho			0.57	0.57	0.56	0.72	0.64	0.64	0.95	
Er			1.74	1.74	1.78	2.13	1.95	1.95	2.50	
Tm			0.24	0.24	0.23	0.28	0.26	0.26	0.29	
Yb			1.70	1.70	1.75	1.99	1.88	1.88	2.05	
Lu			0.27	0.27	0.27	0.32	0.33	0.33	0.32	
Sc			50.28	50.28	47.06	41.96	43.29	43.29	35.80	
V	289	363	261	260	253	271	261	262	308	182
Cr	629	58	493	491	182	81	131	129	133	380
Co			53	53	50	45	43	43	41	
Ni	137	56	208	207	163	100	91	92	88	274
Cu			98	98	110	116	85	85	151	
Zn	102	127	74	73	78	88	98	98	100	64
Ga	18	17	13	13	13	15	14	14	19	10
Rb	18.3	0.5	0.9	0.6	0.8	0.4	2	1.9	2.6	0.9
Sr	801	58	151	150	141	198	170	170	231	114
Y	16.7	32.6	15.5	15.5	15.5	18.5	17.2	17.2	23	11.8
Zr	65	43	18	17	19	28	26	26	102	19
Nb	4	4.8	1.1	1	1	1.4	1.3	1.3	8.8	1.3
Cs			0.17	0.17	0.12	0.12	0.18	0.18	0.09	
Ba	674	39	62	62	62	33	75	78	59	102
Hf			0.66	0.66	0.66	0.96	0.88	0.88	2.84	
Ta			0.04	0.04	0.05	0.06	0.10	0.10	0.59	
Pb			0.23	0.23	0.44	0.26	0.63	0.63	0.76	
Th			0.09	0.09	0.27	0.30	0.28	0.28	0.78	
U			0.04	0.04	0.10	0.09	0.12	0.12	0.24	
La(XRF)	8	3	1	0	2	3	3	0	6	2
Ce(XRF)	20	7	3	1	3	7	2	4	19	3

The Nikolai Formation in Alaska has similar major- and trace-element chemistry to Nikolai basalts from Yukon, which also have high- and low-titanium basalts (Fig. 3.10). Nikolai basalts in Alaska are notably lower in total alkalis than basalts from Yukon due to alkali metasomatism during alteration of the Yukon basalts (see chapter 4).

The low-titanium basalts are characterized by a range of flat and slightly light rare earth element (LREE)-depleted chondrite-normalized REE patterns (mean  $\text{La/Sm}_{\text{CN}} = 0.8 \pm 0.5$ , except one LREE-enriched sample) with flat, parallel heavy REE (HREE) segments (mean  $\text{Dy/Yb}_{\text{CN}} = 1.0 \pm 0.2$ ; Fig. 3.11). The high-titanium basalts form a tight range of parallel LREE-enriched patterns (mean  $\text{La/Yb}_{\text{CN}} = 2.3 \pm 0.9$ ) with higher REE abundances (mean  $\text{Yb}_{\text{CN}} = 16.1 \pm 6.4$ ) than the low-titanium basalts (mean  $\text{Yb}_{\text{CN}} = 11.0 \pm 2.2$ ; Fig. 3.11). Several low-titanium basalts from the Amphitheater Mountains have positive Eu anomalies (Fig. 3.11). Several high-titanium basalts from the Wrangell Mountains have patterns with flatter HREE segments. The basal flow-conglomerate from the Wrangell Mountains has a distinct LREE-enriched pattern ( $\text{La/Sm}_{\text{CN}} = 2.7$ ) with a flat HREE segment ( $\text{Dy/Yb}_{\text{CN}} = 1.2$ ). The Rainy Creek picrites are LREE-enriched ( $\text{La/Yb}_{\text{CN}} = 2.8\text{--}3.1$ ) and the REE pattern of the Clearwater picrite is LREE-enriched ( $\text{La/Sm}_{\text{CN}} = 1.9$ ) with a flat HREE segment ( $\text{Dy/Yb}_{\text{CN}} = 1.0$ ).

The low-titanium basalts have mostly parallel, primitive mantle-normalized trace-element patterns with pronounced HFSE depletions, especially for Nb, Ta, and Zr, relative to LILE and REE (Fig. 3.11), and HFSE (Nb and Zr) form linear trends (Fig. 3.12). The large negative Zr anomalies in the low-titanium basalts are not accompanied by comparably low Hf (Fig. 3.11d). The LILE segments of trace-element patterns for low-titanium basalts are parallel and each of the patterns has a pronounced positive Sr anomaly, relative to Nd and Sm. The high-titanium basalts form a tight range of parallel, concave-downward trace-element patterns with negative Pb anomalies, relative to Ce and Pr, and small negative K anomalies, relative to U and Nb (Fig. 3.11). The LILE in the high-titanium basalts are slightly depleted relative to the HFSE and LREE. The Clearwater picrite is depleted in HFSE with a positive Sr anomaly, similar to the low-titanium basalts, whereas Rainy Creek picrites have gently negative-sloping patterns with negative Sr anomalies (Fig. 3.11).

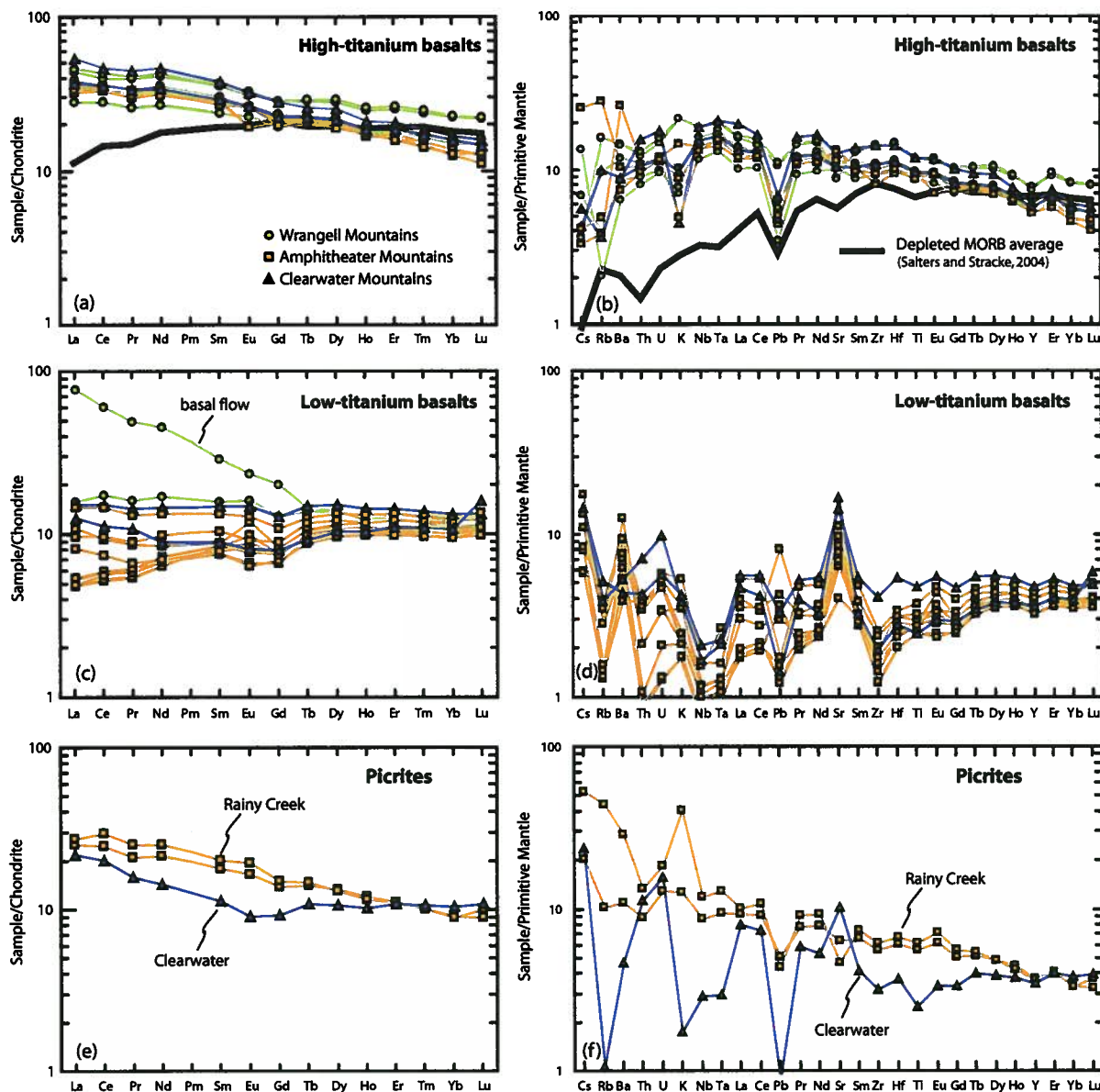


**Figure 3.11** Whole-rock REE and other incompatible-element concentrations for the Nikolai Formation in Alaska. (a), (c), and (e) are chondrite-normalized REE patterns for high-titanium basalts, low-titanium basalts, and picrites, respectively, from field areas in southern Alaska. (b), (d), and (f) are primitive mantle-normalized trace-element patterns for high-titanium basalts, low-titanium basalts, and picrites, respectively. All normalization values are from McDonough and Sun (1995). Depleted MORB average from Salters and Stracke (2004). Note the clear distinction between LREE-enriched high-titanium basalt and mostly LREE-depleted low-titanium basalts. Trace-element patterns for the basal flow-conglomerate and one Clearwater sample are not shown in panel d for clarity.

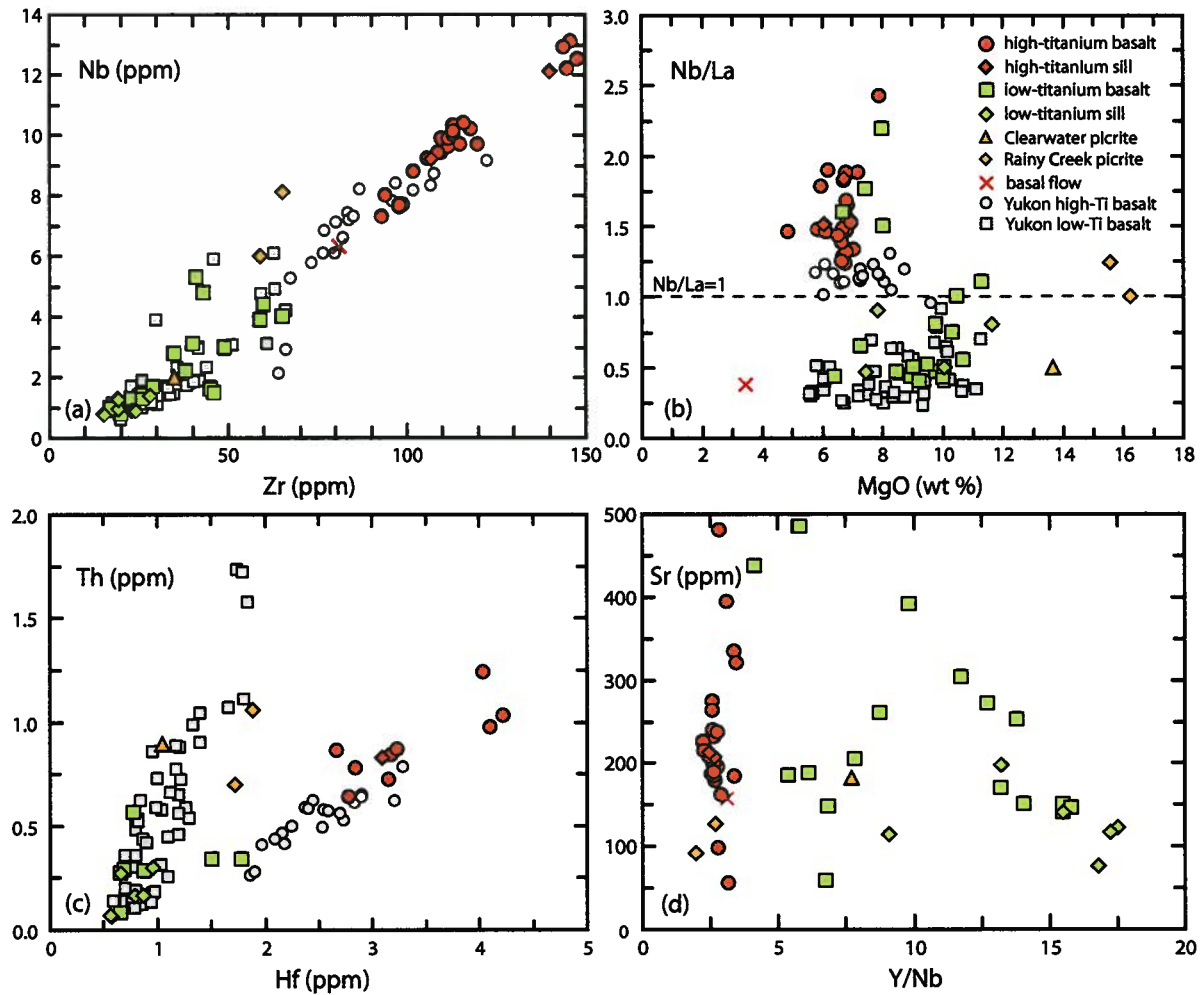


**Figure 3.12** Whole-rock trace-element concentration variations and ratios for the Nikolai Formation in Alaska (except panel b is versus MgO), with data for the Nikolai Formation in Yukon. (a) Nb vs. Zr. (b) Nb/La vs. MgO. (c) Th vs. Hf. (d) Sr vs. Y/Nb. Note the clear distinction between the high- and low-titanium basalt in each of the plots.

### **Sr-Nd-Hf-Pb isotopic compositions**

The high- and low-titanium Wrangellia basalts in Alaska have distinct Hf and Sr isotope ratios (Fig. 3.13). The low-titanium basalts have higher initial  $\epsilon_{\text{Hf}}$  (+13.7 to +18.4) and  $^{87}\text{Sr}/^{86}\text{Sr}$  (0.70422-0.70554) than the high-titanium basalts (initial  $\epsilon_{\text{Hf}}$  = +9.7 to +10.7, initial  $^{87}\text{Sr}/^{86}\text{Sr}$  = 0.70302-0.70376), except for sample 5715A5, which has anomalous chemistry (Fig. 3.13; Tables 3.3 and 3.4). The low-titanium basalts have a narrower range in initial  $\epsilon_{\text{Nd}}$  (+4.6 to +5.4) than the high-titanium basalts (initial  $\epsilon_{\text{Nd}}$  = +6.0 to +8.1) and a wider range in initial  $\epsilon_{\text{Hf}}$ , except for three low-titanium samples with higher initial  $\epsilon_{\text{Nd}}$  (+7.0 to +7.6). The basal flow-conglomerate in the Wrangell Mountains has similar initial Sr, Nd, and Hf isotopic compositions to the high-titanium basalts. The Clearwater picrite lies between the high- and low-titanium basalts in initial  $\epsilon_{\text{Hf}}$ , and has the lowest initial  $\epsilon_{\text{Nd}}$  and initial  $^{87}\text{Sr}/^{86}\text{Sr}$  at the upper end of the range of all samples. The two Rainy Creek picrites have similar Sr, Nd, and Hf isotope ratios to high-titanium basalts with slightly lower initial  $\epsilon_{\text{Nd}}$  (Fig. 3.13).

The high- and low-titanium basalts have indistinguishable age-corrected Pb isotopic compositions, although the high-titanium basalts show a narrower range (Fig. 3.14). The range of initial Pb isotopic compositions for low-titanium basalts is  $^{206}\text{Pb}/^{204}\text{Pb}$  = 18.421-19.418,  $^{207}\text{Pb}/^{204}\text{Pb}$  = 15.568-15.609, and  $^{208}\text{Pb}/^{204}\text{Pb}$  = 37.962-38.481 and the high-titanium basalts have  $^{206}\text{Pb}/^{204}\text{Pb}$  = 18.504-18.888,  $^{207}\text{Pb}/^{204}\text{Pb}$  = 15.556-15.587, and  $^{208}\text{Pb}/^{204}\text{Pb}$  = 38.008-38.451 (Fig. 3.14; Table 3.5). The basal flow-conglomerate has a slightly lower initial Pb isotopic composition than the high- and low-titanium basalts. The Clearwater picrite has a lower initial Pb isotope ratio than the basalts and the Rainy Creek picrites have noticeably higher initial Pb isotope ratios than the basalts (Fig. 3.14).

### **ALTERATION**

The Nikolai basalts generally preserve primary mineralogical, textural, and volcanological features and have retained most of their primary magmatic composition. Secondary minerals have replaced variable, but generally small, proportions of primary minerals in the Nikolai Formation and the basalts contain zeolite to prehnite-pumpellyite facies alteration minerals (prehnite + pumpellyite + epidote + chlorite + quartz  $\pm$



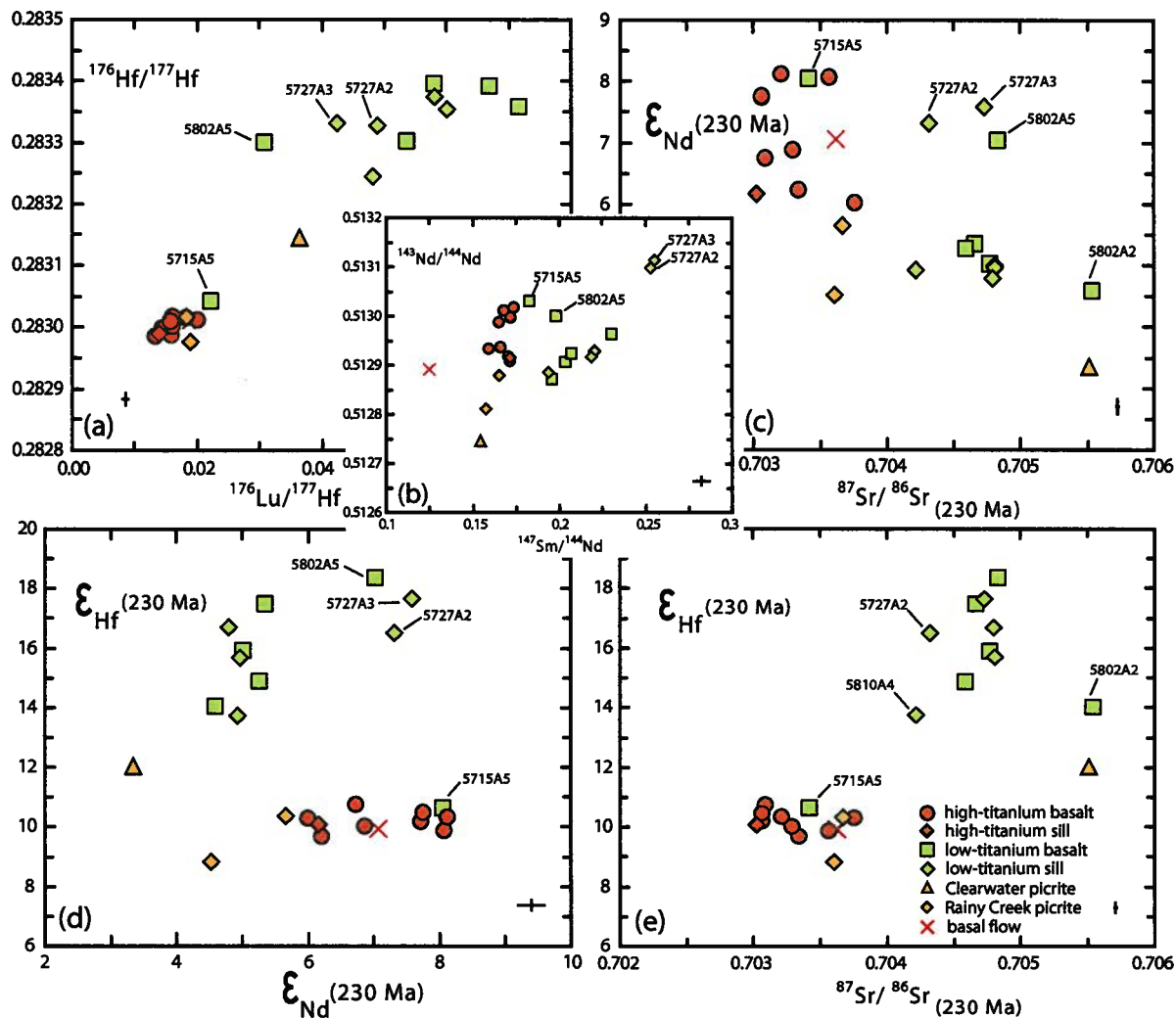


**Figure 3.13** Whole-rock Sr, Nd, and Hf isotopic compositions for the Nikolai Formation in Alaska. (a)  $^{176}\text{Hf}/^{177}\text{Hf}$  vs.  $^{176}\text{Lu}/^{177}\text{Hf}$ . (b)  $^{143}\text{Nd}/^{144}\text{Nd}$  vs.  $^{147}\text{Sm}/^{144}\text{Nd}$ . (c) Initial  $\epsilon_{\text{Nd}}$  vs.  $^{87}\text{Sr}/^{86}\text{Sr}$ . Age correction to 230 Ma. (d) Initial  $\epsilon_{\text{Hf}}$  vs.  $\epsilon_{\text{Nd}}$ . (e) Initial  $\epsilon_{\text{Hf}}$  vs.  $^{87}\text{Sr}/^{86}\text{Sr}$ . Average  $2\sigma$  error bars are shown in a corner of each panel.

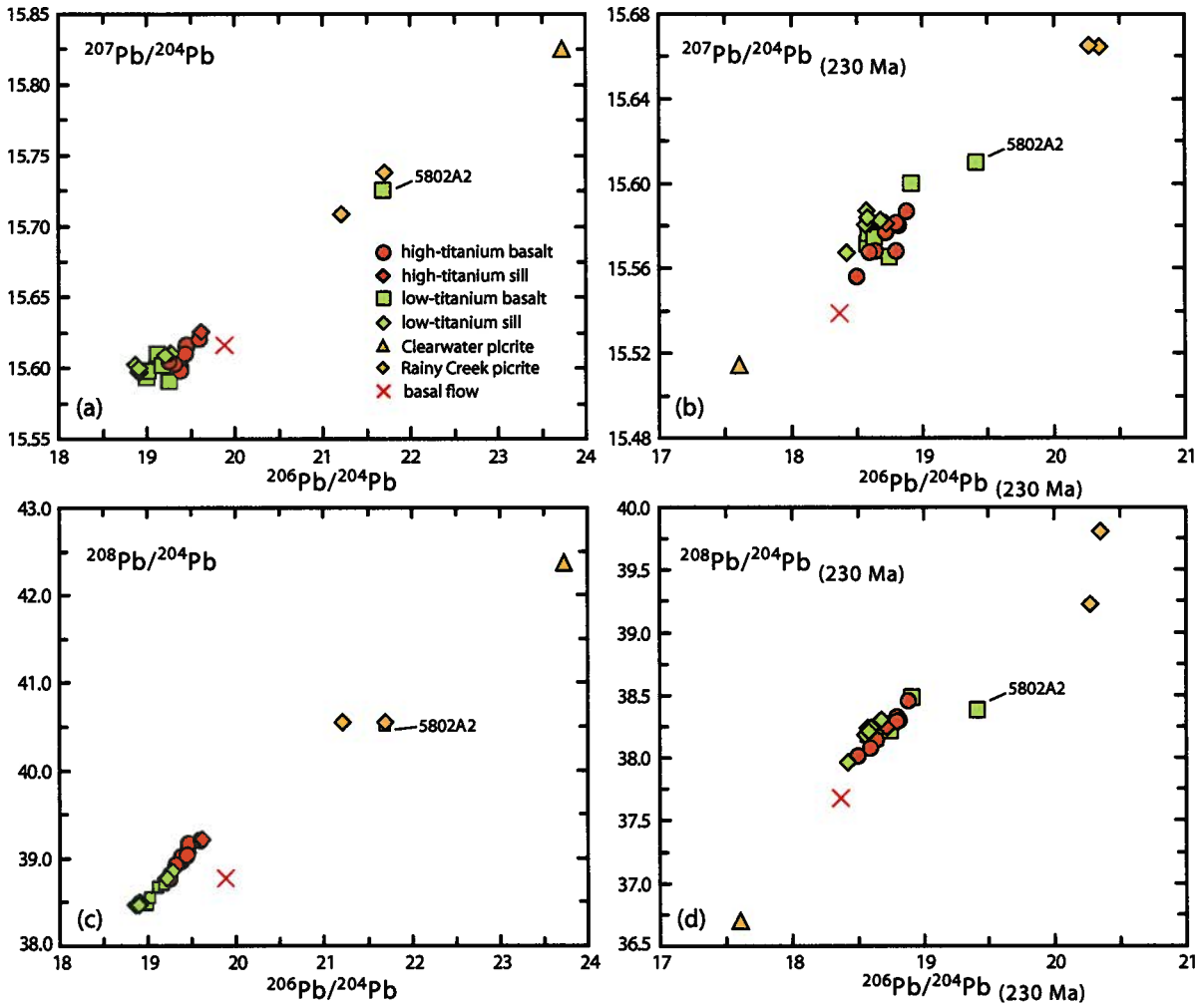


**Figure 3.14** Pb isotopic compositions of leached whole-rock samples by MC-ICP-MS for the Nikolai Formation in Alaska. Error bars are smaller than symbols. (a) Measured  $^{207}\text{Pb}/^{204}\text{Pb}$  vs.  $^{206}\text{Pb}/^{204}\text{Pb}$ . (b) Initial  $^{207}\text{Pb}/^{204}\text{Pb}$  vs.  $^{206}\text{Pb}/^{204}\text{Pb}$ . Age-correction to 230 Ma. (c) Measured  $^{208}\text{Pb}/^{204}\text{Pb}$  vs.  $^{206}\text{Pb}/^{204}\text{Pb}$ . (d) Initial  $^{208}\text{Pb}/^{204}\text{Pb}$  vs.  $^{206}\text{Pb}/^{204}\text{Pb}$ .

Table 3.3 Sr and Nd isotopic geochemistry of whole rock samples of Nikolai basalts, Alaska

Sample	Group <sup>a</sup>	Area <sup>b</sup>	Rb	Sr	<sup>87</sup> Sr/ <sup>86</sup> Sr	2σ <sub>m</sub>	<sup>87</sup> Rb/ <sup>86</sup> Sr	<sup>87</sup> Sr/ <sup>86</sup> Sr	Sm	Nd	<sup>143</sup> Nd/ <sup>144</sup> Nd	2σ <sub>m</sub>	ε <sub>Nd</sub>	<sup>147</sup> Sm/ <sup>144</sup> Nd	<sup>143</sup> Nd/ <sup>144</sup> Nd	ε <sub>Nd</sub> (t)
			(ppm)	(ppm)					(ppm)	(ppm)					230 Ma	
5708A2	HI-Ti	WM	9.7	162	0.703776	7	0.1733	0.70321	5.22	18.83	0.513011	5	7.3	0.1677	0.51276	8.1
5801A2	HI-Ti	CL	1.7	225	0.703365	8	0.0219	0.70329	5.55	21.10	0.512934	7	5.8	0.1592	0.51269	6.9
5719A5	HI-Ti	WM	5.9	200	0.703344	8	0.0854	0.70306	4.45	16.26	0.512988	6	6.8	0.1653	0.51274	7.7
5801A5	HI-Ti	CL	5.9	187	0.703389	8	0.0913	0.70309	4.25	15.51	0.512937	6	5.8	0.1659	0.51269	6.7
5712A2	HI-Ti	WM	2.2	184	0.703179	8	0.0346	0.70307	4.19	14.73	0.512987	6	7.0	0.1720	0.51274	7.7
5726A1	HI-Ti	TA	2.1	239	0.703844	7	0.0254	0.70376	4.07	14.35	0.512908	7	5.3	0.1713	0.51265	6.0
5810A10	HI-Ti	TA	2.6	231	0.703448	9	0.0326	0.70334	3.95	13.98	0.512918	6	5.5	0.1707	0.51266	6.2
5715A1	HI-Ti	WM	1.0	184	0.703619	7	0.0157	0.70357	3.51	12.20	0.513017	7	7.4	0.1738	0.51276	8.1
5715A5	Low-Ti	WM	8.5	437	0.703602	8	0.0563	0.70342	2.32	7.68	0.513030	5	7.6	0.1829	0.51275	8.1
5802A5	Low-Ti	CL	3.0	252	0.704942	6	0.0345	0.70483	2.19	6.68	0.513000	6	7.1	0.1980	0.51270	7.0
5810A6	Low-Ti	TA	2.0	170	0.704704	7	0.0340	0.70459	1.55	4.52	0.512924	6	5.6	0.2070	0.51261	5.3
5810A1	Low-Ti	TA	0.9	151	0.704721	7	0.0172	0.70466	1.26	3.31	0.512963	5	6.3	0.2303	0.51262	5.4
5727A7	Low-Ti	TA	1.5	155	0.704865	9	0.0280	0.70477	1.30	3.86	0.512906	7	5.2	0.2038	0.51260	5.0
5802A2	Low-Ti	CL	2.1	303	0.705604	8	0.0201	0.70554	1.31	4.04	0.512872	7	4.6	0.1959	0.51258	4.6
5719A1	Basal	WM	25.4	158	0.705138	7	0.4652	0.70362	4.26	20.65	0.512892	6	5.0	0.1248	0.51270	7.1
5725A4	SIII (HI-Ti)	TA	16.5	207	0.703775	8	0.2306	0.70302	4.30	15.16	0.512916	7	5.4	0.1715	0.51266	6.2
5727A2	SIII (Low-Ti)	TA	1.7	76	0.704532	8	0.0647	0.70432	1.22	2.92	0.513098	6	9.0	0.2531	0.51272	7.3
5727A3	SIII (Low-Ti)	TA	1.8	117	0.704872	8	0.0445	0.70473	1.23	2.92	0.513115	8	9.3	0.2553	0.51273	7.6
5727A6	SIII (Low-Ti)	TA	0.6	123	0.704857	10	0.0141	0.70481	1.11	3.05	0.512930	7	5.7	0.2203	0.51280	5.0
5727A6 (dup)	SIII (Low-Ti)	TA	0.6	123	0.704851	8	0.0141	0.70480	1.13	3.09	0.512928	10	5.7	0.2202	0.51280	5.0
5810A2	SIII (Low-Ti)	TA	0.8	141	0.704846	7	0.0164	0.70479	1.16	3.21	0.512917	6	5.4	0.2187	0.51259	4.8
5810A4	SIII (Low-Ti)	TA	0.4	198	0.704235	8	0.0058	0.70422	1.96	6.12	0.512886	6	4.8	0.1937	0.51259	4.9
5802A4	Picrite	CL	0.4	183	0.705530	9	0.0063	0.70551	1.69	6.61	0.512746	6	2.1	0.1544	0.51251	3.3
5808A2	Picrite	RC	6.1	127	0.704124	10	0.1395	0.70367	2.69	9.85	0.512880	6	4.7	0.1649	0.51263	5.7
5808A3	Picrite	RC	26.4	93	0.706307	9	0.8265	0.70360	3.01	11.57	0.512811	6	3.4	0.1576	0.51257	4.5

<sup>a</sup>HI-Ti, high-titanium basalt; Low-Ti, low-titanium basalt; Basal, basal flow-conglomerate. <sup>b</sup>Abbreviations for area are: WM, Wrangell Mountains; TA, Tangle Lake; GG, Glacier Gap Lake; CL, Clearwater Mountains; RC, Rainy Creek. (dup) indicates complete chemistry duplicate. All trace-element and isotopic analyses were carried out at the PCIGR. The analytical methods are described in Appendix D.

Table 3.4 Hf isotopic compositions of whole rock samples of Nikolai basalts, Alaska

Sample	Group <sup>a</sup>	Area <sup>b</sup>	Lu	Hf	<sup>177</sup> Hf/ <sup>178</sup> Hf	2σ <sub>m</sub>	ε <sub>Hf</sub>	<sup>176</sup> Lu/ <sup>177</sup> Hf	<sup>177</sup> Hf/ <sup>176</sup> Hf <sub>i</sub>	ε <sub>Hf</sub> (t)
			(ppm)	(ppm)					230 Ma	
5708A2	HI-TI	WM	0.53	4.10	0.28302	5	8.6	0.0184	0.28293	10.3
5801A2	HI-TI	CL	0.38	4.03	0.28299	6	7.6	0.0134	0.28293	10.0
5719A5	HI-TI	WM	0.36	3.23	0.28301	6	8.4	0.0159	0.28294	10.5
5801A5	HI-TI	CL	0.36	3.17	0.28302	7	8.7	0.0161	0.28295	10.7
5712A2	HI-TI	WM	0.36	3.15	0.28300	6	8.2	0.0162	0.28293	10.2
5726A1	HI-TI	TA	0.27	2.66	0.28300	6	8.0	0.0146	0.28293	10.3
5810A10	HI-TI	TA	0.32	2.84	0.28299	6	7.6	0.0160	0.28292	9.7
5715A1	HI-TI	WM	0.40	2.78	0.28301	5	8.5	0.0202	0.28292	9.9
5715A5	Low-TI	WM	0.28	1.79	0.28304	6	9.6	0.0223	0.28294	10.6
5802A5	Low-TI	CL	0.33	1.51	0.28330	14	18.6	0.0309	0.28316	18.4
5810A6	Low-TI	TA	0.33	0.88	0.28330	6	18.7	0.0537	0.28306	14.9
5810A1	Low-TI	TA	0.27	0.66	0.28340	5	22.1	0.0581	0.28314	17.5
5727A7	Low-TI	TA	0.33	0.70	0.28339	7	21.9	0.0670	0.28309	15.9
5802A2	Low-TI	CL	0.39	0.78	0.28336	7	20.7	0.0717	0.28304	14.0
5719A1	Basal	WM	0.31	2.30	0.28301	6	8.3	0.0188	0.28292	9.9
5725A4	SIII (HI-TI)	TA	0.30	3.08	0.28299	5	7.7	0.0141	0.28293	10.1
5727A2	SIII (Low-TI)	TA	0.27	0.80	0.28333	7	19.7	0.0489	0.28311	16.5
5727A3	SIII (Low-TI)	TA	0.26	0.87	0.28333	9	19.8	0.0425	0.28314	17.7
5727A6	SIII (Low-TI)	TA	0.24	0.57	0.28335	8	20.6	0.0602	0.28309	15.7
5810A2	SIII (Low-TI)	TA	0.27	0.66	0.28337	6	21.3	0.0581	0.28311	16.7
5810A4	SIII (Low-TI)	TA	0.32	0.96	0.28325	8	16.7	0.0481	0.28303	13.7
5802A4	Picrite	CL	0.27	1.05	0.28315	6	13.2	0.0365	0.28298	12.0
5808A2	Picrite	RC	0.22	1.71	0.28302	7	8.7	0.0184	0.28294	10.3
5808A3	Picrite	RC	0.25	1.88	0.28298	6	7.2	0.0189	0.28289	8.8

<sup>a</sup>HI-TI, high-titanium basalt; Low-TI, low-titanium basalt; Basal, basal flow-conglomerate. <sup>b</sup>Abbreviations for area are: WM, Wrangell Mountains; TA, Tangle Lake; GG, Glacier Gap Lake; CL, Clearwater Mountains; RC, Rainy Creek. All trace-element and isotopic analyses were carried out at the PCIGR. The analytical methods are described in Appendix D.

Table 3.5 Pb isotopic compositions of whole rock samples of Nikolai basalts, Alaska

Sample	Group <sup>a</sup>	Area <sup>b</sup>	U	Th	Pb	(ppm)											
						<sup>206</sup> Pb/ <sup>204</sup> Pb	2σ <sub>m</sub>	<sup>207</sup> Pb/ <sup>204</sup> Pb	2σ <sub>m</sub>	<sup>208</sup> Pb/ <sup>204</sup> Pb	2σ <sub>m</sub>	<sup>238</sup> U/ <sup>204</sup> Pb	<sup>235</sup> U/ <sup>204</sup> Pb	<sup>232</sup> Th/ <sup>204</sup> Pb	<sup>206</sup> Pb/ <sup>204</sup> Pb <sub>i</sub>	<sup>207</sup> Pb/ <sup>204</sup> Pb <sub>i</sub>	<sup>208</sup> Pb/ <sup>204</sup> Pb <sub>i</sub>
5708A2	HI-Ti	WM	0.31	0.98	1.59	19.2557	0.0006	15.6040	0.0005	38.7613	0.0014	12.39	0.09	40.95	18.806	15.581	38.289
5801A2	HI-Ti	CL	0.36	1.24	1.01	19.4404	0.0008	15.6100	0.0007	39.0217	0.0019	23.11	0.17	82.17	18.601	15.567	38.074
5719A5	HI-Ti	WM	0.25	0.87	0.85	19.3198	0.0007	15.6023	0.0006	38.9183	0.0013	18.64	0.14	67.86	18.643	15.568	38.136
5801A5	HI-Ti	CL	0.24	0.84	0.72	19.6020	0.0008	15.6197	0.0007	39.1955	0.0019	21.58	0.16	78.29	18.818	15.580	38.293
5712A2	HI-Ti	WM	0.20	0.72	0.81	19.3834	0.0011	15.5974	0.0009	39.0093	0.0024	16.00	0.12	59.61	18.802	15.568	38.322
5726A1	HI-Ti	TA	0.23	0.86	0.95	19.4594	0.0008	15.6158	0.0007	39.1506	0.0018	15.73	0.11	60.68	18.888	15.587	38.451
5810A10	HI-Ti	TA	0.24	0.78	0.76	19.4551	0.0007	15.6141	0.0005	39.0577	0.0014	20.20	0.15	68.74	18.721	15.577	38.265
5715A1	HI-Ti	WM	0.19	0.64	0.52	19.3815	0.0009	15.6002	0.0008	38.9557	0.0021	24.15	0.18	82.22	18.504	15.556	38.008
5715A5	Low-Ti	WM	0.09	0.34	0.44	19.2520	0.0008	15.5908	0.0007	38.8096	0.0027	13.88	0.10	51.33	18.748	15.565	38.218
5802A5	Low-Ti	CL	0.11	0.34	0.50	19.1708	0.0012	15.6019	0.0011	38.6861	0.0024	14.80	0.11	45.79	18.633	15.575	38.158
5810A6	Low-Ti	TA	0.12	0.28	0.63	19.0178	0.0007	15.5980	0.0006	38.5428	0.0017	11.84	0.09	29.87	18.588	15.576	38.198
5810A1	Low-Ti	TA	0.04	0.09	0.23	19.0025	0.0008	15.5927	0.0007	38.4697	0.0018	11.64	0.08	24.48	18.580	15.571	38.188
5727A7	Low-Ti	TA	0.10	0.29	1.21	19.1190	0.0007	15.6099	0.0005	38.6667	0.0014	5.54	0.04	16.07	18.918	15.600	38.481
5802A2	Low-Ti	CL	0.20	0.56	0.21	21.6909	0.0009	15.7248	0.0009	40.5119	0.0025	62.57	0.45	185.21	19.418	15.609	38.376
5719A1	Basal	WM	1.91	4.18	2.96	19.8855	0.0007	15.6160	0.0006	38.7767	0.0020	41.91	0.30	94.93	18.363	15.539	37.682
5725A4	SIII (HI-Ti)	TA	0.25	0.83	0.66	19.6092	0.0010	15.6258	0.0009	39.2093	0.0018	24.33	0.18	84.22	18.725	15.581	38.238
5727A2	SIII (Low-Ti)	TA	0.07	0.17	0.55	18.8625	0.0008	15.6021	0.0007	38.4711	0.0019	8.05	0.06	20.11	18.570	15.587	38.239
5727A3	SIII (Low-Ti)	TA	0.07	0.17	0.50	18.9004	0.0009	15.5998	0.0008	38.4641	0.0024	8.68	0.06	22.04	18.585	15.584	38.210
5727A6	SIII (Low-Ti)	TA	0.03	0.07	0.20	18.9076	0.0007	15.5967	0.0006	38.4960	0.0017	8.37	0.06	22.36	18.603	15.581	38.238
5727A6 (dup)	SIII (Low-Ti)	TA	0.03	0.07	0.18	18.9015	0.0005	15.5978	0.0005	38.4883	0.0014	9.40	0.07	25.99	18.580	15.581	38.189
5810A2	SIII (Low-Ti)	TA	0.10	0.27	0.44	19.1968	0.0008	15.6089	0.0007	38.7776	0.0016	14.21	0.10	40.97	18.681	15.583	38.305
5810A4	SIII (Low-Ti)	TA	0.09	0.30	0.26	19.2638	0.0008	15.6103	0.0007	38.8501	0.0018	23.20	0.17	77.04	18.421	15.568	37.962
5802A4	Picrite	CL	0.32	0.89	0.13	23.7352	0.0018	15.8255	0.0013	42.3716	0.0043	168.73	1.22	491.95	17.806	15.514	36.699
5808A2	Picrite	RC	0.26	0.70	0.76	21.2095	0.0014	15.7083	0.0012	40.5540	0.0030	23.59	0.17	64.96	20.353	15.665	39.805
5808A3	Picrite	RC	0.38	1.06	0.65	21.7002	0.0009	15.7379	0.0008	40.5468	0.0024	39.32	0.29	114.80	20.272	15.665	39.223

<sup>a</sup>HI-Ti, high-titanium basalt; Low-Ti, low-titanium basalt; Basal, basal flow-conglomerate. <sup>b</sup>Abbreviations for area are: WM, Wrangell Mountains; TA, Tangle Lake; GG, Glacier Gap Lake; CL, Clearwater Mountains; RC, Rainy Creek. (dup) Indicates complete chemistry duplicate. All trace-element and isotopic analyses were carried out at the PCIGR. The analytical methods are described in Appendix D.

laumonite), primarily making up the amygdules (Stout, 1976; Smith, 1981; MacKevett *et al.*, 1997). Many of the Nikolai basalts in the synform in the Amphitheater Mountains are exceptionally unaltered compared to flows in the Wrangell and Clearwater Mountains. Vesicles and interpillow voids in the Amphitheater Mountains commonly remain unfilled and secondary minerals are less common.

Seventeen of the 21 low-titanium basalts have LOI greater than 2.5 wt % and greater than 8 wt % MgO, whereas only four high-titanium basalts have greater than 2.5 wt % LOI and all have less than 8 wt % MgO (Fig. 3.15). Three of the four high-titanium basalts that lie within the alkalic field are plagioclase-rich, highly amygdaloidal, and were collected near a mineralized area at the top of the Nikolai Formation. Tight linear arrays are apparent on plots of HFSE and REE (not shown) indicating negligible affect of element mobility. Only a limited group of samples (5808A3, 5802A4, 5802A2, 5725A4, 5726A1) have LILE concentrations outside the narrow range of most high- and low-titanium basalts (Fig. 3.11) and there is no correlation between LOI and LILE. All of the low-titanium basalts have positive Sr anomalies that are complemented with small positive Eu anomalies in most samples, and none of the high-titanium basalts have Sr anomalies (Fig. 3.11), which indicates Sr concentrations probably represent primary values. U and Th show a linear relationship, whereas Pb and Th do not show a clear relationship (not shown), indicating some secondary mobility of Pb, especially in the low-titanium basalts.

Almost all initial Nd and Hf, and to a lesser extent Sr and Pb isotopic compositions represent close to magmatic compositions. Several of the more altered samples were not selected for isotopic analyses and leaching effectively removed most of the secondary alteration products (Weis *et al.*, 2006; Nobre Silva *et al.*, in revision). A single exception is the Clearwater picrite (5802A4), which was significantly affected by Pb loss and has less radiogenic age-corrected Pb isotopic ratios (Figs 3.11 and 3.14). The correlation of LOI and  $^{87}\text{Sr}/^{86}\text{Sr}$ ,  $^{206}\text{Pb}/^{204}\text{Pb}$ , and  $^{238}\text{U}/^{204}\text{Pb}$  in the low- and high-titanium basalts is a primary feature that is not apparent with age correction (Fig. 3.15). The rather small range of initial Pb and distinct initial Hf and Sr isotopic compositions for high- and low-titanium basalts clearly reflect the isotopic compositions of the sources of Wrangellia flood basalts in Alaska.

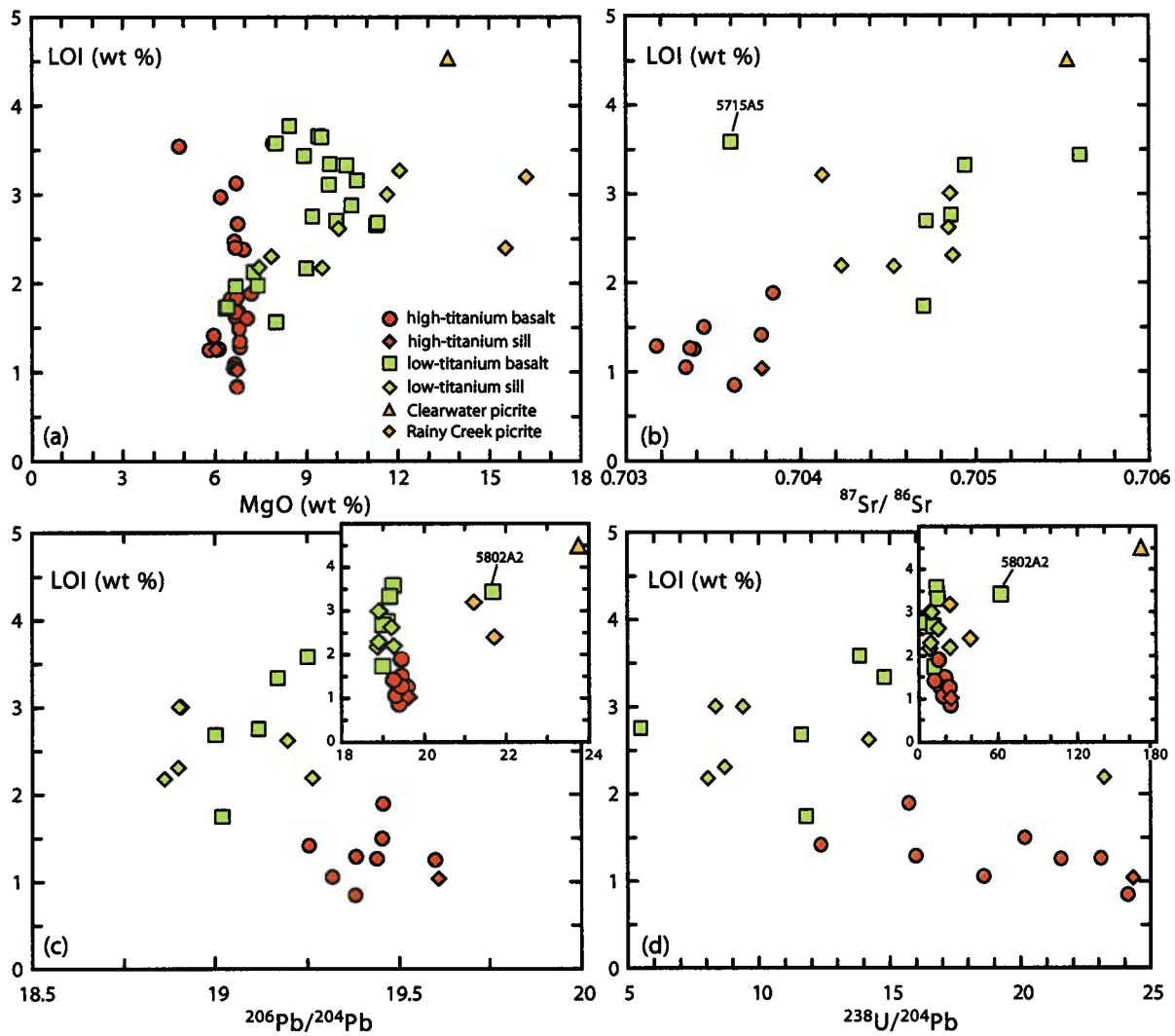


**Figure 3.15** Loss-on-ignition versus MgO and isotopic ratios for the Nikolai Formation in Alaska. (a) LOI vs. MgO. (b) LOI vs. measured  $^{87}\text{Sr}/^{86}\text{Sr}$ . (c) LOI vs. measured  $^{206}\text{Pb}/^{204}\text{Pb}$ . (d) LOI vs. measured  $^{238}\text{U}/^{206}\text{Pb}$ . The two insets show the expanded x-axis for  $^{206}\text{Pb}/^{204}\text{Pb}$  and  $^{238}\text{U}/^{206}\text{Pb}$ . Note the generally higher LOI and MgO for the low-titanium basalts. The differences in measured  $^{87}\text{Sr}/^{86}\text{Sr}$  and  $^{206}\text{Pb}/^{204}\text{Pb}$  within the suites of high- and low-titanium basalts are mostly not apparent after age-correction.

## FLOOD BASALT CHEMOSTRATIGRAPHY

Samples of the Nikolai Formation were collected going up or downsection through the volcanic stratigraphy to provide an estimate of the relative stratigraphic position of each sample and to determine the relationship between stratigraphic position and chemical composition. Figure 3.16 shows sample numbers, lithologies, relative stratigraphic height, and  $\text{TiO}_2$  and  $\text{MgO}$  contents for Nikolai basalts from the three main areas of Alaska where fieldwork was undertaken (Fig. 3.1). Each stratigraphic column is a combination of multiple traverses (separated by dashed lines in Figure 3.16). We are confident in the relative position of each section of stratigraphy because of the continuous exposure and minimal disruption by faults in these areas. Since the trace-element and isotopic variation of the basalts generally correspond with variation in  $\text{TiO}_2$  (Figs 3.10-3.13), only  $\text{TiO}_2$  and  $\text{MgO}$  are shown in Figure 3.16.

In the Clearwater and Amphitheater Mountains, there is a clear relationship between stratigraphic position and chemical composition of the flood basalts (Fig. 3.16). The low-titanium basalts form the lowermost several hundred meters of flows (10-15% of stratigraphy) and the high-titanium basalts form the majority of the flows (~85-90% of stratigraphy) above the lowest several hundred meters. More of the low-titanium basalts and sills were sampled, partly because lower sections of volcanic stratigraphy were more easily accessible and partly because there are more interesting relationships with pre-Nikolai sediments and mafic sills and submarine units preserved lower in the stratigraphy. The transition from low- to high-titanium basalts does not appear to coincide with the transition from submarine to subaerial flows, but almost all of the low-titanium basalts that were sampled are submarine flows.

In the Wrangell Mountains, there do not appear to be any low-titanium basalts, except for two anomalous samples (Fig. 3.16). A single sample of the basal flow-conglomerate has a low titanium content (0.67 wt %), similar initial  $\epsilon_{\text{HF}}$  to the high-titanium basalts, and anomalous  $\text{La/Yb}_{\text{CN}}$  (6.4),  $\text{Ba}$  (1277 ppm), and  $\text{Th}$  (4.18 ppm; Figs 3.10 and 3.13; Tables 3.2 and 3.4). Field observations and several other geochemical characteristics indicate the chemistry of this basal flow-conglomerate is the result of considerable assimilation (~30 vol %) of material derived from underlying Paleozoic



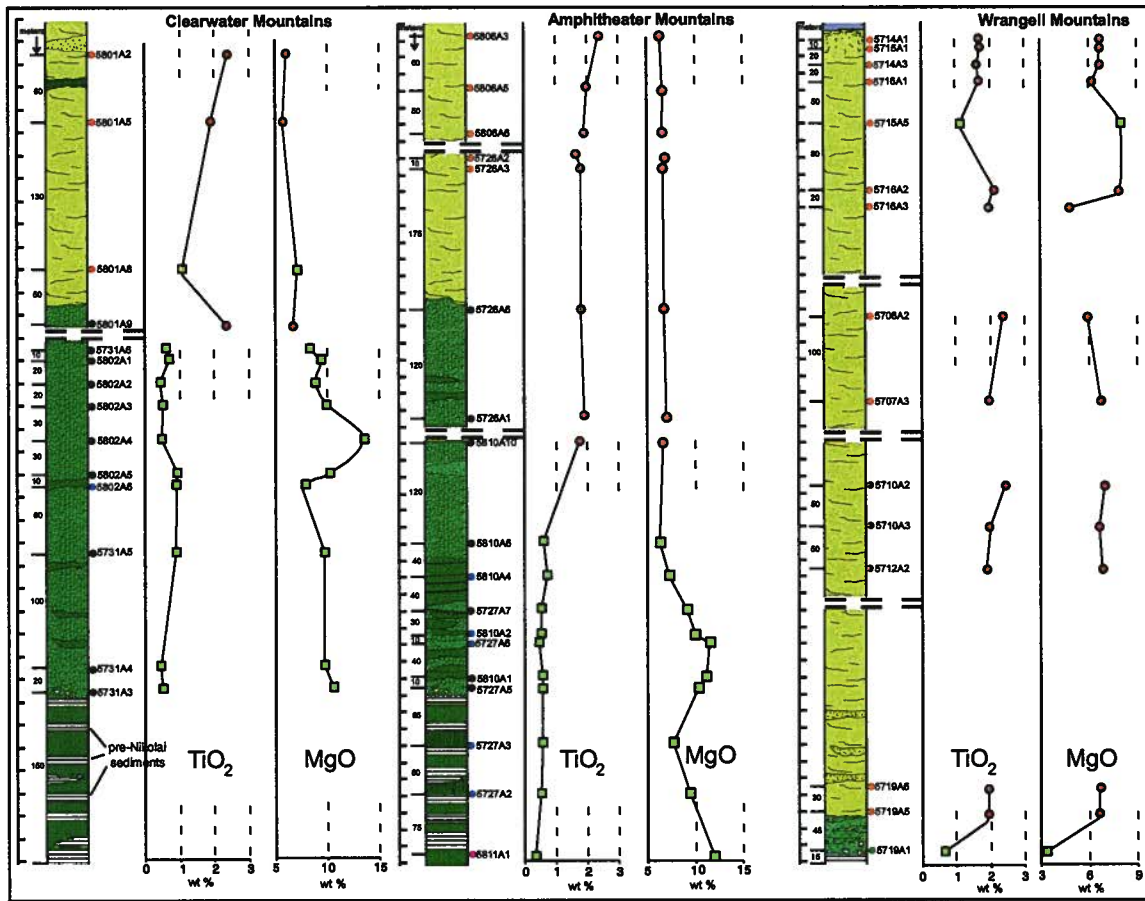


**Figure 3.16** Chemostratigraphy of the Nikolai Formation in three areas of Alaska (Clearwater, Amphitheater, and Wrangell Mountains). Each column shows lithology, sample numbers, relative stratigraphic height, and  $\text{TiO}_2$  and  $\text{MgO}$  contents (in wt %). Dashed lines in each column separate individual traverses.

sequences. The next sample going upsection, ~20 m above the uppermost exposure of basal flow conglomerate in the Wrangell Mountains, does not have visible assimilated material and is high-titanium basalt with unexceptional chemistry. A single sample with a low titanium content (1.14 wt %TiO<sub>2</sub>; 5715A5) was collected from near the top of the stratigraphy in the Wrangell Mountains, but this sample has similar isotopic composition to the high-titanium basalts, atypical petrographic texture, and is at the upper range of TiO<sub>2</sub> of low-titanium basalts.

## DISCUSSION

### Source of Nikolai basalts

The Nikolai Formation in Alaska has two main lava types with distinct isotopic compositions. The high-titanium basalts in Alaska have depleted Hf and Nd isotopic compositions that are not as depleted as most Pacific and Indian mid-ocean ridge basalts (MORB) and are displaced just below the ocean island basalt (OIB) mantle array (Fig. 3.17). The high-titanium basalts have similar initial Sr and Nd isotopic compositions to Ontong Java Plateau, Hawaii, and Caribbean Plateau basalts and similar initial  $\epsilon_{\text{Hf}}$  to Ontong Java, with slightly lower initial  $\epsilon_{\text{Hf}}$  than most Hawaii and Caribbean basalts (Fig. 3.17). In contrast, the low-titanium basalts are displaced well above the OIB mantle array in a  $\epsilon_{\text{Hf}}(t)$ - $\epsilon_{\text{Nd}}(t)$  correlation diagram and have a similar range of initial  $\epsilon_{\text{Hf}}$  to Pacific MORB, with initial  $\epsilon_{\text{Nd}}$  2 to 5 epsilon units lower than Pacific MORB. The Hf isotopic compositions of the low-titanium basalts are 2 to 6 epsilon units higher than for most samples from Ontong Java, with slightly lower initial  $\epsilon_{\text{Nd}}$ . Sr isotopic compositions for low-titanium basalts extend to significantly higher initial  $^{87}\text{Sr}/^{86}\text{Sr}$  than Ontong Java and Hawaii. Three low-titanium basalts with particularly high initial  $\epsilon_{\text{Nd}}$  lie within a field for Indian MORB in  $\epsilon_{\text{Hf}}(t)$ - $\epsilon_{\text{Nd}}(t)$  space. Two Rainy Creek picrite samples lie close to the  $\epsilon_{\text{Hf}}(t)$ - $\epsilon_{\text{Nd}}(t)$  OIB mantle array with lower initial  $\epsilon_{\text{Nd}}$  than the high-titanium basalts (Fig. 3.17). The high- and low-titanium basalts have uniform initial Pb isotopic compositions that overlap a field for Caribbean basalts and have more radiogenic initial  $^{207}\text{Pb}/^{204}\text{Pb}$  than Ontong Java, Hawaii, and a field for the East Pacific Rise (EPR; Fig. 3.18). Pb isotopic compositions form a linear trend in  $^{208}\text{Pb}$ - $^{206}\text{Pb}$  space which intersects the field of Pacific MORB compositions and is slightly offset towards lower  $^{208}\text{Pb}/^{204}\text{Pb}$  from

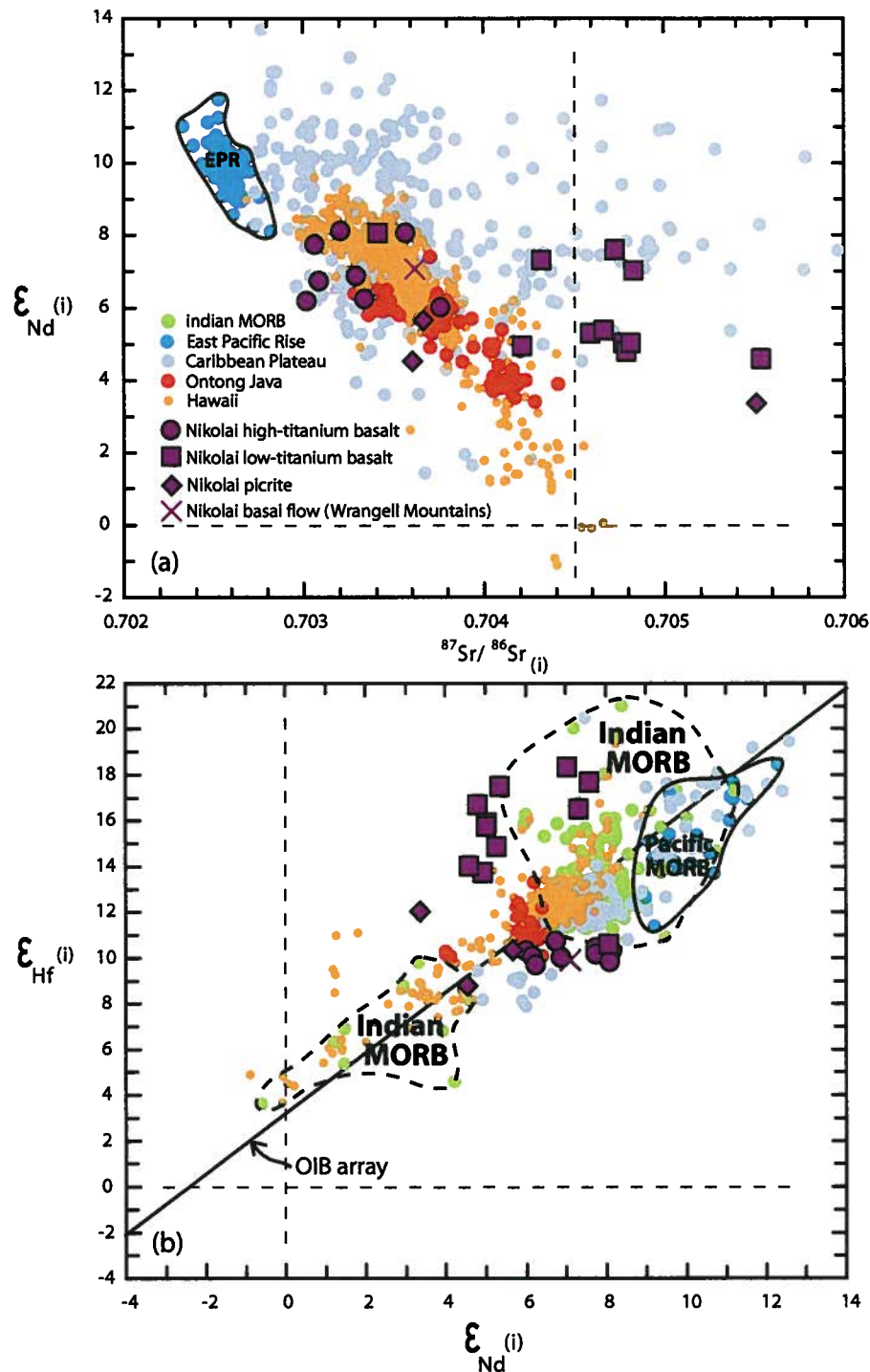


**Figure 3.17** Comparison of age-corrected (230 Ma) Sr-Nd-Hf isotopic compositions for Nikolai basalts in Alaska to age-corrected OIB and MORB. (a) Initial  $\epsilon_{\text{Nd}}$  vs.  $^{87}\text{Sr}/^{86}\text{Sr}$ . (b) Initial  $\epsilon_{\text{Hf}}$  vs.  $\epsilon_{\text{Nd}}$ . Both fields with dashed lines are Indian MORB. All of the references for the compiled data are too numerous to cite here. Most of the compiled data was extracted from the GEOROC database (<http://georoc.mpch-mainz.gwdg.de/georoc/>). Data for Ontong Java from Mahoney *et al.* (1993), Babbs (1997), and Tejada *et al.* (2004); Indian MORB from Salters (1996), Kempton *et al.* (2002), and Janney *et al.* (2005); Pacific MORB from Mahoney *et al.* (1992, 1994), Nowell *et al.* (1998), Salters and White, and Chauvel and Blichert-Toft (2001); Explorer Ridge data from Cousens and Weis (pers. comm., 2007); OIB array line from Vervoort (1999). EPR is East Pacific Rise. Dashed lines indicate Bulk Silicate Earth (BSE). An extended reference list is available upon request.

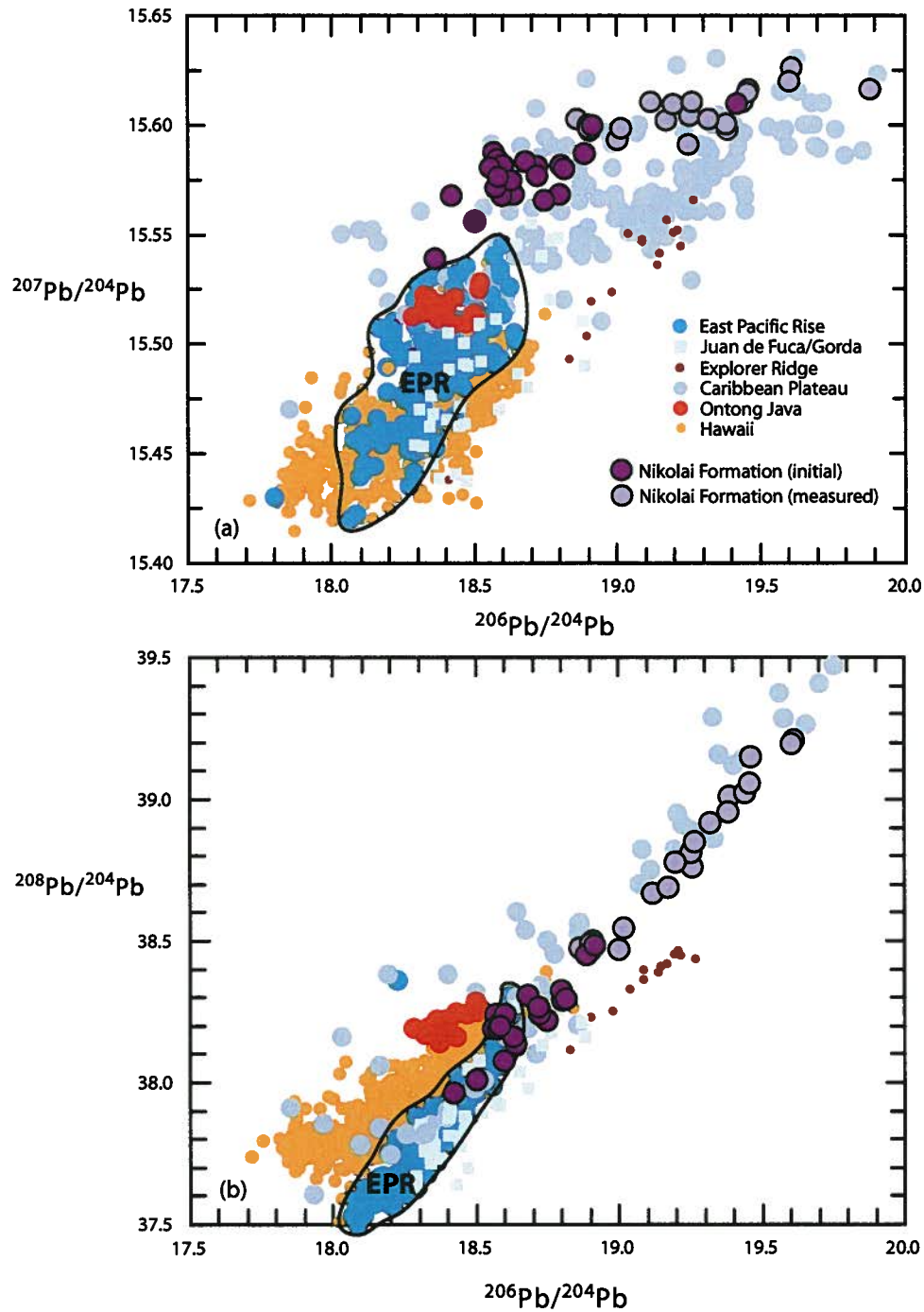


**Figure 3.18** Comparison of Pb isotopic compositions of the Nikolai Formation in Alaska to OIB and MORB. (a) Measured and initial  $^{207}\text{Pb}/^{204}\text{Pb}$  vs.  $^{206}\text{Pb}/^{204}\text{Pb}$ . (b) Measured and initial  $^{208}\text{Pb}/^{204}\text{Pb}$  vs.  $^{206}\text{Pb}/^{204}\text{Pb}$ . See figure caption for Figure 3.17 for references for OIB and MORB data.

Ontong Java and Hawaii. The Pb in Nikolai basalts is more enriched in radiogenic Pb than MORB, Ontong Java, and OIB from Hawaii, but similar to basalts of the Caribbean Plateau.

The initial Hf and Nd isotopic compositions of high-titanium basalts indicate a uniform OIB-type Pacific mantle source derived from a long-term depleted source, distinct from the source of MORB. In contrast, the low-titanium basalts have initial Hf isotopic compositions that are clearly distinct from OIB and initial Nd isotopic compositions that are distinct from the Pacific MORB source. The displacement of the low-titanium basalts well above the OIB array indicates involvement of a depleted component (mantle or crust), distinct from depleted MORB mantle, early in the formation of Nikolai basalts in Alaska. The origin of the distinct isotopic and geochemical signature of the low-titanium basalts is the focus of subsequent discussion sections.

### **Lithospheric involvement in derivation of the low-titanium basalts**

The stratigraphic relationship of the two contrasting lava types in the Nikolai Formation preserve a record of a shift in composition of the source of Nikolai basalts in Alaska and provide a rare opportunity to evaluate the role of oceanic arc lithosphere in the formation of an oceanic plateau. Thus far, the low-titanium basalts have primarily been recognized in the lowermost part of the stratigraphy in the western part of Wrangellia in Alaska, where there is a substantial section of submarine flows (~500 m). The low-titanium basalts possess distinct negative-HFSE anomalies in normalized trace-element patterns and have high initial  $\epsilon_{\text{Hf}}$  and high initial  $^{87}\text{Sr}/^{86}\text{Sr}$  compared to the high-titanium basalts. This compositional and stratigraphic evidence suggests that the underlying Paleozoic arc lithosphere may have played a significant role in the generation of early-erupted low-titanium basalts in the Wrangellia oceanic plateau of Alaska.

### *Nature of underlying Paleozoic arc lithosphere*

The Paleozoic arc (320-285 Ma) and marine sedimentary sequences (Early Permian to Middle Triassic) exposed underlying the Nikolai basalts in Alaska are >2.5 km thick in areas. Recent geophysical studies in southern Alaska by Saltus *et al.* (2007) indicate Wrangellia crust is at least 50 km thick between the Denali and Border Ranges

Faults (Fig. 3.1). The arc crust that the Wrangellia oceanic plateau was built upon may have been 20-30 km thick and this would have included a substantial sub-arc mantle lithosphere that was metasomatized during arc activity.

In the Alaska Range, the Nikolai basalts are underlain, in decreasing order of depth, by the Paleozoic Tetelna Volcanics, the Slana Spur and Eagle Creek Formations. Tetelna Volcanics (<1000 m) are andesitic and dacitic flows, tuffs interbedded with volcanoclastic rocks, and debris-flow deposits; the Slana Spur Formation (~1400 m) is marine volcanoclastics, with lesser limestone and sandstone; and the Eagle Creek Formation (~900 m) is Permian argillite and limestone (Nokleberg *et al.*, 1985). Numerous comagmatic intermediate to felsic plutonic rocks intrude Tetelna Volcanics and the Slana Spur Formation (Nokleberg *et al.*, 1994). In the Wrangell Mountains, the Paleozoic sequences include the Station Creek Formation (~1200 m of mostly basaltic and andesitic flows and 800 m of volcanoclastic sequences) and the sedimentary Hasen Creek Formation (~500 m of chert, black shale, sandstone, bioclastic limestone, and conglomerate) (Smith & MacKevett, 1970; Fig. 3.2).

#### *Trace-element and isotopic source constraints of the low-titanium basalts*

The trace element and isotopic compositions of the early-erupted low-titanium basalts are not typical of OIB and indicate involvement of a HFSE-depleted component that was different than the plume-type source of the high-titanium basalts. The arc lithosphere is a key suspect for derivation of the low-titanium basalts because: 1) the geochemical and isotopic signature of the low-titanium basalts is similar to rocks formed in subduction settings (e.g. Kelemen *et al.*, 2003); 2) arc crust is exposed beneath the Nikolai basalts in Alaska; and 3) the low-titanium basalts only form ~10-15% of the lowest part of the volcanic stratigraphy.

Figure 3.19 highlights differences in trace elements and isotopic compositions between the high- and low-titanium basalts and indicates a strong arc lithospheric, or subduction-modified mantle, component in the low-titanium basalts. The high-titanium basalts form a concentrated cluster of points in each of the plots and show a remarkably small degree of variation, whereas the low-titanium basalts have a noticeably wider range of variation, which mostly does not overlap the range for the high-titanium basalts (Fig.

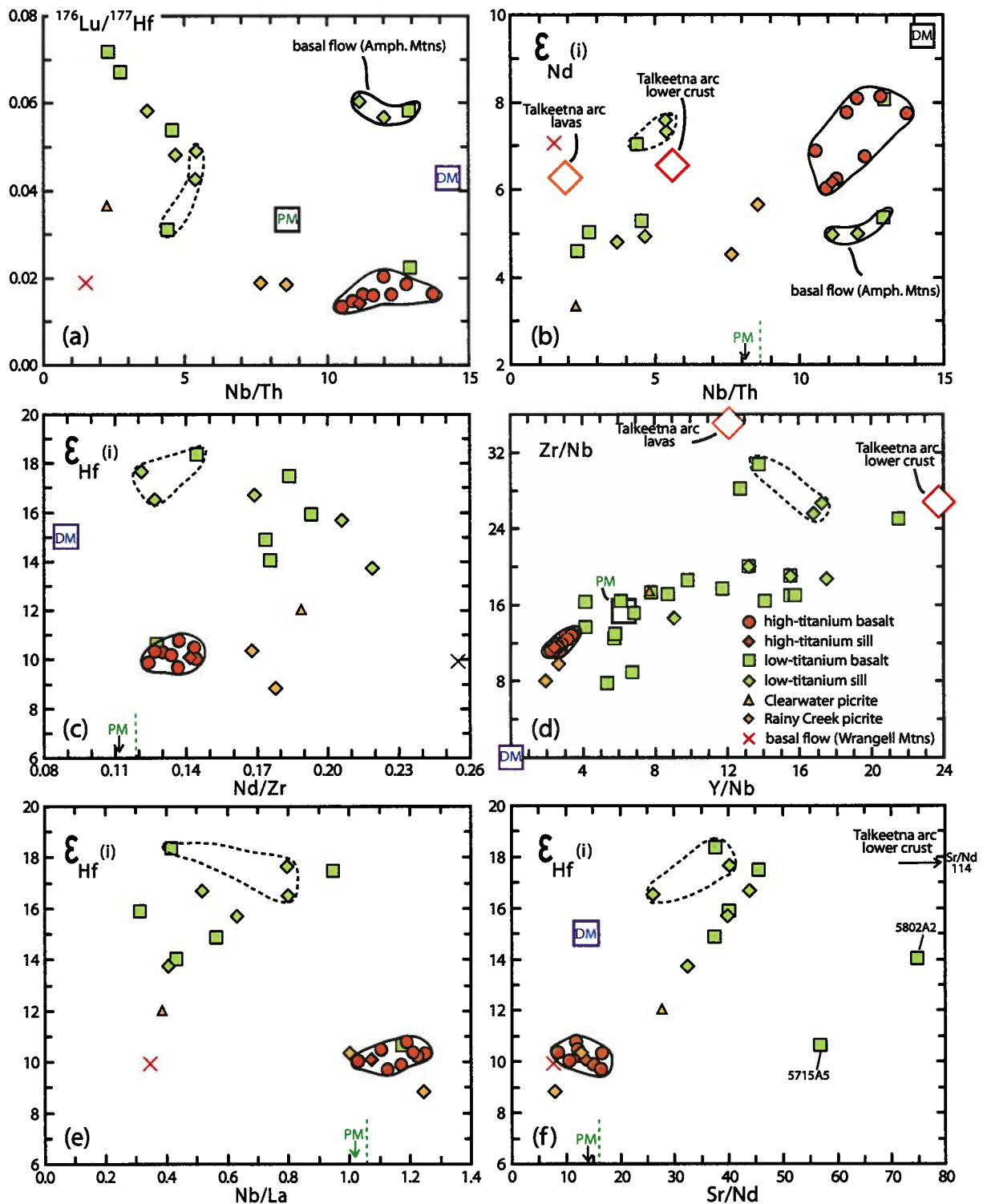


**Figure 3.19** Trace-element ratios and isotopic compositions of the Nikolai Formation in Alaska. (a)  $^{176}\text{Lu}/^{177}\text{Hf}$  vs. Nb/Th. (b) Initial  $\epsilon_{\text{Nd}}^{(i)}$  vs. Nb/Th. (c) Initial  $\epsilon_{\text{Hf}}^{(i)}$  vs. Nd/Zr. (d) Zr/Nb vs. Y/Nb. (e) Initial  $\epsilon_{\text{Hf}}^{(i)}$  vs. Nb/La. (f) Initial  $\epsilon_{\text{Hf}}^{(i)}$  vs. Sr/Nd. Primitive mantle (PM) from McDonough and Sun (1995), depleted mantle (DM) trace-element and isotopic composition estimates from Salters and Stracke (2004). Talkeetna arc lower crust compositions from Greene *et al.* (2006) and Talkeetna arc lavas from Clift *et al.* (2005). Dashed circle in each panel outlines samples 5727A2, 5727A3, and 5802A5.

3.19). The low-titanium basalts have low Nb/Th and Nb/La relative to primitive mantle, which is characteristic of subduction-related rocks (Pearce, 1982). Except for three analyses from the basal flow in the Amphitheater Mountains, which has pelagic sediment between pillow tubes derived from the directly underlying strata and has similar Nb/Th to the high-titanium basalts, the low-titanium basalts have similar Nb/Th and Nb/La to accreted arc crust from the Early Jurassic Talkeetna arc exposed in southern Alaska ~50 km south of the Amphitheater Mountains (Fig. 3.19; Greene *et al.*, 2006). Low Nb/Th in arc magmas is commonly attributed to inheritance from subducted sediments (e.g. Kelemen *et al.*, 2003). Low Nb/La may be related to a process whereby migration of REE into magma takes place, but mobilization of Nb is inhibited, such as by reaction between magmas and metasomatized peridotite (e.g. Kelemen *et al.*, 1990, 1993). The low-titanium basalts have high Sr/Nd and Nd/Zr relative to primitive mantle and the high-titanium basalts (Fig. 3.19). Elevated Sr relative to REE may indicate addition of Sr to arc lithosphere through aqueous fluids, since Sr is more soluble than REE at high pressure (e.g. Johnson & Plank, 1999) or addition from Sr-enriched cumulates from gabbroic lower crust (e.g. Kelemen *et al.*, 2003). The trace-element and isotopic compositions of the low-titanium basalts have an arc-type geochemical signature.

Figure 3.20 utilizes proxies described by Pearce (2008) for identifying lithospheric input (Th-Nb) and assessing depth of melting (Ti-Yb). For the Th-Nb proxy, all the high-titanium basalts lie within a diagonal MORB-OIB array parallel to a melting vector, whereas most of the low-titanium basalts are displaced above the array, oblique to the melting vector. The low-titanium basalts follow a trend for lavas that have a subduction component, or have interacted with continental crust, and they are consistent with a small amount of assimilation ( $F < 0.9$ ;  $F$  is melt fraction) combined with fractional crystallization (AFC), shown by the modeling curve of Pearce (2008; Fig. 3.20). A Nb-Th depleted source is indicated for the low-titanium basalts, which also have similar Th-Nb to Talkeetna arc lavas and lower crust. For the Ti-Yb proxy, high Ti/Yb ratios for high-titanium basalts indicate residual garnet from melting at high pressure, within the OIB melting array, whereas low-titanium basalts lie along a complementary mantle melt depletion trend indicating shallow melting, similar to compositions of Talkeetna arc lavas (Pearce, 2008; Fig. 3.20).



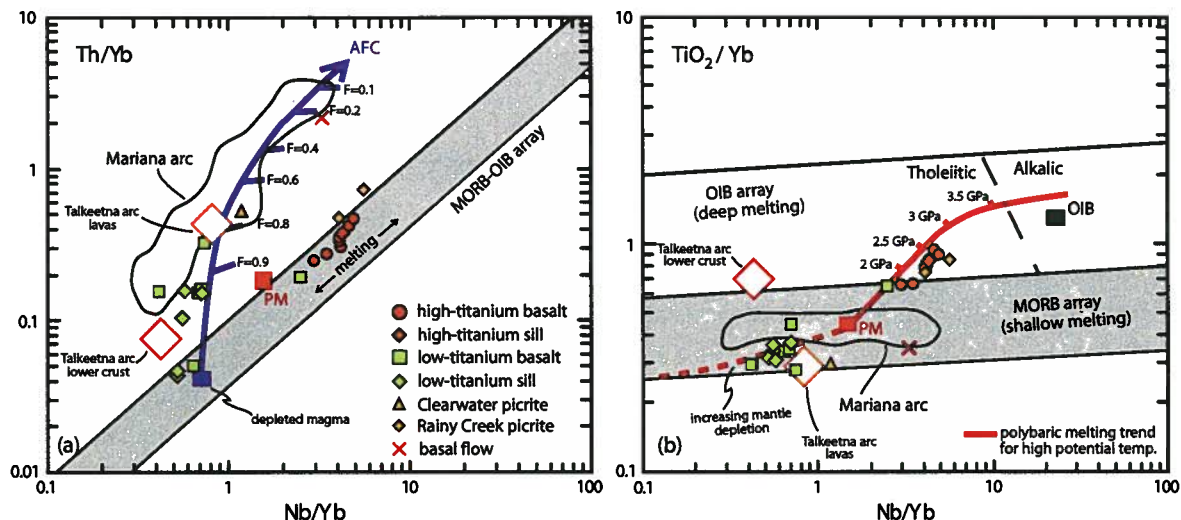


**Figure 3.20** Th-Nb and Ti-Yb proxies of the Nikolai Formation in Alaska with data compilation and modeling results from Pearce (2008). See Pearce (2008) for full reference list used to create MORB and OIB arrays, and OIB average in panel b. Primitive mantle (PM) estimate in panel a from McDonough & Sun (1995). (a) Th/Yb vs. Nb/Yb. MORB-OIB array and assimilation-fractional crystallization (AFC) model from Pearce (2008). (b) TiO<sub>2</sub>/Yb vs. Nb/Yb. Talkeetna arc lower crust from Greene *et al.* (2006) and Talkeetna arc lavas from Clift *et al.* (2005). Mariana arc data from Pearce *et al.* (2007) and Woodhead *et al.* (2001). The low-titanium basalts indicate a depleted source and interaction with a subduction component combined with fractional crystallization, whereas the high-titanium basalts lie within an OIB array in panel b, parallel to a melting vector that indicates higher pressure melting. See Pearce (2008) for parameters of polybaric melting and assimilation-fractional crystallization (AFC) modeling. Blue line in panel A represents an AFC model following the modeling of DePaolo (1981). Red line in panel b illustrates a polybaric melting trend (with changing composition of pooled melt extracted from the mantle that undergoes decompression from the solidus to the pressure marked) for high and lower mantle potential temperatures which correspond to representative conditions for the generation of present-day MORB and OIB (Pearce, 2008).

Lassiter *et al.* (1995) suggested a minor role for the arc lithosphere in formation of the Wrangellia flood basalts based on a suite of nine samples from the Wrangell Mountains in Alaska. They inferred that assimilation of low  $\epsilon_{Nd}$ , low Nb/Th arc material may have affected the composition of the Wrangellia basalts, but that mixing of MORB mantle with low  $\epsilon_{Nd}$  arc material did not reproduce the trends in the Wrangellia basalts. Rather, Lassiter *et al.* (1995) suggested mixing of a plume-type source, with  $\epsilon_{Nd}$  +6 to +7, with arc material with low Nb/Th could reproduce variations in the Wrangellia flood basalts. They noted that the absence of low Nb/La ratios in flood basalts from their dataset suggests a restricted amount of lithospheric involvement. The lower FeO content for most of the low-titanium basalts also may reflect melting generated from refractory arc lithosphere (Lassiter & DePaolo, 1997). The widespread sampling of Nikolai basalts in Alaska in this study supports the interpretation of Lassiter *et al.* (1995), that arc lithosphere was involved in formation of the Nikolai basalts in Alaska.

The low-titanium basalts may have developed an arc-type signature by substantial melting of subduction-modified mantle, interaction of plume-derived melts with melts or material derived from the arc lithospheric, and/or reaction of magmas and metasomatized arc peridotite early in generation of the Nikolai basalts. All CFBs show compositional evidence of involvement of continental crust or lithospheric mantle in parts of their volcanic stratigraphy (e.g. Saunders *et al.*, 1992). Several CFBs and volcanic rifted margins show a transition in the eruptive sequence from a lithospheric to a plume-derived signature [e.g. Siberia (Wooden *et al.*, 1993); Parana (Peate & Hawkesworth, 1996); North Atlantic Igneous Province (Kerr, 1994); Ethiopia (Pik *et al.*, 1999)] and a number of influential studies have examined the role of plume-lithosphere interactions in the formation of flood basalt provinces (e.g. Arndt & Christensen, 1992; Menzies, 1992; Saunders *et al.*, 1992; Turner *et al.*, 1996; Lassiter & DePaolo, 1997). White and McKenzie (1995) presented geochemical evidence for continental lithospheric contribution to flood basalts, but indicated that the conduction of heat to the lithosphere from the plume is too slow to produce large volumes of magma in short timespans. Arndt and Christensen (1992) found that >96% of melt in CFBs comes from the asthenosphere and only minor amounts of melt (<5%) may originate in the lithosphere. Although there are conflicts with anhydrous melting models for the lithosphere, Lassiter and DePaolo

(1997) found evidence for lithospheric mantle melting and typically these melts are more abundant during early phases of flood volcanism, as they usually represent a minor volume (10-20%) of the eruptive sequences (e.g. Siberia). Pik *et al.* (1999) proposed melting of a shallow-level, depleted source for low-titanium basalts from Ethiopia, with a strong, but variable, lithospheric contribution.

For certain conditions (e.g. lithospheric thickness, duration of heating, and temperature), modeling predicts that small volumes of lithosphere-derived basalts may be overlain by larger volumes of asthenospheric basalts (Turner *et al.*, 1996). Turner *et al.* (1996) concluded that the lithospheric mantle can contribute melt if it is less than 100 km thick and if the solidus is lowered from addition of volatiles at some time in the past. Saunders *et al.* (1992) suggested that, although conduction alone may not cause melting of the lithosphere, rifting and decompression, the presence of hydrous phases (e.g. Gallagher & Hawkesworth, 1992), melt injection from the plume into the lithosphere, and thermal and mechanical erosion of the lithosphere may all facilitate melting. Numerical modeling of d'Acremont *et al.* (2003) involving plume head-lithosphere interaction and the formation of oceanic plateaus indicates thermal weakening may be less important than mechanical weakening at timescales of plume head flattening and related strain rates. Farnetani and Richards (1994) found from numerical modeling, partly applied to Triassic Wrangellia stratigraphy, that without extension, melting would likely be entirely sublithospheric, however, they note that they did not examine complexities of arc lithosphere and the presence of hydrous phases that would enhance melting.

The combination of chemostratigraphy and trace-element and isotopic compositions suggests involvement of a subduction-modified mantle component early in the formation of the Nikolai basalts in Alaska. The compositions of Nikolai basalts in Yukon show the same characteristics and are interpreted as having formed from a similar degree of involvement of subduction-modified mantle, as part of the same oceanic plateau (Greene *et al.*, 2008, submitted-a).

#### *Origin of decoupled Hf and Nd isotopic compositions of low-titanium basalts*

The initial Hf isotopic compositions of the low-titanium basalts indicate involvement of a component that evolved with high Lu/Hf over time, but not

corresponding high Sm/Nd. There are only a few processes that are known to be able to fractionate the parent-daughter elements Lu and Hf, but not Sm and Nd, and the combined use of  $^{176}\text{Hf}/^{177}\text{Hf}$  and  $^{143}\text{Nd}/^{144}\text{Nd}$  is an indicator of these processes (Salters and White, 1998). Parent isotopes  $^{176}\text{Lu}$  and  $^{147}\text{Sm}$  are more compatible during melting than their daughter isotopes  $^{176}\text{Hf}$  and  $^{143}\text{Nd}$ , respectively (Salters and White, 1998), and show a close coupling in the crust-mantle system; when plotting Hf versus Nd isotopes they form the “terrestrial array” (Vervoort & Blichert-Toft, 1999; van de Flierdt *et al.*, 2004; Fig. 3.21). Decoupling of the Hf and Nd isotope system has been attributed to processes that involve zircon or garnet, which result in larger fractionation of Lu/Hf than of Sm/Nd (Patchett *et al.*, 1984; Vervoort *et al.*, 2000). These processes may involve pelagic sediment, ancient melt extraction, or oceanic lithosphere modified by subduction (e.g. Geldmacher *et al.*, 2003). Pelagic sediment can acquire high Lu/Hf compared to Sm/Nd because of the sedimentary fractionation of zircon (Patchett *et al.*, 1984). Ancient melt extraction can result in high Lu/Hf relative to Sm/Nd from a source with a high garnet/clinopyroxene ratio (Geldmacher *et al.*, 2003). The arc mantle wedge can develop high Lu/Hf, compared to Sm/Nd, that will evolve over time to high  $^{176}\text{Hf}/^{177}\text{Hf}$  relative to  $^{143}\text{Nd}/^{144}\text{Nd}$  and displace compositions above the OIB array (e.g. Barry *et al.*, 2006). Kempton *et al.* (2002) and Janney *et al.* (2005) have presented models that involve subduction-modified mantle to explain high  $\epsilon_{\text{Hf}}$  for Indian MORB. Subduction-modified mantle may lead to greater decoupling of Hf and Nd isotopic compositions than pelagic sediment alone, and this may initially lead to a more significant decrease in  $^{143}\text{Nd}/^{144}\text{Nd}$  than  $^{176}\text{Hf}/^{177}\text{Hf}$ , which then evolve along a similar path to depleted compositions well above the mantle array (Kempton *et al.*, 2002; Janney *et al.*, 2005).

The high  $\epsilon_{\text{Hf}}$  and HFSE-depleted characteristics of the low-titanium basalts were probably not intrinsic to the plume source of Wrangellia flood basalts in Alaska; the isotopic and trace element compositions indicate involvement of subduction-modified lithospheric mantle. Along with high Hf isotope ratios, high primary Sr isotopic compositions of the low-titanium basalts suggest a degree of seawater influence (Hauff *et al.*, 2003) or influence from high Rb/Sr arc mantle. Figure 3.22 shows Sr, Nd, and Hf isotopic compositions of the Nikolai basalts compared to modern Pacific arcs and sediments. The low-titanium basalts have comparable initial  $\epsilon_{\text{Hf}}$  to modern Pacific arcs

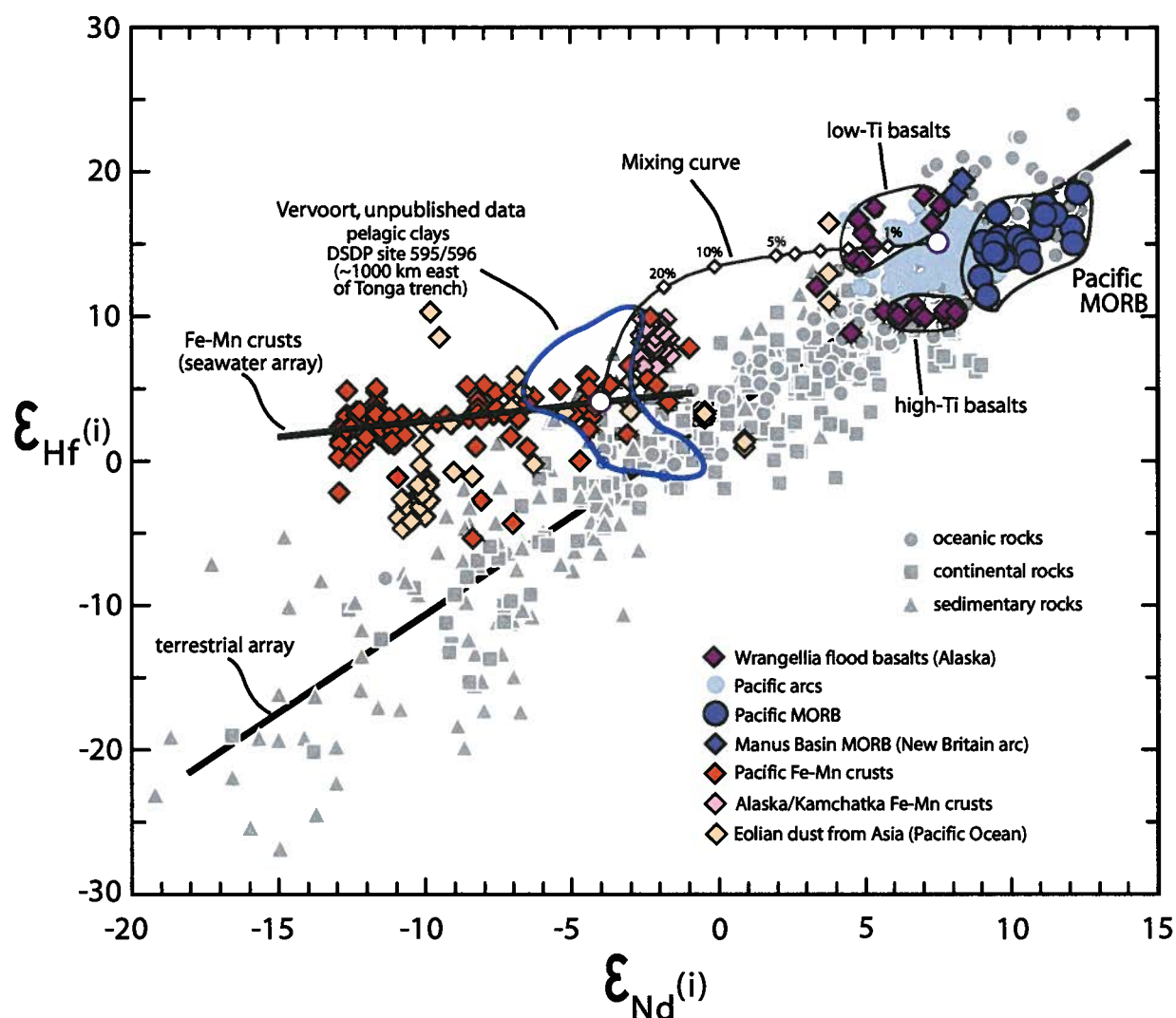


**Figure 3.21** Global Hf-Nd isotope systematics with age-corrected data of the Nikolai Formation in Alaska. Data for terrestrial array are from Vervoort and Blichert-Toft (1999) and references therein. Data for the seawater array, mostly from Fe-Mn crusts, and are too numerous to cite here. Pelagic sediment data from DSDP 595/596 provided courtesy of J. Vervoort. The mixing curve shown is for mixing of pelagic sediment with arc basalt. Average pelagic sediment composition used for mixing curve is initial  $\epsilon_{\text{Hf}} = +5.0 \pm 4.0$  and initial  $\epsilon_{\text{Nd}} = -4.5 \pm 2.4$ . Average arc basalt from Pearce *et al.* (2007) and Woodhead *et al.* (2001). Pacific MORB from Nowell *et al.* (1998), Salters and White (1998), and Chauvel and Blichert-Toft (2001). An extended reference list is available upon request.

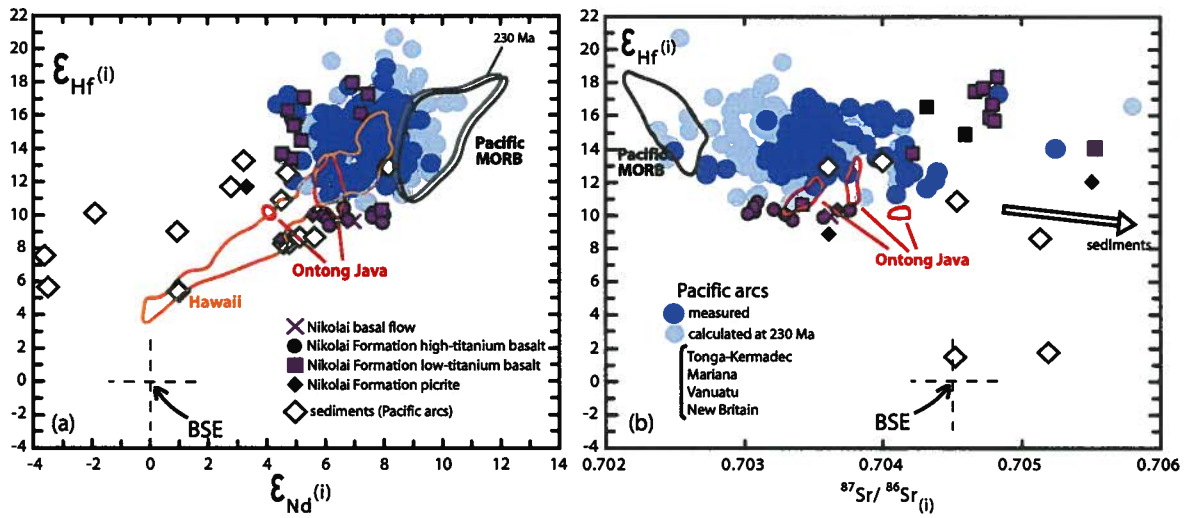


**Figure 3.22** Comparison of initial Hf, Nd, and Sr isotopic compositions of the Nikolai Formation in Alaska to Pacific arcs (Tonga-Kermadec, Mariana, Vanuatu, New Britain) and Pacific MORB. Compiled Pacific arc and sediment data from Pearce *et al.* (2007) and Woodhead *et al.* (2001). See figure caption for Figure 3.17 for references for Pacific MORB. Ontong Java data from Tejada *et al.* (2004). Hawaii data from numerous references. Dashed lines indicate Bulk Silicate Earth (BSE).

(and Pacific MORB) with lower initial  $\epsilon_{\text{Nd}}$  and higher initial  $^{87}\text{Sr}/^{86}\text{Sr}$ . High Sr isotope ratios, in combination with high Hf ratios, indicate a significant degree of Rb/Sr and Lu/Hf fractionation, which are characteristic of fractionations produced in the mantle wedge. The trace-element compositions of the low-titanium basalts indicate they probably did not originate from a source with a high garnet/clinopyroxene ratio.

A binary mixing curve between average Pacific arc basalt composition and pelagic sediments, from ~1000 km east of the Tonga trench (DSDP site 595/596; Vervoort, pers. comm.), in a plot of initial  $\epsilon_{\text{Hf}}$  versus  $\epsilon_{\text{Nd}}$  suggests involvement of a pelagic sediment component with high Lu/Hf could generate high initial Hf isotopic compositions similar to those of the low-titanium basalts (Fig. 3.21). This does not preclude the role of subduction-modified mantle. The addition of a small amount of a pelagic component that underwent radiogenic ingrowth from high Lu/Hf could explain the displacement of low-titanium basalts above the OIB mantle array from a source more depleted than that of the high-titanium basalts (Fig. 3.21). The pelagic sediment component is different than the local contamination of the basal pillowed flows in the Alaska Range which contain sediment filling interpillow voids. The trace-element and isotopic geochemistry of the low-titanium basalts is consistent with involvement of a subduction-modified mantle component, possibly including a pelagic sediment component, which may have evolved with high  $^{176}\text{Hf}/^{177}\text{Hf}$  (and  $^{87}\text{Sr}/^{86}\text{Sr}$ ) relative to  $^{143}\text{Nd}/^{144}\text{Nd}$ .

### **Melting conditions and estimated major-element composition of primary low-Ti magma**

The conditions of partial melting and composition of primary melts can be estimated using a modeling technique of Herzberg *et al.* (2007). All of the high-titanium basalts have MgO contents that are too low to represent direct partial melts of mantle peridotite and underwent significant fractional crystallization. The low-titanium basalts extend to higher MgO contents, but several high-MgO basalts and picrites have been sampled in the Alaska Range and are the best candidates for least-modified partial melts of the mantle source. In addition to several high-MgO, low-titanium basalts (samples 5727A6, 5810A2, 5802A3), we use one Rainy Creek picrite (sample 5808A2; Fig. 3.9) to

estimate melting conditions and major-element primary magma composition because it is available. However, this sample is from outside the main flood basalt stratigraphy and has a distinct LREE-enriched trace-element composition, and a slightly offset isotopic composition. Several high-MgO, low-titanium basalts are more typical of the volcanic stratigraphy. Herzberg *et al.* (2007) have provided a thorough description of a technique for inverse and forward modeling for estimating mantle temperature, melt fraction, primary magma composition, and source residue composition using major elements.

The estimated melting conditions and primary magma compositions for several high-MgO lavas from the Nikolai Formation, and a brief summary of the modeling method, are presented in Figure 3.23 and Table 3.6. Calculated mantle potential temperatures for several Nikolai picrites (~1495°C) are significantly higher than ambient mantle that produces MORB (~1280-1400°C; Herzberg *et al.*, 2007). If the Nikolai basalts were derived from accumulated fractional melting of fertile peridotite, the primary magmas would have 15-17 wt % MgO and 10-11 wt % CaO, formed from 25-29% partial melting, and would have crystallized olivine with a Fo content of ~91 (Fig. 3.23; Table 3.6). A picrite from the Rainy Creek area requires very little addition of olivine, however, it has a trace-element and isotopic composition that is distinct from the basalts (e.g. sample 5808A2; Table 3.6). The estimated primary magma compositions and melting conditions for Nikolai picrites are similar to estimates for Ontong Java, where Herzberg (2004) found that primary magmas would have formed by 27% partial melting with mantle potential temperatures of ~1500°C (Table 3.6). The estimated melting conditions of several Nikolai picrites indicate high-degree melting of unusually hot mantle peridotite, which is consistent with a plume initiation model for the Nikolai basalts. The geochemical data for the low-titanium basalts reflects significant involvement of subduction-modified lithospheric mantle, or even has its source in the lithospheric mantle; however, this would lead to the formation of comparatively small-degree melts since lithospheric mantle is cold relative to plume-derived magmas at the same pressure. This raises the question for future studies as to whether the low-titanium basalts may have involved mixing of plume-derived melts and low-degree partial melts of the arc lithospheric mantle.



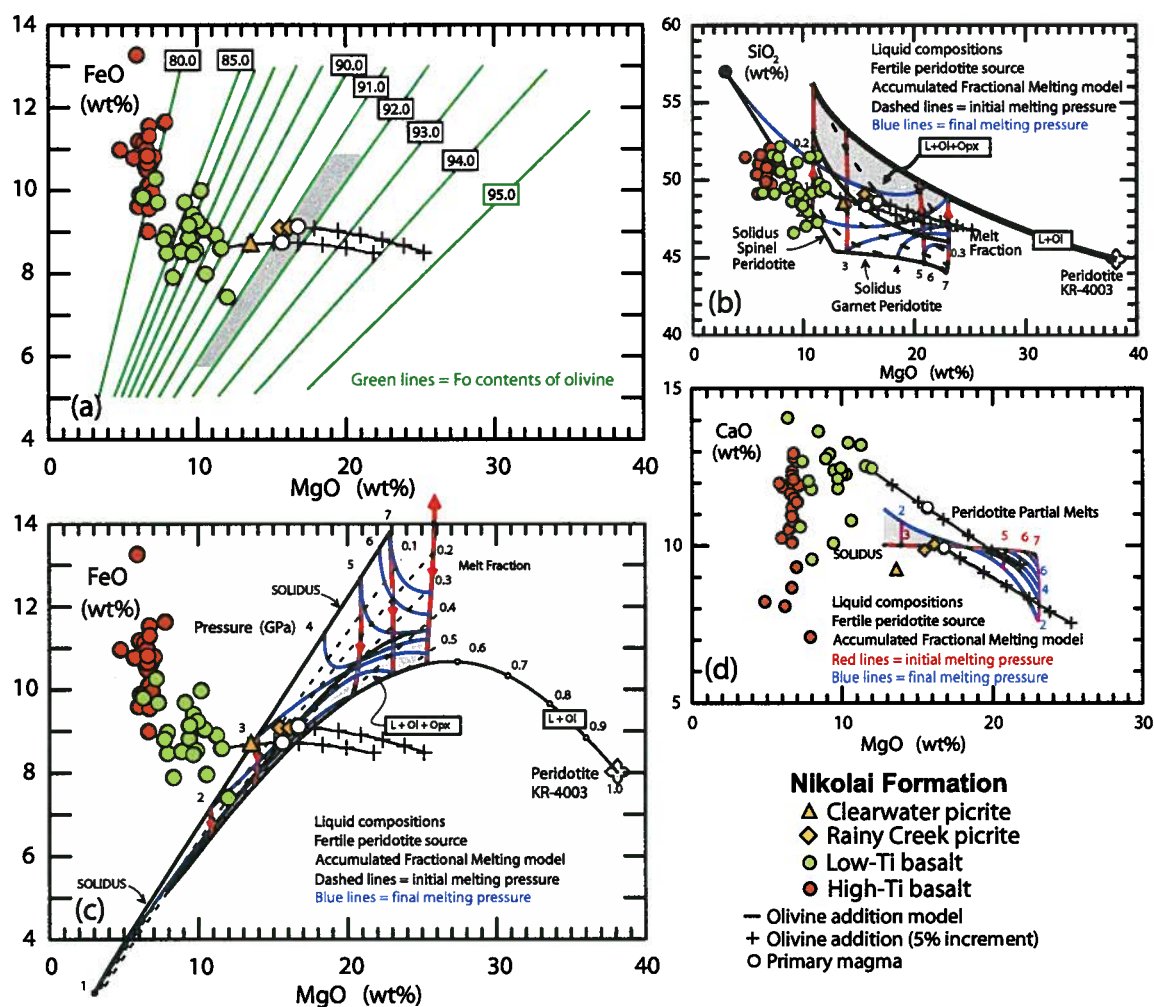


**Figure 3.23** Estimated primary magma compositions for two picrites from the Nikolai Formation (samples 5808A2, 5727A6) using the forward and inverse modeling technique of Herzberg *et al.* (2007). Nikolai basalt and picrite compositions and modeling results are overlain on diagrams provided by C. Herzberg. (a) Whole-rock FeO vs. MgO for Nikolai samples from this study. Total iron estimated to be FeO is 0.90. Green lines show olivine compositions that would precipitate from liquid of a given MgO-FeO composition. Black lines with crosses show results from olivine addition (inverse model) using PRIMELT1 (Herzberg *et al.*, 2007). (b) SiO<sub>2</sub> vs. MgO with Nikolai basalt and model results. (c) FeO vs. MgO with Nikolai lava compositions and results of forward model for accumulated fractional melting of fertile peridotite. (d) CaO vs. MgO with Nikolai basalt compositions and model results. See Herzberg *et al.* (2007) for complete description of the modeling technique. Potential parental magma compositions for the high-MgO lava series were selected (highest MgO and appropriate CaO) and, using PRIMELT1 software, olivine was incrementally added to the selected compositions to show an array of potential primary magma compositions (inverse model). Then, using PRIMELT1, the results from the inverse model were compared to a range of accumulated fractional melts for fertile peridotite, derived from parameterization of the experimental results of Walter (1998) (forward model; Herzberg & O'Hara, 2002). A melt fraction was sought that was unique to both the inverse and forward models (Herzberg *et al.*, 2007). A unique solution was found when there was a common melt fraction for both models in FeO-MgO and CaO-MgO-Al<sub>2</sub>O<sub>3</sub>-SiO<sub>2</sub> (CMAS) projection space. This modeling assumes olivine was the only phase crystallizing and ignores chromite precipitation, and possible augite fractionation in the mantle (Herzberg & O'Hara, 2002). Results are best for a residue of spinel lherzolite (not pyroxenite). The high- and low-titanium basalts cannot be used for modeling because they are all plag + cpx + ol saturated.

Table 3.6 Estimated primary magma compositions for Nikolai basalts and other oceanic plateaus/islands

Sample	5727A6	5808A2	5810A2	5802A3	Average	OJP <sup>a</sup>	Mauna Kea <sup>b</sup>	Gorgona <sup>c</sup>
Area	Tangle	Rainy Creek	Tangle	Clearwater				
<i>(Weight %):</i>								
SiO <sub>2</sub>	48.4	48.7	47.1	47.2	47.8	48.0	46.3	46.1
TiO <sub>2</sub>	0.43	1.09	0.44	0.45	0.60	0.62	1.93	0.56
Al <sub>2</sub> O <sub>3</sub>	13.5	11.1	13.1	14.5	13.0	12.3	9.6	11.7
Cr <sub>2</sub> O <sub>3</sub>	0.07	0.20	0.05	0.06	0.09	0.07	0.26	0.16
Fe <sub>2</sub> O <sub>3</sub>	0.94	1.11	0.91	0.90	0.97	0.90	1.08	1.18
FeO	8.7	9.1	9.5	8.8	9.0	9.2	10.3	10.1
MnO	0.18	0.16	0.20	0.18	0.18	0.17	0.18	0.18
MgO	15.7	16.8	17.6	15.7	16.4	16.8	18.3	18.8
CaO	11.2	9.9	9.9	10.7	10.4	10.3	10.1	10.0
Na <sub>2</sub> O	0.71	1.39	0.99	1.03	1.03	1.36	1.67	1.04
K <sub>2</sub> O	0.04	0.36	0.06	0.51	0.24	0.08	0.41	0.03
NiO	0.06	0.09	0.08	0.03	0.07	0.10	0.08	0.11
Eruption T(°C)	1361	1385	1401	1361	1377	1382	1415	1422
Potential T(°C)	1476	1503	1521	1476	1494	1500		1606
Fo content (olivine)	91.1	91.3	91.5	91.2	91.3	90.5	91.38	90.6
Melt fraction	0.27	0.29	0.28	0.25	0.27	0.27		0.28
%ol addition	11.7	1.8	22.2	16.1	13.0	18		

<sup>a</sup> Ontong Java primary magma composition for accumulated fraction melting (AFM) from Herzberg (2004).

<sup>b</sup> Mauna Kea primary magma composition is average of 4 samples in Table 1 of Herzberg (2006).

<sup>c</sup> Gorgona primary magma composition for AFM for 1F, fertile source, in Table 4 of Herzberg and O'Hara (2002).

Area: Tangle, Tangle Lakes area; Rainy Creek, Rainy Creek area (Fig. 6); Clearwater, Clearwater Mountains (Fig. 3.8)

## CONCLUSION

The Nikolai Formation in southern Alaska forms an arcuate belt ~450 km long that extends eastward into southwest Yukon. The volcanic stratigraphy of the Nikolai Formation in the Wrangell Mountains and Alaska Range (Amphitheater and Clearwater Mountains) is approximately 3.5-4 km thick and formed as part of an extensive oceanic plateau in the Middle to Late Triassic during a single, short-lived phase of volcanism lasting <5 Myr. The Nikolai Formation is bounded by marine sedimentary sequences and unconformably overlies Late Paleozoic volcanic arc sequences. The volcanic stratigraphy is predominantly subaerial flows in Alaska, but consists of ~500 m of submarine flows and basal sills intruding pre-existing shale in the southern Alaska Range.

The Nikolai Formation is composed of high- and low-titanium basalts that record a change in the source of magmas that constructed the Wrangellia oceanic plateau in Alaska. The low-titanium basalts form the lowest ~400 m of volcanic stratigraphy in the Alaska Range, and the remainder of the volcanic stratigraphy in the Alaska Range and all of the sampled stratigraphy in the Wrangell Mountains is high-titanium basalt. The geochemistry of the erupted sequences of the Wrangellia oceanic plateau in Alaska provide a way of detecting the different contributions from the crust and lithospheric mantle, and plume-type mantle. The high-titanium basalts were derived from a uniform OIB plume-type Pacific mantle source, with similar initial Hf and Nd isotopic ratios to Ontong Java. The low-titanium basalts require involvement of a HFSE-depleted, high  $\epsilon\text{Hf}$  source component that is distinct from OIB and MORB and was only involved during the early phase of this major melting event. There is no indication as yet discovered of a transitional lava type, nor do the high-titanium basalts indicate significant assimilation or interaction of lithospheric material so as to be detectable with geochemistry relative to the volume of the magmas erupted.

Whereas almost all CFBs, and at least one oceanic plateau (e.g. Kerguelen), record involvement of continental lithosphere, Wrangellia flood basalts in Alaska do not indicate involvement of low  $\epsilon\text{Nd}$ , low  $\epsilon\text{Hf}$  continental material. However, the low-titanium basalts have compositions that indicate melting and/or interaction with subduction-modified mantle was involved in their formation. A large thermal anomaly,

indicated by estimates of melting conditions of low-titanium picrites, may have mobilized the lithosphere and/or caused interaction of plume-derived melts and lithosphere that would have initially caused mechanical erosion, and possibly thermal erosion, of the base of the lithosphere, whereafter plume-derived lavas dominated construction of the Wrangellia plateau in Alaska.

## ACKNOWLEDGEMENTS

We are grateful to Jeff Trop and Danny Rosenkrans for their advice on geology and logistics within Wrangell-St. Elias National Park. Jeanine Schmidt was very helpful with field advice and information about Wrangellia geology. We also appreciate insights from Jeff Vervoort and Julian Pearce, and assistance from Claude Herzberg with modeling. Bruno Kieffer and Jane Barling assisted with some lab work. Funding was provided by NSERC Discovery Grants to J. Scoates and D. Weis. A. Greene was supported by a University Graduate Fellowship at UBC.

## REFERENCES

- Armstrong, A. K. & MacKevett, E. M., Jr. (1977). The Triassic Chitistone Limestone, Wrangell Mountains, Alaska. *U. S. Geological Survey. Open-File Report 77-217*, D49-D62 p.
- Armstrong, A. K. & MacKevett, E. M., Jr. (1982). Stratigraphy and diagenetic history of the lower part of the Triassic Chitistone Limestone, Alaska. *U. S. Geological Survey. Professional Paper 1212-A*, 26 p.
- Arndt, N. T. & Christensen, U. (1992). The role of lithospheric mantle in continental flood volcanism: thermal and geochemical constraints. *Journal of Geophysical Research* **97**(B7), 10,967-10,981.
- Arndt, N. T., Czamanske, G. K. & Wooden, J. L. (1993). Mantle and crustal contributions to continental flood volcanism. *Tectonophysics* **223**(1-2), 39-52.
- Babbs, T. L. (1997). Geochemical and petrological investigations of the deeper portions of the Ontong Java Plateau: Malaita, Solomon Islands. Unpublished Ph.D. dissertation, Leicester University, U.K., 254 pp.
- Barry, T. L., Pearce, J. A., Leat, P. T., Millar, I. L. & le Roex, A. P. (2006). Hf isotope evidence for selective mobility of high-field-strength elements in a subduction setting: South Sandwich Islands. *Earth and Planetary Science Letters* **252**(3-4), 223.
- Bittenbender, P. E., Bean, K. W., Kurtak, J. M. & Deninger, J., Jr (2007). Mineral assessment of the Delta River Mining District area, East-central Alaska. *U. S. Bureau of Land Management-Alaska. Technical Report*.

- Chauvel, C. & Blichert-Toft, J. (2001). A hafnium isotope and trace element perspective on melting of the depleted mantle. *Earth and Planetary Science Letters* **190**, 137-151.
- Clift, P., Draut, A., Kelemen, P., Blusztajn, J. & Greene, A. (2005). Stratigraphic and geochemical evolution of the Jurassic Talkeetna Volcanic Formation, south-central Alaska. *Geological Society of America Bulletin* **117**(7/8), 902-925.
- Coffin, M. F., Duncan, R. A., Eldholm, O., Fitton, J. G., Frey, F. A., Larsen, H. C., Mahoney, J. J., Saunders, A. D., Schlich, R. & Wallace, P. J. (2006). Large igneous provinces and scientific ocean drilling: Status quo and a look ahead. *Oceanography* **19**(4), 150-160.
- Cox, K. G., MacDonald, R. & Hornung, G. (1967). Geochemical and petrographic provinces in the Karoo basalts of southern Africa. *American Mineralogist* **52**, 1451-1474.
- d'Acremont, E., Leroy, S. & Burov, E. B. (2003). Numerical modelling of a mantle plume: the plume head-lithosphere interaction in the formation of an oceanic large igneous province. *Earth and Planetary Science Letters* **206** (3-4), 379-396.
- DePaolo, D. J. (1981). Trace element and isotopic effects of combined wallrock assimilation and fractional crystallization. *Earth and Planetary Science Letters* **53**, 189-202.
- Farnetani, C. G. & Richards, M. A. (1994). Numerical investigations of the mantle plume initiation model for flood basalt event. *Journal of Geophysical Research* **99**, 13,813-13,834.
- Gallagher, K. & Hawkesworth, C. (1992). Dehydration melting and the generation of continental flood basalts. *Nature* **358**, 57-59.
- Gardner, M. C., Bergman, S. C., Cushing, G. W., MacKevett, E. M., Jr., Plafker, G., Campbell, R. B., Dodds, C. J., McClelland, W. C. & Mueller, P. A. (1988). Pennsylvanian pluton stitching of Wrangellia and the Alexander terrane, Wrangell Mountains, Alaska. *Geology* **16**, 967-971.
- Geldmacher, J., Hanan, B. B., Blichert-Toft, J., Harpp, K., Hoernle, K., Hauff, F., Werner, R. & Kerr, A. C. (2003). Hafnium isotopic variations in volcanic rocks from the Caribbean Large Igneous Province and Galapagos hot spot tracks. *Geochemistry Geophysics Geosystems* **4**(7)(1062), doi:10.1029/2002GC000477.
- Glen, J. M. G., Schmidt, J. M. & Morin, R. (2007). Gravity and magnetic studies of the Talkeetna Mountains, Alaska: constraints on the geological and tectonic interpretation of southern Alaska, and implications for mineral exploration. In: Ridgway, K. D., Trop, J. M., O'Neill, J. M. & Glen, J. M. G. (eds.) *Tectonic Growth of a Collisional Continental Margin: Crustal Evolution of Southern Alaska*. Geological Society of America Special Paper 431, pp. 593-622.
- Greene, A. R., DeBari, S. M., Kelemen, P. B., Blusztajn, J. & Clift, P. D. (2006). A detailed geochemical study of island arc crust: the Talkeetna Arc section, south-central Alaska. *Journal of Petrology* **47**(6), 1051-1093, 10.1093/petrology/egl002.
- Greene, A. R., Scoates, J. S., Weis, D. & Israel, S. (2008, submitted-a). Geochemistry of flood basalts from the Yukon (Canada) segment of the accreted Wrangellia oceanic plateau. *Lithos*.
- Greene, A. R., Scoates, J. S., Weis, D., Nixon, G. T. & Kieffer, B. (2008, submitted-b). Wrangellia flood basalts on Vancouver Island: Significance of picritic and

- tholeiitic lavas for the melting history and magmatic evolution of a major oceanic plateau. *Journal of Petrology*.
- Hauff, F., Hoernle, K. & Schmidt, A. (2003). Sr-Nd-Pb composition of Mesozoic Pacific oceanic crust (Site 1149 and 801, ODP Leg 185): Implications for alteration of ocean crust and the input into the Izu-Bonin-Mariana subduction system. *Geochemistry Geophysics Geosystems* 4(8), doi:10.1029/2002GC000421.
- Herzberg, C. (2004). Partial melting below the Ontong Java Plateau. In: Fitton, J. G., Mahoney, J. J., Wallace, P. J. & Saunders, A. D. (eds.) *Origin and Evolution of the Ontong Java Plateau*. Geological Society Special Publication 229, pp. 179-183.
- Herzberg, C., Asimow, P. D., Arndt, N., Niu, Y., Leshner, C. M., Fitton, J. G., Cheadle, M. J. & Saunders, A. D. (2007). Temperatures in ambient mantle and plumes: Constraints from basalts, picrites, and komatiites. *Geochemistry Geophysics Geosystems* 8(Q02006), doi:10.1029/2006GC001390.
- Herzberg, C. & O'Hara, M. J. (2002). Plume-associated ultramafic magmas of Phanerozoic age. *Journal of Petrology* 43(10), 1857-1883.
- Hooper, P. R. & Hawkesworth, C. J. (1993). Isotopic and geochemical constraints on the origin and evolution of the Columbia River Basalt. *Journal of Petrology* 34(6), 1203-1246.
- Hornig, I. (1993). High-Ti and low-Ti tholeiites in the Jurassic Ferrar Group, Antarctica. *Geologisches Jahrbuch Reihe E: Geophysik* 47, 335-369.
- Janney, P. E., Le Roex, A. P. & Carlson, R. W. (2005). Hafnium isotope and trace element constraints on the nature of mantle heterogeneity beneath the Central Southwest Indian Ridge (13°E to 47°E). *Journal of Petrology* 46(12), 2427-2464, doi:10.1093/petrology/egi060.
- Johnson, M. C. & Plank, T. (1999). Dehydration and Melting Experiments Constrain the Fate of Subducted Sediments. *Geochemistry Geophysics Geosystems* 1(13 December), 1999GC000014.
- Jones, D. L., Silberling, N. J. & Hillhouse, J. (1977). Wrangellia; a displaced terrane in northwestern North America. *Canadian Journal of Earth Sciences* 14(11), 2565-2577.
- Kelemen, P. B., Hanghøj, K. & Greene, A. R. (2003). One view of the geochemistry of subduction-related magmatic arcs, with emphasis on primitive andesite and lower crust. In: Rudnick, R. (ed.) *The Crust*. Elsevier-Pergamon: Oxford Treatise on Geochemistry Vol. 3 Holland, H. D. & Turekian, K. K. (eds.), pp. 593-659.
- Kelemen, P. B., Johnson, K. T. M., Kinzler, R. J. & Irving, A. J. (1990). High-field-strength element depletions in arc basalts due to mantle-magma interaction. *Nature* 345, 521-524.
- Kelemen, P. B., Shimizu, N. & Dunn, T. (1993). Relative depletion of niobium in some arc magmas and the continental crust: partitioning of K, Nb, La and Ce during melt/rock reaction in the upper mantle. *Earth and Planetary Science Letters* 120, 111-134.
- Kempton, P. D., Pearce, J. A., Barry, T. L., Fitton, J. G., Langmuir, C. H. & Christie, D. M. (2002). Sr-Nd-Pb-Hf isotope results from ODP Leg 187: Evidence for mantle dynamics of the Australian-Antarctic Discordance and origin of the Indian MORB

- source. *Geochemistry Geophysics Geosystems* **3**(12), 1074, doi:10.1029/2002GC000320.
- Kerr, A. C. (1994). Lithospheric thinning during the evolution of continental large igneous provinces: A case study from the North Atlantic Tertiary province. *Geology* **22**, 1027-1030.
- Kerr, A. C. & Mahoney, J. J. (2007). Oceanic plateaus: Problematic plumes, potential paradigms. *Chemical Geology* **241**, 332-353.
- Lassiter, J. C. (1995). Geochemical investigations of plume-related lavas : constraints on the structure of mantle plumes and the nature of plume/lithosphere interactions. Ph.D. thesis, unpublished chapter, University of California, Berkeley, 231 pp.
- Lassiter, J. C. & DePaolo, D. J. (1997). Plume/lithosphere interaction in the generation of continental and oceanic flood basalts: chemical and isotopic constraints. In: Mahoney, J. J. & Coffin, M. F. (eds.) *Large Igneous Provinces: Continental, Oceanic, and Planetary Flood Volcanism*. American Geophysical Union: Washington Geophysical Monograph 100, pp. 335-355.
- Lassiter, J. C., DePaolo, D. J. & Mahoney, J. J. (1995). Geochemistry of the Wrangellia flood basalt province: Implications for the role of continental and oceanic lithosphere in flood basalt genesis. *Journal of Petrology* **36**(4), 983-1009.
- MacDonald, G. A. & Katsura, T. (1964). Chemical composition of Hawaiian lavas. *Journal of Petrology* **5**, 82-133.
- MacKevett, E. M., Jr. (1978). Geologic map of the McCarthy Quadrangle, Alaska. U. S. Geological Survey. Miscellaneous Investigations Series Map I-1032 scale 1:250,000.
- MacKevett, E. M., Jr., Cox, D. P., Potter, R. P. & Silberman, M. L. (1997). Kennecott-type deposits in the Wrangell Mountains, Alaska: High-grade copper ores near a basalt-limestone contact. In: Goldfarb, R. J. & Miller, L. D. (eds.) *Mineral Deposits of Alaska*. Economic Geology Monograph 9, pp. 66-89.
- Mahoney, J., LeRoex, A. P., Peng, Z., Fisher, R. L. & Natland, J. H. (1992). Southwestern Limits of Indian Ocean Ridge Mantle and the Origin of Low  $^{206}\text{Pb}/^{204}\text{Pb}$  Mid-Ocean Ridge Basalt: Isotope Systematics of the Central Southwest Indian Ridge (17°-50°E). *Journal of Geophysical Research* **97**(B13), 19771-19790.
- Mahoney, J., Storey, M., Duncan, R., Spencer, K. & Pringle, M. (1993). Geochemistry and age of the Ontong Java Plateau. In: Pringle, M., Sager, W. & Sliter, W. (eds.) *AGU Monograph on the Mesozoic Pacific: Geology, Tectonics, and Volcanism*. 77 AGU: Washington, pp. 233-261.
- Mahoney, J. J., Sinton, J. M., Kurz, M. D., MacDougall, J. D., Spencer, K. J. & Lugmair, G. W. (1994). Isotope and trace element characteristics of a super-fast spreading ridge: East Pacific rise, 13-23°S. *Earth and Planetary Science Letters* **121**, 173-193.
- McDonough, W. F. & Sun, S. (1995). The composition of the Earth. *Chemical Geology* **120**, 223-253.
- Melluso, L., Beccaluva, L., Brotzu, P., Gregnanin, A., Gupta, A. K., Morbidelli, L. & Traversa, G. (1995). Constraints on the mantle sources of the Deccan Traps from the petrology and geochemistry of the basalts of Gujarat State (Western India). *Journal of Petrology* **36**(5), 1393-1432, 10.1093/petrology/36.5.1393.

- Menzies, M. A. (1992). The lower lithosphere as a major source for continental flood basalts: a re-appraisal. In: Storey, B. C., Alabaster, T. & Pankhurst, R. J. (eds.) *Magmatism and the Causes of Continental Break-up*. Geological Society Special Publication No. 68, pp. 31-39.
- Nobre Silva, I. G., Weis, D., Barling, J. & Scoates, J. S. (in revision). Leaching systematics for the determination of high-precision Pb isotope compositions of ocean island basalts. *Geochemistry Geophysics Geosystems*, doi:2007GC001891.
- Nokleberg, W. J., Aleinikoff, J. N., Dutro, J. T. J., Lanphere, M. A., Silberling, N. J., Silva, S. R., Smith, T. E. & Turner, D. L. (1992). Map, tables, and summary fossil and isotopic age data, Mount Hayes quadrangle, eastern Alaska Range, Alaska. *U. S. Geological Survey Miscellaneous Field Studies Map* 1996-D, 1:250,000 scale.
- Nokleberg, W. J., Jones, D. L. & Silberling, N. J. (1985). Origin and tectonic evolution of the Maclaren and Wrangellia terranes, eastern Alaska Range, Alaska. *Geological Society of America Bulletin* **96**, 1251-1270.
- Nokleberg, W. J., Plafker, G. & Wilson, F. H. (1994). Geology of south-central Alaska. In: Plafker, G. & Berg, H. C. (eds.) *The Geology of North America*. Geological Society of America: Boulder, CO The Geology of Alaska G-1, pp. 311-366.
- Nowell, G. M., Kempton, P. D., Noble, S. R., Fitton, J. G., Saunders, A., Mahoney, J. J. & Taylor, R. N. (1998). High precision Hf isotope measurements of MORB and OIB by thermal ionisation mass spectrometry: insights into the depleted mantle. *Chemical Geology* **149**, 211-233.
- Patchett, P. J., White, W. M., Feldmann, H., Kielinczuk, S. & Hofmann, A. W. (1984). Hafnium/rare earth element fractionation in the sedimentary system and crustal recycling into the Earth's mantle. *Earth and Planetary Science Letters* **69**, 365-378.
- Pearce, J. A. (1982). Trace element characteristics of lavas from destructive plate boundaries. In: Thorpe, R. S. (ed.) *Andesites: Orogenic Andesites and Related Rocks*. John Wiley & Sons: Chichester, UK, pp. 526-547.
- Pearce, J. A. (2008). Geochemical fingerprinting of oceanic basalts with applications to ophiolite classification and the search for Archean oceanic crust. *Lithos* **100**, 14-48.
- Pearce, J. A., Kempton, P. D. & Gill, J. B. (2007). Hf-Nd evidence for the origin and distribution of mantle domains in the SW Pacific. *Earth and Planetary Science Letters* **260**(1-2), 98-114, doi:10.1016/j.epsl.2007.05.023
- Peate, D. W. (1997). The Parana-Etendeka Province. In: Coffin, M. F. & Mahoney, J. (eds.) *Large Igneous Provinces: Continental, Oceanic, and Planetary Flood Volcanism*. American Geophysical Union Geophysical Monograph 100, pp. 217-245.
- Peate, D. W. & Hawkesworth, C. (1996). Lithospheric to asthenospheric transition in low-Ti flood basalts from southern Parana, Brazil. *Chemical Geology* **127**, 1-24.
- Pik, R., Deniel, C., Coulom, C., Yirgu, G. & Marty, B. (1999). Isotopic and trace element signatures of Ethiopian flood basalts: Evidence for plume-lithosphere interaction. *Geochimica et Cosmochimica Acta* **63**, 2263-2279.
- Pik, R., Deniel, C., Coulon, C., Yirgu, G., Hofmann, C. & Ayalew, D. (1998). The northwestern Ethiopian Plateau flood basalts: Classification and spatial



- distribution of magma types. *Journal of Volcanology and Geothermal Research* **81**(1-2), 91.
- Plafker, G., Moore, J. C. & Winkler, G. R. (1994). Geology of the southern Alaska margin. In: Plafker, G. & Berg, H. C. (eds.) *The Geology of North America*. Geological Society of America: Boulder, CO The Geology of Alaska G-1, pp. 389-449.
- Plafker, G., Nokleberg, W. J. & Lull, J. S. (1989). Bedrock geology and tectonic evolution of the Wrangellia, Peninsular, and Chugach terranes along the Trans-Alaskan Crustal Transect in the northern Chugach Mountains and southern Copper River basin, Alaska. *Journal of Geophysical Research* **94**, 4,255-4,295.
- Richards, M. A., Jones, D. L., Duncan, R. A. & DePaolo, D. J. (1991). A mantle plume initiation model for the Wrangellia flood basalt and other oceanic plateaus. *Science* **254**, 263-267.
- Richter, D. H., Smith, J. G., Lanphere, M. A., Dalrymple, G. B., Reed, B. L. & Shew, N. (1990). Age and progression of volcanism, Wrangell volcanic field, Alaska. *Bulletin of Volcanology* **53**, 29-44.
- Rioux, M., Hacker, B., Mattinson, J., Kelemen, P., Blusztajn, J. & Gehrels, G. (2007). Magmatic development of an intra-oceanic arc: High-precision U-Pb zircon and whole-rock isotopic analyses from the accreted Talkeetna arc, south-central Alaska. *Geological Society of America Bulletin* **119**(9-10), 1168-1184, doi:10.1130/b25964.1.
- Salters, V. J. & White, W. (1998). Hf isotope constraints on mantle evolution. *Chemical Geology* **145**, 447-460.
- Salters, V. J. M. (1996). The generation of mid-ocean ridge basalts from the Hf and Nd isotope perspective. *Earth and Planetary Science Letters* **141**, 109-123.
- Salters, V. J. M. & Stracke, A. (2004). Composition of the depleted mantle. *Geochemistry Geophysics Geosystems* **5**(Q05B07), doi:10.1029/2003GC000597.
- Saltus, R. W., Hudson, T. & Wilson, F. H. (2007). The geophysical character of southern Alaska: Implications for crustal evolution. In: Ridgway, K. D., Trop, J. M., O'Neill, J. M. & Glen, J. M. G. (eds.) *Tectonic Growth of a Collisional Continental Margin: Crustal Evolution of Southern Alaska*. Geological Society of America Special Paper 431, pp. 1-20.
- Saunders, A. D. (2005). Large igneous provinces: Origin and environmental consequences. *Elements* **1**, 259-263.
- Saunders, A. D., Storey, M., Kent, R. W. & Norry, M. J. (1992). Consequences of plume-lithosphere interactions. In: Storey, B. C., Alabaster, T. & Pankhurst, R. J. (eds.) *Magmatism and the Causes of Continental Breakup*. Geological Society of London Special Publication 68: London, pp. 41-60.
- Schmidt, J. M. & Rogers, R. K. (2007). Metallogeny of the Nikolai large igneous province (LIP) in southern Alaska and its influence on the mineral potential of the Talkeetna Mountains. In: Ridgway, K. D., Trop, J. M., O'Neill, J. M. & Glen, J. M. G. (eds.) *Tectonic Growth of a Collisional Continental Margin: Crustal Evolution of Southern Alaska*. Geological Society of America Special Paper 431, pp. 623-648.
- Silberling, N. J., Richter, D. H., Jones, D. L. & Coney, P. C. (1981). Geologic map of the bedrock part of the Healy A-1 Quadrangle south of the Talkeetna-Broxon Gulch

- fault system, Clearwater Mountains, Alaska. *U.S. Geological Survey Open-File Report 81-1288*, 1 sheet, 1:63,360 scale.
- Smith, J. G. & MacKevett, E. M., Jr. (1970). The Skolai Group in the McCarthy B-4, C-4, C-5 Quadrangles, Wrangell Mountains, Alaska. *U. S. Geological Survey. Bulletin 1274-Q*, Q1-Q26 p.
- Smith, T. E. (1981). Geology of the Clearwater Mountains, south-central Alaska. *Alaska Division of Geological and Geophysical Surveys. Geologic Report 60*, 72 p.
- Stout, J. H. (1976). Geology of the Eureka Creek area, east-central Alaska Range. *Alaska Division of Geological and Geophysical Surveys. Geologic Report 46*, 32 p.
- Tejada, M. L. G., Mahoney, J. J., Castillo, P. R., Ingle, S. P., Sheth, H. C. & Weis, D. (2004). Pin-pricking the elephant: evidence on the origin of the Ontong Java Plateau from Pb-Sr-Hf-Nd isotopic characteristics of ODP Leg 192 basalts. In: Fitton, J. G., Mahoney, J. J., Wallace, P. J. & Saunders, A. D. (eds.) *Origin and Evolution of the Ontong Java Plateau*. Geological Society of London, Special Publication 229, pp. 133-150.
- Turner, S., Hawkesworth, C., Gallagher, K., Stewart, K., Peate, D. & Mantovani, M. (1996). Mantle plumes, flood basalts, and thermal models for melt generation beneath continents: Assessment of a conductive heating model and application to the Paraná. *Journal of Geophysical Research* **101**(B5), 11,503-11,518.
- van de Flierdt, T., Frank, M., Lee, D.-C., Halliday, A. N., Reynolds, B. C. & Hein, J. R. (2004). New constraints on the sources and behavior of neodymium and hafnium in seawater from Pacific Ocean ferromanganese crusts. *Geochimica et Cosmochimica Acta* **68**(19), 3827.
- Vervoort, J. D. & Blichert-Toft, J. (1999). Evolution of the depleted mantle: Hf isotope evidence from juvenile rocks through time. *Geochimica et Cosmochimica Acta* **63**, 533-556.
- Vervoort, J. D., Patchett, P. J., Albarède, F., Blichert-Toft, J., Rudnick, R. L. & Downes, H. (2000). Hf-Nd isotopic evolution of the lower crust. *Earth and Planetary Science Letters* **181**, 115-129.
- Vervoort, J. D., Patchett, P. J., Blichert-Toft, J. & Albarède, F. (1999). Relationships between Lu-Hf and Sm-Nd isotopic systems in the global sedimentary system. *Earth and Planetary Science Letters* **168**, 79-99.
- Walter, M. J. (1998). Melting of garnet peridotite and the origin of komatiite and depleted lithosphere. *Journal of Petrology* **39**(1), 29-60.
- Weis, D., Kieffer, B., Maerschalk, C., Barling, J., de Jong, J., Williams, G. A., Hanano, D., Mattielli, N., Scoates, J. S., Goolaerts, A., Friedman, R. A. & Mahoney, J. B. (2006). High-precision isotopic characterization of USGS reference materials by TIMS and MC-ICP-MS. *Geochemistry Geophysics Geosystems* **7**(Q08006), doi:10.1029/2006GC001283.
- White, R. S. & McKenzie, D. (1995). Mantle plumes and flood basalts. *Journal of Geophysical Research* **100**, 17,543-17,585.
- Wilson, F. H., Dover, J. D., Bradley, D. C., Weber, F. R., Bundtzen, T. K. & Haeussler, P. J. (1998). Geologic map of Central (Interior) Alaska. *U. S. Geological Survey Open-File Report 98-133-A*, <http://wrgis.wr.usgs.gov/open-file/of98-133-a/>.
- Wilson, F. H., Labay, K. A., Shew, N. B., Preller, C. C., Mohadjer, S. & Richter, D. H. (2005). Digital Data for the Geology of Wrangell-Saint Elias National Park and

- Preserve, Alaska *U. S. Geological Survey Open-File Report 2005-1342*,  
<http://pubs.usgs.gov/of/2005/1342/>.
- Wooden, J. L., Czamanske, G. K., Fedorenko, V. A., Arndt, N. T., Chauvel, C., Bouse, R. M., King, B. S. W., Knight, R. J. & Siems, D. F. (1993). Isotopic and trace-element constraints on mantle and crustal contributions to Siberian continental flood basalts, Noril'sk area, Siberia. *Geochimica et Cosmochimica Acta* **57**, 3,677-3,704.
- Woodhead, J. D., Hergt, J. M., Davidson, J. P. & Eggins, S. M. (2001). Hafnium isotope evidence for 'conservative' element mobility during subduction zone processes. *Earth and Planetary Science Letters* **192**, 331-346.
- Xu, Y., Chung, S.-L., Jahn, B.-m. & Wu, G. (2001). Petrologic and geochemical constraints on the petrogenesis of Permian-Triassic Emeishan flood basalts in southwestern China. *Lithos* **58**(3-4), 145.

## **CHAPTER 4**

### **Geochemistry of Flood Basalts from the Yukon (Canada) Segment of the Accreted Wrangellia Oceanic Plateau**

<sup>1</sup>A version of this chapter has been submitted for publication.

## INTRODUCTION

Oceanic plateaus cover ~10% of the seafloor (Ben-Avraham *et al.*, 1981) and form from melting events that are distinct from melting at mid-ocean ridges. The largest Phanerozoic examples of oceanic plateaus largely formed below sea-level (Ontong Java Plateau), or subsided below sea-level after their formation (Kerguelen Plateau), and the basement rock and direct evidence of the tectonic setting they formed in remains hidden beneath the surface of the ocean and the thick sequence of flood basalts. Oceanic plateaus and flood basalts are constructed on rifted margins, extinct mid-ocean ridges, old oceanic lithosphere, rifted parts of continental crust, or extinct or active oceanic arcs.

Geochemical and stratigraphical studies of accreted oceanic plateaus where the base of the volcanic stratigraphy is exposed provide a means of discerning the tectonic setting during formation and its effect on the generation of magmas and their geochemical and isotopic characteristics. The erupted flood basalts preserve a record of the interaction between a plume and the oceanic lithosphere, without complications from thicker and geochemically distinct continental lithosphere (Saunders *et al.*, 1992).

The Wrangellia flood basalts in the Pacific Northwest of North America are part of an enormous oceanic plateau that formed in the Middle to Late Triassic and accreted to western North America in the Late Jurassic or Early Cretaceous (Jones *et al.*, 1977). Parts of the volcanic stratigraphy of this oceanic plateau extend over 2300 km in British Columbia (BC), Yukon, and Alaska where the flood basalts overlie Paleozoic arc volcanic and marine sedimentary sequences and are overlain by Late Triassic limestone. In Yukon, Canada, a significant part of the Wrangellia flood basalts (Nikolai Formation) are exposed in a belt that extends more than 500 km westward into Alaska and consists predominantly of well-layered subaerial flows. A companion study in Alaska has revealed two geochemically distinct groups of lavas that record a shift in the source region that produced the erupted basalts (see Chapter 3).

In this study, we characterize the geochemical and isotopic variations of the Nikolai Formation in Yukon to provide insights about the construction and tectonic setting of this part of the Wrangellia oceanic plateau and to assess the source regions that were involved in the generation of the magmas. The geochemistry of underlying

Paleozoic volcanic arc sequences is also examined to evaluate whether the lower arc mantle lithosphere may have had a role in the formation of the Nikolai basalts. This work is used to support interpretations made about geochemical variations of the Nikolai Formation in Alaska, and also describes some of the key differences between these two areas. There are no previously published geochemical and Sr-Nd-Hf-Pb isotopic data of Wrangellia flood basalts in Yukon and this work substantially adds to our dataset as part of a larger project on the Wrangellia oceanic plateau in BC, Yukon, and Alaska. Previous work on Wrangellia flood basalts in Alaska and Vancouver Island by Richards *et al.* (1991) proposed a plume initiation model for the origin of Wrangellia flood basalts based on the large volumetric output of lavas over a short timespan, evidence of uplift preceding volcanism, and an absence of evidence of rifting.

## GEOLOGIC SETTING AND AGE CONSTRAINTS

In the southwest corner of Yukon, Wrangellia forms a southeast- to northwest-trending linear belt (<20 km wide and 300 km long), bordered by Alaska to the west and British Columbia to the south (Fig. 4.1). In the Kluane Ranges, Wrangellia stratigraphy lies adjacent to older units of the Alexander terrane, in a southeast-tapering wedge between the Duke River and Denali Faults (Fig. 4.1). Late Mesozoic and Cenozoic strike-slip faulting that juxtaposed parts of the Wrangellia and Alexander Terranes resulted in extensive folding, faulting, and low-grade metamorphism of Wrangellia stratigraphy (Israel *et al.*, 2006). The Denali Fault is a major terrane boundary between Wrangellia and the Nisling and Windy-McKinley Terranes to the northeast, where there has been ~370 km of right-lateral displacement since the mid-Cretaceous (Lowey, 1998).

The oldest definitive units of Wrangellia in Yukon are Late Paleozoic arc volcanic sequences and marine sediments of the Skolai Group (Station Creek and Hasen Creek Formations; Fig. 4.2). The Nikolai Formation unconformably overlies the Hasen Creek Formation in most areas in Yukon and there are isolated occurrences of Middle Triassic argillite-chert-siltstone-limestone (<100 m thick; Hoge Creek succession) between the Skolai Group and Nikolai Formation (Read & Monger, 1976; Israel *et al.*, 2006). The Paleozoic formations are intruded by mafic and ultramafic sills related to the overlying Nikolai Formation (Hulbert, 1997). The Nikolai Formation covers ~700 km<sup>2</sup> (<3% of all

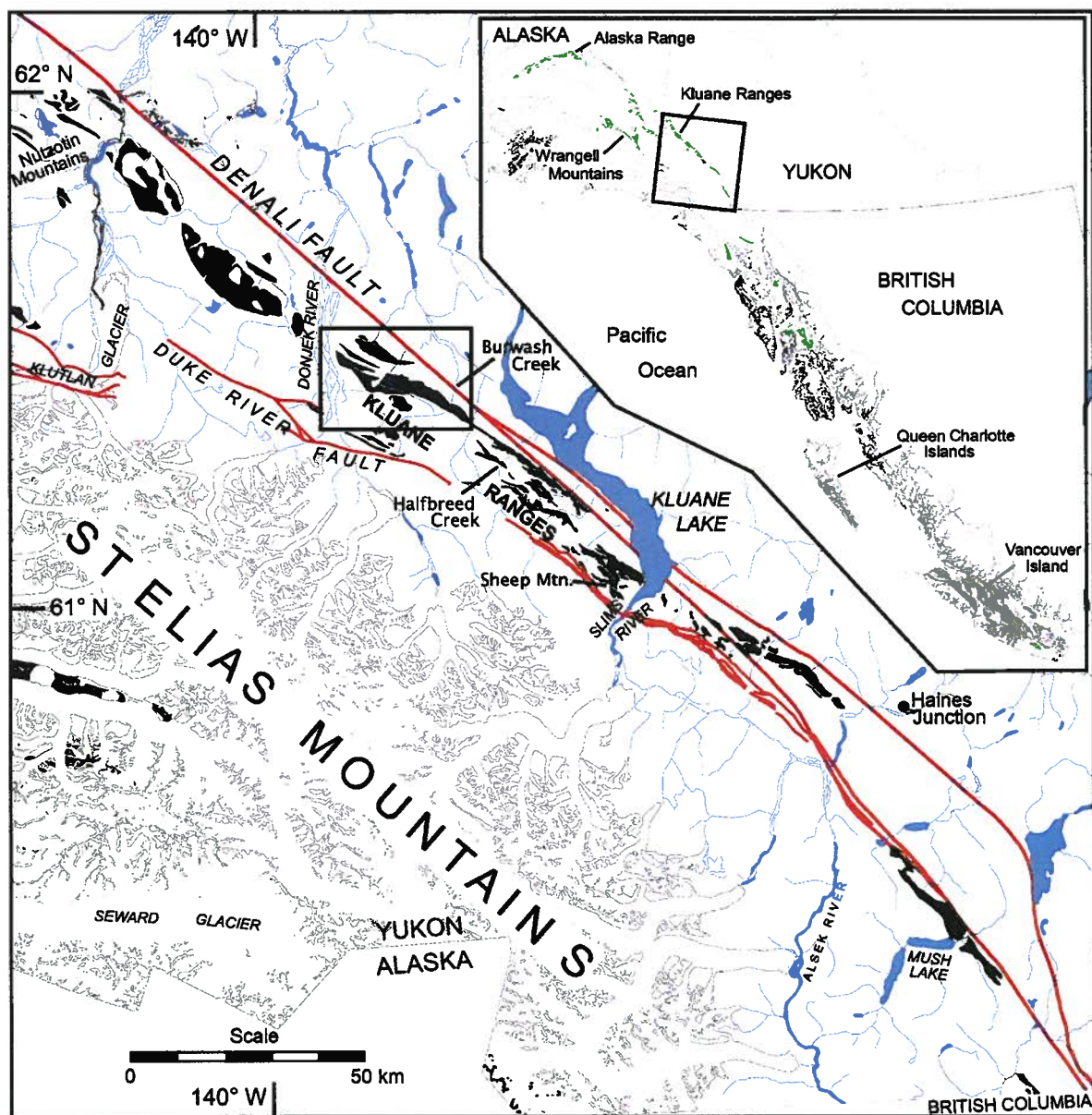


**Figure 4.1** Simplified map of southwest Yukon showing the distribution of the Nikolai Formation (black; after Israel, 2004; Israel & Van Zeyl, 2004; Israel *et al.*, 2005). The main area of field study in the Kluane Ranges is specified with a black box. The inset shows the extent of the Wrangellia flood basalts (green) in BC, Yukon, and Alaska.

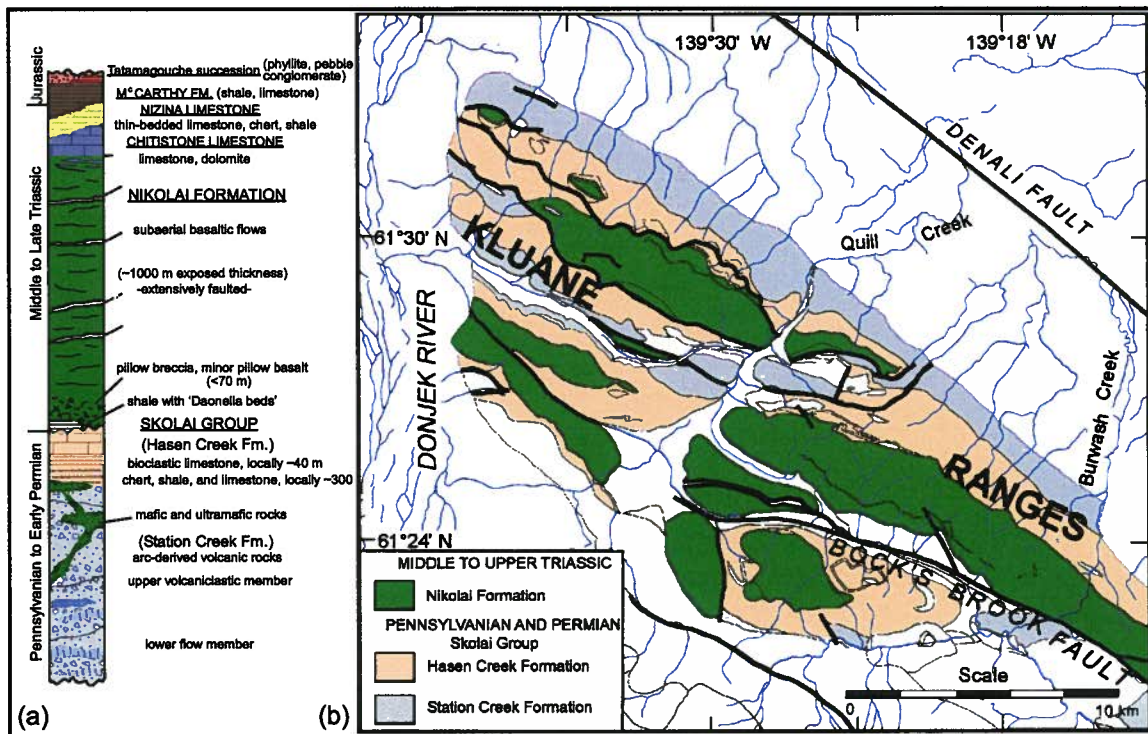


**Figure 4.2** Geologic map and stratigraphy of the northern part of the Kluane Ranges, Yukon (location of map shown in Fig. 4.1). (a) Stratigraphic column of Wrangellia units exposed in the Kluane Ranges, derived from the works of (Read & Monger, 1976; Israel & Van Zeyl, 2004; Israel *et al.*, 2005). (b) Simplified geologic map of the Kluane Ranges (1:50,000 scale) between the Donjek River and Burwash Creek, derived from (Israel & Van Zeyl, 2004; Israel *et al.*, 2005).



Wrangellia flood basalts from Vancouver Island to central Alaska) from the Mush Lake area to the Nutzotin Mountains and is best preserved in the Kluane Ranges where the total estimated thickness is ~1000 m (accurate estimation of the thickness is not possible because of extensive faulting and folding) (Figs 4.1 and 4.2). The Nikolai Formation is capped by shallow-water to deep-water limestone and shale of the Upper Triassic to Lower Jurassic Chitistone and Nizina Limestones and McCarthy Formation (Read & Monger, 1976; Armstrong & MacKevett, 1977; MacKevett, 1978) (Fig. 4.2). Thick deep marine fan deposits of the Jurassic Dezadeash Formation overlap the Wrangellia and Alexander Terranes (Read & Monger, 1976) and mid-Cretaceous arc plutonic rocks of the Kluane Ranges suite intrude parts of Wrangellia (Plafker & Berg, 1994).

Detailed regional mapping in southwest Yukon was accomplished by Muller (1967), Read and Monger (1976), and Dodds and Campbell (1992a, b, c) and recent mapping in the Kluane Ranges (1:50,000 scale) is by Israel *et al.* (2004; 2005; 2007a, b). *Daonella* imprints in shale immediately underlying the Nikolai Formation and conodonts in limestone overlying the Nikolai Formation, in Yukon and Alaska, indicate Late Ladinian to Late Carnian-Early Norian ages (ca 227-216 Ma; Ogg, 2004; Furin *et al.*, 2006), respectively (Smith & MacKevett, 1970; Read & Monger, 1976; MacKevett, 1978; Israel *et al.*, 2006). U-Pb dating of zircon separated from a gabbro sill possibly related to the Nikolai Formation yielded a Ladinian age of  $232.2 \pm 1.0$  Ma (average  $^{207}\text{Pb}/^{206}\text{Pb}$  age of 3 discordant (1.6 to 2.4%) analyses from multi-grain zircon fractions) (Mortensen & Hulbert, 1991). Five  $^{40}\text{Ar}/^{39}\text{Ar}$  ages of hornblende and biotite from intrusive rocks in the Alaska Range, interpreted to be comagmatic with Nikolai basalts, indicate formation of these rocks at ca. 231-225 Ma (Bittenbender *et al.*, 2007; Schmidt & Rogers, 2007). In addition, three Nikolai basalt samples from the Wrangell Mountains yielded  $^{40}\text{Ar}/^{39}\text{Ar}$  step-heating ages of  $228.3 \pm 5.2$ ,  $232.8 \pm 11.5$ , and  $232.4 \pm 11.9$  Ma (Lassiter, 1995).

## FIELD RELATIONS AND PETROGRAPHY

Fieldwork was undertaken from Mush Lake to the Donjek River to examine and sample the volcanic stratigraphy of the Nikolai Formation and underlying Paleozoic sequences (Fig. 4.1). Complete sections of the original volcanic stratigraphy are not

preserved in any one area because of the pervasive faulting in southwest Yukon. The basal flows of the Nikolai Formation in Yukon are composed of volcanic breccia and minor pillow lava less than 70 meters in total thickness (Fig. 4.3). Conglomerate with rounded clasts derived from the underlying Paleozoic formations also occurs along the base. The basal conglomerate is laterally discontinuous, and bound by faults in several localities (Read & Monger, 1976; Israel & Cobbett, 2008), and these structures are interpreted as grabens associated with uplift or rifting during the initial phase of Nikolai volcanism. Above these basal units, almost all the flood basalts (90-95%) are subaerial flows that form monotonous maroon- and green-colored sequences marked primarily by amygdaloidal-rich horizons (Fig. 4.3). No discernible erosional surfaces are preserved along flow contacts and rarely are any sediments found between flows (Fig. 4.3). Several occurrences of hematite-rich tuff and breccia are preserved between massive flows (Read and Monger, 1976). The massive lava flows are commonly <10 m thick and rarely exhibit columnar jointing. Close to the top of the flood basalt sequence, the basalt flows are commonly interbedded with thin lenticular beds of marine limestone (<1 meter thick). Several occurrences of the interbedded limestone reach close to 30 m in thickness (e.g. Read and Monger, 1976). There is no evidence of detrital material from a continental source anywhere associated with the flood basalts.

The Nikolai Formation in Yukon is divided into high- and low-titanium basalts, based on geochemistry; the two types also have distinct petrographic differences (Table 1). Much of the Nikolai Formation in Yukon is intensely altered; eighteen of the 59 samples (16 of 42 low-titanium basalts; 2 of 17 high-titanium basalts) are pervasively altered with no remaining primary igneous texture or minerals (Table 1). Seventeen of the 41 low-titanium samples with discernible igneous texture exhibit glomeroporphyritic to porphyritic texture (plagioclase phenocrysts) and 8 samples are aphyric with intersertal to intergranular texture (Table 1; Fig. 4.4). Fourteen of the 17 high-titanium samples are coarse-grained with subophitic textures and contain plagioclase laths (1-2 mm long) and Fe-Ti oxides (>1 mm), which are more abundant in the high-titanium basalts (Table 1; Fig. 4.4). Plagioclase is commonly replaced by epidote, chlorite, sericite, clinozoisite, and clay minerals and clinopyroxene is mostly unaltered. Fe-Ti oxides are altered to sphene and leucoxene mineral. Hematitic staining is common throughout most subaerial flows

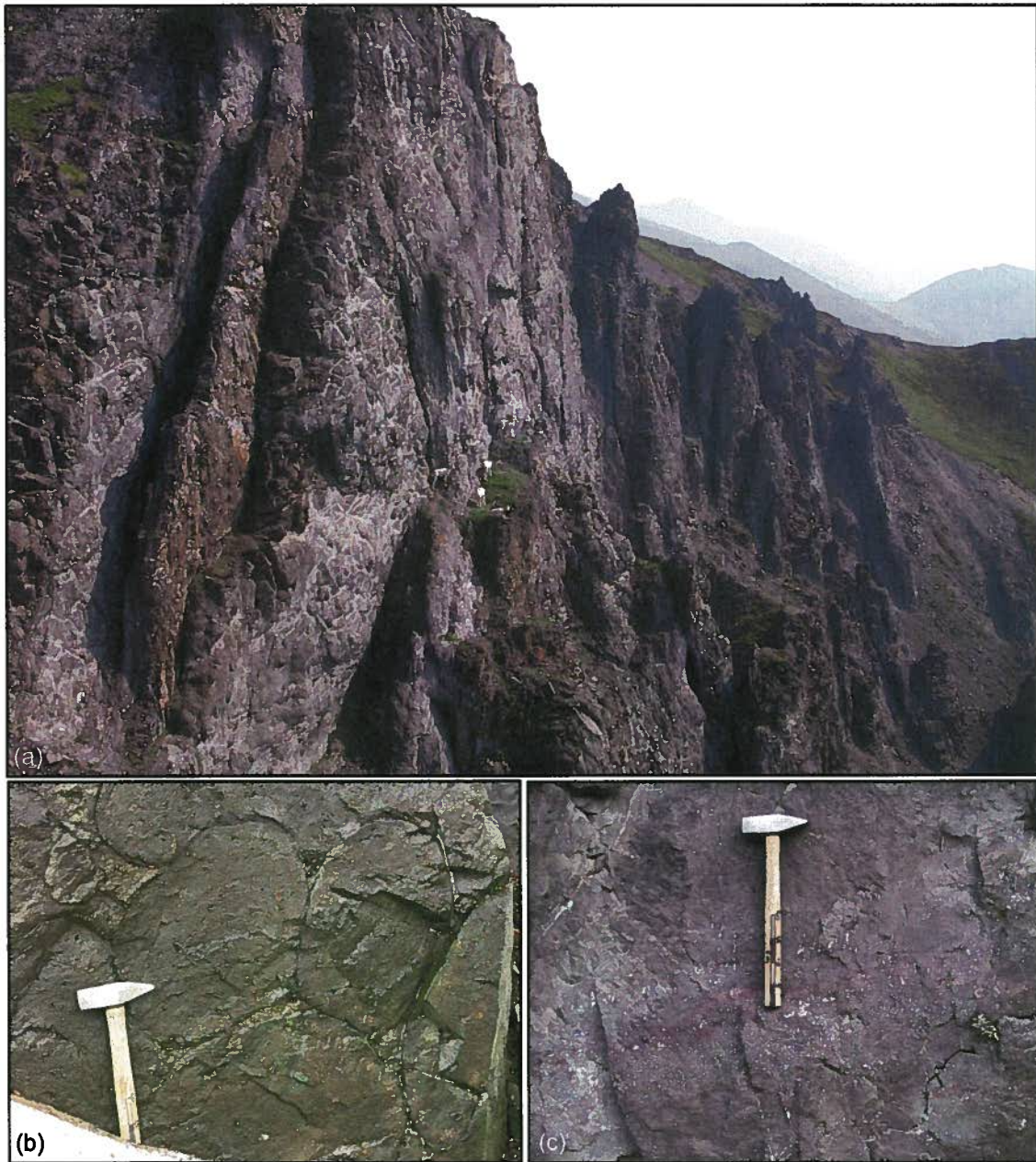


**Figure 4.3** Photographs of the Nikolai Formation in the Kluane Ranges, Yukon. (a) Vertically-oriented subaerial basalt flows south of Quill Creek, above the headwaters of the Tatamagouche Creek. Dall sheep (white dots) in center of photograph for scale. (b) Pillow basalt at the base of the Nikolai Formation. Hammer (45 cm) for scale. (c) Massive amygdaloidal basalt typical of the Nikolai Formation in Yukon. Hammer (45 cm) for scale.



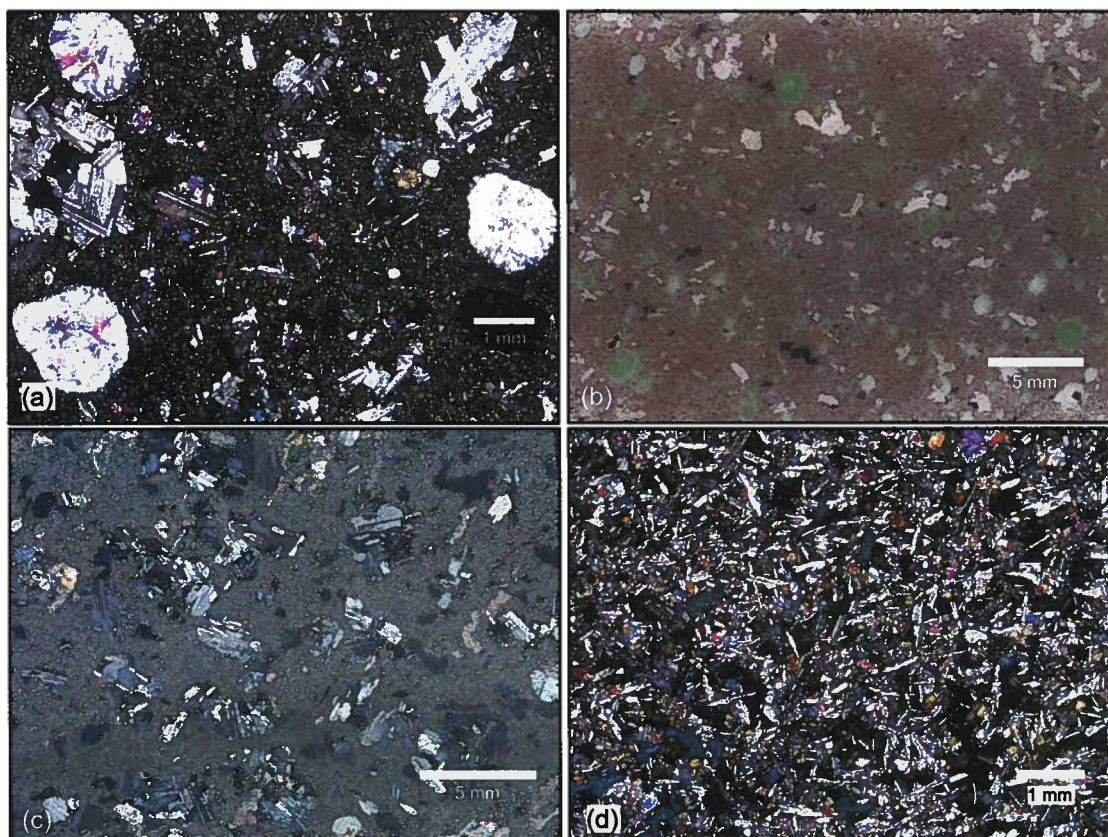


**Figure 4.4** Photomicrographs of representative Nikolai basalts in southwest Yukon. (a) Glomeroporphyritic pillow basalt with abundant zeolite-filled amygdules in cross-polarized transmitted light (sample 2151; low-titanium basalt). (b) Thin-section scan of typical red-stained amygdaloidal basalt in plane-polarized transmitted light (sample 4821A4; no chemistry). (c) Abundant plagioclase glomerocrysts in a fine-grained intersertal groundmass in cross-polarized transmitted light (sample 4810A10; low-titanium basalt). (d) Aphyric basalt with abundant Fe-Ti oxides in cross-polarized transmitted light (sample 4812A6; high-titanium basalt). Scale bars are labeled in each of the photographs. Table 4.1 contains detailed descriptions of the petrographic characteristics of Nikolai samples.

Table 4.1 Summary of petrographic characteristics and phenocryst proportions of Nikolai basalts in Yukon

Sample <sup>a</sup>	Area <sup>b</sup>	Flow <sup>c</sup>	Group <sup>d</sup>	Igneous texture <sup>e</sup>	vol% Plag	Cpx	Ox	Alt <sup>f</sup>	Notes <sup>g</sup>
231	QC	FLO	high-Ti	relict c.g. intergranular			15	5	abund ox, alt plag <2 mm, relict cpx <0.5 mm
4820A1	HC	FLO	high-Ti	relict c.g. intergranular			10	5	alt plag laths <2 mm, fresh cpx <0.5 mm
1801	QC	FLO	high-Ti	c.g. intergranular	5		15	3	very ox-rich, alt plag laths <1.5 mm
1691	QC	PIL	high-Ti	relict c.g. intergranular			10	4	alt plag <2 mm, ox <0.5 mm, few unalt cpx <0.5 mm
1451	QC	FLO	high-Ti	relict c.g. intergranular				5	faint outline plag <2 mm
4807A9	QC	FLO	high-Ti	relict glomero	10		20	4	very ox-rich <0.5 mm, alt plag glcr <3 mm
821	QC	FLO	high-Ti	perv alt, relict c.g.				5	relict c.g. plag deformed
4807A7	QC	FLO	high-Ti	c.g. intergranular			7	4	alt plag laths <1.5 mm, fresh cpx <0.5 mm
4810A11	DJ	FLO	high-Ti	c.g. intergranular			10	4	patchy zones alt, fresh cpx <1 mm, alt plag <2 mm
4816A3	ML	FLO	high-Ti	relict c.g. intergranular			5	4	fresh cpx <2 mm, highly alt plag
4816A2	ML	FLO	high-Ti	c.g. intergranular			10	3	fresh cpx <1 mm, alt plag laths <2 mm
1561	QC	FLO	high-Ti	subophitic, intergranular			15	3	ox-rich, fresh cpx <1 mm enc plag <0.5 mm
4807A8	QC	FLO	high-Ti	c.g. glomero, intergranular	20		15	4	ox-rich, very c.g., cpx <2 mm, plag glcr <5 mm
4808A4	QC	FLO	high-Ti	c.g. intergranular			15	4	c.g., fresh cpx <1 mm, ox <1 mm, alt plag laths
4807A3	QC	FLO	high-Ti	pervasive alteration				5	no primary texture or minerals
4808A8	QC	FLO	high-Ti	c.g. intergranular			10	3	c.g., abund ox <1 mm, alt plag laths <1 mm, fresh cpx
4821A1	BC	FLO	high-Ti	c.g. intergranular			10	3	c.g., abund ox <0.5 mm
4806A6	QC	FLO	low-Ti	glomero, amygdaloidal	3		3		amylg <5 mm, few plag glcr <2 mm
4811A1	DJ	FLO	low-Ti	intergranular			1		Fe-ox alt, patchy zones alt, few plag phenos <2 mm
561	DJ	PIL	low-Ti	relict glomero, perv alt	2		5	1	relict plag glcr <2 mm
4810A10	DJ	FLO	low-Ti	glomero, amygdaloidal	15		2		plag glcr <2 mm
4810A1	DJ	FLO	low-Ti	porphyritic	20		2		tabular plag phenos <2 mm, pl laths <1 mm in gm
4806A2	QC	FLO	low-Ti	relict porphyritic	5		3		outline of plag phenos <2 mm, f.g. plag needles
2221	QC	FLO	low-Ti	pervasive alteration			5		faint outline of plag needles <0.5 mm
4810A5	DJ	FLO	low-Ti	glomero	30		2		abund plag glcr <2 mm, alt felty f.g. gm
1381	QC	FLO	low-Ti	pervasive alteration			5		no primary texture or minerals
1321	QC	FLO	low-Ti	perv alt, relict glomero			5		faint sign of plag glcr <3 mm, f.g. gm
4810A3	DJ	FLO	low-Ti	c.g. intergranular	3		3		few alt plag phenos <2 mm, patchy alt
1141	QC	FLO	low-Ti	perv alt, relict glomero			5		relict deformed plag phenos <2 mm
4812A8	DJ	FLO	low-Ti	aphyric, intergranular			10	2	ox-rich, plag laths <1 mm, patchy zones alt
4811A5	DJ	FLO	low-Ti	glomero, amygdaloidal	20		1		~25% amylg, plag glc and phenos <2 mm
961	QC	FLO	low-Ti	relict glomero	15		4		fresh cpx <0.5 mm, alt plag glcr <3 mm
1241	QC	PIL	low-Ti	relict intersertal, aphyric			4		plag needles <0.5 mm, patchy zones alt
4806A7	QC	FLO	low-Ti	relict glomero	10		3		plag replaced, cpx <0.5 mm, relict plag glcr <3 mm
4806A4	QC	FLO	low-Ti	intersertal, intergranular			2		plag needles <0.5 mm, few plag glcr <2 mm
1391	QC	FLO	low-Ti	aphyric w/ chilled margin	5		3		chilled margin w/ microphenos <0.5 mm
4806A5	QC	FLO	low-Ti	porphyritic, intersertal	20		2		plag phenos <2 mm, f.g. gm
1131	QC	FLO	low-Ti	perv alt			5		hint of plag glomerocrysts
4811A6	DJ	FLO	low-Ti	intergranular, glomero	5		2		plag laths <1 mm, few pl glcr <3 mm, fresh cpx
2131	QC	FLO	low-Ti	pervasive alteration			5		no primary texture or minerals
1741	QC	FLO	low-Ti	pervasive alteration			5		no primary texture or minerals
4811A8	DJ	FLO	low-Ti	porphyritic, plag-phyric	10		2		plag phenos <2 mm, intergranular gm, plag laths <1 mm
4816A5A	ML	FLO	low-Ti	pervasive alteration			5		no primary texture or minerals
2151	QC	PIL	low-Ti	glomero, intersertal	40		3		f.g. gm of plag needles, abund plag glcr <5 mm
4811A3	DJ	FLO	low-Ti	glomero, intergranular	10		3		plag glcr <3 mm, patchy zones alt
4816A9	ML	FLO	low-Ti	pervasive alteration			5		little primary texture or minerals, few relict cpx
1301	QC	FLO	low-Ti	aphyric			4		felty plag microlites, plag <0.3 mm
4812A5	DJ	FLO	low-Ti	subophitic, ophimottled			3		Fe-ox alt, plag <0.5 mm, cpx <1.5 mm enc plag
4816A7	ML	FLO	low-Ti	pervasive alteration			4		no primary texture or minerals
2191	QC	FLO	low-Ti	pervasive alteration			5		hint of plag glomerocrysts
441	QC	FLO	low-Ti	intergranular, aphyric			3		cpx partially enc pl, plag <1 mm
881	QC	FLO	low-Ti	pervasive alteration			5		no primary texture or minerals
4816A4	ML	FLO	low-Ti	pervasive alteration			4		no primary texture or minerals
4810A8	DJ	FLO	low-Ti	glomero, intersertal	10		2		plag glcr <3 mm, patchy zones alt
2291	QC	FLO	low-Ti	pervasive alteration			5		no primary texture or minerals, few patches plag needles
851	QC	FLO	low-Ti	aphyric			3		patchy zones alt, plag <0.5 mm, amylg-rich (~25%)
4816A11	ML	FLO	low-Ti	pervasive alteration			5		no primary texture or minerals, amylg
4810A7	DJ	FLO	low-Ti	aphyric, intersertal	2		3		patchy zones alt, Fe-ox alt, 1 plag pheno <4 mm
1031	QC	PBRE	basal	aphyric, intersertal			3		patchy zones alt, 1 plag <0.5 mm

<sup>a</sup>Sample numbers beginning with 4: last digit year, month, day, initial, sample station. <sup>b</sup>QC, Quill Creek; ML, Mush Lake; DJ, Donjek River; BC, Burwash Creek; HC, Halfbreed Creek. <sup>c</sup>PIL, pillow; PBRE, pillow breccia; FLO, flow. <sup>d</sup>high-Ti, high-titanium basalt; low-Ti, low-titanium basalt; basal, basal flow. <sup>e</sup>glomero, glomeroporphyritic; perv alt, pervasive alteration; c.g., coarse-grained. <sup>f</sup>Visual alteration index based primarily on degree of plagioclase alteration, alteration distribution, textural preservation, and secondary mineralization (after Gilkins et al., 2005; Table 2.5, page 27); 1, subtle, 2, weak, 3, moderate, 4, strong, 5, intense. <sup>g</sup>glcr, glomerocrysts; f.g., fine-grained; enc, enclosing; gm, groundmass; alt, alteration, amylg, amygdulites; phenos, phenocrysts, abund, abundant, Fe-ox, iron oxyhydroxide. Mineral abbreviations: plag, plagioclase; cpx, clinopyroxene; ox, oxides (includes ilmenite + titanomagnetite). High- and low-titanium basalts are listed from highest (top) to lowest (bottom) TiO<sub>2</sub>.

and growth of iron oxyhydroxides is prevalent. Amygdules (<25 volume %) are usually filled with quartz, calcite, epidote, prehnite and pumpellyite. Sample preparation and analytical methods for 60 of the 85 collected samples of the Nikolai Formation and 11 samples of underlying Paleozoic arc sequences are described in Electronic Appendix 1.

## WHOLE-ROCK CHEMISTRY

### Major- and trace-element compositions

The Nikolai Formation in Yukon contains low-titanium basalts (0.5-1.0 wt %  $\text{TiO}_2$ ; 5.6-11.3 wt % MgO) and high-titanium basalts (1.4-2.3 wt %  $\text{TiO}_2$ ; 5.8-8.7 wt % MgO, except for one outlier) that overlap the boundary between the alkalic and tholeiitic fields of MacDonald and Katsura (1964) (Fig. 4.5; Table 2). High- and low-titanium basalts have similar loss-on-ignition (LOI; 1.1-6.7 wt %; mean  $3.8 \pm 1.6$  wt %; Table 2) and major and trace elements do not correlate with LOI. The composition of the high- and low-titanium basalts in Yukon is similar to those of the Nikolai Formation in Alaska, but they have noticeably higher alkali contents and mostly lower CaO and FeO(T) (Fig. 4.5). Nikolai basalts in Yukon are higher in total alkalis than basalts from Alaska due to alkali metasomatism during alteration of the Yukon basalts.

The high-titanium basalts form a tight range of parallel, rare earth element (REE) patterns sloping downward to the right (mean  $\text{La/Yb}_{\text{CN}} = 2.0 \pm 0.4$ ; except for two LREE-depleted samples); this range is distinct from the broader range of flat and light REE (LREE)-enriched patterns of the low-titanium basalts (Fig 4.6). The LREE segments of the low-titanium basalts flatten with decreasing REE abundance ( $\text{La/Sm}_{\text{CN}} = 0.6$ -2.8; mean  $1.4 \pm 0.8$ ) and are flat and parallel through the middle and heavy REE (HREE) (mean  $\text{Dy/Yb}_{\text{CN}} = 1.0 \pm 0.15$ ;  $10$ - $16 \times$  chondrite), with the exception of two LREE-depleted ( $\text{La/Sm}_{\text{CN}} = 0.6$ -0.8) and two LREE-enriched ( $\text{La/Sm}_{\text{CN}} = 2.5$ -2.8) samples (Fig. 4.6). The low-titanium basalts (mean  $\text{Yb}_{\text{CN}} = 11.9 \pm 4.4$ ) lie at the low end of the range and have lower REE abundances than the high-titanium basalts (mean  $\text{Yb}_{\text{CN}} = 14.6 \pm 4.9$ ).

A key feature of all the low-titanium basalts is negative high field strength element (HFSE; Nb, Ta, Zr, Hf, Ti) anomalies relative to the large ion lithophile elements (LILE) and REE on primitive mantle-normalized trace-element patterns (Fig 4.6). Most of the low-titanium basalts have high Sr relative to Nd and Sm and high concentrations and

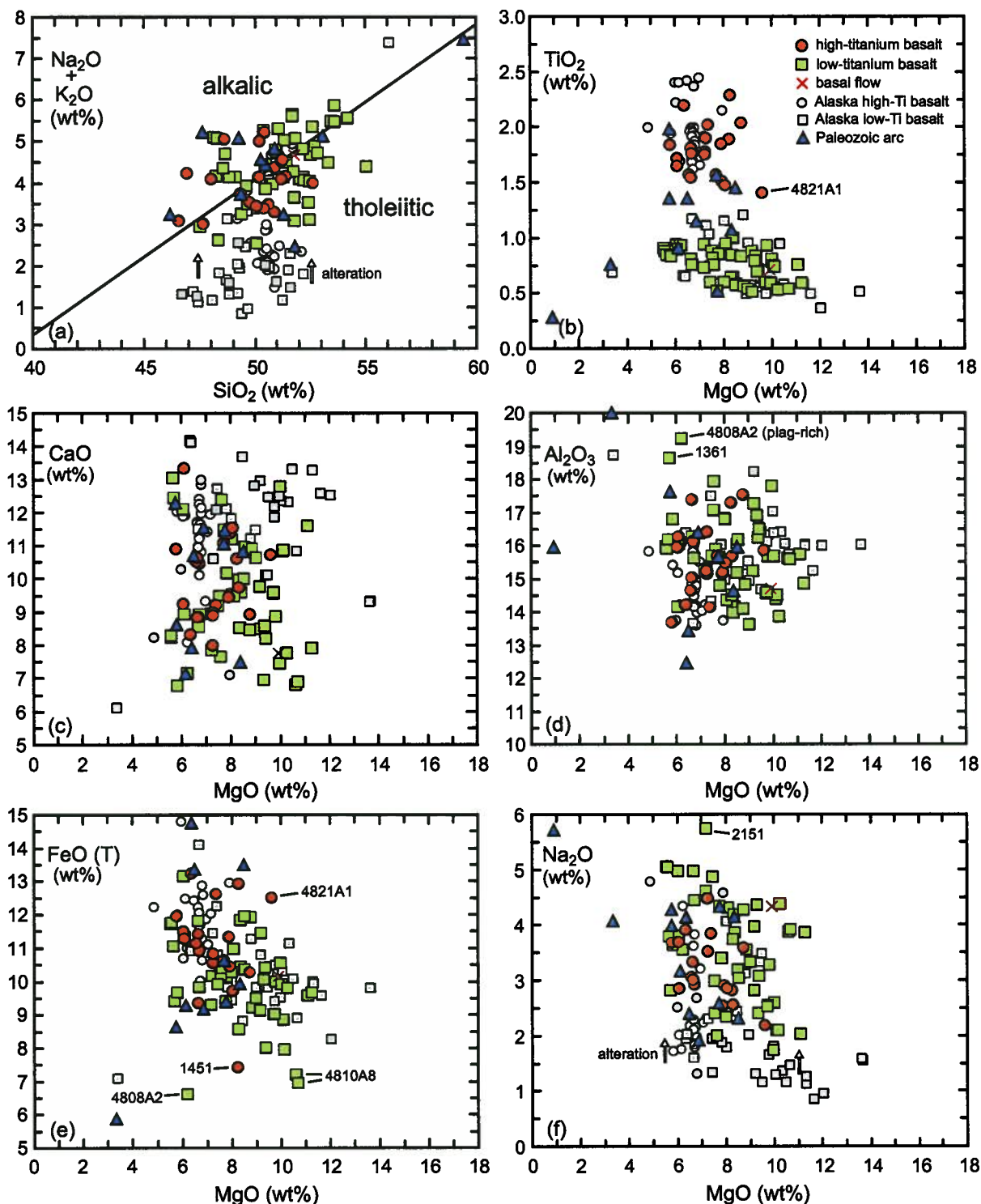


**Figure 4.5** Whole-rock major-element variation diagrams for the Nikolai Formation in Yukon with data for the Nikolai Formation in Alaska (Greene et al., submitted). The boundary of the alkaline and tholeiitic fields is that of MacDonald and Katsura (1964). Total iron expressed as FeO. Oxides are plotted on an anhydrous, normalized basis. Note the difference in alkali contents between the Nikolai Formation in Yukon and Alaska and the clear separation between high- and low-titanium basalts. Arrows indicate the effect of alteration on whole-rock alkali contents.

Table 4.2 Major element (wt% oxide) and trace element (ppm) abundances in whole rock samples of Nikolai basalts, Yukon

Sample	231	441	561	820	851	881	961	1031	1131	1141
Group	HI-TI	LOW-TI	LOW-TI	HI-TI	LOW-TI	LOW-TI	LOW-TI	BASAL	LOW-TI	LOW-TI
Area	QC	QC	DJ	QC	QC	QC	QC	QC	QC	QC
Flow	FLO	FLO	PIL	FLO	FLO	FLO	FLO	BRE	FLO	FLO
UTM EW	6817374	6817574	6800729	6816007	6817880	6819358	6817296	6815519	6815507	6815545
UTM NS	581357	576917	576969	582331	577003	576411	579513	573780	583741	584009
Unnormalized Major Element Oxides (Weight %):										
SiO <sub>2</sub>	45.16	45.94	46.98	46.78	50.65	47.4	49.48	49.03	48.74	52.23
TiO <sub>2</sub>	2.17	0.55	0.88	1.74	0.5	0.55	0.78	0.67	0.75	0.8
Al <sub>2</sub> O <sub>3</sub>	14.82	16.88	14.96	16.69	13.26	14.49	16.41	13.93	16.15	16.17
Fe <sub>2</sub> O <sub>3</sub> *	13.6	11.14	10.6	12.18	10.42	12.66	10.89	10.69	10.66	10.33
MnO	0.248	0.206	0.195	0.159	0.194	0.211	0.195	0.168	0.142	0.181
MgO	7.85	9.48	9.37	6.4	9.83	8.13	7.28	9.37	8.91	5.62
CaO	9.21	7.08	8.46	8.48	7.43	9.53	7.35	7.36	6.63	6.53
Na <sub>2</sub> O	2.42	1.65	3.13	3.2	4.19	3.04	2.31	4.11	4.16	3.5
K <sub>2</sub> O	0.42	3.17	0.82	1.64	0.32	0.71	2.52	0.3	0.42	1.84
P <sub>2</sub> O <sub>5</sub>	0.18	0.07	0.19	0.15	0.09	0.07	0.18	0.19	0.14	0.2
LOI	3.92	4.01	3.52	2.73	3.12	3.02	2.96	4.13	3.45	2.55
Total	100.00	100.18	99.11	100.15	100.00	99.81	100.36	99.95	100.15	99.95
Trace Elements (ppm):										
La	9.32	1.10	7.58	6.58	2.70	1.58	7.78	12.10	2.71	8.26
Ce	22.4	2.7	15.5	15.8	6.5	4.0	16.0	23.8	6.3	19.1
Pr	3.29	0.43	2.06	2.36	0.86	0.58	2.11	2.88	0.93	2.35
Nd	16.8	2.7	9.3	11.8	4.6	3.2	9.8	11.6	5.1	10.8
Sm	4.97	1.14	2.53	3.59	1.47	1.27	2.62	2.74	1.76	2.87
Eu	1.68	0.48	0.94	1.35	0.55	0.46	0.94	0.79	0.68	0.95
Gd	5.81	1.72	2.87	3.95	1.96	1.88	3.02	2.68	2.17	2.98
Tb	1.01	0.34	0.53	0.69	0.37	0.39	0.49	0.44	0.40	0.54
Dy	6.23	2.30	3.40	4.06	2.53	2.56	3.19	2.74	2.44	3.28
Ho	1.28	0.53	0.70	0.82	0.57	0.56	0.69	0.58	0.53	0.69
Er	3.83	1.74	2.10	2.48	1.82	1.86	2.24	1.81	1.63	2.16
Tm	0.55	0.27	0.33	0.36	0.27	0.28	0.33	0.27	0.24	0.33
Yb	3.29	1.61	2.12	2.12	1.75	1.73	2.01	1.63	1.43	2.08
Lu	0.47	0.24	0.32	0.30	0.26	0.26	0.31	0.25	0.22	0.33
Sc	40.0	36.6	39.5	29.0	35.8	39.8	33.8	35.4	33.6	29.4
V	446	181	233	237	284	323	294	195	225	325
Cr	214	201	370	154	1,000	310	138	274	179	60
Co	49	44	29	35	61	55	38	41	32	38
Ni	78	139	100	72	335	101	67	114	63	65
Cu	230	56	30	77	35	68	24	73	35	48
Zn	202	71	50	79	77	94	91	79	54	208
Ga	22	15	12	21	14	17	18	10	13	22
Ge	1.5	1.3	1	1.3	1.2	1.5	1.4	0.8	0.9	1.5
Rb	7	38	16	36	4	13	36	4	4	33
Sr	171	174	219	249	113	102	184	296	236	235
Y	33.1	14.8	19.2	21.7	16.3	16.8	18.9	16.8	14.6	21.1
Zr	113	21	46	87	26	26	49	62	20	66
Nb	9.7	1	5.9	8.2	1.1	1	2.9	3.2	0.6	4.2
Cs	1.4	2		5.2	1.2	1.1	2	0.7	0.2	1.7
Ba	83	258	376	149	56	160	311	624	134	370
Hf	3.2	0.7	1.4	2.4	0.8	0.8	1.4	1.5	0.6	1.8
Ta	0.59	0.02	0.36	0.49	0.04	0.03	0.16	0.13	0.04	0.21
Th	0.62	0.14	0.90	0.58	0.52	0.30	1.04	1.39	0.14	1.72
U	0.19	0.07	0.47	0.17	0.24	0.15	0.43	0.44	0.06	0.73

Abbreviations for group are: HI-TI, high-titanium basalt; LOW-TI, low-titanium basalt; BASAL, basal pillow breccia. Abbreviations for area are: QC, Quill Creek; ML, Mush Lake; DJ, Donjek River; BC, Burwash Creek; HC, Halfbreed Creek. Abbreviations for flow are: FLO, subaerial flow; PIL, pillow basalt; BRE, breccia. Sample locations are given using the Universal Transverse Mercator (UTM) coordinate system (NAD83; zones 7 and 8). Analyses were performed at Activation Laboratory (ActLabs). Fe<sub>2</sub>O<sub>3</sub>\* is total iron expressed as Fe<sub>2</sub>O<sub>3</sub>. LOI is loss-on-ignition. All major elements, Sr, V, and Y were measured by ICP quadrupole OES on solutions of fused samples; Cu, Ni, Pb, and Zn were measured by total dilution ICP; Cs, Ga, Ge, Hf, Nb, Rb, Ta, Th, U, Zr, and REE were measured by magnetic-sector ICP on solutions of fused samples; Co, Cr, and Sc were measured by INAA. Blanks are below detection limit. See Appendix E for sample preparation and analytical methods.



Sample	1241	1301	1321	1361	1391	1451	1561	1691	1741	1801
Group	LOW-TI	LOW-TI	LOW-TI	LOW-TI	LOW-TI	HI-TI	HI-TI	HI-TI	LOW-TI	HI-TI
Area	QC	QC	QC	QC	QC	QC	QC	QC	QC	QC
Flow	PIL	FLO	FLO	FLO	FLO	FLO	FLO	PIL	FLO	FLO
UTM EW	6812929	6814635	6814283	6814881	6813656	6811576	6806001	6807411	6807894	6810271
UTM NS	583591	586217	573054	571429	572922	575121	593450	590665	592808	588559
<i>Unnormalized Major Element Oxides (Weight %):</i>										
SiO <sub>2</sub>	48.52	49.31	46.05	47.67	45.16	49.68	48.41	45.76	45.95	48.18
TiO <sub>2</sub>	0.78	0.56	0.83	0.84	0.76	1.84	1.65	1.94	0.71	1.94
Al <sub>2</sub> O <sub>3</sub>	13.69	14.26	16.45	17.96	14.87	16.86	15.34	16.67	14.92	13.57
Fe <sub>2</sub> O <sub>3</sub> *	10.42	10.29	12.11	10.08	10.44	8.06	12.31	10.85	10.11	13.46
MnO	0.122	0.178	0.147	0.178	0.203	0.208	0.168	0.223	0.164	0.15
MgO	7.23	10.83	8.77	5.51	9.52	8.05	5.85	8.32	10.54	7.08
CaO	9.39	7.6	8.09	12	12.11	10.35	8.9	8.49	10.99	8.83
Na <sub>2</sub> O	3.14	3.7	2.69	2.71	2.46	2.74	3.55	3.41	1.93	3.69
K <sub>2</sub> O	0.13	0.27	1.28	0.42	0.34	0.46	1.26	0.48	0.55	0.28
P <sub>2</sub> O <sub>5</sub>	0.18	0.1	0.16	0.16	0.12	0.18	0.15	0.17	0.12	0.17
LOI	6.68	3.2	3.69	2.51	4.27	1.63	2.67	3.81	4.1	2.77
Total	100.28	100.30	100.27	100.04	100.25	100.06	100.26	100.12	100.08	100.12
<i>Trace Elements (ppm):</i>										
La	5.32	2.43	4.54	6.19	4.58	6.37	2.86	7.31	4.97	6.80
Ce	12.1	5.7	10.3	13.5	10.5	18.6	7.7	18.6	12.5	17.3
Pr	1.7	0.85	1.48	1.94	1.52	2.59	1.32	2.73	1.67	2.53
Nd	8.1	4.7	7.4	9.7	8.0	13.2	8.4	14.3	8.2	13.2
Sm	2.44	1.56	2.32	2.64	2.26	3.83	3.06	4.22	2.30	3.92
Eu	0.85	0.60	0.81	0.94	0.85	1.43	1.21	1.48	0.81	1.43
Gd	2.74	2.02	2.56	2.85	2.56	4.03	4.03	4.56	2.38	4.62
Tb	0.49	0.41	0.49	0.46	0.41	0.71	0.72	0.78	0.43	0.81
Dy	2.88	2.53	2.98	2.86	2.68	4.16	4.57	4.63	2.53	4.89
Ho	0.61	0.54	0.63	0.62	0.55	0.83	0.96	0.92	0.52	1.01
Er	1.89	1.70	2.05	1.91	1.78	2.42	2.88	2.76	1.70	3.11
Tm	0.29	0.26	0.31	0.28	0.25	0.34	0.42	0.39	0.25	0.44
Yb	1.84	1.54	1.90	1.71	1.52	1.97	2.46	2.32	1.56	2.58
Lu	0.26	0.23	0.27	0.24	0.23	0.26	0.35	0.33	0.22	0.38
Sc	33.9	40.2	34.5	28.5	37.1	30.5	36.9	29.7	27.8	42.8
V	238	248	226	316	291	371	384	264	281	327
Cr	198	440	115	83	476	273	286	195	938	234
Co	32	47	36	30	43	46	52	38	49	37
Ni	63	129	58	29	139	93	113	67	235	76
Cu	82	102	49	169	53	19	11	1,050		89
Zn	51	69	60	70	63	118	100	94	73	69
Ga	17	11	16	19	17	25	22	23	18	20
Ge	1.5	1	1.8	1.8	1.8	1.4	1.6	2	1.5	1.7
Rb	3	4	8	2	4	7	14	4	5	4
Sr	52	103	221	478	213	317	115	298	174	197
Y	16.5	14.1	17.6	16.2	15.7	23.3	25.7	25.3	15.6	27.6
Zr	34	23	36	42	39	107	66	108	45	96
Nb	1.4	1.7	2.3	1.9	1.8	8.3	2.9	8.7	1.7	7.8
Cs	1.3	0.5	0.2		0.4	0.4	1.3	0.3	0.3	0.3
Ba	20	62	135	144	200	87	64	27	94	30
Hf	1.1	0.7	1.1	1.3	1.2	2.9	1.9	2.9	1.2	2.7
Ta	0.09	0.04	0.09	0.08	0.06	0.52	0.12	0.55	0.07	0.52
Th	0.45	0.36	0.26	0.54	0.46	0.65	0.28	0.64	0.65	0.56
U	0.18	0.14	0.10	0.24	0.20	0.83	0.12	0.23	0.30	0.17

Sample	2131	2151	2191	2221	4806A4	4806A5	4806A6	4806A7	4807A7	4807A8
Group	LOW-TI	LOW-TI	LOW-TI	LOW-TI	LOW-TI	LOW-TI	LOW-TI	LOW-TI	HI-TI	HI-TI
Area	QC	QC	QC	QC	QC	QC	QC	QC	QC	QC
Flow	FLO	PIL	FLO	FLO	FLO	FLO	FLO	FLO	FLO	FLO
UTM EW	6806210	6807691	6807196	6807640	6817548	6817593	6817691	6817717	6817253	6817138
UTM NS	583857	582824	580433	581895	576922	576901	576954	577019	581187	581034
<i>Unnormalized Major Element Oxides (Weight %):</i>										
SiO <sub>2</sub>	48.42	50.98	48.69	44.39	47.99	47.54	47.75	47.56	48.43	43.56
TiO <sub>2</sub>	0.72	0.69	0.55	0.86	0.777	0.753	0.931	0.778	1.729	1.528
Al <sub>2</sub> O <sub>3</sub>	15.34	14.48	15.83	13.02	13.25	15.32	13.29	15.27	12.88	15.06
Fe <sub>2</sub> O <sub>3</sub> *	11.14	9.81	11.28	13.43	12.46	12.35	12.34	10.9	12.5	11.61
MnO	0.191	0.142	0.177	0.161	0.151	0.123	0.154	0.126	0.152	0.135
MgO	7.37	6.84	8.37	5.57	8.23	6.28	7.88	8.81	5.45	5.65
CaO	11.95	7.45	10.72	11.13	7.96	8.06	9	8.06	10.25	12.36
Na <sub>2</sub> O	1.92	5.44	2.98	4.57	4.01	4.67	3.62	2.27	3.45	2.64
K <sub>2</sub> O	0.54	0.12	0.42	0.11	0.44	0.28	0.11	1.36	0.47	1.27
P <sub>2</sub> O <sub>5</sub>	0.19	0.14	0.11	0.19	0.11	0.17	0.14	0.12	0.13	0.12
LOI	1.98	4.03	1.1	6.53	3.65	3.71	3.89	4.52	4.44	5.29
Total	99.76	100.12	100.23	99.96	99.03	99.25	99.11	99.78	99.89	99.21
<i>Trace Elements (ppm):</i>										
La	5.64	4.24	2.47	5.54	3.99	6.92	3.56	3.82	6.98	4.97
Ce	11.8	8.2	5.9	12.5	8.9	20.3	8.3	8.9	17.9	12.6
Pr	1.63	1.15	0.82	1.76	1.28	1.95	1.29	1.34	2.68	1.86
Nd	7.8	5.9	4.2	8.8	6.6	8.6	6.9	6.7	13.2	9.2
Sm	2.33	1.91	1.41	2.61	2.12	2.36	2.17	2.00	3.74	2.63
Eu	0.83	0.70	0.54	0.96	0.85	0.88	0.90	0.85	1.44	1.06
Gd	2.53	2.20	1.83	2.96	2.88	3.13	2.85	2.65	4.72	3.28
Tb	0.47	0.41	0.35	0.54	0.56	0.57	0.54	0.46	0.81	0.56
Dy	2.97	2.62	2.35	3.53	3.76	3.58	3.52	2.91	4.85	3.34
Ho	0.66	0.60	0.52	0.76	0.83	0.76	0.73	0.61	0.96	0.66
Er	2.12	1.79	1.76	2.45	2.57	2.36	2.20	1.83	2.74	1.88
Tm	0.32	0.27	0.27	0.38	0.39	0.36	0.33	0.27	0.38	0.26
Yb	1.98	1.62	1.68	2.41	2.50	2.29	2.14	1.69	2.33	1.62
Lu	0.29	0.24	0.26	0.35	0.38	0.33	0.30	0.25	0.33	0.23
Sc	35.0	29.8	40.6	41.8	60.0	50.5	56.7	45.2	37.9	34.2
V	217	173	330	235	364	304	370	312	332	309
Cr	186	244	390	162	148	140	208	201	180	291
Co	35	32	51	40	43.8	39.3	46.7	44	34	51
Ni	76	110	135	67	64	61	66	79	57	161
Cu	70	26	56	119	121	80	28	23	96	130
Zn	69	70	86	61	53	48	58	52	65	68
Ga	15	11	15	16	16	14	16	16	18	15
Ge	1.4	1	1.4	1.2	1.6	1.6	1.5	1.1	1.6	1.1
Rb	6	1	10	2	4	3	1	15	15	15
Sr	352	73	370	57	116	93	62	302	229	415
Y	18.6	15.1	15.7	20.9	24	24	20	17	27	21
Zr	30	25	20	44	26	36	29	26	102	80
Nb	3.9	1.4	1.1	2.3	1.1	1.8	1.1	1.2	8.1	6.1
Cs		0.1	0.6		1.0	0.4	0.5	1.4	2.0	1.8
Ba	135	25	256	17	86	62	39	186	84	170
Hf	1	0.8	0.7	1.2	0.9	1.2	1.0	0.9	2.8	2.1
Ta	0.08	0.04	0.04	0.12	0.05	0.10	0.06	0.05	0.55	0.43
Th	0.73	0.19	0.20	0.56	0.42	0.78	0.19	0.12	0.61	0.44
U	0.23	0.09	0.11	0.19	0.19	0.26	0.06	0.04	0.14	0.15

Sample	4807A9	4808A2	4808A4(1)	4808A4(2)	4808A8(1)	4808A8(2)	4810A1	4810A3	4810A5 (1)	4810A5 (2)
Group	HI-TI	LOW-TI	HI-TI	HI-TI	HI-TI	HI-TI	LOW-TI	LOW-TI	LOW-TI	LOW-TI
Area	QC	QC	QC	QC	QC	QC	DJ	DJ	DJ	DJ
Flow	FLO	FLO	FLO	FLO	FLO	FLO	FLO	FLO	FLO	FLO
UTM EW	6816898	6811612	6811993	6811993	6811620	6811620	6814777	6815040	6815192	6815192
UTM NS	581012	582220	582329	582329	582622	582622	573586	573688	573642	573642
<i>Unnormalized Major Element Oxides (Weight %):</i>										
SiO <sub>2</sub>	47.48	51.85	48.79	47.12	47.1	49.88	48.24	45.6	48.52	48.6
TiO <sub>2</sub>	1.785	0.865	1.495	1.385	1.427	1.46	0.873	0.816	0.841	0.815
Al <sub>2</sub> O <sub>3</sub>	15.43	18.07	13.94	14.55	14.37	14.22	15.14	16.8	14.96	14.95
Fe <sub>2</sub> O <sub>3</sub> *	11.04	6.93	11.79	10.15	10.96	9.85	11.9	10.86	12.21	12.25
MnO	0.15	0.069	0.163	0.179	0.182	0.16	0.155	0.194	0.134	0.128
MgO	6.84	5.87	6.28	7.58	7.5	6.31	5.76	7.06	5.22	5.26
CaO	7.51	6.72	10.01	10.84	10.73	10.07	8.41	8.88	7.72	7.79
Na <sub>2</sub> O	3.3	3.33	2.91	2.68	2.74	2.85	3.59	2.79	4.74	4.73
K <sub>2</sub> O	1.6	0.8	0.99	0.55	0.6	0.92	1.41	1.6	0.58	0.53
P <sub>2</sub> O <sub>5</sub>	0.12	0.32	0.1	0.06	0.09	0.06	0.18	0.18	0.16	0.16
LOI	4.16	4.46	2.9	3.5	3.56	2.98	3.88	4.7	3.58	3.58
Total	99.41	99.28	99.35	98.59	99.25	98.75	99.54	99.48	98.63	98.80
<i>Trace Elements (ppm):</i>										
La	7.02	12.28	6.02	4.77	5.01	5.49	7.76	4.52	5.95	5.61
Ce	17.7	24.8	15.2	12.2	12.7	14.1	17.1	10.4	12.9	12.1
Pr	2.64	3.08	2.3	1.84	1.93	2.13	2.36	1.5	1.76	1.66
Nd	12.7	13.1	11.2	9.5	9.7	10.7	10.5	7.2	8.5	7.9
Sm	3.65	3.07	3.38	2.79	2.92	3.19	2.83	2.15	2.48	2.33
Eu	1.46	1.18	1.31	1.12	1.16	1.24	1.02	0.83	0.97	0.90
Gd	4.68	3.62	4.36	3.58	3.86	4.24	3.37	2.72	3.37	3.19
Tb	0.80	0.63	0.75	0.62	0.67	0.74	0.58	0.47	0.60	0.58
Dy	4.78	3.84	4.63	3.92	4.12	4.49	3.65	2.92	3.84	3.63
Ho	0.93	0.81	0.94	0.78	0.83	0.93	0.77	0.60	0.84	0.78
Er	2.63	2.55	2.75	2.21	2.39	2.66	2.35	1.81	2.57	2.38
Tm	0.37	0.40	0.41	0.32	0.35	0.38	0.35	0.27	0.39	0.36
Yb	2.28	2.58	2.49	1.98	2.08	2.30	2.26	1.70	2.48	2.31
Lu	0.33	0.40	0.34	0.28	0.28	0.33	0.35	0.25	0.37	0.35
Sc	38.9	44.3	45.6	40.2	41.2	41.5	38.2	43.3	44.8	
V	341	261	313	280	291	307	304	313	284	265
Cr	185	149	251	356	355	250	88	211	112	
Co	41.1	26.9	46.4	50.2	49.8	47.6	40.2	43.4	38.9	
Ni	75	37	89	119	125	88	59	69	46	45
Cu	49	40	102	12	13	102	74	14	111	103
Zn	77	99	74	69	69	75	59	68	50	47
Ga	20	17	18	15	18	13	18	15	17	11
Ge	1.4	1.4	1.3	1.1	1.5	0.5	1.4	1.0	1.2	-0.5
Rb	29	14	15	7	8	15	21	25	5	7
Sr	230	451	238	209	213	232	256	412	165	160
Y	27	21	26	22	23	27	22	19	25	23
Zr	97	63	82	68	73	77	61	30	40	33
Nb	8.4	6.1	6.6	5.3	5.8	6.1	3.1	1.7	1.8	1.6
Cs	3.1	0.9	2.2	1.3	1.4	2.0	0.6	2.2	0.2	0.3
Ba	217	203	98	69	70	96	184	395	109	103
Hf	2.7	1.7	2.5	2.0	2.2	2.3	1.8	1.0	1.2	1.1
Ta	0.57	0.35	0.44	0.37	0.40	0.43	0.19	0.08	0.10	0.10
Th	0.52	1.07	0.50	0.41	0.41	0.50	1.11	0.18	0.73	0.66
U	0.14	1.44	0.14	0.12	0.13	0.12	0.44	0.07	0.25	0.22

Sample	4810A7	4810A8(1)	4810A8(2)	4810A10	4810A11	4811A1	4811A3	4811A5	4811A8	4812A5
Group	LOW-Ti	LOW-Ti	LOW-Ti	LOW-Ti	Hi-Ti	LOW-Ti	LOW-Ti	LOW-Ti	LOW-Ti	LOW-Ti
Area	DJ	DJ	DJ	DJ	DJ	DJ	DJ	DJ	DJ	DJ
Flow	FLO	FLO	FLO	FLO	FLO	FLO	FLO	FLO	FLO	FLO
UTM EW	6815402	6815462	6815462	6815458	6815848	6814759	6814766	6814788	6814894	6818593
UTM NS	573659	573674	573674	573228	572400	575267	574545	574779	575325	575987
<i>Unnormalized Major Element Oxides (Weight %):</i>										
SiO <sub>2</sub>	48.84	50.77	50.66	49.35	47.53	48.78	48.99	46.11	49.89	45.74
TiO <sub>2</sub>	0.473	0.501	0.498	0.877	1.728	0.893	0.642	0.789	0.706	0.56
Al <sub>2</sub> O <sub>3</sub>	14.35	14.8	14.73	14.31	14.2	13.61	15.48	15.25	14.8	15.79
Fe <sub>2</sub> O <sub>3</sub> *	9.57	7.6	7.3	10.6	11.8	11.54	8.34	11.57	10.35	10.74
MnO	0.149	0.193	0.193	0.137	0.167	0.145	0.166	0.138	0.115	0.144
MgO	8.65	10.09	10.11	6.76	7.4	7.68	8.82	5.35	6.37	7.55
CaO	9.21	6.46	6.51	8.4	8.85	8.97	7.69	12.29	8.44	10.52
Na <sub>2</sub> O	3.73	3.68	3.69	4.32	2.39	4.07	2.88	3.57	4.2	2.2
K <sub>2</sub> O	0.29	1.53	1.47	0.07	0.88	0.18	1.63	0.32	0.87	1.88
P <sub>2</sub> O <sub>5</sub>	0.06	0.09	0.08	0.15	0.1	0.14	0.06	0.15	0.13	0.1
LOI	3.98	3.91	3.88	4.09	3.63	3.5	3.99	4.26	3.9	4.07
Total	99.31	99.63	99.11	99.04	98.68	99.51	98.67	99.79	99.76	99.30
<i>Trace Elements (ppm):</i>										
La	4.06	3.39	3.41	4.79	6.30	3.84	2.16	3.02	6.08	4.56
Ce	8.7	7.9	7.9	11.3	16.1	9.1	5.3	7.0	12.4	9.8
Pr	1.2	1.14	1.11	1.67	2.42	1.42	0.85	1.06	1.64	1.34
Nd	5.4	5.5	5.3	8.0	11.8	7.1	4.7	5.5	7.5	6.4
Sm	1.48	1.58	1.49	2.47	3.52	2.24	1.41	1.67	2.14	1.82
Eu	0.57	0.56	0.56	0.96	1.37	0.88	0.61	0.76	0.88	0.70
Gd	2.03	2.05	1.96	3.20	4.51	2.83	2.01	2.34	2.77	2.20
Tb	0.38	0.38	0.38	0.60	0.79	0.50	0.36	0.42	0.50	0.42
Dy	2.50	2.53	2.46	3.95	4.85	3.26	2.26	2.70	3.16	2.76
Ho	0.55	0.54	0.53	0.84	0.98	0.68	0.47	0.58	0.66	0.57
Er	1.72	1.67	1.60	2.62	2.80	2.06	1.43	1.72	2.02	1.72
Tm	0.26	0.24	0.24	0.40	0.41	0.31	0.21	0.25	0.30	0.26
Yb	1.73	1.57	1.55	2.57	2.53	1.93	1.37	1.61	1.92	1.66
Lu	0.26	0.24	0.22	0.37	0.36	0.28	0.20	0.25	0.29	0.25
Sc	44.4	44.2	47.6	48.1	42.6	52.2	43.2	42.9	40.4	38.7
V	242	197	197	373	361	354	266	318	293	234
Cr	349	328	323	88	138	278	337	158	82.7	152
Co	48.7	49.7	47.5	39.7	45.2	47.6	45.1	38.2	37.3	53
Ni	119	107	105	60	61	78	110	62	56	133
Cu	43	1337	1297	40	79	50	27	122	20	44
Zn	63	97	98	50	93	52	50	49	44	64
Ga	13	7	7	17	18	13	11	17	14	14
Ge	1.4	1.0	1.0	1.5	1.3	1.1	0.9	2.1	1.5	1.4
Rb	4	23	20		9	3	25		8	27
Sr	171	376	375	75	228	131	610	42	119	233
Y	16	15	16	23	27	20	13	17	21	16
Zr	30	24	28	29	85	30	19	23	35	30
Nb	1.5	1.1	1.3	1.4	7.3	1.4	0.9	1.0	1.5	1.1
Cs	0.5	1.9	1.6	0.1	0.4	0.2	1.0		0.3	1.3
Ba	74	782	778	22	83	46	519	10	147	273
Hf	1.0	0.8	0.8	1.0	2.6	0.9	0.6	0.8	1.0	0.9
Ta	0.09	0.06	0.05	0.07	0.52	0.06	0.04	0.04	0.08	0.06
Th	0.86	0.52	0.53	0.32	0.57	0.13	0.08	0.13	0.59	0.44
U	0.33	0.19	0.17	0.13	0.16	0.05	0.03	0.05	0.24	0.16

Sample	4812A6	4816A2(1)	4816A2(2)	4816A3	4816A4	4816A5A(1)	4816A5A(2)	4816A7 (1)	4816A7 (2)	4816A9
Group	LOW-TI	HI-TI	HI-TI	HI-TI	LOW-TI	LOW-TI	LOW-TI	LOW-TI	LOW-TI	LOW-TI
Area	DJ	ML	ML	ML	ML	ML	ML	ML	ML	ML
Flow	FLO	FLO	FLO	FLO	FLO	FLO	FLO	FLO	FLO	FLO
UTM EW	6818439	6688127	6688127	6687963	6689140	6689693	6689693	6689745	6689745	6689706
UTM NS	576165	370621	370621	370998	372554	372597	372597	372438	372438	372367
<i>Unnormalized Major Element Oxides (Weight %):</i>										
SiO <sub>2</sub>	50.2	48.48	48.39	47.47	49.18	49.62	48.99	49.23	49.28	50.39
TiO <sub>2</sub>	0.793	1.651	1.679	1.653	0.532	0.694	0.695	0.555	0.56	0.599
Al <sub>2</sub> O <sub>3</sub>	13.31	14.38	14.29	15.17	14.07	13.7	13.59	13.73	13.72	13.67
Fe <sub>2</sub> O <sub>3</sub> *	11.04	11.36	11.34	11.41	9.7	8.36	9.3	9.43	9.44	9
MnO	0.163	0.146	0.146	0.17	0.205	0.142	0.14	0.159	0.16	0.16
MgO	7.96	6.86	6.84	6.32	8.4	9.6	9.56	9.19	9.17	7.84
CaO	8.1	8.41	8.48	9.83	10.34	10.25	10.23	9.03	9.01	9.39
Na <sub>2</sub> O	3.98	4.23	4.22	2.75	3.37	1.99	1.99	2.37	2.4	3.52
K <sub>2</sub> O	0.66	0.06	0.04	0.44	0.08	0.94	0.93	1.46	1.49	0.71
P <sub>2</sub> O <sub>5</sub>	0.16	0.11	0.21	0.09	0.03	0.08	0.08	0.05	0.06	0.06
LOI	2.87	3.54	3.5	3.57	3.8	3.43	3.39	3.91	3.91	4.4
Total	99.24	99.21	99.13	98.86	99.72	98.79	98.90	99.11	99.19	99.74
<i>Trace Elements (ppm):</i>										
La	6.17	6.66	6.39	6.43	2.90	7.83	7.62	4.44	4.38	4.84
Ce	14.2	16.6	16.2	16.0	6.2	16.1	16.1	9.6	9.5	10.3
Pr	1.99	2.46	2.36	2.32	0.86	2.05	2.04	1.29	1.27	1.37
Nd	9.2	12.0	11.7	11.3	4.2	8.8	8.8	5.7	5.7	6.3
Sm	2.53	3.44	3.34	3.06	1.27	2.27	2.23	1.55	1.61	1.63
Eu	0.98	1.31	1.28	1.28	0.53	0.72	0.74	0.55	0.56	0.66
Gd	3.44	4.20	4.18	3.71	2.00	2.92	2.89	2.24	2.18	2.30
Tb	0.63	0.73	0.72	0.66	0.41	0.57	0.54	0.44	0.43	0.42
Dy	4.05	4.45	4.31	4.05	2.84	3.56	3.50	2.77	2.77	2.80
Ho	0.87	0.88	0.85	0.80	0.63	0.75	0.77	0.60	0.59	0.61
Er	2.70	2.55	2.40	2.32	1.92	2.39	2.34	1.87	1.88	1.86
Tm	0.41	0.37	0.35	0.33	0.31	0.37	0.36	0.29	0.30	0.29
Yb	2.64	2.24	2.15	2.02	1.98	2.40	2.34	1.92	1.92	1.90
Lu	0.39	0.31	0.30	0.28	0.28	0.35	0.34	0.28	0.29	0.27
Sc	48.3	39.8	45.3	33.9	45.4	42.0	46.8	44.5		39.2
V	332	333	338	327	243	212	215	225	227	219
Cr	127	200	222	100	597	984	1010	509		314
Co	45.3	42.2	44.9	44.4	50.7	52.6	51.9	47.6		38.3
Ni	55	71	68	97	125	196	191	44		7
Cu	20	202	197	181	96	69	68	18		2
Zn	73	74	73	74	51	66	67	65		63
Ga	12	17	16	17	13	13	13	13	13	12
Ge	1.4	1.4	1.2	1.2	1.0	0.9	1.4	1.1	1.3	1.1
Rb	9			8	2	22	18	34	35	14
Sr	210	55	56	280	55	220	220	119	121	125
Y	24	23	23	22	18	21	22	17	18	18
Zr	39	84	84	80	33	59	63	42	42	51
Nb	1.7	7.4	7.2	7.1	1.7	4.7	4.9	3.0	2.9	3.1
Cs	1.5	0.2	0.2	0.2	0.7	0.9	0.8	1.2	1.3	0.5
Ba	154	21	22	78	72	399	393	337	339	207
Hf	1.3	2.5	2.4	2.4	1.0	1.8	1.7	1.2	1.2	1.3
Ta	0.08	0.51	0.52	0.66	0.10	0.31	0.31	0.19	0.20	0.22
Th	0.59	0.58	0.62	0.59	0.58	1.57	1.73	0.88	0.89	0.99
U	0.21	0.16	0.16	0.18	0.29	0.71	0.66	0.42	0.42	0.48

Sample	4816A11	4820A1	4821A1
Group	LOW-TI	HI-TI	HI-TI
Area	ML	HC	BC
Flow	FLO	FLO	FLO
UTM EW	6689726	6796214	6806060
UTM NS	372328	607850	593494
<i>Unnormalized Major Element Oxides (Weight %):</i>			
SiO <sub>2</sub>	48.88	48.54	43.95
TiO <sub>2</sub>	0.494	2.087	1.317
Al <sub>2</sub> O <sub>3</sub>	12.66	13.53	14.92
Fe <sub>2</sub> O <sub>3</sub> *	9.82	13.99	13.1
MnO	0.185	0.231	0.193
MgO	8.39	6.07	9.07
CaO	9.89	7.92	10.1
Na <sub>2</sub> O	3.1	3.72	2.05
K <sub>2</sub> O	0.65	0.43	0.85
P <sub>2</sub> O <sub>5</sub>	0.04	0.2	0.06
LOI	5.52	2.81	3.17
Total	99.64	99.51	98.77
<i>Trace Elements (ppm):</i>			
La	2.76	7.85	2.21
Ce	6.1	19.8	6.5
Pr	0.84	2.96	1.12
Nd	4.3	14.6	6.8
Sm	1.28	4.17	2.56
Eu	0.47	1.57	1.11
Gd	1.92	5.43	3.89
Tb	0.39	0.93	0.71
Dy	2.71	5.57	4.45
Ho	0.61	1.12	0.90
Er	1.89	3.18	2.61
Tm	0.29	0.45	0.38
Yb	1.88	2.84	2.37
Lu	0.27	0.41	0.34
Sc	44.6	43.9	48.5
V	228	435	364
Cr	581	54.1	307
Co	48.6	47	60.2
Ni	103	46	116
Cu	20	122	14
Zn	64	102	84
Ga	11	15	18
Ge	1.1	1.1	1.3
Rb	14	6	13
Sr	149	266	104
Y	17	35	26
Zr	32	123	64
Nb	1.5	9.1	2.1
Cs	0.4	1.2	1.8
Ba	203	82	73
Hf	0.8	3.3	1.9
Ta	0.10	0.70	0.12
Th	0.62	0.79	0.27
U	0.25	0.24	0.06

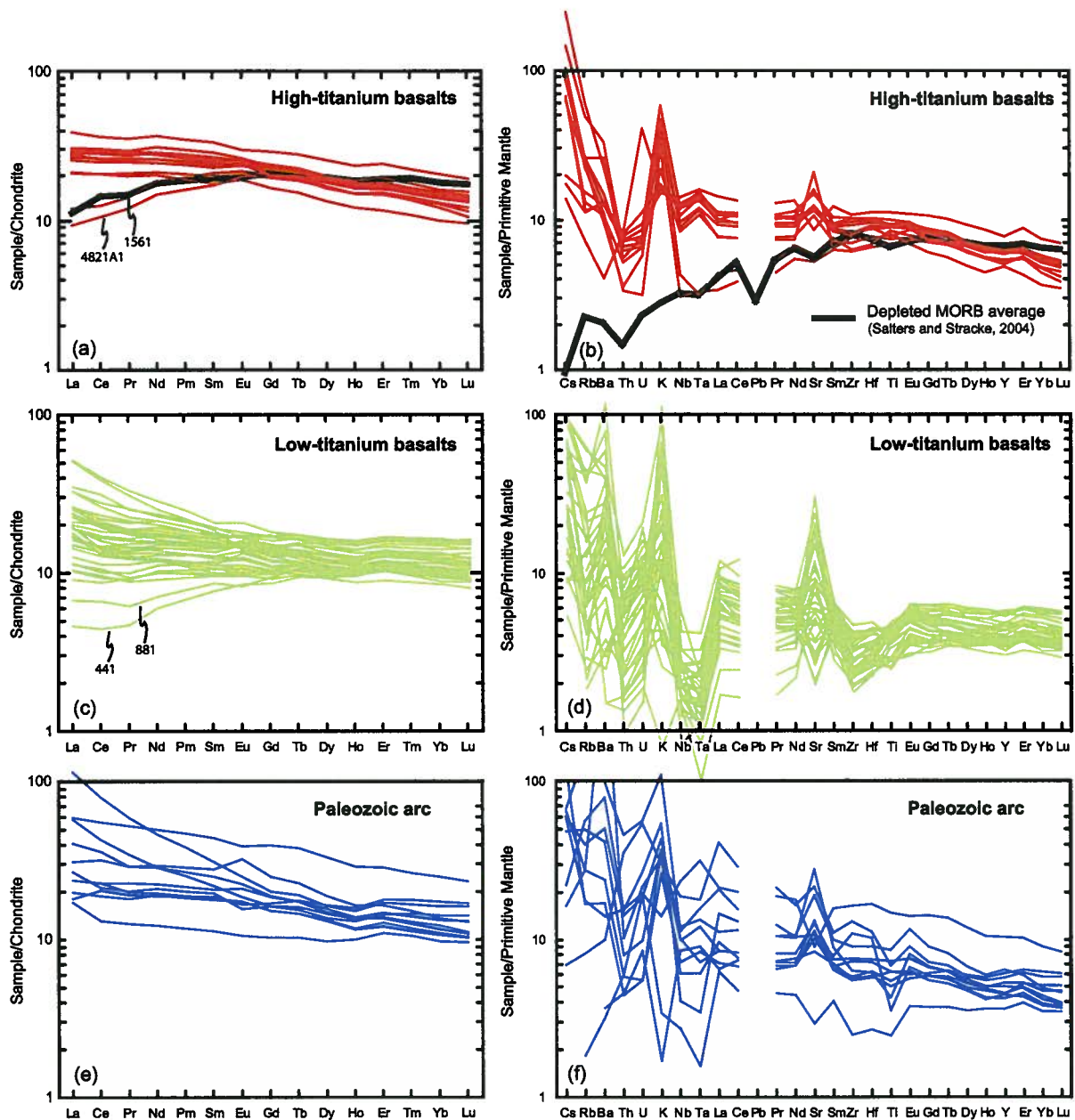


**Figure 4.6** Whole-rock REE and trace-element concentrations for the Nikolai Formation in Kluane Ranges, Yukon. (a), (c), and (e) are chondrite-normalized REE patterns for high-titanium basalts, low-titanium basalts, and Paleozoic arc volcanics from the Kluane Ranges. (b), (d), and (f) are primitive mantle-normalized trace-element patterns for high-titanium, low-titanium basalts, and Paleozoic arc volcanics from the Kluane Ranges. All normalization patterns are from McDonough and Sun (1995). Depleted MORB average from Salters and Stracke (2004). Note the clear distinction between the high- and low-titanium basalts.

degree of variability of LILE (Cs, Rb, Ba, K). The high- and low-titanium basalts form two distinct trends on plots of Nb vs. Zr and Th vs. Hf (Fig. 4.7).

### **Sr-Nd-Hf-Pb isotopic compositions**

The low-titanium basalts have mostly higher initial  $\epsilon_{\text{Hf}}$  (+11.1 to +15.8) and lower initial  $\epsilon_{\text{Nd}}$  (+2.3 to +6.8) than the high-titanium basalts (initial  $\epsilon_{\text{Hf}}$  = +10.4 to +12.0; initial  $\epsilon_{\text{Nd}}$  = +6.6 to +9.0). One low-titanium basalt sample (4808A2) lies within the range of initial  $\epsilon_{\text{Hf}}$  for the high-titanium basalts and a separate sample (4816A5a) from outside the Kluane Ranges has particularly low initial  $\epsilon_{\text{Hf}}$  (+9.3) and initial  $\epsilon_{\text{Nd}}$  (+2.3) (Fig. 4.8; Tables 3 and 4). The high- and low-titanium basalts have wide ranges of overlapping initial Sr isotopic compositions, which is likely due to the effects of secondary alteration. Two Paleozoic arc samples overlap the range of Sr and Nd isotopic compositions of the high- and low-titanium basalts and have similar  $^{176}\text{Hf}/^{177}\text{Hf}$  and  $^{176}\text{Lu}/^{177}\text{Hf}$  to the high-titanium basalts (Fig. 4.8). A single sample of the basal pillow breccia lies at the low end of the ranges of high- and low-titanium basalts in Hf and Nd, and close to the upper end of the ranges in Sr. The range of present-day Pb isotope ratios are similar for high and low-titanium basalts, with low-titanium basalts extending to slightly lower Pb isotope ratios (high-titanium basalt:  $^{206}\text{Pb}/^{204}\text{Pb}$  = 19.008-20.297,  $^{207}\text{Pb}/^{204}\text{Pb}$  = 15.579-15.627,  $^{208}\text{Pb}/^{204}\text{Pb}$  = 38.453-39.090; low-titanium basalt:  $^{206}\text{Pb}/^{204}\text{Pb}$  = 18.561-19.836,  $^{207}\text{Pb}/^{204}\text{Pb}$  = 15.559-15.646,  $^{208}\text{Pb}/^{204}\text{Pb}$  = 38.118-38.755 ) (Fig. 4.8; Table 5). Both the basal pillow breccia and Paleozoic arc samples lie within the range of Pb isotopic compositions for the high- and low-titanium basalts (Fig. 4.8).

## **DISCUSSION**

### **Effects of alteration and comparison to Nikolai basalts in Alaska**

Since eruption of the Nikolai Formation at ca. 230 Ma, the flood basalts have undergone burial metamorphism during subsidence of the Wrangellia plateau (Late Triassic-Early Jurassic), a pre-mid-Cretaceous contraction event related to accretion of Wrangellia (Late Jurassic-Early Cretaceous), and post-mid-Cretaceous strike-slip faulting during northward transport of Wrangellia along the continental margin (MacKevett *et al.*, 1997; Israel *et al.*, 2006). More than 3600 m of marine sediments accumulated on top of



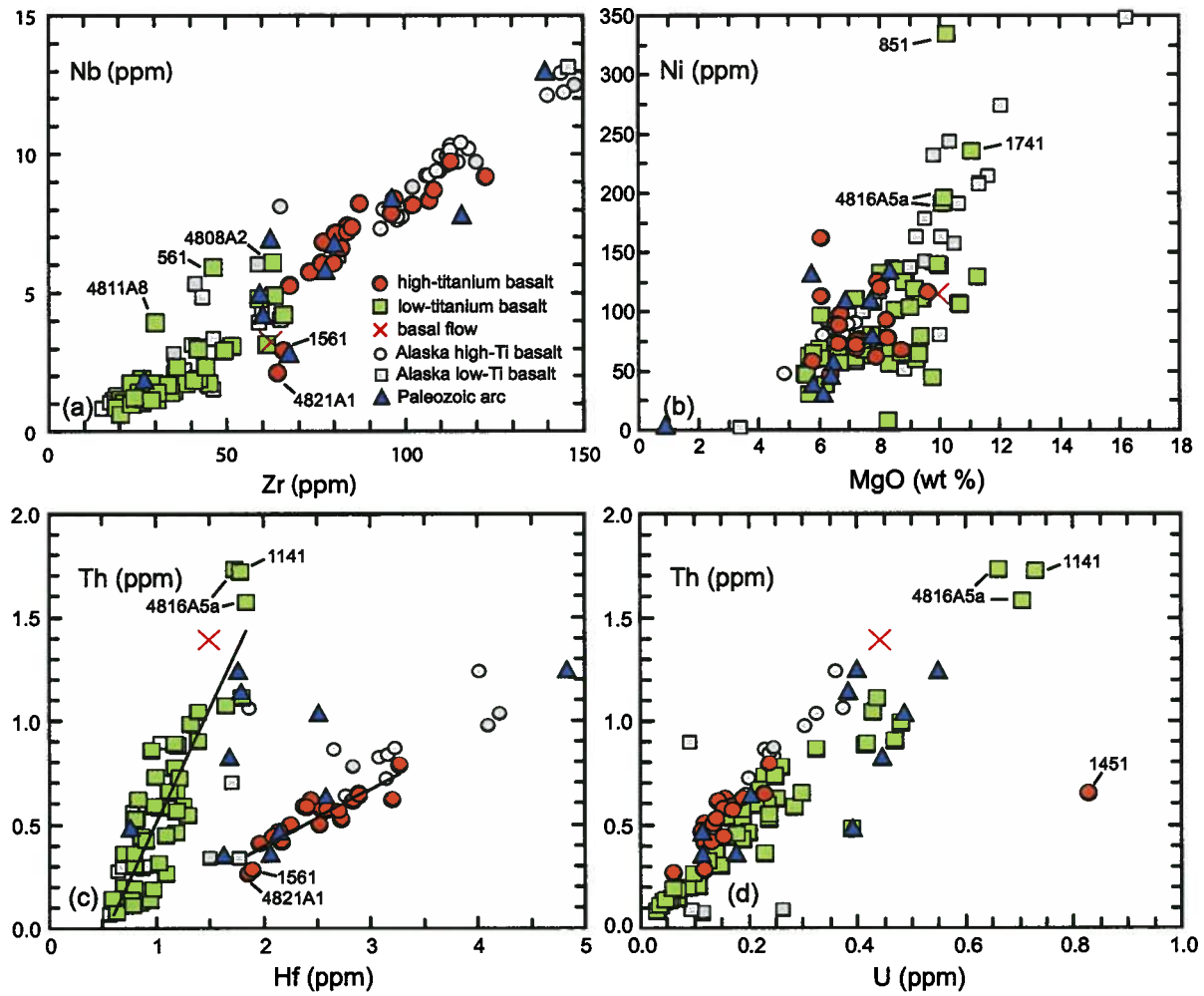


**Figure 4.7** Whole-rock trace-element concentrations for the Nikolai Formation in Yukon, with data for the Nikolai Formation in Alaska (Greene *et al.*, submitted). (a) Nb vs. Zr. (b) Ni vs. MgO. (c) Th vs. Hf. (d) Th vs. U.

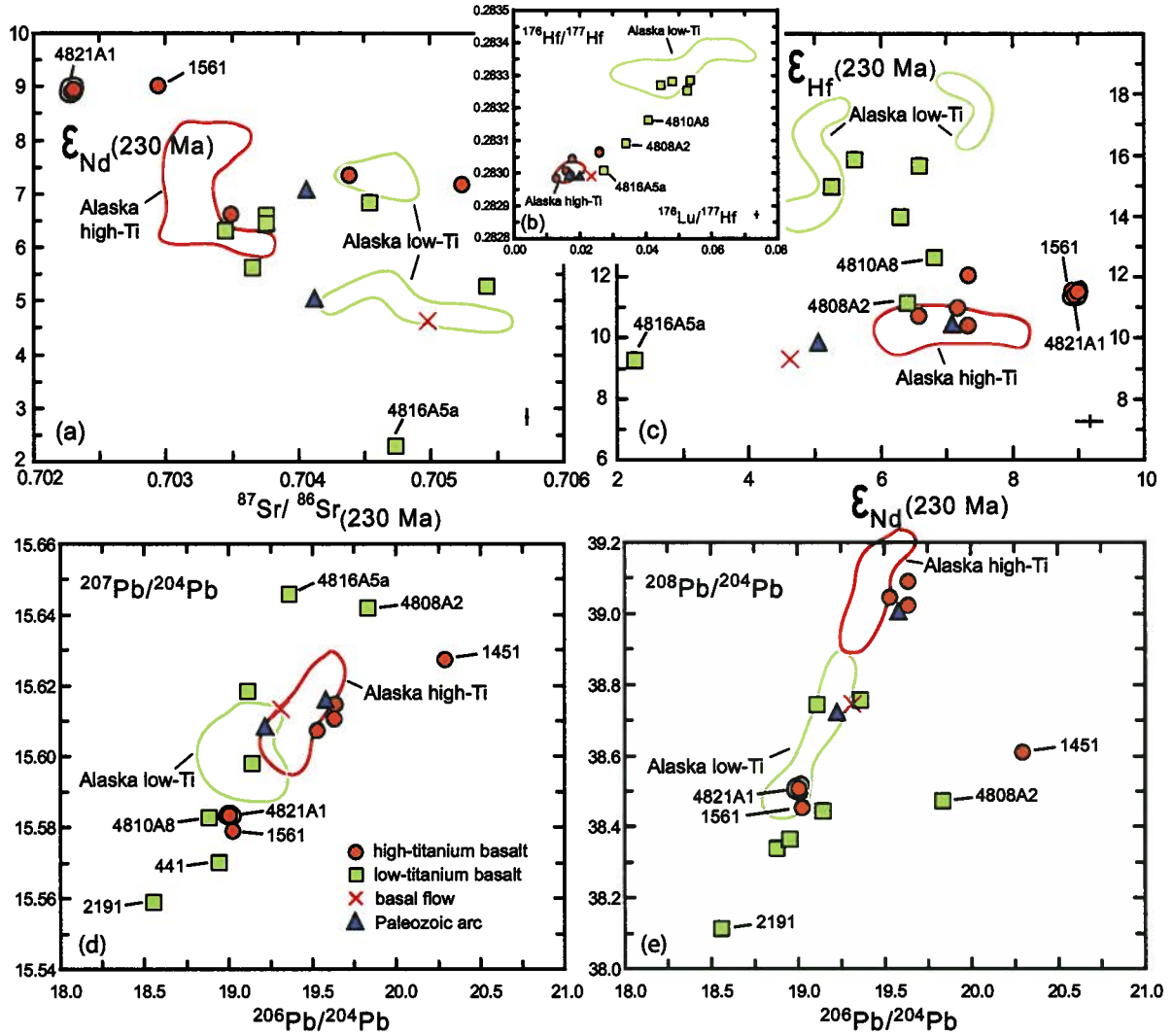


**Figure 4.8** Whole-rock Sr, Nd, and Hf isotopic compositions for the Nikolai Formation in Yukon, with fields for high- and low-titanium basalts of the Nikolai Formation in Alaska (Greene *et al.*, 2008, submitted). (a) Initial  $\epsilon_{Nd}$  vs.  $^{87}Sr/^{86}Sr$ . Age-correction to 230 Ma. (b) Measured  $^{176}Hf/^{177}Hf$  vs.  $^{176}Lu/^{177}Hf$ . (c) Initial  $\epsilon_{Hf}$  vs.  $\epsilon_{Nd}$ . (d) Measured  $^{207}Pb/^{204}Pb$  vs.  $^{206}Pb/^{204}Pb$ . (e) Measured  $^{208}Pb/^{204}Pb$  vs.  $^{206}Pb/^{204}Pb$ . Average  $2\sigma$  error bars shown in lower right corner of panels; they are smaller than symbols in the Pb isotope ratio plots. Results from a complete chemistry duplicate, shown in Tables 3, 4, and 5 (sample 4821A1), are circled in each plot (except panel b).

Table 4.3 Sr and Nd isotopic geochemistry of Nikolai basalts, Yukon

Sample	Group <sup>a</sup>	Area <sup>b</sup>	Rb (ppm)	Sr (ppm)	<sup>87</sup> Sr/ <sup>86</sup> Sr	2σ <sub>m</sub>	<sup>87</sup> Rb/ <sup>86</sup> Sr	<sup>87</sup> Sr/ <sup>86</sup> Sr <sub>i</sub> 230 Ma	Sm (ppm)	Nd (ppm)	<sup>143</sup> Nd/ <sup>144</sup> Nd	2σ <sub>m</sub>	ε <sub>Nd</sub>	<sup>147</sup> Sm/ <sup>144</sup> Nd	<sup>143</sup> Nd/ <sup>144</sup> Nd <sub>i</sub> 230 Ma	ε <sub>Nd(t)</sub>
4820A1	HI-Ti	HC	5.93	266	0.704596	6	0.064	0.70439	4.17	14.55	0.512979	5	6.7	0.1733	0.51272	7.3
1691	HI-Ti	QC	4.27	298	0.705370	7	0.041	0.70523	4.22	14.29	0.512978	6	6.6	0.1785	0.51271	7.2
1451	HI-Ti	QC	6.70	317	0.703692	8	0.061	0.70349	3.83	13.15	0.512945	7	6.0	0.1760	0.51268	6.6
4816A2	HI-Ti	ML	N/A	55	0.703988	8			3.44	12.04	0.512978	9	6.6	0.1726	0.51272	7.3
1561	HI-Ti	QC	13.91	115	0.704085	8	0.349	0.70284	3.06	8.35	0.513137	8	9.7	0.2218	0.51280	9.0
4821A1	HI-Ti	BC	13.35	104	0.703505	7	0.371	0.70229	2.56	6.81	0.513141	7	9.8	0.2277	0.51280	8.9
4821A1 (dup)	HI-Ti	BC	13.35	104	0.703525	7	0.371	0.70231	2.56	6.81	0.513143	7	9.9	0.2277	0.51280	8.9
4808A2	Low-Ti	QC	13.60	451	0.704041	7	0.087	0.70376	3.07	13.07	0.512885	6	4.8	0.1421	0.51267	6.4
4816A5A	Low-Ti	ML	21.79	220	0.705677	8	0.287	0.70474	2.27	8.76	0.512695	8	1.1	0.1565	0.51246	2.3
1301	Low-Ti	QC	3.78	103	0.704001	7	0.106	0.70365	1.56	4.67	0.512934	6	5.8	0.2020	0.51263	5.6
441	Low-Ti	QC	37.72	174	0.705510	7	0.629	0.70345	1.14	2.73	0.513047	7	8.0	0.2534	0.51267	6.3
881	Low-Ti	QC	12.75	102	0.704944	9	0.363	0.70376	1.27	3.22	0.513037	7	7.8	0.2376	0.51268	6.6
2191	Low-Ti	QC	10.00	370	0.705677	8	0.078	0.70542	1.41	4.18	0.512920	6	5.5	0.2048	0.51261	5.3
4810A8	Low-Ti	DJ	22.62	376	0.705106	6	0.174	0.70454	1.58	5.46	0.512955	6	6.2	0.1748	0.51269	6.8
1031	Basal	QC	3.94	296	0.705096	6	0.038	0.70497	2.74	11.57	0.512794	6	3.0	0.1429	0.51258	4.6
4807A4	Paleozoic	QC	10.80	182	0.704625	7	0.172	0.70406	6.52	22.74	0.512966	6	6.4	0.1733	0.51271	7.1
1191	Paleozoic	QC	24.48	265	0.704994	8	0.267	0.70412	2.69	8.98	0.512874	7	4.6	0.1814	0.51260	5.1

<sup>a</sup>HI-Ti, high-titanium basalt; Low-Ti, low-titanium basalt; Basal, basal pillow breccia; Paleozoic, Paleozoic arc (Station Creek Formation). <sup>b</sup>Abbreviations for area are: QC, Quill Creek; ML, Mush Lake; DJ, Donjek River; BC, Burwash Creek; HC, Halfbreed Creek. (dup) Indicates complete chemistry duplicate. N/A is no analysis. All isotopic analyses carried out at the PCIGR. Trace element analyses were performed at Activation Laboratories (ActLabs). Analytical methods given in Appendix E.

Table 4.4 Hf isotopic compositions of Nikolai basalts, Yukon

Sample	Group <sup>a</sup>	Area <sup>b</sup>	Lu (ppm)	Hf (ppm)	<sup>177</sup> Hf/ <sup>178</sup> Hf	2σ <sub>m</sub>	ε <sub>Hf</sub>	<sup>176</sup> Lu/ <sup>177</sup> Hf	<sup>177</sup> Hf/ <sup>178</sup> Hf <sub>i</sub>	ε <sub>Hf</sub> (t)
230 Ma										
4820A1	HI-TI	HC	0.41	3.28	0.283044	6	9.6	0.0179	0.28296	12.0
1691	HI-TI	QC	0.33	2.89	0.283006	5	8.3	0.0161	0.28293	11.0
1451	HI-TI	QC	0.26	2.89	0.282984	5	7.5	0.0129	0.28293	10.7
4816A2	HI-TI	ML	0.31	2.54	0.282995	5	7.9	0.0172	0.28292	10.4
1561	HI-TI	QC	0.35	1.93	0.283065	5	10.4	0.0260	0.28295	11.5
4821A1	HI-TI	BC	0.34	1.86	0.283067	7	10.4	0.0261	0.28295	11.5
4821A1 (dup)	HI-TI	BC	0.34	1.86	0.283063	4	10.3	0.0261	0.28295	11.4
4808A2	Low-TI	QC	0.40	1.66	0.283090	6	11.2	0.0341	0.28294	11.1
4816A5A	Low-TI	ML	0.35	1.84	0.283008	5	8.3	0.0273	0.28289	9.3
1301	Low-TI	QC	0.23	0.73	0.283270	4	17.6	0.0446	0.28307	15.8
441	Low-TI	QC	0.24	0.66	0.283253	6	17.0	0.0527	0.28302	13.9
881	Low-TI	QC	0.26	0.77	0.283280	5	18.0	0.0481	0.28307	15.6
2191	Low-TI	QC	0.26	0.69	0.283285	6	18.1	0.0535	0.28305	15.0
4810A8	Low-TI	DJ	0.24	0.82	0.283162	6	13.8	0.0409	0.28298	12.6
1031	Basal	QC	0.25	1.52	0.282991	5	7.7	0.0234	0.28289	9.3
4807A4	Paleozoic	QC	0.57	4.84	0.282995	6	7.9	0.0168	0.28292	10.5
1191	Paleozoic	QC	0.25	1.79	0.282993	5	7.8	0.0200	0.28290	9.9

<sup>a</sup>HI-TI, high-titanium basalt; Low-TI, low-titanium basalt; Basal, basal pillow breccia, Paleozoic, Paleozoic arc (Station Creek Formation). <sup>b</sup>Abbreviations for area are: QC, Quill Creek; ML, Mush Lake; DJ, Donjek River; BC, Burwash Creek; HC, Halfbreed Creek. (dup) indicates complete chemistry duplicate. All isotopic analyses carried out at PCIGR. Trace element analyses were performed at Activation Laboratories (ActLabs). Analytical methods given in Appendix E.

Table 4.5 Pb isotopic compositions of Nikolai basalts, Yukon

Sample	Group <sup>a</sup>	Area <sup>b</sup>	U (ppm)	Th (ppm)	<sup>206</sup> Pb/ <sup>204</sup> Pb	2σ <sub>m</sub>	<sup>207</sup> Pb/ <sup>204</sup> Pb	2σ <sub>m</sub>	<sup>208</sup> Pb/ <sup>204</sup> Pb	2σ <sub>m</sub>
4820A1	HI-TI	HC	0.24	0.79	19.6386	0.0010	15.6144	0.0007	39.0899	0.0019
1691	HI-TI	QC	0.23	0.64	19.6362	0.0008	15.6103	0.0007	39.0232	0.0021
1451	HI-TI	QC	0.83	0.65	20.2967	0.0009	15.6272	0.0007	38.6070	0.0017
4816A2	HI-TI	ML	0.16	0.58	19.5320	0.0008	15.6073	0.0007	39.0425	0.0017
1561	HI-TI	QC	0.12	0.28	19.0263	0.0009	15.5790	0.0008	38.4525	0.0022
4821A1	HI-TI	BC	0.06	0.27	19.0089	0.0011	15.5831	0.0010	38.5045	0.0019
4821A1 (dup)	HI-TI	BC	0.06	0.27	19.0075	0.0007	15.5833	0.0006	38.5049	0.0018
4808A2	Low-TI	QC	1.44	1.07	19.8356	0.0006	15.6419	0.0007	38.4723	0.0018
4816A5A	Low-TI	ML	0.71	1.57	19.3641	0.0011	15.6456	0.0008	38.7554	0.0022
1301	Low-TI	QC	0.14	0.36	19.1146	0.0006	15.6184	0.0007	38.7403	0.0022
441	Low-TI	QC	0.07	0.14	18.9507	0.0013	15.5698	0.0011	38.3631	0.0029
881	Low-TI	QC	0.15	0.30	19.1467	0.0007	15.5979	0.0006	38.4415	0.0014
2191	Low-TI	QC	0.11	0.20	18.5606	0.0007	15.5588	0.0008	38.1117	0.0019
4810A8	Low-TI	DJ	0.19	0.52	18.8847	0.0006	15.5825	0.0005	38.3364	0.0015
1031	Basal	QC	0.44	1.39	19.3089	0.0008	15.6133	0.0007	38.7445	0.0017
4807A4	Paleozoic	QC	0.40	1.25	19.5791	0.0009	15.6160	0.0008	39.0046	0.0021
1191	Paleozoic	QC	0.38	1.14	19.2205	0.0010	15.6084	0.0009	38.7223	0.0024

<sup>a</sup>HI-TI, high-titanium basalt; Low-TI, low-titanium basalt; Basal, basal pillow breccia, Paleozoic, Paleozoic arc (Station Creek Formation).

<sup>b</sup>Abbreviations for area are: QC, Quill Creek; ML, Mush Lake; DJ, Donjek River; BC, Burwash Creek; HC, Halfbreed Creek. (dup) Indicates complete chemistry duplicate. All isotopic analyses carried out at PCIGR. Trace element analyses were performed at Activation Laboratories (ActLabs). Analytical methods given in Appendix E.

the Nikolai Formation (MacKevett *et al.*, 1997), at least 2 km by the end of the Triassic (Armstrong & MacKevett, 1977). This systematic decrease in the accumulation rate of marine sediments during the Late Triassic (~200 m/Myr to ~20 m/Myr) may have been controlled by cooling and deflation of the lithosphere following eruption of the flood basalts (Saltus *et al.*, 2007) or related to rifting. Seven whole rock K-Ar ages of the Nikolai Formation in the Wrangell Mountains yield an isochron age of  $112 \pm 11$  Ma and indicate resetting of K-Ar systematics during tectonism related to northward transport of Wrangellia (MacKevett, 1978; Plafker *et al.*, 1989).

The least-altered samples were selected for chemistry and, although alteration and low-grade metamorphism has dramatically affected the primary igneous texture and mineralogy of the sampled Nikolai basalts, many of the analyzed basalt samples appear to have retained a large part of their primary geochemistry. There is no clear correlation between petrographic alteration index and chemical alteration indices (e.g. Ba/Rb vs.  $K_2O/P_2O_5$ ) or LOI and any of the measured or age-corrected isotopic ratios; compositions of more mobile elements (Cs, Rb, Ba, and K) show some coherence with compositions of immobile elements (Nb, Zr, HREE).

The Nikolai Formation in Yukon and Alaska formed as part of the same contiguous flood basalt province and the chemistry of most of the basalt flows in Alaska has not been significantly affected by alteration and metamorphism (see chapter 3). The similarity in volcanic stratigraphy, underlying and overlying formations, age, petrography, and chemistry between these two areas provides an excellent opportunity to compare the flood basalts that have undergone different degrees of alteration (Fig. 4.9). Figure 4.9 shows trace element concentrations of high- and low-titanium basalts in Yukon normalized to a mean for high- and low-titanium basalts from Alaska to help distinguish the general differences in compositions of the Nikolai basalts from these two areas. LILE show a higher degree of scatter in normalized trace-element patterns than HFSE and REE, especially for the low-titanium basalts (Figs 4.6 and 4.9). The high-titanium basalts in Yukon have similar concentrations to Alaska high-titanium basalts, with the exception of the LILE (Fig. 4.9). The differences in low-titanium basalt trace-element concentrations between Yukon and Alaska increase systematically from moderately incompatible to highly incompatible trace elements with almost all trace

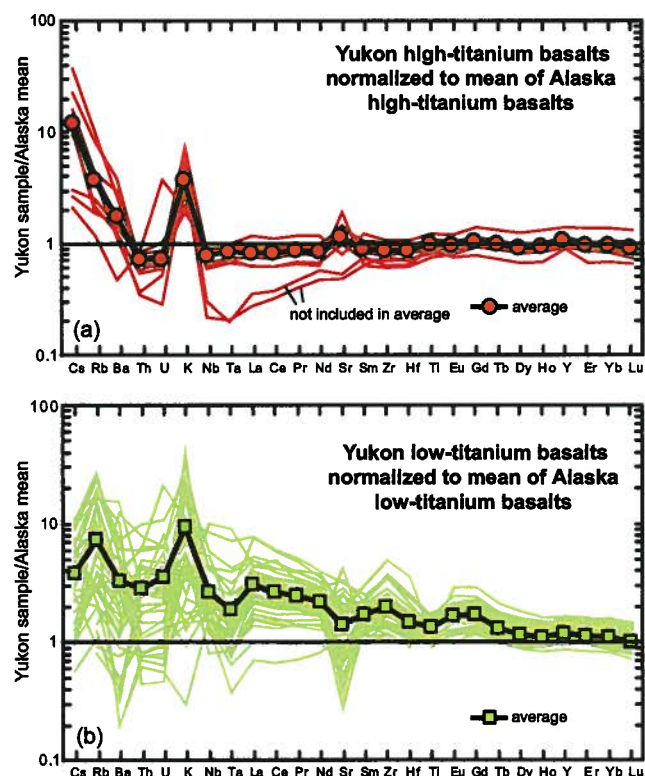


**Figure 4.9** Comparison of trace-element compositions of the Nikolai basalts in Yukon to averages for high- and low-titanium basalts from Alaska (Greene *et al.*, submitted). (a) High-titanium basalts from Yukon divided by the mean of high-titanium basalts from Alaska. (b) Low-titanium basalts from Yukon divided by the mean of low-titanium basalts from Alaska. Averages for all of the normalized patterns (except two indicated in panel a) are shown by the patterns with symbols in each of the two panels. Note the close similarity of the trace-element concentrations of high-titanium basalts from Yukon and Alaska (panel a), except for LILE (Cs, Rb, Ba, K). The trace-element concentrations of low-titanium basalts in Yukon are systematically higher than the average concentration of low-titanium basalts in Alaska for the more incompatible elements, with the most significant differences in Rb and K relative to adjacent elements.

elements, except the HREE, having higher concentrations in Yukon basalts (Fig. 4.9). The low-titanium basalts in Yukon and Alaska both have HFSE depletions, but on average the Yukon low-titanium basalts have higher concentrations of HFSE. Similar to the high-titanium basalts, the LILE (mostly Rb and K) show the largest differences in low-titanium basalts from Yukon and Alaska and Sr shows considerable scatter (Fig. 4.9). The systematic differences between the low-titanium basalts in Yukon and Alaska are not simply the result of alteration. The low-titanium basalts in Yukon on average are more enriched in incompatible elements, which reflects differences in lava compositions erupted in Yukon and Alaska.

Sr isotopic compositions are highly sensitive to alteration and metamorphism in oceanic basalts and the relatively high initial Sr isotopic compositions for the Nikolai basalts in Yukon (up to 0.7054) are probably due to an increase in  $^{87}\text{Sr}/^{86}\text{Sr}$  through addition of seawater Sr and/or an increase in  $^{87}\text{Rb}/^{86}\text{Sr}$  through preferential addition of Rb relative to Sr during low-temperature alteration (Hauff *et al.*, 2003). The Sr isotopic compositions of the Nikolai basalts in Yukon cannot be used to assess magmatic processes and clear differences are apparent between Sr isotopic compositions from Yukon and Alaska (Fig. 4.8a). Several measured Pb isotopic compositions lie well outside the expected range of variation (samples 4808A2, 4816A5a, 2191, and 1451) and cover a greater range, but several of the present-day Pb isotopic compositions from Yukon are similar to those of Nikolai basalts from Alaska.

### **Relationship between chemistry and stratigraphic position**

In Yukon, unless volcanic stratigraphy is in unfaulted contact with underlying or overlying units, it is extremely challenging to be confident of the exact stratigraphic position of flows. The relative stratigraphic positions of 31 of the 60 analyzed basalt samples were estimated using a ranking system (1-near base; 5-near top). Six analyzed basalts from two traverses from the base of the Nikolai Formation several hundred meters upward into the volcanic stratigraphy were all low-titanium basalts. A total of 13 basalts appear to be located near the base of the volcanic stratigraphy and all of these samples are low-titanium basalts. Only three samples were estimated to come from near the upper contact with overlying Chitistone Limestone and each of these samples is high-titanium



basalt. Several samples from the vertically-oriented subaerial stratigraphy above Tatamagouche Creek (Fig. 4.3a) are high-titanium basalt; this section of stratigraphy does not appear to be close to the base of the Nikolai Formation and several interflow limestones are present, which are typically found between flows in the upper part of the stratigraphy. Lastly, each traverse contained either high-titanium basalt or low-titanium basalt; both lava types were not collected in the same traverse. In Alaska, low-titanium basalts comprise the lower part of the volcanic stratigraphy (~500 m) in the Alaska Range and high-titanium flows form most of the remainder of the ~3 km of stratigraphy (see manuscript 2). Given these constraints on the chemostratigraphy, and the connection to stratigraphically distributed high- and low-titanium basalts in Alaska, a similar transition from low-titanium to high-titanium basalt is inferred in Yukon. Primarily the lower parts of the stratigraphy appear to be preserved in the Kluane Ranges. However, as seen in Figures 4.6 and 4.9, the trace-element concentrations of low-titanium basalts in Yukon extend to higher abundances than the low-titanium basalts in Alaska.

#### **Source characteristics of Nikolai basalts in Yukon**

The trace-element and isotopic compositions of the Nikolai basalts in Yukon indicate a Pacific ocean-island type mantle source for the high-titanium basalts and the involvement of a different component for the low-titanium basalts. The high-titanium basalts have depleted Hf and Nd isotopic compositions that are distinct from mid-ocean ridge basalts (MORB) and there is no indication of involvement of low- $\epsilon_{\text{Nd}}$ , low- $\epsilon_{\text{Hf}}$  continental material (Fig. 4.10). The high-titanium basalts from Yukon and Alaska are displaced just below the OIB mantle array and broadly overlap fields for the Ontong Java Plateau, Hawaii, and the Caribbean Plateau (Fig. 4.10b). Two high-titanium basalts (samples 4821A1, 1561) exhibit a mid-ocean ridge basalt (MORB)-like composition (Fig. 4.10). These two LREE-depleted basalts have similar trace-element concentrations to a depleted MORB average (Fig. 4.6; Salters & Stracke, 2004) and Sr-Nd-Hf isotopic compositions that place them at the edge of the Pacific MORB field (Fig. 4.10).

Five of seven low-titanium basalts from Yukon with initial  $\epsilon_{\text{Hf}}$  values that are 1 to 4 epsilon units higher than those of the high-titanium basalts are displaced above the OIB mantle array and indicate involvement of a source that evolved with high Lu/Hf, but not

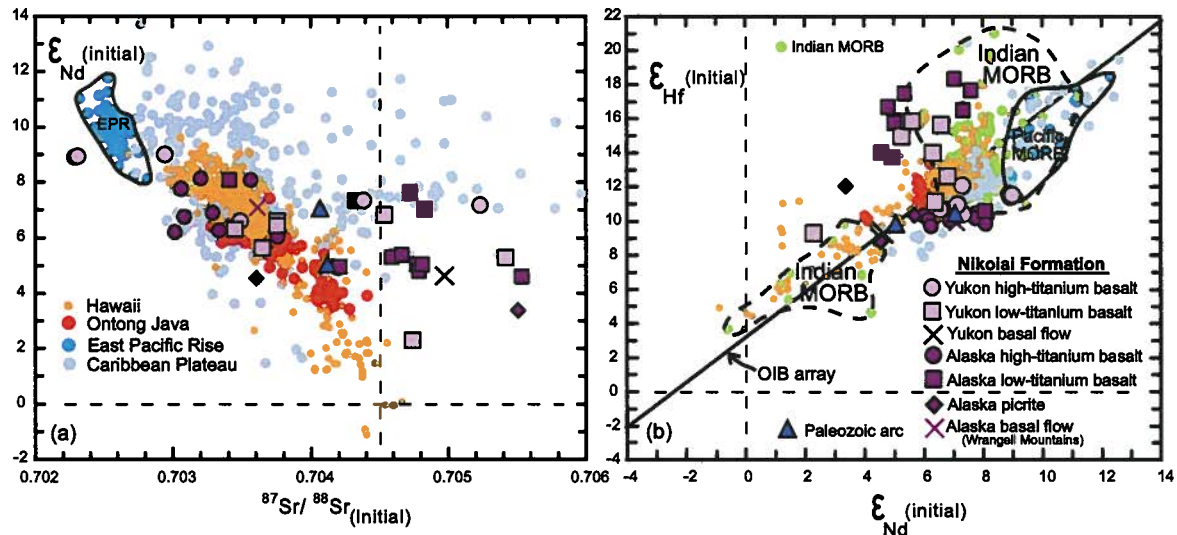


**Figure 4.10** Comparison of age-corrected (230 Ma) Sr-Nd-Hf isotopic compositions of the Nikolai Formation in Yukon and Alaska to age-corrected OIB and MORB. (a) Initial  $\epsilon_{\text{Nd}}$  vs.  $^{87}\text{Sr}/^{86}\text{Sr}$ . (b) Initial  $\epsilon_{\text{Hf}}$  vs.  $\epsilon_{\text{Nd}}$ . The complete references for the compiled data are too numerous to cite here; most of the compiled data was extracted from the GEOROC database (<http://georoc.mpch-mainz.gwdg.de/georoc/>). Data for Ontong Java from Mahoney *et al.* (1993), Babbs (1997), and Tejada *et al.* (2004); Indian MORB from Salters (1996), Kempton *et al.* (2002), and Janney *et al.* (2005); Pacific MORB from Mahoney *et al.* (1992, 1994), Nowell *et al.* (1998), Salters and White (1998), and Chauvel and Blichert-Toft (2001); OIB array line from Vervoort (1999). EPR is East Pacific Rise. Dashed lines indicate Bulk Silicate Earth (BSE). Note the two LREE-depleted high-titanium basalts (4821A1, 1561) that lie at the edge of the field of Pacific MORB.

correspondingly high Sm/Nd (Fig. 4.10b). The Hf and Nd isotopic compositions of the low-titanium basalts from Yukon generally follow the trend of the low-titanium basalts from Alaska, which are 4 to 8 epsilon-Hf units higher than the high-titanium basalts from Alaska and Yukon and (Fig. 4.10b). The displacement of low-titanium basalts above the OIB mantle array could have involved the addition of a small amount of a pelagic component that underwent radiogenic ingrowth from high Lu/Hf because of the sedimentary fractionation of zircon (Patchett *et al.*, 1984). Several low-titanium basalts (samples 4808A2 and 4810A8) have initial  $\epsilon_{\text{Hf}}$  and  $\epsilon_{\text{Nd}}$  that lie between the high- and low-titanium basalt fields (Fig 4.8c), and, together with some low-titanium basalts with high La/Yb, may indicate a transitional lava type. Overall, the low-titanium basalts are mostly distinct from OIB and the source of MORB and require a different depleted source than the source of the high-titanium basalts, early in the formation of Nikolai basalts. The negative HFSE anomalies in the low-titanium basalts are also markedly different from basalts produced from OIB- or MORB-type mantle. Proxies of mantle-crust interaction (Th-Nb) and melting depth (TiO<sub>2</sub>-Nb) of Pearce (2008) suggest involvement of arc mantle or crust in generation of the low-titanium basalts (Fig. 4.11). Additional trace-element ratios also distinguish the low-titanium basalts from OIB and N-MORB-type mantle (Fig. 4.12). The following section examines the origin of the low-titanium basalts as indicated by their chemistry.

### **Melting of arc mantle in formation of the low-titanium basalts**

A shift in the source region that produced the Nikolai basalts is apparent in the major- and trace-element and isotopic compositions. The chemistry of the low-titanium basalts indicates involvement of an arc-type source (or subduction-modified mantle) during the early part of the eruptive history of the Nikolai Formation (Fig. 4.13). The Nikolai basalts erupted through a thick succession of Late Paleozoic arc volcanics, presumably consisting of complementary sub-arc mantle lithosphere, which may have played a key role in the development of the geochemical signature of the low-titanium basalts (here, lithosphere indicates a region that was not involved in the convective flow of the mantle). The high-titanium basalts have compositions that suggest they originated

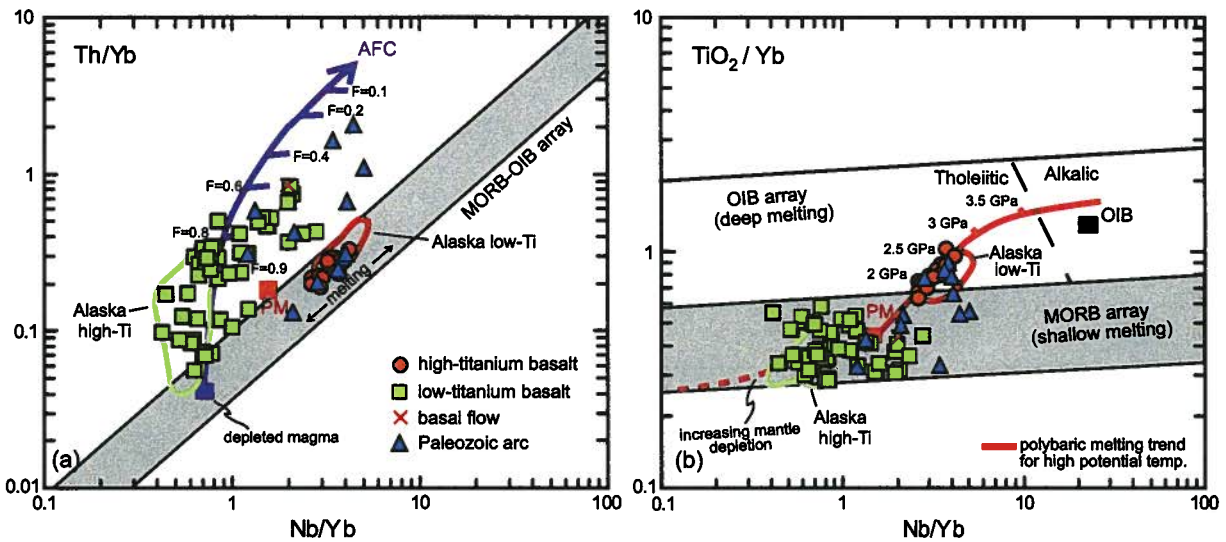


**Figure 4.11** Th-Nb and Ti-Yb systematics for the Nikolai Formation in Yukon with data compilation and modeling results from Pearce (2008). (a) Th/Yb vs. Nb/Yb. MORB-OIB array and assimilation-fractional crystallization (AFC) model trend from Pearce (2008). (b)  $\text{TiO}_2/\text{Yb}$  vs. Nb/Yb. MORB-OIB array and assimilation-fractional crystallization (AFC) model from Pearce (2008). Talkeetna arc lower crust from Greene *et al.* (2006) and Talkeetna arc lavas from Clift *et al.* (2005). Mariana arc data from Pearce *et al.* (2007) and Woodhead *et al.* (2001). The low-titanium basalts indicate a depleted source and interaction with a subduction component combined with fractional crystallization, whereas the high-titanium basalts lie within an OIB array in panel b, parallel to a melting vector that indicates higher pressure melting. See Pearce (2008) for parameters of polybaric melting and assimilation-fractional crystallization (AFC) modeling. Blue line in panel A represents an AFC model following the modeling of DePaolo (1981). Red line in panel b illustrates a polybaric melting trend (with changing composition of pooled melt extracted from the mantle that undergoes decompression from the solidus to the pressure marked) for high and lower mantle potential temperatures which correspond to representative conditions for the generation of present-day MORB and OIB (Pearce, 2008).

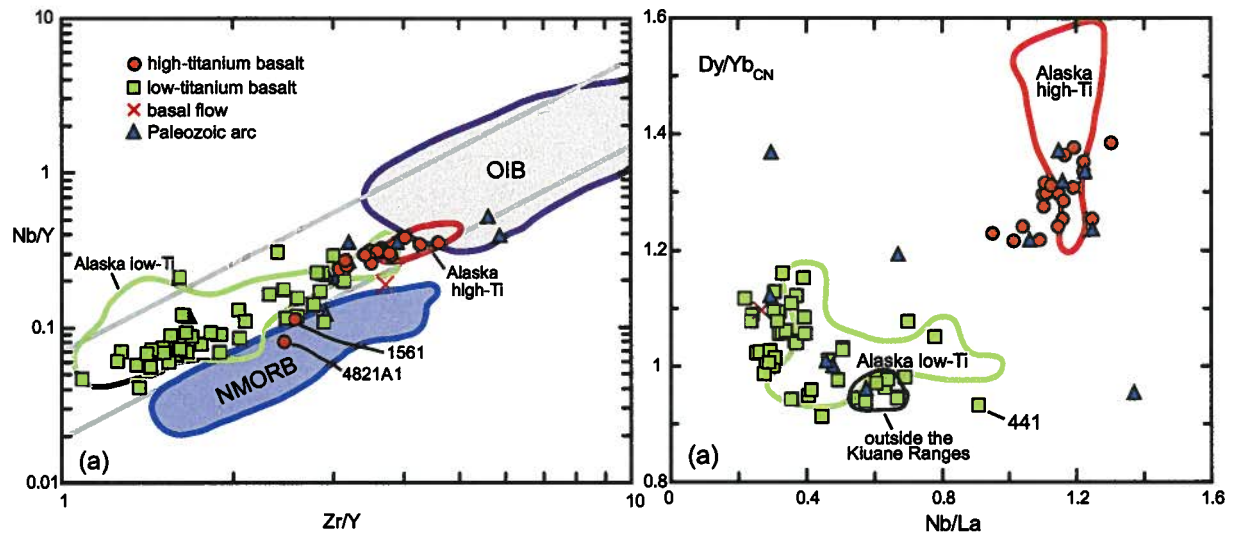


**Figure 4.12** Trace-element ratios of high- and low-titanium basalts of the Nikolai Formation in Yukon with Paleozoic arc samples and fields for Nikolai basalts in Alaska. (a) Nb/Y and Zr/Y variation (after Fitton *et al.*, 1997). (b) Dy/Yb<sub>CN</sub> vs. Nb/La. The NMORB and OIB fields, not including Icelandic OIB, are from data compilations of Fitton *et al.* (1997; 2003). Note the two LREE-depleted high-titanium basalts (4821A1, 1561) that lie within the field for NMORB in panel a. The two parallel gray lines are the limits of data for Icelandic rocks.



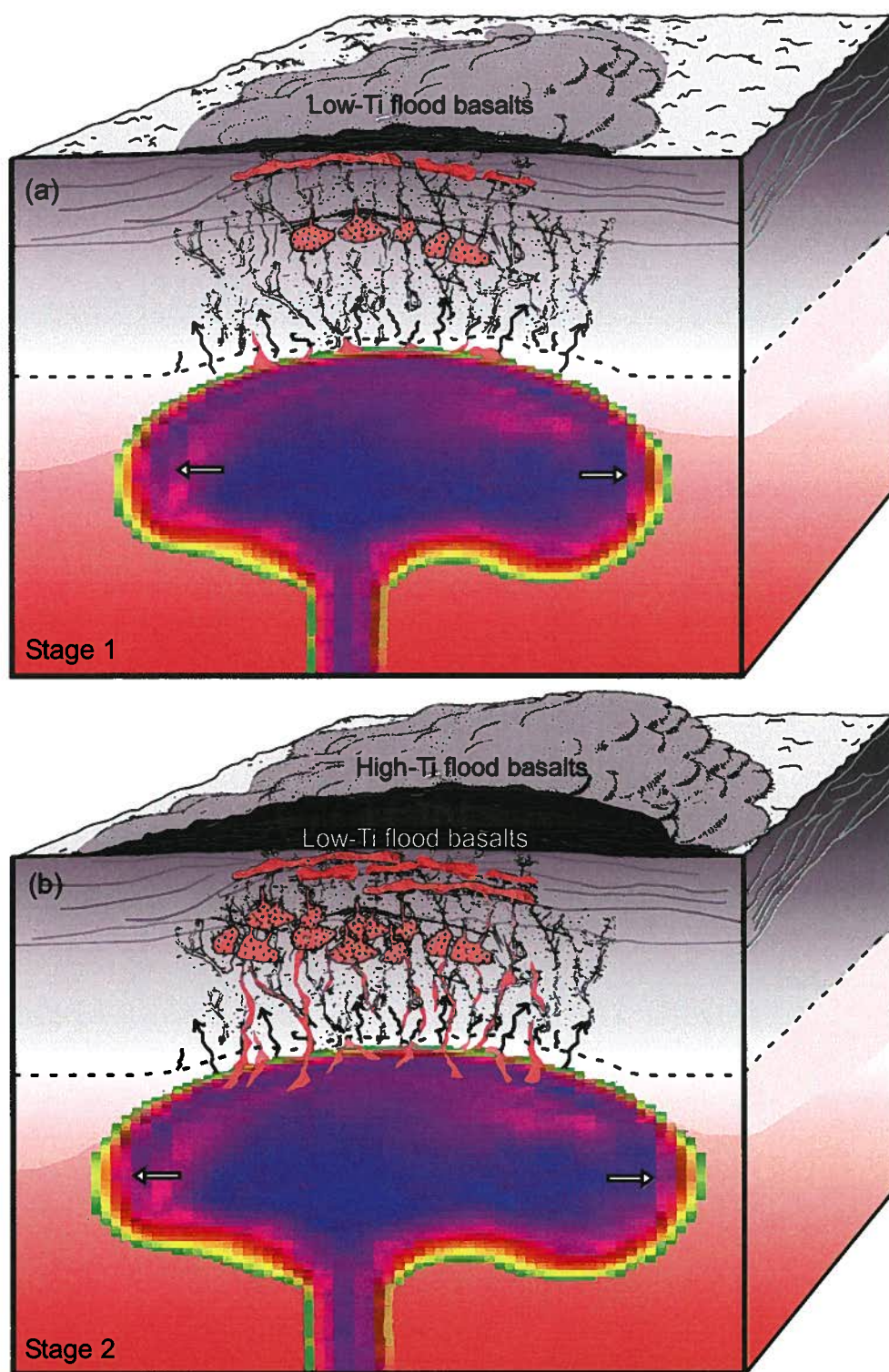


**Figure 4.13** Schematic diagrams of two stages of melting of Nikolai basalts in Yukon and Alaska that produced the low- and high-titanium basalts in Yukon and Alaska. Parts of the diagrams were adapted from a drawing by J. Holden in Fodor (1987) and Farnetani and Samuel (2005). (a) Low-titanium basalts form the lower parts of the stratigraphy in parts of Yukon and Alaska. In this scenario, a plume head impinging on the base of arc lithosphere leads to the formation of small-degree, HFSE-depleted low-titanium melts from a source in the arc mantle. (b) High-titanium basalts, which dominate the remainder of the volcanic stratigraphy, were derived from an OIB plume-type source. White arrows indicate flattening of the plume head. Black arrows indicate heat conduction from the plume head into the base of the lithosphere. The dashed line represents the base of the mechanical boundary layer. Vertical exaggeration =  $\sim 10:1$ .

from an OIB plume-type source and followed the eruption of most of the low-titanium basalts (Fig. 4.13).

The arc-type signature of the low-titanium basalts may have been generated from substantial melting of subduction-modified mantle, interaction of plume-derived melts with melts or material derived from the arc mantle, and/or reaction of magmas and metasomatized arc peridotite early in generation of the Nikolai basalts. Thus, we modelled melting of arc mantle compositions to determine if magma compositions similar to the low-titanium basalts can be produced by melting of ultramafic arc mantle rocks. The trace element concentrations of the low-titanium basalts were simulated using the incongruent dynamic melting model developed by Zou & Reid (2001) and source compositions of exposed arc mantle peridotite from the Early to Middle Jurassic Talkeetna arc in south-central Alaska (Kelemen *et al.*, 2003).

The modeling results indicate that small degrees of melting (<5%) of arc mantle can produce HFSE-depleted trace-element signatures similar to those of low-titanium basalts of the Nikolai Formation (Fig. 4.14). Negative Nb and Zr-Hf anomalies are generally not found in samples of metasomatized mantle peridotite (Arndt & Christensen, 1992), but they are present in mantle samples of exposed oceanic arc sections such as the Talkeetna arc. Small-degree melting of HFSE-depleted arc mantle offers one of the best explanations for the origin of the chemical signature of the low-titanium basalts. These modeling results require a fairly high proportion of cpx in the source (<30 vol. %). Modeling results depend highly on the average trace-element composition of the source, which caused the model compositions of partial melts of 10% or greater to be more LREE-depleted than most of the low-titanium basalts. Mixing of high- and low-titanium magmas would not significantly change the trace-element concentrations of either lava type unless >25 vol. % of the other lava type was mixed (Fig. 4.14). Assimilation of subduction-modified mantle is a less likely scenario because the amount of contaminant necessary to account for the trace-element and isotopic compositions of the low-titanium basalts would be unreasonably large. The compositions of the Late Paleozoic arc volcanic sequences are variable and partially overlap the compositions of both the high- and low-titanium basalts; therefore, they are not ideally-suited as assimilants responsible for the geochemical variation of the low-titanium basalts.

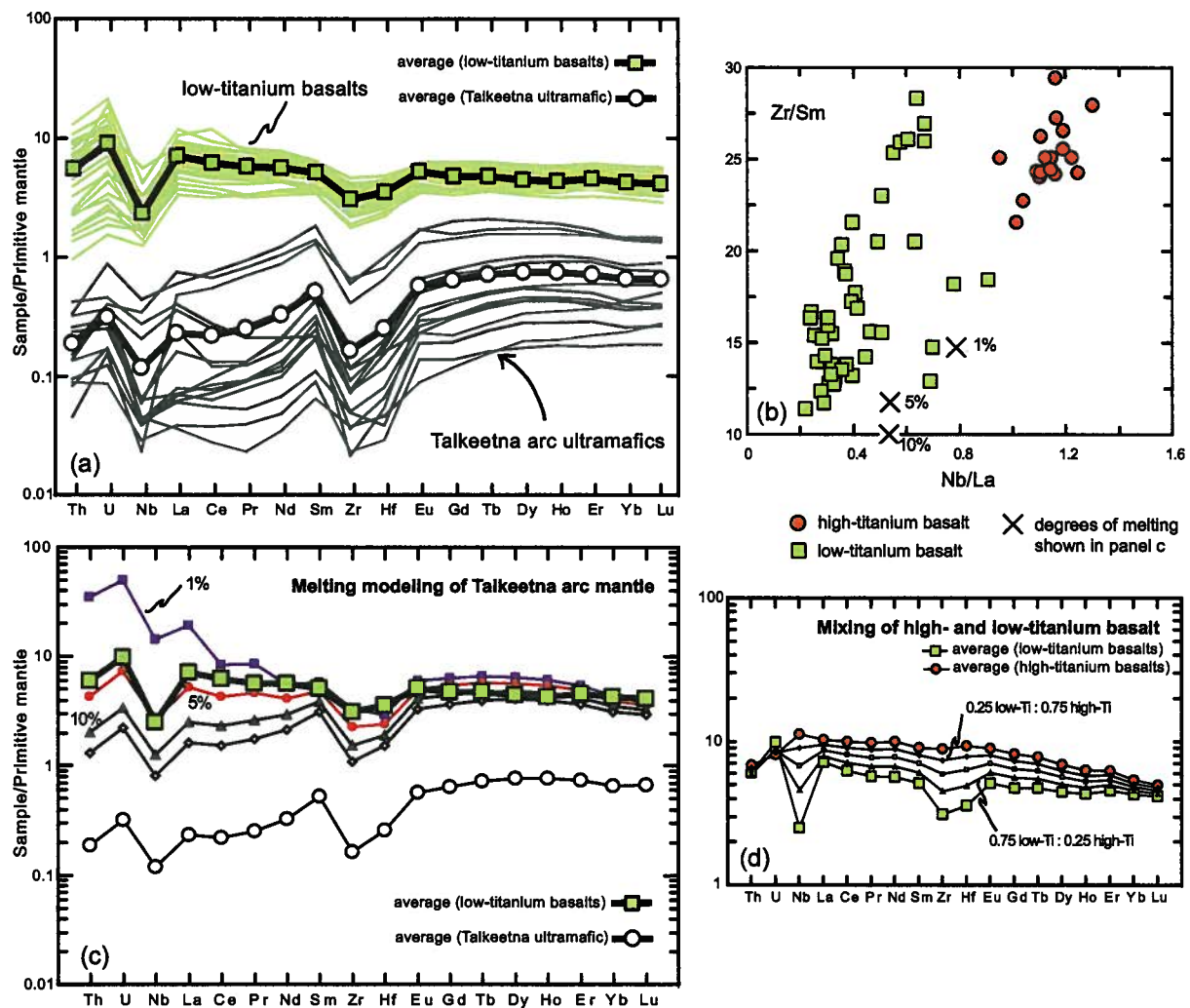


**Figure 4.14** Trace-element abundances of low-titanium basalts from Yukon compared to arc mantle compositions of the Early to Middle Jurassic Talkeetna arc and incongruent dynamic melting modeling results. (a) Primitive mantle-normalized trace-element patterns for low-titanium basalts from Yukon and Talkeetna arc ultramafic rocks (harzburgite, websterite, wherlite, and dunite) from south-central Alaska (Kelemen *et al.*, 2003), with averages denoted in the legend. (b) Zr/Sm vs. Nb/La for high- and low-titanium basalts from Yukon with melting modeling results, shown in panel c. (c) Melting modeling of the average Talkeetna arc ultramafic composition using the formulation for incongruent dynamic melting of Zou and Reid (2001), an example calculation is shown in their Appendix. Melting increments are labelled next to patterns. (d) Mixing modeling of high- and low-titanium melts. A range of melt reaction coefficients were used from Kinzler and Grove (1992) and Kelemen *et al.* (1990) and slight changes do not significantly affect the results. Partition coefficients from Salters and Stracke (2004) for 2 GPa were kept constant. Source mineralogy ranges from 0.28cpx:0.15opx:0.55ol:0.02sp to 0.18cpx:0.27opx:0.52ol:0.03sp. Higher proportions of cpx in the source yield better fits to the Yukon low-titanium basalt compositions. The results serve to illustrate that small degrees of melting (<5%) of arc mantle compositions may produce HFSE-depleted trace-element compositions similar to those of low-titanium basalts.



Studies of plume-lithosphere interaction suggest that, although conduction alone may not cause melting of the lithosphere, rifting and decompression, the presence of hydrous phases (e.g. Gallagher & Hawkesworth, 1992), melt injection from the plume into the lithosphere, and thermal and mechanical erosion of the lithosphere may all facilitate melting (Saunders *et al.*, 1992). Lassiter and DePaolo (1997) found geochemical evidence indicating that lavas with a lithospheric geochemical signature are commonly erupted during the early stages of flood basalt sequences and are often followed by lavas with more plume-type signatures. Lassiter *et al.* (1995) also suggested that a minimal amount of involvement of arc material was indicated by geochemistry in the generation of Nikolai basalts in Alaska. Geochemistry indicates melting of subduction-modified mantle in the Yukon and Alaska segments of the Wrangellia oceanic plateau, possibly from intrusion of the plume into the lithosphere or erosion and melting of cooler subduction-modified mantle along the edge of the plume head.

## CONCLUSION

Parts of the volcanic stratigraphy of the accreted Middle to Late Triassic Wrangellia oceanic plateau are exposed in a linear belt (~300 km long) in southwest Yukon, which extends westward over large areas of southern Alaska. Approximately 1000 m of predominantly massive subaerial basalt flows of the Nikolai Formation consist of pillow breccia and close-packed pillows (<70 m) along the base. The Nikolai Formation is bounded by Middle to Late Triassic marine sediments and unconformably overlies Paleozoic arc volcanic sequences. This northerly part of the Wrangellia oceanic plateau formed mostly above sea-level during a single short-lived magmatic phase (ca. 230 Ma). Importantly, these voluminous basaltic lavas erupted through a Late Paleozoic oceanic arc assemblage which presumably was underlain by a complementary region of metasomatized arc mantle.

This study presents the first set of geochemical and Sr-Nd-Hf-Pb isotopic compositions of Wrangellia flood basalts and Paleozoic arc sequences in Yukon and, along with a comparable study in Alaska, has provided a clear understanding of the source and temporal evolution of magmas that constructed the Wrangellia oceanic plateau in Yukon and Alaska. Similar to Alaska, the Nikolai basalts in Yukon have two

fundamentally distinct lava types. The high-titanium basalts that generally form the upper parts of the volcanic stratigraphy have compositions that are characteristic of OIB and distinct from N-MORB. The low-titanium basalts that generally form the lower part of the volcanic stratigraphy are depleted in HFSE and have relatively high Hf isotopic compositions that strongly differ from OIB and MORB, and are similar to lavas produced in arc settings. The involvement of lithosphere created and modified by prolonged subduction-related magmatism, and possible incorporation of a high Lu/Hf sediment component, offers the best explanation for derivation of the early-erupted low-titanium basalts. The low-titanium basalts in Yukon extend to more LREE-enriched compositions than in Alaska and may indicate a transitional lava type between the high- and low-titanium basalts. There is minor evidence of extension preserved in the underlying units directly beneath the Nikolai Formation and evidence of prolonged subsidence (>20 Myr) in sediments overlying the Nikolai Formation. The intrusion or erosion of the base of the lithosphere by the impinging plume head may have led to melting of subduction-modified mantle or interaction of plume-derived melts and arc material.

## ACKNOWLEDGEMENTS

Funding for field work and some of the analytical work for this study was generously provided by the Yukon Geological Survey and NSERC Discovery Grants to J. Scoates and D. Weis. Assistance with field work was provided by Bruno Kieffer. A. Greene was supported by a University Graduate Fellowship at UBC.

## REFERENCES

- Armstrong, A. K. & MacKevett, E. M., Jr. (1977). The Triassic Chitistone Limestone, Wrangell Mountains, Alaska. *U. S. Geological Survey*. Open-File Report 77-217, D49-D62 p.
- Arndt, N. T. & Christensen, U. (1992). The role of lithospheric mantle in continental flood volcanism: thermal and geochemical constraints. *Journal of Geophysical Research* **97**(B7), 10,967-10,981.
- Babbs, T. L. (1997). Geochemical and petrological investigations of the deeper portions of the Ontong Java Plateau: Malaita, Solomon Islands. Unpublished Ph.D. dissertation, Leicester University, U.K., 254 pp.
- Ben-Avraham, Z., Nur, A., Jones, D. L. & Cox, A. (1981). Continental accretion: From oceanic plateaus to allochthonous terranes. *Science* **213**, 47-54.

- Bittenbender, P. E., Bean, K. W., Kurtak, J. M. & Deninger, J., Jr (2007). Mineral assessment of the Delta River Mining District area, East-central Alaska. *U. S. Bureau of Land Management-Alaska*. Technical Report.
- Chauvel, C. & Blichert-Toft, J. (2001). A hafnium isotope and trace element perspective on melting of the depleted mantle. *Earth and Planetary Science Letters* **190**, 137-151.
- Dodds, C. J. & Campbell, R. B. (1992a). Geology, Mount St. Elias map area [115B & C[E1/2]], Yukon Territory. *Geological Society of Canada*. Open File Report 2189, 85 p.
- Dodds, C. J. & Campbell, R. B. (1992b). Geology, SW Dezadeash map area [115A], Yukon Territory. *Geological Society of Canada*. Open File Report 2190, 85 p.
- Dodds, C. J. & Campbell, R. B. (1992c). Geology, SW Kluane Lake map area [115G & F [E1/2]], Yukon Territory. *Geological Society of Canada*. Open File Report 2188, 85 p.
- Farnetani, C. G. & Samuel, H. (2005). Beyond the thermal plume paradigm. *Geophysical Research Letters* **32**(L07311), doi:10.1029/2005GL022360.
- Fitton, J. G., Saunders, A. D., Kempton, P. D. & Hardarson, B. S. (2003). Does depleted mantle form an intrinsic part of the Iceland plume? *Geochemistry Geophysics Geosystems* **4**(3), 1032, doi:10.1029/2002GC000424.
- Fitton, J. G., Saunders, A. D., Norry, M. J., Hardarson, B. S. & Taylor, R. N. (1997). Thermal and chemical structure of the Iceland plume. *Earth and Planetary Science Letters* **153**, 197-208.
- Fodor, R. V. (1987). Low- and high-TiO<sub>2</sub> flood basalts of southern Brazil: origin from picritic parentage and a common mantle source. *Earth and Planetary Science Letters* **84**, 423-430.
- Furin, S., Preto, N., Rigo, M., Roghi, G., Gianolla, P., Crowley, J. L. & Bowring, S. A. (2006). High-precision U-Pb zircon age from the Triassic of Italy: Implications for the Triassic time scale and the Carnian origin of calcareous nannoplankton and dinosaurs. *Geology* **34**(12), 1009-1012, doi:10.1130/g22967a.1.
- Gallagher, K. & Hawkesworth, C. (1992). Dehydration melting and the generation of continental flood basalts. *Nature* **358**, 57-59.
- Greene, A. R., Scoates, J. S. & Weis, D. (submitted). Wrangellia flood basalts in Alaska: A record of plume-lithosphere interaction in a Late Triassic accreted oceanic plateau. *Geochemistry Geophysics Geosystems*.
- Hauff, F., Hoernle, K. & Schmidt, A. (2003). Sr-Nd-Pb composition of Mesozoic Pacific oceanic crust (Site 1149 and 801, ODP Leg 185): Implications for alteration of ocean crust and the input into the Izu-Bonin-Mariana subduction system. *Geochemistry Geophysics Geosystems* **4**(8), doi:10.1029/2002GC000421.
- Hulbert, L. J. (1997). Geology and metallogeny of the Kluane mafic-ultramafic belt, Yukon Territory, Canada : eastern Wrangellia - a new Ni-Cu-PGE metallogenic terrane. *Geological Survey of Canada Bulletin*. Bulletin 506, Ottawa, 265 p.
- Israel, S. (2004). Geology of Southwestern Yukon (1:250 000 scale). *Yukon Geological Survey Open File* 2004-16.
- Israel, S. & Cobbett, R. (2008). Kluane Ranges bedrock geology, White River area (Parts of NTS 115F/9, 15 and 16; 115G/12 and 115K/1, 2). In: Emond, D. S., Blackburn,

- L. R., Hill, R. P. & Weston, L. H. (eds.) *Yukon Exploration and Geology 2007*. Yukon Geological Survey, pp. 153-167.
- Israel, S., Cobbett, R. & Fozard, C. (2007a). Bedrock geology of the Koidern River area (parts of NTS 115F/9, 15, 16 and 115G/12), Yukon (1:50 000 scale). *Yukon Geological Survey*. Open File 2007-8.
- Israel, S., Cobbett, R. & Fozard, C. (2007b). Bedrock geology of the Miles Ridge area (parts of NTS 115F/15, 16 and 115K/1, 2), Yukon (1:50 000 scale). *Yukon Geological Survey*. Open File 2007-7.
- Israel, S., Tizzard, A. & Major, J. (2005). Geological map of the Duke River area (parts of NTS 115G/2, 3, 5, 6, 7), Yukon (1:50 000 scale). *Yukon Geological Survey*. Open File 2005-11.
- Israel, S., Tizzard, A. & Major, J. (2006). Bedrock geology of the Duke River area, parts of NTS 115G/2, 3, 4, 6 and 7, southwestern Yukon. In: Emond, D. S., Bradshaw, G. D., Lewis, L. L. & Weston, L. H. (eds.) *Yukon Exploration and Geology 2005*. Yukon Geological Survey, pp. 139-154.
- Israel, S. & Van Zeyl, D. (2004). Preliminary geological map of the Quill Creek area (parts of NTS 115G/5,6,12), southwest Yukon (1:50,000 scale). *Yukon Geological Survey*. Open File 2004-20.
- Janney, P. E., Le Roex, A. P. & Carlson, R. W. (2005). Hafnium isotope and trace element constraints on the nature of mantle heterogeneity beneath the Central Southwest Indian Ridge (13°E to 47°E). *Journal of Petrology* 46(12), 2427-2464, 10.1093/petrology/egi060.
- Jones, D. L., Silberling, N. J. & Hillhouse, J. (1977). Wrangellia; a displaced terrane in northwestern North America. *Canadian Journal of Earth Sciences* 14(11), 2565-2577.
- Kelemen, P. B., Hanghøj, K. & Greene, A. R. (2003). One view of the geochemistry of subduction-related magmatic arcs, with emphasis on primitive andesite and lower crust. In: Rudnick, R. (ed.) *The Crust*. Elsevier-Pergamon: Oxford Treatise on Geochemistry Vol. 3 Holland, H. D. & Turekian, K. K. (eds.), pp. 593-659.
- Kelemen, P. B., Johnson, K. T. M., Kinzler, R. J. & Irving, A. J. (1990). High-field-strength element depletions in arc basalts due to mantle-magma interaction. *Nature* 345, 521-524.
- Kempton, P. D., Pearce, J. A., Barry, T. L., Fitton, J. G., Langmuir, C. H. & Christie, D. M. (2002). Sr-Nd-Pb-Hf isotope results from ODP Leg 187: Evidence for mantle dynamics of the Australian-Antarctic Discordance and origin of the Indian MORB source. *Geochemistry Geophysics Geosystems* 3(12), 1074, doi:10.1029/2002GC000320.
- Kinzler, R. J. & Grove, T. L. (1992). Primary magmas of mid-ocean ridge basalts 1. Experiments and methods. *Journal of Geophysical Research* 97(B5), 6,885-6,906.
- Lassiter, J. C. (1995). Geochemical investigations of plume-related lavas : constraints on the structure of mantle plumes and the nature of plume/lithosphere interactions. Ph.D. thesis, unpublished chapter, University of California, Berkeley, 231 pp.
- Lassiter, J. C. & DePaolo, D. J. (1997). Plume/lithosphere interaction in the generation of continental and oceanic flood basalts: chemical and isotopic constraints. In: Mahoney, J. J. & Coffin, M. F. (eds.) *Large Igneous Provinces: Continental,*

- Oceanic, and Planetary Flood Volcanism*. American Geophysical Union: Washington Geophysical Monograph 100, pp. 335-355.
- Lassiter, J. C., DePaolo, D. J. & Mahoney, J. J. (1995). Geochemistry of the Wrangellia flood basalt province: Implications for the role of continental and oceanic lithosphere in flood basalt genesis. *Journal of Petrology* **36**(4), 983-1009.
- Lowey, G. (1998). A new estimate of the amount of displacement on the Denali fault system based on the occurrence of carbonate megaboulders in the Dezadeash formation (Jura-Cretaceous), Yukon, and the Nutzotin Mountains sequence (Jura-Cretaceous), Alaska. *Bulletin of Canadian Petroleum Geology* **46**(3), 379-386.
- MacDonald, G. A. & Katsura, T. (1964). Chemical composition of Hawaiian lavas. *Journal of Petrology* **5**, 82-133.
- MacKevett, E. M., Jr. (1978). Geologic map of the McCarthy Quadrangle, Alaska. *U. S. Geological Survey*. Miscellaneous Investigations Series Map I-1032 scale 1:250,000.
- MacKevett, E. M., Jr., Cox, D. P., Potter, R. P. & Silberman, M. L. (1997). Kennecott-type deposits in the Wrangell Mountains, Alaska: High-grade copper ores near a basalt-limestone contact. In: Goldfarb, R. J. & Miller, L. D. (eds.) *Mineral Deposits of Alaska*. Economic Geology Monograph 9, pp. 66-89.
- Mahoney, J., LeRoex, A. P., Peng, Z., Fisher, R. L. & Natland, J. H. (1992). Southwestern Limits of Indian Ocean Ridge Mantle and the Origin of Low  $^{206}\text{Pb}/^{204}\text{Pb}$  Mid-Ocean Ridge Basalt: Isotope Systematics of the Central Southwest Indian Ridge (17°-50°E). *Journal of Geophysical Research* **97**(B13), 19771-19790.
- Mahoney, J., Storey, M., Duncan, R., Spencer, K. & Pringle, M. (1993). Geochemistry and age of the Ontong Java Plateau. In: Pringle, M., Sager, W. & Sliter, W. (eds.) *AGU Monograph on the Mesozoic Pacific: Geology, Tectonics, and Volcanism*. 77 AGU: Washington, pp. 233-261.
- Mahoney, J. J., Sinton, J. M., Kurz, M. D., MacDougall, J. D., Spencer, K. J. & Lugmair, G. W. (1994). Isotope and trace element characteristics of a super-fast spreading ridge: East Pacific rise, 13-23°S. *Earth and Planetary Science Letters* **121**, 173-193.
- McDonough, W. F. & Sun, S. (1995). The composition of the Earth. *Chemical Geology* **120**, 223-253.
- Mortensen, J. K. & Hulbert, L. J. (1991). A U-Pb zircon age for a Maple Creek gabbro sill, Tatamagouche Creek area, southwestern Yukon Territory. *Geological Survey of Canada*. Radiogenic Age and Isotopic Studies: Report 5 Paper 91-2, 175-179 p.
- Muller, J. E. (1967). Kluane Lake map area, Yukon Territory (115G, 115F/E 1/2). *Geological Survey of Canada*. Memoir 340, 137 p.
- Nowell, G. M., Kempton, P. D., Noble, S. R., Fitton, J. G., Saunders, A., Mahoney, J. J. & Taylor, R. N. (1998). High precision Hf isotope measurements of MORB and OIB by thermal ionisation mass spectrometry: insights into the depleted mantle. *Chemical Geology* **149**, 211-233.
- Ogg, J. G. (2004). The Triassic Period. In: Gradstein, F. M., Ogg, J. G. & Smith, A. G. (eds.) *A Geologic Time Scale 2004*. Cambridge University Press: Cambridge. pp. 271-306.

- Patchett, P. J., White, W. M., Feldmann, H., Kielinczuk, S. & Hofmann, A. W. (1984). Hafnium/rare earth element fractionation in the sedimentary system and crustal recycling into the Earth's mantle. *Earth and Planetary Science Letters* **69**, 365-378.
- Pearce, J. A. (2008). Geochemical fingerprinting of oceanic basalts with applications to ophiolite classification and the search for Archean oceanic crust. *Lithos* **100**, 14-48.
- Plafker, G. & Berg, H. C. (1994). Overview of the geology and tectonic evolution of Alaska. In: G., P. & H.C., B. (eds.) *The Geology of North America*. Geological Society of America: Boulder, CO The Geology of Alaska G-1, pp. 989-1021.
- Plafker, G., Nokleberg, W. J. & Lull, J. S. (1989). Bedrock geology and tectonic evolution of the Wrangellia, Peninsular, and Chugach terranes along the Trans-Alaskan Crustal Transect in the northern Chugach Mountains and southern Copper River basin, Alaska. *Journal of Geophysical Research* **94**, 4,255-4,295.
- Read, P. B. & Monger, J. W. H. (1976). Pre-Cenozoic volcanic assemblages of the Kluane and Alsek Ranges, southwestern Yukon Territory. *Geological Survey of Canada*. Open-File Report 381, 96 p.
- Richards, M. A., Jones, D. L., Duncan, R. A. & DePaolo, D. J. (1991). A mantle plume initiation model for the Wrangellia flood basalt and other oceanic plateaus. *Science* **254**, 263-267.
- Salters, V. J. & White, W. (1998). Hf isotope constraints on mantle evolution. *Chemical Geology* **145**, 447-460.
- Salters, V. J. M. (1996). The generation of mid-ocean ridge basalts from the Hf and Nd isotope perspective. *Earth and Planetary Science Letters* **141**, 109-123.
- Salters, V. J. M. & Stracke, A. (2004). Composition of the depleted mantle. *Geochemistry Geophysics Geosystems* **5**(Q05B07), doi:10.1029/2003GC000597.
- Saltus, R. W., Hudson, T. & Wilson, F. H. (2007). The geophysical character of southern Alaska: Implications for crustal evolution. In: Ridgeway, K. D., Trop, J. M., O'Neill, J. M. & Glen, J. M. G. (eds.) *Tectonic Growth of a Collisional Continental Margin: Crustal Evolution of Southern Alaska*. Geological Society of America Special Paper 431, pp. 1-20.
- Saunders, A. D., Storey, M., Kent, R. W. & Norry, M. J. (1992). Consequences of plume-lithosphere interactions. In: Storey, B. C., Alabaster, T. & Pankhurst, R. J. (eds.) *Magmatism and the Causes of Continental Breakup*. Geological Society of London Special Publication 68: London, pp. 41-60.
- Schmidt, J. M. & Rogers, R. K. (2007). Metallogeny of the Nikolai large igneous province (LIP) in southern Alaska and its influence on the mineral potential of the Talkeetna Mountains. In: Ridgeway, K. D., Trop, J. M., O'Neill, J. M. & Glen, J. M. G. (eds.) *Tectonic Growth of a Collisional Continental Margin: Crustal Evolution of Southern Alaska*. Geological Society of America Special Paper 431, pp. 623-648.
- Smith, J. G. & MacKevett, E. M., Jr. (1970). The Skolai Group in the McCarthy B-4, C-4, C-5 Quadrangles, Wrangell Mountains, Alaska. *U. S. Geological Survey*. Bulletin 1274-Q, Q1-Q26 p.
- Tejada, M. L. G., Mahoney, J. J., Castillo, P. R., Ingle, S. P., Sheth, H. C. & Weis, D. (2004). Pin-pricking the elephant: evidence on the origin of the Ontong Java

- Plateau from Pb-Sr-Hf-Nd isotopic characteristics of ODP Leg 192 basalts. In: Fitton, J. G., Mahoney, J. J., Wallace, P. J. & Saunders, A. D. (eds.) *Origin and Evolution of the Ontong Java Plateau*. Geological Society of London, Special Publication 229, pp. 133-150.
- Vervoort, J. D., Patchett, P. J., Blichert-Toft, J. & Albarède, F. (1999). Relationships between Lu-Hf and Sm-Nd isotopic systems in the global sedimentary system. *Earth and Planetary Science Letters* **168**, 79-99.
- Zou, H. & Reid, M. R. (2001). Quantitative modeling of trace element fractionation during incongruent dynamic melting. *Geochimica et Cosmochimica Acta* **65**(1), 153-162.

## **CHAPTER 5**

### **The Age and Volcanic Stratigraphy of the Accreted Wrangellia Oceanic Plateau in Alaska, Yukon, and British Columbia**



## INTRODUCTION

Approximately 10% of the ocean floor is covered with oceanic plateaus or flood basalts, mostly in the western Pacific and Indian Oceans (Fig. 5.1; Ben-Avraham *et al.*, 1981). These regions can rise thousand of meters above the ocean floor and rarely exhibit magnetic lineations like the surrounding seafloor (Ben-Avraham *et al.*, 1981). Oceanic plateaus are produced from high volumetric output rates generated by high-degree melting events which are distinct from melting beneath mid-ocean ridges. Most of what we know about the architecture of oceanic plateaus is based on obducted portions of oceanic plateaus, drilling of the volcanic sequences of extant oceanic plateaus, and geophysical studies of the seismic properties of oceanic plateaus. The study of oceanic plateaus furthers our understanding of the relationship between large igneous provinces (LIPs) and mantle plumes, mass extinctions, and continental growth.

Oceanic plateaus have formed near spreading ridges, extinct arcs, fragments of continental crust, and in intraplate settings. They form crustal emplacements 20-40 km thick with flood basalt sequences up to 6 km thick that cover up to 2 million km<sup>2</sup> of the ocean floor (Coffin & Eldholm, 1994). Detailed studies of the volcanic stratigraphy of oceanic plateaus are rare because of the inaccessibility of oceanic plateaus in the ocean basins. Some of the best evidence for understanding the construction of oceanic plateaus, other than studies of the age, composition, and stratigraphy of the volcanic rocks themselves, is to examine the eruption record in conjunction with observations of inter-relationships between sedimentation, erosion, and magmatism (Saunders *et al.*, 2007). Stratigraphic and geochronological studies of an obducted oceanic plateau, where the base and top of the volcanic stratigraphy are exposed as well as the underlying and overlying sediments, provide a means for understanding the construction of an oceanic plateau (e.g. the emplacement of flows, eruption environment, the tectonic setting during formation, the timescale of volcanism, the palaeoenvironment directly preceding and following the eruptions, and the uplift and subsidence history).

Wrangellia flood basalts are the remnants of one of the best exposed accreted oceanic plateaus on Earth. Dissected sections of extensive Triassic flood basalts form a major part of Wrangellia, one of the largest terranes accreted to western North America. Wrangellia contains a rare example of an accreted oceanic plateau where parts of the

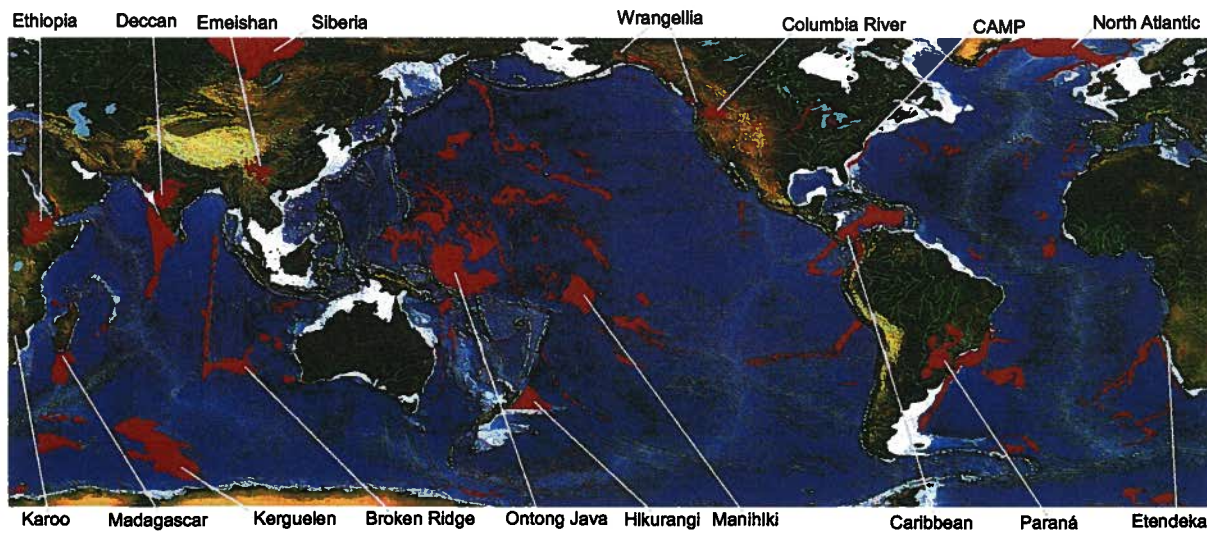


**Figure 5.1** Map showing the distribution of Phanerozoic large igneous provinces in red (Mahoney & Coffin, 1997). Oceanic plateaus and flood basalts are mostly concentrated in the western Pacific and Indian Oceans. Map modified from base map by A. Goodlife and F. Martinez in Mahoney and Coffin (1997).

entire volcanic stratigraphy as well as the pre- and post-volcanic stratigraphy are preserved. The stratigraphy of this oceanic plateau is exposed in numerous fault-bound blocks in a belt extending from Vancouver Island, British Columbia (BC) to south-central Alaska. Detailed descriptions of the volcanic and pre- and post-volcanic stratigraphy of Wrangellia are presently dispersed in hundreds of geologic maps, geologic survey reports in BC, Yukon, and Alaska.

In this contribution, we integrate new observations on the volcanic stratigraphy and pre- and post-volcanic stratigraphy of Wrangellia, including geochronology and biostratigraphy with previously published data, to evaluate the construction and age of the Wrangellia oceanic plateau. This material is presented in the form of detailed descriptions of Wrangellia stratigraphy, compiled geologic maps, photographic databases, interactive Google Earth files, and a review and compilation of previous research on Wrangellia. The maps, photographs, and archiving of information offer tools to visualize and fully explore the large body of information about Wrangellia, bringing together past and present research on Wrangellia to provide an overview of the origin and evolution of the Wrangellia oceanic plateau (Greene *et al.*, 2008a, 2008b, 2008c, submitted).

## **WRANGELLIA FLOOD BASALTS: THE VOLCANIC STRATIGRAPHY OF AN OCEANIC PLATEAU**

A large part of Wrangellia formed as an oceanic plateau, or transient LIP, that accreted to western North America in the Late Jurassic to Early Cretaceous (e.g. Trop & Ridgway, 2007). Wrangellia flood basalts are the defining unit of Wrangellia, in conjunction with underlying and overlying sediments with age-diagnostic fossils (Jones *et al.*, 1977). The flood basalts are defined as the Karmutsen Formation on Vancouver and Queen Charlotte Islands, and the Nikolai Formation in southwest Yukon and south-central Alaska (Fig. 5.2). Smaller elements of Middle to Late Triassic basalt stratigraphy in southeast Alaska are also believed to correlate with the Wrangellia flood basalts (Plafker & Hudson, 1980).

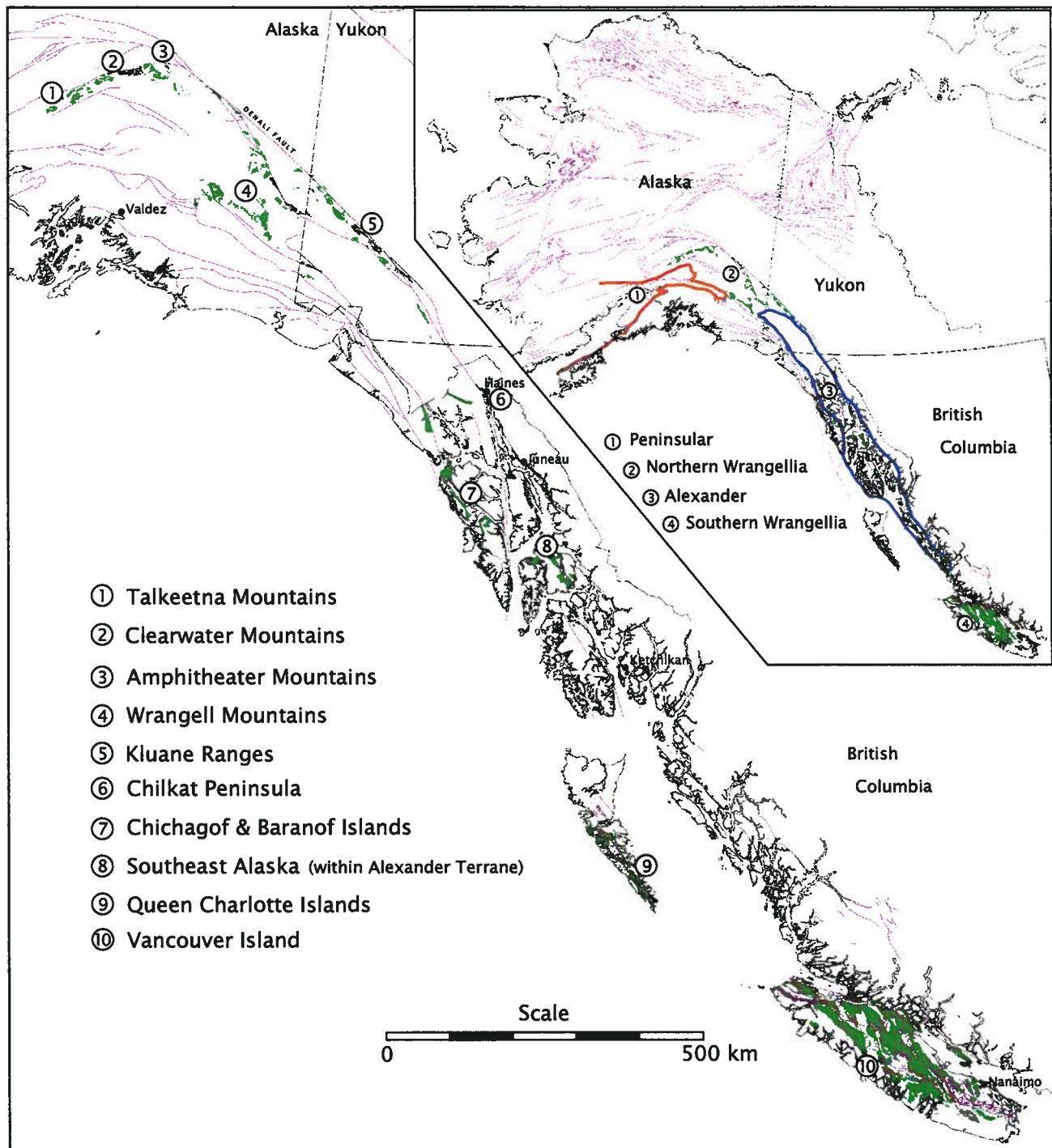


**Figure 5.2** Simplified map showing the distribution of Wrangellia flood basalts in Alaska, Yukon, and British Columbia. Map derived from (Wilson *et al.*, 1998; Israel, 2004; Massey *et al.*, 2005a, b; Wilson *et al.*, 2005; Brew, 2007, written comm.). Inset shows northwest North America with Wrangellia flood basalts, and outlines for the Peninsular (orange) and Alexander (blue) Terranes. Purple lines are faults in Alaska and parts of Yukon. Circled numbers indicated in the legend refer to areas mentioned in the text. Basalts indicated in southeast Alaska are mostly part of the Alexander Terrane.

### **Geographic distribution and aerial extent of the Wrangellia flood basalts**

The Wrangellia flood basalts in BC, Yukon, and Alaska have been identified by geologic mapping and regional geophysical surveys. Exposures of Wrangellia flood basalts extend over 2300 km from Vancouver Island to south-central Alaska (Fig. 5.2; Supplementary Google Earth files). Exposures of the Karmutsen Formation cover ~58% of Vancouver Island, BC. In southern Alaska, elements of Wrangellia have a well-defined northern boundary along the Denali fault and extend southwards to the outboard Peninsular Terrane (Fig. 5.2). In southeast Alaska and southwest Yukon, Wrangellia is mostly limited to slivers of intensely dissected crustal fragments with minimal aerial extent (Fig. 5.2).

From recently compiled digital geologic maps, the aerial exposure of the Wrangellia flood basalts is ~20,000 km<sup>2</sup> on Vancouver Island, ~800 km<sup>2</sup> in southwest Yukon and southeast Alaska, and ~2,000 km<sup>2</sup> across southern Alaska (Table 5.1). The original areal distribution was considerably greater and these estimates of outcrop extent do not consider areas of flood basalt covered by younger strata and surficial deposits. The boundaries and crustal structure of Wrangellia in southern Alaska, as defined by recent magnetic and gravity surveys, indicate a distinct magnetic high interpreted as due to the presence of thick, dense crust from Triassic mafic magmatism (Glen *et al.*, 2007a, 2007b; Saltus *et al.*, 2007). Wrangellia crust beneath Vancouver Island (~25-30 km thick) has seismic properties corresponding to mafic plutonic rocks extending to depth that are underlain by a strongly reflective zone of high velocity and density, which has been interpreted as a major shear zone where lower Wrangellia lithosphere was detached (Clowes *et al.*, 1995).

### **Geologic history of Wrangellia**

A note about the terminology used in this contribution. Wrangellia (or the Wrangellia Terrane) refers to fault-bound sections of the upper crust that contain successions of diagnostic Middle to Late Triassic flood basalts and Paleozoic formations that underlie the flood basalts (as originally defined by Jones *et al.* (1977)). The areas of Wrangellia in Alaska and Yukon are referred to as Northern Wrangellia and areas in British Columbia are referred to as Southern Wrangellia. The Wrangellia Composite

Table 5.1 Areal extent and volumetric estimates for the Wrangellia flood basalts

Quadrangle	Area (km <sup>2</sup> )	% Area	Estimated thickness (km)		Estimated volume (km <sup>3</sup> )		% Volume
			min	max	min	max	
British Columbia							
Southern VI (NM10)	10,581	41.9	4	6	42,323	63,485	45.2
Northern VI (NM9)	8,561	33.9	4	6	34,245	51,368	36.6
Queen Charlotte Is (NN8)	1,773	7.0	3	4.5	5,319	7,979	5.7
Queen Charlotte Is (NN9)	1,827	7.2	3	4.5	5,481	8,221	5.9
Northern BC (NO8)	86	0.3	1	3	86	257	0.2
Yukon							
Kluane South	705	2.8	1	3	705	2,115	1.5
Alaska							
McCarthy	720	2.9	3	4	2,161	2,882	2.1
Nabesna	275	1.1	3	4	824	1,098	0.8
Valdez	55	0.2	1	2	55	110	0.1
Gulkana	7	0.0	1	2	7	14	0.0
Mt Hayes	356	1.4	3	4.5	1,067	1,601	1.1
Healy	205	0.8	3	4.5	616	924	0.7
Talkeetna Mtns	105	0.4	3	4.5	314	471	0.3
Totals	25,256				93,204	140,525	

Estimates for British Columbia are calculated from Massey *et al.* (2005). Estimates for Yukon are calculated from Israel *et al.* (2004). Estimates for Alaska are calculated from Wilson *et al.* (2005) and Wilson *et al.* (1998).

Terrane refers to three distinct terranes (Wrangellia, Alexander, Peninsular; Fig. 5.2) that share similar elements or have a linked geologic history (as defined by Plafker *et al.*, 1989b; Nokleberg *et al.*, 1994; Plafker & Berg, 1994; Plafker *et al.*, 1994). The connections between the Wrangellia, Alexander, and Peninsular Terranes are not well-established, although the age from a single pluton in Alaska is proposed to link the Proterozoic to Triassic Alexander Terrane to Wrangellia by late Pennsylvanian time (Gardner *et al.*, 1988). This paper specifically focuses on Wrangellia and does not examine the relationship of Wrangellia to the Alexander and Peninsular terranes.

Wrangellia has a geologic history spanning a large part of the Phanerozoic prior to its accretion with western North America. The geologic record beneath the flood basalts contains Paleozoic oceanic arc and sedimentary sequences with a rich marine fossil assemblage. Paleontological studies indicate that Wrangellia was located in cool-temperate northern paleolatitudes ( $\sim 25^{\circ}\text{N}$ ) during the Permian and not far from the North American continent (Katvala & Henderson, 2002). The geologic record is sparse to absent in the Middle Permian to Early Triassic throughout Wrangellia. A major, short-lived phase of tholeiitic flood volcanism occurred in the Middle to Late Triassic in submarine and subaerial environments. The Wrangellia flood basalts subsided during and after their emplacement. Paleomagnetic studies of Wrangellia flood basalts indicate eruption in equatorial latitudes (Irving & Yole, 1972; Hillhouse, 1977; Hillhouse & Gromme, 1984) and Late Triassic bivalves indicate an eastern Panthalassan position in the Late Triassic (Newton, 1983). Previous geochronological and biostratigraphic studies indicate magmatism occurred between  $\sim 230$  and  $225$  Ma (e.g. Parrish and McNicoll, 1992; Slaggett, 2003; Bittenbender *et al.*, 2007). A mantle plume origin for the Wrangellia flood basalts was initially proposed by Richards *et al.* (1991) and is supported by ongoing geochemical and petrological studies (Greene *et al.*, 2008, submitted-c). Late Triassic to Early Jurassic arc magmatism is preserved as intrusions within and volcanic sequences overlying Wrangellia flood basalts throughout areas on Vancouver Island. Paleobiogeographic studies indicate Wrangellia was located in the northeast Pacific Ocean during the Early Jurassic (Smith, 2006) and probably accreted to western North America in the Late Jurassic to Early Cretaceous (Csejtey *et al.*, 1982; McClelland *et al.*, 1992; Nokleberg *et al.*, 1994; Umhoefer & Blakey, 2006; Trop & Ridgway, 2007).

The following overview of the stratigraphy of Wrangellia covers the Paleozoic and early Mesozoic formations pre-dating Triassic flood volcanism, but focuses primarily on the volcanic stratigraphy of the Wrangellia flood basalts and their relationship with the immediately underlying and overlying sedimentary formations. Descriptions below are presented from northwest (Alaska) to southeast (BC) and generally from the oldest to the youngest strata in each area. A summary of previous research related to Wrangellia is given in Appendix G and Supplementary data files 1 and 2 contain a compilation of ~500 references related to Wrangellia.

## **STRATIGRAPHY OF WRANGELLIA**

### **Wrangellia in southern Alaska**

The accretion and northward migration of parts of Wrangellia, followed by the oroclinal bending of Alaska, has left Wrangellia flood basalts exposed in an arcuate belt extending ~450 km across south-central Alaska (Fig. 5.3). Wrangellia stratigraphy underlies most of the Wrangell Mountains in the eastern part of southern Alaska and extends westward in a wide belt immediately south of the Denali Fault, along the southern flank of the eastern Alaska Range and in the northern Talkeetna Mountains (Fig. 5.3). Recent mapping and geophysical studies have recognized Wrangellia basalts (Nikolai Formation) southwest of previously mapped exposures, in the Talkeetna Mountains (Schmidt *et al.*, 2003b; Glen *et al.*, 2007a). Triassic flood basalt stratigraphy may extend several hundred kilometers to the southwest of the Talkeetna Mountains on the Alaska Peninsula (Cottonwood Bay Greenstone of Detterman and Reed, 1980), however, the relationship between these basalts and the Nikolai Formation has not been explored.

Geophysical studies and detailed work on sedimentary basins along the margins of Wrangellia have helped define the boundaries of Wrangellia and led to the development of a model for the accretionary history of southern Alaska (Glen *et al.*, 2007b; Trop & Ridgway, 2007). The northwestern boundary of Wrangellia corresponds with a prominent steeply-dipping structure (Talkeetna Suture Zone), which may represent the original suture between Wrangellia and the former continental margin (Glen *et al.*, 2007). Mesozoic and Cenozoic sedimentary basins along the inboard margin of



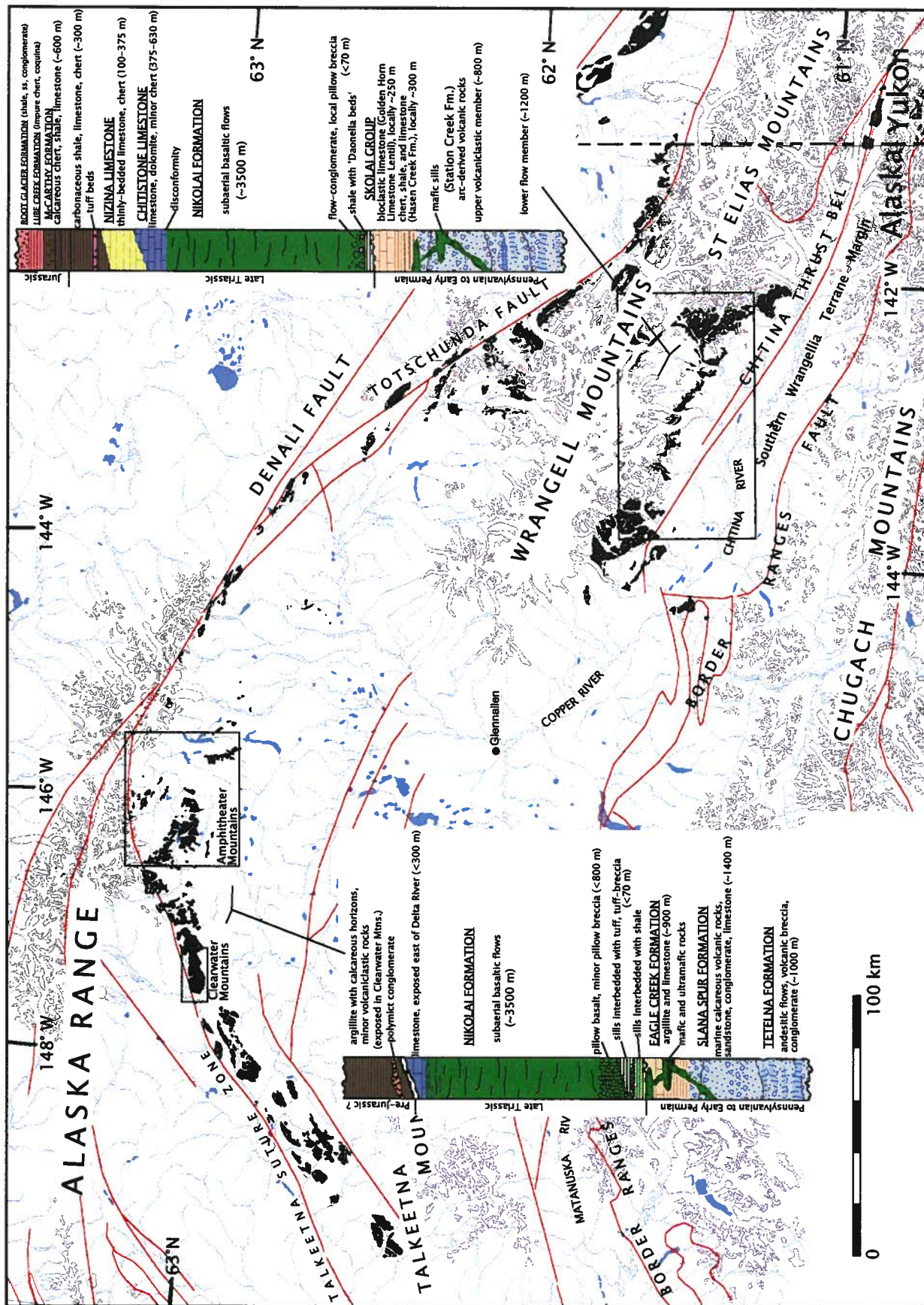


Figure 5.3 Simplified map of eastern south-central Alaska showing the distribution of Wrangellia flood basalts and stratigraphic columns. Map derived from Wilson *et al.* (1998) and Wilson *et al.* (2005), with unpublished mapping from Schmidt (pers. comm., 2006). Stratigraphic columns depict Late Paleozoic to Jurassic units on the south side of the Wrangell Mountains, derived from Smith and MacKevett (1970) and MacKevett (1978), and the east-central Alaska Range, derived partly from Nokleberg *et al.* (1992).

Wrangellia, adjacent to and overlying the Talkeetna Suture Zone and Denali Fault, record the uplift and collisional history of Wrangellia and the former continental margin, north of the Denali Fault (Trop *et al.*, 2002; Ridgeway *et al.*, 2002; Trop and Ridgeway, 2007). The southern boundary of Wrangellia in Alaska is interpreted to lie along a prominent northeast-trending geophysical gradient separating Wrangellia units to the north from parts of the Peninsular Terrane to the south (Glen *et al.*, 2007b).

### ***Talkeetna Mountains and Eastern Alaska Range***

The westernmost Wrangellia stratigraphy in the Talkeetna Mountains consists of Paleozoic strata that are intruded by mafic sills associated with Nikolai basalts. The Wrangellia basement consists of siliceous argillite, siltstone, and chert interbedded with limestone, which are similar to Paleozoic sedimentary units elsewhere in Alaska (Schmidt & Rogers, 2007). The arc sequences that are typical of Wrangellia basement in the Alaska Range and Wrangell Mountains are absent or unexposed in the Talkeetna Mountains. A rare quartz-pebble conglomerate has been recognized in the Talkeetna Mountains that has not been reported elsewhere beneath the flood basalts (Schmidt *et al.*, 2003a). The overall thickness of Nikolai basalts is limited in the Talkeetna Mountains (~300 m) and only minor occurrences of overlying sedimentary rocks have been reported (Schmidt & Rogers, 2007).

From southwest of the Clearwater Mountains eastward to the Amphitheater Mountains, volcanic stratigraphy of the Nikolai Formation approaching 4 km thick is exposed in a discontinuous belt (Fig. 5.3). There are limited exposures of underlying Paleozoic units in this area. In the Clearwater Mountains, the base of the volcanic stratigraphy consists of pillowed flows overlying interlayered shale and mafic sills. The pillow basalt contains sediment derived from directly underlying beds filling voids between small-diameter pillows (<1 m). The total thickness of the pillowed flows is less than several hundred meters and they are overlain by predominantly massive subaerial flows. Picritic pillow lavas with abundant olivine pseudomorphs occur within the basal pillowed flows (Greene *et al.*, 2008, submitted-c).

In the Clearwater Mountains, the upper parts of the volcanic stratigraphy is primarily subaerial flows (and rarely sills) with columnar jointing preserved in several of

the thicker flows (<25 m). Smith (1981) described minor occurrences of tuff, flow breccia, and limestone and argillite lenses within the volcanic stratigraphy. These rare interbedded horizons are mainly found in the lower parts or at the top of the volcanic stratigraphy (Smith, 1981). Tuffaceous layers (or redistributed hyaloclastite) occur within rhythmically layered carbonaceous argillite or are a mixture of volcanic clasts and carbonaceous matter (Smith, 1981). Diagnostic index fossils (the bivalve *Halobia* and the ammonoid *Tropites*) have been found in intervalvolcanic sedimentary lenses at the top of the volcanic stratigraphy and in strata overlying the basalts (Smith, 1981). The complex interbedding of volcanic and sedimentary horizons gives way to fine-grained marine sedimentary strata above the flood basalts.

In the eastern Alaska Range, Paleozoic volcanic and volcanoclastic rocks of the Tetelna Volcanics form isolated exposures east of the Amphitheater Mountains, where they are intruded by plutonic rocks related to the Nikolai basalts (Nokleberg *et al.*, 1992). Pre-flood basalt sedimentary units are mostly non-fossiliferous carbonaceous black shale and siliceous argillite (Blodgett, 2002). Some of the best exposures of Wrangellia flood basalt stratigraphy are preserved as part of an east-west-trending synform underlain by mafic and ultramafic plutonic rocks in the Amphitheater Mountains (Fig. 5.4). The synform is dissected by several north-south-trending U-shaped glacial valleys filled with elongate lakes that provide access to kilometer-high exposures of volcanic stratigraphy. The Amphitheater Mountains synform is largely intact and much of the stratigraphy lacks pervasive faulting. Five large sheet-like mafic-ultramafic intrusions, which occur within argillites underlying the flood basalts, are exposed around the Amphitheater Mountains (Schmidt & Rogers, 2007).

The volcanic stratigraphy in the Amphitheater Mountains is very similar to the Clearwater Mountains. The lowest exposures are argillite and shale underlying the pillowed flows and intruded by numerous massive sills (Fig. 5.5). The lowermost pillowed flows engulf sediment of underlying strata and only occur in the lowest several hundred meters of stratigraphy (~10-15% of the total section). Tuffs and breccia are preserved in the submarine part of the stratigraphic section below the transition from submarine to subaerial flows. Mafic sills form parts of the lower volcanic stratigraphy and are locally interbedded with tuff and breccia (Fig. 5.5). There are approximately 3



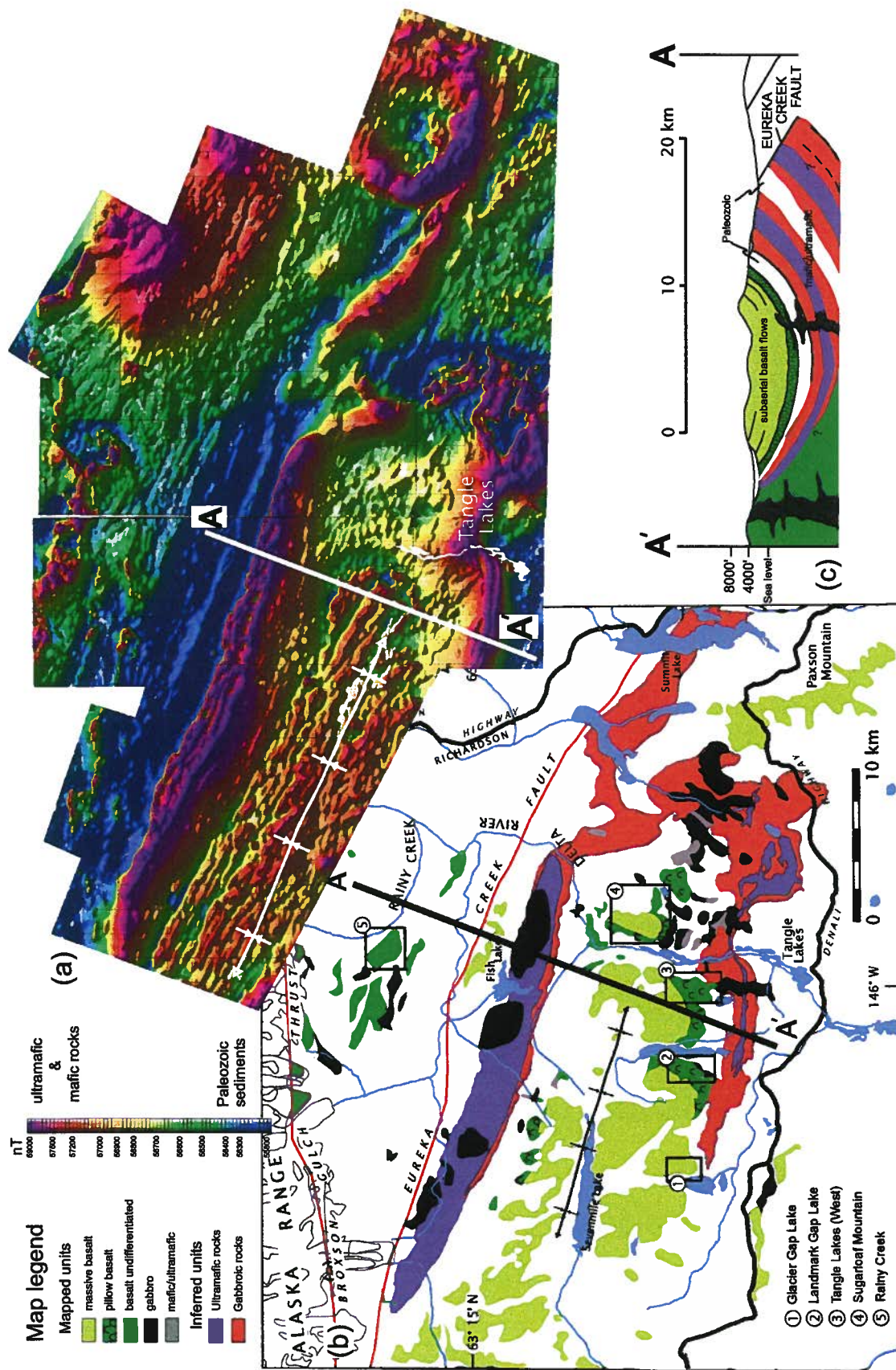


**Figure 5.4** Geology and magnetic map of the Amphitheater Mountains, Alaska (location shown in Figure 5.3). (a) Color shadow total magnetic field map of part of the Amphitheater Mountains. A summary of the magnetic survey is provided in Burns *et al.* (2003) and the full color shadow map is presented in Burns *et al.* (2003). Details of the data acquisition, interpretation, publications, and data formats are provided in Prichard (2003). The surveys (1995 and 2002) mapped the magnetic and conductive properties of the area to detect conductive mineralization. This was accomplished by using a DIGHEM(V) multi-coil, multi-frequency electromagnetic system, supplemented by a high sensitivity cesium magnetometer and GPS system (Burns & Clautice, 2003). The rocks with the highest magnetic susceptibility (Fe-rich magnetic minerals; mafic and ultramafic rocks) dampen the magnetic signal and produce highs and lows, measured in nanoTeslas (nT). The high nT values are purple and orange in color, indicating magnetic rocks, and the low values are blue and green. The purple and red areas are assumed to be coincident with mafic and ultramafic rocks, and the blue areas are inferred to be Paleozoic sediments. (b) Generalized geology of the Nikolai Formation and related plutonic rocks in the Amphitheater Mountains. Five main field areas are outlined with numbered boxes (denoted in map). Map derived from Nokleberg *et al.* (1992) and digital compilation of Wilson *et al.* (1998). Inferred units from Burns *et al.* (2003). (c) Schematic cross-section of Amphitheater Mountains from A to A' (shown in panels a and b), adapted from Nokleberg *et al.* (1985).



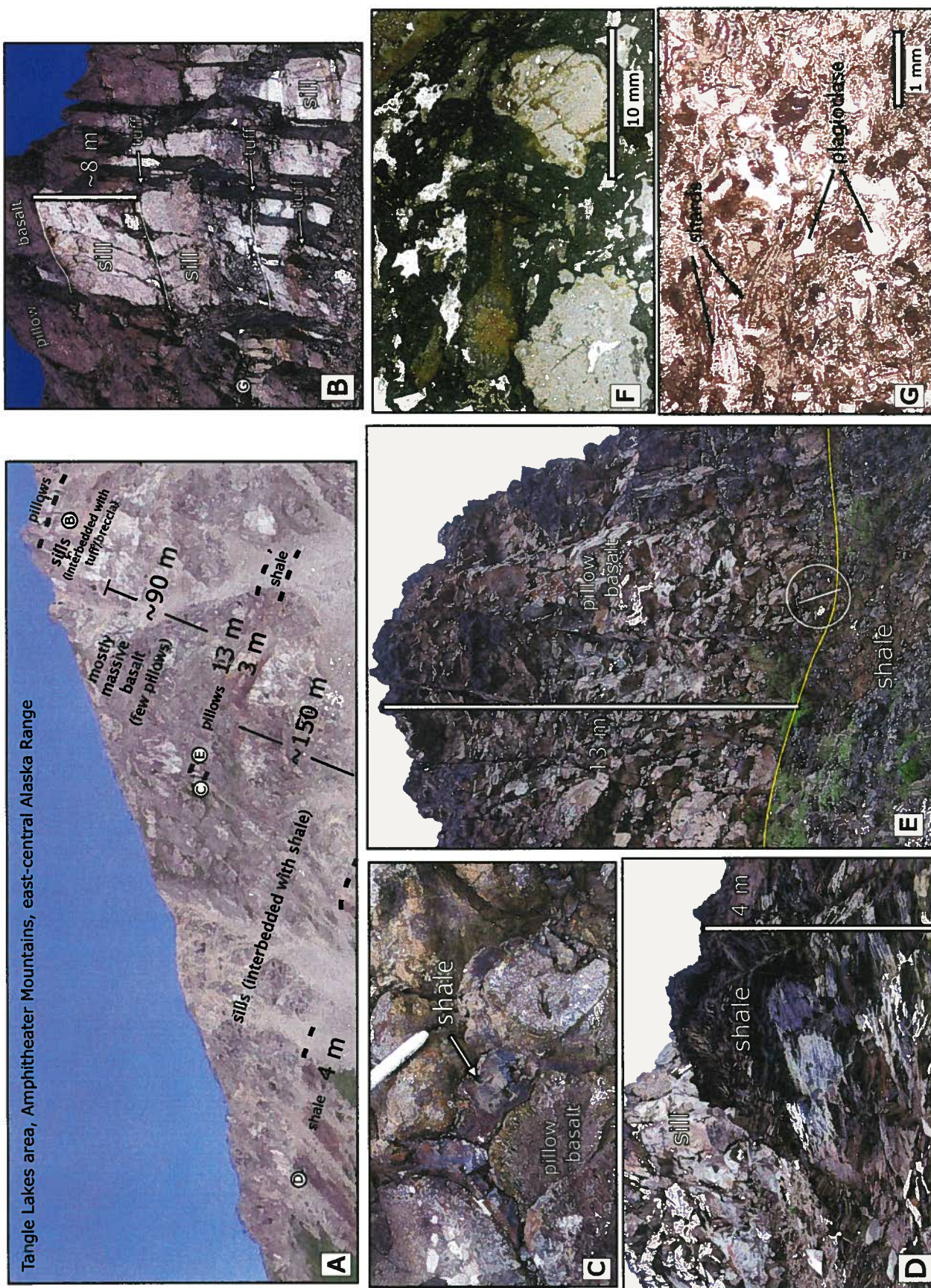


**Figure 5.5** Photographs of base of Nikolai Formation in Tangle Lakes area of the Amphitheater Mountains (location shown in Figure 5.4). (A) Sediment-sill complex and base of flood basalts on the west side of Lower Tangle Lake. Circled letters mark the location of the lowermost flow of the submarine section. (C) Pillow basalt in the lowermost flow with fine-grained sediment filling spaces between pillows (marker for scale). (D) Carbonaceous non-fossiliferous black shale with parallel laminations overlain by mafic sill. (E) Lowermost flow directly overlying shale. (F) Thin-section scan of tuffaceous layers just below the base of sills in photograph B. (G) Photomicrograph of tuff from between sills, location indicated in photograph B.



km of subaerial flows overlying the submarine stratigraphy. Neither the top of the flood basalts or significant sections of Late Triassic or Jurassic formations are well exposed in the Amphitheater Mountains.

North of the Eureka Creek Fault is a small area with mafic and ultramafic plutonic rocks and volcanic stratigraphy different from that south of the Eureka Creek Fault within the synform (Fig. 5.4). Although originally mapped as a separate subterrane from assemblages in the Amphitheater synform by Nokelberg *et al.* (1985), age constraints indicate that it is in fact part of Wrangellia (Bittenbender *et al.*, 2007). This area contains a complex sequence of vertically-dipping limestone, shale, and picritic tuff cross-cut by numerous mafic and ultramafic dikes.

### ***Wrangell Mountains***

Wrangellia flood basalts form two northwest- to southeast-trending belts along the northeast and southwest margins of the Wrangell Mountains, between the Totschunda Fault and Chitina Thrust Belt (Fig. 5.3). Large Miocene to Recent volcanoes of the Wrangell Mountains volcanic field, Tertiary continental sedimentary rocks, and glaciers overlie most of the central portion of the Wrangell Mountains, covering most of the pre-Cenozoic Wrangellia stratigraphy.

The type Wrangellia Terrane lies in the area between the Totschunda Fault and the Chitina Thrust Belt, although similar assemblages are exposed to the south between the Chitina Thrust Belt and the Border Ranges Fault (Fig 5.3). Paleozoic sequences south of the Chitina Thrust Belt have different character than sequences north of the thrust belt. Plafker *et al.* (1989b) interpreted this area between the Chitina Thrust Belt and the Border Ranges Fault, referred to as the Southern Wrangellia Terrane Margin, as a deeper, more metamorphosed equivalent of the type Wrangellia Terrane in the Wrangell Mountains. There are exposures of Nikolai basalts in this area, but these units are not addressed in this paper.

Wrangellia stratigraphy is well-exposed in a shallow northwest-trending syncline along the south side of the Wrangell Mountains. The entire stratigraphy is not exposed in one area, but different areas contain sections of the base, middle, and top of Wrangellia flood basalt stratigraphy (Figs 5.6, 5.7, and 5.8). The base of the volcanic stratigraphy is

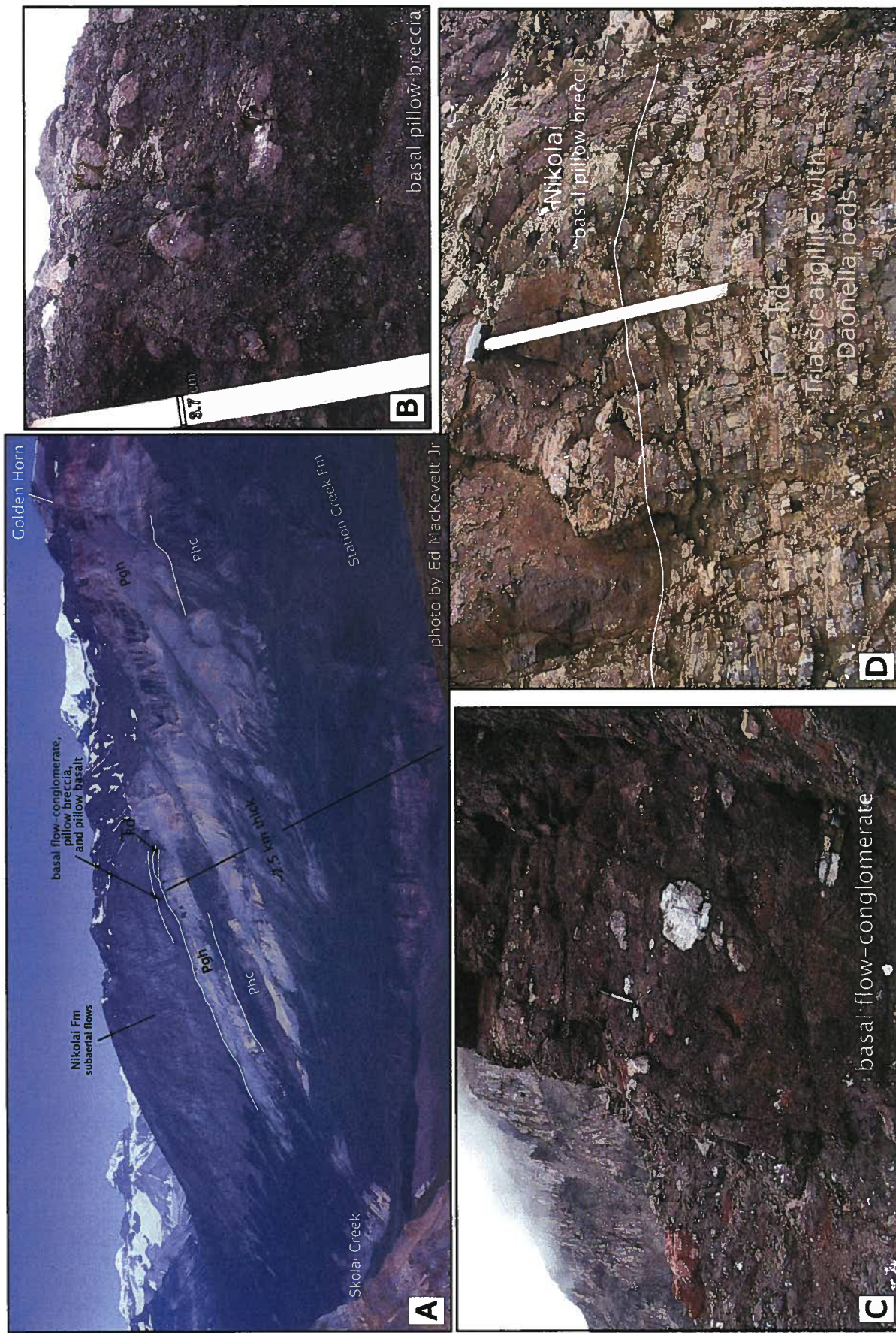


**Figure 5.6** Photographs of the base of Nikolai Formation north of Skolai Creek in Wrangell-St. Elias National Park. (A) Paleozoic arc rocks and marine sedimentary sequences underlying Nikolai basalts. Photograph by Ed MacKevett, Jr. (Phc, Hasen Creek Formation; Pgh, Golden Horn Limestone Lentil; TRd, Middle Triassic 'Daonella-beds'). (B) Basal pillow breccia just above Middle Triassic argillite and shale with *Daonella*. (C) Basal flow-conglomerate with rounded clasts of white limestone (<20 cm) derived from Golden Horn Limestone Lentil and red basalt (<40 cm) from Station Creek Formation. Marker (14 cm) for scale. (D) Argillite overlain by pillow breccia above the Golden Horn Limestone. The location of photographs B, C, and D are from the area just above TRd in photograph A.



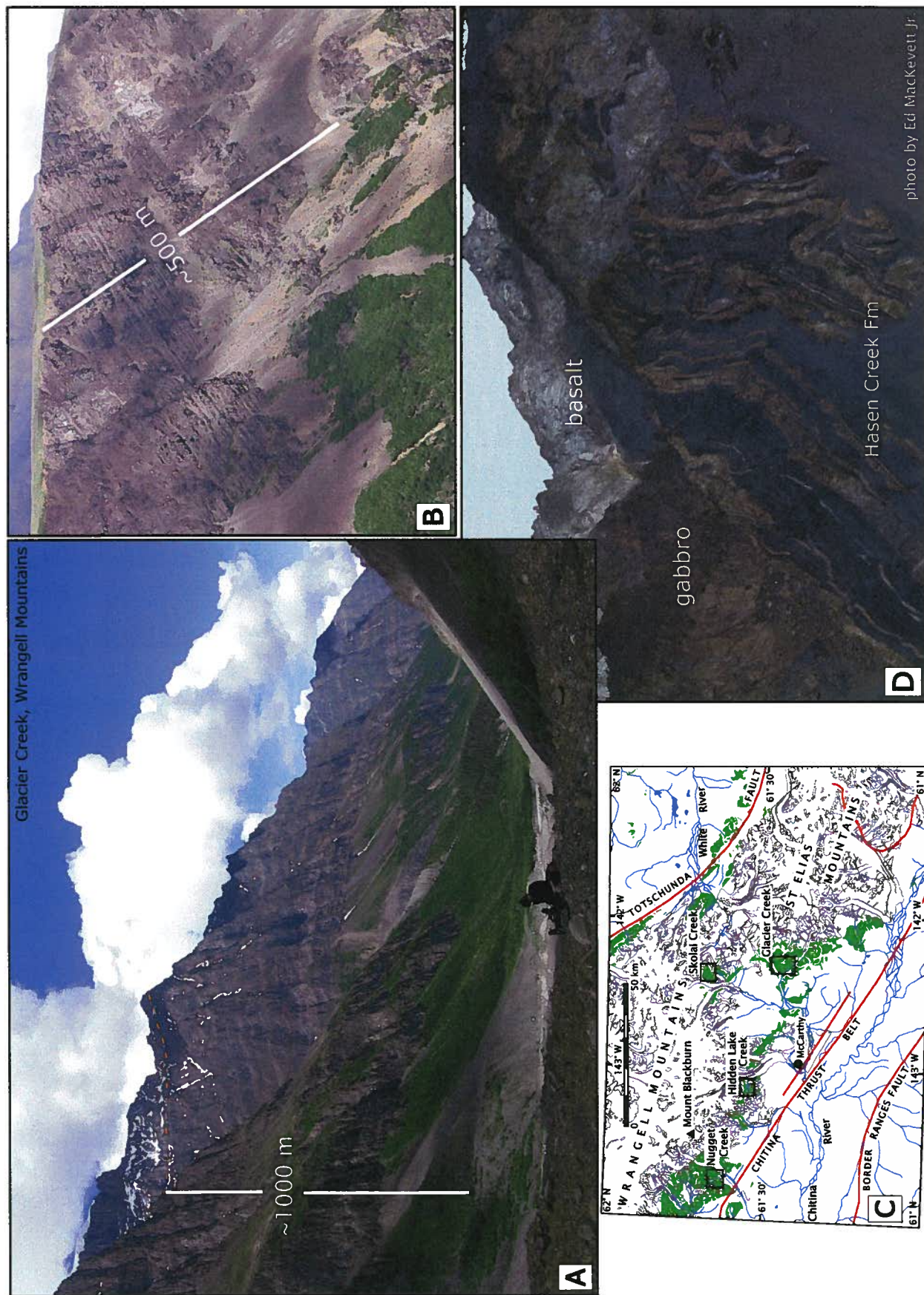


**Figure 5.7** Photographs of flood basalts in the Glacier Creek area in Wrangell-St. Elias National Park and map of the southern part of the Wrangell Mountains. (A) Photograph of ~1000 m of subaerial basalt flows overlain by Chitstone Limestone (dashed orange line indicates the contact). Flows appear as a layer-cake stratigraphy but may vary in thickness and locally appear to terminate. (B) Photograph of ~500 m of thin and thick basalt flows. (C) Simplified map showing the distribution of the Nikolai Formation (green) in the Wrangell Mountains, derived from Wilson *et al.* (2005). The four areas of field study are outlined with labeled boxes. (D) Photograph of Hasen Creek Formation intruded and deformed by gabbroic rocks related to the Nikolai Formation. Photograph by Ed MacKevett, Jr.



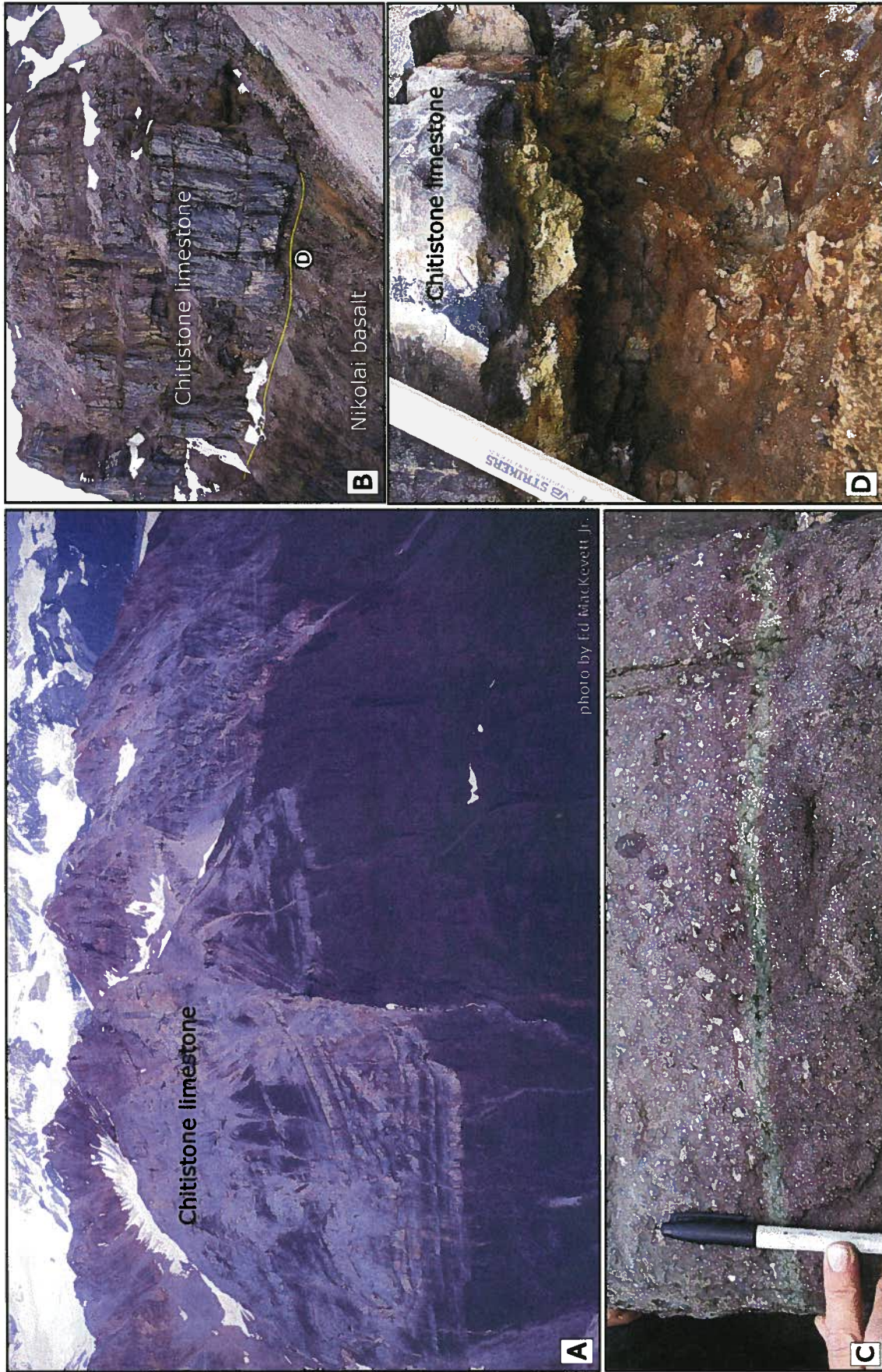


**Figure 5.8** Photographs of the top of the Nikolai Formation around Hidden Lake Creek in Wrangell-St. Elias National Park. (A) Photograph of the top of the Nikolai Formation and overlying Chitistone Limestone, taken by Ed MacKevett, Jr. Several faults offset the contact. (B) Close-up photograph of massive micritic limestone overlying the Nikolai basalts. Location of photo D shown. (C) Close-up photograph of a contact between subaerial flows in the upper Nikolai Formation. Marker (14 cm) for scale. (D) Cobbles (<10 cm long) along the contact between the Chitistone Limestone and Nikolai Formation. The oxidized cobbles are subangular, closely packed, aligned along their long axis, and are glomeroporphyritic basalt identical to the uppermost flows of the Nikolai Formation. Sledgehammer handle (4 cm wide) for scale.

exposed on the north side of Skolai Creek, where Paleozoic arc volcanic rocks of the Skolai Group form the lowest stratigraphic level exposed of Wrangellia in Alaska (MacKevett, 1978) (Figs 5.6 and 5.7). The type section of the Skolai Group north of Skolai Creek is ~2400 m thick (Smith and MacKevett, 1970; Fig. 5.6; Supplementary photo file). The Skolai Group consists of a basal volcanic flow member (~1200 m) and volcanoclastic unit (~750 m) comprising the Station Creek Formation, and a sedimentary package that includes the Hasen Creek Formation (~300 m) and the Golden Horn Limestone Lenticle (~250 m locally; Fig. 5.3). The transition between the lower flow and volcanoclastic members consists of interbedded lava flows and volcanoclastic beds (Smith and MacKevett, 1970). The Hasen Creek is a heterogeneous assemblage of chert, shale, sandstone, bioclastic limestone, and conglomerate, all with very little volcanic-derived material (Smith and MacKevett, 1970). The Golden Horn Limestone is bioclastic grainstone and packstone, locally with 75% of the clasts consisting of crinoid stems, and is also rich in bryozoans, brachiopods, foraminifera, and corals (Smith & MacKevett, 1970). In most places, the Golden Horn Limestone is unconformably overlain by Nikolai basalts with little discordance. In several areas, between the top of the Skolai Group and the base of the Nikolai, there is Middle Triassic argillite (<30 m thick) with fissile shale beds containing imprints of *Daonella* bivalves. Sills and discordant gabbroic intrusions related to the Nikolai occur within the Skolai Group, and sedimentary units of the Hasen Creek may be significantly deformed around these intrusions (MacKevett, 1978; Fig. 5.7; Supplementary photo file 2).

The Nikolai Formation in the Wrangell Mountains is estimated to be ~3.5 km in total thickness and is almost entirely subaerial flows (MacKevett, 1978). In several areas on the south side of the Wrangell Mountains a thin zone of interbedded flow-conglomerate, pillow breccia, and pillow basalt, typically less than 70 m thick, forms the lowest flow unit of the Nikolai (Fig. 5.6). The basal flow unit lies directly on shale and contains abundant subrounded pebble- and cobble-sized clasts derived from the Golden Horn Limestone and volcanic rocks of the underlying Skolai Group in a basalt-rich matrix (Fig. 5.6; Supplementary photo file 2). Contacts between the basal flow-conglomerate and overlying flows are mostly sharp, but locally conglomerate-rich beds



and basaltic lava are interbedded along the upper part of the basal flow unit (MacKevett, 1970).

The flood basalt stratigraphy forms continuous sections over 1000 m thick of monotonous sequences of massive amygdaloidal flows with few discernible features (Fig. 5.7). There are no interflow sediments or submarine volcanic features within the Nikolai in the Wrangell Mountains (except in the basal flow-conglomerate unit). Amygdules and clusters of plagioclase phenocrysts are typically the only distinguishing features within flows (Supplementary photo file 2).

A cumulative thickness of over 3.5 km of marine sedimentary rocks, which range in age from Late Triassic to Late Jurassic, overlie the Nikolai basalts. These marine sedimentary strata form impressive cliff-forming sequences in the Wrangell Mountains and the contact between the strongly contrasting black Nikolai basalts and the overlying white Chitistone Limestone is featured along many of the cliffs (Fig. 5.8; Supplementary photo file 2). Late Triassic to Early Jurassic limestone and shale successions above the Nikolai have been divided into three formations in the Wrangell Mountains, from oldest to youngest: Chitistone Limestone (350-600 m), Nizina Limestone (100-375 m), and McCarthy Formation (~900 m). The Chitistone disconformably overlies the Nikolai Formation and is gradational into the overlying Nizina Limestone. Faults commonly offset the contact between the uppermost basalt flows and the lowermost Chitistone Limestone; however, the top of the Nikolai is mostly a smooth flat surface (Fig. 5.8; Supplementary photo files). There are local occurrences of regolith between the top of the Nikolai and the base of the Chitistone (Fig. 5.8; Armstrong *et al.*, 1969). The carbonates in the lowermost 130 m of the Chitistone indicate deposition in a supratidal to intertidal environment and the stratigraphically higher parts of the Chitistone, up into the Nizina and McCarthy, indicate progressively deeper water marine deposition (Armstrong & MacKevett, 1977).

Wrangellia stratigraphy documented on the northern side of the Wrangell Mountains is similar to that in the southern Wrangell Mountains (Richter, 1976). The Eagle Creek Formation, which underlies the Nikolai basalts, is correlative with the Hasen Creek Formation on the south side of the Wrangell Mountains and has a richly fossiliferous Early Permian limestone member, similar to the Golden Horn Limestone

Lentil (Richter, 1976). Richter (1976) documented and mapped (Nabesna A3 and A4 quadrangles) extensive mafic sills intruding the Eagle Creek Formation which make up approximately 70 % of the section beneath the Nikolai basalts. Thin discontinuous lenses of shale and argillite containing imprints of Middle Triassic bivalve *Daonella* are found in several localities between the Eagle Creek and the base of the Nikolai. Richter (1976) describes a basal Nikolai flow unit that is discontinuous volcanic conglomerate-breccia containing fragments of basalt and sedimentary rock derived from the underlying Paleozoic formations. In one area on the north side of the Wrangell Mountains, Richter (1976) describes Permian limestone fragments incorporated in flows as large lenses and masses, up to hundreds of meters long, which may represent flow-rafted debris. The volcanic stratigraphy on the northern side of the Wrangell Mountains is also predominantly subaerial flows. Late Triassic limestone and shale overlying the Nikolai in the northern Wrangell Mountains are correlative with the Chitistone, Nizina, and McCarthy Formations on the south side of the Wrangell Mountains (Richter, 1976).

### **Wrangellia in southwest Yukon**

From the Nutzotin Mountains along the Alaska-Yukon border to southeast Alaska, Wrangellia forms a thin northwest- to southeast-trending belt in the southwest corner of Yukon (Figs 5.2 and 5.9). This belt is separated from several small discontinuous exposures of Wrangellia to the southwest by rocks of the Alexander Terrane (Figs 5.2 and 5.9). The best exposures of Wrangellia are in the Kluane Ranges, where the stratigraphy is similar in most aspects to stratigraphy in the Wrangell Mountains, and it has been described using the same nomenclature (Fig. 5.9; Muller, 1967; Read & Monger, 1976). The key difference between these two areas is that Wrangellia stratigraphy in Yukon is intensely folded and faulted, and the stratigraphic relationships are commonly difficult to determine. Discontinuous sections of Wrangellia stratigraphy exposed south of the Kluane Ranges have limited exposures of Nikolai basalts.

Paleozoic arc volcanic and marine sedimentary rocks of the Skolai Group are the oldest units of Wrangellia in Yukon (Fig. 5.9). The Skolai Group consists of lower flow and upper volcanoclastic members of the Station Creek Formation conformably overlain

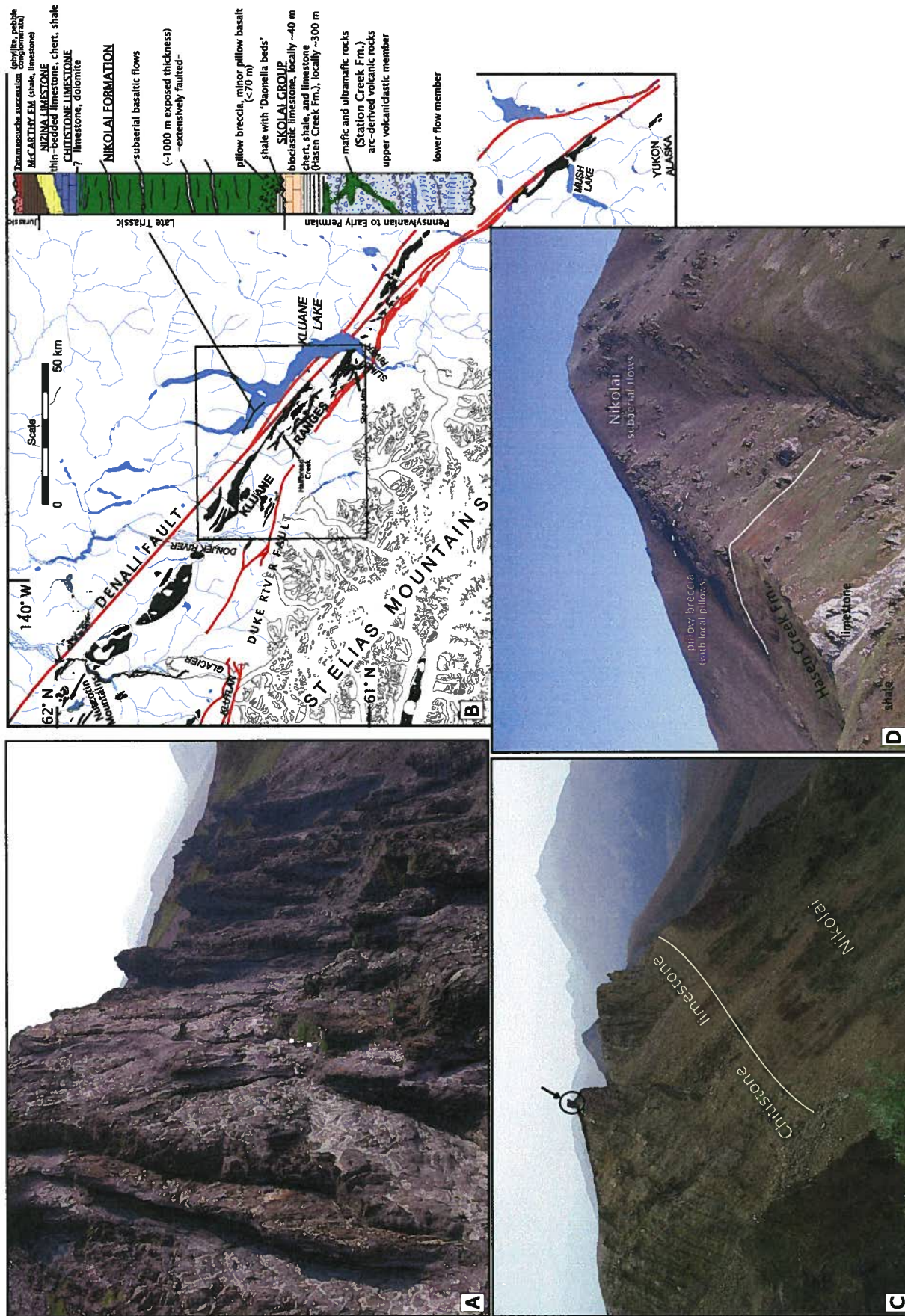


**Figure 5.9** Photographs and map of the Nikolai Formation in southwest Yukon. (A) Vertically-oriented subaerial flows (<10 m thick) in the Kluane Ranges. Dall sheep (white dots) in center of photograph for scale. (B) Simplified map of southwest Yukon showing the distribution of the Nikolai Formation (black; after Israel, 2004; Israel & Van Zeyl, 2004; Israel *et al.*, 2005). Stratigraphic column for Kluane Ranges derived from Read & Monger (1976) Israel *et al.* (2006), Israel & Van Zeyl (2005), and fieldwork. (C) Nikolai Formation overlain by Chitstone Limestone with Donjek River valley in far background. Dave Van Zeyl in center of photograph for scale. (D) Photograph of base of flood basalts in Wellgreen area, with Hasen Creek Formation overlain by pillow breccia and subaerial basalt flows of the Nikolai Formation.

by sedimentary units of the Hasen Creek Formation, similar to those described by Smith and MacKevett (1970) in the Wrangell Mountains. Numerous mafic and ultramafic intrusions related to the Nikolai basalts intrude the Skolai Group in Yukon (Carne, 2003). Several occurrences of thin lenses of alternating beds of argillite, siltstone, and sandstone containing Middle Triassic *Daonella* imprints underlie the Nikolai Formation (Read & Monger, 1976). The Middle Triassic unit is very similar to the underlying Hasen Creek Formation and the presence of the *Daonella* is the only discerning characteristic between the two units.

Everywhere in the Kluane Ranges where Middle Triassic sedimentary rocks have been identified they are overlain by a conglomerate and breccia unit assigned to the base of the Nikolai Formation (Read & Monger, 1976; Israel & Cobbett, 2008). The lithological character of the conglomerate/breccia unit is highly variable, ranging from clast supported boulder and pebble conglomerate to matrix supported cobble and pebble breccia. The clasts are primarily derived from the underlying Skolai Group and include the whole spectrum of volcanic and sedimentary rocks observed in the underlying units. Rounded to sub-rounded boulders and pebbles of augite and plagioclase phyric basaltic andesite and lithic tuffs of the Station Creek Formation are common, as are subrounded to subangular mudstone, siltstone and cherty pebbles from the Hasen Creek Formation. The basal conglomerate/breccia and the underlying Middle Triassic sedimentary units are laterally discontinuous and they are bound by faults in several localities (Read & Monger, 1976; Israel & Cobbett, 2008). These structures are interpreted as laterally discontinuous grabens associated with uplift or rifting during the initial stage of Nikolai volcanism.

The Nikolai Formation, in southwest Yukon, includes a marine basal flow unit overlain by a thick succession of dominantly subaerial flows capped by a shallow submarine flow unit. The basal flow unit is predominantly pillow breccia with occurrences of pillow basalt, which is less than 100 m thick (Greene *et al.*, 2005; Israel *et al.*, 2006). The volcanic stratigraphy in Yukon is ~1 km in total thickness. The subaerial flows (1-10 m thick) are strongly amygdaloidal in zones and are dominantly maroon to olive green. Local thin tuffs and breccias have been reported within the volcanic stratigraphy. In numerous locations within the uppermost portions of the Nikolai Formation, limestone and argillite are interbedded with basalt flows. These thin,

discontinuous beds are usually less than 1 meter thick, but locally as thick as 30 m. Microfossils collected from the interbedded limestone units yield a Late Carnian to Late Norian age (Read and Monger, 1976; Israel *et al.*, 2006).

Above the highest stratigraphic flows, massive limestone, including horizons of gypsum, dominates the stratigraphy. The limestone and gypsum are correlatives to the Chitistone Limestone described by MacKevett (1971, 1978) in the Wrangell Mountains. The limestone is often brecciated near the base and includes large blocks of the underlying basalt. The Chitistone Limestone ranges from hundreds of meters thick to less than 10 m thick as discontinuous lenses. Macrofossils are extremely rare in the Chitistone Limestone; however, there are abundant microfossils that yield Late Norian ages (Read & Monger, 1976; Israel & Van Zeyl, 2005). Conformably overlying the Chitistone Limestone is a Late Triassic to Early Jurassic, thinly-bedded argillite and limestone unit assigned to the McCarthy Formation. The McCarthy Formation is easily identifiable in outcrop by alternating light and dark grey calcareous and carbonaceous beds. Abundant macrofossils from the calcareous beds give Late Norian ages (Read & Monger, 1976). An Early Jurassic age for the uppermost McCarthy Formation is suggested by the presence of ammonite-bearing horizons.

### **Wrangellia in southeast Alaska**

Triassic basaltic and sedimentary rocks with similarities to Wrangellia sequences in southern Alaska are exposed in several areas of southeast Alaska (Fig. 5.10). Most of these sequences occur as elongate fault-bound slivers within a large and complex fault system. Not all of these sequences are definitively established as part of Wrangellia. Most of these sections occur within the Alexander Terrane.

Two areas in the northern part of southeast Alaska with thick Triassic basalt sequences (Chilkat Peninsula, Chichagof and Baranof Islands) are probably correlative with Wrangellia flood basalts in southern Alaska (Fig. 5.10). The Chilkat Peninsula area contains Triassic metavolcanic sequences that form a thin (<5 km wide) belt northwest and southeast of Haines, Alaska, along the east side of the Chilkat River and on the Chilkat Peninsula (Plafker & Hudson, 1980) (Fig. 5.10). These Triassic basaltic sequences are steeply dipping and are approximately 3000 m in total thickness (Plafker



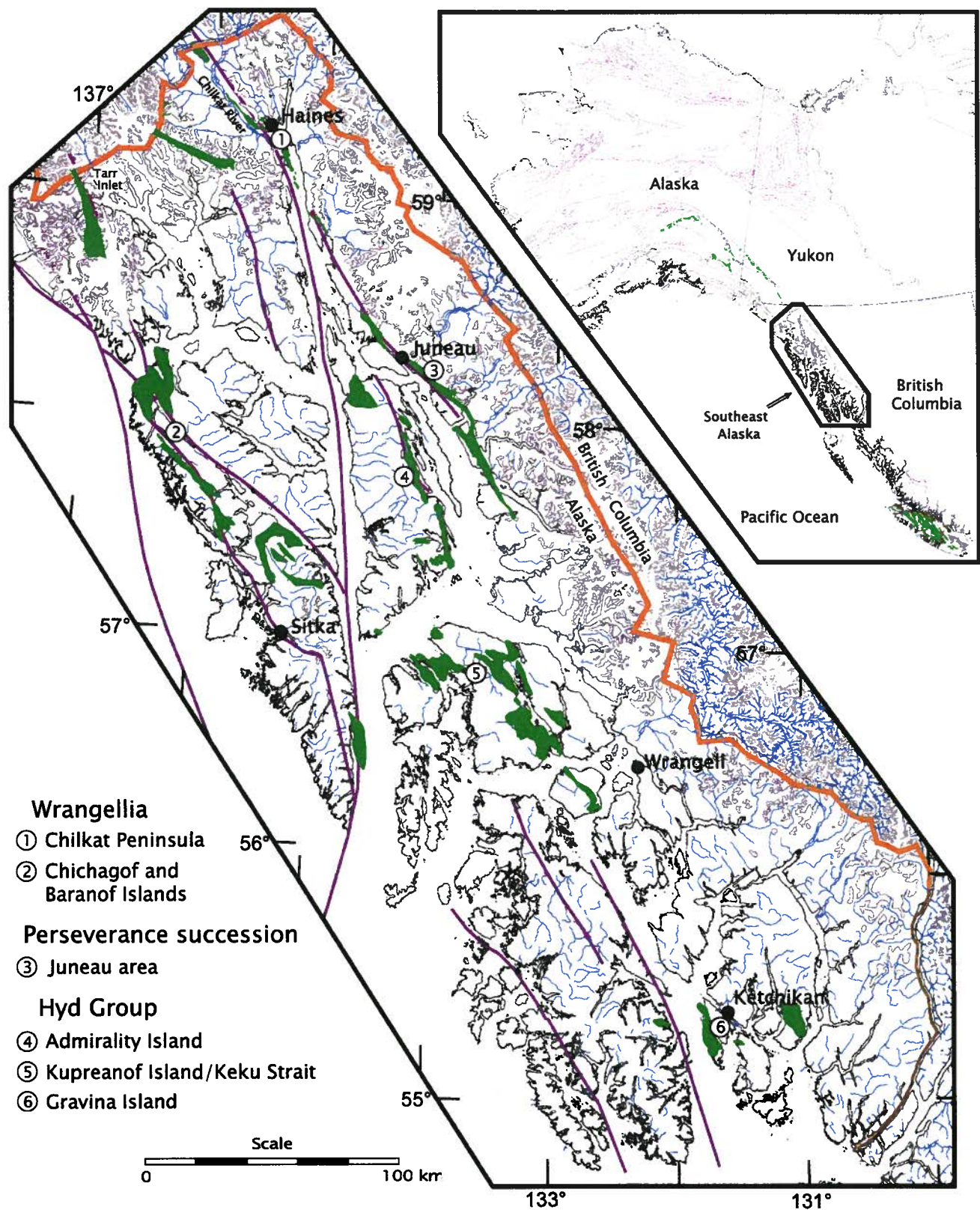


**Figure 5.10** Simplified map of southeast Alaska showing the distribution of Triassic basalts which may be correlative with Wrangellia flood basalts. Most of these basalts are in the Alexander Terrane. Orange line is Alaska-BC border. Purple lines are faults. See text for description of units. Map adapted from a map provided courtesy of Brew (written comm., 2007). Inset shows location of map in northwestern North America.

and Hudson, 1980). The metabasalt flows are primarily massive layered amygdaloidal flows with local occurrences of pillow basalt, pillow breccia, and tuff (Plafker and Hudson, 1980). The base of the basaltic sequence is not exposed, but a 300-400 m-thick section in the upper part of the stratigraphy contains abundant pillowed flows and breccia, locally with thin (<1 m) lenses of limestone (Plafker *et al.*, 1989a). Diagnostic Late Carnian macrofossils (Ammonites and Bivalves) occur just above the top of the basalt sequence in overlying limestone (Plafker *et al.*, 1989a). The basalt is overlain by ~1700 m of mostly limestone, carbonaceous argillite, siltstone, and volcanic sandstone (Plafker and Hudson, 1980). These sedimentary sequences are slightly different than the inner-platform carbonate rocks overlying Nikolai basalts in the Wrangell Mountains (Plafker and Hudson, 1980). Late Triassic radiolarians from the overlying sequences on Chilkat Peninsula are identical to species found above Wrangellia flood basalts in the Queen Charlotte Islands (Plafker *et al.*, 1989b). A thin belt of metabasalt northwest and southeast of Juneau, Alaska, is also lithologically and geochemically similar to Wrangellia flood basalts and may be a continuation of the belt on the Chilkat Peninsula (Fig. 5.10; Gehrels & Barker, 1992).

The stratigraphy on Chichagof and Baranof Islands, which is similar to Wrangellia, may also extend northward along the west side of Tarr Inlet (Decker, 1981; Fig. 5.10). The metabasalt in this area, called the Goon Dip Greenstone, is mostly massive subaerial flows (<1000 m in total thickness) with local pillows (Decker, 1981). The Goon Dip is lithologically and geochemically similar to the Nikolai basalts in the Wrangell Mountains (Decker, 1981). The Goon Dip is overlain by Whitestripe Marble, similar to the Chitistone Limestone in the Wrangell Mountains, but no age-diagnostic fossils have been found in the uppermost Goon Dip or Whitestripe Marble (Decker, 1981).

Metabasaltic sequences of Triassic age, with underlying Paleozoic and overlying Late Triassic sedimentary sequences, are found in several other areas of southeast Alaska (Brew, 2007, written comm.; Fig. 5.10). These areas are believed to be within the Alexander Terrane and they may not be correlative with Wrangellia stratigraphy. These units belong to the Hyd Group, mainly exposed on Admiralty, Kupreanof Islands and other assorted islands, and the Perseverance succession of Brew (written comm., 2007)

(Fig. 5.10). The Hyd and Perseverance volcanic rocks contain Triassic basalt ranging from pillow lava, breccia, and tuff to massive flows (Brew, 2007, written comm.), but most of the Hyd Group is non-volcanic (Loney, 1964; Muffler, 1967). Basalt sequences do not exceed 600-700 m in thickness and are more variable and heterogeneous in composition than flood basalt stratigraphy in the main portions of Wrangellia. The basalts are Late Triassic in age and the only fossils associated with the basalts are Early and Middle Norian; Early Norian rocks underlie the basalts and Late Norian rocks overlie them (Muffler, 1967; Katvala & Stanley, 2008, in press). A variety of thin (<200 m) limestone and calcareous clastic sedimentary rocks with Late Carnian and Norian fossils have been found associated with some of the metabasalts in southeast Alaska (Brew, 2007, written comm.).

#### **Wrangellia in the Queen Charlotte Islands (Haida Gwaii)**

Wrangellia stratigraphy forms a large part of the southern Queen Charlotte Islands and is very similar to Wrangellia stratigraphy on Vancouver Island (Fig. 5.2). Permian chert, carbonate, and volcanoclastic rocks form the deepest level of exposure of Wrangellia stratigraphy (Hesthammer *et al.*, 1991; Lewis *et al.*, 1991). The Paleozoic marine sequences are overlain by flood basalts of the Karmutsen Formation, but the base of the Karmutsen is not exposed in the Queen Charlotte Islands. The Karmutsen Formation in the Queen Charlotte Islands is similar to basalt stratigraphy on Vancouver Island; however, a section of ~4300 m of Karmutsen basalts measured by Sutherland-Brown (1968) consisted of 95 % submarine flows, with a ratio of pillow basalt to fragmental basalt of ~8:2. Rare occurrences of shale and lenses of tuffaceous crinoidal limestone (<30 m thick), grading between limestone and lapilli tuff, occur in the lowest exposed part of the Karmutsen Formation (Sutherland-Brown, 1968).

The Karmutsen Formation is overlain by Late Triassic and Early Jurassic marine limestone and sedimentary rocks of the Kunga and Maude groups (Lewis *et al.*, 1991). Limestone lenses (1-60 m thick), similar to the overlying Kunga limestone, are locally overlain by tuff in the upper part of the Karmutsen Formation along discontinuous horizons (Sutherland-Brown, 1968). Local interfingering of flows and limestone also occurs in the lowest part of the overlying Kunga Group of Sutherland-Brown (1968). The

Kunga Group contains identical fossils and is lithologically indistinguishable from the micritic Quatsino limestone which overlies Karmutsen basalts on Vancouver Island (Sutherland-Brown, 1968).

### **Wrangellia on Vancouver Island**

Northern and central Vancouver Island is underlain by Wrangellia stratigraphy which forms the uppermost sheet of a thick sequence of northeast-dipping thrust sheets that constitute the upper crust of Vancouver Island (Fig. 5.11; Monger & Journeay, 1994; Yorath *et al.*, 1999). The cumulative thickness of Wrangellia stratigraphy exposed on Vancouver Island is more than 10 km (Yorath *et al.*, 1999). Wrangellia lies in fault contact with the Pacific Rim Terrane and West Coast Crystalline Complex to the west, and is intruded by the predominantly Cretaceous Coast Plutonic Complex to the east (Wheeler & McFeely, 1991). Most of the structures and contacts between units on Vancouver Island are northwest-trending. Two prominent northwest- to southeast-trending anticlinoria (Buttle Lake and Cowichan anticlinoria) are cored by Paleozoic rocks, which are not exposed on northern Vancouver Island (Fig. 5.11; Brandon *et al.*, 1986; Yorath *et al.*, 1999). Jurassic and Cretaceous sedimentary strata overlap Wrangellia stratigraphy on parts of Vancouver Island (Muller *et al.*, 1974).

### ***Central and Southern Vancouver Island***

The deepest levels of Wrangellia stratigraphy, mostly exposed in the Buttle Lake and Cowichan anticlinoria, comprise the lower to middle Paleozoic Sicker Group and the upper Paleozoic Buttle Lake Group (Fig. 5.11). The Devonian to Mississippian Sicker Group consists of volcanics, volcanoclastics, and minor chert (Brandon *et al.*, 1986; Massey & Friday, 1988; Yorath *et al.*, 1999). The overlying Mississippian Buttle Lake Group comprises chert, argillite, and limestone, and Pennsylvanian to Permian limestone, argillite, and chert overlain by minor clastics (Yole, 1969; Brandon *et al.*, 1986; Massey & Friday, 1988; Yorath *et al.*, 1999). The Buttle Lake Group overlies the Sicker Group with some conformable contacts and is unconformably overlain by Triassic strata of the Vancouver Group (Karmutsen and Quatsino formations; Massey and Friday, 1988; Yorath *et al.*, 1999; Nixon and Orr, 2007). The combined total thickness of the Sicker



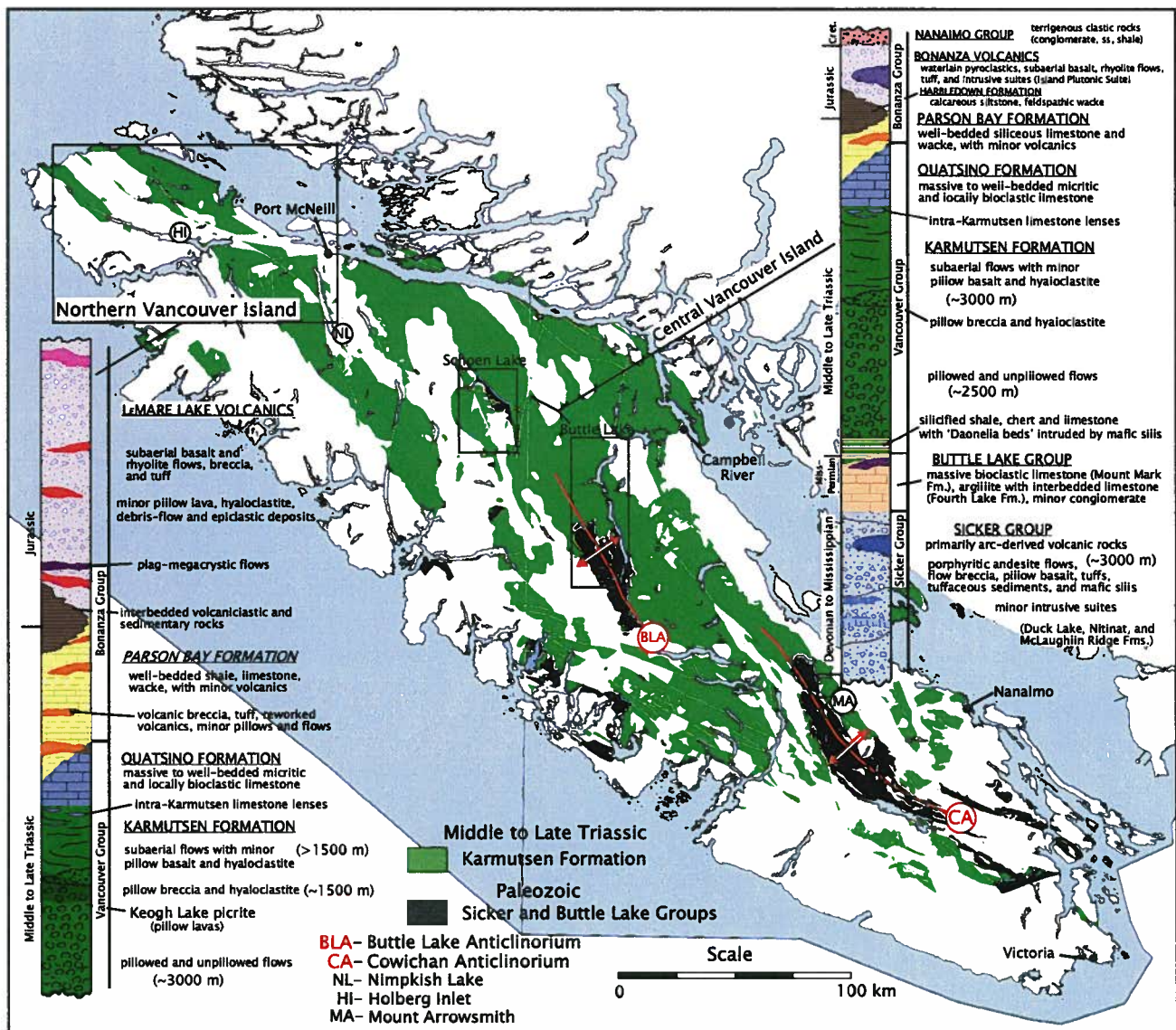


**Figure 5.11** Simplified map of Vancouver Island showing the distribution of the Karmutsen Formation (green) and underlying Paleozoic formations (black; after Massey *et al.*, 2005a, b). The main areas of field study are indicated with boxes or circles with capital letters (see legend). Stratigraphic columns are shown for northern and central Vancouver Island. Column for northern Vancouver Island adapted from Nixon & Orr (2007). Column for central Vancouver Island is derived from Carlisle (1972), Juras (1987), Massey (1995), and from fieldwork.

and Buttle Lake Groups is estimated to be ~5000 m (Massey, 1995; Yorath *et al.*, 1999; Fig. 5.11).

The oldest known rocks on Vancouver Island are pillowed and massive basalt flows of the Devonian Duck Lake Formation (Sicker Group). The Duck Lake Formation is conformably overlain by Upper Devonian interbedded andesitic volcanic and volcanoclastic strata of the Nitinat and McLaughlin Ridge Formations (Massey, 1995). The Buttle Lake Group contains three units (Fourth Lake, Mount Mark, and St. Mary Lake formations) which crop out across Vancouver Island in association with the Sicker Group (Fig. 5.11). The Fourth Lake Formation (Cameron River Formation of Massey & Friday, 1988) is the lowest and contains mostly thin-bedded, commonly cherty sediments including chert, argillite, possible tuffs, siltstones, volcanic sandstones and minor breccia at the base (Massey & Friday, 1988; Yorath *et al.*, 1999). The overlying Mount Mark Formation either conformably overlies and laterally interfingers with the Fourth Lake Formation or unconformably overlies the Sicker Group (Massey & Friday, 1988; Yorath *et al.*, 1999). This formation comprises massive bioclastic limestone beds dominated by crinoid clasts (<2 cm across), with minor argillite and chert interbeds (Yole, 1969; Massey & Friday, 1988; Yorath *et al.*, 1999; Katvala & Henderson, 2002). The Mount Mark and Fourth Lake Formations may alternate in vertical sections as laterally adjacent facies throughout the entire Pennsylvanian to Early Permian succession (Katvala & Henderson, 2002), although the traditional definitions (Massey and Friday, 1988; Yorath *et al.*, 1999) are maintained in this paper for consistency. The St. Mary Lake Formation comprises sandstone, argillite, conglomerates, and chert that conformably overlie the Mount Mark Formation (Massey & Friday, 1988; Yorath *et al.*, 1999). Exposures of the St. Mary Lake Formation are rare and generally removed by the sub-Triassic unconformity (Massey & Friday, 1988). Conodonts indicate Mississippian to Permian ages in the Buttle Lake Group (Orchard fide Brandon *et al.*, 1986; Henderson & Orchard, 1991; Katvala & Henderson, 2002). Paleontologic age determinations can be found in Supplemental data table 5. The upper parts of the Buttle Lake Group (Mount Mark Formation) are commonly intruded by mafic sills related to the Karmutsen basalts (Massey, 1995; Yorath *et al.*, 1999).

The Karmutsen Formation covers large areas of central Vancouver Island, where it forms an emergent oceanic plateau sequence (~6 km). On central Vancouver Island, the base and lower parts of the volcanic stratigraphy are well-exposed in three general areas (Buttle Lake and Cowichan anticlinoria, and the Schoen Lake area; Fig. 5.11). In each of these areas, thick sediment-sill complexes occur at the base of the Karmutsen basalts, which unconformably overlie Buttle Lake Group limestone and Middle Triassic sedimentary strata.

In the Schoen Lake area, a sediment-sill complex and each of the three subdivisions of the Karmutsen Formation (pillow basalt, pillow breccia and hyaloclastite, and subaerial flows) are preserved (Fig. 5.12). Massive mafic sills intrude siltstone, chert, and interbedded limestone with Middle Triassic *Daonella* occurring near the top of the unit. The sediment-sill complex is approximately 1000 m thick and sedimentary layers between the sills range from 1 to 60 m thick. The sills commonly deform and envelop sediments along contacts (Carlisle, 1972; Fig. 5.12; Supplementary photo file 5). The sediment-sill complex is overlain by a thick succession (~2000 m) of pillow basalt (Supplementary photo file 5). Some of the lowest pillowed flows contain sediment in pillow interstices, which is absent higher in the volcanic stratigraphy (Carlisle, 1972).

The volcanic stratigraphy around Buttle Lake is proposed to be the type section for the Karmutsen Formation because close to a complete stratigraphic section (~6000 m thick) is preserved (Yorath *et al.*, 1999; Fig. 5.13; Supplementary photo file 5). Basal sills and lower pillowed flows are well-exposed and accessible on the east side of Buttle Lake (Fig. 5.13). Permian limestone of the Buttle Lake Group (90-120 m thick) on the west side of Buttle Lake is intruded by Karmutsen sills and overlain by pillow lavas (Fig. 5.13). The lower part of the submarine strata at Buttle Lake is intruded by mafic sills 30-40 m thick (Surdam, 1967). Pillowed flows contain large-diameter pillows (1-4 m) and sediments are rarely present between flows.

Above the submarine flows at Buttle Lake are <1500 m of pillow breccia and hyaloclastite and over 2000 m of massive subaerial flows (Surdam, 1967). Marine fossils were found at one locality within the pillow breccia in the lower part of the Karmutsen (Surdam, 1967). The lower part of the subaerial flow member contains thinner flows than the upper part. The upper parts of the Karmutsen Formation around Buttle Lake contain



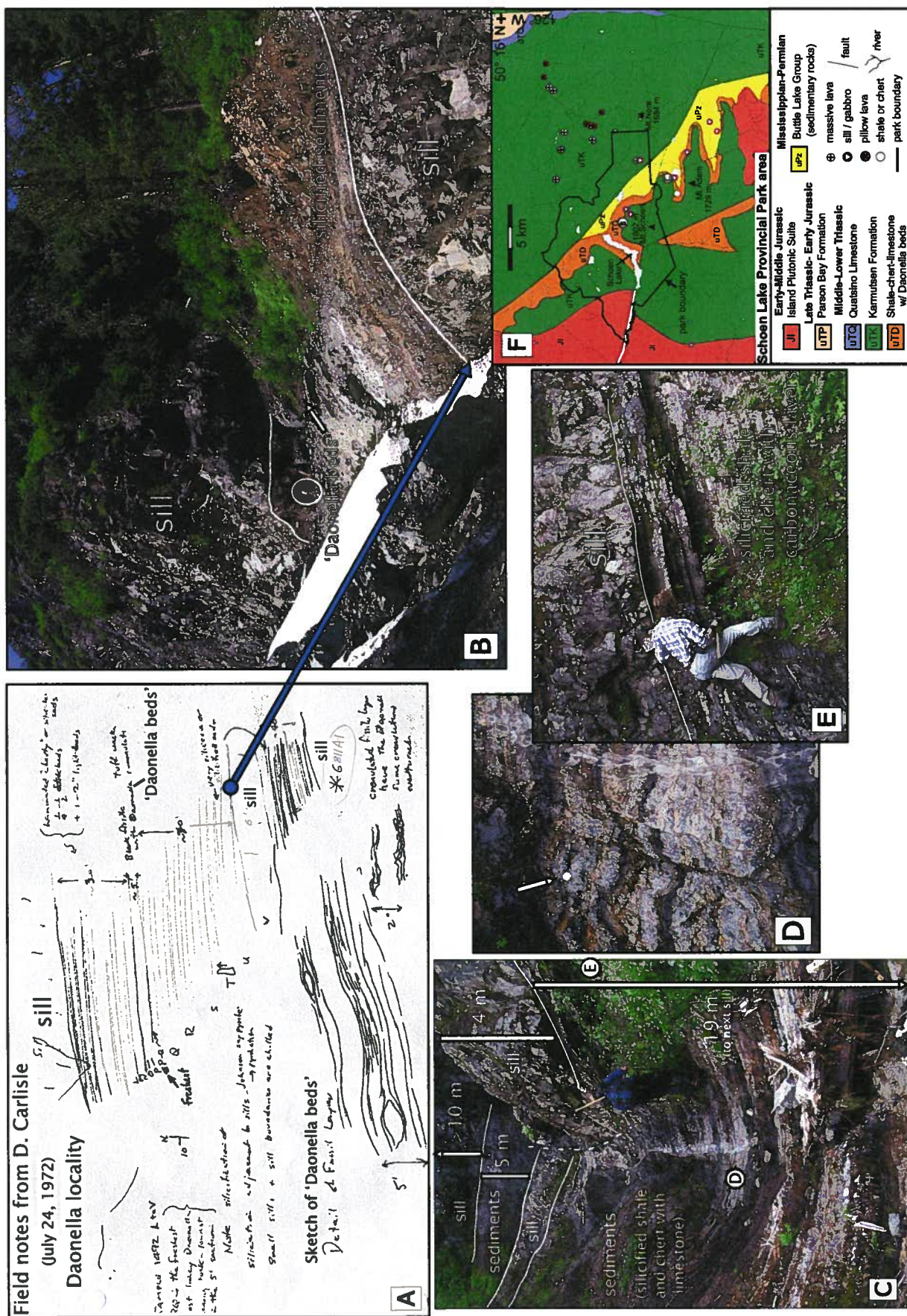


**Figure 5.12** Field notes, photographs, and geologic map for the Schoen Lake area, Vancouver Island (location shown in Figure 5.11). (A) Field notes courtesy of Don Carlisle, taken at the *Daonella* fossil locality within the sediment-sill complex on the north side of Mount Schoen. (B) Photograph of *Daonella* locality depicted by field notes in A. (C) Silicified shale and chert with carbonaceous layers interbedded with mafic sills. (D) Deformed chert with carbonaceous layers (location of photo shown in A). (E) Contact between sill and sedimentary sequences (location of photo shown in C). (F) Generalized geology for the Schoen Lake area with photograph and sample locations. Map derived from Massey *et al.* (2005a).



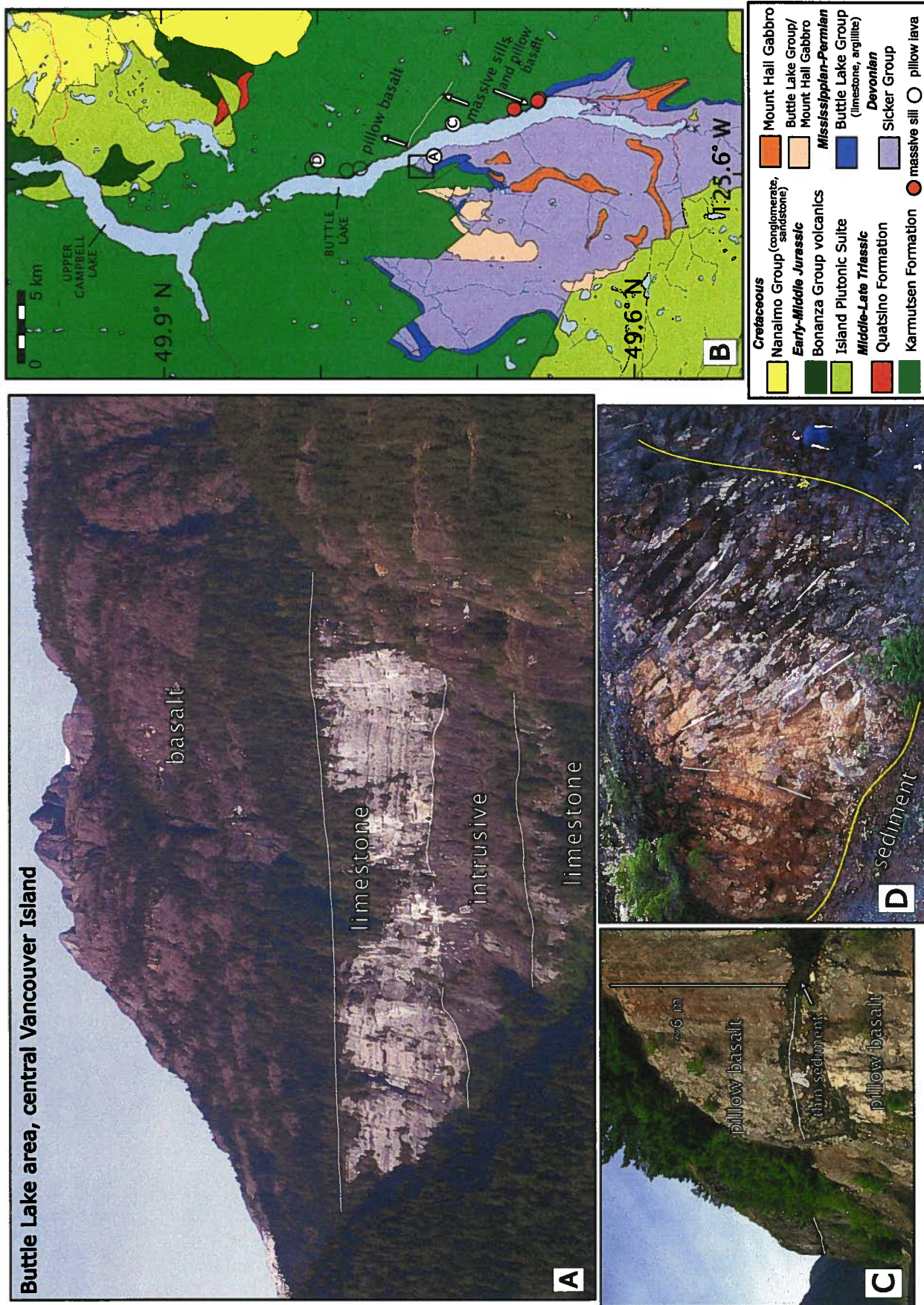


**Figure 5.13** Generalized geology and photographs of Buttle Lake area, Vancouver Island. (A) Photograph of contact between limestone of the upper Paleozoic Buttle Lake Group intruded by mafic sills, related to Karmutsen basalts, and overlain by pillow basalt. (B) Geologic map of the Buttle Lake area showing locations of photographs. Map derived from Massey *et al.* (2005a). (C) Photograph of contact between two pillowed flows with thin sediment layer along the contact. (D) Photograph of an unpillowed flow in the submarine section with radially-oriented columnar jointing and shale (<1 m thick) along the base.

discontinuous alternations of pillow basalt, pillow breccia, and hyaloclastite typically <30 m thick, but a single, more widespread subaqueous unit is 1-120 m thick (Surdam, 1967). This subaqueous section overlies limestone and tuff up to 30 m thick (Surdam, 1967).

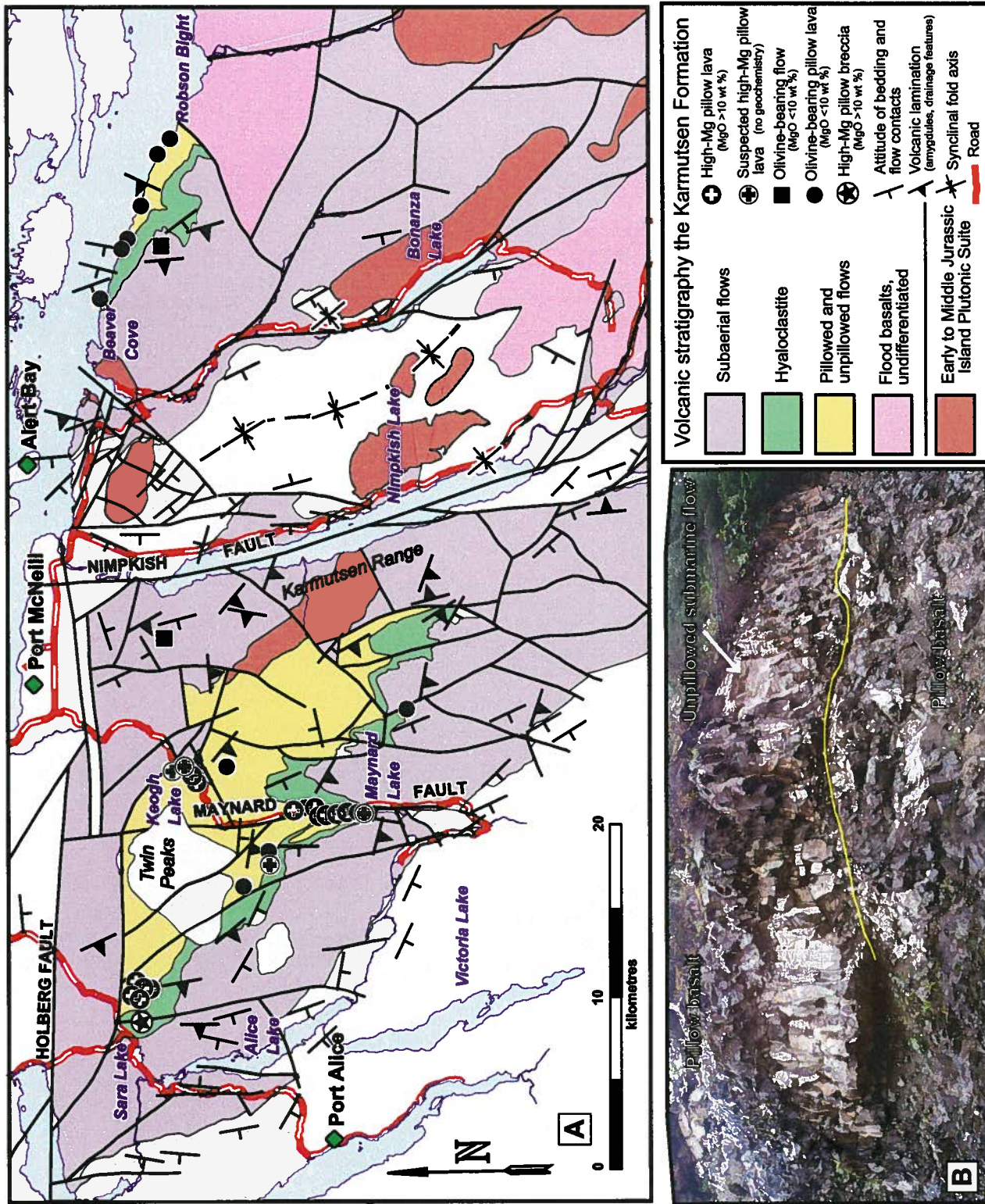
The overlying Quatsino limestone at Buttle Lake lies directly on a Karmutsen basalt flow (Surdam, 1967); however, occurrences of paleosols between the Karmutsen and Quatsino Formations have been reported elsewhere on central Vancouver Island (Yorath *et al.*, 1999). Evidence of molding of limestone around basalt and disaggregation of limestone lenses during interaction with basalt flows is described by Surdam (1967). The basal part of the Quatsino Formation west of Buttle Lake is intercalated with pillow basalt in several areas (Surdam, 1967).

### *Northern Vancouver Island*

Stratigraphy on northern Vancouver Island extends from Middle to Late Triassic flood basalts (lower part of Karmutsen Formation) up through Middle Jurassic arc volcanics (Fig. 5.11). This sequence of lithostratigraphic units is divided into the Vancouver Group and the Bonanza Group (Parson Bay Formation, Volcaniclastic-sedimentary unit, and LeMare Lake volcanics; Muller *et al.*, 1981; Nixon *et al.*, 2006c; Nixon and Orr, 2007; Fig. 5.11). The base of the Karmutsen basalts is not exposed on northern Vancouver Island.

Recent mapping on part of northern Vancouver Island has established a three-part volcanic stratigraphy of pillowed lava sequences, hyaloclastite, and subaerial flows. The stratigraphy has established a structural and stratigraphic framework for volcanic stratigraphy (Nixon *et al.*, 2008; Fig. 5.14). The lower pillowed lava sequence is approximately 3000 m thick and contains closely-packed pillowed flows and unpillowed flows. The unpillowed flows typically have lensoidal geometry, convolute lower contacts with underlying pillowed flows, and rarely exhibit irregular, hackly columnar jointing (Fig. 5.14). Interpillow voids are rarely filled with non-volcanic sediment and display a variety of submarine volcanogenic features (Fig. 5.14). The hyaloclastite unit is estimated to vary in thickness from approximately 1550 m in the west to less than 400 m in the Maynard Lake area (Nixon *et al.*, 2008). The hyaloclastite is predominantly poorly-sorted clasts of pillow basalt in a finely-comminuted matrix of basaltic shards, fragments, and





pillow rinds. The hyaloclastite and pillow breccia is composed of a matrix of dark brown, variably palagonatized shards of devitrified basaltic glass with clasts of pillow fragments. Well-bedded basaltic sandstone occurs locally and exhibits soft-sediment deformation features (Nixon *et al.*, 2008). High-Mg picritic pillow lavas have been identified in the lower part of the Karmutsen Formation (Greene *et al.*, 2006; Nixon *et al.*, 2008). Recent mapping and geochemistry of the internal stratigraphy place the high-Mg lavas in the upper part of the submarine section, near the transition between the pillowed lavas and the overlying hyaloclastite unit (Nixon *et al.*, 2008).

The subaerial flow unit appears conformable with the underlying hyaloclastite unit and is approximately 1500 m thick (Nixon *et al.*, 2008). The subaerial flow sequences have a well-layered, sheet-like appearance. The subaerial flows vary in flow thickness, grain size ( $\leq 5$  mm), and proportion of amygdules, and they rarely exhibit columnar jointing and paleosols are absent between flows. Interflow sedimentary lenses are found mostly near the top of the subaerial flow unit and are commonly associated with pillowed flows and hyaloclastite. Most of these interflow lenses consist of limestone, but rarely comprise siliciclastic sediments (Carlisle and Suzuki, 1974; Nixon *et al.*, 2006; Fig. 5.15). Carlisle and Suzuki (1974) describe small-scale emergent sequences ( $<30$  m thick) of pillow basalt, pillow breccia and hyaloclastite, and massive flows which overlie some limestone lenses. Some of these lenses contain Late Carnian fossil assemblages identical those found in the overlying Quatsino limestone (Carlisle and Suzuki, 1974). Some subaerial flows near the top of the Karmutsen Formation contain abundant (20-40 %) aligned plagioclase megacrysts (1-2 cm laths), and these can be used as stratigraphic markers (Nixon *et al.*, 2006, 2007; Fig. 5.13).

The relationship between the top of the Karmutsen flood basalts and the base of the overlying Quatsino limestone is a sharp, flat-lying contact with minimal evidence of erosion (Fig. 5.16; Supplementary photo file 5). Locally, a thin ( $<25$  cm) layer of brownish-orange basaltic siltstone and sandstone is preserved along the contact (Fig. 5.16). The thin beds of calcareous siltstone grade laterally into limestone.

The overlying Quatsino limestone varies in thickness (40-500 m) and age (Carnian to Early Norian) across northern Vancouver Island (Muller *et al.*, 1981; Nixon *et al.*, 2006, 2007, 2008). The Quatsino Formation immediately above the Karmutsen is



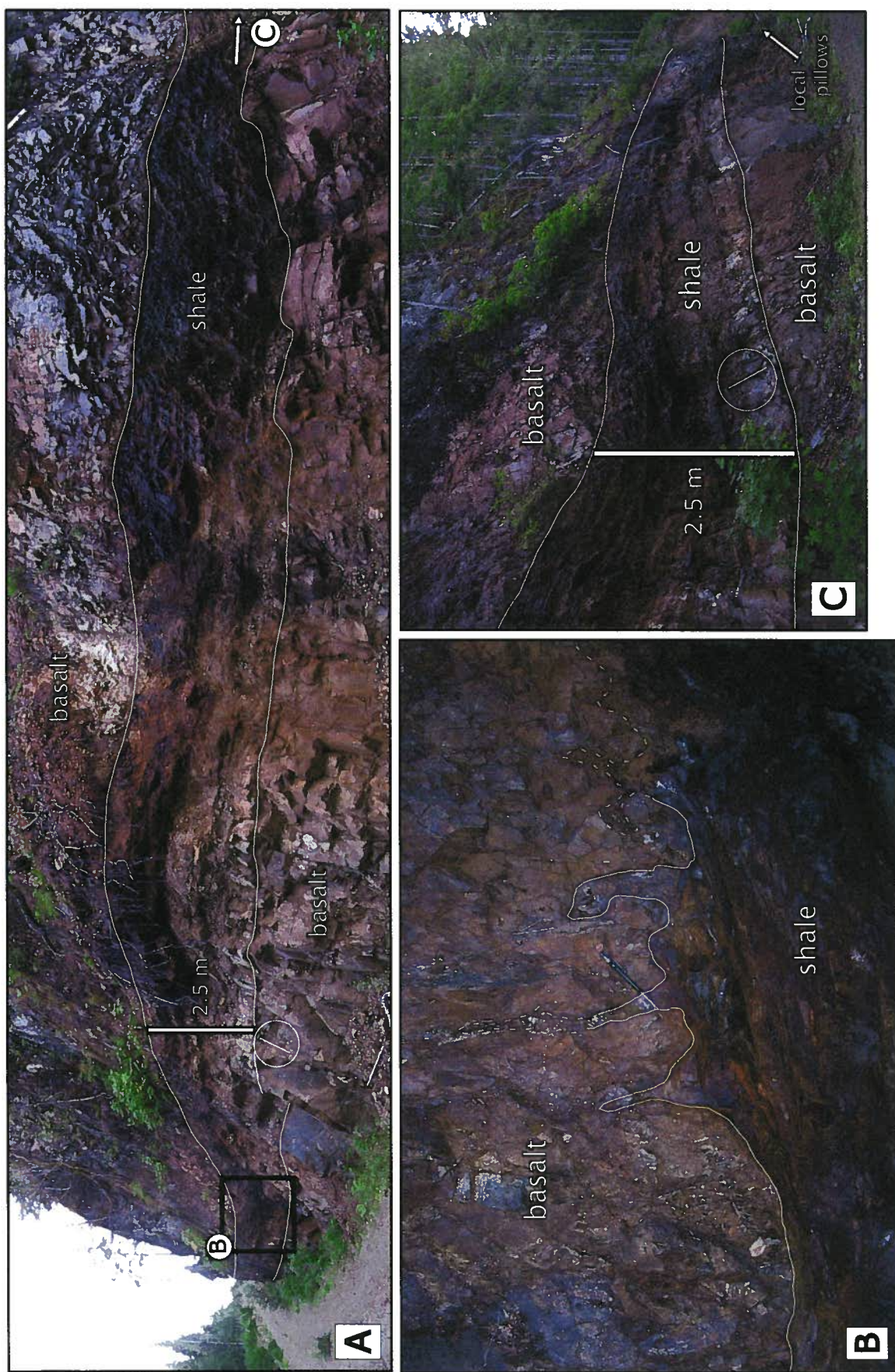


**Figure 5.15** Photographs of intra-Karmutsen sedimentary lens near the top of the Karmutsen southwest of Nimkish Lake, northern Vancouver Island (location shown in Figure 5.11). (A) Panoramic photograph of lens of shale between two unpillowed flows. Circled sledgehammer for scale. (B) Deformed shale with dewatering structures along the top of the lens (location shown in photo A). (C) Photograph of right side of lens, just to the right edge of A. Local pillow basalt occurs along the base.



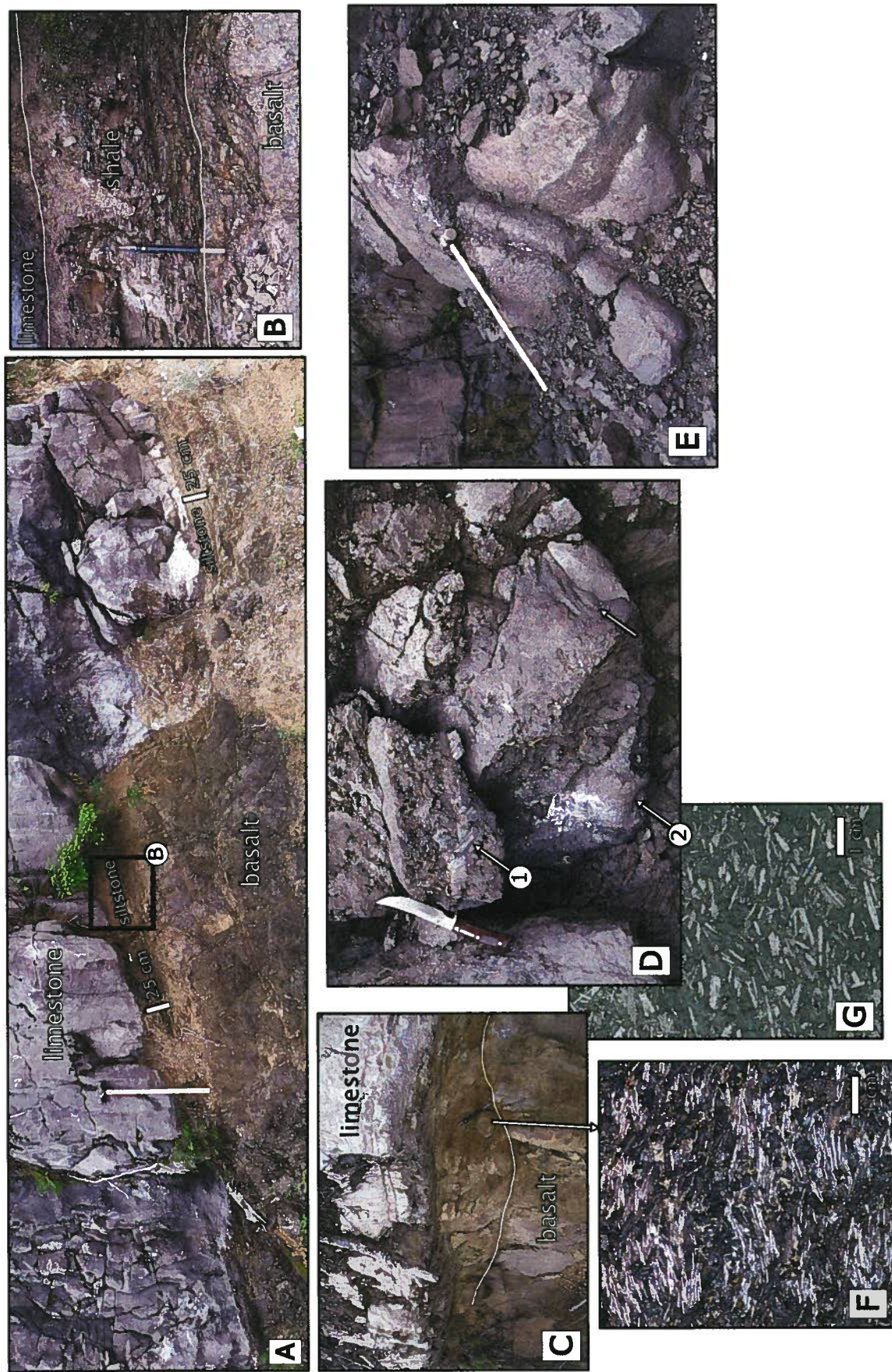


**Figure 5.16** Photographs from near Holberg Inlet, northern Vancouver Island (location shown in Figure 5.11). (A) Panoramic photograph of contact between top of the Karmutsen Formation and overlying Quatsino limestone. (B) Thin layers of siltstone between the Karmutsen basalts and Quatsino limestone (pen for scale; location shown in A). (C) Basalt-limestone contact with possible regolith along the contact (log ~1.5 m long for scale). (D) Close-up of ropy festoons (1) and the edge of a pahoe-hoe lobe (2) within Karmutsen Formation. Knife for scale. (E) Photograph of margin of pahoe-hoe lobe from same location as D. (F) Photomicrograph of plagioclase-rich, trachytic-textured basalt from C. (G) Photograph of cut slab of plagioclase megacrystic basalt flow common in upper part of the Karmutsen Formation.



mostly a non-fossiliferous massive micritic limestone. The upper part of the Quatsino locally contains a diverse fossil assemblage (Muller *et al.*, 1974; Jeletzky, 1976) and is intercalated and overlain by carbonate clastic sediments, as well as volcanic flows and volcanoclastic deposits of the Parson Bay Formation (Nixon *et al.*, 2006, 2007).

Overlying and intercalated with the Parson Bay Formation on northern Vancouver Island are volcanics of the Early to Middle Jurassic Bonanza arc (LeMare Lake volcanics), and equivalent plutonic rocks (Island Plutonic Suite) intrude Wrangellia stratigraphy (Nixon *et al.*, 2006; Nixon and Orr, 2007).

## **GEOCHRONOLOGY OF WRANGELLIA**

### **Previous geochronology for Wrangellia flood basalts and related plutonic rocks**

Samples of Wrangellia flood basalts and related plutonic rocks from BC, Yukon, and Alaska were previously dated in 8 separate studies and these results are summarized in Table 5.2. All ages below are quoted with  $2\sigma$  uncertainty. A total of 15 ages (4 U-Pb, 9  $^{40}\text{Ar}/^{39}\text{Ar}$ , and 2 K-Ar) of variable quality include 4 basalts and 11 plutonic rocks. In Southern Wrangellia, three U-Pb ages from gabbroic rocks on southern Vancouver Island are available based on (1) a single concordant analysis of a multi-grain baddeleyite fraction that yielded a  $^{206}\text{Pb}/^{238}\text{U}$  age of  $227.3 \pm 2.6$  Ma (Parrish & McNicoll, 1992), and (2) two unpublished  $^{206}\text{Pb}/^{238}\text{U}$  baddeleyite ages of  $226.8 \pm 0.5$  Ma (5 fractions) and  $228.4 \pm 2.5$  (2 fractions) (Table 5.2; Sluggett, 2003). A single whole rock  $^{40}\text{Ar}/^{39}\text{Ar}$  age of Karmutsen basalt from Buttle Lake on Vancouver Island yielded a plateau age of  $224.9 \pm 13.2$  Ma (Lassiter, 1995).

In Northern Wrangellia, zircon separated from a gabbro sill possibly related to the Nikolai basalts in southwest Yukon yielded an age of  $232.2 \pm 1.0$  Ma (average  $^{207}\text{Pb}/^{206}\text{Pb}$  age of 3 discordant (1.6 to 2.4%) analyses from multi-grain zircon fractions) (Table 5.2; Mortensen & Hulbert, 1991). K-Ar analyses of two biotite separates from peridotite in the Kluane mafic-ultramafic complex provided ages of  $224 \pm 8$  and  $225 \pm 7$  Ma (Campbell, 1981). In Alaska, three samples of Wrangellia flood basalts from the Wrangell Mountains yielded whole rock  $^{40}\text{Ar}/^{39}\text{Ar}$  plateau ages of  $228.3 \pm 5.2$ ,  $232.8 \pm 11.5$ , and  $232.4 \pm 11.9$  Ma (Lassiter, 1995). Five  $^{40}\text{Ar}/^{39}\text{Ar}$  plateau and isochron ages of variable precision have been determined for hornblende and biotite separates from mafic

Table 5.2 Compilation of previous geochronology of Wrangellia flood basalts and associated plutonic rocks

Sample No.	Age	Error, $\pm$ (2 $\sigma$ )	Method	Material	Reference	Rock description/ location	Comment
<b>Alaska Range</b>							
00AG022	231.1	11	Ar/Ar	Hornblende	Schmidt and Rogers, 2007	Gabbro; Tangle Lakes area, SW Gitzzy Ridge	Total fusion; plateau age. No analytical information available. Analysis by L. Shue (USGS). 62.7°N, 148.5°W.
PB1	230.4	2.3	Ar/Ar	Biotope	Blittensbender et al., 2003 <sup>2</sup>	Gabbro; Tangle Lakes area	No analytical information available.
AK25515	228.3	2.2	Ar/Ar	Biotope	Blittensbender et al., 2007 <sup>2</sup>	Gabbro with poikilitic biotite, including olivine; Rainy Creek Complex	Plateau age, 5 fractions, 81% <sup>39</sup> Ar released. Integrated age: 226.0 $\pm$ 1.1 Ma; Interpreted as age of magnetism.
HBD-2003-29	225.7	4	Ar/Ar	Hornblende	Blittensbender et al., 2007 <sup>2</sup>	Olivine basalt; Rainy Creek Complex	Plateau age, 8 fractions, 97% <sup>39</sup> Ar released. Integrated age: 226.4 $\pm$ 2.0 Ma; Interpreted as age of magnetism.
10830	225.2	13	Ar/Ar	Hornblende <sup>1</sup>	Blittensbender et al., 2007 <sup>2</sup>	Olivine peridotite; Rainy Creek Complex	Isotron age; Interpreted as an alteration age, maximum age for a reset event. Impure separate, excess Ar.
<b>Wrangell Mountains</b>							
92LNG-19	228.3	5.2	Ar/Ar	Whole rock	Lassiter, 1995 <sup>3</sup>	Nikolai basalt flow from the upper third of the volcanic stratigraphy; Glacier Creek	<sup>40</sup> Ar/ <sup>39</sup> Ar step-heating technique; isotron age: 224.8 $\pm$ 5.2 Ma; 56% <sup>39</sup> Ar released; n=5/7
92LNG-42	232.8	11.5	Ar/Ar	Whole rock	Lassiter, 1995 <sup>3</sup>	Nikolai basalt flow, ~100 m above the base of the basalt stratigraphy; Skolai Creek	<sup>40</sup> Ar/ <sup>39</sup> Ar step-heating technique; isotron age: 230.5 $\pm$ 27.8 Ma; 57% <sup>39</sup> Ar released; n=4/7
92LNG-47	232.4	11.9	Ar/Ar	Whole rock	Lassiter, 1995 <sup>3</sup>	Nikolai basalt flow, from the lower part of the basalt stratigraphy; Skolai Creek	<sup>40</sup> Ar/ <sup>39</sup> Ar step-heating technique; isotron age: 228.1 $\pm$ 11.8 Ma; 69% <sup>39</sup> Ar released; n=5/7
<b>Yukon</b>							
HDB88-TAT22	232.2	1	U/Pb	Zircon	Mortensen et al., 1992	Maple Creek gabbro; Kuane Ranges	Average <sup>207</sup> Pb/ <sup>235</sup> Pb ages of 3 discordant (1.6 to 2.4%) analyses from multi-grain zircon fractions.
SC1	224	8	K/Ar	Biotope	Campbell, 1981	Peridotite; Tatamagouche Creek, Kuane Ranges	K-Ar age. No analytical information available. Analysis at University of British Columbia by J. E. Harekai.
SC2	225	7	K/Ar	Biotope	Campbell, 1981	Peridotite; White River, Kuane Ranges	K-Ar age. No analytical information available. Analysis by M. Lanphere (USGS).
<b>Vancouver Island</b>							
02-CS-14	228.4	2.5	U/Pb	Zircon	Sluggatt, 2003	Mount Tuam Gabbro; Sallspring Island	<sup>206</sup> Pb/ <sup>238</sup> U age for 2 concordant fractions yielded ages of 229.4 $\pm$ 2.5 and 228.4 $\pm$ 1.6 Ma. Crystallization age interpreted to be 228.4 $\pm$ 2.5 Ma.
84822-1C	227.3	2.6	U/Pb	Beddelyite	Parish and McNeil, 1982	Porphyritic gabbroic rock; Crofton, southern Vancouver Island	<sup>206</sup> Pb/ <sup>238</sup> U age from a single concordant analysis of a multi-grain beddelyite fraction.
02-CS-11	226.8	0.5	U/Pb	Zircon	Sluggatt, 2003	Mount Tuam Gabbro; Sallspring Island	<sup>206</sup> Pb/ <sup>238</sup> U age for 1 of 5 fractions interpreted as the crystallization age. <sup>206</sup> Pb/ <sup>238</sup> U ages of other fractions are 219.8 $\pm$ 0.7, 223.3 $\pm$ 0.5, 221.9 $\pm$ 0.6, and 233.9 $\pm$ 1.4 Ma, which were interpreted to indicate post-crystallization Pb-loss.
91LKB-46	224.9	13.2	Ar/Ar	Whole rock	Lassiter, 1995 <sup>2</sup>	Karmutsen basalt flow, Buttle Lake, central Vancouver Island	<sup>40</sup> Ar/ <sup>39</sup> Ar step-heating technique; isotron age: 213.7 $\pm$ 20.5; 69% <sup>39</sup> Ar; n=5/7

<sup>1</sup> Replaces clinopyroxene. <sup>2</sup> Analyses provided courtesy of P. Blittensbender. Analyses performed at the University of Alaska, Fairbanks. Monitor mineral MIMB-1 (Samson and Alexander, 1987) with an age of 513.9 Ma (Lanphere and Dalrymple, 2000) was used to monitor neutron flux. <sup>3</sup> Analyses provided courtesy of R. Duncan (Oregon State University), originally interpreted in Lassiter (1995). <sup>40</sup>Ar/<sup>39</sup>Ar ages are reported relative to biotope standard FCT-3 (28.03  $\pm$  0.16 Ma, Renne et al., 1998), calculated with ArArCalc (Koppers, 2002). n = number of heating steps used/total. <sup>4</sup> Errors are 2 $\sigma$ .

and ultramafic plutonic rocks in the Amphitheater Mountains in the Alaska Range (Table 5.2). Three samples with ages of  $225.2 \pm 6.5$ ,  $225.7 \pm 2$ , and  $228.3 \pm 1.1$  Ma are from the Rainy Creek area, which lies to the north across a major fault from typical volcanic stratigraphy of Wrangellia flood basalts (Bittenbender *et al.*, 2007). The Rainy Creek area is a steeply-dipping sequence of picritic tuff and volcanoclastic rocks, mafic and ultramafic intrusives and dikes, and limestone that is distinct from the volcanic stratigraphy of the Nikolai Formation and these units may be older than the Wrangellia flood basalts (Bittenbender *et al.*, 2003) or may be younger intrusions (Nokleberg *et al.*, 1992). Analytical information is not available for two  $^{40}\text{Ar}/^{39}\text{Ar}$  analyses of gabbro related to Wrangellia flood basalts in the Tangle Lakes area of the Amphitheater Mountains with reported ages of  $230.4 \pm 2.3$  and  $231.1 \pm 11$  Ma (Bittenbender *et al.*, 2003; Schmidt & Rogers, 2007).

#### **Information about samples dated by $^{40}\text{Ar}/^{39}\text{Ar}$ in this study**

A total of 20 mineral separates, including 14 plagioclase, 5 hornblende, and 1 biotite mineral separates, were processed from 19 samples from throughout Wrangellia for  $^{40}\text{Ar}/^{39}\text{Ar}$  dating. Thirteen samples are Wrangellia flood basalts or intrusive equivalents and six are from younger, cross-cutting intrusive rocks. Of the 13 Wrangellia flood basalts or intrusive samples, nine are basalt flows and four are mafic sills or gabbroic rocks (Supplementary data file 3 and 4). One biotite separate is from an ultramafic plutonic rock from the Kluane Ranges, Yukon (sample 05-SIS-751). The five hornblende separates are all from younger dikes and intrusions that cross-cut Wrangellia basalts and were selected because they provide minimum ages for eruption. All ages indicated below are cooling ages that correspond to the bulk closure temperature ( $T_{\text{cb}}$ ) of the different minerals to Ar diffusion ( $\sim 200^\circ\text{C}$  plag;  $\sim 550^\circ\text{C}$  hbl;  $\sim 350^\circ\text{C}$  biotite; as summarized in Hodges, 2003).

Petrographic textures and major- and trace-element chemistry for all of the geochronological samples are listed in Supplementary data file 3 and described in detail in chapters 2, 3, and 4. The samples that are younger, cross-cutting intrusive units are clearly distinguishable from the Wrangellia flood basalts by their different textures and whole-rock chemistry (Supplementary data file 3).

#### **$^{40}\text{Ar}/^{39}\text{Ar}$ geochronological results**

Analytical methods for  $^{40}\text{Ar}/^{39}\text{Ar}$  dating are described in Appendix H. Age spectra are shown in Figures 5.17 to 5.20 and the analytical results are summarized in Table 5.3. The analytical data are available in Supplementary data file 4.

Plagioclase separates from three basalt flows (two submarine and one subaerial flow) and one gabbro from Vancouver Island were analyzed. The incremental heating data of the three basalt flows form plateaus over 67-96% of the  $^{39}\text{Ar}$  released with ages of  $72.5 \pm 1.2$ ,  $180.9 \pm 3.1$ , and  $161.1 \pm 7.3$  Ma (Fig. 5.17; Table 5.3); inverse correlation diagrams ( $^{39}\text{Ar}/^{40}\text{Ar}$  vs.  $^{36}\text{Ar}/^{40}\text{Ar}$ ) yield isochron ages that are concordant with the plateau ages. The gabbro from the Alice-Nimkish Lake area displays a disturbed saddle-shaped age spectrum, which may have been affected by excess  $^{40}\text{Ar}$  (e.g. Lanphere & Dalrymple, 1976; Harrison & McDougall, 1981). The cross-cutting mafic dike (sample 4718A3) with 54% of the  $^{39}\text{Ar}$  released had an age of  $193 \pm 26$  Ma and a broadly concordant isochron age of  $186 \pm 13$  Ma (Fig. 5.17; Table 5.3).

The biotite separate from a peridotite in Yukon yielded a well-defined plateau over ~60% of the  $^{39}\text{Ar}$  released with an age of  $227.5 \pm 1.2$  Ma and a concordant isochron age of  $226.1 \pm 3$  Ma (Fig. 5.18; Table 5.3). Plagioclase separates from two basalt flows from different levels of the volcanic stratigraphy of the Nikolai Formation in Yukon display disturbed age spectra (Fig. 5.18).

Plagioclase separates from five basalt flows and one mafic sill in Alaska (two Wrangell Mountains, four Alaska Range) yield age spectra with a total of four interpretable ages with 62-99% of the  $^{39}\text{Ar}$  released and plateau or integrated ages of  $191 \pm 11$ ,  $160.7 \pm 1.3$ ,  $160.57 \pm 8.64$ , and  $169.0 \pm 2.4$  Ma (Fig. 5.19; Table 5.3). Three of these samples (samples 5719A5, 5802A6, 5810A6) form well-defined plateaus that correspond with isochron ages. Two samples of basalt flows (samples 5715A1, 5810A10) showed disturbed  $^{40}\text{Ar}/^{39}\text{Ar}$  systematics.

Incremental heating data of hornblende separates from four younger intrusive samples from Alaska (two Wrangell Mountains, two Alaska Range) yielded well-defined plateau ages of  $29.7 \pm 1.1$ ,  $123.13 \pm 0.77$ ,  $148.80 \pm 0.83$ , and  $149.86 \pm 0.93$  Ma characterized by 54-95% of the  $^{39}\text{Ar}$  released (Fig. 5.20; Table 5.3); these plateau ages

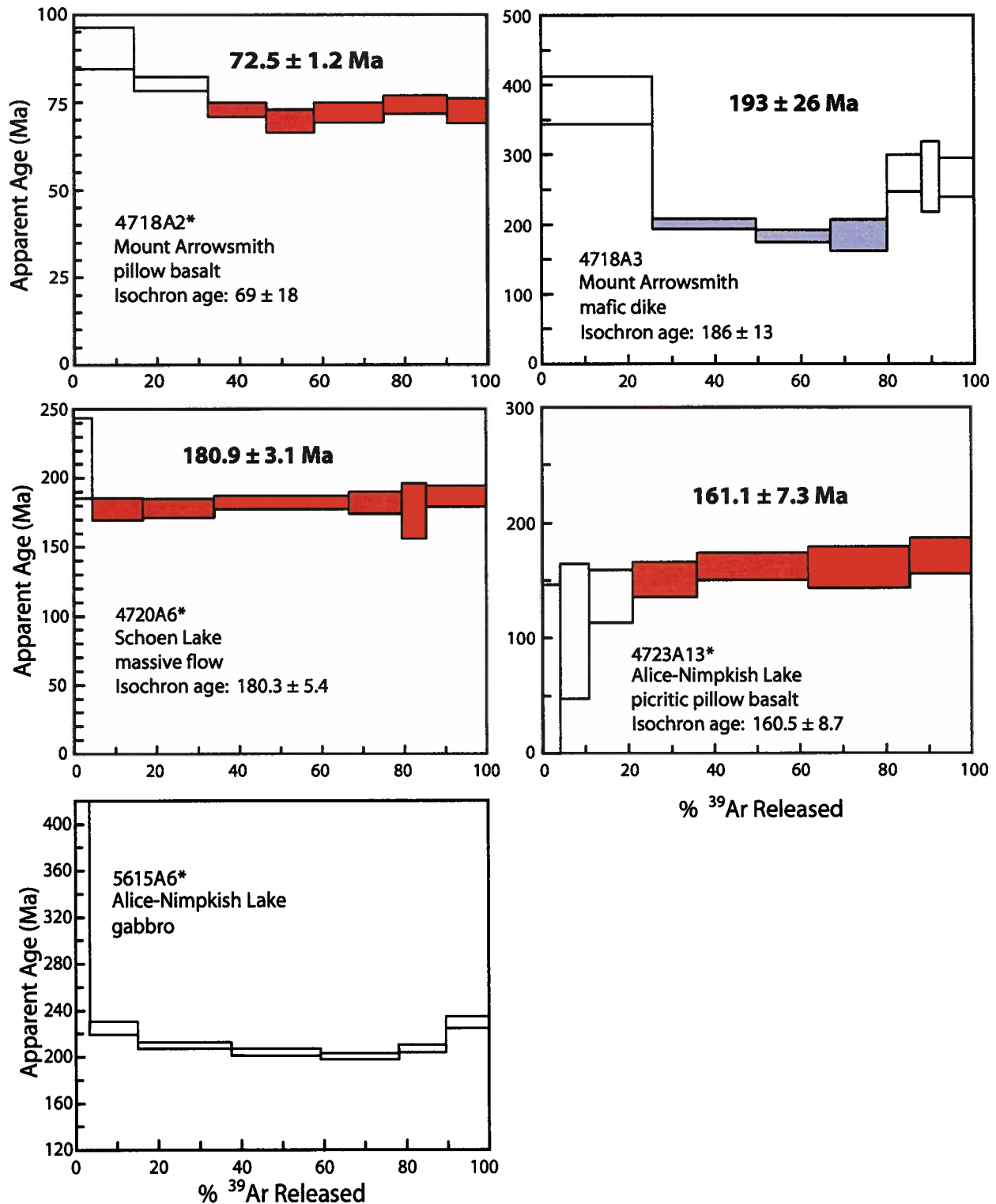


**Figure 5.17**  $^{40}\text{Ar}/^{39}\text{Ar}$  age spectra for six analyses of plagioclase separates from Vancouver Island. Errors on plateaus are  $2\sigma$ . Samples with red plateau steps are Wrangellia flood basalts. The sample with blue plateau steps is not a Wrangellia flood basalt. Plateau steps included in age calculation are colored red. Asterisks after the sample number indicates Wrangellia flood basalt or associated intrusive. Samples with all white steps do not meet the criteria for a plateau age, defined in Appendix H. Analytical data are presented in Supplementary data file 4 and summarized in Table 5.3.

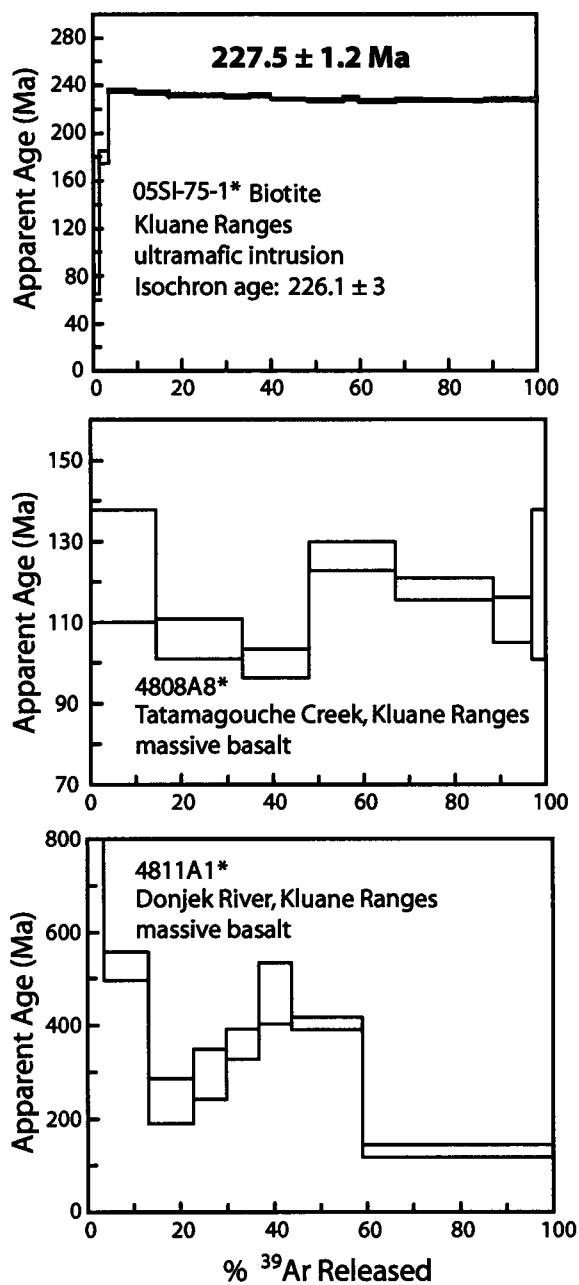


**Figure 5.18**  $^{40}\text{Ar}/^{39}\text{Ar}$  age spectra of one biotite and two plagioclase separates from Yukon. Errors on plateaus are  $2\sigma$ . Sample 05SI-75-1 is an ultramafic plutonic rock and samples 4808A8 and 4811A1 are Nikolai basalts. Plateau steps included in age calculation are colored red. Asterisks after the sample number indicates Wrangellia flood basalt or associated intrusive. Samples with all white steps do not meet the criteria for a plateau age, defined in Appendix H. Analytical data is presented in Supplementary data file 4 and summarized in Table 5.3.



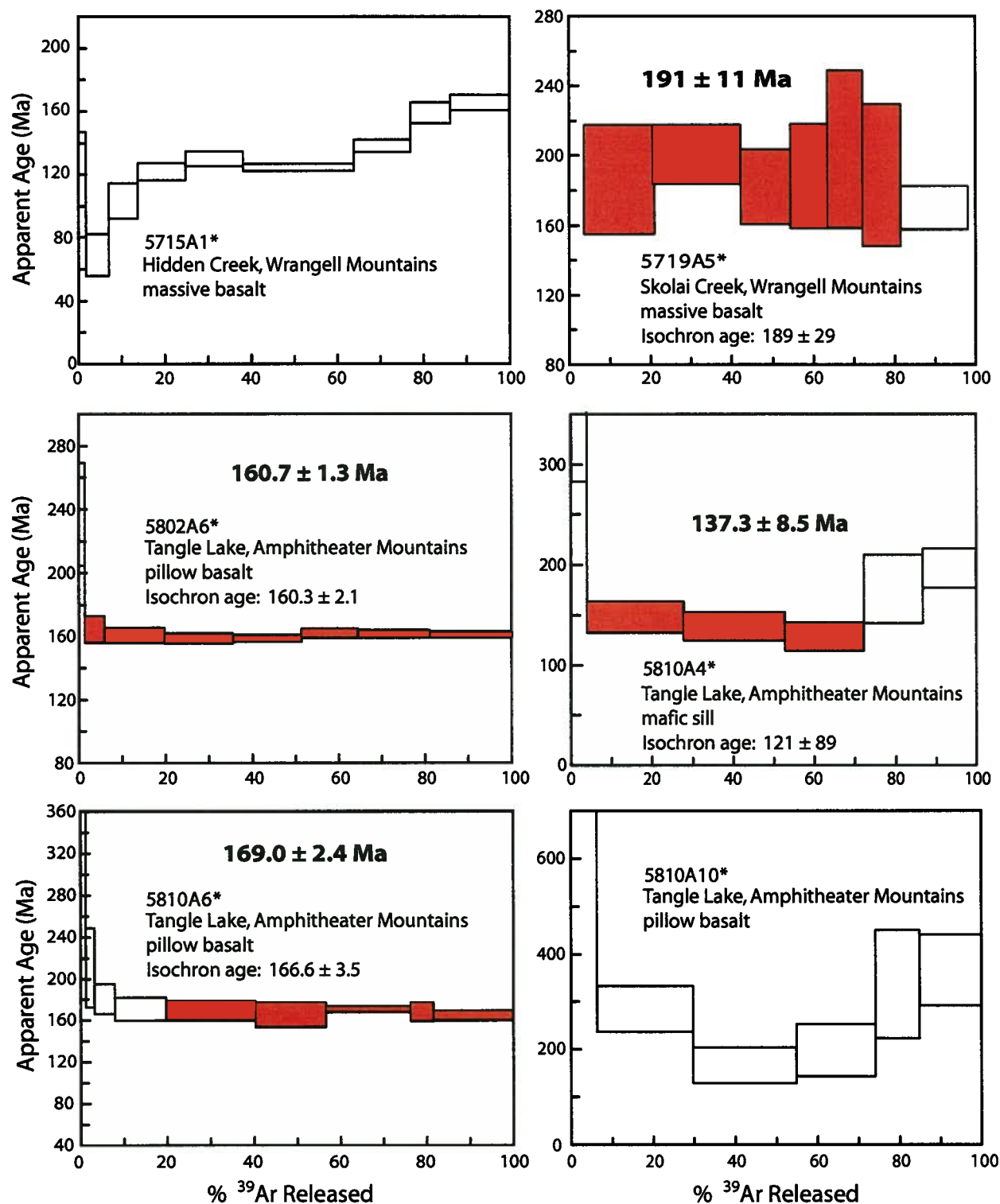


**Figure 5.19**  $^{40}\text{Ar}/^{39}\text{Ar}$  age spectra for six analyses of plagioclase separates from Alaska. Errors on plateaus are  $2\sigma$ . Plateau steps included in age calculation are colored red. Asterisks after the sample number indicates Wrangellia flood basalt or associated intrusive. Samples with all white steps do not meet the criteria for a plateau age, defined in Appendix H. Analytical data is presented in Supplementary data file 4 and summarized in Table 5.3.

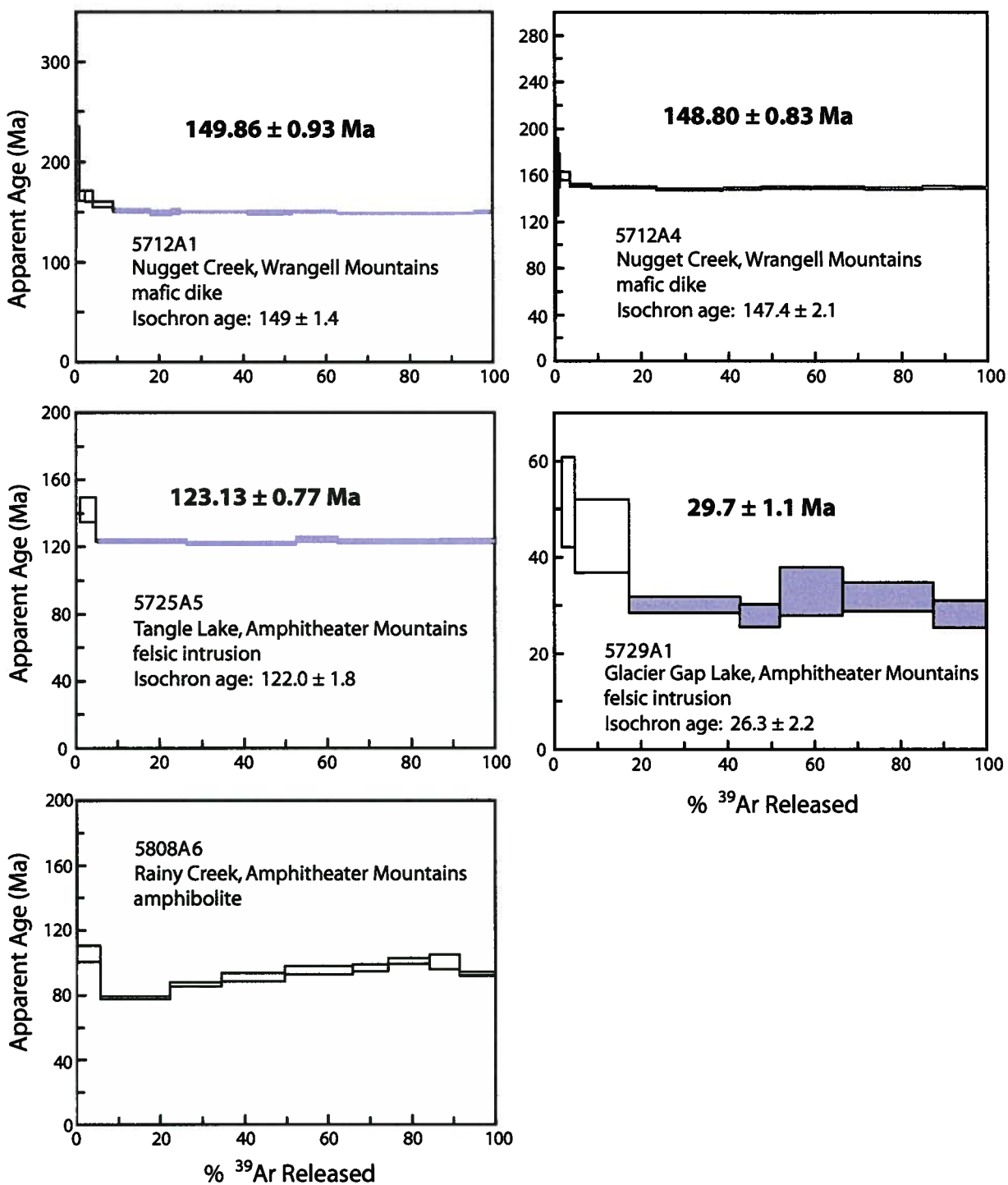


**Figure 5.20**  $^{40}\text{Ar}/^{39}\text{Ar}$  age spectra for six analyses of hornblende separates from plutonic rocks that are younger than Wrangellia basalts in Alaska. Errors on plateaus are  $2\sigma$ . Samples with blue plateau steps are not Wrangellia flood basalts and do meet the criteria for a plateau age. Samples with all white steps do not meet the criteria for a plateau age, defined in Appendix H. Analytical data are presented in Supplementary data file 4 and summarized in Table 5.3.

**Table 5.3  $^{40}\text{Ar}/^{39}\text{Ar}$  dating results for 13 samples of Wrangellia flood basalts\* and 6 samples from the Wrangellia Terrane**

Sample <sup>a</sup>	Mineral <sup>b</sup>	Integrated Age (Ma)	Plateau Age (Ma) <sup>c</sup>	Plateau Information <sup>d</sup>	Isochron <sup>e</sup>	Note
<b>Vancouver Island</b>		(2 $\sigma$ )	(2 $\sigma$ )			
4718A2*	Plag	76.31 $\pm$ 1.32	<b>72.5 <math>\pm</math> 1.2</b>	5 steps 67.6% $^{39}\text{Ar}$ release MSWD=1.3	69 $\pm$ 16 ( $^{40}\text{Ar}/^{39}\text{Ar}$ ) <sub>i</sub> = 307 $\pm$ 65 MSWD = 1.14, n=5 186 $\pm$ 13	tholeiitic, pillowed flow
4718A3	Plag (1)	255.99 $\pm$ 10.86	<b>193 <math>\pm</math> 26</b>	3 steps 54.3% $^{39}\text{Ar}$ release MSWD=5.1	( $^{40}\text{Ar}/^{39}\text{Ar}$ ) <sub>i</sub> = 322.4 $\pm$ 9.6 MSWD = 2.6, n=7 177.1 $\pm$ 3.1	mafic dike
4718A3	Plag (2)	224.51 $\pm$ 10.33	NP		( $^{40}\text{Ar}/^{39}\text{Ar}$ ) <sub>i</sub> = 327.5 $\pm$ 6.2 MSWD = 1.02, n=8 177.6 $\pm$ 3.0	last step: 231 $\pm$ 13 Ma
4718A3	Plag (C)	255.99 $\pm$ 10.86	NP		( $^{40}\text{Ar}/^{39}\text{Ar}$ ) <sub>i</sub> = 325.3 $\pm$ 4.5 MSWD = 1.4, n=9 180.3 $\pm$ 5.4	combined high-T run #1, all run #2 inverse isochron
4720A6*	Plag	182.31 $\pm$ 3.20	<b>180.9 <math>\pm</math> 3.1</b>	6 steps 95.6% $^{39}\text{Ar}$ release MSWD=0.93	( $^{40}\text{Ar}/^{39}\text{Ar}$ ) <sub>i</sub> = 307 $\pm$ 16 MSWD = 0.39, n=7 180.5 $\pm$ 6.7	tholeiitic, massive flow
4723A13*	Plag	150.24 $\pm$ 8.50	<b>161.1 <math>\pm</math> 7.3</b>	4 steps 79.1% $^{39}\text{Ar}$ release MSWD=1.3	( $^{40}\text{Ar}/^{39}\text{Ar}$ ) <sub>i</sub> = 280 $\pm$ 15 MSWD = 1.5, n=7	slightly upstepping plateau, picritic pillow lava
5615A6*	Plag	220.98 $\pm$ 2.15	NP		NI	coarse-grained gabbroic rock
<b>Yukon</b>						
0581-75-1*	Biotite	226.08 $\pm$ 0.53	<b>227.5 <math>\pm</math> 1.2</b>	9 steps 60.1% $^{39}\text{Ar}$ release MSWD=1.6	226.1 $\pm$ 3 ( $^{40}\text{Ar}/^{39}\text{Ar}$ ) <sub>i</sub> = 462 $\pm$ 380 MSWD = 1.7, n=9	nine steps in plateau, peridotite
4808A8*	Plag	114.88 $\pm$ 2.60	NP		NI	high-TI massive flow
4811A1*	Plag	361.37 $\pm$ 11.01	NP		NI	low-TI massive flow
<b>Wrangell Mountains</b>						
5712A1	Plag	144.23 $\pm$ 1.08	<b>145.6 <math>\pm</math> 1.2</b>	6 steps 84.6% $^{39}\text{Ar}$ release MSWD=0.91	146.5 $\pm$ 2.1 ( $^{40}\text{Ar}/^{39}\text{Ar}$ ) <sub>i</sub> = 267 $\pm$ 48 MSWD = 0.72, n=8 149.0 $\pm$ 1.4	hbl-phyric hypabyssal rock
5712A1	Hbl	150.71 $\pm$ 0.53	<b>149.86 <math>\pm</math> 0.93</b>	6 steps 53.5% $^{39}\text{Ar}$ release MSWD=0.56	( $^{40}\text{Ar}/^{39}\text{Ar}$ ) <sub>i</sub> = 359 $\pm$ 23 MSWD = 1.3, n=9 147.4 $\pm$ 2.1	hbl-phyric mafic intrusive rock
5712A4	Hbl	152.51 $\pm$ 0.83	<b>148.80 <math>\pm</math> 0.83</b>	6 steps 61.4% $^{39}\text{Ar}$ release MSWD=0.87	( $^{40}\text{Ar}/^{39}\text{Ar}$ ) <sub>i</sub> = 378 $\pm$ 96 MSWD = 2.9, n=12	hbl-phyric mafic intrusive rock
5715A1*	Plag	131.21 $\pm$ 1.92	NP		NI	high-TI massive flow
5719A5*	Plag	167.20 $\pm$ 10.44	<b>191 <math>\pm</math> 11</b>	6 steps 82.4% $^{39}\text{Ar}$ release MSWD=0.48	189 $\pm$ 29 ( $^{40}\text{Ar}/^{39}\text{Ar}$ ) <sub>i</sub> = 296 $\pm$ 21 MSWD = 0.16, n=6	high-TI massive flow
<b>Alaska Range</b>						
5725A5	Hbl	124.38 $\pm$ 0.69	<b>123.13 <math>\pm</math> 0.77</b>	6 steps 95.2% $^{39}\text{Ar}$ release MSWD=1.5	122.0 $\pm$ 1.6 ( $^{40}\text{Ar}/^{39}\text{Ar}$ ) <sub>i</sub> = 334 $\pm$ 18 MSWD = 0.51, n=9	hbl-phyric felsic intrusive rock
5729A1	Hbl	37.59 $\pm$ 2.41	<b>29.7 <math>\pm</math> 1.1</b>	5 steps 82.6% $^{39}\text{Ar}$ release MSWD=1.9	26.3 $\pm$ 2.2 ( $^{40}\text{Ar}/^{39}\text{Ar}$ ) <sub>i</sub> = 362 $\pm$ 20 MSWD = 0.46, n=8 160.3 $\pm$ 2.1	U-Pb zircon age 31.2 $\pm$ 0.2 Ma, hbl-phyric felsic intrusive rock
5802A6*	Plag	161.86 $\pm$ 1.31	<b>160.7 <math>\pm</math> 1.3</b>	7 steps 98.6% $^{39}\text{Ar}$ release MSWD=1.13	( $^{40}\text{Ar}/^{39}\text{Ar}$ ) <sub>i</sub> = 299 $\pm$ 16 MSWD = 0.88, n=7	low-TI sill
5808A6	Hbl (1)	92.77 $\pm$ 0.88	NP		NI	low-TI dike, Rainy Creek
5808A6	Hbl (2)	87.14 $\pm$ 0.6	NP		NI	low-TI dike, Rainy Creek
5810A4*	Plag	<b>160.57 <math>\pm</math> 8.64</b>	137.3 $\pm$ 8.5	3 steps 68.3% $^{39}\text{Ar}$ release MSWD=1.7	121 $\pm$ 89 ( $^{40}\text{Ar}/^{39}\text{Ar}$ ) <sub>i</sub> = 379 $\pm$ 470 MSWD = 0.17, n=3 166.6 $\pm$ 3.5	integrated age is preferred, low-TI sill
5810A6*	Plag	180.30 $\pm$ 3.65	<b>169.0 <math>\pm</math> 2.4</b>	5 steps 80.3% $^{39}\text{Ar}$ release MSWD=1.3	( $^{40}\text{Ar}/^{39}\text{Ar}$ ) <sub>i</sub> = 321 $\pm$ 21 MSWD = 0.80, n=8	low-TI pillow basalt
5810A10*	Plag	325.39 $\pm$ 26.68	NP		NI	high-TI pillow basalt

\*Wrangellia flood basalt or intrusive equivalent, based on field relations, petrography, and geochemistry. <sup>a</sup>Sample number: last digit year, month, day, initial, sample, except sample 0581-75-1. <sup>b</sup>Mineral separate and run # in parentheses, or (C) for combined result of multiple runs. Mineral abbreviations: hbl, hornblende; plag, plagioclase. <sup>c</sup>Bold italicized age is preferred age, error reported for  $\pm 2\sigma$ . NP, no plateau. <sup>d</sup>Number of steps used for calculating age. Criteria for plateau age are described in the analytical methods in Appendix H. <sup>e</sup>Inverse isochron ( $^{39}\text{Ar}/^{40}\text{Ar}$  vs.  $^{39}\text{Ar}/^{40}\text{Ar}$ ) age, initial  $^{40}\text{Ar}/^{39}\text{Ar}$  ratio, and MSWD. n is number of points included in isochron. MSWD refers to mean sum of the weighted deviates, which is a measure of the scatter compared to that which is expected from analytical uncertainties. NI, no isochron. See Supplementary data file 3 for petrographic and geochemical data for all samples, and coordinates for sample locations. Supplementary data file 4 presents the complete analytical results for  $^{40}\text{Ar}/^{39}\text{Ar}$  analyses as an Excel workbook.

correspond with isochron ages. Two analyses of an amphibolite dike in the Rainy Creek area of the Amphitheater Mountains showed disturbed  $^{40}\text{Ar}/^{39}\text{Ar}$  systematics (Fig. 5.20).

Among the 13 samples of Wrangellia flood basalt that were analyzed in this study, eight analyses satisfy the age spectra and isochron criteria to be geologically interpretable ages (see Appendix H). The plateau age of  $227.5 \pm 1.2$  Ma from biotite in peridotite from Yukon is the only sample inferred to have retained a magmatic age corresponding to cooling of the ultramafic intrusion through the  $T_{cb}$  of biotite ( $\sim 350^\circ\text{C}$ ), and is thus a minimum age of crystallization. The remaining seven ages from the basalts range from 191 to 73 Ma, indicating open-system behavior of the  $^{40}\text{Ar}/^{39}\text{Ar}$  systematics (Table 5.3). The low closure temperature of plagioclase to  $^{40}\text{Ar}$  ( $< 200^\circ\text{C}$  for Ar diffusion (Cohen, 2004)) resulted in these samples degassing  $^{40}\text{Ar}$  under lower greenschist facies metamorphic conditions and they record a reset age of metamorphism. Karmutsen basalts on Vancouver Island experienced prehnite-pumpellyite facies metamorphic conditions (1.7 kbar;  $\sim 300^\circ\text{C}$ ) and higher metamorphic gradients where proximal to granitoid intrusions increases (Cho & Liou, 1987). The mineralogy of Nikolai basalts in Alaska indicates a similar degree of metamorphism.

Despite modification of the original trapped Ar, the seven reset plagioclase  $^{40}\text{Ar}/^{39}\text{Ar}$  ages are geologically meaningful and provide important information about the geologic history of the Wrangellia Terrane. Briefly, three of the reset  $^{40}\text{Ar}/^{39}\text{Ar}$  ages of Karmutsen basalts from Vancouver Island (191, 181, and 161 Ma) are within the age range of Bonanza arc intrusions and volcanic sequences (197-167 Ma), that intrude and overlie the Karmutsen basalts on Vancouver Island (Table 5.3; Fig. 5.14; Nixon & Orr, 2007). The three reset ages of Nikolai basalts from the Amphitheater Mountains (169, 161, 161 Ma) are similar to ages of felsic plutonic rocks in close proximity ( $< 30$  km) to the south (168-150 Ma). Schmidt and co-workers (2003a; written comm., 2006) found that reset plagioclase  $^{40}\text{Ar}/^{39}\text{Ar}$  ages (174-152 Ma) for eight Nikolai basalts and gabbroic rocks in the Amphitheater and Talkeetna Mountains are similar to ages for these felsic plutonic rocks assigned to the Peninsular Terrane. Seven whole rock K-Ar ages of Nikolai basalts in the Wrangell Mountains yielded an isochron age of  $112 \pm 11$  Ma and indicated resetting of K-Ar systematics during tectonism related to northward transport of Wrangellia (MacKevett, 1978; Plafker *et al.*, 1989b). The hornblende  $^{40}\text{Ar}/^{39}\text{Ar}$  ages are

coincident with regional magmatic events reported from other studies in the areas in which these samples were collected. Two Late Jurassic ages of  $148.8 \pm 0.83$  and  $149.86 \pm 0.93$  Ma from mafic dikes in the Wrangell Mountains correspond with ages of Late Jurassic plutons of the Chitina arc (140-160 Ma, with most ages between 145-150 Ma), which are synchronous with a major regional orogeny related to subduction (Grantz *et al.*, 1966; MacKevett, 1978; Hudson, 1983; Dodds & Campbell, 1988; Plafker *et al.*, 1989b; Roeske *et al.*, 2003).

### **Summary of isotopic age determinations for Wrangellia flood basalts**

The ages of Wrangellia flood basalts and intrusives with errors <10 Myr (n=9) range from  $225.7 \pm 2$  to  $232.2 \pm 1$  Ma (Fig. 5.21; Tables 5.2 and 5.3). The three U-Pb ages from mafic sills from Vancouver Island are within error of each of the four  $^{40}\text{Ar}/^{39}\text{Ar}$  ages from Alaska, as well as the  $^{40}\text{Ar}/^{39}\text{Ar}$  biotite plateau age of a peridotite of  $227.5 \pm 1.2$  Ma from this study. The slightly older age of  $232.2 \pm 1$  Ma from Yukon (average  $^{207}\text{Pb}/^{206}\text{Pb}$  age based on results from 3 discordant fractions; Mortensen and Hulbert (1991)) is the only age which falls outside the range for the Vancouver Island samples. This gabbroic sill in Yukon may represent an earlier phase of magmatism. The relatively narrow range of ages for Wrangellia flood basalts and associated intrusive rocks indicates that the duration of the majority of the volcanism was likely less than 5 Myr, occurring between ca. 230 and 225 Ma.

### **Paleontological studies**

Fossils in sedimentary strata directly underlying and overlying the Wrangellia flood basalts also provide constraints on the age and duration of volcanism. In 1964, MacKevett and co-workers (1964) reported that shale directly beneath Nikolai basalts on Golden Horn Peak in the Wrangell Mountains contained abundant Middle Triassic index fossils identified as *Daonella frami* kittl. In 1971, a mineral exploration party discovered a sedimentary layer (<2 m thick) of fissile black shale between sills of Karmutsen basalts on Mount Schoen on Vancouver Island that contained imprints of *Daonella tyrolensis* (Carlisle, 1972). In this study, samples of *Daonella* were collected from Golden Horn Peak in Alaska and on Mount Schoen on Vancouver Island. The *Daonella* from both

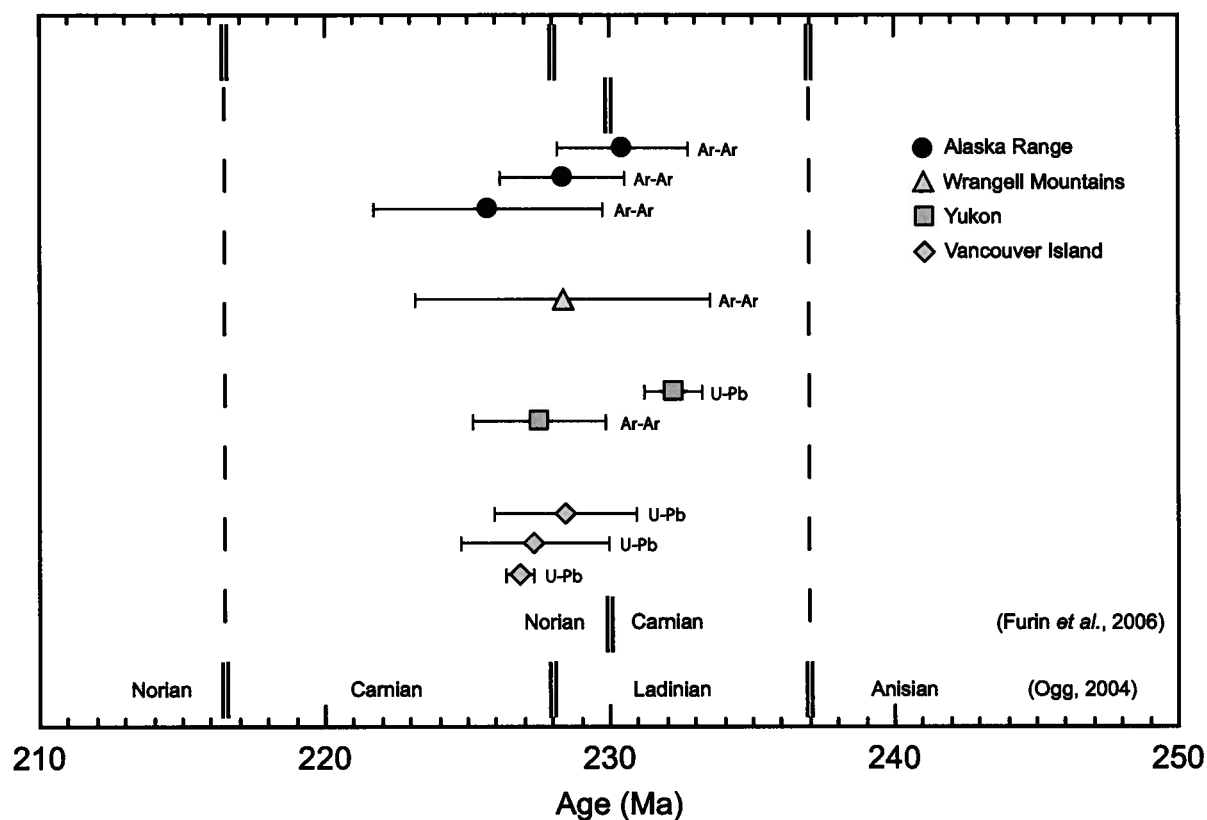


**Figure 5.21** Summary diagram showing  $^{40}\text{Ar}/^{39}\text{Ar}$  and U/Pb ages of Wrangellia flood basalts and plutonic rocks with analytical uncertainty <10 Myr. The results are shown from north (top) to south (bottom) and are distinguished by region. Analytical details are presented in Tables 5.2 and 5.3. Two schemes are shown for the boundaries of part of the Triassic, from Furin *et al.* (2006) and Ogg (2004). Errors are  $2\sigma$ .



localities appear to have similar forms and are closely related to *Daonella frami* kittl (C. A. McRoberts, 2006, pers. comm.). The *Daonella* appear older than Upper Ladinian forms and are likely of middle Ladinian age (Poseidon Zone, ca. 235-232 Ma; C. A. McRoberts, 2006, pers. comm.). Conodont *Neospathodus* in the *Daonella* beds from Vancouver Island confirms this age.

## DISCUSSION

### Overview of the geology and age of Northern and Southern Wrangellia

The stratigraphy and age of different areas of the Wrangellia oceanic plateau provide constraints on the construction of the volcanic stratigraphy, the paleoenvironments existing at the time of eruption, and the duration of volcanism. A summary of observed and previously reported field relationships of Wrangellia flood basalts, and the pre- and post-volcanic rock record, is presented in Table 5.4. A compilation of ages and biostratigraphy for Paleozoic through Triassic rocks of Wrangellia is presented in Figure 5.22 and Supplementary data file 5.

The basement of Wrangellia has different age strata in Alaska and Yukon than on Vancouver Island (Fig. 5.22). The basement of Wrangellia was originally defined as a Pennsylvanian to Permian volcanic arc sequence that may have been deposited on oceanic crust (Jones *et al.*, 1977) and this is maintained by numerous authors (Smith & MacKevett, 1970; MacKevett, 1978; Coney *et al.*, 1980; Monger *et al.*, 1982; Saleeby, 1983; Beard & Barker, 1989). However, while Pennsylvanian to Permian volcanic arcs are preserved in Alaska (Smith & MacKevett, 1970; MacKevett, 1978; Beard & Barker, 1989), older Paleozoic rocks make up much of Vancouver Island (Muller, 1977; Brandon *et al.*, 1986), and there is no arc volcanism in the Pennsylvanian to Permian of Vancouver Island (Fig. 5.22; Massey & Friday, 1988; Yorath *et al.*, 1999). The Paleozoic volcanic sequences on Vancouver Island are considerably older (~380-355 Ma) than presently-dated volcanic sequences in Alaska (~312-280 Ma, mostly from the Wrangell Mountains; Fig. 5.22). Paleozoic limestones beneath Wrangellia basalts in Alaska contain Early Permian bryozoans, brachiopods, foraminifera, and corals (Smith & MacKevett, 1970). On Vancouver Island, conodonts in the Buttle Lake Group indicate Mississippian to

Table 5.4 Comparison of geology and ages of Northern and Southern Wrangellia

Northern Wrangellia	Southern Wrangellia
<b><u>Rocks overlying the Nikolai Formation</u></b>	<b><u>Rocks overlying the Karmutsen Formation</u></b>
clastic sedimentary sequences above Nikolai span Triassic-Jurassic boundary	clastic sedimentary sequences above Karmutsen span Triassic-Jurassic boundary
Late Carnian to Early Norian fossils in overlying limestone overlying limestone grades upward from shallow water to deeper water facies Nikolai basalts interbedded with limestone and argillite (Yukon) limestone is commonly brecciated near the base	Late Carnian to Early Norian fossils in overlying limestone overlying limestone grades upward from shallow water to deeper water facies limestone and sedimentary rocks of the Kunga and Maude Groups on Haida Gwaii Kunga Formation contains identical fossils to Quatsino limestone Karmutsen basalt, or younger basalt, locally intrudes the Quatsino limestone mostly micritic limestone directly overlying the basalts thin (<25 cm) layer of siltstone immediately overlying basalt in several locations no evidence of erosion between Karmutsen and Quatsino limestone
thin layer of siltstone in several locations along Nikolai-Chitstone contact occurrences of regolith between the top of the Nikolai and the base of the Chitstone	thin (<25 cm) siltstone layers between top of Karmutsen and Quatsino interflow limestone/clastic lenses near top formed in shallow submarine areas Late Carnian to Early Norian fossils in lenses within uppermost Karmutsen plagioclase megacrystic flows near the top of the basalt succession
<b><u>Nikolai Formation</u></b> 4 U-Pb and Ar-Ar ages (error <10 Myr) of 225-230 Ma (with one Yukon outlier) Late Carnian to Early Norian fossils in limestone lenses in Yukon trachytic-textured plug-rich flows near top of Nikolai in Wrangell Mtns rare dikes predominantly massive subaerial flows	<b><u>Karmutsen Formation</u></b> 3 U-Pb ages (error <10 Myr) of 226-228 Ma  regolith above uppermost flow thin (<25 cm) siltstone layers between top of Karmutsen and Quatsino interflow limestone/clastic lenses near top formed in shallow submarine areas Late Carnian to Early Norian fossils in lenses within uppermost Karmutsen plagioclase megacrystic flows near the top of the basalt succession
<b>Alaska Range (Amphitheater and Clearwater Mountains)</b> ~7% of lowest part of stratigraphy is pillow basalt (<500 m), and ~3000 m subaerial flows pillows tend to have mostly small diameter (<1 m) pillows have abundant vesicles (20-30 vol%) indicating eruption in shallow water (<800 m) vesicles in pillows are spherical (<1 mm) and evenly distributed throughout pillows megapillows rare in Alaska minor amounts of breccia and tuff within submarine section interbedded limestone/clastic near top of Nikolai in Clearwater Mtns and in Yukon thick sediment-sill complex large area of complementary plutonic rocks represent feeder system for flood basalts no sheeted dike complexes, sill-dominated feeder system	<b>Vancouver Island</b> flood basalts form emergent basalt sequence subaerial stage-subaerial flows (>2500 m on CVI, <1500 m on NVI) shallower-water stage-pillow breccia/hyaloclastite (40-1500 m on NVI) deeper-water stage-pillowed and unpillowed basalt flows (>2500 m)  pillow basalts erupted in deeper marine setting than in Northern Wrangellia most pillows are commonly large diameter (>1 m) pillows are more commonly non-vesicular or have radially-oriented pipe vesicles megapillows (>4 m) within pillowed flows on VI volcaniclastic rocks formed primarily via cooling-contraction granulation volcaniclastics mostly between pillow basalt and subaerial flow units peperites in submarine section subaerial flow unit is conformable with the underlying hyaloclastite unit interflow sedimentary lenses are found near the top of the subaerial flow unit interflow lenses contain Late Carnian to Early Norian fossil rare occurrences of interflow sediments, besides lenses between upper flows columnar jointing is rare rare dikes, no sheeted dike complexes thick sediment-sill complexes where base is exposed on VI increase in vesicularity and proportion of volcaniclastics upwards in submarine unit pahoehoe structures (e.g. rope festoons), within flows and just below Quatsino picritic pillow lavas in upper part of the submarine section on Northern VI marine fossils in pillow breccia, Butte Lake area pillow basalt engulfs fine-grained sediment in lowermost pillowed flows submarine basalts form volumetrically minor component of the subaerial stratigraphy no indication of uplift prior to eruption on VI
black shale within sediment-sill complex, non-fossiliferous (starved, anoxic environment) picritic pillow lava near base of submarine section in Clearwater Mtns pillow basalt engulfs fine-grained sediment in lowermost pillowed flows picritic tuff found outside the main area of flood basalts, but likely related to Nikolai basalts	<b>Queen Charlotte Islands (Haida Gwaii)</b> one measured section (~4300 m) 95% submarine, pillow to fragmental ratio (8:2) local tuffaceous crinoidal limestone lenses in lowermost flows  Permian chert, carbonate, and volcaniclastic rocks form deepest level of exposure
<b>Wrangell Mountains and Kluane Ranges</b> almost no pillow basalt in basalt stratigraphy (only in lowermost ~70 m) pillow breccia and polymictic flow-conglomerate in lowermost ~70 m basal flow-conglomerate sits directly on argillite with fissile <i>Daonella</i> beds abundant rounded clasts derived from underlying Paleozoic formations larger pendants (>100 m long) of Paleozoic rocks in lowermost flows occurrences of regolith between top of Nikolai and overlying Chitstone limestone rare thin argillite (<10 cm) on top of uppermost flow interflow limestone lenses (1-30 m thick) near top formed in shallow submarine areas plagioclase megacrystic flows near the top of the basalt succession  ~3500 m of subaerial sheet flows; columnar jointing is rare  very rare occurrences of interflow sediments, other than lenses in upper part quartz-pebble conglomerate in sediments beneath Nikolai in Talkeetna Mtns Paleozoic arc sequences not exposed in Talkeetna Mtns beneath Nikolai	<b><u>Rocks underlying the Karmutsen Formation</u></b>  <i>Daonella</i> imprints in shale within sediment-sill complex on Mount Schoen, VI <i>Daonella</i> imply dysoxic bottom waters typical of mud-dwellers on soupy sediments  coarse-grained mafic rocks intrude and deform underlying sedimentary sequences mafic sills intrude siliceous argillite, shale, chert, and limestone  Paleozoic sequences mostly exposed in two anticlinoria on central and southern VI  Conodonts indicate Mississippian to Permian ages in the Butte Lake Group underlying Karmutsen flood basalts Paleozoic arc sequences underlying Karmutsen ages 380-355 Ma oldest known rocks on Vancouver Island are the Devonian Duck Lake Formation
<b><u>Rocks underlying the Nikolai Formation</u></b> <b>Wrangell Mountains and Kluane Ranges</b> evidence of erosional surface beneath Nikolai, rounded clasts from underlying sequences rounded pebble- to cobble-size clasts indicate subaerial or shallow submarine reworking indication of uplift prior to eruption in Wrangell Mountains c.g. mafic rocks intrude and deform underlying sedimentary sequences <i>Daonella</i> imprints in fissile shale underlying lowermost pillow breccia erosional unconformity between <i>Daonella</i> beds and underlying Paleozoic limestone formation of laterally discontinuous grabens along base in Kluane Ranges <b>Alaska Range (Amphitheater and Clearwater Mountains)</b> Pre-Nikolai black shale deposited in starved, anoxic marine setting no bioturbation (parallel laminations) and no biogenic structures (trace fossils) coarse-grained mafic rocks intrude and deform underlying sedimentary sequences limestone (with Early Permian fossils), chert, argillite underlying Nikolai basalts Paleozoic arc sequences underlying Nikolai ages 312-280 Ma no rocks dated older than Pennsylvanian in Wrangellia in Alaska	
references not included in this table, see text for references VI, Vancouver Island; CVI, Central Vancouver Island; NVI, Northern Vancouver Island	

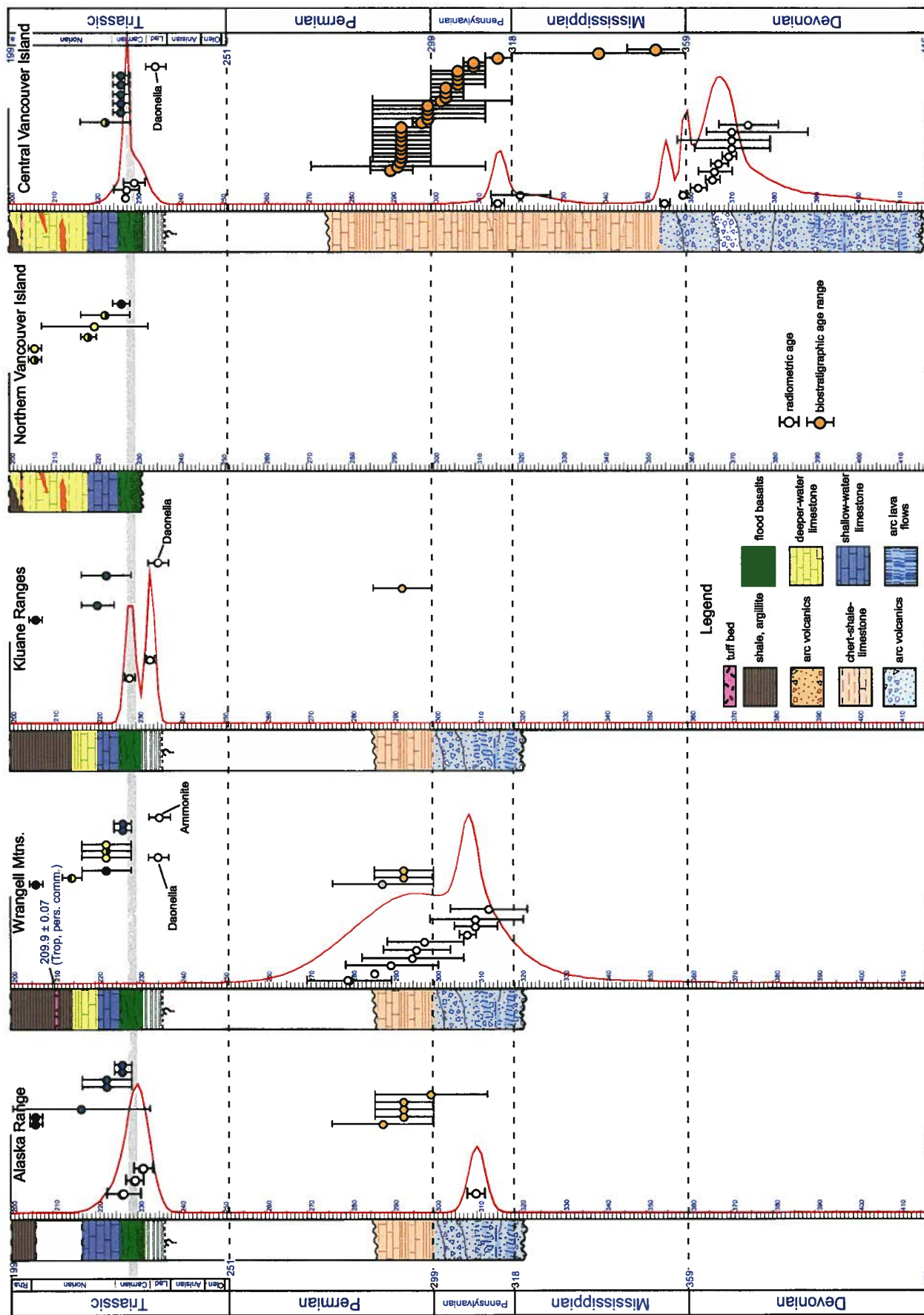


Figure 5.22 Summary of ages and biostratigraphy for Wrangellia, divided into 5 areas. Radiometric ages are white circles. Fossil ages are colored according to formation in stratigraphic column, unless colored gray. Information for age data and biostratigraphy are presented in Supplementary data file 5. Age probability density distribution plots for each area are calculated from the plotted ages using AgeDisplay (Sircombe, 2004). The ages for the period boundaries are from Gradstein *et al.* (2004). Ages for epoch boundaries of the Triassic are adjusted using Furin *et al.* (2006).

Permian ages (Orchard *fide* Brandon *et al.*, 1986; Orchard, 1986; Fig. 5.22; Supplementary data file 5).

The volcanic stratigraphy on Vancouver Island consists of a tripartite succession of submarine flows (50-60%), volcanoclastics, and subaerial flows, whereas volcanic stratigraphy in Alaska and Yukon is predominantly subaerial flows (>90%; Table 5.4; Fig. 5.22). In the Alaska Range, the lowest ~500 m of stratigraphy is submarine flows that were emplaced on non-fossiliferous black shale. In the Wrangell Mountains, the basal flow-conglomerate lies directly on shale with *Daonella* beds and contains erosional remnants from the underlying Paleozoic units. Laterally discontinuous zones of basal conglomerate along the base of the Nikolai in Yukon are interpreted as syntectonic deposits and flows related to the formation of grabens. On Vancouver Island, the lowest pillow basalts were emplaced on unconsolidated fine-grained sediments and mafic sills intrude marine strata with *Daonella* beds. However, the submarine section on Vancouver Island (~3000 m) is substantially thicker than in the Alaska Range (~500 m).

The overlying limestone and interflow sedimentary lenses in Northern and Southern Wrangellia are lithologically similar and have a similar range of fossil ages (Table 5.4; Fig. 5.22). In Southern Wrangellia, interflow sedimentary lenses are common in upper parts of the Karmutsen Formation and the overlying limestone contains Late Carnian to Norian fossils. Within upper Nikolai stratigraphy in Northern Wrangellia, interflow sedimentary lenses occur in southwest Yukon and the Clearwater Mountains and Nikolai basalts are overlain by limestone with age-diagnostic Late Carnian to Early Norian fossils. Sedimentary strata extend up through the Triassic-Jurassic boundary in Northern and Southern Wrangellia.

### **Eruption environment for Wrangellia flood basalts**

#### ***Northern Wrangellia***

The Nikolai basalts in Alaska were emplaced as quiet effusive eruptions in a shallow marine and subaerial environment. Sediments directly beneath the flood basalts in the Alaska Range are mostly siliceous argillites, carbonaceous black shales, and mudstones, with the upper part of the 200-250 m sequence having a higher proportion of black carbonaceous shale and carbonate (Blodgett, 2002). In this area, Blodgett (2002)

interpreted the total absence of fossils and biogenic sedimentary structures (trace fossils), and even, parallel laminations (indicating lack of bioturbation), as indicative of deposition in a starved, anoxic shallow submarine environment. The higher proportion of black carbonaceous shale and calcareous component for sediments higher in the sequence may indicate a shallower depositional environment for the younger sediments than for the older sediments, possibly due to uplift prior to eruption (Blodgett, 2002). The pillow basalts in the Alaska Range (~500 m) are highly vesicular, consistent with eruption in shallow water (Jones, 1969; Kokelaar, 1986). Volcaniclastic flows intercalated with pillow basalt also indicate eruption in shallow water; this transition usually occurs in <200 m water depth for tholeiitic magmas (Kokelaar, 1986). The subaerial flows (>3000 m) were emplaced as inflated compound pahoehoe flow fields during prolonged, episodic eruptions similar to those in most continental flood basalts (Self *et al.*, 1997).

In the Wrangell Mountains and Yukon, the basal flow-conglomerate and pillow breccia (<100 m thick) erupted in shallow water (<200 m). Rounded clasts in the basal flow-conglomerate indicate an area of relief near sea-level in the Wrangell Mountains. Above the basal flow unit in the Wrangell Mountains is ~3500 m of subaerial sheet flows that lack features of submarine emplacement. The proportion of amygdules in the massive flows is variable, but generally high, similar to many continental flood basalts. Submarine sheet flows exposed in accreted portions of the Ontong Java Plateau in the Solomon Islands rarely have significant proportions of amygdules and pillowed and unpillowed flows are preserved throughout the stratigraphy (Pettersen, 2004). Individual flow structures are indicative of emplacement by the inflation of effusive subaerial flows.

### *Southern Wrangellia*

The tripartite Karmutsen stratigraphy on Vancouver Island formed as an emergent basalt sequence during a deeper-water, shallow-water, and subaerial stage, similar to those described in formation of emergent seamounts (Schmidt & Schmicke, 2000) and Hawaiian volcanoes (Garcia *et al.*, 2007). Sills obscure relationships at the sediment-basalt interface at the base of the Karmutsen, and there may have been sediments on top that are no longer preserved, but most of the fine-grained strata underlying the Karmutsen were deposited below storm-wave base. Carlisle (1972) reported that pre-Karmutsen

sediments show a progressive change from coarse bioclastic limestone to laminated and silicified shale, indicating transition from an organically rich, shallow-water environment to a starved, pelagic deeper-water depositional environment prior to initiation of volcanism. *Daonella* in fine black shale from near the top of this unit imply dysoxic bottom waters typical of mud-dwellers that float on soupy sediments (Schatz, 2005).

The deeper-water stage (>200 m water depth) of the Karmutsen was dominated by quiescent effusive activity that formed pillowed and unpillowed flows. The pillowed flows are interconnected tubes and lobes that contain large-diameter pillows (>2 m) and have low abundances of amygdules. The unpillowed flows may be some of the master tubes for delivery to distal parts of flow fields or locally increased effusive rates, due to topography, as evinced by concave basal contacts. The basalts increase in vesicularity as does the proportion of volcaniclastics upwards in the submarine stratigraphy (Nixon *et al.*, 2008).

The shallow-water stage of the Karmutsen preserves an increasing proportion of volcaniclastic units (pillow breccia and hyaloclastite) conformably overlying mostly close-packed pillows. The pillow breccias are commonly associated with pillowed flows and contain aquagene tuff (Carlisle, 1963), or redeposited hyaloclastite. The transition from close-packed pillowed flows to pillow breccia and hyaloclastite probably occurred in <500 m water depth; however, in certain areas on northern Vancouver Island the volcaniclastic unit is >1500 m thick (Nixon *et al.*, 2008). Sedimentary structures (e.g. graded bedding, fluidization structures) are present locally and indicate resedimentation processes. Pyroclastic deposits containing lapilli tuff and volcanic bombs do not appear to be common (Carlisle, 1963). The volcaniclastic rocks likely formed primarily via cooling-contraction granulation, magma-water-steam interaction, autobrecciation, and mass-wasting, rather than pyroclastic eruption.

The emergent subaerial stage is marked by the relative absence of volcaniclastic and pillowed flow units and dominance of massive amygdaloidal sheet flows. The sheet flows were emplaced as inflated compound pahoehoe flow fields atop an enormous oceanic plateau. There are isolated sections of submarine flood basalts (<200 m thick) within the uppermost subaerial Karmutsen stratigraphy (Surdam, 1967; Carlisle and Suzuki, 1974); however, these units form a volumetrically minor component of the



subaerial stratigraphy. The intra-Karmutsen sedimentary lenses formed in isolated, low-lying areas in a predominantly subaerially-exposed plateau (Carlisle and Suzuki, 1974).

There are similarities between stratigraphy of Karmutsen basalts and stratigraphy of Hawaii Scientific Drilling Project core (HSDP2; Garcia *et al.*, 2007). The stratigraphies in both the Karmutsen basalts and HSDP2 are predominantly pillowed flows in the lower parts of the submarine stratigraphy and give way to increasing proportions of volcanoclastic units upsection, below the submarine-subaerial transition. Vesiculated pillows of the Karmutsen Formation on Northern Vancouver Island are more common near the top of the pillow unit and in the hyaloclastite unit. HSDP2 drill core shows an increase in vesicularity with decreasing depth in the submarine lava flows (Garcia *et al.*, 2007). Intrusives more commonly intrude lower parts of the stratigraphy within both submarine sections and, although more difficult to identify, they appear to be less common within the subaerial sections.

#### **The accumulation and subsidence of the Wrangellia basalts**

The geology, age and biostratigraphy of Wrangellia can be used to estimate the rate of accumulation of Wrangellia basalts and the subsidence of the Wrangellia oceanic plateau. Carlisle and Suzuki (1974) originally estimated an accumulation rate for the Karmutsen basalts of 0.17-0.27 cm/yr over 2.5-3.5 Myr. This yielded a total erupted volume of basalt of  $3.7\text{--}4.0 \times 10^5 \text{ km}^3$  (they assumed an area 400 km by 150 km, roughly the size of Vancouver Island, or 60,000 km<sup>2</sup>, and a stratigraphic thickness of 6 km) and a volumetric output rate of 0.10-0.16 km<sup>3</sup>/yr (Carlisle & Suzuki, 1974). In this study, an estimate of volcanic output rate ( $\sim 0.03 \text{ km}^3/\text{yr}$ ) and total erupted volume of Karmutsen basalts ( $1.4\text{--}1.5 \times 10^5 \text{ km}^3$ ) are lower than the estimates of Carlisle and Suzuki (1974). The area of exposure of Karmutsen basalts in this study was calculated using digital geology maps for Vancouver Island and the Queen Charlotte Islands (shown in Figure 5.11), and thus represents a minimum estimate. The estimated total erupted volume and volumetric output rate were calculated using a stratigraphic thickness of 6 km and a duration of volcanism of 5 Myr. Even using this conservative estimate for the area of exposure, the volumetric output rate is comparable to recent estimates of long-term

volumetric eruption rates for ocean islands such as Iceland (0.02-0.04 km<sup>3</sup>/yr) and Hawaii (0.02-0.08 km<sup>3</sup>/yr) (White *et al.*, 2006).

The subsidence of the Karmutsen basalts during volcanism was recorded by the deposition of interflow sedimentary lenses between the upper flows during the waning stages of volcanism as low-lying areas of the plateau were submerged. The occurrence of interflow lenses indicates that by the end of Karmutsen flood volcanism (~5 Myr in duration) most of the top of the basalt plateau had subsided and submerged below sea-level. This implies that over the duration of subaerial volcanism, the rate of accumulation of basalt flows was comparable to the rate of subsidence. Carbonate deposition was occurring during the waning stages of volcanism, and there was no significant break after volcanism ceased. There are few signs of erosion between the Quatsino limestone and Karmutsen Formation (in places only a <25 cm thick siltstone/sandstone layer is preserved), and interflow lenses have identical fossils to the lower part of the Quatsino limestone.

Post-volcanic subsidence of the Wrangellia oceanic plateau is recorded by hundreds of meters to >1000 m of Late Triassic marine sedimentary rocks overlying the basalt stratigraphy. The Quatsino limestone was deposited on top of the plateau as it began to submerge beneath sea-level, and while volcanism waned. Deposition continued as the plateau became fully submerged and the sea transgressed over the entire plateau. Initially, intertidal to supratidal limestones were deposited in shallow-water, high-energy areas with some of the limestones reflecting quieter, subtidal conditions (Carlisle and Suzuki, 1974). Upsection, the Quatsino Formation reflects a slightly deeper-water depositional environment and abruptly grades into the overlying Parson Bay Formation (Carlisle & Suzuki, 1974; Nixon & Orr, 2007).

In Alaska and Yukon, the carbonates overlying the Nikolai basalts (>1000 m; Chitistone and Nizina limestones) preserve a record of the gradual submergence of the extensive Nikolai basalt platform. There are only rare occurrences of thin (<0.5 m) weathered zones or discontinuous, intervening clastic deposits at the top of ~3500 m of subaerial basalt flows in the Wrangell Mountains (Fig. 5.7; Armstrong *et al.*, 1969). The absence of significant erosion or deposition of clastic sediment, and the age of the Chitistone Limestone (Fig. 5.22), indicates only a brief interval of non-deposition

between the end of volcanism and carbonate deposition. Following volcanism, several cycles of shaley to argillaceous limestone were deposited in a high-energy, intertidal to supratidal (sahbka) environment, similar to the modern Persian Gulf, and form the lowest 100 m of the Chitistone (Armstrong *et al.*, 1969). Limey mudstone and wackestone with abundant disintegrated shelly material (~300 m thick) indicate gradual transition to low-energy shallow-water deposition with intermittent high-energy shoaling deposition. The upper part of the Chitistone and overlying Nizina Limestone reflect deeper-water deposition on a drowned carbonate platform (Armstrong *et al.* 1969). Gray to black shale and chert of the overlying McCarthy Formation represent submergence of the carbonate platform below the carbonate compensation depth (CCD; Armstrong *et al.* 1969). A thin tuff bed in the lower part of the McCarthy Formation has been dated at  $209.9 \pm 0.07$  Ma (J. Trop, 2006, pers. comm.) and the Triassic-Jurassic boundary is preserved in the upper McCarthy Formation (Fig. 5.22). Between the end of basaltic volcanism and the end of the Triassic (~25 Myr), approximately 2000 m of shallow- to deep-water marine sediments accumulated on top of the Nikolai basalts. Neglecting sediment compaction, this indicates a minimum subsidence rate of ~80 m/Myr. This subsidence decreased substantially, to less than 20 m/Myr, in the Early Jurassic (Saltus *et al.*, 2007).

Several oceanic plateaus and ocean islands worldwide preserve evidence of rapid subsidence after their formation (Detrick *et al.*, 1977) and mantle plume models predict subsidence following the formation of oceanic plateaus (e.g. Campbell & Griffiths, 1990). Subsidence may result from: dispersion of the mantle buoyancy anomaly above a plume; decay of the thermal anomaly and cooling and contraction of the lithosphere; removal of magma from the plume source, causing deflation of the plume head; and/or depression of the surface from loading of volcanic and plutonic material on the lithosphere (e.g. Detrick *et al.*, 1977; Campbell & Griffiths, 1990). Hawaiian volcanoes undergo rapid subsidence during their growth due to the response from loading of intrusive and extrusive magmas on the lithosphere (Moore & Clague, 1992). In Hawaii, subsidence, rather than rising sea level, accounts for the submergence of the volcanoes (Clague & Dalrymple, 1987). Pacific Cretaceous plateaus, such as Ontong Java, Manihiki and Shatsky, underwent significantly less subsidence than predicted by current models, with post-flood basalt subsidence comparable to that of normal ocean seafloor

(Ito & Clift, 1998; Roberge *et al.*, 2005). Drilling of the Kerguelen Plateau indicates subaerial flows, perhaps originally 1-2 km above sea level, subsided below sea level and paleoenvironments of the overlying sediments changed from intertidal to pelagic (Coffin, 1992; Frey *et al.*, 2000; Wallace, 2002). Subsidence estimates for the Northern Kerguelen Plateau (Site 1140) indicate ~1700 m of subsidence occurred since eruption of the basalts at 34 Ma (~50 m/Myr; Wallace, 2002). The subsidence history of Wrangellia may be more fully reconstructed by future studies that estimate the depth of sedimentation and age from microfossil data collected from sediments overlying the Karmutsen and Nikolai Formations.

## CONCLUSION

The volcanic stratigraphy of the obducted Wrangellia flood basalts records the construction of a major oceanic plateau. The Wrangellia basalts cover ~27,000 km<sup>2</sup> along the western edge of North America and are ~3.5 km thick in Alaska and ~6 km thick on Vancouver Island. The Wrangellia basalts in Alaska and Yukon are bounded by Middle to Late Triassic marine sediments and unconformably overlie Pennsylvanian and Permian marine sediments and volcanic arc sequences (ca. 312-280 Ma). The earliest flows were emplaced in a shallow marine environment, but the main phase of volcanism consisted of compound pahoehoe flow fields that form a tabular, shingled architecture. Grabens formed along the base of Wrangellia basalts in Yukon. The flows erupted from a limited number of eruption sites that are rarely observed, except for a large eruptive center in the Amphitheater Mountains.

Wrangellia basalts on Vancouver Island are bounded by Middle to Late Triassic marine sediments and unconformably overlie a basement of Devonian to Mississippian arc rocks and Mississippian to Permian marine sedimentary strata. Early growth of the volcanic stratigraphy on Vancouver Island was dominated by extrusion of pillow lavas and intrusion of sills into sedimentary strata. The plateau grew from the ocean floor and accumulated >3000 m of submarine flows, which were overlain by 400-1500 m of hyaloclastite and minor pillow basalt before the plateau breached sea level. The hyaloclastite formed primarily by quench fragmentation of effusive flows under low hydrostatic pressure. The plateau then grew above sea level as more than 1500 m of

subaerial flows were emplaced. The plateau subsided during its construction and intervolcanic sedimentary lenses formed in shallow water in local areas as eruptions waned. After volcanism ceased, the plateau continued to subside for more than 25 Myr and was overlain by hundreds to >1000 m of limestone and siliciclastic deposits.

The absence of intervening sediments in the volcanic stratigraphy and magnetic reversals preserved in the basalts attests to the brief duration of volcanism. Middle Ladinian *Daonella* just beneath the basalts in Alaska and Vancouver Island, and conodonts in limestones overlying the basalts, restrict volcanism to a maximum duration of less than ~10 Myr. The duration of volcanism in Northern and Southern Wrangellia was probably less than 5 Myr, and the ages of eruptions appear to overlap between ca. 230 and 225 Ma.

## ACKNOWLEDGEMENTS

This manuscript was influenced from discussions with Travis Hudson and material that he provided. We are grateful to Jeff Trop for his advice. Jeanine Schmidt and Peter Bittenbender were very helpful with data and ideas about Alaskan geology. Don Carlisle thoughtfully provided maps and notes that helped with fieldwork on Vancouver Island. Andrew Caruthers and Chris Ruttan helped with fieldwork on Vancouver Island. David Brew was very helpful with information about southeast Alaska. Funding was provided by research grants from the BC Geological Survey and Yukon Geological Survey, the Rocks to Riches Program administered by the BC & Yukon Chamber of Mines, and NSERC Discovery Grants to James Scoates and Dominique Weis. A. Greene was supported by a University Graduate Fellowship at UBC.

## REFERENCES

- Armstrong, A. K. & MacKevett, E. M., Jr. (1977). The Triassic Chitistone Limestone, Wrangell Mountains, Alaska. *U. S. Geological Survey. Open-File Report 77-217*, D49-D62 p.
- Armstrong, A. K., MacKevett, E. M., Jr. & Silberling, N. J. (1969). The Chitistone and Nizina limestones of part of the southern Wrangell Mountains—a preliminary report stressing carbonate petrography and depositional environments. *U. S. Geological Survey. Professional Paper 650-D*, D49-D62 p.

- Beard, J. S. & Barker, F. (1989). Petrology and tectonic significance of gabbros, tonalites, shoshonites, and anorthosites in a Late Paleozoic arc-root complex in the Wrangellia Terrane, southern Alaska. *Journal of Geology* **97**, 667-683.
- Ben-Avraham, Z., Nur, A., Jones, D. L. & Cox, A. (1981). Continental accretion: From oceanic plateaus to allochthonous terranes. *Science* **213**, 47-54.
- Bittenbender, P. E., Bean, K. W. & Gensler, E. G. (2003). Mineral Investigations in the Delta River Mining District, East-Central Alaska 2001-2002. *U. S. Bureau of Land Management-Alaska*. Open-File Report 91, 88 pages p.
- Bittenbender, P. E., Bean, K. W., Kurtak, J. M. & Deninger, J., Jr (2007). Mineral assessment of the Delta River Mining District area, East-central Alaska. *U. S. Bureau of Land Management-Alaska*. Technical Report 57, 676 p.  
[http://www.blm.gov/pgdata/etc/medialib/blm/ak/aktest/tr.Par.86412.File.dat/BLM\\_TR57.pdf](http://www.blm.gov/pgdata/etc/medialib/blm/ak/aktest/tr.Par.86412.File.dat/BLM_TR57.pdf).
- Blodgett, R. B. (2002). Paleontological Inventory of the Amphitheater Mountains, Mt. Hayes A-4 and A-5 Quadrangles, southcentral Alaska. *Alaska Division of Geological and Geophysical Surveys*. Report of Investigations 2002-3, 11 p.
- Brandon, M. T., Orchard, M. J., Parrish, R. R., Sutherland-Brown, A. & Yorath, C. J. (1986). Fossil ages and isotopic dates from the Paleozoic Sicker Group and associated intrusive rocks, Vancouver Island, British Columbia. *Geological Survey of Canada Paper 86-1A*. Current Research, Part A, 683-696 p.
- Brew, D. A. C. (2007, written comm.). Unpublished map showing the distribution of the Late Triassic Wrangellia, Hyd Group, and Perserverance group rocks in southeastern Alaska, scale 1:600,000 (Based on Brew, D. A. (Compiler), Unpublished bedrock geologic map of southeastern Alaska.)
- Burns, L. E., U. S. Bureau of Land Management, Fugro Airborne Surveys, & Stevens Exploration Management Corp. (2003). Color shadow magnetic map of the southern Delta River area, east-central Alaska. *Alaska Division of Geological and Geophysical Surveys*. Geophysical Report 2003-5-1C, 2 sheets, scale 1:63,360
- Burns, L. E. & Clautice, K. H. (2003). Portfolio of aeromagnetic and resistivity maps of the southern Delta River area, east-central Alaska. *Alaska Division of Geological and Geophysical Surveys*. Geophysical Report 2003-8, 16 p.
- Campbell, I. H. & Griffiths, R. W. (1990). Implications of mantle plume structure for the evolution of flood basalts. *Earth and Planetary Science Letters* **99**, 79-93.
- Campbell, S. W. (1981). Geology and genesis of copper deposits and associated host rocks in and near the Quill Creek area, southwestern Yukon. Unpublished Ph.D. dissertation, University of British Columbia, 215 pp.
- Carlisle, D. (1963). Pillow breccias and their aquagene tuffs, Quadra Island, British Columbia. *Journal of Geology* **71**, 48-71.
- Carlisle, D. (1972). Late Paleozoic to Mid-Triassic sedimentary-volcanic sequence on Northeastern Vancouver Island. *Geological Society of Canada Report of Activities 72-1*, Part B, 24-30 p.
- Carlisle, D. & Suzuki, T. (1974). Emergent basalt and submergent carbonate-clastic sequences including the Upper Triassic Dilleri and Welleri zones on Vancouver Island. *Canadian Journal of Earth Sciences* **11**, 254-279.
- Carne, R. C. (2003). Metallogeny of the Kluane Ranges, southwest Yukon Territory. <http://www.geology.gov.yk.ca/metallogeny/kluane/index.html>.



- Cho, M. & Liou, J. G. (1987). Prehnite-pumpellyite to greenschist facies transition in the Karmutsen Metabasites, Vancouver Island, B. C. *Journal of Petrology* **28**(3), 417-443.
- Clague, D. A. & Dalrymple, G. B. (1987). The Hawaiian-Emperor Volcanic Chain Part 1: geologic evolution. *U. S. Geological Survey Professional Paper* **1350**, 5-54.
- Clowes, R. M., Zelt, C. A., Amor, J. R. & Ellis, R. M. (1995). Lithospheric structure in the southern Canadian Cordillera from a network of seismic refraction lines. *Canadian Journal of Earth Sciences* **32**(10), 1485-1513.
- Coffin, M. F. (1992). Subsidence of the Kerguelen Plateau: the Atlantis concept. In: Wise Jr, S. W., Schlich, R. & al, e. (eds.) *Proceedings of Ocean Drilling Program, Scientific Results, 120*. Ocean Drilling Program: College Station, TX. pp. 945-949.
- Coffin, M. F. & Eldholm, O. (1994). Large igneous provinces: Crustal structure, dimensions, and external consequences. *Reviews of Geophysics* **32**(1), 1-36.
- Cohen, B. A. (2004). Can granulite metamorphic conditions reset  $^{40}\text{Ar}/^{39}\text{Ar}$  ages in lunar rocks? *Lunar and Planetary Science Conference XXXV*, abstract #1009.
- Coney, P. J., Jones, D. L. & Monger, J. W. H. (1980). Cordilleran suspect terranes. *Nature* **288**(5789), 329.
- Csejtei, B., Jr., Cox, D. P., Evarts, R. C., Stricker, G. D. & Foster, H. L. (1982). The Cenozoic Denali fault system and the Cretaceous accretionary development of southern Alaska. *Journal of Geophysical Research* **87**, 3741-3754.
- Decker, J. E. (1981). Geochemical signature of the Goon Dip Greenstone on Chichagof Island, southeastern Alaska. *Alaska Division of Geological & Geophysical Surveys*. Geologic Report 73G, 29-35 p.
- Detrick, R. S., Sclater, J. G. & Thiede, J. (1977). The subsidence of aseismic ridges. *Earth and Planetary Science Letters* **34**, 185-198.
- Detterman, R. L. & Reed, B. L. (1980). Stratigraphy, structure, and economic geology of the Iliamna quadrangle, Alaska. *U. S. Geological Survey*. Bulletin 1368-B, 86 p.
- Dodds, C. J. & Campbell, R. B. (1988). Potassium-argon ages of mainly intrusive rocks in the Saint Elias Mountains, Yukon and British Columbia. *Geological Society of Canada*. Paper 87-16, 43 p.
- Frey, F. A., Coffin, M. F., Wallace, P. J., Weis, D., Zhao, X., Wise, S. W., Jr., Wähnert, V., Teagle, D. A. H., Saccoccia, P. J., Reusch, D. N., Pringle, M. S., Nicolaysen, K. E., Neal, C. R., Müller, R. D., Moore, C. L., Mahoney, J. J., Keszthelyi, L., Inokuchi, H., Duncan, R. A., Delius, H., Damuth, J. E., Damasceno, D., Coxall, H. K., Borre, M. K., Boehm, F., Barling, J., Arndt, N. T. & Antretter, M. (2000). Origin and evolution of a submarine large igneous province: the Kerguelen Plateau and Broken Ridge, southern Indian Ocean. *Earth and Planetary Science Letters* **176**, 73-89.
- Furin, S., Preto, N., Rigo, M., Roghi, G., Gianolla, P., Crowley, J. L. & Bowring, S. A. (2006). High-precision U-Pb zircon age from the Triassic of Italy: Implications for the Triassic time scale and the Carnian origin of calcareous nannoplankton and dinosaurs. *Geology* **34**(12), 1009-1012, 10.1130/g22967a.1.
- Garcia, M. O., Haskins, E. H., Stolper, E. M. & Baker, M. (2007). Stratigraphy of the Hawai'i Scientific Drilling Project core (HSDP2): Anatomy of a Hawaiian shield

- volcano. *Geochemistry Geophysics Geosystems* 8(Q02G20), doi:10.1029/2006GC001379.
- Gardner, M. C., Bergman, S. C., Cushing, G. W., MacKevett, E. M., Jr., Plafker, G., Campbell, R. B., Dodds, C. J., McClelland, W. C. & Mueller, P. A. (1988). Pennsylvanian pluton stitching of Wrangellia and the Alexander terrane, Wrangell Mountains, Alaska. *Geology* 16, 967-971.
- Gehrels, G. E. & Barker, F. (1992). Reconnaissance geochemistry of Permian and Triassic basalts of the Taku and Wrangellia terranes, Southeastern Alaska. *U. S. Geological Survey Geologic Circular*. Geologic studies in Alaska by the U. S. Geological Survey, 1992, 218-227 p.
- Glen, J. M. G., Schmidt, J. M. & Morin, R. (2007a). Gravity and magnetic studies of the Talkeetna Mountains, Alaska: constraints on the geological and tectonic interpretation of southern Alaska, and implications for mineral exploration. In: Ridgway, K. D., Trop, J. M., O'Neill, J. M. & Glen, J. M. G. (eds.) *Tectonic Growth of a Collisional Continental Margin: Crustal Evolution of Southern Alaska*. Geological Society of America Special Paper 431, pp. 593-622.
- Glen, J. M. G., Schmidt, J. M., Pellerin, L., O'Neill, M. & McPhee, D. K. (2007b). Crustal structure of Wrangellia and adjacent terranes inferred from geophysical studies along a transect through the northern Talkeetna Mountains. In: Ridgway, K. D., Trop, J. M., O'Neill, J. M. & Glen, J. M. G. (eds.) *Tectonic Growth of a Collisional Continental Margin: Crustal Evolution of Southern Alaska*. Geological Society of America Special Paper 431. pp. 21-42.
- Gradstein, F. M., Ogg, J. G. & Smith, A. G. (eds.) (2004). *A Geologic Time Scale 2004*. Cambridge University Press 610 pp.
- Grantz, A., Jones, D. L. & Lanphere, M. A. (1966). Stratigraphy, paleontology, and isotopic ages of upper Mesozoic rocks in the southwestern Wrangell Mountains, Alaska. *U. S. Geological Survey Professional Paper* 550-C, 39-47 p.
- Greene, A. R., Scoates, J. S., Weis, D. & Israel, S. (2005). Flood basalts of the Wrangellia Terrane, southwest Yukon: Implications for the formation of oceanic plateaus, continental crust and Ni-Cu-PGE mineralization. In: Emond, D. S., Lewis, L. L. & Bradshaw, G. D. (eds.) *Yukon Exploration and Geology 2004*. Yukon Geological Survey. pp. 109-120.
- Greene, A. R., Scoates, J. S., Nixon, G. T. & Weis, D. (2006). Picritic lavas and basal sills in the Karmutsen flood basalt province, Wrangellia, northern Vancouver Island. In: Grant, B. (ed.) *Geological Fieldwork 2005*. British Columbia Ministry of Energy, Mines and Petroleum Resources. Paper 2006-1, pp. 39-52.
- Greene, A. R., Scoates, J. S. & Weis, D. (2008, submitted-a). Wrangellia flood basalts in Alaska: A record of plume-lithosphere interaction in a Late Triassic accreted oceanic plateau. *Geochemistry Geophysics Geosystems*.
- Greene, A. R., Scoates, J. S., Weis, D. & Israel, S. (2008, submitted-b). Geochemistry of flood basalts from the Yukon (Canada) segment of the accreted Wrangellia oceanic plateau. *Lithos*.
- Greene, A. R., Scoates, J. S., Weis, D., Nixon, G. T. & Kieffer, B. (2008, submitted-c). Wrangellia flood basalts on Vancouver Island: Significance of picritic and tholeiitic lavas for the melting history and magmatic evolution of a major oceanic plateau. *Journal of Petrology*.

- Harrison, T. M. & McDougall, I. (1981). Excess  $^{40}\text{Ar}$  in metamorphic rocks from Broken Hill, New South Wales: Implications for  $^{40}\text{Ar}/^{39}\text{Ar}$  age spectra and the thermal history of the region. *Earth and Planetary Science Letters* **55**, 123-149.
- Henderson, C. M. & Orchard, M. J. (1991). Gondolelloides, a new Lower Permian conodont genus from western and northern Canada. In: Orchard, M. J. & McCracken, A. D. (eds.) *Ordovician to Triassic Conodont Paleontology of the Canadian Cordillera*. Geological Survey of Canada Bulletin 417. pp. 253-267.
- Hesthammer, J., Indrelid, J., Lewis, P. D. & Orchard, M. J. (1991). Permian strata on the Queen Charlotte Islands, British Columbia. Current Research, Part A, Cordillera and Pacific margin. *Geological Survey of Canada*. Report 91-01A, 321-329 p.
- Hillhouse, J. W. (1977). Paleomagnetism of the Triassic Nikolai Greenstone, McCarthy Quadrangle, Alaska. *Canadian Journal of Earth Sciences* **14**, 2578-3592.
- Hillhouse, J. W. & Gromme, C. S. (1984). Northward displacement and accretion of Wrangellia: New paleomagnetic evidence from Alaska. *Journal of Geophysical Research* **89**, 4461-4467.
- Hodges, K. V. (2003). Geochronology and thermochronology in orogenic systems. In: Rudnick, R. (ed.) *The Crust*. Elsevier-Pergamon: Oxford. Treatise on Geochemistry Vol. 3, Holland, H. D. & Turekian, K. K. (eds.), pp. 263-292.
- Hudson, T. (1983). Calk-alkaline plutonism along the Pacific Rim of southern Alaska. In: Roddick, J. A. (ed.) *Circum-Pacific Plutonic Terranes*. Geological Society of America Memoir 159. pp. 159-169.
- Irving, E. & Yule, R. W. (1972). Paleomagnetism and kinematic history of mafic and ultramafic rocks in fold mountain belts. *Earth Physics Branch Publications* **42**, 87-95.
- Israel, S. (2004). Geology of Southwestern Yukon (1:250 000 scale). *Yukon Geological Survey* Open File 2004-16.
- Israel, S. & Cobbett, R. (2008). Kluane Ranges bedrock geology, White River area (Parts of NTS 115F/9, 15 and 16; 115G/12 and 115K/1, 2). In: Emond, D. S., Blackburn, L. R., Hill, R. P. & Weston, L. H. (eds.) *Yukon Exploration and Geology 2007*. Yukon Geological Survey. pp. 153-167.
- Israel, S., Tizzard, A. & Major, J. (2005). Geological map of the Duke River area (parts of NTS 115G/2, 3, 5, 6, 7), Yukon (1:50 000 scale). *Yukon Geological Survey*. Open File 2005-11
- Israel, S., Tizzard, A. & Major, J. (2006). Bedrock geology of the Duke River area, parts of NTS 115G/2, 3, 4, 6 and 7, southwestern Yukon. In: Emond, D. S., Bradshaw, G. D., Lewis, L. L. & Weston, L. H. (eds.) *Yukon Exploration and Geology 2005*. Yukon Geological Survey. pp. 139-154.
- Israel, S. & Van Zeyl, D. (2004). Preliminary geological map of the Quill Creek area (parts of NTS 115G/5,6,12), southwest Yukon (1:50,000 scale). *Yukon Geological Survey*. Open File 2004-20
- Israel, S. & Van Zeyl, D. P. (2005). Preliminary geology of the Quill Creek map area, southwest Yukon parts of NTS 115G/5, 6 and 12. In: Emond, D. S., Lewis, L. L. & Bradshaw, G. D. (eds.) *Yukon Exploration and Geology 2004*. Yukon Geological Survey. pp. 129-146.
- Ito, G. & Clift, P. D. (1998). Subsidence and growth of Pacific Cretaceous plateaus. *Earth and Planetary Science Letters* **161**, 85-100.

- Jeletzky, J. A. (1976). Mesozoic and Tertiary rocks of Quatsino Sound, Vancouver Island, British Columbia. *Geological Survey of Canada*. Bulletin 242, 243 p.
- Jerram, D. A. & Widdowson, M. (2005). The anatomy of Continental Flood Basalt Provinces: geological constraints on the processes and products of flood volcanism. *Lithos* 79(3-4), 385.
- Jones, D. L., Silberling, N. J. & Hillhouse, J. (1977). Wrangellia; a displaced terrane in northwestern North America. *Canadian Journal of Earth Sciences* 14(11), 2565-2577.
- Jones, J. G. (1969). Pillow lavas as depth indicators. *American Journal of Science* 267, 181-195.
- Juras, S. J. (1987). Geology of the polymetallic volcanogenic Buttle Lake Camp, with emphasis on the Prince Hillside, Vancouver Island, British Columbia, Canada. Unpublished Ph.D. dissertation, University of British Columbia, 279 pp.
- Katvala, E. C. & Henderson, C. M. (2002). Conodont sequence biostratigraphy and paleogeography of the Pennsylvanian-Permian Mount Mark and Fourth Lake Formations, southern Vancouver Island. In: Hills, L. V., Henderson, C. M. & Bamber, E. W. (eds.) *Carboniferous and Permian of the World*. Canadian Society of Petroleum Geologists Memoir 19. pp. 461-478.
- Katvala, E. C. & Stanley, G. D., Jr. (2008, in press). Conodont biostratigraphy and facies correlations in a Late Triassic island arc, Keku Strait, Southeast Alaska. In: Blodgett, R. B. & Stanley, G. D., Jr. (eds.) *The Terrane Puzzle: New Perspectives on Paleontology and Stratigraphy from the North American Cordillera*. Geological Society of America. Special Paper 442, pp.
- Kokelaar, P. (1986). Magma-water interactions in subaqueous and emergent basaltic volcanism. *Bulletin of Volcanology* 48, 275-289.
- Koppers, A. A. P. (2002). ArArCALC—software for  $^{40}\text{Ar}/^{39}\text{Ar}$  age calculations. *Computers & Geosciences* 28(5), 605-619.
- Lanphere, M. A. & Dalrymple, G. B. (1976). Identification of excess  $^{40}\text{Ar}$  by the  $^{40}\text{Ar}/^{39}\text{Ar}$  age spectrum technique. *Earth and Planetary Science Letters* 32, 141-148.
- Lassiter, J. C. (1995). Geochemical investigations of plume-related lavas: constraints on the structure of mantle plumes and the nature of plume/lithosphere interactions. Unpublished Ph.D. dissertation (chapter 2), University of California, Berkeley, 231 pp.
- Lewis, P. D., Haggart, J. W., Anderson, R. G., Hickson, C. J., Thompson, R. I., Dietrich, J. R. & Rohr, K. M. M. (1991). Triassic to Neogene geological evolution of the Queen Charlotte region. *Canadian Journal of Earth Sciences* 28(6), 854-869.
- Loney, R. A. (1964). Stratigraphy and petrography of the Pybus-Gambier area, Admiralty Island, Alaska. *U. S. Geological Survey*. Bulletin 1178
- MacKevett, E. M., Jr. (1970). Geology of the McCarthy B-4 quadrangle, Alaska. *U.S. Geological Survey*. Bulletin 1333, 31 p.
- MacKevett, E. M., Jr. (1971). Stratigraphy and general geology of the McCarthy C-5 Quadrangle, Alaska. *U. S. Geological Survey*. Bulletin 1323, 35 p.
- MacKevett, E. M., Jr. (1978). Geologic map of the McCarthy Quadrangle, Alaska. *U. S. Geological Survey*. Miscellaneous Investigations Series Map I-1032 scale 1:250,000

- MacKevett, E. M., Jr., Berg, H. C., Plafker, G. & Jones, D. L. (1964). Preliminary geologic map of the McCarthy C-4 quadrangle, Alaska. *U. S. Geological Survey. Miscellaneous Geological Investigations Map I-423*, scale 1:63,360
- Mahoney, J. J. & Coffin, M. F. (eds.) (1997). *Large Igneous Provinces: Continental, Oceanic, and Planetary Flood Volcanism*. AGU Geophysical Monograph 100. 438 pp.
- Massey, N. W. D. (1995). Geology and mineral resources of the Alberni-Nanaimo Lakes sheet, Vancouver Island 92F/1W, 92F/2E, and part of 92F/7E. *B.C. Ministry of Energy, Mines and Petroleum Resources. Paper 1992-2*, 132 p.
- Massey, N. W. D. & Friday, S. J. (1988). Geology of the Chemainus River-Duncan Area, Vancouver Island (92C/16; 92B/13). In: *Geological Fieldwork 1987*. B.C. Ministry of Energy, Mines and Petroleum Resources Paper 1988-1. pp. 81-91.
- Massey, N. W. D., MacIntyre, D. G., Desjardins, P. J. & Cooney, R. T. (2005a). Digital Geology Map of British Columbia: Tile NM9 Mid Coast, B.C. *B.C. Ministry of Energy and Mines Geofile 2005-2*.
- Massey, N. W. D., MacIntyre, D. G., Desjardins, P. J. & Cooney, R. T. (2005b). Digital Geology Map of British Columbia: Tile NM10 Southwest B.C. *B.C. Ministry of Energy and Mines Geofile 2005-3*.
- McClelland, W. C., Gehrels, G. E. & Saleeby, J. B. (1992). Upper Jurassic-Lower Cretaceous basinal strata along the Cordilleran margin: Implication for the accretionary history of the Alexander-Wrangellia-Peninsular terranes. *Tectonics* **11**, 823-835.
- Monger, J. W. H. & Journeay, J. M. (1994). Basement geology and tectonic evolution of the Vancouver region. In: Monger, J. W. H. (ed.) *Geology and Geological Hazards of the Vancouver Region, Southwestern British Columbia*. Geological Survey of Canada Bulletin, 481. pp. 3-25.
- Monger, J. W. H., Price, R. A. & Tempelman-Kluit, D. J. (1982). Tectonic accretion and the origin of the two major metamorphic and plutonic belts in the Canadian Cordillera. *Geology* **10**(2), 70-75.
- Moore, J. G. & Clague, D. A. (1992). Volcano growth and evolution of the island of Hawaii. *Geological Society of America Bulletin* **104**, 1471-1484.
- Mortensen, J. K. & Hulbert, L. J. (1991). A U-Pb zircon age for a Maple Creek gabbro sill, Tatamagouche Creek area, southwestern Yukon Territory. *Geological Survey of Canada. Radiogenic Age and Isotopic Studies: Report 5 Paper 91-2*, 175-179 p.
- Muffler, L. J. P. (1967). Stratigraphy of the Keku Islets and neighboring parts of Kuiu and Kupreanof Islands, southeastern Alaska. *U.S. Geological Survey. Bulletin* **1241-C**, 52 p.
- Muller, J. E. (1967). Kluane Lake map area, Yukon Territory (115G, 115F/E 1/2). *Geological Survey of Canada. Memoir* **340**, 137 p.
- Muller, J. E. (1977). Geology of Vancouver Island. *Geological Survey of Canada Open File Map* **463**.
- Muller, J. E., Northcote, K. E. & Carlisle, D. (1974). Geology and mineral deposits of Alert Bay - Cape Scott map area, Vancouver Island, British Columbia. *Geological Survey of Canada, Paper* **74-8**, 77 pp.
- Newton, C. R. (1983). Paleozoogeographic affinities of Norian bivalves from the Wrangellian, Peninsular, and Alexander terranes, northwestern North America.

- In: Stevens, C. H. (ed.) *Pre-Jurassic Rocks in Western North American Suspect Terranes*. Pacific Section, Society of Economic Paleontologists and Mineralogists. pp. 37-48.
- Nixon, G. T., Laroque, J., Pals, A., Styan, J., Greene, A. R. & Scoates, J. S. (2008). High-Mg lavas in the Karmutsen flood basalts, northern Vancouver Island (NTS 092L): Stratigraphic setting and metallogenic significance. In: Grant, B. (ed.) *Geological Fieldwork 2007*. B.C. Ministry of Energy, Mines and Petroleum Resources Paper 2008-1. pp. 175-190.
- Nixon, G. T. & Orr, A. J. (2007). Recent revisions to the Early Mesozoic stratigraphy of Northern Vancouver Island (NTS 102I; 092L) and metallogenic implications, British Columbia. In: Grant, B. (ed.) *Geological Fieldwork 2006*. B.C. Ministry of Energy, Mines and Petroleum Resources Paper 2007-1. pp. 163-177.
- Nokleberg, W. J., Aleinikoff, J. N., Dutro, J. T. J., Lanphere, M. A., Silberling, N. J., Silva, S. R., Smith, T. E. & Turner, D. L. (1992). Map, tables, and summary fossil and isotopic age data, Mount Hayes quadrangle, eastern Alaska Range, Alaska. *U. S. Geological Survey Miscellaneous Field Studies Map 1996-D*, 1:250,000 scale.
- Nokleberg, W. J., Jones, D. L. & Silberling, N. J. (1985). Origin and tectonic evolution of the Maclaren and Wrangellia terranes, eastern Alaska Range, Alaska. *Geological Society of America Bulletin* **96**, 1251-1270.
- Nokleberg, W. J., Plafker, G. & Wilson, F. H. (1994). Geology of south-central Alaska. In: Plafker, G. & Berg, H. C. (eds.) *The Geology of North America*. Geological Society of America: Boulder, CO. The Geology of Alaska G-1, pp. 311-366.
- Ogg, J. G. (2004). The Triassic Period. In: Gradstein, F. M., Ogg, J. G. & Smith, A. G. (eds.) *A Geologic Time Scale 2004*. Cambridge University Press: Cambridge. pp. 271-306.
- Orchard, M. J. (1986). Conodonts from Western Canadian Chert: Their Nature, Distribution and Stratigraphic Application. In: Austin, R. L. (ed.) *Conodonts, Investigative Techniques and Applications: Proceeding of the Fourth European Conodont Symposium (ECOS IV)*. Ellis-Horwood, U.K., pp. 96-121.
- Parrish, R. R. & McNicoll, V. J. (1992). U-Pb age determinations from the southern Vancouver Island area, British Columbia. *Geological Survey of Canada. Radiogenic Age and Isotopic Studies: Report 5 Paper 91-2*, 79-86 p.
- Petterson, M. G. (2004). The geology of north and central Malaita, Solomon Islands: the thickest and most accessible part of the world's largest (Ontong Java) oceanic plateau. In: Fitton, J. G., Mahoney, J. J., Wallace, P. J. & Saunders, A. D. (eds.) *Origin and Evolution of the Ontong Java Plateau*. Geological Society. Special Publication 229, pp. 63-81.
- Plafker, G. & Berg, H. C. (1994). Overview of the geology and tectonic evolution of Alaska. In: G., P. & H.C., B. (eds.) *The Geology of North America*. Geological Society of America: Boulder, CO. The Geology of Alaska G-1, pp. 989-1021.
- Plafker, G., Blome, C. D. & Silberling, N. J. (1989a). Reinterpretation of lower Mesozoic rocks on the Chilkat Peninsula, Alaska, as a displaced fragment of Wrangellia. *Geology* **17**, 3-6.
- Plafker, G. & Hudson, T. (1980). Regional implications of the Upper Triassic metavolcanic and metasedimentary rocks on the Chilkat Peninsula, southeastern Alaska. *Canadian Journal of Earth Sciences* **17**(6), 681-689.

- Plafker, G., Moore, J. C. & Winkler, G. R. (1994). Geology of the southern Alaska margin. In: Plafker, G. & Berg, H. C. (eds.) *The Geology of North America*. Geological Society of America: Boulder, CO. The Geology of Alaska G-1, pp. 389-449.
- Plafker, G., Nokleberg, W. J. & Lull, J. S. (1989b). Bedrock geology and tectonic evolution of the Wrangellia, Peninsular, and Chugach terranes along the Trans-Alaskan Crustal Transect in the northern Chugach Mountains and southern Copper River basin, Alaska. *Journal of Geophysical Research* **94**, 4,255-4,295.
- Prichard, R. A. (2003). Project report of the airborne geophysical survey for the southern Delta River area, east-central Alaska. *Alaska Division of Geological and Geophysical Surveys* Geophysical Report 2003-7, 2 sheets, scale 1:63,360, 252 p.
- Read, P. B. & Monger, J. W. H. (1976). Pre-Cenozoic volcanic assemblages of the Kluane and Alsek Ranges, southwestern Yukon Territory. *Geological Survey of Canada*. Open-File Report 381, 96 p.
- Renne, P. R., Swisher, C. C., III, Deino, A. L., Karner, D. B., Owens, T. & DePaolo, D. J. (1998). Intercalibration of standards, absolute ages and uncertainties in  $^{40}\text{Ar}/^{39}\text{Ar}$  dating. *Chemical Geology* **145**(1-2), 117-152.
- Richards, M. A., Jones, D. L., Duncan, R. A. & DePaolo, D. J. (1991). A mantle plume initiation model for the Wrangellia flood basalt and other oceanic plateaus. *Science* **254**, 263-267.
- Richter, D. H. (1976). Geologic map of the Nabesna Quadrangle, Alaska. *U. S. Geological Survey*. Miscellaneous Geologic Investigations Map I-932, scale 1:250,000
- Roberge, J., Wallace, P. J., White, R. V. & Coffin, M. F. (2005). Anomalous uplift and subsidence of the Ontong Java Plateau inferred from  $\text{CO}_2$  contents of submarine basaltic glasses. *Geology* **33**(6), 501-504.
- Roeske, S. M., Snee, L. W. & Pavlis, T. L. (2003). Dextral-slip reactivation of an arc-forearc boundary during Late Cretaceous-Early Eocene oblique convergence in the northern Cordillera. In: Sisson, V. B., Roeske, S. M. & Pavlis, T. L. (eds.) *Geology of a Transpressional Orogen Developed During Ridge-Trench Interaction Along the North Pacific Margin*. Geological Society of America: Boulder, Colorado. 371, pp. 141-169.
- Saleeby, J. B. (1983). Accretionary tectonics of the North American cordillera. *Annual Review of Earth and Planetary Sciences* **15**, 45-73.
- Saltus, R. W., Hudson, T. & Wilson, F. H. (2007). The geophysical character of southern Alaska: Implications for crustal evolution. In: Ridgeway, K. D., Trop, J. M., O'Neill, J. M. & Glen, J. M. G. (eds.) *Tectonic Growth of a Collisional Continental Margin: Crustal Evolution of Southern Alaska*. Geological Society of America Special Paper 431, pp. 1-20.
- Samson, S. D. & Alexander, E. C. (1987). Calibration of the interlaboratory  $^{40}\text{Ar}/^{39}\text{Ar}$  dating standard, MMhb1. *Chemical Geology* **66**, 27-34.
- Saunders, A. D., Jones, S. M., Morgan, L. A., Pierce, K. L., Widdowson, M. & Xu, Y. G. (2007). Regional uplift associated with continental large igneous provinces: The roles of mantle plumes and the lithosphere. *Chemical Geology* **241**(3-4), 282.



- Schatz, W. (2005). Palaeoecology of the Triassic black shale bivalve *Daonella*--new insights into an old controversy. *Palaeogeography, Palaeoclimatology, Palaeoecology* **216**(3-4), 189.
- Schmidt, J. M., O'Neill, J. M., Snee, L. W., Blodgett, R. B., Ridgeway, K. D., Wardlaw, B. R. & Blome, C. D. (2003a). The Northwestern edge of Wrangellia: Stratigraphic and intrusive links between crustal block from the Peninsular Terrane to Broad Pass. *Geological Society of America Cordilleran Section*, Volume 35, No. 6, p. 560.
- Schmidt, J. M. & Rogers, R. K. (2007). Metallogeny of the Nikolai large igneous province (LIP) in southern Alaska and its influence on the mineral potential of the Talkeetna Mountains. In: Ridgway, K. D., Trop, J. M., O'Neill, J. M. & Glen, J. M. G. (eds.) *Tectonic Growth of a Collisional Continental Margin: Crustal Evolution of Southern Alaska*. Geological Society of America Special Paper 431, pp. 623-648.
- Schmidt, J. M., Weldon, M. B. & Wardlaw, B. (2003b). New mapping near Iron Creek, Talkeetna Mountains, indicates presence of Nikolai greenstone. In: Clautice, K. H. & Davis, P. K. (eds.) *Short Notes on Alaska Geology 2003*. Alaska Division of Geological & Geophysical Surveys Professional Report 120J, pp. 101-108.
- Schmidt, R. & Schmicke, H. U. (2000). Seamounts and island building. In: Sigurdsson, H. (ed.) *Encyclopedia of Volcanoes*. Academic Press: San Diego. pp. 383-402.
- Self, S., T., T. & L., K. (1997). Emplacement of continental flood basalt lava flows. In: Mahoney, J. J. & Coffin, M. F. (eds.) *Large Igneous Provinces: Continental, Oceanic, and Planetary Flood Volcanism*. American Geophysical Union: Washington. Geophysical Monograph 100, pp. 381-410.
- Sircombe, K. N. (2004). AGEDISPLAY: an EXCEL workbook to evaluate and display univariate geochronological data using binned frequency histograms and probability density distributions. *Computers & Geosciences* **30**(1), 21.
- Sluggett, C. L. (2003). Uranium-lead age and geochemical constraints on Paleozoic and Early Mesozoic magmatism in Wrangellia Terrane, Salt Spring Island, British Columbia. Unpublished B.Sc. thesis, University of British Columbia, 84 pp.
- Smith, J. G. & MacKevett, E. M., Jr. (1970). The Skolai Group in the McCarthy B-4, C-4, C-5 Quadrangles, Wrangell Mountains, Alaska. *U. S. Geological Survey. Bulletin* 1274-Q, Q1-Q26 p.
- Smith, P. L. (2006). Paleobiogeography and Early Jurassic molluscs in the context of terrane displacement in western Canada. In: Haggart, J. W., Enkin, R. J. & Monger, J. W. H. (eds.) *Paleogeography of the North American Cordillera: Evidence For and Against Large-Scale Displacements*. Geological Association of Canada. Special Paper 46, pp. 81-94.
- Smith, T. E. (1981). Geology of the Clearwater Mountains, south-central Alaska. *Alaska Division of Geological and Geophysical Surveys. Geologic Report* 60, 72 p. <http://www.dggs.dnr.state.ak.us/scan2/gr/text/GR60.PDF>.
- Sutherland Brown, A. (1968). Geology of the Queen Charlotte Islands, British Columbia. *BC Department of Mines and Petroleum Resources, Bulletin* **54**, 226 p.
- Trop, J. M. & Ridgway, K. D. (2007). Mesozoic and Cenozoic tectonic growth of southern Alaska: A sedimentary basin perspective. In: Ridgway, K. D., Trop, J. M., O'Neill, J. M. & Glen, J. M. G. (eds.) *Tectonic Growth of a Collisional*

- Continental Margin: Crustal Evolution of Southern Alaska*. Geological Society of America Special Paper 431, pp. 55-94.
- Umhoefer, P. J. & Blakey, R. C. (2006). Moderate (1600 km) northward translation of Baja British Columbia from southern California: An attempt at reconciliation of paleomagnetism and geology. In: Haggart, J. W., Enkin, R. J. & Monger, J. W. H. (eds.) *Paleogeography of the North American Cordillera: Evidence For and Against Large-Scale Displacements*. Geological Association of Canada. Special Paper 46, pp. 307-329.
- Wallace, P. J. (2002). Volatiles in submarine basaltic glasses from the Northern Kerguelen Plateau (ODP Site 1140): implications for source region compositions, magmatic processes, and plateau subsidence. *Journal of Petrology* **43**, 1311-1326.
- Wheeler, J. O. & McFeely, P. (1991). Tectonic assemblage map of the Canadian Cordillera and adjacent part of the United States of America. *Geological Survey of Canada* Map 1712A.
- White, S. M., Crisp, J. A. & Spera, F. J. (2006). Long-term volumetric eruption rates and magma budgets. *Geochemistry Geophysics Geosystems* **7**, Q03010, doi:10.1029/2005GC001002.
- Wilson, F. H., Dover, J. D., Bradley, D. C., Weber, F. R., Bundtzen, T. K. & Haeussler, P. J. (1998). Geologic map of Central (Interior) Alaska. *U. S. Geological Survey Open-File Report 98-133-A* <http://wrgis.wr.usgs.gov/open-file/of98-133-a/>.
- Wilson, F. H., Labay, K. A., Shew, N. B., Preller, C. C., Mohadjer, S. & Richter, D. H. (2005). Digital Data for the Geology of Wrangell-Saint Elias National Park and Preserve, Alaska *U. S. Geological Survey Open-File Report 2005-1342*. <http://pubs.usgs.gov/of/2005/1342/>.
- Yole, R. W. (1969). Upper Paleozoic stratigraphy of Vancouver Island, British Columbia. *Proceedings of the Geological Association of Canada* **20**, 30-40.
- Yorath, C. J., Sutherland Brown, A. & Massey, N. W. D. (1999). LITHOPROBE, southern Vancouver Island, British Columbia. *Geological Survey of Canada*. LITHOPROBE, southern Vancouver Island, British Columbia Bulletin 498, 145 p.

## **CHAPTER 6**

### **Conclusions**

## CONCLUSIONS AND DIRECTIONS FOR FUTURE RESEARCH

There have been considerable gains made in understanding of the origin and growth of the Wrangellia oceanic plateau as a result of this project, yet a great deal continues to remain elusive and is ideally suited for prospective research. The obducted parts of an accreted oceanic plateau offer the best way to observe and sample the volcanic stratigraphy of oceanic plateaus, in a similar way that ophiolites provide a way to examine rocks that form in mid-ocean ridges. The development of a complete understanding of the architecture, source and evolution of basaltic magmas, and timescale of formation of oceanic plateaus is essential for furthering our understanding of the origin and evolution of oceanic plateaus.

The ideas presented in the four main chapters in this dissertation represent some of the more recent advances in understanding the formation of the Wrangellia oceanic plateau. The contributions in this study include: (1) extensive reconnaissance fieldwork in BC, Yukon, and Alaska; (2) geologic map compilations of the entire extent of Wrangellia flood basalts; (3) photographic database (>1000 photographs); (4) reference database on Wrangellia (>500 references); (5) archived samples of the volcanic stratigraphy (>300 samples and thin-sections); (6) major- and trace-element analyses of 175 samples; (7) Sr-Nd-Hf-Pb isotopic analyses of 75 samples; (8) assessment of alteration of the basalts; (9) characterization of the composition of the source of Wrangellia basalts; (10) major-element modeling of melting conditions, primary melt compositions, and magmatic evolution; (11) trace-element dynamic melting modeling; (12) flood basalt chemostratigraphy in Alaska and studies of plume-lithosphere interaction; (13) detailed description and photographic illustration of volcanic stratigraphy and relationships with underlying and overlying units throughout Wrangellia; (14) Google Earth archiving of sample locations, mapped flood basalts, and field photographs. (15) Ar-Ar geochronology of 20 samples from throughout Wrangellia; (16) sampling of fossils and paleontological age determinations of bivalves in sediments beneath the flood basalts; (17) comprehensive summary of previous research on Wrangellia; (18) publication of 3 geological survey field reports (Greene *et al.* 2005a, 2005b, 2006); (19) abstracts and presentations at 8 scientific conferences; (20) co-author on 4 conference proceedings and 1 geological survey report; (21) preparation/submittal of 4 manuscripts for publication.

The four main chapters of this dissertation have each yielded an important set of interpretations about the source, generation, and emplacement of basalts of the Wrangellia oceanic plateau. The geochemistry of picritic and tholeiitic basalts that form the Karmutsen Formation provide constraints about the melting history of plume-derived magmas where continental lithosphere and significant source heterogeneity were not involved. The tripartite stratigraphy on Vancouver Island is constructed largely of tholeiitic basalt with a restricted major- and trace-element, and isotopic composition. The high-Mg picritic pillow lavas on northern Vancouver Island are depleted in LREE and have similar initial isotopic compositions to the tholeiitic basalts. Modeling results for the picrites, utilizing the technique of Herzberg *et al.* (2007), support that the Karmutsen Formation originated from high degrees of partial melting (25-30%) of unusually hot mantle (~1450°C) during the start-up phase of a mantle plume. The picrites developed a depleted trace-element signature, likely during melting of the plume. The isotopic compositions of the tholeiitic basalts and picrites indicate a homogeneous, OIB-type enriched Pacific mantle source, less depleted than the source of MORB, and comparable to the source that produced basalts of the Caribbean oceanic plateau. Decompression melting within the mantle plume initiated within the garnet stability field (>2.7 GPa; 80 km) and proceeded beneath oceanic lithosphere where more extensive degrees of melting occurred within the spinel stability field (<60 km). The trace-element compositions of the Wrangellia flood basalts are best explained by a peridotite source rather than a source consisting of a high proportion of eclogite. The major-element compositions of Karmutsen tholeiitic basalts (low Mg#, MgO, etc.) indicate an important role for fractional crystallization of melts at low pressure and some of the crystalline residues from partially crystallized Karmutsen magmas may be present beneath Vancouver Island.

The geochemistry of Wrangellia basalts in Alaska and Yukon has helped to improve our understanding of the relationship between mantle plumes and oceanic lithosphere through which the basaltic magmas erupted. The volcanic stratigraphy in Alaska and Yukon preserves a shift from low-titanium to high-titanium basalts and provides compositional evidence of plume-lithosphere interaction during the formation of the northern part of the Wrangellia oceanic plateau. The trace-element and isotopic compositions of the high- and low-titanium basalts are distinct and indicate involvement

of arc lithospheric mantle in the formation of the low-titanium basalts. In a similar way that CFBs acquire geochemical characteristics from the lithosphere through which they erupt, basalts erupted in oceanic plateaus can acquire geochemical properties of oceanic arc lithosphere when present. Results from geochemical modeling suggest that small-degree melting (1-5%) of arc mantle may explain the trace-element signature of the low-titanium basalts. Based on isotopic compositions, the high-titanium basalts in Alaska and Yukon originated from an OIB-type mantle source compositionally similar to Karmutsen basalts on Vancouver Island and the source of ocean islands (e.g. Hawaii) and plateaus (e.g. Ontong Java and Caribbean) in the Pacific Ocean. Basalts from the Wrangellia plateau, together with Hawaii and the Ontong Java and Caribbean Plateaus, provide a sampling of OIB-type mantle emanating from the Pacific mantle in the last 230 Myr.

The volcanic stratigraphy of the Wrangellia flood basalts records the evolution of a major oceanic plateau (Nixon *et al.*, 2008). The duration of volcanism in Northern and Southern Wrangellia was probably less than 5 Myr, between ca. 231 and 225 Ma (e.g. Parrish & McNicoll, 1992; Slaggett, 2003; Bittenbender *et al.*, 2007). The Wrangellia basalts in Alaska and Yukon overlie Late Pennsylvanian and Permian sediments and arc volcanic sequences (ca. 320-285 Ma), whereas basalts on Vancouver Island overlie a basement of Mississippian to Permian marine sedimentary strata and Devonian to Mississippian age (~380-355 Ma) arc rocks (e.g. Muller *et al.*, 1974). The earliest flows in Alaska were emplaced in a shallow marine environment followed by accumulation of ~3.5 km of subaerial flows. On Vancouver Island, the early growth of the plateau was dominated by extrusion of pillow lavas, which accumulated more than 3000 m thick and were overlain by 40-1500 m of pillow basalt and hyaloclastite, before the plateau emerged above sea level. The accumulation of approximately 1500 m of sheet flows continued above sea level and intervolcanic sedimentary lenses formed as the plateau subsided and volcanism waned. The plateau continued to subside for more than 25 Myr following volcanism and is overlain with minimal disconformity by hundreds to thousands of meters of limestone and shale.

The Wrangellia oceanic plateau is one of the best natural laboratories available on land to study and sample the entire volcanic stratigraphy of a well-preserved Phanerozoic oceanic plateau. A combined in-depth geochemical, geochronological, and

sedimentological study is needed to further elucidate the processes that led to volcanism, uplift and subsidence of the plateau, and the precise duration of volcanism. The following short list is a plan for prospective research of the Wrangellia oceanic plateau:

- Widespread geochemical studies from sampling and portable XRF analysis to determine the spatial and stratigraphic distribution of high- and low-titanium basalts, as well as newly discovered picritic lavas, in Alaska and Yukon.
- Widespread geochemical studies from sampling and portable XRF analysis to determine the spatial and stratigraphic distribution of picritic lavas on Vancouver Island and the Queen Charlotte Islands.
- Identification of the tripartite stratigraphy throughout the entire Karmutsen Formation on Vancouver Island and the Queen Charlotte Islands (Haida Gwaii).
- Fieldwork and sampling of correlative flood basalts in southeast Alaska, and examination of their relationship with underlying and overlying strata.
- Studies of osmium and helium isotopic ratios to further determine the composition and origin of the source that produced Wrangellia basalts and whether lower mantle or core material was involved.
- U-Pb geochronology of basal sills and coarse-grained thick flows to better constrain the duration of volcanism in Wrangellia.
- Paleontological and sedimentological analysis of underlying and overlying sedimentary sequences to assess the environmental setting immediately preceding and following volcanism, the uplift and subsidence history of the Wrangellia plateau, and to provide additional age constraints.
- Geochemical studies of underlying Paleozoic arc volcanic sequences on Vancouver Island and in Alaska to determine the role of arc lithosphere in the evolution of Wrangellia basalts erupted in these areas and the tectonic history of the Wrangellia Terrane.
- Detailed mineralogical and whole-rock geochemical studies of the mafic and ultramafic plutonic rocks exposed within Wrangellia, particularly of the exposures in the Amphitheater Mountains, Alaska and the base of the Nikolai Formation in Yukon.
- Studies of the environmental impact of eruption of the Wrangellia flood basalts in the Late Ladinian and Carnian stages of the Triassic.

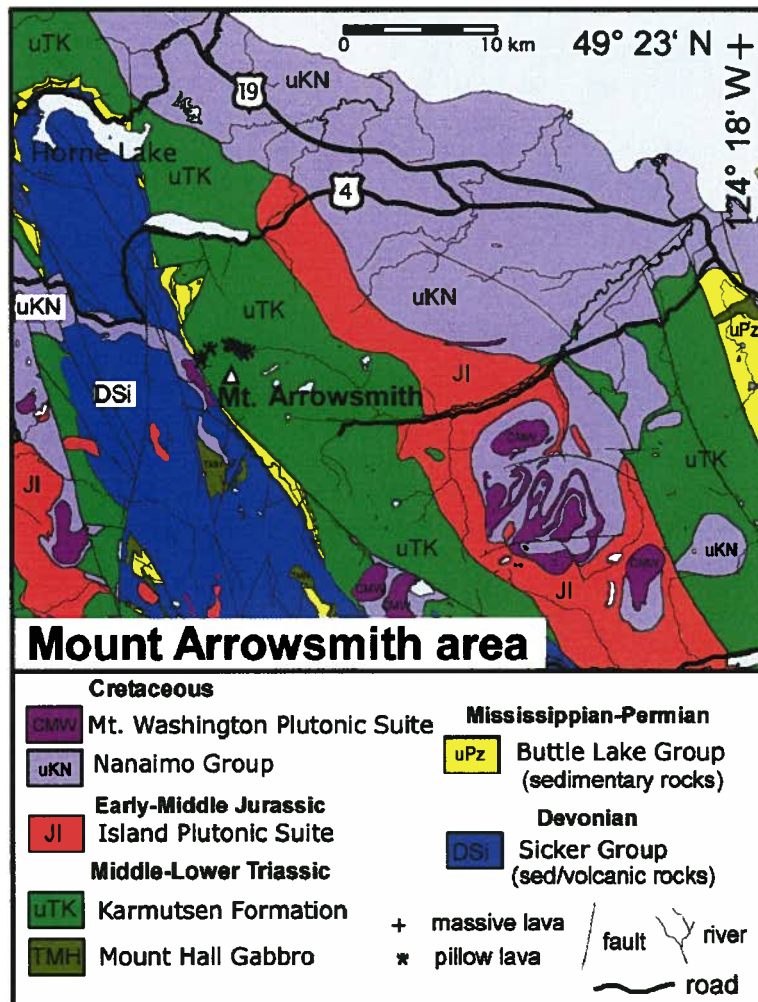


The Wrangellia oceanic plateau is ripe for future research and may hold answers to some of the important questions about the development of oceanic plateaus that remain mostly hidden beneath the surface of the ocean.

## REFERENCES

- Bittenbender, P. E., Bean, K. W., Kurtak, J. M. & Deninger, J., Jr (2007). Mineral assessment of the Delta River Mining District area, East-central Alaska. *U. S. Bureau of Land Management-Alaska*. Technical Report 57, 676 p.  
[http://www.blm.gov/pgdata/etc/medialib/blm/ak/aktest/tr.Par.86412.File.dat/BLM\\_TR57.pdf](http://www.blm.gov/pgdata/etc/medialib/blm/ak/aktest/tr.Par.86412.File.dat/BLM_TR57.pdf).
- Greene, A. R., Scoates, J. S. & Weis, D. (2005a). Wrangellia Terrane on Vancouver Island: Distribution of flood basalts with implications for potential Ni-Cu-PGE mineralization. In: Grant, B. (ed.) *Geological Fieldwork 2004*. British Columbia Ministry of Energy, Mines and Petroleum Resources Paper 2005-1, pp. 209-220.
- Greene, A. R., Scoates, J. S., Weis, D. & Israel, S. (2005b). Flood basalts of the Wrangellia Terrane, southwest Yukon: Implications for the formation of oceanic plateaus, continental crust and Ni-Cu-PGE mineralization. In: Emond, D. S., Lewis, L. L. & Bradshaw, G. D. (eds.) *Yukon Exploration and Geology 2004*. Yukon Geological Survey, pp. 109-120.
- Greene, A. R., Scoates, J. S., Nixon, G. T. & Weis, D. (2006). Picritic lavas and basal sills in the Karmutsen flood basalt province, Wrangellia, northern Vancouver Island. In: Grant, B. (ed.) *Geological Fieldwork 2005*. British Columbia Ministry of Energy, Mines and Petroleum Resources Paper 2006-1, pp. 39-52.
- Herzberg, C., Asimow, P. D., Arndt, N., Niu, Y., Leshner, C. M., Fitton, J. G., Cheadle, M. J. & Saunders, A. D. (2007). Temperatures in ambient mantle and plumes: Constraints from basalts, picrites, and komatiites. *Geochemistry Geophysics Geosystems* 8(Q02006), doi:10.1029/2006GC001390.
- Muller, J. E., Northcote, K. E. & Carlisle, D. (1974). Geology and mineral deposits of Alert Bay - Cape Scott map area, Vancouver Island, British Columbia. *Geological Survey of Canada, Paper 74-8*, 77 pp.
- Nixon, G. T., Laroque, J., Pals, A., Styan, J., Greene, A. R. & Scoates, J. S. (2008). High-Mg lavas in the Karmutsen flood basalts, northern Vancouver Island (NTS 092L): Stratigraphic setting and metallogenic significance. In: Grant, B. (ed.) *Geological Fieldwork 2007*. B.C. Ministry of Energy, Mines and Petroleum Resources Paper 2008-1. pp. 175-190.
- Parrish, R. R. & McNicoll, V. J. (1992). U-Pb age determinations from the southern Vancouver Island area, British Columbia. *Geological Survey of Canada*. Radiogenic Age and Isotopic Studies: Report 5 Paper 91-2, 79-86 p.
- Sluggett, C. L. (2003). Uranium-lead age and geochemical constraints on Paleozoic and Early Mesozoic magmatism in Wrangellia Terrane, Saltspring Island, British Columbia. Unpublished B.Sc. thesis, University of British Columbia, 84 pp.

## **APPENDICES**



**Appendix A.** Geologic map of the Mount Arrowsmith area with sample locations (location of map shown in Figure 2.1), south-central Vancouver Island. Map derived from Massey *et al.* (2005b).

Appendix B. XRF whole-rock analyses of a subset of Karmutsen basalts, Vancouver Island, B.C.

Sample	4722A2	4722A4	4722A5	4723A2	4723A3	4723A4	4723A13	5614A1	5614A3	5614A5
Group	THOL	PIC	OUTLIER	HI-MG	PIC	PIC	PIC	PIC	HI-MG	HI-MG
Area	KR	KR	KR	KR	KR	KR	KR	KR	KR	KR
Flow	Flow	Pillow	Flow	Pillow	Pillow	Pillow	Pillow	Pillow	Pillow	Breccia
UTM EW	5590769	5595528	5595029	5588266	5588274	5586081	5599233	5599183	5599183	5599192
UTM NS	634318	629490	627605	626698	626641	626835	616507	616472	616472	614756
Unnormalized Major Element Oxides (Weight %):										
SiO <sub>2</sub>	48.48	46.05	48.20	48.47	47.43	46.38	46.91	48.79	51.03	49.84
TiO <sub>2</sub>	1.89	0.47	2.43	0.67	0.61	0.72	0.50	0.52	0.51	0.56
Al <sub>2</sub> O <sub>3</sub>	14.23	12.47	13.10	16.33	13.99	16.26	14.77	15.11	15.35	15.45
Fe <sub>2</sub> O <sub>3</sub> *	13.96	11.37	16.50	10.85	11.12	11.03	10.90	9.88	8.80	9.48
MnO	0.21	0.19	0.22	0.19	0.18	0.17	0.17	0.17	0.16	0.16
MgO	7.18	18.67	6.15	10.66	16.14	13.56	15.02	12.43	10.90	10.95
CaO	11.87	9.71	9.33	10.43	9.57	10.32	10.21	11.55	11.35	11.27
Na <sub>2</sub> O	2.06	0.57	3.40	2.19	0.69	1.47	1.04	1.17	1.24	1.96
K <sub>2</sub> O	0.11	0.12	0.33	0.37	0.04	0.07	0.05	0.05	0.07	0.04
P <sub>2</sub> O <sub>5</sub>	0.16	0.04	0.22	0.06	0.06	0.07	0.05	0.05	0.05	0.04
LOI	1.49	5.28	1.71	3.52	5.46	4.77	5.21	4.04	3.63	4.00
Total	100.15	99.66	99.88	100.22	99.83	100.05	99.61	99.72	99.46	99.75
Trace Elements (ppm):										
La	5	2	6	1	3	1	2	1	1	0
Ce	16	1	21	3	3	4	3	2	3	3
Pr										
Nd										
Sm										
Eu										
Gd										
Tb										
Dy										
Ho										
Er										
Tm										
Yb										
Lu										
Sc										
V	351	184	485	235	201	205	208	217	211	185
Cr	160	1784	100	396	1787	912	1541	1625	1549	814
Co										
Ni	95	755	59	163	656	339	583	564	551	315
Cu										
Zn	126	62	124	73	74	71	68	64	60	62
Ga	19	10	18	13	12	14	11	11	11	12
Ge										
Rb	1.4	5.4	5.4	10.3	1.6	1.7	1.5	0.7	1.5	0.3
Sr	182	95	226	276	65	134	74	122	133	144
Y	25.7	14.2	36.6	18.5	16.7	17.4	16.5	17.0	16.7	15.3
Zr	109	19	148	37	33	42	27	28	29	23
Nb	9.4	1.0	11.5	1.8	1.7	1.6	1.0	1.1	1.0	0.8
Cs										
Ba	39	37	95	98	21	25	20	30	28	18
Hf										
Ta										
Pb	0	1	2	0	1	1	1	1	1	1
Th	0	0	2	0	1	0	0	1	0	0
U	1	1	1	1	1	1	1	1	1	1

Abbreviations for group are: THOL, tholeiitic basalt; PIC, picrite; HI-MG, high MgO basalt; CG, coarse-grained (sill or gabbro); OUTLIER, anomalous pillowed flow in plots. Abbreviations for area are: SL, Schoen Lake; KR, Karmutsen Range. Sample locations are given using the Universal Transverse Mercator (UTM) coordinate system (NAD83; zones 9 and 10). Analyses were performed at University of Massachusetts Ronald B. Gilmore XRF Laboratory. Fe<sub>2</sub>O<sub>3</sub>\* is total iron expressed as Fe<sub>2</sub>O<sub>3</sub>. LOI is loss-on-ignition.

Sample	5615A7	5615A12	5616A1	5617A5
Group	PIC	PIC	PIC	CG
Area	KR	KR	KR	SL
Flow	Pillow	Pillow	Pillow	Sill
UTM EW	5595569	5586126	5598448	5557712
UTM NS	629573	626824	616507	700905
<i>Unnormalized Major Element Oxides (Weight %):</i>				
SiO <sub>2</sub>	46.28	48.46	46.89	49.10
TiO <sub>2</sub>	0.47	0.70	0.48	1.80
Al <sub>2</sub> O <sub>3</sub>	12.26	14.96	14.75	14.02
Fe <sub>2</sub> O <sub>3</sub> *	11.53	10.83	10.86	12.72
MnO	0.19	0.17	0.19	0.20
MgO	18.83	12.78	15.75	7.49
CaO	9.65	9.68	9.39	12.39
Na <sub>2</sub> O	0.39	1.97	1.00	1.63
K <sub>2</sub> O	0.12	0.07	0.05	0.25
P <sub>2</sub> O <sub>5</sub>	0.04	0.06	0.05	0.15
LOI	5.23	4.58	5.84	1.42
Total	99.76	99.68	99.42	99.75
<i>Trace Elements (ppm):</i>				
La	7	0	3	7
Ce	18	4	4	18
Pr				
Nd				
Sm				
Eu				
Gd				
Tb				
Dy				
Ho				
Er				
Tm				
Yb				
Lu				
Sc				
V	329	198	199	329
Cr	279	998	4059	279
Co				
Ni	100	368	559	100
Cu				
Zn	99	72	62	99
Ga	18	13	12	18
Ge				
Rb	6.6	2.1	1.1	6.6
Sr	258	193	114	258
Y	23.0	16.8	15.3	23.0
Zr	102	41	26	102
Nb	9.5	1.5	1.1	9.5
Cs				
Ba	49	24	29	49
Hf				
Ta				
Pb	1	0	0	1
Th	1	0	0	1
U	1	1	1	1

Appendix C. PCIGR trace-element concentrations of Karmutsen basalts, Vancouver Island, B.C.

Sample	4718A2(1)	4718A7	4719A2	4719A3	4720A4	4720A6	4720A7	4720A7dup	4720A10	4721A2
Group	THOL	THOL	THOL	THOL	THOL	CG	CG	CG	CG	THOL
Area	MA	MA	MA	MA	SL	SL	SL	SL	SL	SL
Flow	Pillow	Pillow	Pillow	Pillow	Flow	Flow	Flow	Flow	Sill	Flow
UTM EW	5455150	5455280	5454625	5454625	5566984	5566161	5566422	5566422	5560585	5563936
UTM NS	384260	382261	381761	381761	707626	704411	703056	703056	702230	704941
Trace Elements (ppm):										
La	10.32	9.44	9.12	8.36	12.48	10.02	10.13	9.39	2.68	8.64
Ce	26.11	24.25	23.70	22.00	31.35	25.17	26.05	23.93	7.16	21.94
Pr	3.66	3.53	3.41	3.17	4.46	3.56	3.68	3.38	1.10	3.07
Nd	16.79	16.65	16.06	14.84	20.99	16.80	17.28	16.02	5.67	14.60
Sm	4.60	4.79	4.48	4.22	5.77	4.75	4.96	4.56	2.05	4.05
Eu	1.63	1.79	1.65	1.57	2.05	1.67	1.76	1.63	0.87	1.44
Gd	5.25	5.72	5.35	4.98	6.87	5.65	5.81	5.31	3.08	4.77
Tb	0.86	0.98	0.87	0.80	1.14	0.96	0.99	0.91	0.58	0.78
Dy	5.39	5.91	5.52	5.12	6.87	6.03	6.17	5.63	3.91	4.90
Ho	1.11	1.27	1.14	1.06	1.46	1.25	1.29	1.20	0.88	0.99
Er	3.01	3.42	3.16	2.85	4.01	3.50	3.58	3.28	2.57	2.78
Tm	0.41	0.48	0.43	0.40	0.55	0.48	0.49	0.45	0.37	0.39
Yb	2.51	2.96	2.69	2.46	3.42	2.93	3.10	2.86	2.38	2.47
Lu	0.38	0.46	0.40	0.37	0.53	0.45	0.46	0.43	0.36	0.36
Sc	41.2	54.2	45.2	39.3	58.0	44.5	50.9	43.8	26.5	42.8
V	376	386	359	353	472	357	384	376	313	330
Cr										
Co	41.0	43.9	44.1	43.1	51.5	41.7	40.6	40.7	37.6	48.4
Ni	55.9	77.3	62.9	66.7	67.2	57.1	53.0	51.5	78.4	79.5
Cu	156	142	147	138	193	162	164	164	111	182
Zn	77.8	76.6	73.5	74.5	94.7	72.0	77.7	75.2	48.6	93.6
Ga	15.1	15.5	14.7	14.5	18.0	14.0	14.8	14.4	9.8	19.0
Rb	1.28	3.78	3.27	3.49	2.54	6.11	2.18	1.79	0.11	1.58
Sr	202	283	244	229	215	123	157	140	60	209
Y	26.6	29.7	27.6	25.1	35.2	29.8	31.8	28.6	19.9	24.1
Zr	103	98	88	90	126	97	93	98	40	118
Nb	8.64	7.01	5.76	5.75	10.23	5.54	5.50	6.00	1.32	7.36
Cs	0.19	0.23	0.13	0.15	0.23	0.55	0.24	0.20	0.02	0.26
Ba	41.2	61.4	125.6	115.7	37.3	34.1	37.8	37.8	55.5	41.6
Hf	2.53	2.41	2.16	2.12	3.04	2.38	2.23	2.35	1.00	2.99
Ta	0.53	0.49	0.37	0.38	0.70	0.36	0.36	0.41	0.09	0.49
Pb	0.71	0.54	0.68	0.52	0.65	0.56	0.61	0.61	0.51	0.91
Th	0.56	0.52	0.47	0.45	0.72	0.45	0.48	0.44	0.11	0.72
U	0.18	0.17	0.18	0.14	0.21	0.13	0.13	0.14	0.05	0.25

Abbreviations for group are: THOL, tholeiitic basalt; PIC, picrite; HI-MG, high MgO basalt; CG, coarse-grained (sill or gabbro); OUTLIER, anomalous pillowed flow in plots. Abbreviations for area are: MA, Mount Arrowsmith; SL, Schoen Lake; KR, Karmutsen Range. Sample locations are given using the Universal Transverse Mercator (UTM) coordinate system (NAD83; zones 9 and 10). All analyses were performed at the Pacific Centre for Isotopic and Geochemical Research (PCIGR) at UBC by HR-ICP-MS. Fe<sub>2</sub>O<sub>3</sub>\* is total Iron expressed as Fe<sub>2</sub>O<sub>3</sub>. \*Samples marked with asterisk are not from the Karmutsen Formation, their age is unknown.

Sample	4721A4	4722A4	4722A4dup	4722A5	4723A2	4723A3	4723A4	4723A13	4724A3	4718A3*
Group	THOL	PIC	PIC	OUTLIER	HI-MG	PIC	PIC	PIC	CG	
Area	SL	KR	KR	KR	KR	KR	KR	KR	SL	MA
Flow	Flow	Pillow	Pillow	Flow	Pillow	Pillow	Pillow	Pillow	Flow	Flow
UTM EW	5584285	5595528	5595528	5595029	5588266	5588274	5586081	5599233	5581870	5455174
UTM NS	704896	629490	629490	627605	626698	626641	626835	616507	704472	383960
<i>Trace Elements (ppm):</i>										
La	11.73	1.29	1.25	11.00	2.99	3.10	2.83	1.83	7.09	22.12
Ce	28.92	3.49	3.07	30.57	7.83	8.39	7.18	4.72	19.33	46.72
Pr	4.16	0.51	0.47	4.41	1.15	1.19	1.12	0.70	2.76	5.93
Nd	19.58	2.70	2.48	21.00	5.79	5.91	5.90	3.54	13.21	25.32
Sm	5.48	1.07	0.97	6.10	1.99	2.09	2.14	1.33	3.84	5.97
Eu	1.97	0.44	0.41	1.95	0.73	0.79	0.88	0.55	1.44	1.95
Gd	6.58	1.73	1.64	7.31	2.98	3.08	3.21	2.09	4.52	6.08
Tb	1.11	0.35	0.33	1.25	0.57	0.61	0.61	0.43	0.77	0.96
Dy	6.88	2.53	2.43	7.76	3.96	4.09	4.05	3.03	4.75	5.66
Ho	1.47	0.61	0.56	1.63	0.93	0.98	0.90	0.73	1.00	1.26
Er	4.03	1.88	1.77	4.44	2.75	2.87	2.59	2.26	2.71	3.59
Tm	0.57	0.27	0.26	0.60	0.42	0.43	0.38	0.34	0.37	0.52
Yb	3.52	1.83	1.79	3.75	2.70	2.89	2.40	2.19	2.32	3.43
Lu	0.53	0.29	0.29	0.56	0.43	0.45	0.35	0.35	0.34	0.56
Sc	55.6	38.0	41.9	45.2	57.5	59.3	43.3	42.6	38.5	37.3
V	446	211	212	475	371	295	244	237	301	343
Cr										
Co	46.6	63.9	67.7	42.4	52.3	74.9	52.2	59.7	44.6	24.3
Ni	70.6	475.0	522.6	41.8	141.5	567.1	227.7	382.0	136.3	1.7
Cu	178	71	82	92	119	116	82	75	171	50
Zn	81.7	50.2	50.1	84.9	67.2	68.4	50.1	49.7	69.1	84.8
Ga	15.7	7.1	6.1	14.4	12.5	10.8	10.5	8.4	13.7	17.2
Rb	1.65	3.16	0.00	4.46	8.23	1.65	1.43	0.67	1.44	13.94
Sr	172	77	50	191	269	69	110	63	135	356
Y	35.0	14.5	14.3	39.5	21.3	22.3	20.7	17.5	23.6	30.6
Zr	110	16	15	126	42	38	37	24	59	73
Nb	8.96	0.63	0.60	7.11	1.82	1.78	1.13	0.71	4.52	4.81
Cs	0.36	2.26	0.00	0.25	0.39	0.83	0.55	0.47	0.19	0.06
Ba	27.4	15.1	12.3	75.4	88.2	13.8	16.6	10.2	46.8	353.6
Hf	2.79	0.48	0.45	3.15	1.06	0.98	0.90	0.63	1.41	1.80
Ta	0.62	0.05	0.04	0.47	0.12	0.12	0.07	0.05	0.29	0.22
Pb	0.54	0.17	0.16	0.81	0.09	0.32	0.09	0.18	0.60	2.20
Th	0.61	0.07	0.03	0.82	0.19	0.19	0.07	0.11	0.30	1.51
U	0.17	0.05	0.05	0.33	0.06	0.06	0.05	0.03	0.09	0.86



Sample	4718A4*	4723A12*
Group		
Area	MA	KR
Flow	Flow	Flow
UTM EW	5455292	5579914
UTM NS	383790	628268
<i>Trace Elements (ppm):</i>		
La	17.59	7.58
Ce	37.73	21.00
Pr	4.79	2.93
Nd	20.26	13.69
Sm	4.74	3.88
Eu	1.54	1.34
Gd	4.66	4.57
Tb	0.73	0.80
Dy	4.52	5.04
Ho	0.96	1.11
Er	2.77	3.17
Tm	0.40	0.45
Yb	2.66	2.85
Lu	0.42	0.43
Sc	30.1	21.1
V	269	356
Cr		
Co	19.7	37.1
Ni	2.2	21.8
Cu	34	115
Zn	92.4	72.7
Ga	13.7	14.2
Rb	30.59	0.52
Sr	440	116
Y	24.6	21.6
Zr	64	113
Nb	3.75	3.11
Cs	0.23	0.00
Ba	711.9	106.5
Hf	1.44	2.49
Ta	0.17	0.20
Pb	1.95	0.78
Th	1.26	0.21
U	0.65	0.40

## **APPENDIX D.**

### **SAMPLE PREPARATION AND ANALYTICAL METHODS FOR ALASKA SAMPLES**

The least altered samples of the Nikolai Formation were selected for geochemical analysis based on thorough petrographic inspection. Thirty-seven of 68 samples from the Alaska Range and 16 of 36 samples from the Wrangell Mountains were crushed (400 g) into pieces <2 mm in diameter in a Rocklabs hydraulic piston crusher between WC-plates. The coarse-crush was thoroughly mixed and 100 g was powdered in a planetary mill using agate jars and balls that were cleaned with quartz sand between samples.

#### *University of Massachusetts XRF Analytical Methods*

Fifty-three sample powders and 6 duplicate powders were analyzed at the Ronald B. Gilmore X-Ray Fluorescence (XRF) Laboratory at the University of Massachusetts. Major elements were measured on a fused La-bearing lithium borate glass disc using a Siemens MRS-400 spectrometer with a Rh X-ray tube operating at 2700 W. Trace element concentrations (Rb, Sr, Ba, Ce, Nb, Zr, Y, Pb, Zn, Ga, Ni, Cr, V) were measured on a separate powder pellet using a Philips PW2400 sequential spectrometer with a Rh X-ray tube. Loss on ignition (LOI) and ferrous iron measurements were made as described by Rhodes and Vollinger (2004). Precision and accuracy estimates for the data are described by Rhodes (1996) and Rhodes and Vollinger (2004). Results for each sample are the average of two separate analyses. A total of 4 complete duplicates were analyzed for Alaska samples. Eighteen sample duplicate powders of Wrangellia flood basalts were also analyzed at Activation Laboratories and the results for most elements were within analytical error (ActLabs; see Chapter 2 for analytical methods).

#### *PCIGR Trace Element and Isotopic Analytical Methods*

A subset of twenty-four samples was selected for high-precision trace-element analysis and Sr, Nd, Pb, and Hf isotopic analysis at the Pacific Centre for Isotopic and Geochemical Research (PCIGR) at the University of British Columbia (UBC; Table 3.2). Samples were selected from the 53 samples analyzed by XRF, based on major- and trace-element chemistry, alteration (low LOI and petrographic alteration index), sample

location, and stratigraphic position. Samples were prepared for trace-element analysis at the PCIGR by the technique described by Pretorius *et al.* (2006) on unleached rock powders. Sample powders (~100 mg) were weighed in 7 mL screw-top Savillex® beakers and dissolved in 1 mL ~14N HNO<sub>3</sub> and 5 mL 48% HF on a hotplate for 48 hours at 130°C with periodic ultrasonication. Samples were dried and redissolved in 6 mL 6N HCl on a hotplate for 24 hours and then dried and redissolved in 1 mL concentrated HNO<sub>3</sub> for 24 hours before final drying. Trace element abundances were measured with a Thermo Finnigan Element2 High Resolution-Inductively Coupled Plasma-Mass Spectrometer (HR-ICP-MS) following the procedures described by Pretorius *et al.* (2006) within 24 hours of redissolution. High field strength elements (HFSE) and large ion lithophile elements (LILE) were measured in medium resolution mode at 2000x dilution using a PFA teflon spray chamber washed with Aqua Regia for 3 minutes between samples. Rare earth elements (REE) were measured in high resolution mode, and U and Pb in low resolution mode, at 2000x dilution using a glass spray chamber washed with 2% HNO<sub>3</sub> between samples. Total procedural blanks and reference materials (BCR-2, BHVO-2) were analyzed with the batch of samples. Indium was used as an internal standard in all samples and standard solutions. Background and standard solutions were analyzed after every 5 samples to detect memory effects and mass drift.

Sample digestion for purification of Sr, Nd, Hf, and Pb for column chemistry involved weighing each sample powder. All samples were initially leached with 6N HCl and placed in an ultrasonic bath for 15 minutes. Samples were rinsed two times with 18 mega  $\Omega$ -cm H<sub>2</sub>O between each leaching step (15 total) until the supernatant was clear (following the technique of Mahoney, 1987). Samples were then dried on a hotplate for 24 hours and weighed again. Sample solutions were then prepared by dissolving ~100-250 mg of the leached powder dissolved in 1 mL ~14N HNO<sub>3</sub> and 10 mL 48% HF on a hotplate for 48 hours at 130°C with periodic ultrasonication. Samples were dried and redissolved in 6 mL 6N HCl on a hotplate for 24 hours and then dried. Pb was separated using anion exchange columns and the discard was used for Sr, REE, and Hf separation. Nd was separated from the REE and Hf required two additional purification steps. Detailed procedures for column chemistry for separating Sr, Nd, and Pb at the PCIGR are described in Weis *et al.* (2006) and Hf purification is described in Weis *et al.* (2007). Sr

and Nd isotope ratios were measured on a Thermo Finnigan Triton Thermal Ionization Mass Spectrometer (TIMS) in static mode with relay matrix rotation on a single Ta and double Re-Ta filament, respectively. Four to 5 filaments per barrel of 21 were occupied by standards (NIST SRM 987 for Sr and LaJolla for Nd) for each barrel where samples were run. Sample Sr and Nd isotopic compositions were corrected for mass fractionation using  $^{86}\text{Sr}/^{88}\text{Sr} = 0.1194$  and  $^{146}\text{Nd}/^{144}\text{Nd} = 0.7219$ . Each sample was then normalized using the barrel average of the reference material relative to the values of  $^{143}\text{Nd}/^{144}\text{Nd} = 0.511858$  and  $^{87}\text{Sr}/^{86}\text{Sr} = 0.710248$  (Weis *et al.*, 2006). During the period when the Alaska samples were analyzed, the La Jolla Nd standard gave an average value of  $0.511853 \pm 11$  (n=8) and NIST SRM standard gave an average of  $0.710253 \pm 11$  (n=9;  $2\sigma$  error is reported as times  $10^6$ ).  $^{147}\text{Sm}/^{144}\text{Nd}$  ratio errors are approximately  $\sim 1.5\%$ , or  $\sim 0.006$ . Leached powder of United States Geological Survey (USGS) reference material BHVO-2 was processed with the samples and yielded Sr and Nd isotopic ratios of  $0.703473 \pm 8$  and  $0.512980 \pm 6$ , respectively. These are in agreement with the published values of  $0.703479 \pm 20$  and  $0.512984 \pm 11$ , respectively (Weis *et al.*, 2006). USGS reference material BCR-2 was processed with the samples and yielded Sr and Nd isotopic ratios of  $0.705002 \pm 9$  and  $0.512633 \pm 7$ , respectively. These are in agreement with the published values of  $0.705013 \pm 10$  and  $0.512637 \pm 12$ , respectively (Weis *et al.*, 2006).

Pb and Hf isotopic compositions were analyzed by static multi-collection on a Nu Plasma (Nu Instruments) Multiple Collector-Inductively Coupled Plasma-Mass Spectrometer (MC-ICP-MS). The detailed analytical procedure for Pb isotopic analyses on the Nu at the PCIGR is described in Weis *et al.* (2006). The configuration for Pb analyses allows for collection of Pb, Tl, and Hg together. Tl and Hg are used to monitor instrumental mass discrimination and isobaric overlap, respectively. All sample solutions were analyzed with approximately the same Pb/Tl ratio ( $\sim 4$ ) as the reference material NIST SRM 981. To accomplish this, a small aliquot of each sample solution from the Pb columns was analyzed on the Element2 to determine the precise amount of Pb available for analysis on the Nu Plasma. The SRM 981 standard was run after every two samples on the Nu Plasma. During the time samples were run, analyses of the SRM 981 Pb reference material gave values of  $^{206}\text{Pb}/^{204}\text{Pb} = 16.9403 \pm 19$ ,  $^{207}\text{Pb}/^{204}\text{Pb} = 15.4964 \pm 20$ , and  $^{208}\text{Pb}/^{204}\text{Pb} = 36.7142 \pm 53$  (n=124;  $2\sigma$  error is reported as times  $10^4$ ); these values are

in excellent agreement with reported TIMS triple-spike values of Galer and Abouchami (1998). Results were further corrected by the sample-standard bracketing method or the ln-ln correction method described by White *et al.* (2000) and Blichert-Toft *et al.* (2003). Leached powder of USGS reference material BHVO-2 yielded Pb isotopic ratios of  $^{206}\text{Pb}/^{204}\text{Pb} = 18.6500 \pm 7$ ,  $^{207}\text{Pb}/^{204}\text{Pb} = 15.5294 \pm 7$ , and  $^{208}\text{Pb}/^{204}\text{Pb} = 38.2380 \pm 19$ . These values are in agreement with leached residues of BHVO-2 from Weis *et al.*, (2006).

Hf isotopic compositions were analyzed following the procedures detailed in Weis *et al.* (2007). The configuration for Hf analyses monitored Lu mass 175 and Yb mass 172 to allow for interference correction to masses 174 and 176. Hf isotopic ratios were normalized internally for mass fractionation to a  $^{179}\text{Hf}/^{177}\text{Hf}$  ratio of 0.7325 using an exponential correction. Standards were run after every two samples and sample results were normalized to the ratio of the in-run daily average and a  $^{176}\text{Hf}/^{177}\text{Hf}$  ratio for JMC-475 of 0.282160. During the course of analyses, the Hf standard JMC-475 gave an average value  $0.282153 \pm 3$  (n=79). USGS reference materials BCR-2 and BHVO-2 were processed with the samples and yielded Hf isotopic ratios of  $0.282874 \pm 5$  and  $0.283114 \pm 6$ , respectively. Published values for BCR-2 and BHVO-2 are  $0.282871 \pm 7$  and  $0.283104 \pm 8$ , respectively (Weis *et al.*, 2007).

## REFERENCES

- Blichert-Toft, J., Weis, D., Maerschalk, C., Agranier, A. & Albarède, F. (2003). Hawaiian hot spot dynamics as inferred from the Hf and Pb isotope evolution of Mauna Kea volcano. *Geochemistry Geophysics Geosystems* **4**(2), 1-27, doi:10.1029/2002GC000340.
- Galer, S. J. G. & Abouchami, W. (1998). Practical application of lead triple spiking for correction of instrumental mass discrimination. *Mineralogical Magazine* **62A**, 491-492.
- Mahoney, J. J. (1987). An isotopic survey of Pacific oceanic plateaus: implications for their nature and origin. In: Keating, B. H., Fryer, P., Batiza, R. & Boehlert, G. W. (eds.) *Seamounts, Islands, and Atolls*. American Geophysical Union: Washington, D.C. Geophysical Monograph 43, pp. 207-220.
- Pretorius, W., Weis, D., Williams, G., Hanano, D., Kieffer, B. & Scoates, J. S. (2006). Complete trace elemental characterization of granitoid (USGSG-2,GSP-2) reference materials by high resolution inductively coupled plasma-mass spectrometry. *Geostandards and Geoanalytical Research* **30**(1), 39-54.

- Rhodes, J. M. (1996). Geochemical stratigraphy of lava flows samples by the Hawaii Scientific Drilling Project. *Journal of Geophysical Research* **101**(B5), 11,729-11,746.
- Rhodes, J. M. & Vollinger, M. J. (2004). Composition of basaltic lavas sampled by phase-2 of the Hawaii Scientific Drilling Project: Geochemical stratigraphy and magma types. *Geochemistry Geophysics Geosystems* **5**(3), doi:10.1029/2002GC000434.
- Weis, D., Kieffer, B., Hanano, D., Silva, I. N., Barling, J., Pretorius, W., Maerschalk, C. & Mattielli, N. (2007). Hf isotope compositions of U.S. Geological Survey reference materials. *Geochemistry Geophysics Geosystems* **8**(Q06006), doi:10.1029/2006GC001473.
- Weis, D., Kieffer, B., Maerschalk, C., Barling, J., de Jong, J., Williams, G. A., Hanano, D., Mattielli, N., Scoates, J. S., Goolaerts, A., Friedman, R. A. & Mahoney, J. B. (2006). High-precision isotopic characterization of USGS reference materials by TIMS and MC-ICP-MS. *Geochemistry Geophysics Geosystems* **7**(Q08006), doi:10.1029/2006GC001283.
- White, W. M., Albarède, F. & Télouk, P. (2000). High-precision analysis of Pb isotope ratios by multi-collector ICP-MS. *Chemical Geology* **167**, 257-270.

## **APPENDIX E.**

### **SAMPLE PREPARATION AND ANALYTICAL METHODS FOR YUKON SAMPLES**

The freshest rocks possible were sampled in the field and only the least altered samples were selected for analysis based on thorough petrographic inspection. Thirty-four of the 85 Nikolai basalt samples and 3 Station Creek samples were crushed (400 g) into pieces <2 mm in diameter in a Rocklabs hydraulic piston crusher between WC-plates. The coarse-crush was mixed and 100 g was powdered in a planetary mill using agate jars and balls cleaned with quartz sand between samples.

The major- and trace-element compositions of the whole rock powders were determined at Activation Laboratories Ltd. (Actlabs) in Ancaster, Ontario. Twenty-six additional samples of Nikolai basalt and 8 Station Creek samples, provided by S. Israel, were crushed and powdered by Actlabs. Analytical techniques and detection limits are also available from Actlabs ([http://www.actlabs.com/methsub\\_code4ere.htm](http://www.actlabs.com/methsub_code4ere.htm)). The particular analytical method for each of the elements analyzed is indicated in Table 4.2. For the major elements, a 0.2 g sample was mixed with a mixture of lithium metaborate/lithium tetraborate and fused in a graphite crucible. The molten mixture was poured into a 5% HNO<sub>3</sub> solution and shaken until dissolved (~30 minutes). The samples were analyzed for major oxides and selected trace elements on a combination simultaneous/sequential Thermo Jarrell-Ash Enviro II inductively coupled plasma optical emission spectrometer (ICP-OES). Internal calibration was achieved using a variety of international reference materials (e.g. W-2, BIR-1, DNC-1) and independent control samples. Additional trace elements were analyzed by both the INAA (instrumental neutron activation analysis) and ICP-MS (inductively couple plasma mass spectrometry) methods. For the INAA analyses, 1.5-2.5 g of sample was weighed into small polyethylene vials and irradiated with control international reference material CANMET WMS-1 and NiCr flux wires at a thermal neutron flux of  $7 \times 10^{12} \text{ n cm}^{-2} \text{ s}^{-1}$  in the McMaster Nuclear Reactor. Following a 7-day waiting period, the samples were measured on an Ortec high-purity Ge detector linked to a Canberra Series 95 multichannel analyzer. Activities for each element were decay- and weight-corrected and compared to a detector calibration developed from multiple international certified



reference materials. For the ICP-MS analyses, 0.25 g of sample was digested in HF, followed by a mixture of HNO<sub>3</sub> and HClO<sub>4</sub>, heated and taken to dryness. The samples were brought back into solution with HCl. Samples were analyzed using a Perkin Elmer Optima 3000 ICP. In-lab standards or certified reference materials (e.g. W-2, BIR-1, DNC-1) were used for quality control. A total of 12 blind duplicates were analyzed to assess reproducibility.

A subset of 18 samples was selected for Sr, Nd, Pb, and Hf isotopic analysis at the Pacific Centre for Isotopic and Geochemical Research (PCIGR) at the University of British Columbia (UBC). Samples were selected from the 60 samples analyzed for whole-rock chemistry at ActLabs on unleached rock powders, based on major- and trace-element chemistry, alteration (low LOI and petrographic alteration index), sample location, and stratigraphic position. Sample digestion for purification of Sr, Nd, Hf, and Pb for column chemistry involved weighing each sample powder. Column chemistry was performed at the same time as samples from Alaska (Greene *et al.*, submitted manuscript). All samples were initially leached with 6N HCl and placed in an ultrasonic bath for 15 minutes. Samples were rinsed two times with 18 mega  $\Omega$ -cm H<sub>2</sub>O between each leaching step (15 total) until the supernatant was clear (following the technique of Mahoney, 1987). Samples were then dried on a hotplate for 24 hours and weighed again. Sample solutions were then prepared by dissolving ~100-250 mg of the leached powder dissolved in 1 mL ~14N HNO<sub>3</sub> and 10 mL 48% HF on a hotplate for 48 hours at 130°C with periodic ultrasonication. Samples were dried and redissolved in 6 mL 6N HCl on a hotplate for 24 hours and then dried. Pb was separated using anion exchange columns and the discard was used for Sr, REE, and Hf separation. Nd was separated from the REE and Hf required two additional purification steps. Detailed procedures for column chemistry for separating Sr, Nd, and Pb at the PCIGR are described in Weis *et al.* (2006) and Hf purification is described in Weis *et al.* (2007). Sr and Nd isotope ratios were measured on a Thermo Finnigan Triton Thermal Ionization Mass Spectrometer (TIMS) in static mode with relay matrix rotation on a single Ta and double Re-Ta filament, respectively. Four to 5 filaments per barrel of 21 were occupied by standards (NBS 987 for Sr and LaJolla for Nd) for each barrel where samples were run. Sample Sr and Nd isotopic compositions were corrected for mass fractionation using  $^{86}\text{Sr}/^{88}\text{Sr} = 0.1194$  and  $^{146}\text{Nd}/^{144}\text{Nd} = 0.7219$ .

Each sample was then normalized using the barrel average of the reference material relative to the values of  $^{143}\text{Nd}/^{144}\text{Nd} = 0.511858$  and  $^{87}\text{Sr}/^{86}\text{Sr} = 0.710248$  (Weis *et al.*, 2006). While the Yukon samples were analyzed, the La Jolla Nd standard gave an average value of  $0.511853 \pm 11$  (n=8) and the NBS987 standard gave an average of  $0.710253 \pm 11$  (n=9;  $2\sigma$  error is reported as times  $10^6$ ).  $^{147}\text{Sm}/^{144}\text{Nd}$  ratio errors are approximately ~1.5%, or ~0.006. Leached powder of United States Geological Survey (USGS) reference material BHVO-2 was processed with the samples and yielded Sr and Nd isotopic ratios of  $0.703473 \pm 8$  and  $0.512980 \pm 6$ , respectively. These are in agreement with the published values of  $0.703479 \pm 20$  and  $0.512984 \pm 11$ , respectively (Weis *et al.*, 2006). USGS reference material BCR-2 was processed with the samples and yielded Sr and Nd isotopic ratios of  $0.705002 \pm 9$  and  $0.512633 \pm 7$ , respectively. These are in agreement with the published values of  $0.705013 \pm 10$  and  $0.512637 \pm 12$ , respectively (Weis *et al.*, 2006).

Pb and Hf isotopic compositions were analyzed by static multi-collection on a Nu Plasma (Nu Instruments) Multiple Collector-Inductively Coupled Plasma-Mass Spectrometer (MC-ICP-MS). The detailed analytical procedure for Pb isotopic analyses on the Nu at the PCIGR is described in Weis *et al.* (2006). The configuration for Pb analyses allows for collection of Pb, Tl, and Hg together. Tl and Hg are used to monitor instrumental mass discrimination and isobaric overlap, respectively. All sample solutions were analyzed with approximately the same Pb/Tl ratio (~4) as the reference material NIST SRM 981. To accomplish this, a small aliquot of each sample solution from the Pb columns was analyzed on the Element2 to determine the precise amount of Pb available for analysis on the Nu Plasma. The SRM 981 standard was run after every two samples on the Nu Plasma. During the time Yukon and Alaska samples were run, analyses of the SRM 981 Pb reference material gave values of  $^{206}\text{Pb}/^{204}\text{Pb} = 16.9403 \pm 19$ ,  $^{207}\text{Pb}/^{204}\text{Pb} = 15.4964 \pm 20$ , and  $^{208}\text{Pb}/^{204}\text{Pb} = 36.7142 \pm 53$  (n=124;  $2\sigma$  error is reported as times  $10^4$ ); these values are in excellent agreement with reported TIMS triple-spike values of Galer and Abouchami (1998). Results were further corrected by the sample-standard bracketing method or the ln-ln correction method described by White *et al.* (2000) and Blichert-Toft *et al.* (2003). Leached powder of USGS reference material BHVO-2 yielded Pb isotopic ratios of  $^{206}\text{Pb}/^{204}\text{Pb} = 18.6500 \pm 7$ ,  $^{207}\text{Pb}/^{204}\text{Pb} = 15.5294 \pm$

7, and  $^{208}\text{Pb}/^{204}\text{Pb} = 38.2380 \pm 19$ . These values are in agreement with leached residues of BHVO-2 from Weis *et al.*, (2006).

Hf isotopic compositions were analyzed following the procedures detailed in Weis *et al.* (2007). The configuration for Hf analyses monitored Lu mass 175 and Yb mass 172 to allow for interference correction to masses 174 and 176. Hf isotopic ratios were normalized internally for mass fractionation to a  $^{179}\text{Hf}/^{177}\text{Hf}$  ratio of 0.7325 using an exponential correction. Standards were run after every two samples and sample results were normalized to the ratio of the in-run daily average and a  $^{176}\text{Hf}/^{177}\text{Hf}$  ratio for JMC-475 of 0.282160. During the course of analyses of Yukon and Alaska samples, the Hf standard JMC-475 gave an average value  $0.282153 \pm 3$  (n=79). USGS reference materials BCR-2 and BHVO-2 were processed with the samples and yielded Hf isotopic ratios of  $0.282874 \pm 5$  and  $0.283114 \pm 6$ , respectively. Published values for BCR-2 and BHVO-2 are  $0.282871 \pm 7$  and  $0.283104 \pm 8$ , respectively (Weis *et al.*, 2007).

## REFERENCES

- Blichert-Toft, J., Weis, D., Maerschalk, C., Agranier, A. & Albarède, F. (2003). Hawaiian hot spot dynamics as inferred from the Hf and Pb isotope evolution of Mauna Kea volcano. *Geochemistry Geophysics Geosystems* 4(2), 1-27, doi:10.1029/2002GC000340.
- Galer, S. J. G. & Abouchami, W. (1998). Practical application of lead triple spiking for correction of instrumental mass discrimination. *Mineralogical Magazine* 62A, 491-492.
- Mahoney, J. J. (1987). An isotopic survey of Pacific oceanic plateaus: implications for their nature and origin. In: Keating, B. H., Fryer, P., Batiza, R. & Boehlert, G. W. (eds.) *Seamounts, Islands, and Atolls*. American Geophysical Union: Washington, D.C. Geophysical Monograph 43, pp. 207-220.
- Weis, D., Kieffer, B., Hanano, D., Silva, I. N., Barling, J., Pretorius, W., Maerschalk, C. & Mattielli, N. (2007). Hf isotope compositions of U.S. Geological Survey reference materials. *Geochemistry Geophysics Geosystems* 8(Q06006), doi:10.1029/2006GC001473.
- Weis, D., Kieffer, B., Maerschalk, C., Barling, J., de Jong, J., Williams, G. A., Hanano, D., Mattielli, N., Scoates, J. S., Goolaerts, A., Friedman, R. A. & Mahoney, J. B. (2006). High-precision isotopic characterization of USGS reference materials by TIMS and MC-ICP-MS. *Geochemistry Geophysics Geosystems* 7(Q08006), doi:10.1029/2006GC001283.
- White, W. M., Albarède, F. & Télouk, P. (2000). High-precision analysis of Pb isotope ratios by multi-collector ICP-MS. *Chemical Geology* 167, 257-270.

Appendix F. Major element (wt% oxide) and trace element (ppm) abundances in whole rock samples of Late Paleozoic Station Creek Formation, Yukon

Sample	4812A1	4807A3	4807A4	1442	2291	2053	2333	1191	6922
Group	PALEO	PALEO	PALEO	PALEO	PALEO	PALEO	PALEO	PALEO	PALEO
Area	DJ	QC	QC	QC	QC	QC	QC	QC	QC
Flow	VOLC	VOLC	VOLC	VOLC	VOLC	VOLC	VOLC	VOLC	VOLC
UTM EW	6817620	6817581	6817559	6812321	6807024	6807279	6813893	6814658	6821358
UTM NS	575107	582090	581767	574584	580257	584933	579050	582008	570972
Unnormalized Major Element Oxides (Weight %):									
SiO <sub>2</sub>	69.72	46.98	47.77	59.96	49.39	51.24	44.33	49.77	56.82
TiO <sub>2</sub>	0.27	1.489	3.015	0.61	0.5	1.03	1.39	1.11	0.72
Al <sub>2</sub> O <sub>3</sub>	15.51	14.91	11.86	17.48	15.28	14.11	15.29	15.91	19.12
Fe <sub>2</sub> O <sub>3</sub> *	2.09	11.25	15.59	6.44	10.21	10.66	14.4	9.89	6.27
MnO	0.032	0.155	0.192	0.134	0.199	0.225	0.192	0.155	0.142
MgO	0.88	7.33	6.06	2.31	7.59	8.04	8.14	6.67	3.18
CaO	2.72	10.54	7.54	4.17	11.22	7.22	10.39	11.21	2.59
Na <sub>2</sub> O	5.55	2.47	3.94	6.74	4.24	3.99	2.23	1.87	3.9
K <sub>2</sub> O	0.65	1.09	0.41	0.2	0.1	0.96	0.89	1.27	3.23
P <sub>2</sub> O <sub>5</sub>	0.07	0.12	0.24	0.5	0.14	0.1	0.11	0.11	0.23
LOI	2.06	3.08	2.33	1.92	1.38	2.63	2.50	2.33	4.03
Total	99.54	99.41	98.94	100.46	100.25	100.20	99.86	100.29	100.23
Trace Elements (ppm):									
La	7.54	5.58	14.00	6.92	4.09	6.30	27.20	5.60	13.60
Ce	14.35	13.95	33.94	17.00	8.05	13.09	48.82	14.01	26.37
Pr	1.7	2.1	4.84	2.45	1.17	1.87	5.52	1.85	3.19
Nd	6.63	10.28	22.74	12.52	5.63	9.57	21.1	8.98	13.1
Sm	1.38	3.06	6.52	3.78	1.67	2.89	4.56	2.69	3.22
Eu	0.47	1.17	2.18	1.38	0.59	0.884	1.41	0.983	1.04
Gd	1.28	3.7	7.83	4.3	2.04	3.23	3.99	3.02	3.24
Tb	0.2	0.63	1.37	0.75	0.37	0.58	0.69	0.52	0.56
Dy	1.07	3.82	8.12	4.67	2.4	3.59	3.98	3.23	3.34
Ho	0.21	0.76	1.59	0.93	0.55	0.74	0.83	0.63	0.72
Er	0.59	2.18	4.55	2.79	1.77	2.22	2.73	1.93	2.32
Tm	0.08	0.31	0.65	0.4	0.26	0.321	0.412	0.280	0.358
Yb	0.51	1.87	4.03	2.39	1.56	1.97	2.60	1.71	2.27
Lu	0.08	0.27	0.57	0.34	0.24	0.273	0.397	0.253	0.347
Sc	4.1	44.2	53.8	33.3	30.7	32.7	9.5	30.1	16.1
V	32	314	465	294	207	305	50	297	178
Cr	6.4	317	51.6	184	261	437		363	32
Co	4.5	47.1	50.4	38	33	43	9	38	16
Ni	4	111	45	64	79	134		111	
Cu	11	22	98	39	66	115		126	
Zn	49	69	97	65	66	84	77	82	90
Ga	16	16	20	20	16				
Ge	0.7	1.3	1.3	1.2	1.4				
Rb	11	17	11	19	1	17	5	24	93
Sr	389	257	182	269	59	169	435	265	216
Y	6	22	45	24.5	15.8	19.8	24.8	19.3	19.7
Zr	89	77	171	87	26	60	139	62	116
Nb	2.2	6.8	16.2	7.3	1.9	4.2	13.0	7.0	7.8
Cs	0.7	1.4	1.3	0.2		0.3	0.1	1.3	1.4
Ba	190	161	94	97	21	3,730	66	336	688
Hf	2.5	2.2	4.8	2.5	0.8	1.7	3.2	1.8	2.9
Ta	0.17	0.45	1.18	0.45	0.06	0.23	0.67	0.27	0.59
Th	1.04	0.47	1.25	0.5	0.48	0.83	2.84	1.14	3.73
U	0.49	0.11	0.40	0.55	0.39	0.44	1.12	0.38	1.17

Abbreviations for group are: PALEO, Paleozoic Station Creek Formation. Abbreviations for area are: QC, Quill Creek; DJ, Donjek River. Abbreviations for flow are: VOLC, volcanic lava flow or tuff. Sample locations are given using the Universal Transverse Mercator (UTM) coordinate system (NAD83; zones 7 and 8). Analyses were performed at Activation Laboratories (ActLabs). Fe<sub>2</sub>O<sub>3</sub>\* is total iron expressed as Fe<sub>2</sub>O<sub>3</sub>. LOI is loss-on-ignition. All major elements, Sr, V, and Y by Fused ICP quadrupole (ICP-OES); Cu, Ni, Pb, and Zn by Total dilution ICP; Cs, Ga, Ge, Hf, Nb, Rb, Ta, Th, U, Zr, and REE by Fused-magnetic-sector ICP; Co, Cr, and Sc by INAA. Blanks are below detection limit. See Appendix E for sample preparation and analytical methods.

Sample	212	1571	561	11	2121
Group	PALEO	PALEO	PALEO	PALEO	PALEO
Area	QC	QC	QC	QC	QC
Flow	VOLC	VOLC	VOLC	VOLC	VOLC
UTM EW	6817725	6805380	6817757	6818536	6806109
UTM NS	582272	591287	575179	583527	584732
<i>Unnormalized Major Element Oxides (Weight %):</i>					
SiO <sub>2</sub>	46.49	48.87	41.89	49.04	49.16
TiO <sub>2</sub>	1.28	0.87	1.74	1.28	0.56
Al <sub>2</sub> O <sub>3</sub>	19.8	19.5	15.49	12.72	14.84
Fe <sub>2</sub> O <sub>3</sub> *	9.07	9.91	8.98	14.04	10.42
MnO	0.138	0.135	0.14	0.203	0.172
MgO	5.44	5.89	5.05	6.14	7.07
CaO	8.14	6.85	10.79	10.12	8.69
Na <sub>2</sub> O	4.03	3.04	3.51	2.28	4.61
K <sub>2</sub> O	0.77	1.59	1.09	0.05	0.18
P <sub>2</sub> O <sub>5</sub>	0.11	0.31	0.14	0.15	0.11
LOI	4.81	3.33	11.46	4.026	4.2
Total	100.08	100.29	100.28	100.05	100.01
<i>Trace Elements (ppm):</i>					
La	4.68	9.62	7.34	4.28	4.65
Ce	11.47	21.99	19.47	12.48	8.67
Pr	1.68	2.70	2.69	1.77	1.14
Nd	8.70	13.0	13.5	8.64	5.6
Sm	2.64	3.67	4.12	2.76	1.66
Eu	0.977	1.26	1.82	0.941	0.63
Gd	3.04	3.74	5.00	3.37	2.06
Tb	0.53	0.63	0.82	0.63	0.41
Dy	3.28	3.64	4.63	4.06	2.57
Ho	0.64	0.76	0.90	0.86	0.57
Er	2.03	2.36	2.65	2.86	1.84
Tm	0.291	0.347	0.374	0.439	0.28
Yb	1.76	2.13	2.21	2.78	1.68
Lu	0.257	0.323	0.316	0.418	0.26
Sc	23	22.6	36.6	38.5	39
V	215	241	421	405	274
Cr	79	54	347	38	323
Co	23	28	56	54	41
Ni	39	30	132	57	75
Cu	166	89	197	194	176
Zn	64	101	118	97	54
Ga					13
Ge					1
Rb	10	35	30		2
Sr	228	563	382	205	152
Y	18.4	23.0	27.8	26.4	15.9
Zr	59	67	96	77	27
Nb	5.0	2.8	8.4	5.9	1.4
Cs	2.7	0.5	1.0		0.3
Ba	114	530	278	25	89
Hf	1.6	1.8	2.6	2.1	0.8
Ta	0.31	0.13	0.50	0.34	0.05
Th	0.36	1.24	0.64	0.37	0.36
U	0.11	0.55	0.20	0.18	0.23

## **APPENDIX G.**

### **PREVIOUS RESEARCH ON WRANGELLIA**

This brief overview of previous research highlights some of the key references, grouped into three main areas (south-central Alaska, southwest Yukon and southeast Alaska, and British Columbia). Supplementary data files 1 and 2 (an Endnote library and .txt file, respectively) include over 500 references involving research related to Wrangellia.

Early stratigraphic and paleomagnetic studies of Wrangellia significantly influenced the geological research community. One of the earliest modern works on Wrangellia, by Jones *et al.* (1977), had a major influence in the usage of terranes to assist with tectonic reconstructions. Wrangellia was one of the first sets of allochthonous crustal fragments to be referred to as a terrane, and this was based on the distinct stratigraphy and paleomagnetism of Wrangellia flood basalts (Winkler, 2000). Paleomagnetic studies on the flood basalts in Alaska indicated long-distance displacement since their eruption at low latitude (Hillhouse, 1977). The landmark works of Jones *et al.* (1977) and Hillhouse (1977) laid part of the foundation for future research on Wrangellia and spawned paleogeographic reconstructions of other areas of western North America.

#### **Previous research on Wrangellia in south-central Alaska**

There is a remarkable history of exploration and early geological work in southern Alaska. The earliest recorded geological work was conducted by pioneers exploring the expanse of unknown territory in Alaska in the late 1800s and early 1900s (Hunt, 1996). People native to the Wrangell Mountains area used copper implements, which were derived from copper deposits near the contact between the top of the Nikolai flood basalts and the overlying Chitistone Limestone (Winkler, 2000). The search for these copper deposits spurred exploration of the Wrangell Mountains and eventually lead to mining of what were some of the highest-grade copper deposits in the world (Kennicott mill-site) (MacKevett *et al.*, 1997). The Wrangell and St. Elias Mountains are now part of a National Park and World Heritage Site, which is the largest internationally protected area

in the world (Hunt, 1996). Exceptional historical accounts from the Wrangell-St. Elias area are given in books by Winkler (2000), Hunt (1996), and Sherwood (1965).

Modern geologic overviews of southern Alaska are presented by many authors [Plafker *et al.* (1989b), Nokleberg *et al.* (1994), Plafker *et al.* (1994), Winkler (2000), and Trop and Ridgeway (2007)]. The geology of the Wrangell Mountains has been exceptionally well-mapped and described by E. M. MacKevett, Jr. (1978) and D. Richter (1976). The 1:250,000 scale mapping has been compiled in digital format by Wilson *et al.* (2005). Major contributions describing the formations in the Wrangell Mountains include Armstrong *et al.* (1969), Armstrong and MacKevett (1977, 1982), Smith and MacKevett (1970), MacKevett (1970; 1971) and Trop *et al.* (2002). The paleomagnetic character of Wrangellia in Alaska is addressed by Hillhouse (1977), Hillhouse and Gromme (1984), Hillhouse and Coe (1994).

On the southern flank of the east-central Alaska Range, geologic exploration and early mapping was carried out by Mendenhall (1900), Moffit (1912; 1954), Rose (1965, 1966a, b), Rose and Saunders (1965), Stout (1965; 1976), and Richter and Jones (1973). More recent mapping and a geologic overview of the Amphitheater Mountains and Mount Hayes quadrangle was undertaken by Nokleberg *et al.* (1982; 1985; 1992). A digital version of this mapping is included in the work compiled by Wilson *et al.* (1998). A nice summary of sedimentary sequences at the base of the Nikolai in the Amphitheater Mountains is given by Blodgett (2002). In the Clearwater Mountains, in the southeast corner of the Healy quadrangle, mapping was accomplished by Smith (1973), Silberling *et al.* (1981), and Csejtey *et al.* (1992). The geology of the Clearwater Mountains is summarized by Smith (1971; 1973) and Turner and Smith (1974). To the southwest, in the northern Talkeetna Mountains, recent mapping has revealed exposures of Nikolai basalts and sills (Werdon *et al.*, 2000a, b, 2002; Schmidt *et al.*, 2003a; Schmidt *et al.*, 2003b).

The geophysical properties of Wrangellia in southern Alaska are described by Glen *et al.* (2007a; 2007b) and Saltus *et al.* (2007). The character and development of sedimentary basins in the east-central Alaska Range are described by Ridgway *et al.* (2002). An overview of metallogenic prospects related to the Nikolai Formation in southern Alaska is presented by Schmidt and Rogers (2007).



### **Previous research on Wrangellia in southwest Yukon and southeast Alaska**

The earliest geological mapping of the Kluane Ranges was by McConnell (1905), Cairnes (1915), Sharp (1943), Bostock (1952), and Kindle (1953). More recent regional mapping in southwest Yukon was accomplished by Muller (1967), Read and Monger (1976), and Dodds and Campbell (1992a, b, c). Muller (1967) first proposed the correlation between the flood basalts in Yukon and those underlying extensive areas of southern Alaska. Nickel and copper mineralization discovered in the Kluane Ranges in the early 1950's has led to continuous exploration into the mineralization potential of the mafic and ultramafic intrusions related to the Nikolai basalts (Carne, 2003). Campbell (1981) and Miller (1991) completed thesis projects on mineral deposits related to Nikolai basalts near Quill Creek. The Yukon Geological Survey (YGS) recently initiated a bedrock mapping project in the Kluane Ranges (1:50,000 scale) led by Israel *et al.* (2004; 2005; 2006).

Mapping and field studies in southeast Alaska spurred several reports on Triassic basalt sequences in different areas of southeast Alaska. Plafker *et al.* (1976) first recognized Nikolai equivalents in southeast Alaska, and pursued this work with detailed studies of metabasalts on the Chilkat Peninsula area near Haines, Alaska (Plafker & Hudson, 1980; Davis & Plafker, 1985; Plafker *et al.*, 1989a). Other studies that describe the lithologic character and geochemistry of isolated segments of Triassic basalts in southeast Alaska include those by Loney *et al.* (1975), Decker (1981), Ford and Brew (1987, 1992), and Gehrels and Barker (1992). Regional mapping (1:600,000 scale) and an overview of the geology of southeast Alaska are presented by Gehrels and Berg (1992, 1994).

### **Previous research on Wrangellia in British Columbia**

The earliest exploratory geological work in the Queen Charlotte Islands (Haida Gwaii) was made by Dawson (1880). The foundation for the modern geologic framework for the islands was accomplished in an exceptionally-detailed study by Sutherland-Brown (1968). These studies have been expanded upon with works on Mesozoic and younger

strata by Cameron (1988), Lewis (1991), Thompson (1988; 1991), and Woodsworth (1991).

The earliest geologic studies on northern Vancouver Island were made by Selwyn (1872), Dawson (1887), Dolmage (1919), Gunning (1930; 1931; 1932), and Hoadley (1953). On central and southern Vancouver Island, early fieldwork was carried out by Clapp (1909, 1913), Clapp and Cooke (1917), Stevenson (1945), Jeletzky (1950), and Fyles (1955). Early regional mapping and stratigraphic studies on Vancouver Island were accomplished by Muller and co-workers (Muller & Carson, 1969; Muller & Rahmani, 1970; Muller *et al.*, 1974; Muller, 1977, 1980, 1981; Muller *et al.*, 1981) and Jeletzky (1970, 1976). Carlisle supervised four Ph.D. theses related to the Karmutsen Formation (Surdam, 1967; Asihene, 1970; Kuniyoshi, 1972; Lincoln, 1978) that spawned a number of papers on the low-grade metamorphism of the Karmutsen (Surdam, 1968a, b, 1969, 1970; Kuniyoshi & Liou, 1976; Lincoln, 1981; Lincoln, 1986). These studies were impressive in their thoroughness. Carlisle thoroughly documented the stratigraphic relationships and character of the Karmutsen Formation (Carlisle, 1963; Carlisle, 1972; Carlisle & Suzuki, 1974). Low-grade metamorphism of the Karmutsen Formation has also been studied by Cho *et al.* (Cho & Liou, 1987; Cho *et al.*, 1987), Starkey and Frost (1990), Teraybayashi (1993), and Greenwood *et al.* (1991).

Wrangellia sequences have recently been described during regional mapping studies (1:50,000 scale) on northern Vancouver Island by Nixon and co-workers (1993b, a; 1994a, b; 1995a, b; 2006a; 2006b; 2006d; 2006e; 2007; 2008) and on southern Vancouver Island by Massey and co-workers (Massey & Friday, 1987, 1988, 1989; Massey, 1995a, b, c). Paleozoic basement of Wrangellia is well-described in the works by Massey, as well as in studies by Juras (1987), Yole (1963, 1965, 1969), Sutherland-Brown and Yorath (1985), Brandon *et al.* (1986), Yorath *et al.* (1999) and Katvala and Henderson (2002). Irving and Yole (1972), Yole and Irving (1980), and Irving and Wynne (1990) studied the paleomagnetism of the Karmutsen basalts. A digital geologic map for British Columbia has been compiled by Massey *et al.* (2005a, b). The most recent geochemical and isotopic studies of Karmutsen basalts were undertaken by Barker *et al.* (1989), Andrew and Godwin (1989), Lassiter *et al.* (1995), and Yorath *et al.* (1999).

## REFERENCES

- Andrew, A. & Godwin, C. I. (1989). Lead- and strontium-isotope geochemistry of the Karmutsen Formation, Vancouver Island, British Columbia. *Canadian Journal of Earth Sciences* **26**, 908-919.
- Armstrong, A. K. & MacKevett, E. M., Jr. (1977). The Triassic Chitistone Limestone, Wrangell Mountains, Alaska. *U. S. Geological Survey. Open-File Report 77-217*, D49-D62 p.
- Armstrong, A. K. & MacKevett, E. M., Jr. (1982). Stratigraphy and diagenetic history of the lower part of the Triassic Chitistone Limestone, Alaska. *U. S. Geological Survey. Professional Paper 1212-A*, 26 p.
- Armstrong, A. K., MacKevett, E. M., Jr. & Silberling, N. J. (1969). The Chitistone and Nizina limestones of part of the southern Wrangell Mountains-a preliminary report stressing carbonate petrography and depositional environments. *U. S. Geological Survey. Professional Paper 650-D*, D49-D62 p.
- Asihene, K. A. B. (1970). The Texada Formation and its associated magnetite concentrations. Unpublished Ph.D. dissertation, University of California, Los Angeles, 188 pp.
- Barker, F., Brown, A. S., Budahn, J. R. & Plafker, G. (1989). Back-arc with frontal-arc component origin of Triassic Karmutsen basalt, British Columbia, Canada. *Chemical Geology* **75**, 81-102.
- Blodgett, R. B. (2002). Paleontological Inventory of the Amphitheater Mountains, Mt. Hayes A-4 and A-5 Quadrangles, southcentral Alaska. *Alaska Division of Geological and Geophysical Surveys. Report of Investigations 2002-3*, 11 p.
- Bostock, H. S. (1952). Geology of the northwest Shikwak Valley, Yukon Territory. *Geological Survey of Canada. Memoir 267*.
- Brandon, M. T., Orchard, M. J., Parrish, R. R., Sutherland-Brown, A. & Yorath, C. J. (1986). Fossil ages and isotopic dates from the Paleozoic Sicker Group and associated intrusive rocks, Vancouver Island, British Columbia. *Geological Survey of Canada Paper 86-1A. Current Research, Part A*, 683-696 p.
- Cairnes, D. D. (1915). Exploration in southwest Yukon. *Geological Survey of Canada. Summary Report 1913*, 10-37 p.
- Cameron, B. E. B. & Hamilton, T. S. (1988). Contributions to the stratigraphy and tectonics of the Queen Charlotte Basin, British Columbia. *Geological Survey of Canada. Paper 88-1E*, 221-227 p.
- Campbell, S. W. (1981). Geology and genesis of copper deposits and associated host rocks in and near the Quill Creek area, southwestern Yukon. Ph.D., University of British Columbia, 215 pp.
- Carlisle, D. (1963). Pillow breccias and their aquagene tuffs, Quadra Island, British Columbia. *Journal of Geology* **71**, 48-71.
- Carlisle, D. (1972). Late Paleozoic to Mid-Triassic sedimentary-volcanic sequence on Northeastern Vancouver Island. *Geological Society of Canada Report of Activities 72-1, Part B*, 24-30 p.
- Carlisle, D. & Suzuki, T. (1974). Emergent basalt and submergent carbonate-clastic sequences including the Upper Triassic Dilleri and Welleri zones on Vancouver Island. *Canadian Journal of Earth Sciences* **11**, 254-279.

- Carne, R. C. (2003). Metallogeny of the Kluane Ranges Southwest Yukon Territory. <http://www.geology.gov.yk.ca/metallogeny/kluane/index.html>.
- Cho, M. & Liou, J. G. (1987). Prehnite-pumpellyite to greenschist facies transition in the Karmutsen Metabasites, Vancouver Island, B. C. *Journal of Petrology* **28**(3), 417-443.
- Cho, M., Liou, J. G. & Maruyama, S. (1987). Transition from the zeolite to prehnite-pumpellyite facies in the Karmutsen metabasites, Vancouver Island, British Columbia. *Journal of Petrology* **27**(2), 467-494.
- Clapp, C. H. (1909). Southeastern portion of Vancouver Island. *Geological Survey of Canada*. Summary Report 1908, 52-60 p.
- Clapp, C. H. (1913). Southern Vancouver Island. *Geological Survey of Canada*. Memoir 13, 208 p.
- Clapp, C. H. & Cooke, H. C. (1917). Sooke and Duncan map-areas, Vancouver Island. *Geological Survey of Canada*. Memoir 96, 445 p.
- Csejtey, B. J., Mullen, M. W., Cox, D. P. & Stricker, G. D. (1992). Geology and geochronology of the Healy Quadrangle, south-central Alaska. *U. S. Geological Survey Miscellaneous Investigations* 1961, scale 1:360,000, 63 p.
- Davis, A. & Plafker, G. (1985). Comparative geochemistry and petrology of the Triassic basaltic rocks from the Taku terrane on the Chilkat Peninsula and Wrangellia. *Canadian Journal of Earth Sciences* **22**, 183-194.
- Dawson, G. M. (1880). Queen Charlotte Islands. *Geological Survey of Canada*. Report on Progress 1878-1879.
- Dawson, G. M. (1887). Report on a geological examination of the northern part of Vancouver Island and adjacent coasts. *Geological Survey of Canada*. Annual Report, New Series, Vol.2, 1B-107B p.
- Decker, J. E. (1981). Geochemical signature of the Goon Dip Greenstone on Chichagof Island, southeastern Alaska. *Alaska Division of Geological & Geophysical Surveys*. Geologic Report 73G, 29-35 p.
- Dodds, C. J. & Campbell, R. B. (1992a). Geology, Mount St. Elias map area [115B & C[E1/2]], Yukon Territory. *Geological Society of Canada*. Open File Report 2189, 85 p.
- Dodds, C. J. & Campbell, R. B. (1992b). Geology, SW Dezadeash map area [115A], Yukon Territory. *Geological Society of Canada*. Open File Report 2190, 85 p.
- Dodds, C. J. & Campbell, R. B. (1992c). Geology, SW Kluane Lake map area [115G & F [E1/2]], Yukon Territory. *Geological Society of Canada*. Open File Report 2188, 85 p.
- Dolmage, V. (1919). Quatsino Sound and certain mineral deposits of the west coast of Vancouver Island, British Columbia. *Geological Survey of Canada*. Summary Report 1918, 30-38 p.
- Ford, A. B. & Brew, D. A. (1987). Major-element chemistry of metabasalts near the Juneau-Haines region, southeastern Alaska. *U. S. Geological Survey*. Circular 1016, 150-155 p.
- Ford, A. B. & Brew, D. A. (1992). Geochemical character of Upper Paleozoic and Triassic Greenstone and related metavolcanic rocks of the Wrangellia terrane in northern Southeastern Alaska. *U. S. Geological Survey Circular*. Geologic studies in Alaska by the U. S. Geological Survey, 1992, 197-217 p.

- Fyles, J. T. (1955). Geology of the Cowichan Lake area, Vancouver Island, British Columbia. *British Columbia Ministry of Energy, Mines, and Petroleum Resources*. Bulletin 37, 79 p.
- Gehrels, G. E. & Barker, F. (1992). Reconnaissance geochemistry of Permian and Triassic basalts of the Taku and Wrangellia terranes, Southeastern Alaska. *U. S. Geological Survey Geologic Circular*. Geologic studies in Alaska by the U. S. Geological Survey, 1992, 218-227 p.
- Gehrels, G. E. & Berg, H. C. (1992). Geologic map of southeastern Alaska. *U. S. Geological Survey*. Miscellaneous Geologic Investigations Map I-1867, 1 sheet, scale 1:600,000, 24 p.
- Gehrels, G. E. & Berg, H. C. (1994). Geology of southeastern Alaska. In: Plafker, G. & Berg, H. C. (eds.) *The Geology of North America*. Geological Society of America: Boulder, CO The Geology of Alaska G-1, pp. 451-467.
- Glen, J. M. G., Schmidt, J. M. & Morin, R. (2007a). Gravity and magnetic studies of the Talkeetna Mountains, Alaska: constraints on the geological and tectonic interpretation of southern Alaska, and implications for mineral exploration. In: Ridgway, K. D., Trop, J. M., O'Neill, J. M. & Glen, J. M. G. (eds.) *Growth of a Collisional Continental Margin - Crustal Evolution of South-central Alaska*. Geological Society of America Special Paper 431, pp. 593-622.
- Glen, J. M. G., Schmidt, J. M., Pellerin, L., O'Neill, M. & McPhee, D. K. (2007b). Crustal structure of Wrangellia and adjacent terranes inferred from geophysical studies along a transect through the northern Talkeetna Mountains. In: Ridgway, K. D., Trop, J. M., O'Neill, J. M. & Glen, J. M. G. (eds.) *Growth of a collisional continental margin - Crustal evolution of south-central Alaska*. Geological Society of America Special Paper 431, pp. 21-42.
- Greenwood, H. J., Woodsworth, G. J., Read, P. B., Ghent, E. D. & Evenchick, C. A. (1991). Metamorphism; Chapter 16. In: Gabrielse, H. & Yorath, C. J. (eds.) *Geology of the Cordilleran Orogen in Canada*. Geological Survey of Canada Geology of Canada 4, pp. 533-570.
- Gunning, H. C. (1930). Geology and mineral deposits of Quatsino-Nimpkish area, Vancouver Island. *Geological Survey of Canada*. Summary Report 1929, Part A, 94-143 p.
- Gunning, H. C. (1931). Buttle Lake map-area, Vancouver Island, British Columbia. *Geological Survey of Canada*. Summary Report 1930, Part A, 56-78 p.
- Gunning, H. C. (1932). Preliminary report on the Nimpkish Lake Quadrangle, Vancouver Island, B. C. *Geological Survey of Canada*. Summary Report 1931, Part A, 22-35 p.
- Hillhouse, J. W. (1977). Paleomagnetism of the Triassic Nikolai Greenstone, McCarthy Quadrangle, Alaska. *Canadian Journal of Earth Sciences* **14**, 2578-3592.
- Hillhouse, J. W. & Coe, R. S. (1994). Paleomagnetic data from Alaska. In: Plafker, G. & Berg, H. C. (eds.) *The Geology of Alaska*. Geological Society of America Geology of North America G-1, pp. 797-812.
- Hillhouse, J. W. & Gromme, C. S. (1984). Northward displacement and accretion of Wrangellia: New paleomagnetic evidence from Alaska. *Journal of Geophysical Research* **89**, 4461-4467.

- Hoadley, J. W. (1953). Geology and mineral deposits of the Zeballos-Nimpkish area, Vancouver Island, British Columbia. *Geological Survey of Canada*. Memoir 272, 82 p.
- Hunt, W. R. (1996). *Mountain Wilderness: An Illustrated History of the Wrangell-St. Elias National Park and Preserve, Alaska*. Alaska Natural History Association: Anchorage, 224 p.
- Irving, E. & Wynne, P. J. (1990). Paleomagnetic evidence bearing on the evolution of the Canadian Cordillera. *Philosophical Transactions Royal Society of London* **331**, 487-509.
- Irving, E. & Yole, R. W. (1972). Paleomagnetism and kinematic history of mafic and ultramafic rocks in fold mountain belts. *Earth Physics Branch Publications* **42**, 87-95.
- Israel, S., Tizzard, A. & Major, J. (2006). Bedrock geology of the Duke River area, parts of NTS 115G/2, 3, 4, 6 and 7, southwestern Yukon. In: Emond, D. S., Bradshaw, G. D., Lewis, L. L. & Weston, L. H. (eds.) *Yukon Exploration and Geology 2005*. Yukon Geological Survey, pp. 139-154.
- Israel, S. & Van Zeyl, D. (2004). Preliminary geological map of the Quill Creek area (parts of NTS 115G/5,6,12), southwest Yukon (1:50,000 scale). *Yukon Geological Survey*. Open File 2004-20.
- Israel, S. & Van Zeyl, D. P. (2005). Preliminary geology of the Quill Creek map area, southwest Yukon parts of NTS 115G/5, 6 and 12. In: Emond, D. S., Lewis, L. L. & Bradshaw, G. D. (eds.) *Yukon Exploration and Geology 2004*. Yukon Geological Survey, pp. 129-146.
- Jeletzky, J. A. (1950). Stratigraphy of the west coast of Vancouver Island between Kyuquot Sound and Esperanza Inlet, British Columbia. *Geological Survey of Canada*. Paper 50-57.
- Jeletzky, J. A. (1970). Some salient features of Early Mesozoic history of Insular Tectonic Belt, western British Columbia. *Geological Survey of Canada*. Paper 69-14, 26 p.
- Jeletzky, J. A. (1976). Mesozoic and Tertiary rocks of Quatsino Sound, Vancouver Island, British Columbia. *Geological Survey of Canada*. Bulletin 242, 243 p.
- Jones, D. L., Silberling, N. J. & Hillhouse, J. (1977). Wrangellia; a displaced terrane in northwestern North America. *Canadian Journal of Earth Sciences* **14**(11), 2565-2577.
- Juras, S. J. (1987). Geology of the polymetallic volcanogenic Buttle Lake Camp, with emphasis on the Prince Hillside, Vancouver Island, British Columbia, Canada. Unpublished Ph.D. dissertation, University of British Columbia, 279 pp.
- Katvala, E. C. & Henderson, C. M. (2002). Conodont sequence biostratigraphy and paleogeography of the Pennsylvanian-Permian Mount Mark and Fourth Lake Formations, southern Vancouver Island. In: Hills, L. V., Henderson, C. M. & Bamber, E. W. (eds.) *Carboniferous and Permian of the World*. Canadian Society of Petroleum Geologists Memoir 19, pp. 461-478.
- Kindle, E. D. (1953). Dezadeash map-area, Yukon Territory. *Canadian Geological Survey*. Memoir 268, 68 p.

- Kuniyoshi, S. (1972). Petrology of the Karmutsen (Volcanic) Group, northeastern Vancouver Island, British Columbia. Unpublished Ph.D. dissertation, University of California, Los Angeles, 242 pp.
- Kuniyoshi, S. & Liou, J. G. (1976). Contact metamorphism of the Karmutsen volcanics, Vancouver Island, British Columbia. *Journal of Petrology* 17, 73-99.
- Lassiter, J. C., DePaolo, D. J. & Mahoney, J. J. (1995). Geochemistry of the Wrangellia flood basalt province: Implications for the role of continental and oceanic lithosphere in flood basalt genesis. *Journal of Petrology* 36(4), 983-1009.
- Lewis, P. D., Haggart, J. W., Anderson, R. G., Hickson, C. J., Thompson, R. I., Dietrich, J. R. & Rohr, K. M. M. (1991). Triassic to Neogene geological evolution of the Queen Charlotte region. *Canadian Journal of Earth Sciences* 28(6), 854-869.
- Lincoln, T. N. (1978). The redistribution of copper during metamorphism of the Karmutsen Volcanics, Vancouver Island, British Columbia. Published Ph.D., UCLA, 236 pp.
- Lincoln, T. N. (1981). The redistribution of copper during metamorphism of the Karmutsen Volcanics, Vancouver Island, British Columbia. *Economic Geology* 76, 2147-2161.
- Lincoln, T. N. (1986). Minor and trace element chemistry and environment of eruption of Karmutsen pillow lavas, Vancouver Island, B. C. *Geological Association of Canada Program with Abstracts* 11. p. 95
- Loney, A. R., Brew, D. A., Muffler, L. J. P. & Pomeroy, J. S. (1975). Reconnaissance geology of Chichagof, Baranof, and Kruzof Islands, southeastern Alaska. *U. S. Geological Survey. Professional Paper* 792, 105 p.
- MacKevett, E. M., Jr. (1970). Geology of the McCarthy B-4 quadrangle, Alaska. *U.S. Geological Survey. Bulletin* 1333, 31 p.
- MacKevett, E. M., Jr. (1971). Stratigraphy and general geology of the McCarthy C-5 Quadrangle, Alaska. *U. S. Geological Survey. Bulletin* 1323, 35 p.
- MacKevett, E. M., Jr. (1978). Geologic map of the McCarthy Quadrangle, Alaska. *U. S. Geological Survey. Miscellaneous Investigations Series Map* I-1032 scale 1:250,000.
- MacKevett, E. M., Jr., Cox, D. P., Potter, R. P. & Silberman, M. L. (1997). Kennecott-type deposits in the Wrangell Mountains, Alaska: High-grade copper ores near a basalt-limestone contact. In: Goldfarb, R. J. & Miller, L. D. (eds.) *Mineral Deposits of Alaska*. Economic Geology Monograph 9, pp. 66-89.
- Massey, N. W. D. (1995a). Geology and mineral resources of the Alberni-Nanaimo Lakes sheet, Vancouver Island 92F/1W, 92F/2E, and part of 92F/7E. *B.C. Ministry of Energy, Mines and Petroleum Resources. Paper* 1992-2, 132 p.
- Massey, N. W. D. (1995b). Geology and mineral resources of the Cowichan Lake sheet, Vancouver Island 92C/16. *B.C. Ministry of Energy, Mines and Petroleum Resources. Paper* 1992-3, 112 p.
- Massey, N. W. D. (1995c). Geology and mineral resources of the Duncan sheet, Vancouver Island 92B/13. *B.C. Ministry of Energy, Mines and Petroleum Resources. Paper* 1992-4, 112 p.
- Massey, N. W. D. & Friday, S. J. (1987). Geology of the Cowichan Lake Area, Vancouver Island (92C/16). In: *Geological Fieldwork 1986*. B.C. Ministry of Energy, Mines and Petroleum Resources Paper 1987-1, pp. 223-229.



- Massey, N. W. D. & Friday, S. J. (1988). Geology of the Chemainus River-Duncan Area, Vancouver Island (92C/16; 92B/13). In: *Geological Fieldwork 1987*. B.C. Ministry of Energy, Mines and Petroleum Resources Paper 1988-1, pp. 81-91.
- Massey, N. W. D. & Friday, S. J. (1989). Geology of the Alberni-Nanaimo Lakes Area, Vancouver Island (91F/1W, 92F/2E and part of 92F/7). In: *Geological Fieldwork 1987*. B.C. Ministry of Energy, Mines and Petroleum Resources Paper 1989-1, pp. 61-74.
- Massey, N. W. D., MacIntyre, D. G., Desjardins, P. J. & Cooney, R. T. (2005a). Digital Geology Map of British Columbia: Tile NM9 Mid Coast, B.C. *B.C. Ministry of Energy and Mines* Geofile 2005-2.
- Massey, N. W. D., MacIntyre, D. G., Desjardins, P. J. & Cooney, R. T. (2005b). Digital Geology Map of British Columbia: Tile NM10 Southwest B.C. *B.C. Ministry of Energy and Mines* Geofile 2005-3.
- McConnell, R. G. (1905). The Kluane mining district. *Geological Survey of Canada*. Annual Report 1904, v.16, 1A-18A p.
- Mendenhall, W. C. (1900). A reconnaissance from Resurrection Bay to Tanana River, Alaska, in 1898. *U.S. Geological Survey*. Twentieth Annual Report, pt. 7, 271-340 p.
- Miller, S. (1991). Geology, petrology and geochemistry of the host rocks and associated Ni-Cu-PGE disseminated mineralization of the Wellgreen deposit, Kluane Ranges, Yukon Territory. M.Sc., McMaster University, 249 pp.
- Moffit, F. H. (1912). Headwater regions of Gulkana and Susitna River, Alaska, with accounts of the Valdez Creek and Chistochina placer districts. *U. S. Geological Survey*. Bulletin 498, 82 p.
- Moffit, F. H. (1954). Geology of the eastern part of the Alaska Range and adjacent area. *U. S. Geological Survey*. Bulletin 989-C, 65-218 p.
- Muller, J. E. (1967). Kluane Lake map area, Yukon Territory (115G, 115F/E 1/2). *Geological Survey of Canada*. Memoir 340, 137 p.
- Muller, J. E. (1977). Geology of Vancouver Island. *Geological Survey of Canada* Open File Map 463.
- Muller, J. E. (1980). The Paleozoic Sicker Group of Vancouver Island, British Columbia. *Geological Survey of Canada*. Paper 79-30, 22 p.
- Muller, J. E. (1981). Insular and Pacific Belts. In: Price, R. A., Monger, J. W. H. & Muller, J. E. (eds.) *Cordilleran Cross-section-Calgary to Victoria, Field Guide 1981*. Geological Association of Canada Field Guide, pp. 261-334.
- Muller, J. E., Cameron, B. E. B. & Northcote, K. E. (1981). Geology and mineral deposits of Nootka Sound Map-Area, Vancouver Island, British Columbia. *Geological Survey of Canada, Paper 80-16*.
- Muller, J. E. & Carson, D. J. T. (1969). Geology and mineral deposits of the Alberni area, British Columbia. *Geological Survey of Canada, Paper 68-50*, 35pp.
- Muller, J. E., Northcote, K. E. & Carlisle, D. (1974). Geology and mineral deposits of Alert Bay - Cape Scott map area, Vancouver Island, British Columbia. *Geological Survey of Canada, Paper 74-8*, 77 pp.
- Muller, J. E. & Rahmani, R. A. (1970). Upper Triassic sediments of northern Vancouver Island. *Geological Survey of Canada*. Report of Activities, Part B Paper 70-1B, 11-18 p.

- Nixon, G. T., Hammack, J. L., Hamilton, J. V. & Jennings, H. (1993a). Preliminary geology of the Mahatta Creek area, northern Vancouver Island (92L/5). *British Columbia Ministry of Energy, Mines, and Petroleum Resources*. Open File 1993-10, scale 1:50,000.
- Nixon, G. T., Hammack, J. L., Hamilton, J. V. & Jennings, H. (1993b). Preliminary geology of the Mahatta Creek area, northern Vancouver Island (92L/5). In: Grant, B. & Newell, J. M. (eds.) *Geological Fieldwork 1992*. B.C. Ministry of Energy, Mines and Petroleum Resources Paper 1993-1, pp. 17-35.
- Nixon, G. T., Hammack, J. L., Koyanagi, V. M., Payie, G. J., Haggart, J. W., Orchard, M. J., Tozer, T., Friedman, R. M., D.A., A., Palfy, J. & Cordey, F. (2006a). Geology of the Quatsino – Port McNeill area, northern Vancouver Island. *B.C. Ministry of Energy, Mines and Petroleum Resources*. Geoscience Map 2006-2, scale 1:50 000.
- Nixon, G. T., Hammack, J. L., Koyanagi, V. M., Payie, G. J., Panteleyev, A., Massey, N. W. D., Hamilton, J. V. & Haggart, J. W. (1994a). Preliminary geology of the Quatsino - Port McNeill map areas, northern Vancouver Island (92L/12, 11). In: Grant, B. & Newell, J. M. (eds.) *Geological Fieldwork 1993*. B.C. Ministry of Energy, Mines and Petroleum Resources Paper 1994-1, pp. 63-85.
- Nixon, G. T., Hammack, J. L., Koyanagi, V. M., Payie, G. J., Panteleyev, A., Massey, N. W. D., Hamilton, J. V. & Haggart, J. W. (1994b). Preliminary geology of the Quatsino - Port McNeill map areas, northern Vancouver Island (92L/12, 11). *B.C. Ministry of Energy, Mines, and Petroleum Resources*. Open File 1994-26, scale 1:50,000.
- Nixon, G. T., Hammack, J. L., Koyanagi, V. M., Payie, G. J., Snyder, L. D., Panteleyev, A., Massey, N. W. D., Archibald D.A., Haggart, J. W., Orchard, M. J., Friedman, R. M., Tozer, T., Tipper, H. W., Poulton, T. P., Palfy, J., Cordey, F. & Barron, D. J. (2006b). Geology of the Holberg - Winter Harbour area, northern Vancouver Island. *B.C. Ministry of Energy, Mines and Petroleum Resources*. Geoscience Map 2006-3, scale 1:50 000.
- Nixon, G. T., Hammack, J. L., Payie, G. J., Snyder, L. D., Archibald, D. A. & Barron, D. J. (1995a). Quatsino-San Josef map area, Northern Vancouver Island (92L/12W, 102I/8,9). *B.C. Ministry of Energy, Mines and Petroleum Resources*. Open File 1995-9, scale 1:50,000.
- Nixon, G. T., Hammack, J. L., Payie, G. J., Snyder, L. D., Archibald, D. A. & Barron, D. J. (1995b). Quatsino-San Josef map area, Northern Vancouver Island; geological overview (92L/12W, 102I/8,9). In: Grant, B. & Newell, J. M. (eds.) *Geological Fieldwork 1994*. B.C. Ministry of Energy, Mines and Petroleum Resources Paper 1995-1, pp. 9-21.
- Nixon, G. T., Kelman, M. C., Stevenson, D., Stokes, L. A. & Johnston, K. A. (2006c). Preliminary geology of the Nimpkish map area (NTS 092L/07), northern Vancouver Island, British Columbia. In: Grant, B. & Newell, J. M. (eds.) *Geological Fieldwork 2005*. B.C. Ministry of Energy, Mines and Petroleum Resources Paper 2006-1, pp. 135-152.
- Nixon, G. T., Kelman, M. C., Stevenson, D., Stokes, L. A. & Johnston, K. A. (2006d). Preliminary geology of the Nimpkish map area, northern Vancouver Island

- (92L/07). *B.C. Ministry of Energy, Mines and Petroleum Resources*. Open File 2006-5 scale 1:50 000.
- Nixon, G. T., Laroque, J., Pals, A., Styan, J., Greene, A. R. & Scoates, J. S. (2008). High-Mg lavas in the Karmutsen flood basalts, northern Vancouver Island (NTS 092L): Stratigraphic setting and metallogenic significance. In: Grant, B. (ed.) *Geological Fieldwork 2007*. B.C. Ministry of Energy, Mines and Petroleum Resources Paper 2008-1, pp. 175-190.
- Nixon, G. T. & Orr, A. J. (2007). Recent revisions to the Early Mesozoic stratigraphy of Northern Vancouver Island (NTS 102I; 092L) and metallogenic implications, British Columbia. In: Grant, B. (ed.) *Geological Fieldwork 2006*. B.C. Ministry of Energy, Mines and Petroleum Resources Paper 2007-1, pp. 163-177.
- Nixon, G. T., Snyder, L. D., Payie, G. J., Long, S., Finnie, A., Friedman, R. M., D.A., A., Orchard, M. J., Tozer, T., Poulton, T. P. & Haggart, J. W. (2006e). Geology of the Alice Lake area, northern Vancouver Island. *B.C. Ministry of Energy, Mines and Petroleum Resources*. Geoscience Map 2006-1, scale 1:50 000.
- Nokleberg, W. J., Albert, N. R. D., Bond, G. C., Herzon, P. L., Miyaoka, R. T., Nelson, W. H., Richter, D. H., Smith, T. E., Stout, J. H., Yeend, W. & Zehner, R. E. (1982). Geologic map of the southern Mount Hayes Quadrangle, Alaska. *U. S. Geological Survey Open-File Report 82-52*, 1:250,000 scale, 27 p.
- Nokleberg, W. J., Aleinikoff, J. N., Dutro, J. T. J., Lanphere, M. A., Silberling, N. J., Silva, S. R., Smith, T. E. & Turner, D. L. (1992). Map, tables, and summary fossil and isotopic age data, Mount Hayes quadrangle, eastern Alaska Range, Alaska. *U. S. Geological Survey Miscellaneous Field Studies Map 1996-D*, 1:250,000 scale.
- Nokleberg, W. J., Jones, D. L. & Silberling, N. J. (1985). Origin and tectonic evolution of the Maclaren and Wrangellia terranes, eastern Alaska Range, Alaska. *Geological Society of America Bulletin* **96**, 1251-1270.
- Nokleberg, W. J., Plafker, G. & Wilson, F. H. (1994). Geology of south-central Alaska. In: Plafker, G. & Berg, H. C. (eds.) *The Geology of North America*. Geological Society of America: Boulder, CO The Geology of Alaska G-1, pp. 311-366.
- Plafker, G., Blome, C. D. & Silberling, N. J. (1989a). Reinterpretation of lower Mesozoic rocks on the Chilkat Peninsula, Alaska, as a displaced fragment of Wrangellia. *Geology* **17**, 3-6.
- Plafker, G. & Hudson, T. (1980). Regional implications of the Upper Triassic metavolcanic and metasedimentary rocks on the Chilkat Peninsula, southeastern Alaska. *Canadian Journal of Earth Sciences* **17**(6), 681-689.
- Plafker, G., Jones, D. L., Hudson, T. & Berg, H. C. (1976). The Border Ranges fault system in the Saint Elias Mountains and Alexander Archipelago. *U.S. Geological Survey*. U. S. Geological Survey in Alaska: Accomplishments during 1975 751-B, B41-43 p.
- Plafker, G., Moore, J. C. & Winkler, G. R. (1994). Geology of the southern Alaska margin. In: Plafker, G. & Berg, H. C. (eds.) *The Geology of North America*. Geological Society of America: Boulder, CO The Geology of Alaska G-1, pp. 389-449.
- Plafker, G., Nokleberg, W. J. & Lull, J. S. (1989b). Bedrock geology and tectonic evolution of the Wrangellia, Peninsular, and Chugach terranes along the Trans-

- Alaskan Crustal Transect in the northern Chugach Mountains and southern Copper River basin, Alaska. *Journal of Geophysical Research* **94**, 4,255-4,295.
- Read, P. B. & Monger, J. W. H. (1976). Pre-Cenozoic volcanic assemblages of the Kluane and Alsek Ranges, southwestern Yukon Territory. *Geological Survey of Canada*. Open-File Report 381, 96 p.
- Richter, D. H. (1976). Geologic map of the Nabesna Quadrangle, Alaska. *U. S. Geological Survey*. Miscellaneous Geologic Investigations Map I-932, scale 1:250,000.
- Richter, D. H. & Jones, D. L. (1973). Structure and stratigraphy of the eastern Alaska Range, Alaska. In: *Arctic geology*. American Association of Petroleum Geologists **19**, pp. 408-420.
- Ridgway, K. D., Trop, J. M., Nokleberg, W. J., Davidson, C. M. & Eastham, K. R. (2002). Mesozoic and Cenozoic tectonics of the eastern and central Alaska Range: Progressive basin development and deformation in a suture zone. *Geological Society of America Bulletin* **114**, 1,480-1,504.
- Rose, A. W. (1965). Geology and mineral deposits of the Rainy Creek area, Mt. Hayes Quadrangle, Alaska. *Alaska Division of Mines and Minerals*. Geologic Report 14, 51 p.
- Rose, A. W. (1966a). Geological and geochemical investigations in the Eureka Creek and Rainy Creek areas, Mt. Hayes Quadrangle, Alaska. *Alaska Division of Mines and Minerals*. Geologic Report 20, 41 p.
- Rose, A. W. (1966b). Geology of part of the Amphitheatre Mountains, Mt. Hayes Quadrangle, Alaska. *Alaska Division of Mines and Minerals*. Geologic Report 19, 17 p.
- Rose, A. W. & Saunders, R. H. (1965). Geology and geochemical investigations near Paxson, northern Copper River basin, Alaska. *Alaska Division of Mines and Minerals*. Geologic Report 13, 38 p.
- Saltus, R. W., Hudson, T. & Wilson, F. H. (2007). The geophysical character of southern Alaska: Implications for crustal evolution. In: Ridgway, K. D., Trop, J. M., O'Neill, J. M. & Glen, J. M. G. (eds.) *Tectonic Growth of a Collisional Continental Margin: Crustal Evolution of Southern Alaska*. Geological Society of America Special Paper 431, pp. 1-20.
- Schmidt, J. M., O'Neill, J. M., Snee, L. W., Blodgett, R. B., Ridgway, K. D., Wardlaw, B. R. & Blome, C. D. (2003a). The Northwestern edge of Wrangellia: Stratigraphic and intrusive links between crustal block from the Peninsular Terrane to Broad Pass *Geological Society of America Cordilleran Section Abstracts with Programs* Volume 35, No. 6. p. 560
- Schmidt, J. M. & Rogers, R. K. (2007). Metallogeny of the Nikolai large igneous province (LIP) in southern Alaska and its influence on the mineral potential of the Talkeetna Mountains. In: Ridgway, K. D., Trop, J. M., O'Neill, J. M. & Glen, J. M. G. (eds.) *Growth of a Collisional Continental Margin - Crustal Evolution of South-Central Alaska*. Geological Society of America Special Paper 431, pp. 623-648.
- Schmidt, J. M., Weldon, M. B. & Wardlaw, B. (2003b). New mapping near Iron Creek, Talkeetna Mountains, indicates presence of Nikolai greenstone. In: Clautice, K.

- H. & Davis, P. K. (eds.) *Short Notes on Alaska Geology 2003*. Alaska Division of Geological & Geophysical Surveys Professional Report 120J, pp. 101-108.
- Selwyn, A. R. C. (1872). Preliminary explorations in British Columbia. *Geological Survey of Canada*. Report of Progress 1871-1872, 52-53, 63 p.
- Sharp, R. P. (1943). Geology of the Wolf Creek area, St. Elias Range, Yukon Territory, Canada. *Geological Society of America Bulletin* **54**, 625-650.
- Sherwood, M. B. (1965). *Exploration of Alaska, 1865-1900*. Yale Western American Series, vol. VII. Yale University Press: New Haven, Connecticut, 207 p.
- Silberling, N. J., Richter, D. H., Jones, D. L. & Coney, P. C. (1981). Geologic map of the bedrock part of the Healy A-1 Quadrangle south of the Talkeetna-Broxon Gulch fault system, Clearwater Mountains, Alaska. *U.S. Geological Survey Open-File Report* 81-1288, 1 sheet, 1:63,360 scale.
- Smith, J. G. & MacKevett, E. M., Jr. (1970). The Skolai Group in the McCarthy B-4, C-4, C-5 Quadrangles, Wrangell Mountains, Alaska. *U. S. Geological Survey. Bulletin* 1274-Q, Q1-Q26 p.
- Smith, T. E. (1971). Geology, economic geochemistry, and placer gold resources of the western Clearwater Mountains, east-central Alaska. Ph.D., University of Nevada.
- Smith, T. E. (1973). Geologic map of the western Clearwater Mountains. *Alaska Division of Geological & Geophysical Surveys* Alaska Open-File Report 29, 7 p., 1 sheet, scale 1:63,360.
- Starkey, R. J. & Frost, B. R. (1990). Low-grade metamorphism of the Karmutsen Volcanics, Vancouver Island, British Columbia. *Journal of Petrology* **31**(1), 167-195.
- Stevenson, J. S. (1945). Geology and ore deposits of the China Creek area, Vancouver Island, British Columbia. *British Columbia Ministry of Energy, Mines, and Petroleum Resources*. Annual Report, 1944, 5-26 p.
- Stout, J. H. (1965). Bedrock geology between Rainy Creek and the Denali Fault, eastern Alaska Range, Alaska. MS, University of Alaska, 75 pp.
- Stout, J. H. (1976). Geology of the Eureka Creek area, east-central Alaska Range. *Alaska Division of Geological and Geophysical Surveys*. Geologic Report 46, 32 p.
- Surdam, R. C. (1967). Low-grade metamorphism of the Karmutsen Group. Unpublished Ph.D. dissertation, University of California, Los Angeles, 288 pp.
- Surdam, R. C. (1968a). Origin of native copper and hematite in the Karmutsen Group, Vancouver Island, British Columbia. *Economic Geology* **63**, 961-966.
- Surdam, R. C. (1968b). The stratigraphy and volcanic history of the Karmutsen group, Vancouver Island, British Columbia. *University of Wyoming, Contributions to Geology* **7**, 15-26.
- Surdam, R. C. (1969). Electron microprobe study of prehnite and pumpellyite from the Karmutsen Group, Vancouver Island, British Columbia. *American Mineralogist* **54**, 256-266.
- Surdam, R. C. (1970). The petrology and chemistry of the Karmutsen group volcanic rocks. *University of Wyoming, Contributions to Geology* **9**(1), 9-12.
- Sutherland Brown, A. (1968). Geology of the Queen Charlotte Islands, British Columbia. *B.C. Department of Mines and Petroleum Resources, Bulletin* **54**, 226 p.
- Sutherland Brown, A. & Yorath, C. J. (1985). Lithoprobe profile across southern Vancouver Island: Geology and Tectonics. In: Tempelman-Kluit, D. (ed.) *Field*

- guides to geology and mineral deposits in the southern Canadian Cordillera.* Geol. Soc. Amer. Cordilleran section annual meeting, Field Trip Guidebook 8: Vancouver, British Columbia, pp. 8.1-8.23.
- Terabayashi, M. (1993). Compositional evolution in Ca-amphibole in the Karmutsen metabasites, Vancouver Island, British Columbia, Canada. *Journal of Metamorphic Petrology* 11(5), 677-690.
- Thompson, R. I. (1988). Late Triassic through Cretaceous geological evolution, Queen Charlotte Islands, British Columbia. In: *Current Research, part E.* Geological Survey of Canada, Paper 88-1E, pp.
- Thompson, R. I., Haggart, J. W. & Lewis, P. D. (1991). Late Triassic through early Tertiary evolution of the Queen Charlotte Islands: a perspective on hydrocarbon potential. In: Woodsworth, G. J. (ed.) *Evolution and Hydrocarbon Potential of the Queen Charlotte Basin, British Columbia.* Geological Survey of Canada, Paper 90-10, pp.
- Trop, J. M. & Ridgway, K. D. (2007). Mesozoic and Cenozoic tectonic growth of southern Alaska: A sedimentary basin perspective. In: Ridgway, K. D., Trop, J. M., O'Neill, J. M. & Glen, J. M. G. (eds.) *Tectonic growth of a collisional continental margin: Crustal evolution of southern Alaska.* Geological Society of America Special Paper 431, pp. 55-94.
- Trop, J. M., Ridgway, K. D., Manuszak, J. D. & Layer, P. W. (2002). Mesozoic sedimentary-basin development on the allochthonous Wrangellia composite terrane, Wrangell Mountains basin, Alaska: A long-term record of terrane migration and arc construction. *Geological Society of America Bulletin* 114, 693-717.
- Turner, D. L. & Smith, T. E. (1974). Geochronology and generalized geology of the central Alaska Range, Clearwater Mountains and northern Talkeetna Mountains. *Alaska Division of Geological and Geophysical Surveys.* Open-File Report AOF-72, 10 p.
- Weldon, M. B., Riehle, J. R., Schmidt, J. M., Newberry, R. J. & Pessel, G. H. (2000a). Major oxide, minor oxide, trace element, and geochemical data from rocks collected in the Iron Creek area, Talkeetna Mountains B-5 Quadrangle. *Alaska Division of Geological & Geophysical Surveys.* Major oxide, minor oxide, trace element, and geochemical data from rocks collected in the Iron Creek area, Talkeetna Mountains B-5 Quadrangle 2 sheets, scale 1:63,360., 31 p.
- Weldon, M. B., Riehle, J. R., Schmidt, J. M., Newberry, R. J. & Pessel, G. H. (2000b). Preliminary geologic map of the Iron Creek area, Talkeetna Mountains B-5 Quadrangle, Alaska. *Alaska Division of Geological & Geophysical Surveys* Preliminary Interpretive Report 2000-7, 1 sheet, scale 1:63,360.
- Weldon, M. B., Riehle, J. R., Schmidt, J. M., Newberry, R. J. & Pessel, G. H. (2002). Geologic map of the Iron Creek area, Talkeetna Mountains B-5 Quadrangle, Alaska. *Alaska Division of Geological & Geophysical Surveys* Preliminary Interpretive Report 2002-4, 1 sheet, scale 1:63,360.
- Wilson, F. H., Dover, J. D., Bradley, D. C., Weber, F. R., Bundtzen, T. K. & Haeussler, P. J. (1998). Geologic map of Central (Interior) Alaska. *U. S. Geological Survey* Open-File Report 98-133-A <http://wrgis.wr.usgs.gov/open-file/of98-133-a/>.

- Wilson, F. H., Labay, K. A., Shew, N. B., Preller, C. C., Mohadjer, S. & Richter, D. H. (2005). Digital Data for the Geology of Wrangell-Saint Elias National Park and Preserve, Alaska *U. S. Geological Survey Open-File Report 2005-1342* <http://pubs.usgs.gov/of/2005/1342/>.
- Winkler, G. R. (2000). A Geologic Guide to Wrangell-Saint Elias National Park and Preserve, Alaska: A tectonic collage of northbound terranes. *U.S. Geological Survey. Professional Paper 1616*, 166 p.
- Woodsworth, G. J. (ed.) (1991). *Evolution and Hydrocarbon Potential of the Queen Charlotte Basin, British Columbia*. Geological Survey of Canada, Paper 90-10.
- Yole, R. W. (1963). Early Permian fauna from Vancouver Island, British Columbia. *Bulletin of Canadian Petroleum Geology* **11**, 138-149.
- Yole, R. W. (1965). A faunal and stratigraphic study of Upper Paleozoic rocks of Vancouver Island, British Columbia. Ph.D., University of British Columbia, 254 pp.
- Yole, R. W. (1969). Upper Paleozoic stratigraphy of Vancouver Island, British Columbia. *Proceedings of the Geological Association of Canada* **20**, 30-40.
- Yole, R. W. & Irving, E. (1980). Displacement of Vancouver Island, paleomagnetic evidence from the Karmutsen Formation. *Canadian Journal of Earth Sciences* **17**, 1210-1228.
- Yorath, C. J., Sutherland Brown, A. & Massey, N. W. D. (1999). LITHOPROBE, southern Vancouver Island, British Columbia. *Geological Survey of Canada. LITHOPROBE, southern Vancouver Island, British Columbia Bulletin 498*, 145 p.



## APPENDIX H.

### <sup>40</sup>Ar/<sup>39</sup>Ar ANALYTICAL METHODS

Twenty mineral separates (6 hornblende, 1 biotite, and 13 plagioclase) from 19 samples were processed for <sup>40</sup>Ar/<sup>39</sup>Ar geochronology. The least altered samples were selected for <sup>40</sup>Ar/<sup>39</sup>Ar dating based on thorough petrographic inspection of minerals in the basaltic groundmass. For processing plagioclase separates, the samples were first crushed in a Rocklabs hydraulic piston crusher between WC-plates. During crushing, approximately 400 g of each sample was sieved to isolate the fraction of grains between 250 and 450 µm. These grains were then rinsed in deionized water (~10 times). After drying, a hand magnet was used to separate the most magnetic grains. A Frantz magnetic separator was then used to isolate the non-magnetic plagioclase from the groundmass. The remaining grains were then hand-picked to select the least altered, inclusion-free plagioclase grains. A 2 mm-diameter circle of the freshest plagioclase was leached with 3 N cold HCl in an ultrasonic bath for 30 min, followed by rinsing with deionized water. Samples were finally rinsed with 1 N HNO<sub>3</sub> and deionized water and allowed to dry. For hornblende and biotite, samples were crushed, sieved, washed in deionized water and dried at room temperature. Mineral separates from the 0.25 mm to 0.15 mm size fraction were hand-picked, washed in acetone, and dried.

Plagioclase, hornblende, and biotite grains were wrapped in aluminum foil and stacked in an irradiation capsule with similar-aged samples and neutron flux monitors (Fish Canyon Tuff sanidine, 28.02 Ma (Renne *et al.*, 1998)). The samples were irradiated at the McMaster Nuclear Reactor in Hamilton, Ontario, for 90 MWH, with a neutron flux of approximately  $6 \times 10^{13}$  neutrons/cm<sup>2</sup>/s. Analyses (n=57) of 19 neutron flux monitor positions produced errors of <0.5% in the J value.

Samples were analyzed at the Noble Gas Laboratory in the Pacific Centre for Isotopic and Geochemical Research at University of British Columbia. The mineral separates were step-heated at incrementally higher powers in the defocused beam of a 10W CO<sub>2</sub> laser (New Wave Research MIR10) until fused. The gas evolved from each step was analyzed by a VG5400 mass spectrometer equipped with an ion-counting electron multiplier. All measurements were corrected for total system blank, mass spectrometer sensitivity, mass discrimination, radioactive decay during and subsequent to

irradiation, as well as interfering Ar from atmospheric contamination and the irradiation of Ca, Cl and K (Isotope production ratios:  $(^{40}\text{Ar}/^{39}\text{Ar})_{\text{K}}=0.0302\pm0.00006$ ,  $(^{37}\text{Ar}/^{39}\text{Ar})_{\text{Ca}}=1416.4\pm0.5$ ,  $(^{36}\text{Ar}/^{39}\text{Ar})_{\text{Ca}}=0.3952\pm0.0004$ ,  $\text{Ca/K}=1.83\pm0.01(^{37}\text{Ar}_{\text{Ca}}/^{39}\text{Ar}_{\text{K}})$ ).

The analytical data are presented in Supplementary data file 4 and are summarized in Table 5.3. Age spectra and isochron diagrams for each of the samples are shown in Supplementary data file 4. The plateau and correlation ages were calculated using Isoplot ver.3.09 (Ludwig, 2003). Errors are quoted at the 95% confidence level ( $2\sigma$ ) and are propagated from all sources except mass spectrometer sensitivity and age of the flux monitor. Following Ludwig (2003), the best statistically-justified plateau and plateau age were picked based on: (1) a well-defined plateau with at least three or more contiguous steps comprising more than 50% of the  $^{39}\text{Ar}$  released; (2) probability of fit of the weighted mean age greater than 5%; (3) slope of the error-weighted line through the plateau ages equals zero at 95% confidence; (4) ages of the two outermost steps on a plateau are not significantly different from the weighted-mean plateau age (at  $1.8\sigma$ , six or more steps only); (5) outermost two steps on either side of a plateau must not have nonzero slopes with the same sign (at  $1.8\sigma$ , nine or more steps only).

## REFERENCES

- Ludwig, K. R. (2003). Isoplot 3.09, A Geochronological Toolkit for Microsoft Excel. *Berkeley Geochronology Center*. Special Publication No. 4.
- Renne, P. R., Swisher, C. C., III, Deino, A. L., Karner, D. B., Owens, T. & DePaolo, D. J. (1998). Intercalibration of standards, absolute ages and uncertainties in  $^{40}\text{Ar}/^{39}\text{Ar}$  dating. *Chemical Geology* **145**(1-2), 117-152.

Appendix I. Major element (wt% oxide) and trace element (ppm) abundances of reference materials DNC-1 and BIR-1 from ActLabs whole-rock analyses

Sample	DNC-1 Meas	DNC-1 Meas	DNC-1 Meas	DNC-1 Meas	DNC-1 AVE	DNC-1 Cert	%RSD
Run	VI_1	VI_2	VI_3	Yukon	AVERAGE	CERT. VALUE	
Rock	dolerite	dolerite	dolerite	dolerite	dolerite	dolerite	
<i>Unnormalized Major Element Oxides (Weight %):</i>							
SiO <sub>2</sub>	47.00	47.09	47.02	47.26	47.09	47.04	0.1
TiO <sub>2</sub>	0.470	0.48	0.48	0.479	0.48	0.48	0.4
Al <sub>2</sub> O <sub>3</sub>	18.23	18.29	18.29	18.28	18.27	18.3	0.1
Fe <sub>2</sub> O <sub>3</sub> *	9.72	9.88	9.93	9.88	9.85	9.93	0.6
MnO	0.140	0.146	0.147	0.146	0.14	0.149	2.0
MgO	10.07	10.24	10.21	10.28	10.20	10.05	1.0
CaO	11.12	11.3	11.2	11.19	11.20	11.27	0.4
Na <sub>2</sub> O	1.90	1.9	1.97	1.91	1.92	1.87	1.9
K <sub>2</sub> O	0.22	0.15	0.11	0.21	0.17	0.23	20.2
P <sub>2</sub> O <sub>5</sub>	0.07	0.07	0.08	0.05	0.07	0.07	2.6
LOI							
Total							
<i>Trace Elements (ppm):</i>							
La	3.83	3.66	3.93	3.69	3.78	3.80	0.4
Ce	8.2	7.9	8.8	8.0	8.2	11.0	20.3
Pr	1.06	1.08	1.14	1.06	1.08	1.3	12.8
Nd	4.8	4.8	5.0	4.8	4.8	4.9	1.1
Sm	1.40	1.35	1.48	1.35	1.40	1.38	0.8
Eu	0.605	0.628	0.621	0.607	0.62	0.59	3.0
Gd	2.05	2.05	2.06	2.02	2.04	2.00	1.5
Tb	0.4	0.4	0.4	0.4	0.4	0.4	2.3
Dy	2.73	2.86	2.8	2.79	2.80	2.7	2.5
Ho	0.64	0.64	0.6	0.64	0.63	0.62	1.2
Er	1.97	1.96	1.94	2.00	1.97	2	1.2
Tm	0.318	0.325	0.318	0.318	0.32	0.38	12.2
Yb	1.96	2.01	2.00	2.00	1.99	2.01	0.7
Lu	0.286	0.294	0.303	0.296	0.29	0.32	5.8
Sc							
V	139	139	148	139	141	148	3.3
Cr							
Co							
Ni							
Cu							
Zn							
Ga	14	14	15	14	14	15	3.3
Ge	1.1	1.1	1.3	1.1	1.2	1.3	7.9
Rb	4	4	4	4	4	5	18.4
Sr	140	143	143	142	142	145	1.5
Y	18	18	18	17	18	18	1.0
Zr	35	31	33	30	32	41	16.9
Nb	1.3	1.4	1.4	1.4	1.4	3.0	52.5
Cs	0.2	0.2	0.2	0.2	0.20	0.3	28.4
Ba	104	106	106	105	105	114	5.6
Hf	0.9	0.9	1.0	0.9	0.9	1.0	4.4
Ta	0.07			0.08	0.08	0.1	20.0
Pb							
Th	0.24	0.25	0.22	0.24	0.24	0.20	12.0
U	0.06	0.06		0.05	0.06	0.10	9.6

Abbreviations are: VU, Vancouver Island; AVE, average; Cert., certified; Meas, measured. Analyses were performed at Activation Laboratory (ActLabs). Fe<sub>2</sub>O<sub>3</sub>\* is total iron expressed as Fe<sub>2</sub>O<sub>3</sub>. All major elements, Sr, V, and Y by Fused ICP quadrupole (ICP-OES); Cu, Ni, Pb, and Zn by Total dilution ICP; Cs, Ga, Ge, Hf, Nb, Rb, Ta, Th, U, Zr, and REE by Fused-magnetic-sector ICP; Co, Cr, and Sc by INAA. Blanks are below detection limit. See Chapter 2 and Appendix E for sample preparation and analytical methods at Actlabs.

Sample	BIR-1 Meas	BIR-1 Meas	BIR-1 Meas	BIR-1 Meas	BIR-1 AVE	BIR-1 Cert	%RSD
Run	VI_1	VI_2	VI_3	Yukon	AVERAGE	CERT. VALUE	
Rock	basalt	basalt	basalt	basalt	basalt	basalt	
<i>Unnormalized Major Element Oxides (Weight %):</i>							
SiO <sub>2</sub>	47.68	47.73	47.7	47.73	47.71	47.77	0.1
TiO <sub>2</sub>	0.958	0.955	0.959	0.958	0.96	0.96	0.2
Al <sub>2</sub> O <sub>3</sub>	15.33	15.37	15.32	15.36	15.35	15.35	0.0
Fe <sub>2</sub> O <sub>3</sub> *	11.23	11.24	11.14	11.25	11.22	11.26	0.3
MnO	0.167	0.17	0.167	0.169	0.17	0.171	1.1
MgO	9.64	9.64	9.6	9.67	9.64	9.68	0.3
CaO	13.14	13.21	13.09	13.18	13.16	13.24	0.5
Na <sub>2</sub> O	1.83	1.8	1.82	1.82	1.82	1.75	2.7
K <sub>2</sub> O	0.03	0.03	0.03	0.03	0.03	0.03	0.0
P <sub>2</sub> O <sub>5</sub>	0.03	0.04	0.02	0.05	0.04	0.05	25.0
LOI							
Total							
<i>Trace Elements (ppm):</i>							
La	0.78	0.78	0.7	0.74	0.75	0.62	13.5
Ce	2.0	2.0	2.0	2.0	2.0	2.0	0.0
Pr	0.40	0.4	0.38	0.38	0.39	0.38	1.4
Nd	2.4	2.5	2.4	2.4	2.4	2.5	2.1
Sm	1.11	1.09	1.11	1.08	1.10	1.1	0.1
Eu	0.544	0.576	0.564	0.549	0.56	0.54	2.3
Gd	1.89	1.92	1.84	1.89	1.89	1.85	1.4
Tb	0.4	0.4	0.4	0.4	0.4	0.4	8.7
Dy	2.66	2.72	2.63	2.66	2.67	2.5	4.6
Ho	0.61	0.62	0.56	0.59	0.59	0.57	3.0
Er	1.79	1.84	1.71	1.77	1.78	1.7	3.2
Tm	0.282	0.292	0.275	0.278	0.28	0.26	5.7
Yb	1.73	1.76	1.69	1.71	1.72	1.65	3.1
Lu	0.253	0.261	0.253	0.253	0.26	0.26	1.4
Sc							
V	322	322	315	322	320	313	1.6
Cr							
Co							
Ni							
Cu							
Zn							
Ga	17	17	16	16	16	16	1.8
Ge	1.5	1.4	1.5	1.4	1.4	1.5	2.8
Rb							
Sr	106	107	106	107	107	108	1.0
Y	16	17	16	16	16	16	1.1
Zr	16	13	13	15	14	16	8.2
Nb	0.4	0.5	0.5	0.5	0.5	0.6	15.6
Cs							
Ba	8	8	8	8	8	7	9.4
Hf	0.6	0.6	0.6	0.6	0.6	0.6	2.1
Ta	0.04			0.03	0.03	0.04	11.0
Pb							
Th							
U	0.02			0.01	0.01	0.01	9.6

## APPENDIX J.

### DESCRIPTION OF SUPPLEMENTARY ELECTRONIC FILES ON CD-ROM

\*\*\*\*\*

#### **Supplementary data files (SD)**

SD 1- Endnote database for Wrangellia (.enl file)

SD 2- Reference list for Wrangellia (.doc file)

SD 3- Geochemistry for  $^{40}\text{Ar}/^{39}\text{Ar}$  samples (.xls file)

SD 4-  $^{40}\text{Ar}/^{39}\text{Ar}$  analytical data (.xls file)

SD 5- Wrangellia ages and biostratigraphy (.xls file)

SD 1- Endnote database for Wrangellia (.enl file)

This Endnote library is a compilation of approximately 500 references mostly related to research of Wrangellia, or parts of western North America. This .enl file was created with Endnote X1.0.1 (Bld 2682) and should be compatible with older versions of Endnote.

SD 2- Reference list for Wrangellia (.doc file)

This .doc file is an exported version of the Endnote file in Supplementary data file 1 (SD1) and was created with Microsoft Word 2003.

SD 3- Geochemistry for  $^{40}\text{Ar}/^{39}\text{Ar}$  samples (.xls file)

This Microsoft Excel file contains the analytical data for whole-rock analyses for the 19 samples dated by the  $^{40}\text{Ar}/^{39}\text{Ar}$  dating method. Analyses were performed by ActLabs and the analytical methods are summarized in Chapter 2 and Appendix E. Additional information in this table includes: UTM coordinates, geographic location, lithology, mineral proportion, and texture. This file was created with Microsoft Excel 2003.

SD 4-  $^{40}\text{Ar}/^{39}\text{Ar}$  analytical data (.xls file)

This Microsoft Excel file contains the analytical data for the  $^{40}\text{Ar}/^{39}\text{Ar}$  dating method for the 20 mineral separates analyzed at the Noble Gas Laboratory in the Pacific Centre for Isotopic and Geochemical Research at University of British Columbia. Age spectra and isochron diagrams for each of the samples are shown along with all the analytical data from incremental step-heating. The analytical methods are summarized in Appendix H. Where multiple analyses of a single sample were made, all the results for each sample are included in a single worksheet in this workbook. This file was created with Microsoft Excel 2003.

SD 5- Wrangellia ages and biostratigraphy (.xls file)

This Microsoft Excel file contains 3 worksheets that are described separately below.

#### **Age (worksheet)**

The Age worksheet contains ~750 isotopic ages for units assigned to Wrangellia. Most of this data was extracted from the CordAge 2004 database and was supplemented by ~50 ages not in the CordAge database, mostly from Alaska. Samples of the Coast and Insular Belts are included, based on their location, and caution should be used in deciding

whether samples are actually located within Wrangellia. CordAge 2004 (a database of isotopic age determinations for rock units from the Canadian Cordillera) is an MS-Access based database, consisting of the merged datasets of the publically available products BCAGE 2004A-1 (released October 2004; Breitsprecher and Mortensen (2004a)) and YukonAge 2004 (released July, 2004; Breitsprecher and Mortensen (2004b)). The compilation contains all reported non-proprietary isotopic age determinations for bedrock units from British Columbia and Yukon Territory respectively: 9321 age determinations from 5997 rock samples, summarizing 778 published articles, theses, reports or unpublished sources. Katrin Breitsprecher offered assistance with extracting this information. The user is referred to Breitsprecher and Mortensen (2004a, 2004b) for information about the rating system of ages (**Rel\_rating** column; column H) and other details.

The database should not be cited as the source of the age. Age determinations should be cited to the original source, which is provided in each record of the database.

#### **Age\_refs (worksheet)**

This worksheet contains the information of the references for the age compilation listed in the Age worksheet (described above). The **ref no** column (column A) in the Age\_refs worksheet refers to the **Ref No** column (column L) in the Age worksheet.

#### **Biostratigraphy (worksheet)**

This is a compilation of 75 fossil age determinations from published literature related to Wrangellia. The full reference where each determination is published is included in column B and the region is shown in column E. All of the age ranges are plotted in Figure 5.22 according to the region indicated in column E. The low and high ages for each age range use the age boundaries for epochs and stages from Gradstein *et al.* (2004). Age boundaries for the Triassic are from Ogg (2004) and revised based on Furin *et al.* (2006). This file was created with Microsoft Excel 2003.

\*\*\*\*\*

#### **Supplementary Google Earth files (SGE)**

- SGE 1- Mapped Wrangellia flood basalts (.kmz file)
- SGE 2- Major faults in Alaska and Yukon (.kml file)
- SGE 3- Major faults in southwest B.C. (.kml file)
- SGE 4- Alaska sample locations (.kml file)
- SGE 5- Yukon sample locations (.kml file)
- SGE 6- Vancouver Island sample locations (.kml file)
- SGE 7- Alaska Range photograph locations (.kmz file)
- SGE 8- Wrangell Mountains photograph locations (.kmz file)
- SGE 9- Yukon photograph locations (.kml file)
- SGE 10- Vancouver Island photograph locations (.kmz file)

The .kmz and .kml files listed above consist of georeferenced information that are designed to be viewed with the satellite imagery in Google Earth. The Google Earth

application is available for free download at <http://earth.google.com/>. Information about Google Earth can be found at this address.

**SGE 1- Mapped Wrangellia flood basalts (.kmz file)**

This is a red transparent layer that shows the distribution of the Wrangellia flood basalts in Alaska, Yukon, and British Columbia. The map was derived from data in Wilson *et al.* (1998, 2005), Israel (2004), Massey *et al.* (2005a, b), and Brew (2007, written comm.). See Chapter 5 for an overview of the Wrangellia flood basalts in these areas.

**SGE 2- Major faults in Alaska and Yukon (.kml file)**

**SGE 3- Major faults in southwest BC (.kml file)**

These files show the location of faults in parts of Alaska, Yukon, and BC. These files were filtered from original files found at the following locations: Alaska from <http://www.asgdc.state.ak.us/>; Yukon from Israel (2004); BC faults from Massey *et al.* (2005a, b).

**SGE 4- Alaska sample locations (.kml file)**

**SGE 5- Yukon sample locations (.kml file)**

**SGE 6- Vancouver Island sample locations (.kml file)**

These files show the locations, sample numbers, and flow type of samples of Wrangellia flood basalts collected during this project.

**SGE 7- Alaska Range photograph locations (.kmz file)**

**SGE 8- Wrangell Mountains photograph locations (.kmz file)**

**SGE 9- Yukon photograph locations (.kml file)**

**SGE 10- Vancouver Island photograph locations (.kmz file)**

These files contain small versions of georeferenced photographs. Multiple photographs are referenced to a single coordinate. Therefore, in order to view all of the photographs from a single coordinate it is necessary to open the folders for each region in the My Places menu so individual photographs can be selected and viewed. Zooming in also helps to distinguish photograph locations. These photographs and others can be viewed in higher resolution in the Supplementary photo files (described below).

\*\*\*\*\*

**Supplementary photo files (SP)**

**SP 1- Alaska Range photographs (.pdf file)**

**SP 2- Wrangell Mountains photographs (.pdf file)**

**SP 3- Ed MacKevett Jr. Wrangell Mountains photographs (.pdf file)**

**SP 4- Yukon photographs (.pdf file)**

**SP 5- Vancouver Island photos (.pdf file)**

These are .pdf files of field photographs from Alaska, Yukon, and British Columbia. SP3 is a file of photographs taken by Ed MacKevett Jr. The photographs by Ed were taken while mapping parts of the Wrangell Mountains in Alaska in the 1970's. These photographs were provided by Travis Hudson. I would like to thank Travis Hudson for making these photographs available for the purposes of research.



\*\*\*\*\*

Also included on the CD-ROM is an electronic file of this complete dissertation:  
Greene\_2008\_PhD\_dissertation\_UBC (.pdf file)

## REFERENCES

- Breitsprecher, K. and Mortensen, J.K., 2004a. BCAGE 2004A-1 - a database of isotopic age determinations for rock units from British Columbia. *British Columbia Ministry of Energy and Mines, Geological Survey*, Open File 2004-3 (Release 3.0), 7757 records, 9.3 Mb.
- Breitsprecher, K., and Mortensen, J.K. (compilers), 2004b. YukonAge 2004: A database of isotopic age determinations for rock units from Yukon Territory. *Yukon Geological Survey*, CD-ROM.
- Brew, D. A. C. (2007, written comm.). Unpublished map showing the distribution of the Late Triassic Wrangellia, Hyd Group, and Perserverance group rocks in southeastern Alaska, scale 1:600,000 (Based on Brew, D. A. (Compiler), Unpublished bedrock geologic map of southeastern Alaska.)
- Furin, S., Preto, N., Rigo, M., Roghi, G., Gianolla, P., Crowley, J. L. & Bowring, S. A. (2006). High-precision U-Pb zircon age from the Triassic of Italy: Implications for the Triassic time scale and the Carnian origin of calcareous nannoplankton and dinosaurs. *Geology* 34(12), 1009-1012, 10.1130/g22967a.1.
- Gradstein, F. M., Ogg, J. G. & Smith, A. G. (eds.) (2004). *A Geologic Time Scale 2004*. Cambridge University Press 610 pp.
- Israel, S. (2004). Geology of Southwestern Yukon (1:250 000 scale). *Yukon Geological Survey* Open File 2004-16.
- Massey, N. W. D., MacIntyre, D. G., Desjardins, P. J. & Cooney, R. T. (2005a). Digital Geology Map of British Columbia: Tile NM9 Mid Coast, B.C. *B.C. Ministry of Energy and Mines* Geofile 2005-2.
- Massey, N. W. D., MacIntyre, D. G., Desjardins, P. J. & Cooney, R. T. (2005b). Digital Geology Map of British Columbia: Tile NM10 Southwest B.C. *B.C. Ministry of Energy and Mines* Geofile 2005-3.
- Ogg, J. G. (2004). The Triassic Period. In: Gradstein, F. M., Ogg, J. G. & Smith, A. G. (eds.) *A Geologic Time Scale 2004*. Cambridge University Press: Cambridge. pp. 271-306.
- Wilson, F. H., Dover, J. D., Bradley, D. C., Weber, F. R., Bundtzen, T. K. & Haeussler, P. J. (1998). Geologic map of Central (Interior) Alaska. *U. S. Geological Survey* Open-File Report 98-133-A <http://wrgis.wr.usgs.gov/open-file/of98-133-a/>.
- Wilson, F. H., Labay, K. A., Shew, N. B., Preller, C. C., Mohadjer, S. & Richter, D. H. (2005). Digital Data for the Geology of Wrangell-Saint Elias National Park and Preserve, Alaska *U. S. Geological Survey* Open-File Report 2005-1342, <http://pubs.usgs.gov/of/2005/1342/>.